Geochemical and Sr-Nd-Hf-O isotopic constraints on volcanic petrogenesis at the Sunda arc, Indonesia

Heather. . Handley

Geochemical and Sr-Nd-Hf-O isotopic constraints on volcanic petrogenesis at the Sunda arc, Indonesia

A thesis presented for the degree of

Doctor of Philosophy

By

Heather. K. Handley

Department of Earth Sciences

Durham University

April 2006

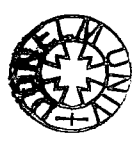

Declaration

No part of this thesis has previously been submitted for a degree at this or any other university. The work described in this thesis is entirely that of the author, except where reference is made to previously published or unpublished work.

Heather. K. Handley

Department of Earth Sciences
University of Durham

April 2006

Abstract

The Sunda island arc of Indonesia formed as a result of the northward subduction of the Indo-Australian Plate beneath the Eurasian Plate. Along-arc variations in the composition and thickness of the overriding Eurasian plate and variation in the type and amount of sediment deposited on the subducting plate create differential effects on Sunda arc lava geochemistry. Detailed study of volcanic rocks from Salak, Gede Volcanic Complex (GVC) in West Java and Ijen Volcanic Complex (IVC) in East Java was carried out in order to establish the relative importance and contributions of various potential source components and composition-modifying processes at individual volcanic centres, prior to investigating petrogenetic variation along the arc.

Differentiation processes play a major role in modifying the geochemical composition of Sunda arc magmas. However, the relative importance and traceable impact of the different processes varies at each volcanic centre. Fractional crystallisation of a typical Javan island arc mineral assemblage exerts the largest control on major and trace element composition of the volcanic rocks. Distinct intra-volcanic complex differentiation trends at IVC and Salak are spatially controlled and are explained by independent conduits and multiple magma reservoirs at different depths in the crust - linked to sub-volcanic structure. Shallow level contamination by typical upper-crustal continental material is insignificant during magmatic differentiation at Salak, GVC and IVC. However, at Salak there is some evidence for assimilation of material similar in composition to the volcanic rocks. Deep fractionation of a phase in which HFSE and HREE are compatible (e.g. amphibole) is inferred in the evolution of most Javan magmas.

Magmatism at Salak, GVC and IVC is the product of shallow, relatively homogeneous, fertile, Indian Ocean MORB-like mantle that has been enriched by slab-derived component(s) sourced from the altered oceanic crust and subducted sediment. Hf and Nd isotope ratios of Javan lavas show that the subducted sedimentary source component is heterogeneous and reflects spatial variations in sediment compositions on the down-going plate along the Java Trench.

A progressive eastward increase in Sr isotope ratio of volcanic rocks across West and Central Java broadly correlates with inferred lithospheric thickness. A significant change in crustal architecture (i.e. thickness) occurs between Central and East Java. This transition may represent the south-eastern boundary of Sundaland (pre-Tertiary arc basement).

Acknowledgements

First and foremost, I would like to thank my supervisors Jon Davidson and Colin Macpherson for all their time, valued advice, discussions and support throughout the project and for shaping my ideas and understanding of arc petrogenesis. I am extremely grateful to Colin for travelling out to Indonesia during fieldwork. NERC is thanked for funding this project. IAVCEI, MinSoc, VMSG and Ustinov College provided financial assistance for me to present this research at national and international conferences. The Ogden Trust, One NE and DEDP are thanked for the 2005-2006 Teaching Fellowship.

I am indebted to Akhmand Zaennudin at the Volcanic Survey of Indonesia for his guidance in the field, extreme kindness and for introducing me to ubi bakar. I also thank: Tis, our driver, who taught me Sundanese so that I could haggle with the Bandung taxi drivers (and win); Super-Komar, for being, well, super; Budi for help in collecting samples and his wife for the daily supply of fried bananas; the Sundanese locals who helped locate outcrops and hammer off samples along the way. Supri Andreastuti and everyone at VSI in Yogya are thanked for terrific hospitality and the trip up Merapi. I am grateful to Diane and Simon at Royal Holloway for helping with fieldwork logistics and Robert Hall and the SEARG for extra financial support, without which, my 80 kg of rocks would still be sat in Bandung.

Chris Ottley and Geoff Nowell are thanked for training and supervision in the lab at Durham. Geoff is also thanked for valuable comments on the analytical techniques section. I thank Dave Sales for the careful preparation of thin sections. Thanks go to Dodie James and Godfrey Fitton for provision of the XRF facility at Edinburgh and Gwylim for accommodation during sample preparation. Dave Plant made trips to the microprobe facility at the University of Manchester very enjoyable and I am grateful to Ben and Chat for accommodation (and Thai Elvis karaoke) during my visits. Dave Mattey is thanked for supervision during oxygen work at Royal Holloway. A huge thanks goes to Ralf Gertisser for supplying Merapi samples and for putting me up during VMSG 2005 in Milton Keynes. Robert Hall, John Gamble, Joel Baker and Ian Smith are thanked for provision of rock powders and samples. I am grateful to Kim Berlo, Jim Stimac and Kurt Knesel for discussions on IVC and Salak. Helen Smyth is thanked for providing Java SRTM data.

I am ever grateful to Shaz, for being a great friend and for making me laugh so many times over the last few years. Thanks also goes to: Ozzy Sarah, for coffee breaks during writing; John E, for housing me for 3 months and creating fun distractions; Darren, for all the 'new life' plans; Gary for all things computer related; Fabio, for chocolate, chats and his jeito brasileira; 'Thousands', for introducing me to North Sea suicide (surfing), meals while writing-up and numerous biscuit and tea breaks; my housemate James, for putting up with my nocturnal lifestyle in the last few months; Janet, Elliot and Mark at Staindrop Comprehensive, for the much appreciated support during my year in school and letting me play with treacle, play-dough and mars bars and call it science!; John Caulfield, for the regular provision of chocolate brownies, dynamite write-up mascot and his family for the great hospitality during VMSG 2006 in Leeds; Neil and Alexis, for extra geochemistry enthusiasm when mine needed a boost; Neil (also), for great encouragement, capoeira and much needed new write-up music; Chris, for the random deadline; The Cat Empire, for Two Shoes, which kept me smiling and dancing while writing on long winter days; Egypt, for shining a light at the end of the tunnel; Karen, for the timely teaching of hieroglyphics and introducing me to grammar I had no idea existed (no comments please).

Last but not least, I am eternally grateful to my Mum and Richard for their constant love and fantastic support in everything I do (and offer of a caravan for writing-up), to our Jude for the clothes and mop-chops, and my Dad, for his unique spirit, amazing support and for keeping me entertained over the last few years with all his latest escapades!

Contents

Data presented in this study are provided on a CD located inside the back cover of this thesis

List of Figures

Chapter 1

Chapter 2

Chapter 3

Chapter 4

Chapter 5

Chapter 6

List of Tables

Chapter 2

Chapter 3

Chapter 4

Common abbreviations and acronyms

AFC - Assimilation and fractional crystallisation

AOC - Altered oceanic crust

cpx - Clinopyroxene

CR - Caldera rim

CVG - Central Vent Group

FC - Fractional crystallisation

GVC - Gede Volcanic Complex

HFSE - High field strength element

IVC - Ijen Volcanic Complex

IC - Intra-caldera

I-MORB - Indian Ocean Mid-Ocean Ridge basalt

LILE - Large ion lithophile element

L/M/HREE - Light/middle/heavy rare earth element

N-MORB - Normal Mid-Ocean Ridge basalt

OG - Old Gede

OIAV - Oceanic island arc volcanic rocks

OIB - Ocean island basalt

ol - Olivine

opx - Orthopyroxene

PAN - Pangrango

plag - Plagioclase

SH - Source heterogeneity

SVG - Side Vent Group

VSI – Volcanic Survey of Indonesia

WBZ - Wadati-Benioff zone

YGKR - Young Gede Kawah Ratu

YGOV - Young Gede Older Volcanic Rocks

Chapter 1

Introduction

Introduction

1.1. General introduction

Destructive plate margins are sites of voluminous magma production and are the major producers of continental crust (Rudnick, 1995, Barth et al., 2000). Therefore, understanding magma genesis and evolution in subduction zone environments is crucial to understanding the origin and growth of the continents and crustal recycling in the mantle. Arc lavas display a wide variation in composition, which reflects both the composition of the primary magma from which they originated and the multitude of differentiation processes magmas experience en route to the Earth's surface (Fig. 1.1).

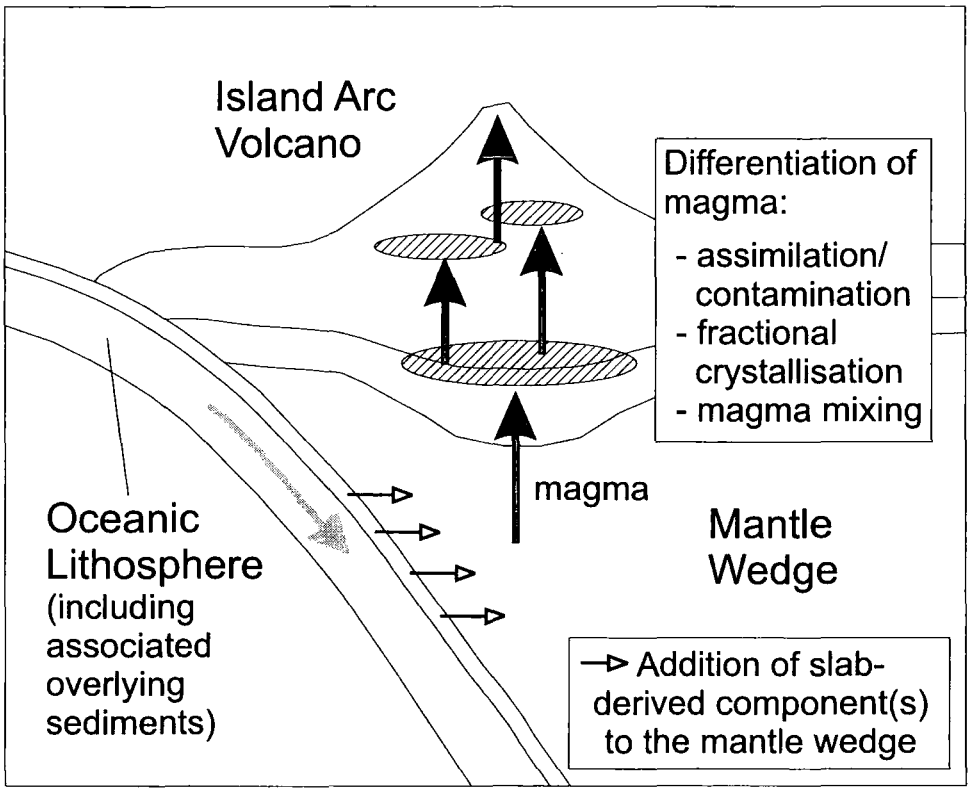

Fig. 1.1. Simple conceptual model of subduction zone petrogenesis. Subduction-related components are added to the mantle wedge from the down-going oceanic lithosphere (McCulloch and Gamble, 1991; Hawkesworth et al., 1991; Pearce and Peate, 1995). En route to the Earth's surface magma created in the mantle wedge may undergo a range of composition modifying processes.

Among the variety of processes capable of masking element concentrations of primary magmas, fractional crystallisation (Gerbe et al., 1992; Reubi and Nicholls, 2004), crustal contamination (Davidson et al., 1987; Hildreth and Moorbath, 1988; Davidson and Harmon, 1989) and magma mixing (Gamble et al., 1999; Tepley et al., 2000) are commonly identified in arc lavas. In most petrogenetic models island arc magmas originate from mantle wedge that is modified by slab-derived components (McCulloch and Gamble, 1991; Hawkesworth et al., 1991; Pearce and Peate, 1995, Fig. 1.1). Several other authors have also highlighted the importance of the subducted component (Tera, et al., 1986; Plank and Langmuir, 1993, 1998; Vroon, 1992) in the petrogenesis of arc lavas.

Indonesia is a classic example of a subduction zone, where the Indo-Australian Plate descends beneath the Eurasian Plate (Fig. 1.2a). The Sunda arc formed above part of this subduction zone and includes around 80% of the region's active volcanoes - many of which have produced eruptions that have had a significant impact on local and global environments (e.g. Toba, Krakatau and Tambora). Despite the apparently simple tectonic setting of the northward subduction of the Indo-Australian Plate beneath the Eurasian Plate, understanding magma genesis and evolution at the Sunda arc is complicated by along-arc changes in the composition and thickness of the overriding Eurasian plate (Hamilton, 1979), the changing age of the subducting oceanic crust and variation in the type and amount of sediment deposited on the subducting plate (Hamilton, 1979; Plank and Langmuir, 1998). Lateral variability in crustal architecture and the nature of the subducting slab at the Sunda arc may create differential effects on Sunda arc lavas. Detailed study of Sunda-arc volcanic centres is, therefore, a prerequisite in order to establish the relative importance and contributions of various potential source components and composition-modifying differentiation processes at individual volcanoes, prior to an along-arc comparative petrogenetic investigation.

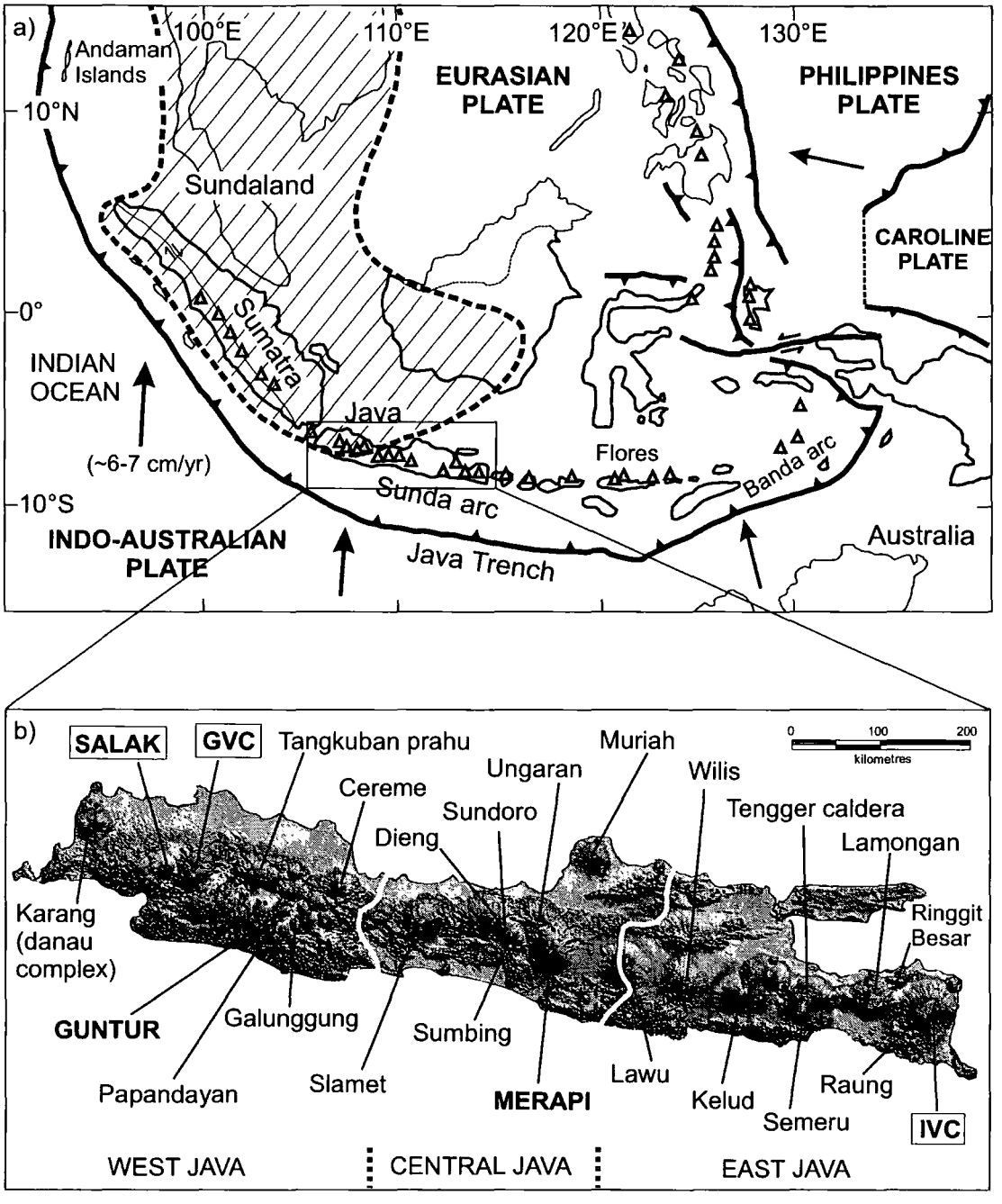

Fig. 1.2. a). Tectonic setting of Indonesia (modified from Hoffmann-Rothe et al., 2001). Solid black arrows represent the directions of plate movement. Convergence rate of the Indo-Australian Plate and Eurasian Plate from DeMets et al. (1990); Chase (1978); Tregoning et al. (1994). Grey triangles indicate active volcanoes. Hashed outline of 'Sundaland' indicates possible extent of continental lithospheric basement (Hamilton, 1979). b) Map of Java showing the location of Javan volcanoes. The main volcanoes of this study (Salak, Gede Volcanic Complex (GVC) and Ijen Volcanic Complex (IVC)) are marked by boxed, bold capitals and other volcanoes for which new Hf data is presented (Guntur and Merapi) are shown in bold capital font. Krakatau is not shown (immediately west of West Java). White lines across Java indicate the geographical boundaries of West, Central and East Java. Digital Elevation Model of Java from SRTM data (Shuttle Radar Topography Mission, NASA data).

At the Sunda arc, debate prevails on the relative importance of source versus crustal contamination. A predominance of subducted sediment at the Sunda arc is suggested from geochemical and isotopic examination of lavas by several authors (e.g. Turner and Foden, 2001; Gertisser and Keller, 2003). Plank and Langmuir (1998) identify an apparent correlation between calculated sediment flux and Sunda-arc volcanic geochemical signature within the global dataset. However, Hamilton (1979) reconciles an eastward along-arc decrease in Sr isotope ratios with decreasing crustal contamination. Gasparon and Varne (1998) argue that crustal assimilation can account for the elevated Sr and lower Nd isotope ratios in western Sunda-arc volcanics relative to MORB.

This study will constrain the relative importance of differentiation processes and source inputs for three volcanic centres situated at the opposing ends of Java (Salak and Gede Volcanic Complex (GVC) in West Java and Ijen Volcanic Complex (IVC) in East Java, Fig. 1.2b). These conclusions will then be compared with data from previous investigations of other Javan volcanoes (e.g. Merapi, Gertisser and Keller, 2003, Andreastuti, 1999; Guntur and Cereme, Edwards, 1990; Galunggung, Harmon and Gerbe, 1992, Gerbe et al., 1992; Slamet, Reubi et al., 2003, Vukadinovic and Sutawidjaja, 1995) and new Hf isotope data for Guntur and Merapi (Fig. 1.2b) to ascertain whether along-arc variations in Javan lava geochemistry are matched by spatial changes in the arc crust or subduction inputs. This study will help elucidate the nature of the transition between the continental and oceanic basement to the arc, which is expected to lie between Sumatra and east Java (Fig. 1.2a). The location of this boundary is particularly important in understanding the tectonic history of southern Indonesia and the distribution of different types of volcanoes.

1.2. The Sunda arc

1.2.1. General setting

The Sunda arc defines the section of the Indonesian arc stretching from the Andaman Islands north of Sumatra to Flores in the Banda Sea (Hamilton, 1979, Fig. 1.2a), which has developed as a result of the Indo-Australian Plate subducting northwards, beneath the Eurasian Plate, at a rate of approximately 6-7 cm/yr (Le Pichon, 1968; DeMets et al., 1990; Tregoning et al., 1994). The tectonic features of the area have been described in detail by Hamilton (1979). The Sunda arc displays a typical arc-type morphological succession of trench, accretionary prism, outer arc ridge, fore-arc basin and active volcanic chain at the islands. Along-arc variations in the nature and composition of the upper and lower plates at the Sunda arc (Hamilton, 1979; Widiyantoro and van der Hilst, 1996; Plank and Langmuir, 1998), have the potential to influence lava geochemistry and therefore these changes are highlighted below.

1.2.2. Along-arc changes of the down-going, Indian Ocean Plate

1.2.2.1. Subduction geometry

The down-going plate beneath the majority of the Sunda arc is composed of Indian Ocean lithosphere (and associated overlying sediments). Further east, at the Banda arc, Australian continental lithosphere is converging with the Eurasian plate. The age of the Indian Ocean Plate approaching the trench varies along the arc, generally increasing eastwards from 50-80 Ma along Sumatra to ~125 Ma south of Flores (Fig. 1.3) (Hamilton, 1979; Widiyantoro and van der Hilst, 1996). Slip vectors in the Benioff Zone (McCaffrey, 1991) indicate that convergence between the Indo-Australian and Eurasian plates, is almost N-S in direction. The curved nature of the arc thus results in oblique subduction along Sumatra, to almost normal

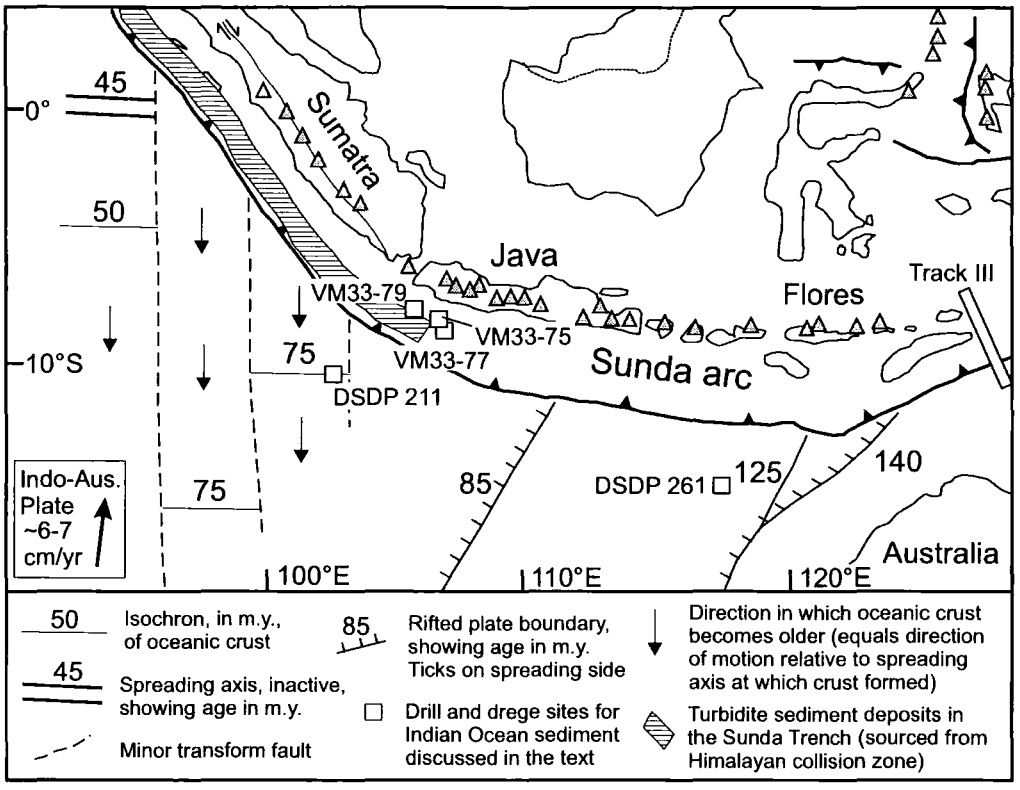

Fig. 1.3. Schematic illustration of Indian Ocean crust age (redrawn from Hamilton, 1979). The suggested southeast limit of terrigenous turbidite deposits in the trench (Anikouchine and Ling, 1967; Hamilton, 1979; Gasparon and Varne, 1998) and provenance of Indian Ocean sediments discussed in this thesis are also indicated (location of drill and dredge sites taken from Gasparon and Varne (1998) and Vroon (1992)).

subduction southwest of Java (Malod et al., 1995). The inclined seismic zone beneath Sumatra tracks Indian Ocean lithosphere to a depth of around 2-300 km, but extends much deeper beneath Java, to a depth of around 650 km. Below 100 km depth the slab dips more steeply beneath Java (~60°) than beneath Sumatra (~30-45°) (Fitch, 1970; Cardwell and Isacks, 1978; Hamilton, 1979; Widiyantoro and van der Hilst, 1996). The lack of deep earthquakes beneath Sumatra in comparison to Java has been attributed to the younger age of the subducting Indian Ocean plate at the former (Wortel and Vlaar, 1988; Kirby et al., 1996).

1.2.2.2. Sediments

Both the amount and the type of sediment deposited on the down-going Indian Ocean plate vary along the Sunda subduction system. Sediments deposited in the trench south of the Sunda arc thin dramatically towards the east: up to 5 km of sedimentary material fills the Sumatra Trench, less than 1 km exists in the western Java Trench and virtually no trench sediments are present in the eastern Java Trench (Plank and Langmuir, 1998). The substantial eastward thinning of trench sediment (largely terrigenous turbiditic material) is attributed to increasing distance from the Himalayan collision zone and deep-sea fans surrounding India in the west (Hamilton, 1979 and references therein; Plank and Langmuir, 1998; Susilohadi et al., 2005, Fig. 1.3). Sediments deposited on the Indian Ocean Plate south of the trench are relatively uniform in thickness along the arc (200-400 m) (Hamilton, 1979; Moore et al., 1980; Plank, 1993) and dominantly pelagic (Hamilton, 1979).

1.2.3. Along-arc changes of the overriding, Eurasian Plate

1.2.3.1. Volcanism

The present Sunda arc has been active since the mid- to late-Tertiary (van Bemmelen, 1949), however subduction related activity is traced back to the late Palaeozoic in Sumatra. The late Cenozoic volcanoes rise mostly above Neogene marine strata in Java, but above outcropping pre-Tertiary complexes in Sumatra (Hamilton, 1979). The evolution of the arc is related to the progressive eastward expansion of a series of subduction zones (Katili, 1975). The style and composition of volcanism changes along the arc; compositions of relatively young volcanic rocks in Java are noticeably more mafic in average composition than those of Sumatra (Hamilton, 1979; Whitford et al., 1979). On Java, the axis of volcanism has moved throughout the Cenozoic. In the early Palaeocene, it was located near the present-day north coast, during the Oligo-Miocene it was along the south coast and from the Pliocene onwards

it has moved to the central part (Hutchinson, 1982). A 200 km long sector of Java between Merapi and Kelud volcanoes (Fig. 1.2b) is classed as volcanologically extinct. Willis and Lawu, the only significant volcanoes located within this sector, show only solfataric activity (Wheller et al., 1987), but their presence indicates that this extinction occurred fairly recently.

1.2.3.2. Arc basement: composition and thickness

Along the length of the arc the composition and thickness of the overriding Eurasian plate is thought to change, from continental in the west to oceanic in the east (Hamilton, 1979), reflecting the eastward growth of the subduction system. Most of Sumatra has been continental in character since the late Palaeozoic, whereas, Java is constructed largely by post-Jurassic subduction-related processes of magmatism and tectonic accretion (Hamilton, 1988) and Palaeozoic age rocks are rare. In Java, rocks of Mesozoic age are limited to polymict melange outcrops in small areas of central and southwest Java. East of Central Java the oldest rocks exposed are calcareous sediments and basaltic to andesitic volcanic rocks of Early-Middle Tertiary age (Wheller et al., 1987).

Seismic refraction studies of the Sunda arc indicate that the crust beneath Sumatra is relatively thick (~25 km). Beneath Java the crust is ~20 km thick and has a seismic velocity structure intermediate between continental and oceanic (quasi-continental) (Ben-Avraham and Emery, 1973, Curray et al., 1977; Jarrard, 1986). Further to the east, seismic data indicate that the crust is ~18 km thick near Bali, and 5-10 km beneath Flores (Curray et al., 1977).

The south-eastern boundary of Sundaland (SE Asian continental part of the Sunda block/Eurasian plate with pre-Tertiary basement) is suggested to be located somewhere between Sumatra and East Java (e.g. Fig.1.2a). However, due to limited knowledge of the precise structure and composition of the Javan crust, the exact location and nature of this boundary is unknown. Hutchinson (1982) places the southeast limit of the Sunda Shelf

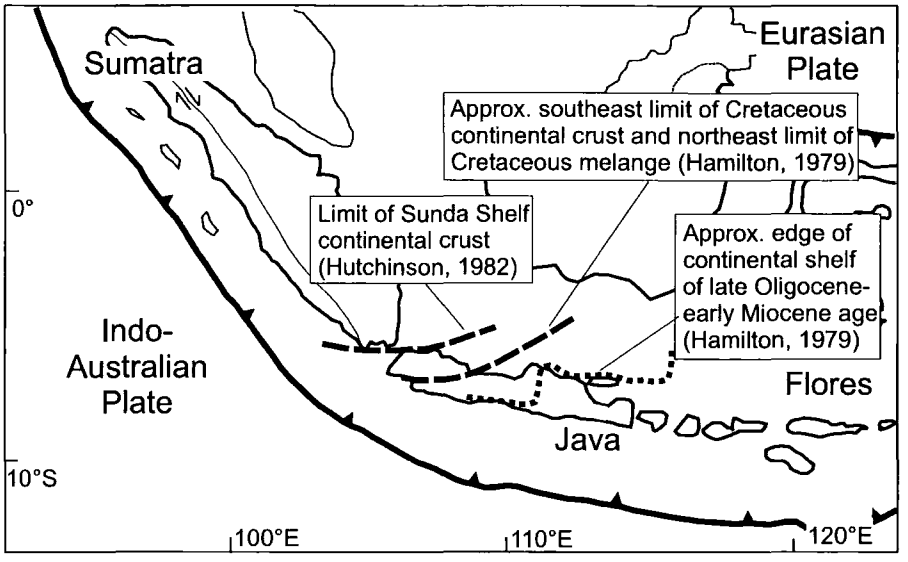

Fig. 1.4. Enlarged section of Fig. 1.2a showing the hypothesised Sundaland continental boundary (Hutcinson, 1982; Hamilton, 1979) and approximate edge of the late-Oligocene-early-Miocene continental shelf (Hamilton, 1979).

continental crust at the northwest tip of Java. However, melange of Late Cretaceous or very early Tertiary age exposed in Central Java leads Hamilton (1979) to suggest that the approximate southeast limit of Cretaceous continental crust and northwest limit of Cretaceous melange lies diagonally through the centre of West Java (Fig. 1.4). This latter location is more frequently quoted in the literature (e.g. Carn and Pyle, 2001; Hoffmann-Rothe et al., 2001; Susilohadi et al., 2005). Based on marine sediment exposures, Hamilton (1979) positions the approximate edge of continental shelf of late Oligocene-early Miocene age through central Java (Fig. 1.4).

1.3. Thesis aims and structure

The three main aims of this thesis are:

1. To evaluate mineralogical and geochemical variations in lavas from volcanic centres in Java and relate these to differentiation processes operating beneath volcanoes (e.g. fractional crystallisation, crustal contamination and magma mixing).

2. Use geochemistry to examine sources of magmatism in Java; in particular to discriminate the relative contributions of sediment subducted beneath Java at the Java Trench from material assimilated as melts pass through the arc lithosphere.
3. Compare major element, trace element and isotopic data of the individual volcanoes to examine how the character of magmatism, the composition and structure of the crust and the processes operating in the mantle vary along the arc. This information will help elucidate the nature of the transition between the continental and oceanic basement to the arc, which is expected to be encountered between Sumatra and east Java.

Chapters 2, 3 and 4 focus on addressing aims 1 and 2, highlighted above, for the individual volcanic complexes of IVC, Salak and GVC, respectively. Chapter 5 then addresses aim 3, comparing the geochemistry of lavas from Salak and GVC in West Java with those from IVC in East Java, in order to establish contrasting East-West Java geochemical traits. The geographical boundaries of West, Central and East Java are used in this study to divide the relatively large Javan lava dataset (particularly in bivariate plots), in order to facilitate the recognition of contrasting East-West geochemical characteristics. The Javan volcanic rock data are used to establish whether variable contributions from the subducting slab, or a change in crustal architecture of the overriding plate, best explain along-arc geochemical variations in Javan volcanic rocks. New Hf-isotope data for Guntur and Merapi is also considered in Chapter 5. Chapter 6 summarises the main conclusions of the thesis and suggests areas for further research.

Chapter 2

Constraining fluid and sediment contributions to subduction-related magmatism in Indonesia: Ijen Volcanic Complex

Constraining fluid and sediment contributions to subduction-related magmatism in Indonesia: Ijen Volcanic Complex

2.1. Introduction

Determining original source compositions of volcanic arc rocks can be challenging, as lavas rarely reach the Earth's surface without experiencing some processes that modify their composition, e.g. crystal fractionation, magma mixing or crustal contamination (Davidson, 1996; Thirlwall et al., 1996; Mandeville et al., 1996; Reubi and Nicholls, 2004, Davidson et al., 2005). In most petrogenetic models island arc magmas originate from mantle wedge that is modified by slab-derived components (McCulloch and Gamble, 1991; Hawkesworth et al., 1991; Pearce and Peate, 1995). The magnitude and nature of the contribution from the subducting slab is debated, although there is a consensus that a slab-derived fluid is involved, consisting of fluids from either the altered oceanic crust (Turner et al., 1997; Turner and Foden, 2001; Hawkesworth et al., 1997) or overlying sediments (Class et al., 2000), and components, possibly partial melts, of subducted sediment (Edwards et al., 1993; Elliot et al., 1997; Vroon et al., 2001; Turner and Foden, 2001).

Despite a number of petrogenetic studies of Javan volcanoes (Gertisser and Keller, 2003; Edwards et al., 1993; Turner and Foden, 2001 and references therein), uncertainty still prevails over the nature of the subduction component and the mechanisms by which it is added to the mantle wedge. For example, Edwards et al. (1993) propose a homogeneous slab contribution along the Sunda arc, while Turner and Foden (2001) identify along-arc heterogeneity in this component. Ijen Volcanic Complex (IVC) is located on the eastern edge of Java within the Quaternary volcanic front of the Sunda arc (Fig. 1.2, Chapter 1), in an ideal location (at the eastern edge of Java) to investigate the mantle source composition beneath Java: the relatively thin (oceanic) crust on which the volcano sits minimises the likelihood of

high-level continental crust contamination (compared to studies in West Java) and potentially allows us to constrain better the crustal contributions in the mantle source. Furthermore, apparent spatial controls on some major and trace element variations at IVC means that the volcanic complex provides a great opportunity to investigate the relationship between volcanic structure and shallow level processes influencing the composition of arc lavas. The aims this chapter are, therefore, 2-fold:

1) to identify the impact, if any, of volcanic and subjacent structure upon magmatic differentiation, and
2) to characterise the IVC magma source and place constraints on the nature of the slab component(s) and the transfer mechanism(s) to the mantle wedge.

2.2. Overview of Ijen Volcano Complex

Ijen volcanic complex consists of several stratovolcanoes and cinder cones constructed within and around a 20-km wide caldera (Fig. 2.1). The complex takes its name from Kawah Ijen volcano, the only volcano of the complex that is currently active. Based on the episode of caldera collapse, the stratigraphic succession has been divided into pre-caldera, caldera and post-caldera groups (van Bemmelen, 1949). Little is known about the age, structure or volcanic history of the pre-caldera cone (Old Ijen); but it is thought to be either early (van Bemmelen, 1949) or late (Sitorus, 1990; K-Ar dating) Pleistocene. Sitorus believes the pre-caldera volcanic structure was a large, single, composite volcano while Berlo (2001), believes that the pre caldera collapse volcano may have had multiple vents. Kemmerling (1921), has suggested the possibility that twin volcanoes made up Old Ijen due to the oval shape of the subsequent caldera. The deposits of Old Ijen disconformably overlie Miocene limestone (van Bemmelen, 1949) and consist of pyroclastic flow deposits, a series of pumice airfall deposits and several lava flows (Sitorus, 1990). The caldera wall forms a prominent, arcuate, ridge in

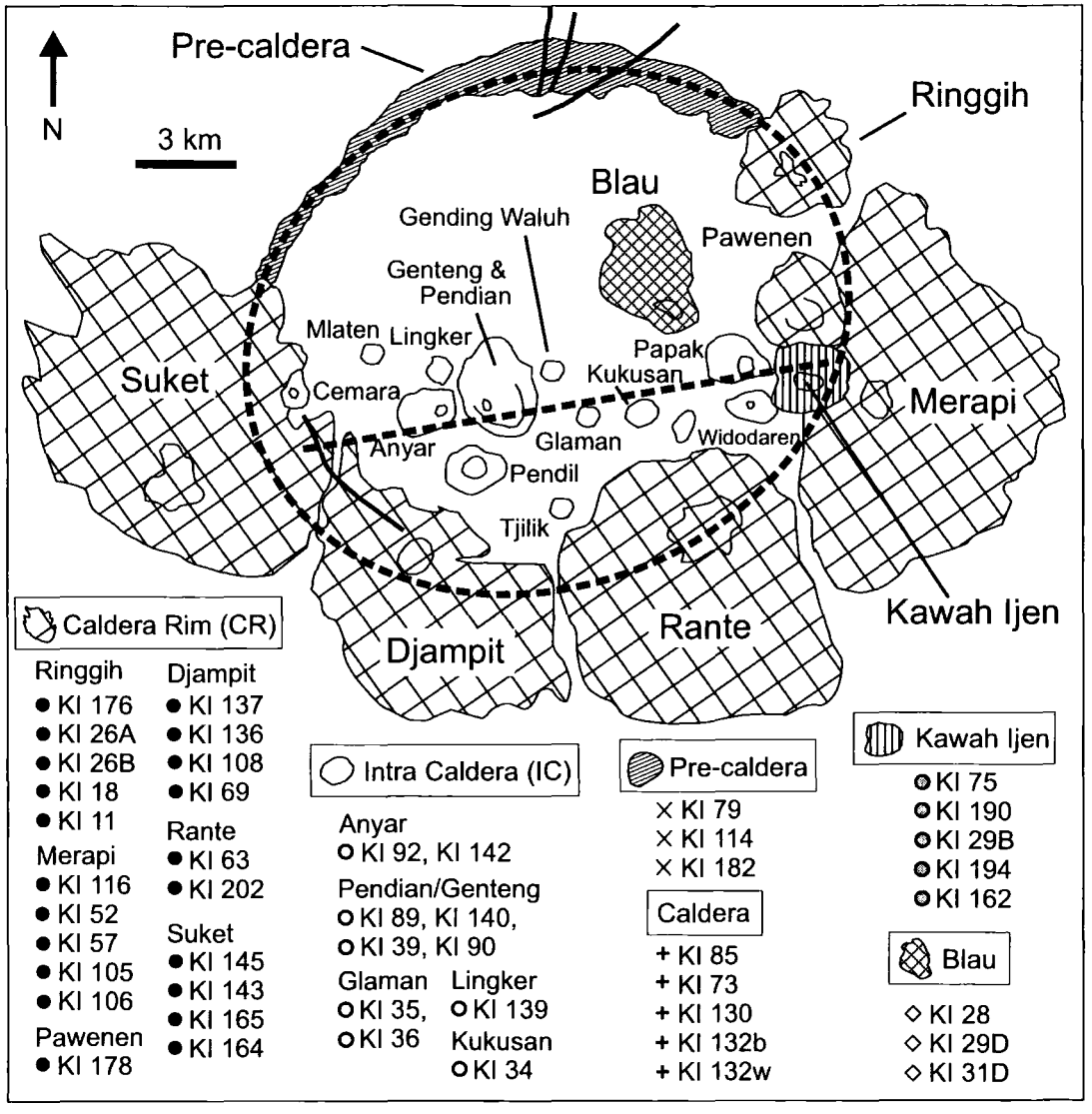

Fig. 2.1. Schematic map of the IVC showing the geographical relationships of the eruptive centres. Oval dashed line denotes the caldera rim (hypothesised in the south). Straight dashed line represents the lineation of intra-caldera volcanoes (based on Berlo, 2001). Solid black lines in the north and south-west indicate faults. Volcano boundaries represent the obvious topographic control exerted by the post-caldera volcanic centres. The general provenance of the samples used in this study (for sample grid references see Sitorus, 1990) is indicated below the map; corresponding data symbols used on subsequent figures are shown.

the north, but elsewhere in the complex the caldera rim is buried by the post-caldera volcanoes (Fig. 2.1). The collapse of the pre-caldera cone(s) is thought to have occurred in stages more than 50,000 years ago (Sitorus, 1990). The caldera group consists of two main units, comprising large volumes of caldera-forming ignimbrite, with minor layers of pumice

airfall and lahar deposits and pumice air fall. Most of the eruptive products were deposited to the north (Sitorus, 1990). Shortly after caldera collapse a resurgent dome (Blau), formed inside the caldera (Berlo, 2001). The post-caldera group is characterised by many types of eruption (phreatomagmatic, phreatic, strombolian and plinian) and comprises 58 lithological volcanic units, erupted from 22 separate vents (Sitorus, 1990). The post-caldera eruptive centres can be further divided on the basis of their geographical position within the complex: those located on the caldera rim (CR); dominantly composite cones, and intra-caldera (IC) centres situated inside the southern part of the caldera along a ENE-WSW lineation (Fig. 2.1); mainly cinder cones, minor composite cones, and a lava dome. The IC volcanoes are generally younger (with the exception of Blau) than the CR volcanoes (Sitorus, 1990; Berlo, 2001). Faulting is evident within the caldera complex in the north (Fig. 2.1) and large faults have affected the caldera-rim volcanoes of Merapi, Ringgih and Djampit. Present volcanic activity is limited to Ijen crater (Kawah Ijen), an acidic crater lake with a maximum diameter of 1.2km, and a depth of around 200-300m. The last major eruption created phreatomagmatic air fall and pyroclastic flow deposits ~2590 yr ago. Historic eruptions, which were mainly phreatic, occurred in 1796, 1817, 1917, 1936, 1952, 1993, 1994, 1999 and 2000.

2.3. Sample Groupings

This study builds on the established stratigraphy and preliminary geochemical work of Sitorus (1990). Few samples were available from the pre-caldera and caldera groups, therefore this paper focuses on the geochemistry of the post-caldera rocks. Based on temporal variations in geochemistry, particularly in SiO_2, FeO, CaO, Ni and Sr contents, Sitorus (1990) divided the post-caldera samples in to 6 separate groups, but admitted that the variations are not entirely consistent through time, either within or between groups. Therefore, in this study the majority of rocks are divided into the 2, afore mentioned groups (CR and IC) based on

their spatial distribution rather than age (Fig. 2.1). The centres of Kawah Ijen and Blau will be considered separately from the two main post-caldera groups. Kawah Ijen is located on the western flank of Merapi (a CR volcano), in line with the other intra-caldera centres and appears to have geochemical affinities to both groups. Blau, although easily identifiable as a volcanic centre inside the caldera, is located north of the linear trend of the other intra-caldera volcanoes and geochemical data show scatter between the two groups. Stratigraphic relationships, geomorphology (deep incised valleys) and K-Ar dating suggest that Blau is significantly older than the rest of the intra-caldera centres (Sitorus, 1990). Samples from IVC were provided as rock powders with the exception of 5 samples, for which hand specimens were also supplied. Petrographic descriptions of thin sections and mineralogical data of IVC rocks are presented in Sitorus (1990).

2.4. Geochemistry

2.4.1. Major Element Data

Major element data are reported in Sitorus (1990) and illustrated in Fig. 2.2. Although SiO_2 is commonly used as the index of differentiation for typically evolved arc lavas (Davidson, et al., 2005), MgO was chosen here as 1) IVC includes a large number of relatively less evolved (SiO_2 <55 wt%) rocks, and 2) there appears to be some division in SiO_2 contents between the CR and IC post-caldera groups at lower MgO content (Fig. 2.2a). Lavas from Ijen Volcanic Complex display a broad range in SiO_2 content from 48-63 wt% and relatively low MgO contents (<5.8 wt %) typical of island arc volcanoes and suggests that no true, primary basalts are erupted from IVC. MgO correlates positively with Fe_2O_3, TiO_2 and CaO, while Na_2O, SiO_2 and K_2O generally increase with decreasing MgO. Al_2O_3 and P_2O_5 data are considerably more scattered, especially at lower MgO contents (Fig. 2.2).

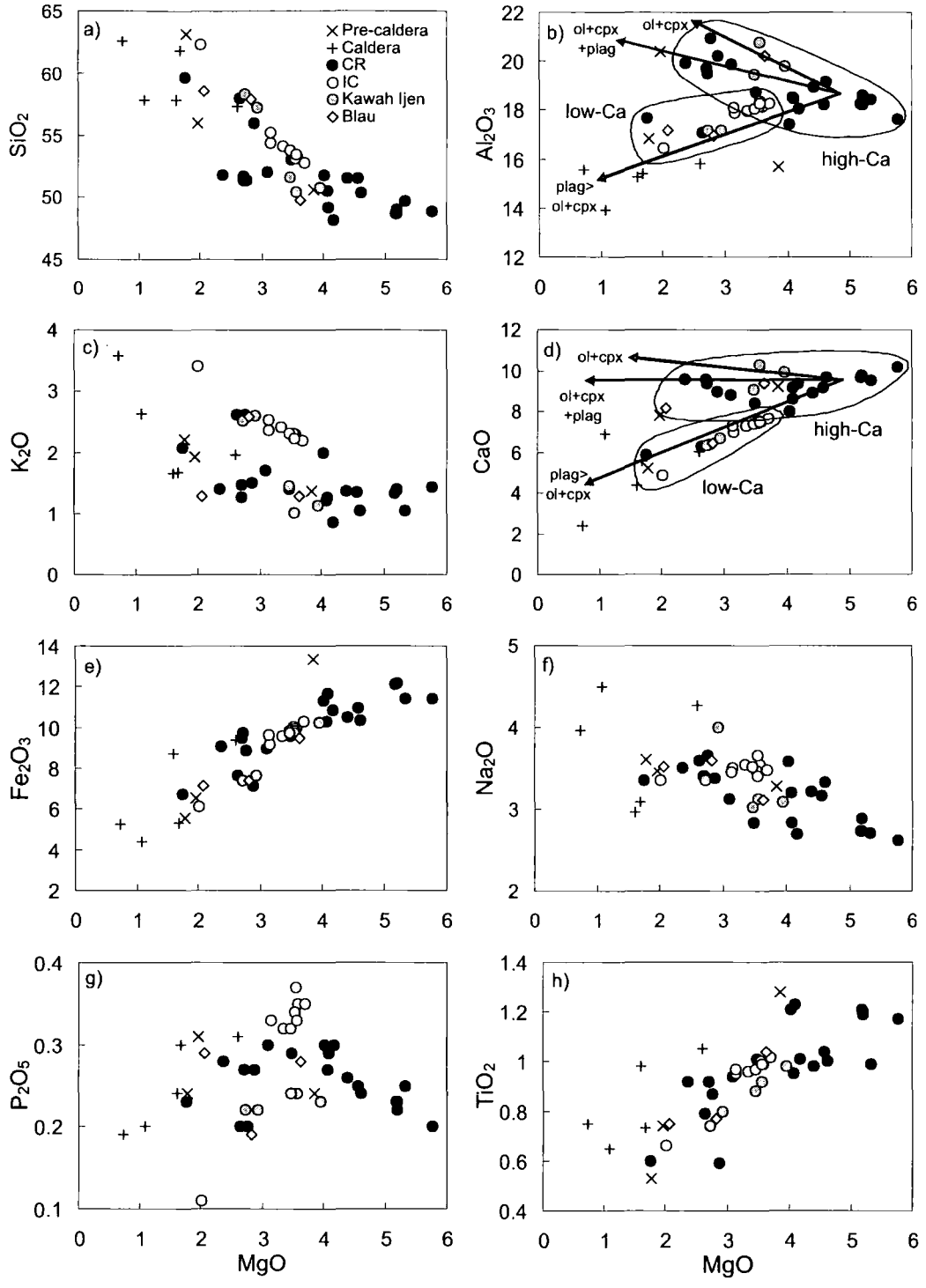

Fig. 2.2. Major element variation diagrams for IVC rocks separated by geographical group. Black arrows on Figs. b and d are general crystallisation vectors indicating the expected direction of magmatic evolution with the crystallisation of varying amounts of olivine (ol), clinopyroxene (cpx) and plagioclase (plag). Vectors were calculated from averaged microprobe mineral data (Sitorus, 1990). Major element data from Sitorus (1990). Vectors indicate potential difference between the two main groups – high Ca (largely CR) and low Ca (largely IC) at Ijen.

The IC samples form a coherent, linear array in the majority of variation diagrams, with a narrower range of SiO_2 and MgO than the CR volcanic rocks. IC and CR rocks generally appear to follow different trends on plots of SiO_2, Al_2O_3, K_2O and CaO against MgO (Figs. 2.2a-d respectively) with the exception of four CR samples (KI 202, KI 136, KI 164 and KI 108) that follow the IC trend. The IC group possess higher SiO_2 and K_2O contents than the CR group at similar MgO and display strong negative correlations, whereas within the CR group, there is a weaker and less obviously negative correlation between SiO_2 and K_2O and MgO (Figs. 2.2a and c). The more differentiated CR rocks (below ~4 wt% MgO) possess elevated CaO and Al_2O_3 contents when compared with the IC samples at the same degree of differentiation (Figs. 2.2b and d). Samples from Kawah Ijen and Blau appear to straddle both trends in the majority of the variation diagrams (e.g. Figs. 2.2b-d).

2.4.2. Trace Element Geochemistry

Ni (< 40 ppm) and Cr (< 60 ppm) concentrations are low in IVC rocks (Appendix B) and are positively correlated with MgO (e.g. Fig. 2.3a). There is a large decrease in Ni (and Cr) abundance from the most mafic rocks to those with intermediate MgO contents, whereas the more evolved lavas display more constant concentrations. Large ion lithophile element (LILE; Rb, Cs, Ba and including U and Th) concentrations (e.g. Figs. 2.3b and c) generally increase with decreasing MgO. Variation of Rb with MgO mirrors that of K_2O (Fig. 2.2b), where IC group contents are higher than the relatively constant concentrations in the CR group. Sr concentrations, on the other hand, are more elevated in the CR group and generally increase with decreasing MgO, whereas Sr concentrations in the IC rocks are in the main lower at similar MgO (Fig. 2.3d); comparable with Al_2O_3 and CaO contents. The IC samples have higher abundances of high field strength elements (HFSE), such as Zr, Hf, Nb and Ta, than the CR rocks at a given MgO (Figs. 2.3e and f). The variation of these elements also

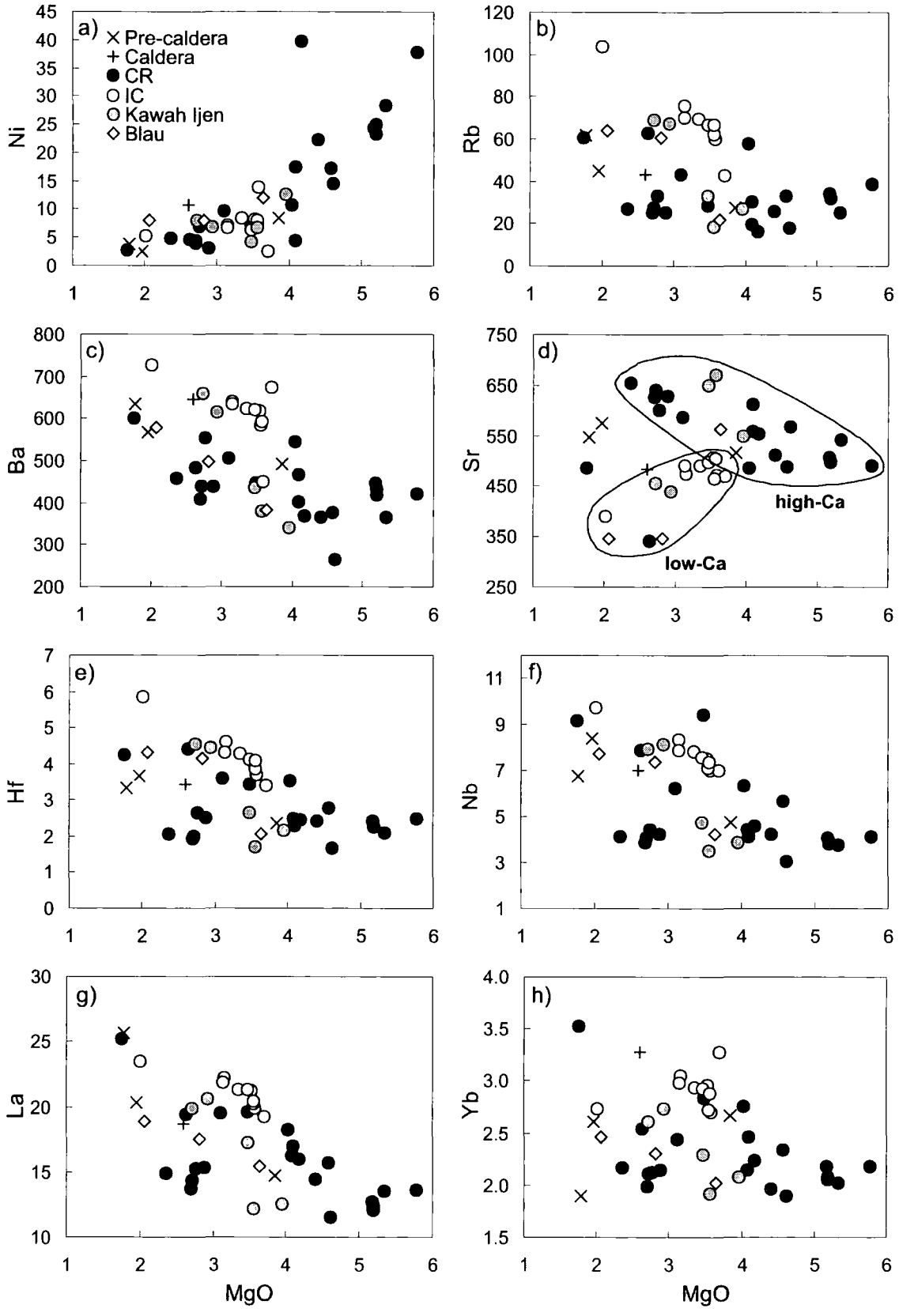

Fig. 2.3 Trace element variation diagrams with differentiation (represented by MgO) for selected trace elements of IVC rocks.

mirrors that of K_2O. REE variation with MgO is exemplified in Figs. 2.3g and h. LREE (e.g. La) concentrations in the IVC rocks generally increase with decreasing MgO (Fig. 2.3g), however HREE variation trends are more difficult to discern; there is a wide variation in Yb at low MgO content (Fig. 2.3h).

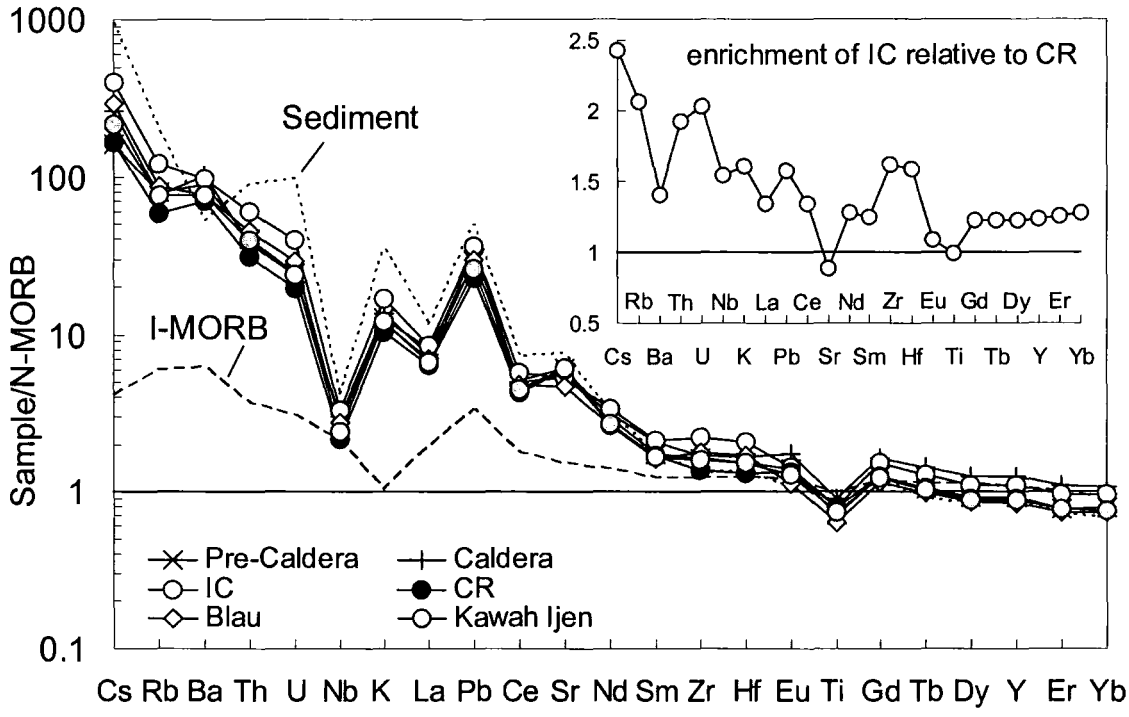

Fig. 2.4. N-MORB normalised trace element diagram for IVC rocks. Inset diagram shows the average enrichment of the IC group relative to the CR group. Data sources: Indian Ocean MORB (I-MORB): Chauvel and Blichert-Toft, 2001; N-MORB normalisation values from Sun and McDonough, 1989; Sediment: Vroon et al. 1995 (Track III).

Normalised trace element abundance patterns (Fig. 2.4) are typical of island arc volcanoes, with enrichment of the more mobile LILE and LREE relative to HFSE and HREE. The highly- to moderately-incompatible elements are all enriched relative to MORB, similar to those from other Sunda arc volcanoes (Turner and Foden, 2001) and local sediment (Vroon, et al., 1995). The IC group are generally more enriched than the CR group. This enrichment is emphasised on the inset diagram of Fig. 2.4, where the IC are normalised to the CR group. There is a general decrease in the degree of enrichment of the IC as element

incompatibility decreases, with the exception of Ba and Sr, which are considerably less enriched relative to their neighbouring elements, and in the case of Sr, actually depleted relative to the CR group. There is greater enrichment of Zr and Hf in the IC group compared to the more compatible elements, while Ti concentrations of the IC and CR rocks are identical.

2.4.3. Radiogenic Isotopes

Sr, Nd, Hf isotope data of the IVC are listed in Appendix C and presented in Figs. 2.5 and 2.6. In contrast to major and trace element data, the intra-caldera and caldera-rim groups cannot be distinguished from one another on the basis of radiogenic isotopes. The relatively large dataset displays a restricted range in $^{87}Sr/^{86}Sr$ (0.704169-0.704483), $^{143}Nd/^{144}Nd$ (0.512814-0.512895) and $^{176}Hf/^{177}Hf$ (0.283078-0.283133) and plots within the range of other island arc volcanoes. Sr and Nd isotope ratios of lavas from the complex are among the least radiogenic Sr and most radiogenic Nd isotopic values reported for Javanese volcanoes (Fig. 2.5); only samples from Guntur (Edwards, 1990) and Galunggung (Gerbe et al., 1992) possess higher $^{143}Nd/^{144}Nd$ and lower $^{87}Sr/^{86}Sr$ ratios. Primitive Sr isotope ratios of IVC lavas conform with the noted eastward decrease in $^{87}Sr/^{86}Sr$ from West Java to Bali (Whitford, 1975). In Nd-Hf isotope space the IVC lavas lie on the edge of the Java field close to the Indian Ocean MORB field (Fig. 2.6). The pre-caldera group has relatively low $^{87}Sr/^{86}Sr$ ratios (0.704169-0.704238) and are indistinguishable from one another in $^{143}Nd/^{144}Nd$ (0.512892-0.512895). However, their range in $^{176}Hf/^{177}Hf$ isotope ratio (0.283081-0.283118) is comparable to the range of Hf isotope ratios seen in the volcanic complex as a whole (Fig. 2.6 inset). IC $^{143}Nd/^{144}Nd$ ratios are similar to the CR group with no obvious division between the two groups. The IC lavas display a more limited range in $^{176}Hf/^{177}Hf$ ratios, but plot in the centre of the larger spread of the CR group (Fig. 2.6 inset).

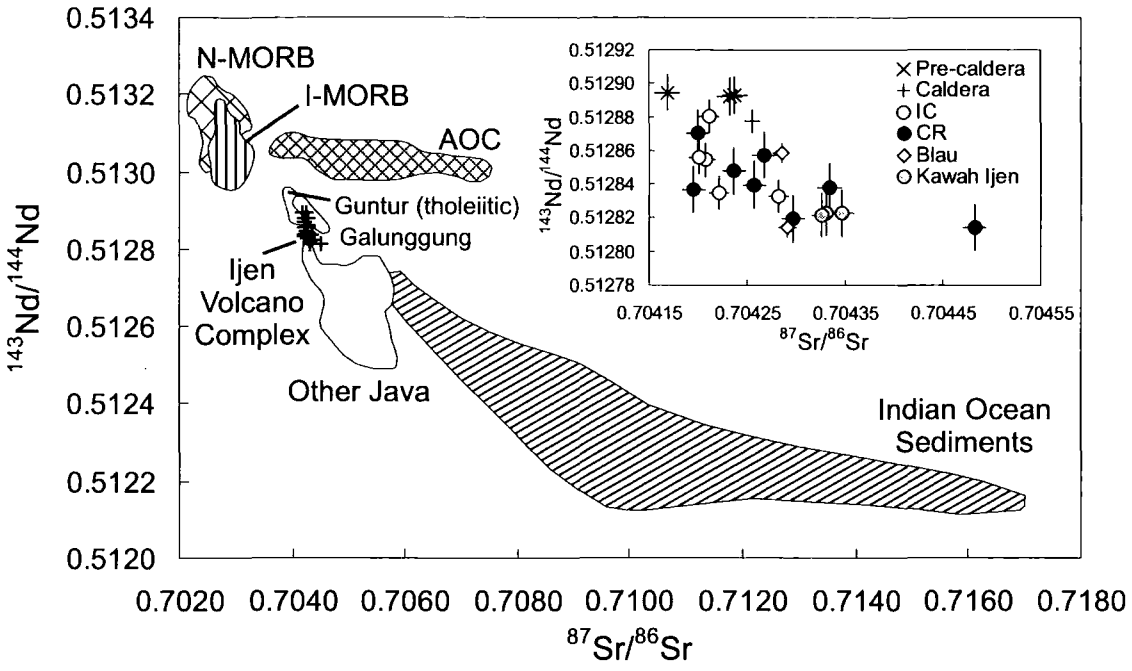

Fig. 2.5. Variation of $^{143}Nd/^{144}Nd$ with $^{87}Sr/^{86}Sr$ for the IVC. Inset: Nd and Sr isotope ratio diagram for the IVC groups. Note the lack of any distinction in isotope ratio between the IC and CR group. Data sources: I-MORB: Rehkämper and Hofmann, 1997; Ito et al., 1987; Price et al., 1986; Chauvel and Blichert-Toft, 2001; N-MORB: Ito et al., 1987; Chauvel and Blichert-Toft, 2001; Altered oceanic crust (AOC): Staudigel et al., 1995; Other Java volcanic rocks: White and Patchett, 1984; Whitford et al, 1981; Edwards, 1990 (inc. Guntur tholeiites); Gertisser and Keller, 2003; Gerbe et al, 1992 (Galunggung); Indian ocean sediments: Ben Othman et al., 1989; Gasparon and Varne, 1998. Errors shown are the maximum 2σ external errors, for each geographical group.

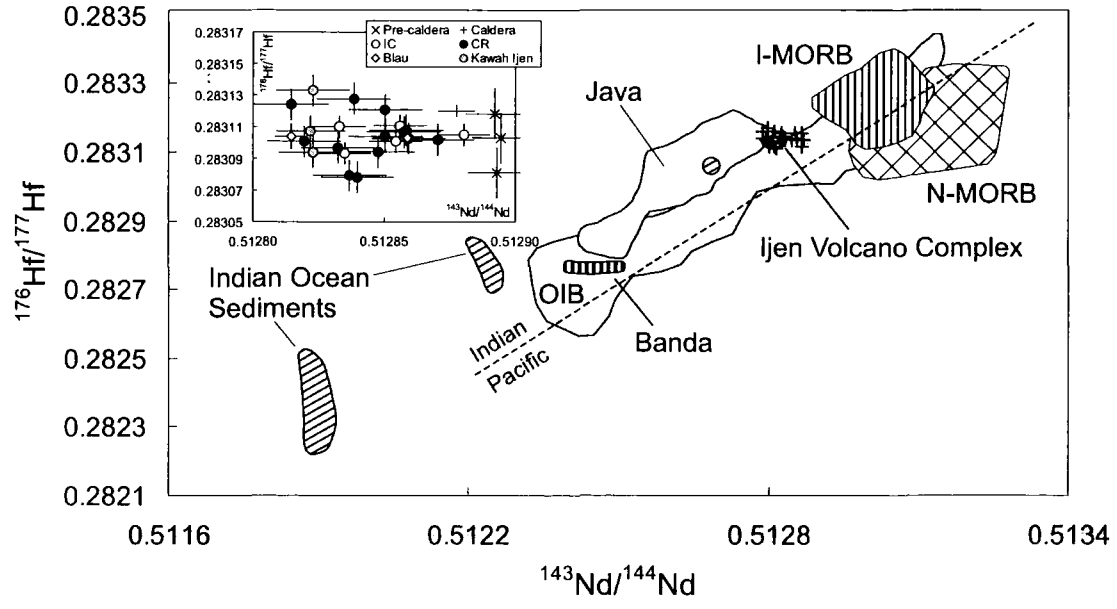

Fig. 2.6. Variation of $^{176}Hf/^{177}Hf$ with $^{143}Nd/^{144}Nd$ for the IVC. Inset: Hf-Nd isotope diagram of IVC volcanic rocks separated by eruptive group. Data sources: I-MORB: Salters, 1996; Nowell et al., 1998; Chauvel and Blichert-Toft, 2001; N-MORB: I-MORB references listed in this caption plus Salters and Hart, 1991; OIB: Salters and Hart, 1991; Salters and White, 1998; Nowell et al., 1998; Patchett and Tatsumoto, 1980; Patchett, 1983; Stille et al., 1986; Java: White and Patchett, 1984; Woodhead et al., 2001; Banda: White and Patchett, 1984; Indian ocean sediments: Ben Othman et al., 1989; White et al., 1986; Vervoort et al., 1999. Dividing line for Indian and Pacific MORB provenance from Pearce et al., 1999. Maximum 2σ external errors in each group are shown on the inset diagram.

2.4.4. Oxygen Isotope Data

The $\delta^{18}O$ values of clinopyroxene, olivine and plagioclase are +5.38 to +5.58‰ (n = 5), +5.02‰ (n = 1) and +6.08‰ (n = 1), respectively (Table 2.1). The range of clinopyroxene $\delta^{18}O$ is narrow and comparable to the average mantle $\delta^{18}O$ value of +5.57 ± 0.32‰ (Mattey et al., 1994; Ionov et al., 1994). IVC $\delta^{18}O$ clinopyroxene values are lower than plagioclase and higher than olivine; with co-existing mineral pair $\Delta_{cpx\text{-}ol}$ and $\Delta_{plag\text{-}cpx}$ values of 0.36‰ and 0.5‰ respectively, suggesting isotopic equilibrium at typical magmatic temperatures for andesite liquids. (Macpherson & Mattey, 1998; Macpherson et al., 1998). The limited data set displays no noticeable difference in cpx $\delta^{18}O$ values of the different geographic groups.

Table 2.1. Oxygen isotope data of IVC

Post-caldera					
	Caldera-rim (CR)	Intra-caldera (IC)			Blau
	Rante	Kukusan	Glaman	Glaman	
sample no.	KI 63	KI 34	KI 35	KI 36	KI 31D
$\delta^{18}O$ cpx. (‰)	+5.38	+5.51	+5.49	+5.58	+5.46
$\delta^{18}O$ ol. (‰)	+5.02				
$\delta^{18}O$ plag. (‰)				+6.08	

$\delta^{18}O$ 1σ errors are given in Appendix E

The oxygen isotope ratios of clinopyroxene phenocrysts from IVC rocks sit within the range reported for clinopyroxene of the primitive Galunggung lavas from West Java (+5.3 to +5.6‰, Harmon and Gerbe, 1992) and clinopyroxene and olivine $\delta^{18}O$ values lie at the lower

end of the Banda arc $\delta^{18}O$ range (+5.18 to +7.04‰ and +4.92 to +5.59‰, respectively; Vroon et al., 2001). The only plagioclase sample analysed from the IVC lies within error of the $\delta^{18}O$ range of Galunggung lavas (+5.6 to +6.0‰; Harmon and Gerbe, 1992) and is lower than $\delta^{18}O$ values recorded in plagioclase phenocrysts of Merapi volcanics (+6.5 to +7.00‰, Gertisser and Keller, 2003). The $\delta^{18}O$ values of the IVC rocks also lie close to the values postulated for the upper mantle in other subduction zones (Smith et al., 1996; Thirlwall et al., 1996; Macpherson and Mattey, 1998; Macpherson et al., 1998, 2000; Eiler et al. 2000).

2.5. Discussion

2.5.1. Differentiation of Magma

Differentiation processes significantly change the composition of magma as it rises through the lithosphere towards the surface. It is important to identify the impact of these processes on the composition of the magma in order to remove uncertainty in establishing the composition and magnitude of slab-derived contributions to the mantle source in subduction zones. Low MgO, Ni and Cr in IVC volcanic rocks indicate that they were not primary mantle melts, and that magma compositions were therefore modified en route to the Earth's surface. Correlations of various major and trace elements with indices of differentiation, such as MgO, in IVC lavas (e.g. Figs. 2.2 and 2.3) suggest that the concentrations of some elements are controlled by shallow level differentiation processes such as fractional crystallisation, magma mixing or contamination. Major and trace element variation for most of the post-caldera samples can be described as one of two trends, which are exemplified in the CaO versus MgO plot (Fig. 2.2d), where a low-Ca group, dominantly consisting of the IC samples, displays a positive correlation and a high-Ca group, comprised of most CR samples along with some Kawah Ijen and Blau samples, showing little change in CaO with decreasing MgO, such that high-Ca lavas possess higher CaO contents than low-Ca lavas at a given

(especially low) MgO content. Similar patterns emerge from plots of Al_2O_3 and Sr against MgO (Figs. 2.2b and 2.3d). Higher modal plagioclase abundances (~10%, Table 2.2), and a less pronounced negative Eu anomaly in high-Ca lavas (Fig. 2.7) suggest that the different geochemical trends exhibited by the low-Ca and high-Ca groups may be due to more extensive plagioclase fractionation in the former, or plagioclase accumulation in the latter. Possible evidence for open-system processes in petrographic and mineral analysis of IVC lavas includes: co-existence of phenocrysts (plagioclase and clinopyroxene) that display normal, oscillatory and reverse zoning (Sitorus, 1990), clinopyroxene overgrowths on orthopyroxene phenocrysts and bimodal distributions in plagioclase core compositions (Sitorus, 1990; Berlo 2001). One group of plagioclase crystal cores cluster below An_{60}, and the other generally above An_{80}. However, bimodal plagioclase compositions are found within

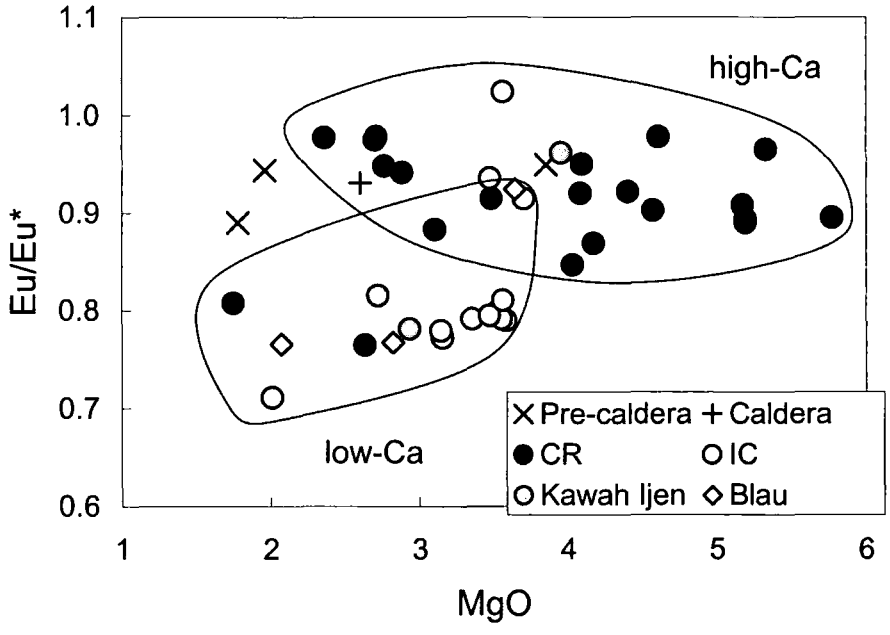

Fig. 2.7. Europium anomaly (Eu/Eu*) versus MgO for IVC rocks.

volcanic rocks from both the high- and low-Ca groups, indicating that although mixing may occur, it is not the dominant control on element variation, otherwise we would only expect to find bimodal plagioclase populations in high-Ca rocks. Also, higher modal plagioclase

abundance does not necessarily indicate accumulation; it may just be a result of a greater degree of crystallisation or more plagioclase in the modal equilibrium assemblage. Variations in the fractionating mineral assemblage can produce contrasting differentiation trends on variation diagrams (e.g. Davidson, 1996). Crystallisation vectors drawn in Figs. 2.2b and d, illustrate the magmatic evolution predicted for a primitive IVC lava during fractionation of different mineral assemblages. Thus, the different trends observed in the high- and low-Ca groups can result from differences in the phases that make up the fractionating assemblage and their proportions. Assemblages consisting of clinopyroxene and olivine ± plagioclase can replicate the high-Ca array (Figs. 2.2b and d), while the same assemblage but with more plagioclase fractionation relative to clinopyroxene and olivine is suggested for the low-Ca trend (see labelled arrows, Figs. 2.2b and d). Less plagioclase fractionation in the evolution of the high-Ca lavas, relative to the low-Ca lavas, is also consistent with the variations of Al_2O_3 and Sr with respect to MgO, along with a smaller negative Eu anomaly.

2.5.1.1. Fractional Crystallisation

The XLFRAC, least squares major element modelling technique (see Stormer and Nicholls, 1978) can be used to test the qualitative observations outlined above. The objectives of major element modelling are 2-fold:

1) to ascertain if the high-Ca and low-Ca differentiation trends can be explained by differences in the amount of plagioclase fractionation,
2) to determine whether compositional variation within and between geographic groups (e.g. IC, CR, Kawah Ijen) can be explained by fractional crystallisation.

The models calculate the proportions of given mineral compositions required to produce a final daughter magma from an initial parent and indicate the discrepancy (residual) between the concentration of each of the nine oxides considered in the modelled and real daughters.

Table 2.2. Results of major element least squares modelling

Model no.		Initial (parent)	Geog. Group	Final (daughter)	Geog. Group	ΔMgO wt %	Σr^2	% removed				%	D thin section abundance			
								Plag	Cpx	Ol	Fe-Ti	Cryst.	Plag %	Cpx %	Ol%	Fe-Ti%
1	Most to low-Ca	**KI 63**	CR	**KI 35**	IC	3.32	0.20	45.2	12.1	7.9	6.2	71	23	6	-	5
2	Least Evolved high-Ca	**KI 11**	CR	**KI 26A**	CR	2.83	0.19	11.8	4.9	8.9	2.6	28	36	7	1	6
3	high-Ca group daughter	**KI 145**	CR	**KI 57**	CR	2.09	0.07	12.4	7.8	3.3	5.8	29	37	4	1	3
4		**KI 63**	CR	**KI 18**	CR	2.62	0.10	11.4	4.3	7.2	1.4	24	34	6	1	4
5		**KI 63**	CR	**KI 26B**	CR	2.63	0.09	10.1	3.7	7.5	1.5	23	33	7	1	5
6		**KI 52**	CR	**KI 57**	CR	1.47	0.16	-	6.4	2.7	1.1	10	37	4	1	3
7	low-Ca group daughter	**KI 63**	CR	**KI 202**	CR	2.7	0.10	37.3	9.0	5.1	7.8	59	25	9	-	7
8		**KI 145**	CR	**KI 108**	CR	1.16	0.07	21.8	6.2	2.5	5.2	36	23	6	1	4
9		**KI 11**	CR	**KI 108**	CR	1.16	0.02	20.4	5.9	2.5	5.5	34	23	6	1	4
10	Within Geog. Groups	**KI 92**	IC	**KI 34**	IC	0.41	0.02	10.3	1.5	2.0	1.3	15	16	6	-	6
11		**KI 190**	K. IJEN	**KI 194**	K. IJEN	1.02	0.04	39.6	6.9	4.8	4.4	56	31	9	-	3
12		**KI 31D**	BLAU	**KI 28**	BLAU	0.82	0.23	50.6	5.1	7.2	4.1	67	25	10	1	4
13	Between Geog. Groups	**KI 31D**	BLAU	**KI 92**	IC	0.08	0.07	39.3	4.2	5.0	2.5	51	28	8	-	5
14		**KI 190**	K. IJEN	**KI 57**	CR	0.85	0.05	15.6	5.9	2.3	2.1	26	37	4	1	3
15		**KI 63**	CR	**KI 162**	K. IJEN	2.61	0.13	39.9	10.8	7.3	5.5	63	28	11	-	4
16		**KI 92**	IC	**KI 18**	CR	0.85	0.07	**36.7**	**12.0**	4.8	**4.9**	58	34	6	1	4
17		**KI 92**	IC	**KI 136**	CR	1.81	1.46	27.8	4.8	5.9	3.9	42	39	9	-	4

ΔMgO wt% = difference calculated between parent and daughter compositions

Plag = plagioclase, Cpx = clinopyroxene, Ol = olivine, Fe-Ti = Fe-Ti oxide

% removed is relative to initial parent magma. Phase percentages in bold font indicate addition rather than removal of that phase

D = daughter

Mineral compositions (Sitorus, 1990) were taken from phenocrysts in the basic and intermediate IVC rocks. Summaries of representative models are shown in Table 2.2. Small values for the sum of all residuals (Σr^2) indicate good agreement between the model and the expected daughter and suggest a more viable model. Models 1 and 2 suggest that the most evolved post-caldera rocks of the high-Ca and low-Ca groups can be produced by fractionation of plagioclase, clinopyroxene, olivine and Fe-Ti oxide from the least evolved samples of their respective groups (Σr^2 = 0.2 and 0.19 respectively). Models of fractionation to other high-Ca and low-Ca group daughter compositions (models 3-6 and 7-9 respectively) yield excellent Σr^2 values (<0.16). All of these models also suggest that significantly less plagioclase fractionation is required from the parent magma to reach high-Ca daughter compositions (10-12%) compared to those of low-Ca (~20-37%). Therefore, we conclude that the different (high- and low-Ca) trends (e.g. Figs. 2.2b and d) are due to a greater amount of plagioclase fractionation in the IC rocks than in the CR rocks.

The second objective of modelling is to assess whether variations seen in major element data within and between each geographical group can be explained by fractional crystallisation alone. Modelling demonstrates that intra-group CR fractionation models yield low Σr^2 values (models 2-9, Table 2.2). A good solution (Σr^2 = 0.02) is also obtained for a model using a less evolved IC sample as parent to a more evolved IC rock (model 10). Low Σr^2 values are obtained in model 11, between the two Kawah Ijen samples, which straddle the high-Ca and low-Ca trends on several major element diagrams. Some inter-group models can also generate very acceptable results (models 13-15), suggesting that members of different geographic groups can be related to each other through fractional crystallisation. However, least squares modelling cannot generate low Σr^2 in models where IC rocks represent the parent magma composition and CR is the daughter, unless crystals are accumulated rather than removed (models 16-17).

To summarise, least squares modelling suggests that the more evolved rocks can be produced by fractionation of plagioclase, clinopyroxene, olivine and Fe-Ti oxide from less evolved members, thus indicating that fractional crystallisation is important in controlling variations in major element data of IVC volcanics. Modelling suggests that the IC rocks are not parental to CR rocks, consistent with the general stratigraphic relationship of the geographical groups (most CR volcanoes are older than IC volcanoes). The high-Ca and low-Ca trends displayed on element variation diagrams are likely to be a result of less plagioclase fractionation in the evolution of the high-Ca group, relative to the low-Ca group, rather than due to the accumulation of plagioclase in high-Ca lavas.

The concentrations of some trace elements are strongly influenced by the crystallising mineral phases. Utilising the phase proportions and degree of crystallisation predicted from major element modelling (Table 2.2) it is possible to test the conclusions of least squares analysis by forward modelling of trace element concentrations during fractional crystallisation. Models are illustrated for those elements seen to vary most widely in concentration between the high-Ca and low-Ca groups. If differences between the fractional crystallisation histories are responsible for the two trends then the trace element modelling should be able to produce calculated values consistent with the trace element concentrations observed in both groups. This method uses the Rayleigh fractionation equation: $C_l = C_o F^{(D-1)}$, where C_l and C_o represent the concentration of an element in the daughter and parental liquids, respectively, F is the fraction of liquid remaining and D is the bulk distribution coefficient. The distribution coefficients used in modelling are given in Appendix F. The results of selected trace element models are shown in Table 2.3 and the difference between calculated and expected concentrations are plotted in Fig. 2.8. If the degree of crystallisation and the phase proportions determined by major element modelling are accurate, the data will have normalised values close to 1, which is generally the case for high-Ca and low-Ca

Table 2.3. Results of trace element modelling

Model no.	3	6	7	8	10	11
Parent	KI 145	KI 52	KI 63	KI 145	KI 92	KI 190
Daughter	KI 57	KI 57	KI 202	KI 108	KI 34	KI 194
Centres	CR-CR	CR-CR	CR-CR	CR-CR	IC-IC	K.Ijen-K.Ijen
To Group	high-Ca	high-Ca	low-Ca	low-ca	low-Ca	high-low Ca
Σr^2	0.07	0.16	0.10	0.07	0.02	0.04
PLAG	12.41	-	37.32	21.81	10.3	39.61
CPX	7.82	6.35	8.99	6.16	1.53	6.94
OL	3.32	2.7	5.14	2.46	2	4.84
FE-Ti	5.75	1.05	7.79	5.18	1.32	4.43
TOTAL	29.30	10.1	59.24	35.61	15.15	55.82
F	0.71	0.90	0.41	0.64	0.85	0.44
Calculated						
Rb	43.7	36.6	57.1	47.4	77.2	56.3
Ba	564	417	677	587	663	584
Th	4.32	4.28	6.54	4.73	7.75	6.34
U	1.22	0.99	1.45	1.32	2.05	1.48
Nb	4.97	6.21	6.98	5.31	8.32	7.00
Ta	0.51	0.48	0.70	0.56	0.72	0.76
Sr	476	536	311	385	447	283
Zr	110	117	161	120	181	162
Hf	2.98	3.00	4.55	3.30	4.72	4.48
Measured						
Rb	43.3	43.3	62.8	57.7	75.7	67.4
Ba	507	507	484	545	639	614
Th	4.85	4.85	7.33	5.64	7.81	7.44
U	1.12	1.12	1.78	1.52	2.01	1.79
Nb	6.22	6.22	7.90	6.37	8.34	8.13
Ta	0.51	0.51	0.77	0.85	0.71	0.65
Sr	586	586	342	487	474	440
Zr	138	138	168	136	177	170
Hf	3.61	3.61	4.41	3.53	4.61	4.44

Σr^2 values and phase proportions (%) taken from Table 2.2.
Trace element concentrations in ppm.

models (models 3 & 6 and 7, 8 & 10 in Table 2.3, respectively). The strongest agreement (model 10) is between the intra-caldera samples KI 92 and KI 34 in the low-Ca group (white squares, Fig. 2.8) where calculated values lie within 10% of the measured concentrations. Modelling the trace element concentrations of Kawah Ijen samples KI 194 from KI 190 (Table 2.3, model 11) overestimates the Ta concentration and underestimates the Sr concentration measured in the actual rocks. These samples plot within the low Ca and high-

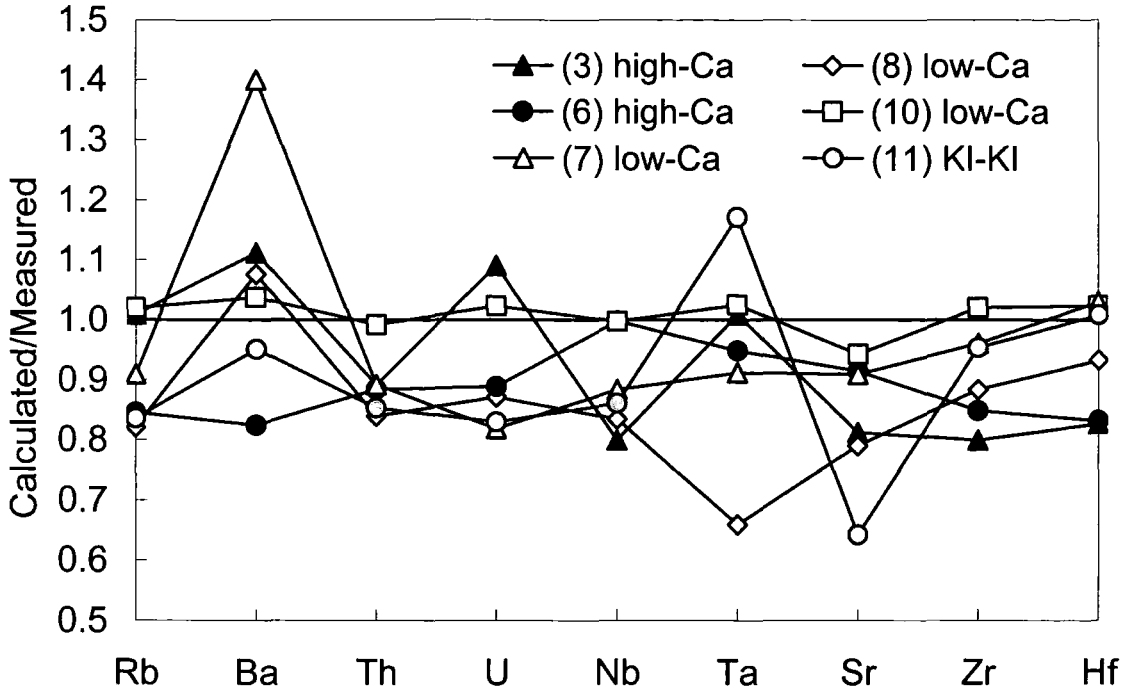

Fig. 2.8. Comparison of trace element concentrations determined by forward modelling with those measured in the rocks. Model numbers correspond to those in Table 2.2. White fill, models using daughter concentrations from the low-Ca group; black fill, models using daughter concentration from the high-Ca group; grey fill, Kawah Ijen parent and daughter compositions used. Mineral phases, abundances and degree of crystallisation used in modelling are those predicted by major element least squares modelling (Table 2.2). Mineral-melt distribution coefficients used are listed in Appendix F. The closer the data lie to 1 the smaller the discrepancy between modelled and measured compositions.

Ca trends respectively, on several major and trace element variation diagrams, and therefore even though major element modelling produced an acceptable Σr^2 value of 0.04, these samples are not consistent with a simple fractional crystallisation relationship. Overall, trace element modelling validates models of fractional crystallisation developed from major element data; suggesting that fractional crystallisation is the main control on melt evolution at IVC. It also confirms that the separate trends of the low-Ca and high-Ca groups are likely to be due to variable influence of plagioclase in the fractionating mineral assemblage and not as a result of plagioclase accumulation in the high-Ca group. This conclusion is consistent with the larger Eu anomalies and lower relative enrichment of Ba and Sr (Fig. 2.4) seen in the IC

group (that dominate the low-Ca group) relative to the CR group (the majority of the high-Ca samples) that are associated with greater involvement of plagioclase.

2.5.1.1.1. Structural controls on magma ascent and storage

The location of the CR volcanoes around the caldera rim, suggests that ring fractures may facilitate the movement of magma below these volcanoes. This has been proposed for other post-caldera vents located along radial fractures of volcanoes e.g. Roccamonfina volcano in Italy (Gianetti, 2001) and Chichontepec volcanic centre in El Salvador (Rotolo and Castorina, 1998). The linear orientation (roughly NE-SW, Berlo, 2001) of the intra-caldera volcanoes also suggests that magma below the central part of the caldera is utilising lines of weakness and further highlights the structural control on the location of post-caldera volcanoes at IVC.

The different fractionation trends exhibited by the low-Ca (dominantly the intra-caldera rocks) and high-Ca (dominantly the caldera-rim rocks) suggest spatial variations in chemistry at the volcanic complex may be linked to sub-volcanic structure. The contrast in geochemistry is proposed to result from differences in the amount of plagioclase fractionation from the respective magmas. Experimental evidence (Grove et al., 2003) suggests that plagioclase crystallisation is suppressed by high water contents and high pressure in basaltic andesite magmas. Therefore, the more extensive plagioclase fractionation inferred for the IC group magmas may result from either shallower level (i.e. lower pressure) storage or lower water contents (or both) in the IC magmas relative to the CR magmas. The volatile content of magma is also controlled by pressure, so the suppression of plagioclase crystallisation in the CR group may be a result of magmatic differentiation at deeper levels in the crust below the caldera-rim volcanoes (Fig. 2.9). Magmas stored at greater depth, with higher volatile contents, may be expected to erupt more explosively than those stored at shallower levels, where eruptions may be more effusive. The presence of large stratovolcanoes on the caldera-

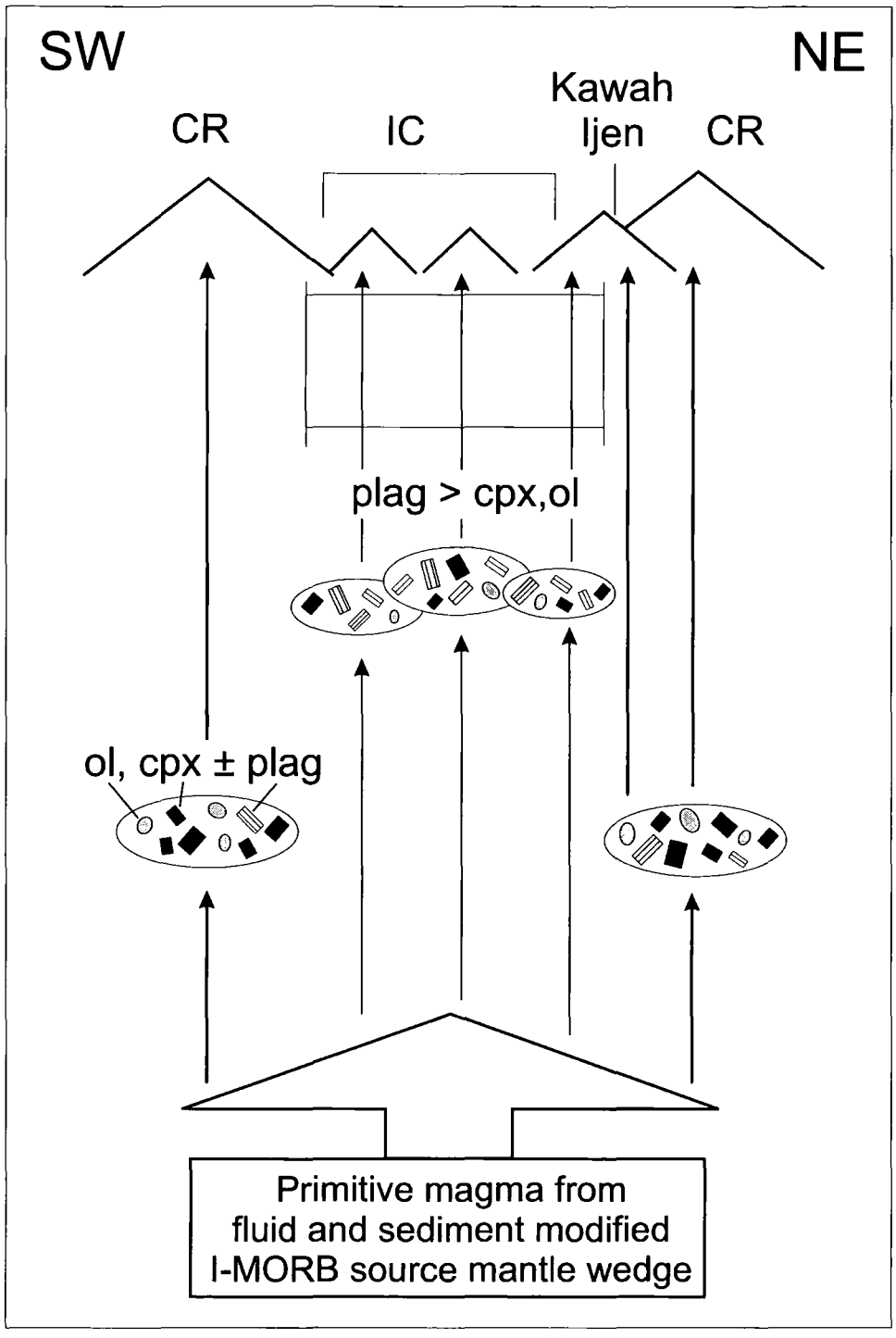

Fig. 2.9. Simplified diagram of rock petrogenesis at IVC, focusing on crustal level fractionation. Cross-section shown is orientated roughly parallel to the lineation of the intra-caldera volcanoes. The diagram shows the envisaged deeper level storage of magma below the CR volcanoes, and shallower level storage plus more extensive plagioclase fractionation below the IC volcanoes. Kawah Ijen is thought to tap both the shallow and deep reservoirs and transport the magma through unconnected pathways. NB. Fe-Ti oxide is also fractionating in both the shallow and deep reservoirs.

rim and dominantly small cinder cones inside the caldera at IVC is consistent with the type of eruption compatible with this interpretation. Therefore, at IVC it is proposed that volcanic structure exerts some control on the depths at which the melts can pond. Kawah Ijen erupts lavas belonging to both the low-Ca and high-Ca trends. Kawah Ijen lies at the intersection between the caldera rim and the northeastern edge of the intra-caldera lineation (Fig. 2.1) and may, therefore, tap both shallow and deeply ponded magmas (Fig. 2.9). There is no temporal division in production of high-Ca and low-Ca lava types at Kawah Ijen, and no evidence for physical mingling/mixing (Berlo, 2001); implying separate magmatic pathways for magmas erupted from different depths (Fig. 2.9).

2.5.1.2. Role of Crustal Contamination

Isotope ratios of IVC lavas are displaced from the MORB fields towards slightly more 'crustal' values (Figs. 2.5 and 2.6). Assuming that the IVC lavas were derived from mantle wedge with initially MORB-like isotope ratios (see next section) this could reflect recycling of a crustal component into the source region, or incorporation of arc lithosphere during ascent (or both). There is considerable evidence from other island arcs (Thirlwall and Graham, 1984; Davidson et al. 1987; Ellam and Harmon, 1990; Smith et al., 1996; Thirlwall et al., 1996; Davidson, 1996; Macpherson et al., 1998) for the contamination of primary magmas by the arc crust. Contamination is also believed to be an important process, responsible for modifying isotope ratios in the western Sunda arc (Gasparon et al., 1994; Gasparon and Varne, 1998) and at Sangeang Api volcano in the East Sunda arc (Turner et al., 2003). It was already noted that the Java crust is transitional in nature, and evidence for explosive, continental-style magmatism, has recently been found in eastern Java (H. Smyth, pers. comm.). Therefore, prior to discussing source compositions it is important to assess the role of crustal contamination at IVC. One method of identifying crustal contributions is to

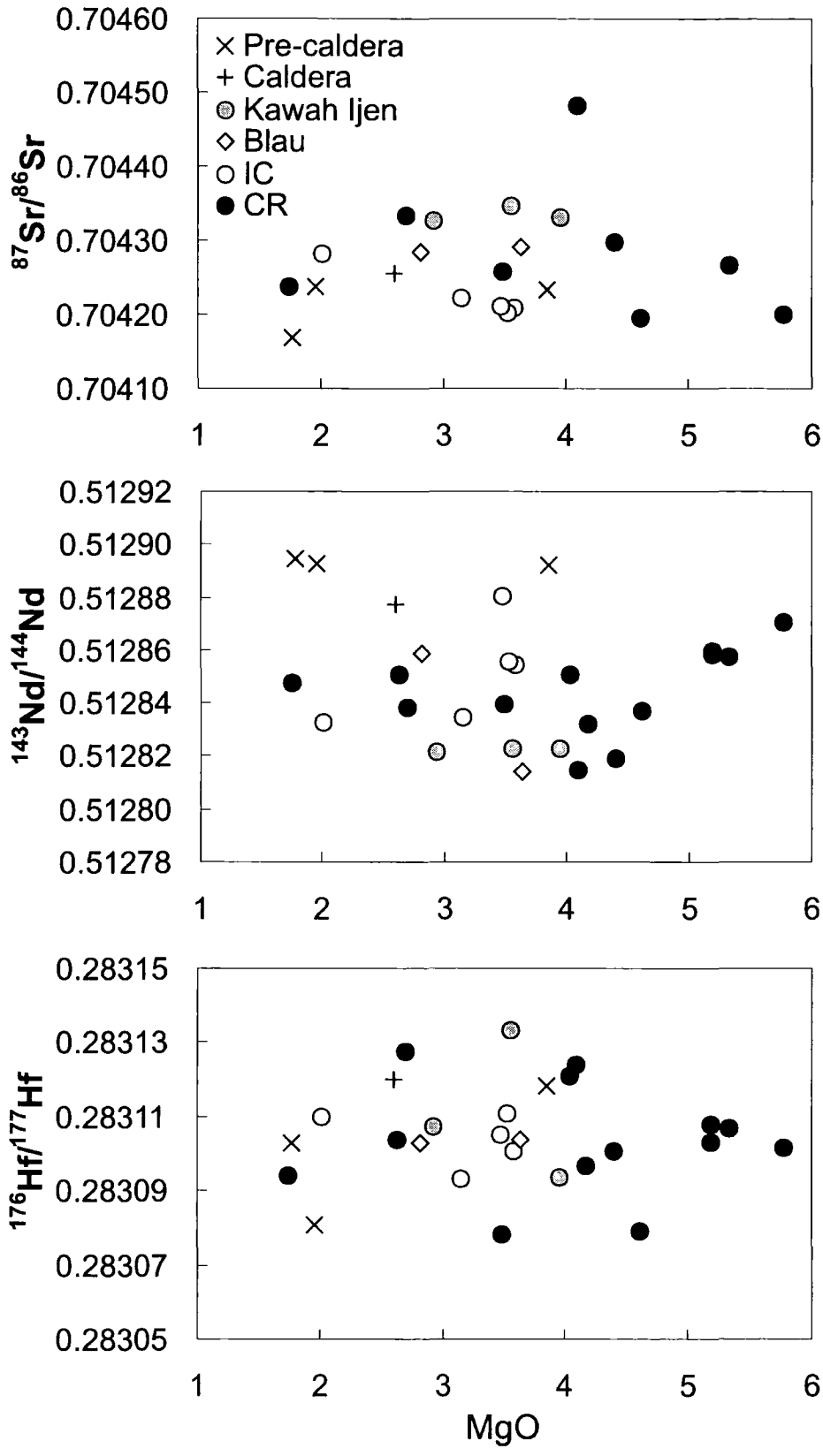

Fig. 2.10. $^{87}Sr/^{86}Sr$, $^{143}Nd/^{144}Nd$, $^{176}Hf/^{177}Hf$ versus MgO for IVC groups. 2σ external errors are less than data symbol size.

examine how isotope ratios vary with indices of differentiation (i.e. SiO_2 and MgO), which works on the principle that the isotope signature of the arc crust is distinguishable from that of the source. If arc crust were assimilated during shallow level differentiation, correlations of isotope ratios with MgO would be expected. Fig. 2.10 shows that there are no such correlations, either within individual geographic groups or in the IVC dataset as a whole. The absence of such correlations and the restricted ranges of Sr, Nd and Hf isotope ratios in IVC samples (Appendix C) are consistent with a negligible input of isotopically-distinct crust during differentiation. This conclusion is similar to those reached in studies of other Sunda arc volcanoes (Elburg et al., 2002; Gerbe et al., 1992; Gertisser and Keller, 2003). However, much of the crust beneath East Java is considered to comprise thickened oceanic crust (Hamilton, 1988) and may possess similar isotopic ratios to the source. Assimilation of this material may be difficult to discern and, therefore, alternative approaches are required to demonstrate that crustal assimilation is inconsequential at IVC.

Clinopyroxene $\delta^{18}O$ values of IVC lavas are homogeneous (+5.38 to +5.58‰, Table 2.1), and low, lying within the range of mantle $\delta^{18}O$ values (+5.57 ± 0.32‰) reported by Mattey et al. (1994) and Ionov et al. (1994). It is, therefore, unlikely that the lavas have been contaminated by upper crustal materials, that typically possess high $\delta^{18}O$ values (> +10‰, e.g. Davidson and Harmon, 1989) due to low temperature interaction with meteoric H_2O. Oceanic crust displays a wide range in oxygen isotope ratios due to interaction between basaltic rocks and seawater over a wide range of temperatures (Muehlenbachs, 1986). Therefore, if interaction with oceanic basement had been a significant process at Ijen we might predict greater scatter in $\delta^{18}O$ values. Similarly, a wide range of oxygen isotope ratios may be predicted to develop in the mafic to intermediate edifices and roots of the Sunda arc magmatism that pre-dates Ijen. A separate line of support is that only igneous, cumulate xenoliths have been found within Ijen complex lavas; no continental-type crustal xenoliths

have been detected (Sitorus, 1990; Berlo, 2001). Monomineralic plagioclase xenoliths are present in lavas erupted from Anyar (IC) and Blau, while cumulate xenoliths containing plagioclase, olivine, clinopyroxene and Ti-magnetite have been found in Rante (CR) and Kawah Ijen lavas. A cumulate containing olivine, ortho- and clinopyroxene was also found in lava from Kukusan (Berlo, 2001).

The evidence above suggests that any interaction of IVC magmas with arc crust during differentiation has had a negligible impact on their geochemistry. Fractional crystallisation therefore appears to be the dominant differentiation process controlling geochemical variations in IVC lavas. Higher Sr and lower Nd and Hf isotope ratios in IVC rocks relative to MORB, point towards contamination of the IVC source by an isotopically distinct crustal component.

2.5.2. Source components

Most models of petrogenesis at island arcs involve three main source components: 1) the mantle wedge, 2) the subducting slab (oceanic crust and associated sediments) and 3) the arc lithosphere. The involvement of the arc lithosphere in magma genesis at Ijen Volcanic Complex has been discussed above and it is concluded that contamination has little, if any, impact on the chemical composition of lavas. Therefore, the following discussion will focus on determining the characteristics of the source region and the role of the subducting slab. The majority of island arc magmas are thought to originate in the mantle wedge (Ringwood, 1974; Ellam and Hawkesworth, 1988; McCulloch and Gamble, 1991), which is inferred by several authors to be similar to the source of MORB (Gamble et al., 1996; Woodhead et al., 1993; Davidson, 1987; Turner et al., 2003). It has been proposed that there may be contribution from an enriched mantle component (OIB source) in some Sunda arc lavas (Wheller et al., 1987; Edwards et al., 1991, 1993; van Bergen et al., 1992), although a

MORB-like mantle source is advocated for the Sunda arc by others (e.g. White and Patchett, 1984; Turner and Foden, 2001; Elburg et al., 2002). Helium isotope values of olivine crystals in mantle xenoliths and island arc volcanics also implicate a MORB-like mantle source in the western Sunda arc (Hilton and Craig, 1989; Gasparon et al., 1994). Before assessing any contribution from the subducting slab in the genesis of IVC magmas it is necessary to characterise the pre-modification mantle wedge below East Java.

2.5.2.1. Mantle source characteristics

The HREE and HFSE are thought to remain relatively immobile compared to other elements, such as LILE, during slab dehydration (Tatsumi et al. 1986; Kessel et al., 2005) and abundances are generally too low in oceanic and continental crust (Taylor and McLennan, 1985) to significantly alter ratios of these elements in magmas derived from the mantle. We can use these trace elements, therefore, to help ascertain the pre-subduction composition of the mantle wedge. HREE concentrations are ~10-15 x chondrite values in IVC lavas and display relatively flat profiles (Fig. 2.11). This suggests that garnet is not an important residual mineral in the source region and that IVC magmas are derived largely from shallow mantle, above the garnet/spinel transition for wet peridotite. The La/Lu ratios of CR (41) and IC (44) lavas are very similar, which is consistent with similar sources and degrees of partial melting for these two post-caldera groups. The large difference in La/Lu ratios within the 3 pre-caldera group samples (34 to 80), when compared with the fairly constant ratio of the post-caldera volcanics (~42) may be due to different degrees of partial melting and/or different source mineralogies of the pre-caldera rocks. If post-caldera rocks from the IC and CR volcanoes, Kawah Ijen and Blau share the same source then they should possess similar ratios of immobile trace elements generally assumed to be unmodified by subduction processes (Table 2.4). Zr/Nb (17-23 (except one CR sample at 14)) and Ta/Nb (0.07-0.13)

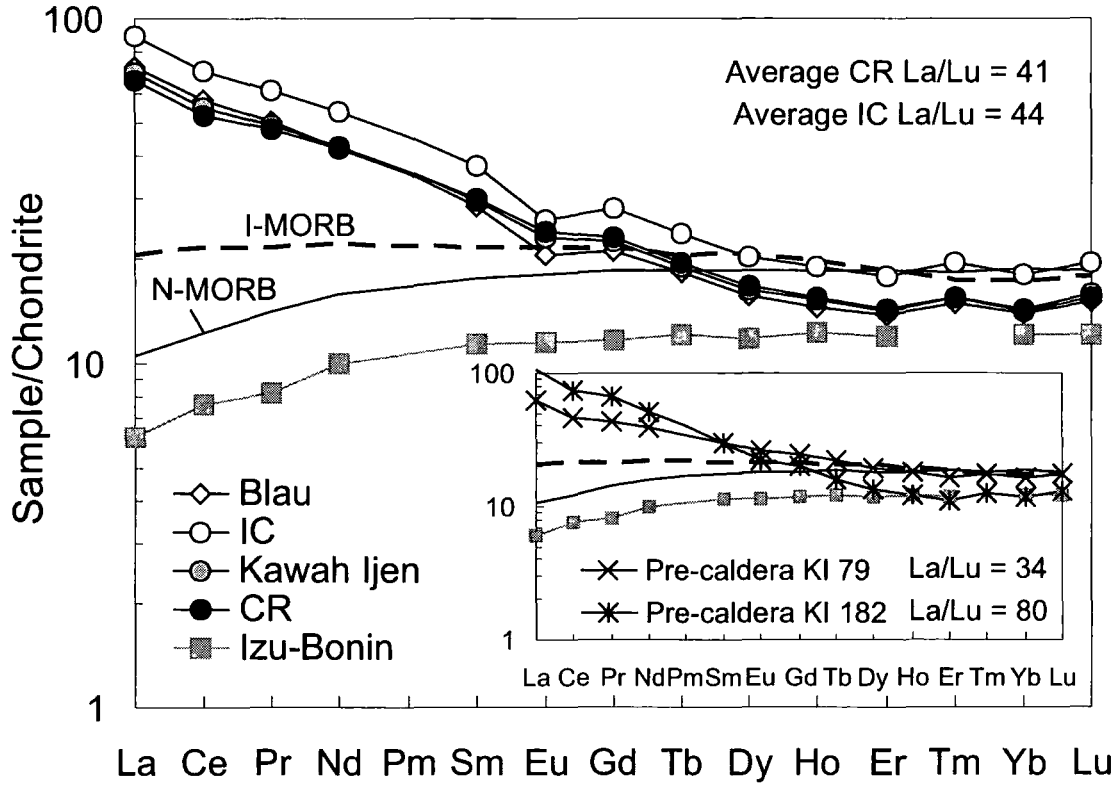

Fig. 2.11. Chondrite normalised rare earth element diagram of post-caldera IVC volcanic rocks. Normalising factors and N-MORB values from Sun and McDonough (1989). Indian MORB (Chauvel and Blichert-Toft, 2001), and Izu-Bonin arc lava compositions (Taylor and Nesbitt, 1998) are shown for comparison. Inset shows the chondrite-normalised abundance of the pre-caldera volcanic rocks. Note the large difference in La/Lu ratios displayed by the pre-caldera group (inset) in comparison with the IC and CR groups.

Table 2.4. Average trace element ratios in I-MORB, N-MORB, Bulk Java Sediment and the range in IVC rocks

Ratio	I-MORB	N-MORB	Bulk Java Sediment	IVC
Ta/Nb	0.07	0.06	0.08	0.07-0.13
Zr/Nb	26	32	13	14-23
Ce/Pb	15	25	3	3-7
Th/Yb	0.17	0.04	3	1-4
Ba/La	7	3	27	23-36
Sr/Nd	14	12	6	16-44

I-MORB: Chauvel and Blichert-Toft, 2001 n = 8; N-MORB: Sun and McDonough, 1989; Bulk Java sediment: Plank and Langmuir, 1998.

ratios do not change with differentiation (Figs. 2.12a and b), and are relatively homogeneous for all IVC eruptive rocks. These ratios are similar to MORB (Normal and Indian type) Ta/Nb ratios compared to OIB (Table 2.4, e.g. Fig. 2.12b), but Zr/Nb ratios of the lavas are lower than Zr/Nb ratios of N-MORB and more closely resemble I-MORB (Table 2.4, e.g. Fig. 2.12a). The similarity between HFSE and HREE concentrations in IVC basalt and I-MORB, rather than N-MORB, is emphasised in Fig. 2.13b. Therefore, we conclude that the mantle wedge beneath IVC is similar to the source of I-MORB. Several studies utilising Pb

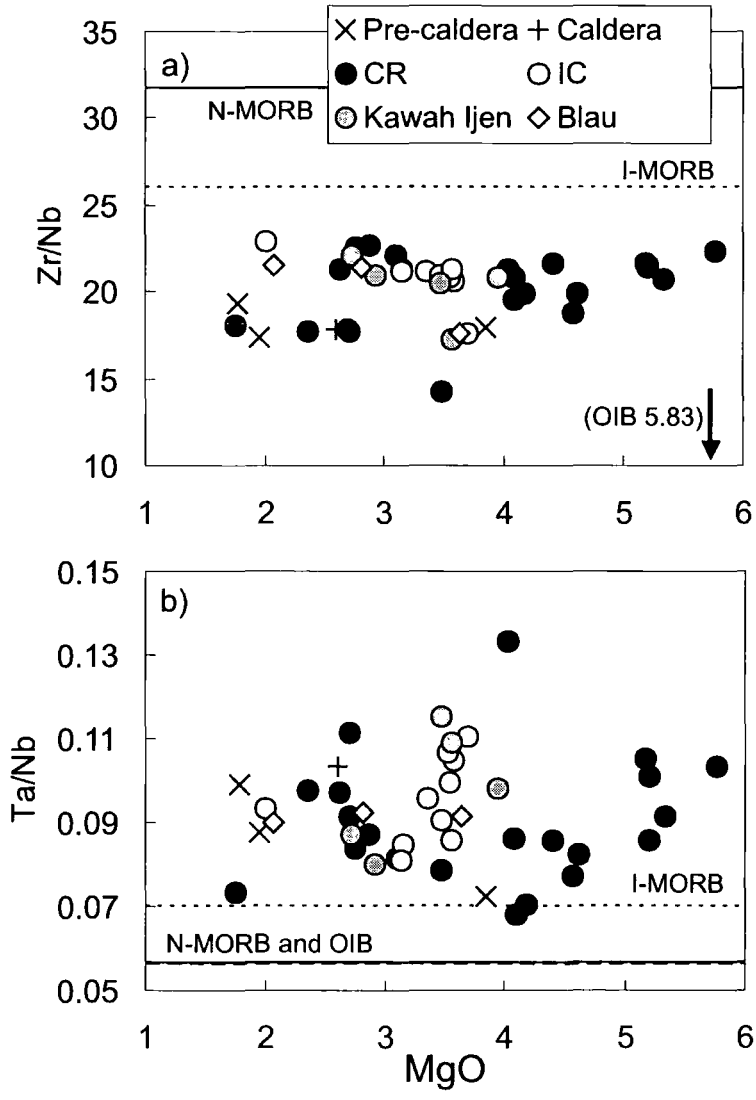

Fig. 2.12. a) Ta/Nb and b) Zr/Nb versus MgO for IVC groups. N-MORB and OIB data from Sun and McDonough (1989). Indian MORB data from Chauvel and Blichert-Toft, 2001.

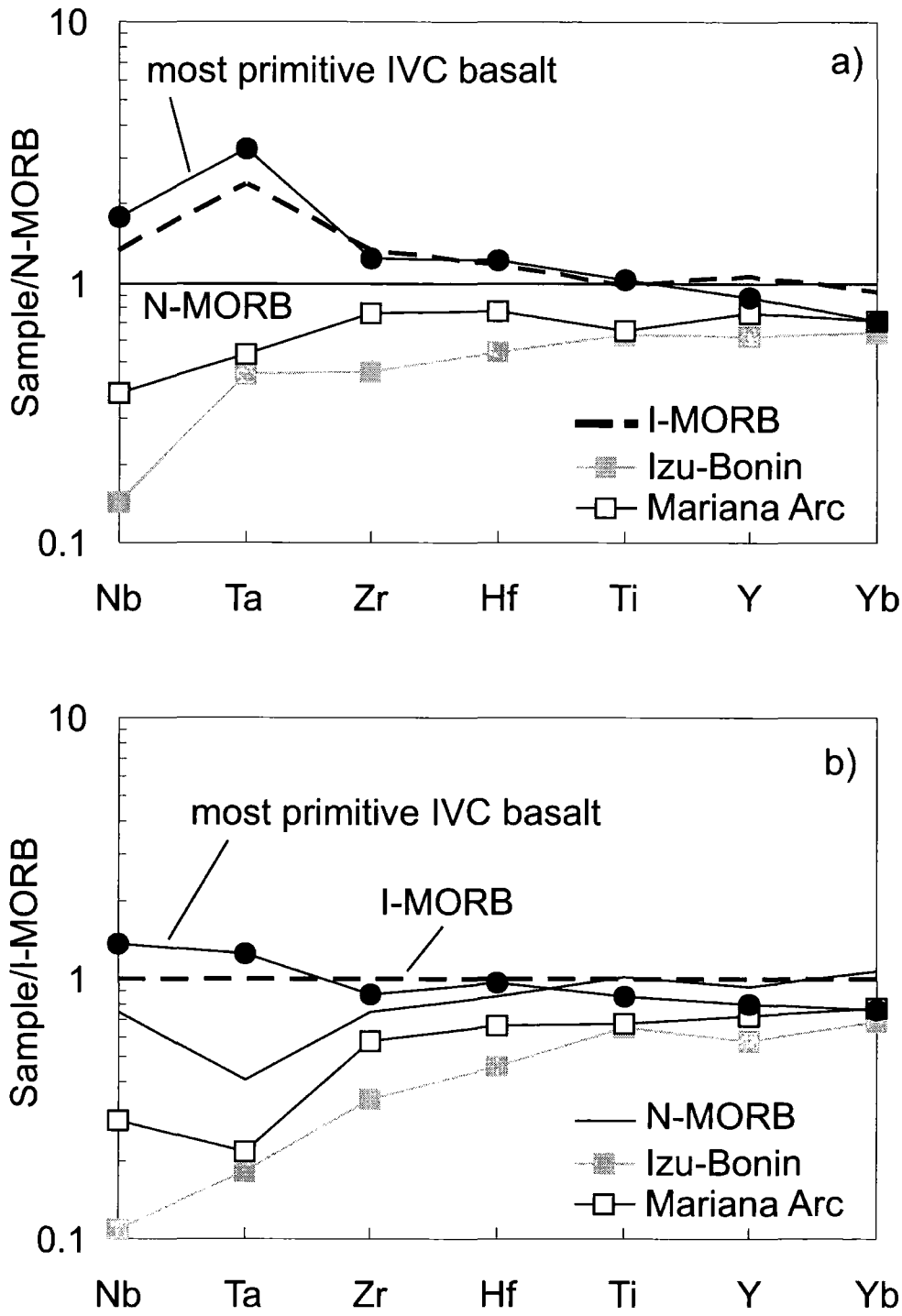

Fig. 2.13. a) Comparison of HFSE, Y and Yb abundances in the most primitive IVC basalt with N-MORB (Sun and McDonough, 1989), I-MORB (Chauvel and Blichert-Toft, 2001; Price et al., 1986; Rekhamper and Hofmann, 1997) and other island arc lavas: Izu-Bonin (Taylor and Nesbitt, 1998) and Mariana arc (Elliot et al., 1997). b) Data (as above) normalised to I-MORB (rather than N-MORB) to emphasise the similarity between I-MORB and IVC element concentrations.

isotopic and trace element ratios have reached a similar conclusion for magmatism in SE Asia throughout the Cenozoic (Taylor et al. 1994; Hickey-Vargas, 1998; Macpherson and Hall, 2001 & 2002; Elburg, et al., 2002; Macpherson et al. 2003). The HFSE and HREE concentrations and ratios of IVC lavas (Fig. 2.13a and b) also indicate that the mantle wedge is not significantly depleted beneath East Java, in contrast to others arcs such as the Izu-Bonin and Mariana arcs, where sources are thought to have experienced melt extraction prior to involvement in arc petrogenesis (Taylor and Nesbitt, 1998; Elliot et al., 1997; Woodhead et al., 1993).

The isotopic ratios of different IVC suites cannot be distinguished from one another, with the exception of Nd isotope ratios of the pre-caldera rocks (Fig. 2.10). It was established above that the arc lithosphere has had a negligible influence on magmatism, therefore the measured isotopic ratios represent the isotopic composition of the mantle source. Since Sr is fluid-mobile during slab dehydration, Sr isotope data are not well suited for identifying the isotopic composition of the pre-modified wedge. Experimental work (You et al., 1996; Tatsumi et al., 1986; Brenan et al., 1995) and studies of arc lavas (McCulloch and Gamble, 1991: Pearce and Peate, 1995; Münker et al., 2004) indicate that Hf and Nd are relatively immobile during slab dehydration, particularly in the formation of aqueous fluids (Kessel et al., 2005). However, Woodhead et al. (2001) cast doubt upon the status of Hf as a truly fluid-immobile element; they see evidence in the New Britain subduction system for the transport of Hf in aqueous fluids when Nd is immobile. Their observations are based on the contrast in Hf isotope ratios of the mantle wedge beneath New Britain and subducting crust of the Woodlark Basin. Since we advocate an I-MORB composition for both the mantle wedge and the down-going plate, any Hf mobility should have negligible impact on the Hf isotope ratios of Ijen sources. Therefore, combined Nd and Hf isotope data can better document source (mantle wedge) characteristics of IVC lavas than combinations of isotope ratios involving

$^{87}Sr/^{86}Sr$ isotope data (e.g. Pearce et al., 1999). IVC lavas display a restricted range in $^{143}Nd/^{144}Nd$ and especially $^{176}Hf/^{177}Hf$ and lie within the Hf isotope range of I-MORB. Lavas from other Javan volcanoes diverge further from typical mantle (MORB) values towards more 'crustal' Hf-Nd isotopic compositions. Therefore, although major element data indicate IVC lavas are moderately fractionated and are not primary magmas, the IVC source appears to be among the least affected by crustal inputs from either the slab or arc lithosphere (noting that the Hf isotope database is slightly more limited in comparison with Sr-Nd isotope data available). Volcanic rocks from IVC and other centres on Java lie above the dividing line that separates MORB of Indian and Pacific provenance, drawn in Hf-Nd isotope space by Pearce et al. (1999) (Fig. 2.6), implying derivation from an I-MORB-like mantle source rather than a source similar to Pacific-MORB, and corroborating conclusions from ratios of immobile trace elements (above).

In summary, restricted variation in isotope ratios and immobile trace element ratios suggests that the mantle sources of different groups of IVC magmatism are not distinct from each other. The mantle wedge beneath East Java is relatively fertile compared to that of many other island arcs, with HFSE (especially Nb and Ta) and HREE concentrations similar to I-MORB. Having constrained the composition of the mantle wedge below IVC and identified that the arc lithosphere has negligible influence upon magma evolution in IVC lavas, we will now determine the modification, if any, imposed upon the mantle source by the subducting slab.

2.5.2.2. Identification of subduction zone components: trace element constraints

Enrichment of LILE and LREE relative to HFSE in arc volcanics has long been attributed to slab involvement (Hawkesworth et al., 1979; Kay, 1980; White and Dupré, 1986; McCulloch and Gamble, 1991; Davidson, 1987). There remains, though, considerable uncertainty as to

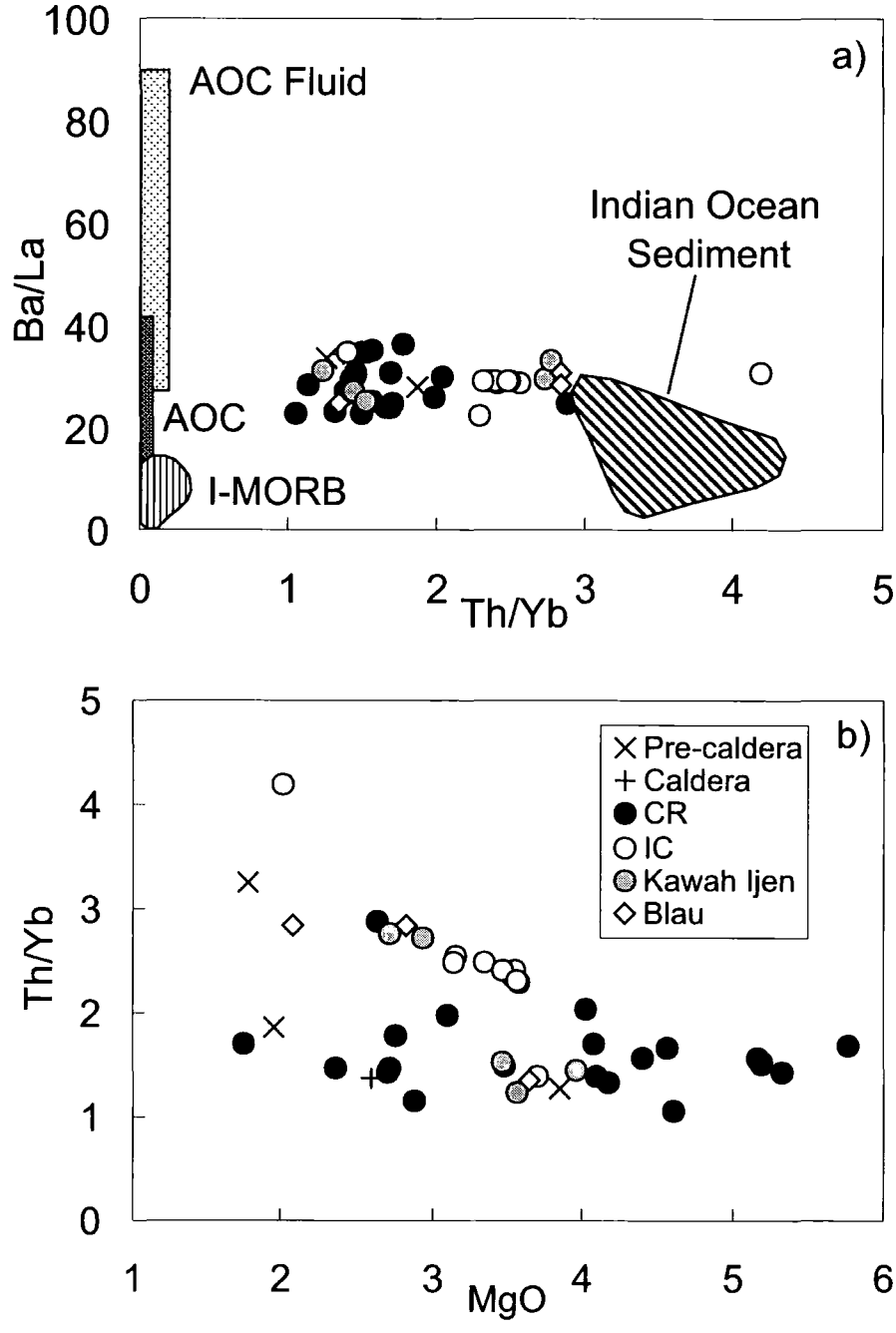

Fig. 2.14. a) Ba/La-Th/Yb diagram highlighting the high Ba/La and Th/Yb ratios of IVC samples compared to I-MORB (Chauvel and Blichert-Toft, 2001). The field of Indian Ocean sediment is defined by 3 of the 4 sediment compositions used in the isotope mixing models in Fig. 2.15a: bulk Java sediment (Plank and Langmuir, 1998), average terrigenous sediment (V33-75, -77, -79) and nanno ooze (Gasparon and Varne, 1998). Altered oceanic crust data from Staudigel et al., 1996. AOC fluid ratios calculated using mobility data of Tatsumi et al., 1986 and shows the significantly higher Ba/La ratios in an AOC fluid relative to bulk AOC. b) Th/Yb versus MgO for IVC groups.

the source of this contribution (altered oceanic crust or sediments or both) and the transfer mechanism of this component to the sub-arc mantle (as a fluid or melt or both).

Th and the LREE are thought to be less mobile in aqueous fluids than the LILE (Tatsumi et al., 1986; Pearce et al., 1999) and, therefore, high Ce/Pb and Th/Yb ratios in arc lavas are taken to indicate a sedimentary contribution from the slab (Gertisser and Keller, 2003; Woodhead et al., 2001). The large contrast in Ce/Pb and Th/Yb ratios between MORB (N- and I-MORB) and Indian Ocean sediments near Java (Table 2.4; Fig. 2.14a), suggests that relatively low Ce/Pb (3-7) and high Th/Yb (1-4) ratios of the IVC may be attributed to a sediment component in the arc mantle source. However, the slightly higher Th/Yb ratios observed in lavas of the low-Ca group, suggests that this ratio was also affected by fractional crystallisation. A plot of Th/Yb versus MgO (Fig. 2.14b), reveals slight elevation and correlation of Th/Yb ratios in the IC group compared to the CR group. The later group display highly restricted variation (Th/Yb ~1.5) over the entire range of MgO, so we infer that this ratio is representative of the IVC source.

Elevation of LILE/LREE ratios in arc lavas compared to MORB are thought to indicate fluid addition to the mantle wedge from dehydration of the subducting slab (Ben Othman et al., 1989; Elliot et al., 1997). Ba/La (23-36) and Sr/Nd (16-44) ratios of IVC lavas are slightly to significantly higher than those seen in Indian Ocean sediment, and also much greater than I-MORB (Table 2.4; Fig. 2.14a), indicating that slab fluids may also be added to the IVC mantle source, possibly from the altered oceanic crust (AOC). However, Ba/La ratios of IVC volcanics are not as high as those found in the Kermadec, Mariana and New Britain arcs where the dominant slab input is thought to be a hydrous fluid (Woodhead et al., 2001). To summarise, trace element ratios suggest that the addition of both aqueous fluid and sediment melt from the subducting plate, to the source region, may be important in producing

primary magma compositions at IVC. Radiogenic isotope modelling will now be explored to place constraints on slab inputs.

2.5.2.3. Modelling slab input: constraints from radiogenic isotopes

2.5.2.3.1. Two-component model: I-MORB + Bulk sediment

Trace element data and Hf isotope ratios of IVC rocks indicate that the mantle source below the Sunda arc is similar to I-MORB, but they possess slightly higher $^{87}Sr/^{86}Sr$ and lower $^{143}Nd/^{144}Nd$. Displacement of Sr-Nd isotope ratios from depleted mantle values has been attributed to the contribution of subducted sediment (White and Patchett, 1984; Vroon, 1992; Ben Othman et al., 1989; White and Dupré, 1986). Fig. 2.15a shows simple mixing between I-MORB source and bulk sediment for a variety of Indian Ocean sediment end members (Table 2.5). Mixing arrays involving three of the four end member sediments: A (Mn nodule, V34-62; Ben Othman et al., 1989), B (nanno ooze, DSDP site 211; Gasparon and Varne, 1998) and C (average Java sediment; Plank and Langmuir, 1998), produce reasonable fits to the general field of Java volcanics (white fill). The terrigenous-biogenic sediment end member (D) has high Sr/Nd and produces a convex-up trend in Sr-Nd isotope space when mixed with I-MORB mantle (Fig. 2.15a). This pattern does not fit the general Java data; therefore, bulk terrigenous-biogenic sediments are unlikely to dominate the sediment contribution to the mantle source of most Java volcanics. This is supported by sediment data collected from the Indian Ocean. Terrigenous sands and silts, such as turbidites, are present in the average composition of the sedimentary column subducted at the Java trench described by Plank and Langmuir (1993), but are minor components compared to clay and siliceous ooze. Boreholes 211 and 261 of DSDP leg 22 (SEATAR, 1981 (Fig. 1.3)), located over Indian Ocean crust south of Java, lack terrigenous sediments, containing nanno-ooze, nanno-claystone, a small amount of volcanic ash and a 12cm thick surface layer of small manganese

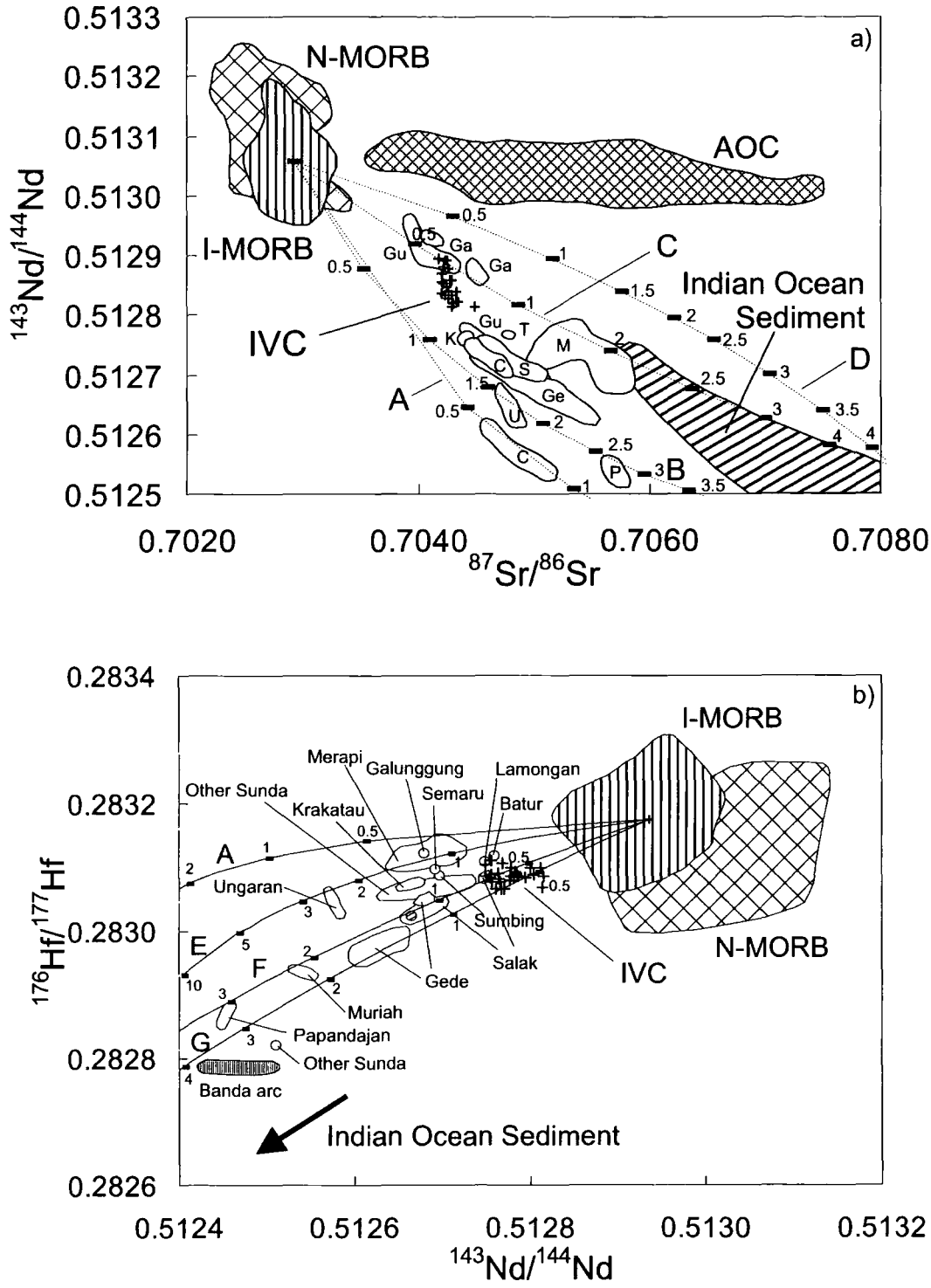

Fig. 2.15. a) $^{143}Nd/^{144}Nd$-$^{87}Sr/^{86}Sr$ diagram showing bulk mixing between I-MORB source (I-MORB*0.1, assuming 10% melting) and bulk sediment. Data sources of I-MORB, N-MORB, AOC and Indian Ocean sediment see Fig. 2.5. Sediments used in mixing: A = Mn nodule; B = nanno ooze; C = bulk Java sediment; D = terrigenous-biogenic. For sediment data sources and compositions see Table 2.5. Ticks along the mixing curves show the percent of sediment in the mixture. Java field: Gu = Guntur, C = Cereme (Edwards, 1990); Ga = Galunggung (Gerbe et al., 1992); S = Salak, Ge = Gede (this study); M = Merapi (Gertisser and Keller,

2001); K = Krakatau (Turner and Foden, 2001); T = Tangkuban Prahu, U = Ungaran, P = Papandayan (Whitford et al., 1981). b) $^{176}Hf/^{177}Hf$ -$^{143}Nd/^{144}Nd$ diagram showing bulk mixing models between I-MORB source and Indian Ocean sediments: Sediments used in mixing: A = Mn nodule (as above); E = pelagic sediment; F and G = terrigenous sediments. Sediment data sources and compositions given in Table 2.5. Other data sources as in Fig. 2.6. Java data: Merapi, Gede and Salak (this study); Other Sunda (White and Patchett, 1984); other named volcanoes (Woodhead et al., 2001). End member compositions are given in Table 2.5.

Table 2.5. End-member compositions used in mixing calculations for Figs.2.15, 2.16 and 2.17.

		Sr (ppm)	Nd (ppm)	Hf (ppm)	$^{87}Sr/^{86}Sr$	$^{143}Nd/^{144}Nd$	$^{176}Hf/^{177}Hf$
Fig. 2.15	I-MORB Source	13.5	0.97	0.25	0.702915	0.513042	0.283211
	Sed A	857	187.9	5.73	0.709117	0.512236	0.282828
	Sed B	126	51.9	-	0.71643	0.512228	-
	Sed C	218	33.95	-	0.71682	0.51216	-
	Sed D	398	15.36	-	0.708875	0.512411	-
	Sed E	-	55.3	3.67	-	0.512278	0.282712
	Sed F	-	35	5.09	-	0.51193	0.282311
	Sed G	-	31.3	5.58	-	0.51191	0.28223
Fig. 2.16	FMM	22.42	0.697	-	0.704584	0.51307	-
Fig. 2.17	IM1	13.9	1.02	0.25	0.702911	0.513044	0.283159
	IM2	13.9	1.02	0.25	0.702819	0.513085	0.283124
	IM3	13.9	1.02	0.25	0.70269	0.512991	0.283124
	IM1 FMM	15.5	1.38	-	0.703502	0.513038	-
	IM2 FMM	15.5	1.38	-	0.703422	0.513067	-
	IM3 FMM	15.5	1.38	-	0.703309	0.513000	-

Mantle wedge represented by I-MORB source (I-MORB/10 assuming 10% melting) I-MORB data from Chauvel and Blichert-Toft (2001).

Data: I-MORB average Sr concentration from Price et al., 1986; Chauvel and Blichert-Toft, 2001; Rekhamper & Hofmann, 1997; I-MORB Nd and Hf concentration, Sr, Nd and Hf isotope data from Chauvel and Blichert-Toft, 2001.

Sediments: A = Mn nodule (V34-62, Ben Othman et al., 1989; White et al., 1986); B = nanno ooze, DSDP site 211 (Gasparon and Varne, 1998); C = average Java sediment (Plank and Langmuir, 1998); D = terrigenous-biogenic, average of V33-75, -77, -79 (Gasparon and Varne, 1998; Ben Othman et al., 1989); E = pelagic sediment (V34-45 White et al., 1986; Ben Othman et al., 1989); F and G = terrigenous sediments V28-357-M (CA30-M) and V28-357-M (CA30-S) respectively (Vervoort et al., 1999).

FMM (fluid modified mantle) mixture in Figs. 2.16 and 2.17 = 3% AOC fluid:97% I-MORB source. AOC end member composition used in fluid calculation from Staudigel et al. (1995): Sr 67.32 ppm, Nd 13.08 ppm, $^{87}Sr/^{86}Sr$ 0.707437, $^{143}Nd/^{144}Nd$ 0.513023.
Fluid created by 0.5% dehydration of AOC using $C_F = C_O/D+F^{(1-D)}$, where C_F is the concentration in the fluid, C_O is the concentration in AOC, D is the distribution coefficient given by Keppler (1996): Sr $D_{fluid/cpx}$ = 2.1, Nd $D_{fluid/cpx}$ estimated at 0.3 (relative to $D_{fluid/cpx}$ La = 1.0, Gd = 0.14 and Lu = 0.11) and F is the fraction of fluid created (0.005).

I-MORB low $^{176}Hf/^{177}Hf$ sources: IM1 = MD37-05-02, Chauvel and Blichert-Toft, 2001; 2 = 54R-1, 115-121, Nowell et al., 1998; 3 = MD34 D2, Chauvel and Blichert-Toft, 2001

nodules. Addition of 0.5-1% average bulk Java sediment (C; Plank and Langmuir, 1998) to I-MORB produces a curve that passes through the most isotopically primitive IVC volcanics (Fig. 2.15a), but that is highly oblique to the IVC array.

There is limited Hf isotope data for the same Indian Ocean sediments modelled in Fig. 2.15a; only the Mn nodule (A) (V34-62, White et al., 1986; Ben Othman et al., 1989; curve A in Fig. 2.15a and b). Hf isotopic data are available for a pelagic sediment (E) (V34-45 White et al., 1986; Ben Othman et al., 1989) and terrigenous sediments (F) V28-357-M (CA30-M) and (G) V28-357-M (CA30-S) (Vervoort et al., 1999). Around 0.5 % addition of deep-sea turbidite from the Java Trench is sufficient to explain the isotopic compositions of some IVC lavas (curves F and G) but, as shown above, Sr-Nd isotopic variation suggests that terrigenous sediments do not significantly contribute to the source IVC magma. Therefore, a more complex, multi-component model may be applicable at IVC to reproduce the isotopic systematics exhibited by the lavas.

2.5.2.3.2. Two-stage, three-component model: I-MORB + AOC component + bulk sediment

Two-component mixing fails to provide a good fit to the isotopic variation of IVC lavas suggesting that an additional, isotopically distinct component may be required in the source. Furthermore, some trace element ratios (e.g. Ba/La) are too high for MORB source mantle and sediment mixtures to explain, but are consistent with a fluid contribution derived from the subducted altered oceanic crust (AOC). Contributions from AOC have been inferred for many Sunda arc lavas (Turner and Foden, 2001) and there is considerable support for 2 separate contributions from the subducting slab to the mantle wedge in the petrogenesis of many other arc lavas (Ellam and Hawkesworth, 1988; White and Patchett, 1984; Taylor and Nesbitt, 1998; Thirlwall et al., 1996; Elliot et al., 1997; Turner et al., 1997; Hawkesworth et

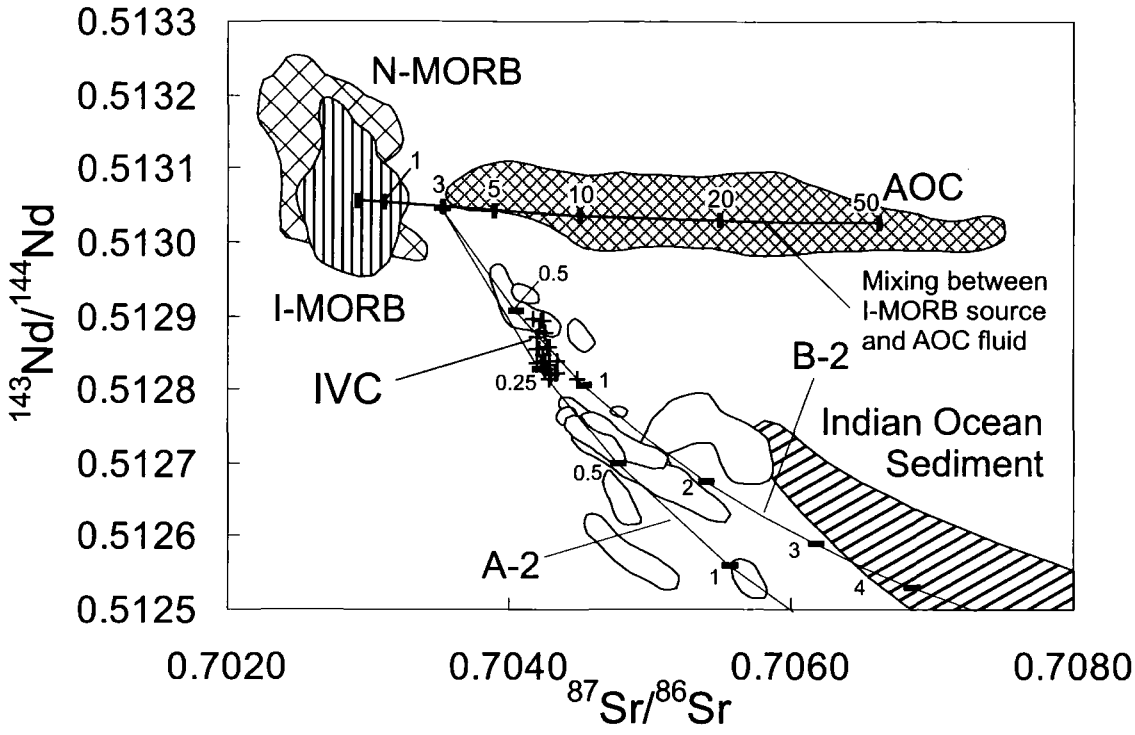

Fig. 2.16. $^{143}Nd/^{144}Nd$-$^{87}Sr/^{86}Sr$ diagram showing 2-stage, 3-component mixing. Data sources as in Figs. 2.5 and 2.15a. Mixing between I-MORB source and a fluid from the altered oceanic crust creates a mixture with higher $^{87}Sr/^{86}Sr$ and near identical $^{143}Nd/^{144}Nd$ to I-MORB source. Mixing of fluid modified mantle with sediments A and B (as in Fig. 2.15a) produces a good fit to the IVC data (curves A-2 and B-2 respectively). Tick marks indicate the percent of sediment added to the fluid modified mantle. End member compositions and fluid calculations are given in Table 2.5.

al., 1997; Turner and Hawkesworth 1997). Interaction of seawater with basalt produces significant chemical and isotopic changes (Hart et al., 1974; White and Patchett, 1984). Altered oceanic crust displays a wide range in $^{87}Sr/^{86}Sr$ ratios while $^{143}Nd/^{144}Nd$ isotope ratios are generally indistinguishable from fresh MORB (Fig. 2.16). Due to the lack of isotopic data reported for altered Indian Ocean MORB we have used data for Atlantic MORB (Staudigel et al., 1996) to consider the effect of adding this component to the mantle wedge. Regardless of how this component is added to the mantle wedge, either as a fluid (most commonly proposed e.g. Ellam and Hawkesworth, 1988; Turner et al., 1997) or melt (particularly where

the subducting crust is young, e.g. Defant and Drummond, 1990), the isotopic composition of the resultant mixture will be generally the same: mixing I-MORB source with AOC fluid or melt will create a mixture with higher Sr isotope ratios and similar Nd isotope ratios to I-MORB. However, the quantity of AOC component required will be dependant on the transfer mechanism, due to higher Sr/Nd ratios in fluids produced from the AOC compared to melts. The trajectory of the IVC data crosscuts any conceivable 2-component mixing curve produced between mantle source and an AOC-sediment mixture, therefore a 2-stage model is explored here. In the mixing models, we have chosen the addition of an AOC component as a fluid, as it is hard to envisage (in a two stage process whereby the mantle source is first contaminated by AOC prior to bulk addition of sediment) (cf. Elliot et al., 1997; Turner and Hawkesworth, 1997) melting of the AOC and addition of this to the mantle wedge without melting the sediments and incorporating them too, simultaneously, to the mantle wedge. Furthermore, the IVC lavas contain none of the geochemical traits thought to record slab melting (Defant and Drummond, 1990; Garrison and Davidson, 2003; Macpherson et al., 2006).

Fig. 2.16 shows the results obtained from models of two-stage source contamination, where an I-MORB source is first contaminated by fluid from the AOC, and then bulk sediment (Mn nodule (curve A-2) and nanno ooze (curve B-2)). These types of sediments are consistent with the findings from DSDP leg 22 boreholes 211 and 261 mentioned above. 3% AOC fluid was added to create the fluid-modified mantle (FMM) component in this model (see Table 2.5 for AOC fluid calculation details). Mixing proportions of AOC and I-MORB are highly dependant on Sr and Nd abundances and isotopic ratios of AOC, which are themselves extremely variable. The fraction of fluid required is smaller if more highly altered basalt compositions are used, and greater if a partial melt/bulk mixing of AOC is considered. The three-component models produce excellent fits not only to the trend of IVC lavas but

also a large proportion of other Java volcanics. Only a small percentage of sediment (0.25% Mn nodule or 0.5-1% nanno ooze) is required to generate the isotopic values seen in IVC volcanics.

2.5.2.3.3. Three-component mixing in Nd and Hf isotope space

Modelling of two-stage source contamination in Nd-Hf isotope space is hampered by the paucity of Hf isotope data reported for altered oceanic crust. Nd isotope ratios remain relatively constant during hydrothermal and low temperature seawater alteration of MORB, therefore, White and Patchett (1984) predict that Hf isotope ratios will also be unaffected by the alteration of oceanic crust. Under these circumstances, contamination of the mantle source by a slab fluid from the AOC would be undetectable using Nd and Hf isotopes.

We will use the good match of the Sr-Nd mixing models to further constrain the nature and amount of sediment added to the fluid-fluxed mantle and investigate the $^{176}Hf/^{177}Hf$ of the mantle end member. Two-component mixing of average I-MORB with the sediment types suggested in Sr-Nd isotope modelling (Mn nodule and pelagic sediment), produced suitable trend shapes to fit the IAV array in Nd-Hf isotope space, however, the mixing curves are located at higher $^{176}Hf/^{177}Hf$ than the IVC lavas (curves, A and E respectively, Fig. 2.15b). The relatively shallow array of IVC lavas project back towards a mantle source with lower $^{176}Hf/^{177}Hf$ ratios than average I-MORB (Fig. 2.15b). Therefore we propose that the mantle wedge beneath IVC is represented by I-MORB with Hf isotope ratios lower than average. Mixing of I-MORB source with lower than average Hf isotope ratios: IM1 (MD34 D2), IM2 (MD37-05-02 D1 N3; Chauvel and Blichert-Toft, 2001) and IM3 (54R-1,115-121; Nowell et al., 1998) with the Mn nodule sample (A) used in Sr-Nd isotope modelling (Hf isotope data is unavailable for the nanno ooze), produces a model that corresponds perfectly with the IVC data array, requiring < 0.5% addition of this sediment (all

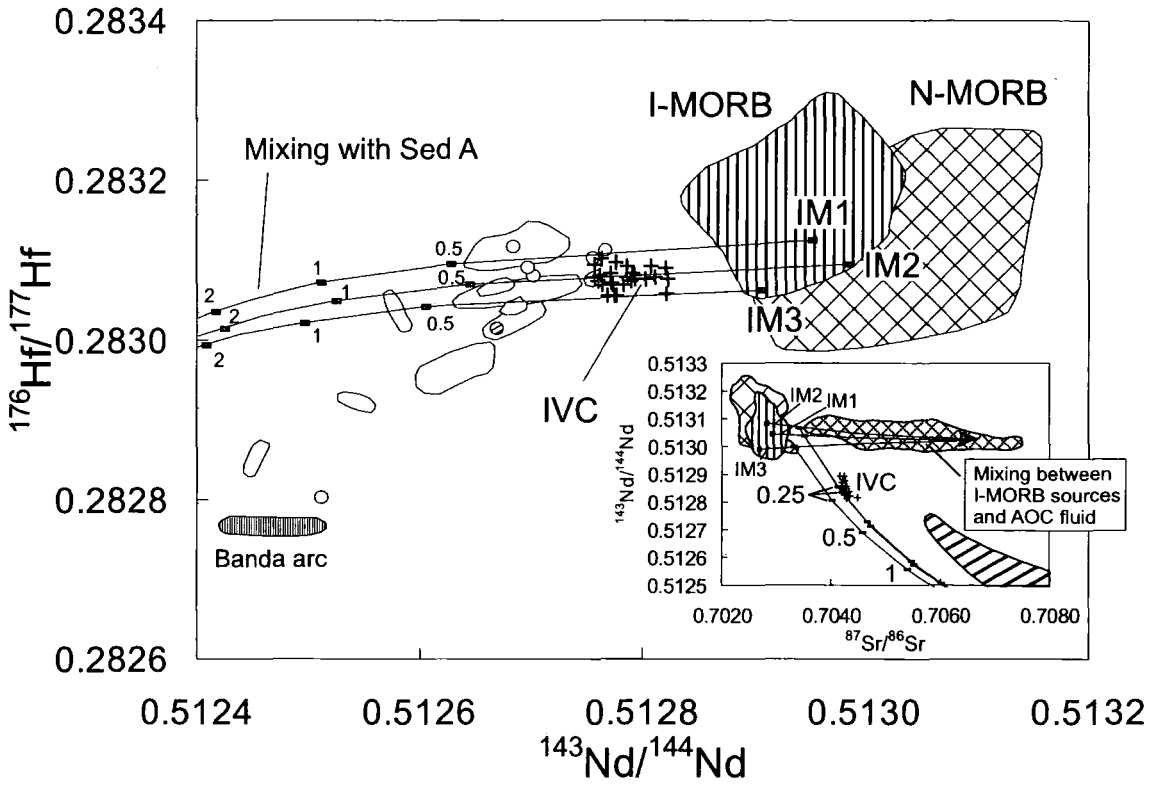

Fig. 2.17. $^{176}Hf/^{177}Hf$-$^{143}Nd/^{144}Nd$ showing mixing curves between three I-MORB source compositions with lower than average $^{176}Hf/^{177}Hf$ isotope ratios: IM1, IM2 and IM3 and sediment A (Mn nodule) . Data sources as in Figs. 2.6 and 2.15b. End member compositions are listed in Table 2.5. Inset diagram shows 3-component mixing in Sr-Nd isotope space using the lower $^{176}Hf/^{177}Hf$ I-MORB source compositions used in the main diagram (rather than average I-MORB), AOC fluid (as in Fig. 2.16) and Mn nodule (sediment A) to represent the sediment. The inset shows that using a lower $^{176}Hf/^{177}Hf$ I-MORB source compositions has little effect on the shape of the mixing curve and the amount of sediment required when compared to curve A in Fig. 2.16, which uses average I-MORB source composition. Data fields as in Fig. 2.5 and end members compositions are given in Table 2.5.

mixing curves Fig. 2.17), matching the percentage of sediment required to explain the IVC data in 3-component Sr-Nd mixing (Fig. 2.16). Using low $^{176}Hf/^{177}Hf$ I-MORB source end members instead of average I-MORB compositions does not affect the conclusions reached from 3-component modelling in Sr-Nd isotope space (Fig. 2.17 inset); almost identical results are obtained (compare with curve A-2 in Fig. 2.16). This implies that, if a hydrous fluid is added to the mantle source from the altered oceanic crust, there is a minimal effect on the resulting Nd and Hf isotope ratios.

In conclusion, radiogenic isotope and trace element data of IVC lavas suggest a 3 component, 2-stage source contamination model is applicable at IVC. In this model I-MORB mantle is metasomatised by slab fluid prior to addition of subducted sediment. Three-component models have also been suggested in geochemical studies of other island arc volcanoes (Ellam and Hawkesworth, 1988; Taylor and Nesbitt, 1998; Elliot et al., 1997; Turner et al., 1997). However, the order in which the two components from the slab (fluid and sediment) are introduced to the mantle wedge beneath IVC differs from that proposed in other models. U-series isotopic compositions of Mariana lavas indicate that addition of a sedimentary component took place at least 350 kyr before fluid addition to the mantle wedge beneath the Mariana arc (Elliot et al., 1997). The authors propose two possible models for the subduction component addition: 1) Shallow (<120 km depth) sedimentary melts produce enriched sub-arc mantle, which is then dragged down to deeper depths, where dehydration of the altered oceanic crust then releases fluid into the enriched sub-arc mantle causing melting. 2) altered oceanic crust dehydrates at shallow depth to produce hydrated peridotite mantle, which is down-dragged and dehydrates at around 120 km depth causing extensive melting. This material then encounters sedimentary material rising from greater depth. The authors acknowledge the inherent problems in their most simplistic model (1) of satisfying thermal models of subduction zones (Peacock, 1991; Johnson and Plank, 1999). The reverse order in the addition of subduction components proposed at IVC i.e. slab dehydration and fluid addition to the mantle wedge prior to sediment addition, appears mechanically more viable. However, in this model, fluid sourced predominantly from the oceanic crust must pass through the overlying sediment and avoid any sedimentary imprint. This is possible as Elliot et al. (1997) point out that the sedimentary pile on top of the oceanic crust is likely to dehydrate and lose its fluid mobile elements at shallower depths before major basaltic dehydration. This earlier fluid addition to the wedge may avoid being down-dragged to the

region of arc magma genesis (Fryer, 1992) and, therefore, not contribute to lava geochemistry. Turner and Hawkesworth (1997) also propose a preferred model in which partial melts of sediment are added to the mantle wedge at relatively shallow levels prior to fluid addition from the slab. The timescale envisaged for fluid addition is in the order of 30,000-50,000 years before eruption.

In comparison, at volcanoes of the Andonara-Pantar section in the East Sunda arc, U-series, Sr-Nd-Pb isotope and trace element data supports a similar transfer order for the addition of fluid and sediment sourced slab components (Hoogewerff et al., 1997), as that proposed at IVC, although differing slightly in the exact nature of the slab components (sediment-derived hydrous fluid and siliceous melt). The hydrous fluid is proposed to dominate the input in the shallow part of the subduction zone, whereas the sedimentary melt dominates the flux at deeper levels. Evidence for relatively recent fluid addition is provided by ^{226}Ra excess in the most arc-front volcanic rocks of the Andonara-Pantar section and also in other Sunda arc lavas (Turner and Foden, 2001; Turner et al., 2003).

2.5.2.4. Comparison of slab contributions

The amount of local sediment incorporated in the source region of IVC lavas (<0.5 Mn nodule or 0.5-1% nanno ooze) is similar to or less than the amount of subducted sediment proposed in magma genesis at other arcs: Lesser Antilles (White and Dupré, 1986), Banda (Vroon, 1992), Izu-Bonin (Taylor and Nesbit, 1998) and Aleutian (McCulloch and Perfit, 1981). Radiogenic isotopic compositions of other Sunda arc lavas are also accounted for by incorporation of similar amounts of subducted Indian Ocean sediment into the mantle wedge as that proposed beneath IVC: 1-2% (Merapi, Gertisser and Keller, 2003); <2% (general Sunda arc lavas, Turner and Foden, 2001); <5% (eastern Sunda arc, Stoltz et al., 1990); 2.5% (Sangeang Api, East Sunda arc, Turner et al., 2003). Several authors propose that the

sedimentary component is added to mantle source in the form of a partial melt (Turner and Foden, 2001; Turner et al., 2003). However, in eastern Sunda arc lavas, calculated melt fractions of pelagic and biogenic sediments at low degrees of melting (1-10%) possess low Sr/Nd values that produce curves which do not fit the volcanic data (even up to 40% melts) (Stoltz et al., 1990). Sediment addition as a partial melt is a possibility beneath IVC, but is not required to explain the data. However, considering this possibility we propose that the bulk sediment to mantle/fluid-modified mantle mixing curves provide an upper estimate of the amount of sediment contribution in the IVC magma source.

2.6. Summary and Conclusions

Differentiation processes can account for the spatial variations observed in geochemistry at Ijen Volcanic Complex. Major element and trace element modelling suggests that trends towards high CaO, Al_2O_3, Sr contents with increasing MgO in the CR group (high-Ca group), and positive correlations of these elements in the IC group (low-Ca group) are a result of slight differences in fractionating mineral assemblages: olivine, clinopyroxene ± plagioclase fractionation dominating the CR group, and plagioclase > clinopyroxene and olivine in the IC group (Fig. 2.9). Spatial variations in lava geochemistry are controlled to some extent by sub-volcanic structure. It is proposed that magmatic storage at shallower depths is prevented beneath volcanoes located on the caldera-rim (cf. the intra-caldera magmas) due to the presence of ring fractures, which focus and facilitate migration of magma towards the surface and inhibit the formation of shallow level storage chambers. As a result, CR magmas do not undergo substantial shallow-level degassing or extensive plagioclase fractionation, like that envisaged for the IC volcanoes (Fig. 2.9). The linear orientation of the IC volcanoes further indicates the importance of sub-volcanic structure for volcanism at IVC. Location of Kawah Ijen at the intersection between the caldera rim and the northeastern edge of the intra-caldera

lineation, combined with the eruption of lavas belonging to both differentiation trends, implies that Kawah Ijen may be sourced by both the shallow and deep magma reservoirs by separate pathways (Fig. 2.9).

Low, mantle-like $\delta^{18}O$ values, and a lack of correlation between isotope ratios and indices of differentiation imply that contamination by continental 'crustal' material is insignificant at IVC, consistent with IVC being located on thickened oceanic crust. Assimilation of isotopically indistinct material (i.e. older volcanic crust) cannot be discounted at IVC.

Despite the variation observed in major and trace element data, HFSE ratios, Nd, Hf isotope ratios and $\delta^{18}O$ values of IVC lavas are remarkably restricted and suggest that the subduction-modified mantle wedge source was relatively homogeneous. IVC lavas have higher Hf and Nd isotope ratios than other Sunda arc volcanoes and lie on the edge of the I-MORB field in Hf-Nd isotope space, suggesting they may best represent the composition of the uncontaminated mantle wedge in East Java.

IVC magma genesis can be explained by 2-stage, 3-component source mixing. In this model, a fertile I-MORB source mantle wedge is infiltrated first by a hydrous slab fluid and then by sediment. Due to the orientation of the ICV array and the shape of the mixing curves produced by different types of sediment in Hf-Nd isotope space (and constraints on sediment type from Sr-Nd isotope modelling) the I-MORB source component proposed has lower than average $^{176}Hf/^{177}Hf$ isotope composition. In the model, I-MORB source is contaminated by a small percentage of fluid created from the dehydration of the subducting slab (dominated by the chemistry of altered oceanic crust); generating a mixture with higher $^{87}Sr/^{86}Sr$, and similar $^{143}Nd/^{144}Nd$ to I-MORB. At a later stage, less than 1% of Indian Ocean sediment is transferred from the slab into the fluid-modified mantle source. The type of subducted

sediment proposed in magma genesis at IVC (nanno ooze and Mn nodule) is consistent with those found as modern deposits on the seabed south of East Java.

Chapter 3

Untangling differentiation in arc lavas: constraints from unusual minor and trace element variations at Salak Volcano

Untangling differentiation in arc lavas: constraints from unusual minor and trace element variations at Salak Volcano

3.1. Introduction

Understanding how geochemical signatures are imparted to arc rocks is problematic. Element compositions in arc lavas are dependent not only on the composition of the primary magma from which they originated, but also on the multitude of differentiation processes primary magma may suffer en route to the Earth's surface. Therefore elucidating composition-modifying processes in arc lavas is a prerequisite before the nature, composition and components of the source can be determined. Among the variety of processes capable of masking element concentrations of primary magmas, fractional crystallisation (Gerbe et al., 1992; Reubi and Nicholls, 2004), crustal contamination (Davidson et al., 1987; Hildreth and Moorbath, 1988; Davidson and Harmon, 1989) and magma mixing (Gamble et al., 1999; Tepley et al., 2000) are commonly identified in arc lavas.

Separate differentiation trends occur in lavas from within the single volcanic centre at Salak Volcano in West Java, and so this volcano provides a great opportunity to study the impact of shallow level processes on the composition of arc lavas. Steeply-sloped, positive correlations of HFSE (high field strength elements) and HREE (heavy rare earth elements) with indices of differentiation are displayed by the Central Vent Group (CVG) of Salak, and are particularly unusual compared to most other Sunda arc volcanic suites. This chapter aims to constrain the relative importance of various differentiation processes at Salak, identifying the reason for the abnormal HFSE-HREE differentiation trends of the CVG, and will ascertain why the differentiation trends are divided at Salak. This information is essential before the characteristics of the source can be investigated. Such a study will aid in elucidating the nature of crust in West Java (Chapter 5), of which relatively little is known.

3.2. Geology of Salak and sampling details

Gunung Salak, 2211m, is a prominent stratovolcano located in the Quaternary volcanic front of the Sunda arc in West Java. It forms the north-eastern part of the Salak-Perbakti-Gagak volcanic massif (Fig. 3.1), which consists of Upper Pleistocene to Recent stratovolcanoes, parasitic vents and phreatomagmatic craters. The Perbakti-Gagak range to the south-west is strongly eroded. Both areas in the north-east and south-west are sites of extensive hydrothermal activity. Intermittent volcanism occurred at Salak between ~0.2 to 1.2 my ago (Stimac, 2003; Volcanic Survey of Indonesia (VSI)). In historic time, volcanic activity at Salak has been limited to a number of phreatic explosions, occurring at side vents on the flanks of the volcano. The Salak summit area is characterised by two large breached craters; one open to the northeast and another to the southwest (Fig. 3.1), which are associated with volcanic sector collapse events. The western most crater was the source of a large debris-avalanche deposit which extends over 10 km from the summit (VSI). Satellitic cones are mainly found on the SW flank of Salak, although they are also present on the eastern side of the volcano on the northern foothills. A late-stage dome (Gunung Sumbul) built on the western crater rim is probably a result of the most recent activity.

The volcanic products of Salak can be divided into two main groups based on eruption location: those erupted from the central vent (CVG), and those erupted from flank or side vents (SVG). The CVG consists of several lava flows and pyroclastic units, which dominate the volcanic deposits at Salak, therefore the majority of samples in this study are collected from this group (filled circles, Fig. 3.1). SVG samples S102 and S103 were taken from lava flows erupted at a side vent on the eastern slope of Salak (unit PD1 on the geological map of Salak (1998) published by the Volcanic Survey of Indonesia (VSI)). S107A and S107B SVG samples were taken from the western flank. Sampling of SVG products for geochemical analysis on the western flank was of limited success due to the

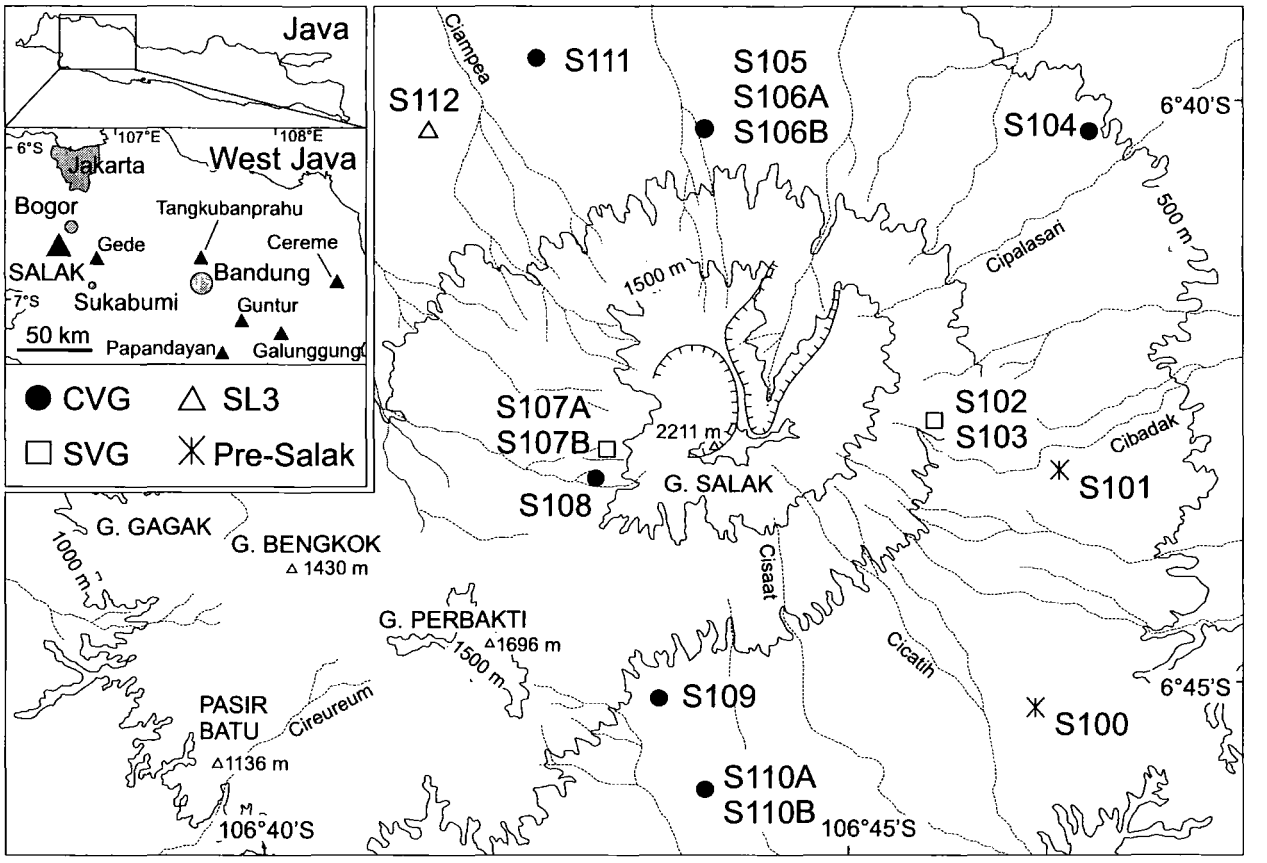

Fig. 3.1. Topographic sketch map of the Salak-Perbakti-Gagak Complex, showing the distribution of samples used in this study and corresponding data symbols used on subsequent figures. CVG = Central Vent Group; SVG = Side Vent Group; SL3 = Salak lava 3 (Zaenudin et al., 1993). Selected rivers are shown in black dash; solid lines with ticks represent escarpments. Inset diagram shows the location of Salak (large black triangle) in West Java, in relation to major centres of population (grey fill) and Quaternary volcanoes (small black triangles).

extensive alteration of lava in this area caused by hydrothermal activity. Sample S112 is from SL3, a lava flow originating from the main vent (CVG) according to the geological map (VSI, 1998). However, this sample is geochemically similar to the SVG samples in major and trace element composition. The SL3 unit is mapped by the VSI to extend down the western flank of Salak, and thus, it is possible that this sample may have been erupted from one of the western side vents. As a result of the uncertainty in the provenance of this sample it is distinguished from the other samples in all diagrams. Two pumice samples collected on the

western slope of Salak (S100 and S101) are from extensive airfall deposits that are thought to be related to pre-Salak activity (VSI) and were overlain by thinner airfall deposits from Salak. Limited dating has been carried out on Salak-Perbakti-Gagak volcanic products (e.g. Stimac, 2003); reliance on geological maps and relative stratigraphy in this study limits a detailed temporal evaluation of Salak lavas and therefore this is not carried out here.

3.3. Petrography and Mineralogy

Modal analyses of Salak lavas and a summary of mineral compositions are given in Appendix A and Table 3.1 (mineral data presented in Appendix D), respectively. Petrographically, samples from the CVG are similar to the lower silica SVG samples (S102 and S103) from the eastern flank. Andesites are the most common rock type sampled at Salak. The andesites of the SVG are generally more phenocryst rich than those of the CVG: total phenocryst abundances range between ~50-60 % and 20-24 % (modal volume), respectively (Appendix A). Both andesite groups contain the same (typical Javan island-arc) mineral assemblage of plagioclase, clinopyroxene, orthopyroxene and Fe-Ti oxide. Basaltic-andesites are restricted to the CVG, and all samples contain olivine phenocrysts, which commonly occur with both clinopyroxene and orthopyroxene. The olivine phenocrysts (Fo_{54-66}) are generally small and subhedral in shape, some showing slight alteration to iddingsite at crystal edges. The SVG rhyolite and Pre-Salak pumice samples are dominated by glassy groundmass and phenocrysts of plagioclase with minor pyroxene. Small amounts of amphibole and quartz ± biotite are also present (Appendix A).

Orthopyroxene phenocrysts in the basaltic-andesites of the CVG are generally subhedral-euhedral and infrequently contain smaller inclusions of early-formed olivine (S104). In some basaltic-andesites (S104, S105 and S108) the orthopyroxene phenocrysts are surrounded by a thin rim, or jacket, of clinopyroxene. This disequilibrium feature appears to

Table 3.1. Ranges of mineral compositions in Salak lavas

		PLAG			CPX				OPX				OL		Fe-Ti OXIDE			
	sample	An(phen)	An(gm)	n	En	Fs	Wo	n	En	Fs	Wo	n	Fo	n	TiO_2	FeO	Fe_2O_3	n
CVG																		
BA	S106B	66-93	57	12	43	15-17	40-42	2	66-68	28-30	3.2-3.4	6	57-66	3	12-16	41-45	39-47	3
BA	S111	58-91	43	9									54-65	7	11-14	41-43	44-48	3
A	S110B	52-72	48	15	40-41	20	39-40	3	61-62	35	3.6-3.8	4			16-19	44-48	33-40	3
SVG																		
A	S102	48-76		14	38-43	17-20	39-43	4	55-60	37-42	2.9-3.0	5			12-14	42-43	44-46	2
	S102XEN	53-80		10	39-43	17-21	40	2	58-66	30-39	2.6-3.3	4			10-50	40-50	0-50	2
SL3																		
A	S112	54-68		10	38-40	19-21	41-43	4	60-63	35-37	2.9-3.4	5			14	43	43	5

PLAG = plagioclase, CPX = clinopyroxene, OPX = orthopyroxene, OL = olivine, phen = phenocryst, gm = groundmass
n = number of spots analysed
BA = basaltic andesite, A = andesite
All data in percentages

be relatively common in arc lavas and has been observed in several Javan lavas: Lamongan (Carn and Pyle, 2001); Slamet (Vukadinovic and Sutawidjaja, 1995); Ijen (Sitorus, 1990); Gede (Chapter 4). Mineralogically, clinopyroxene and orthopyroxene in the basaltic andesites of the CVG lack any evidence suggestive of compositional disequilibrium (e.g. mantled phenocrysts, oscillatory zoning), displaying normal zoning of phenocrysts towards more Fe-rich rims (Appendix D). Orthopyroxene and clinopyroxene compositions in the andesites show slightly more variation in the SVG than the CVG (Figs. 3.2a & b). Pyroxene compositions in the SL3 lava are reasonably homogeneous (Table 3.1).

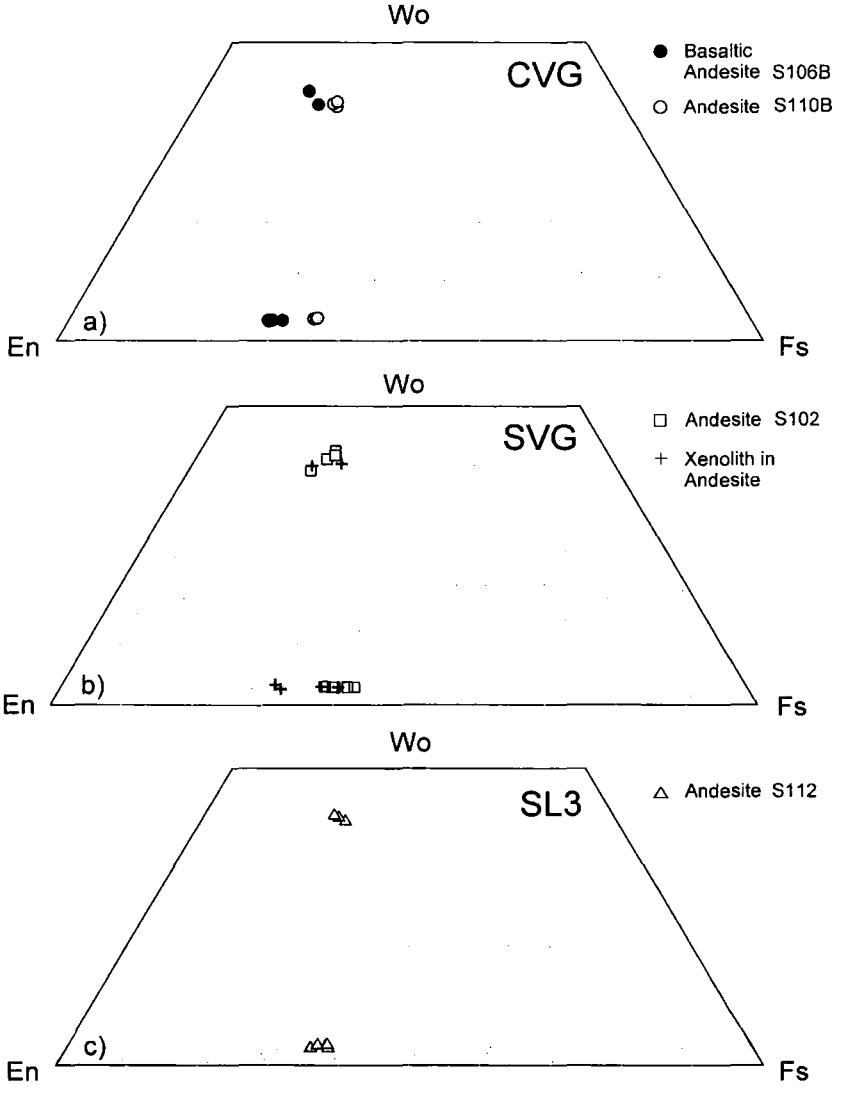

Fig. 3.2. Analyses of pyroxene phenocrysts in Salak lavas. Dashed lines represent 10% increments.

Plagioclase is the most abundant phenocryst phase in all CVG and SVG rocks. Plagioclase phenocrysts exhibit a wide range in composition in the basaltic-andesites of the CVG (Figs. 3.3a & b, Appendix D); plagioclase rims displaying the most variation in anorthite content (An_{58-91}). Analyses from phenocryst interiors are more restricted at fairly primitive An contents (above 80). An contents of some plagioclase rims are higher than those in respective groundmass plagioclase (< An_{55}), indicating that not all phenocrysts were in equilibrium with the host liquid. Disequilibrium textures of plagioclase phenocrysts (sieve textures, oscillatory zoning etc.) are observed in all CVG basaltic-andesite samples. CVG and

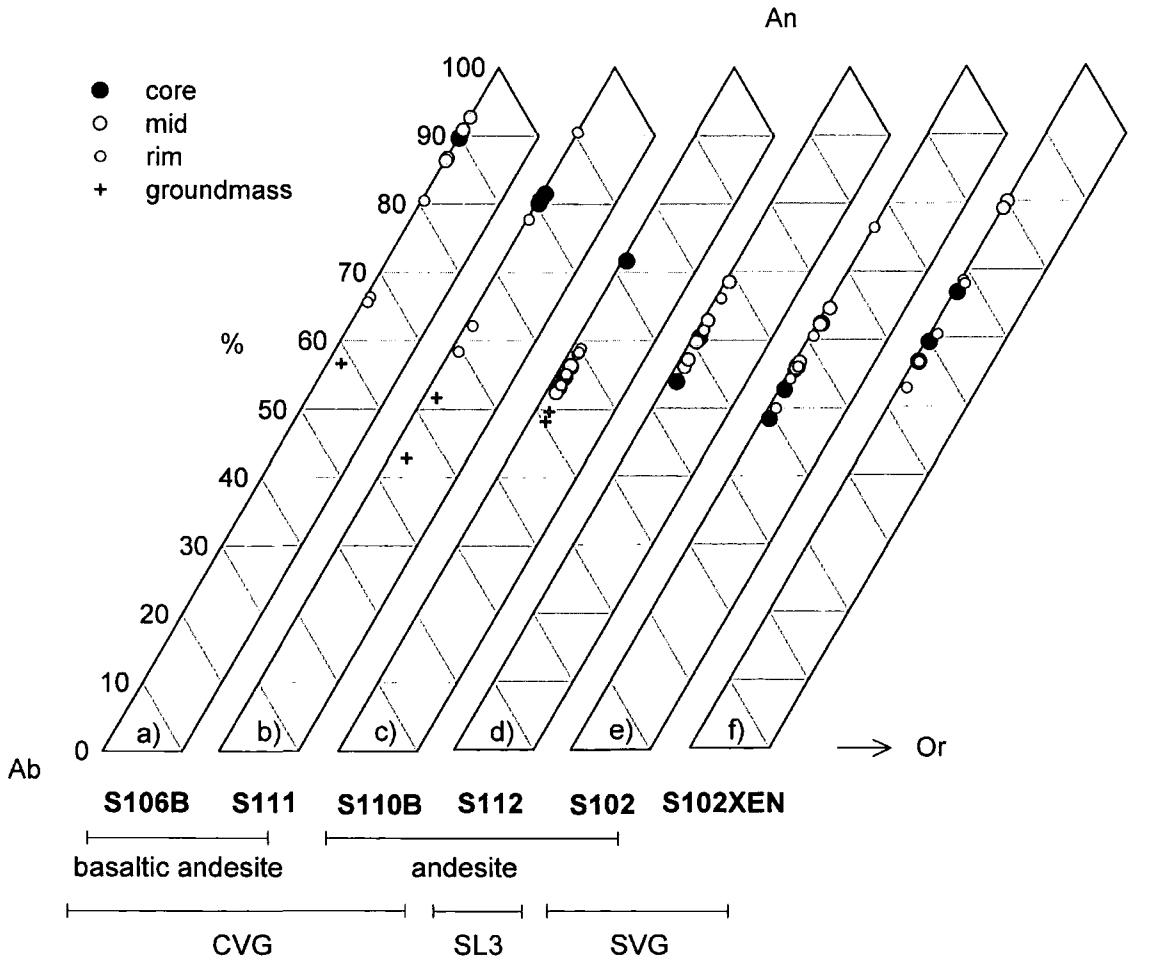

Fig. 3.3. Compositional variation of plagioclase phenocrysts in Salak volcanic rocks.

SVG andesites display similar compositional ranges in plagioclase (Table 3.1). In the CVG (Fig. 3.3c), plagioclase phenocryst and groundmass compositions are extremely homogeneous (An_{48-59}), with the exception of one core analysis (An_{72}). The SVG plagioclases display a slightly wider compositional range and often the core sections possess lower anorthite contents than respective mid and rim sections (Fig. 3.3e; Appendix D). Disequilibrium textures (sieve textures, oscillatory zoning) are common in plagioclase phenocrysts of both groups of andesites. The SL3 andesite displays a fairly restricted range in plagioclase composition (An_{54-68}) similar to the andesite analysed from the CVG (Fig. 3.3d). Some SL3 plagioclase phenocrysts show reverse zoning from less An-rich cores to more An-rich rims.

Fe-Ti oxide (titanomagnetite) occurs as a phenocryst phase in all rocks and is often associated with the other mafic phases, commonly occurring as inclusions within pyroxene, or forming a glomerocrystic texture with pyroxene. The TiO_2 component of titanomagnetite is slightly higher in the CVG andesite (16-19 %) compared to that measured in the SVG (12-14 %; Table 3.1).

Xenoliths of igneous rock fragments are observed in SVG samples from the eastern flank unit, PD1 (S102 and S103) and display sharp contacts with the surrounding lava. The xenoliths are composed of heavily sieve-textured and oscillatory-zoned plagioclase phenocrysts, with clinopyroxene, orthopyroxene and Fe-Ti oxide phenocrysts (titanomagnetite and ilmenite; in close association with ferromagnesian minerals), set in a medium-grained groundmass. The groundmass is dominated by euhedral plagioclase laths, elongate acicular pyroxene, small oxide crystals and minor devitrified glass. Clinopyroxene occasionally forms thick jackets around orthopyroxene phenocrysts. Fig. 3.2b shows there is some overlap in clinopyroxene and orthopyroxene compositions between the xenolith (black crosses) and the host rock (open squares). However, orthopyroxene phenocrysts in the

xenolith also contain significantly more En-rich compositions. Plagioclase compositions in the xenolith (Fig. 3.3f) are scattered, but generally more An-rich than those in the host lava (Fig. 3.3e).

3.4. Geochemistry

3.4.1. Major and trace element variations

Major and trace element data are reported in Appendix B. Salak lavas are reasonably evolved, with MgO contents less than 4 wt %. Similar to other Javan volcanoes, Salak volcanic rocks display negative correlations on diagrams of Al_2O_3, Fe_2O_3, MgO and CaO against SiO_2, and positive correlations between SiO_2 and both Na_2O and K_2O (Fig. 3.4). TiO_2, and P_2O_5 variation is split into two markedly different trends. Lavas erupted from the CVG generally show an increase in TiO_2 and P_2O_5 contents with increasing SiO_2. In contrast, lavas sampled from the SVG possess lower TiO_2 and P_2O_5 contents that decrease as SiO_2 contents increase and plot within the field of other Javan volcanic rocks (Figs. 3.4g and h). TiO_2 and P_2O_5 contents measured in the more evolved CVG rocks (~60% SiO_2), are unusually high, up to 1.18 and 0.48 wt% respectively, when compared to the majority of values reported in other Javan lavas (Fig. 3.4g) and from volcanic rocks of other island arc systems at comparable silica content (e.g. Kermadec, Lesser Antilles, Mariana).

The high field strength elements (HFSE) and the rare earth elements (REE), particularly the heavy REE, also show abnormally high concentrations in the more evolved CVG samples (Y = 32-69 ppm; Yb, 3-6.5 ppm) and display strikingly positively-sloped, linear trends on SiO_2 variation diagrams, contrasting with the SVG rocks and the majority of other volcanic rocks of Java, where concentrations remain relatively constant with increasing SiO_2 (e.g. Fig. 5.2, Chapter 5). High concentrations of Y, P_2O_5, TiO_2 and systematic increases of these elements with SiO_2 are so far only evident at one other volcano in Java; Tengger

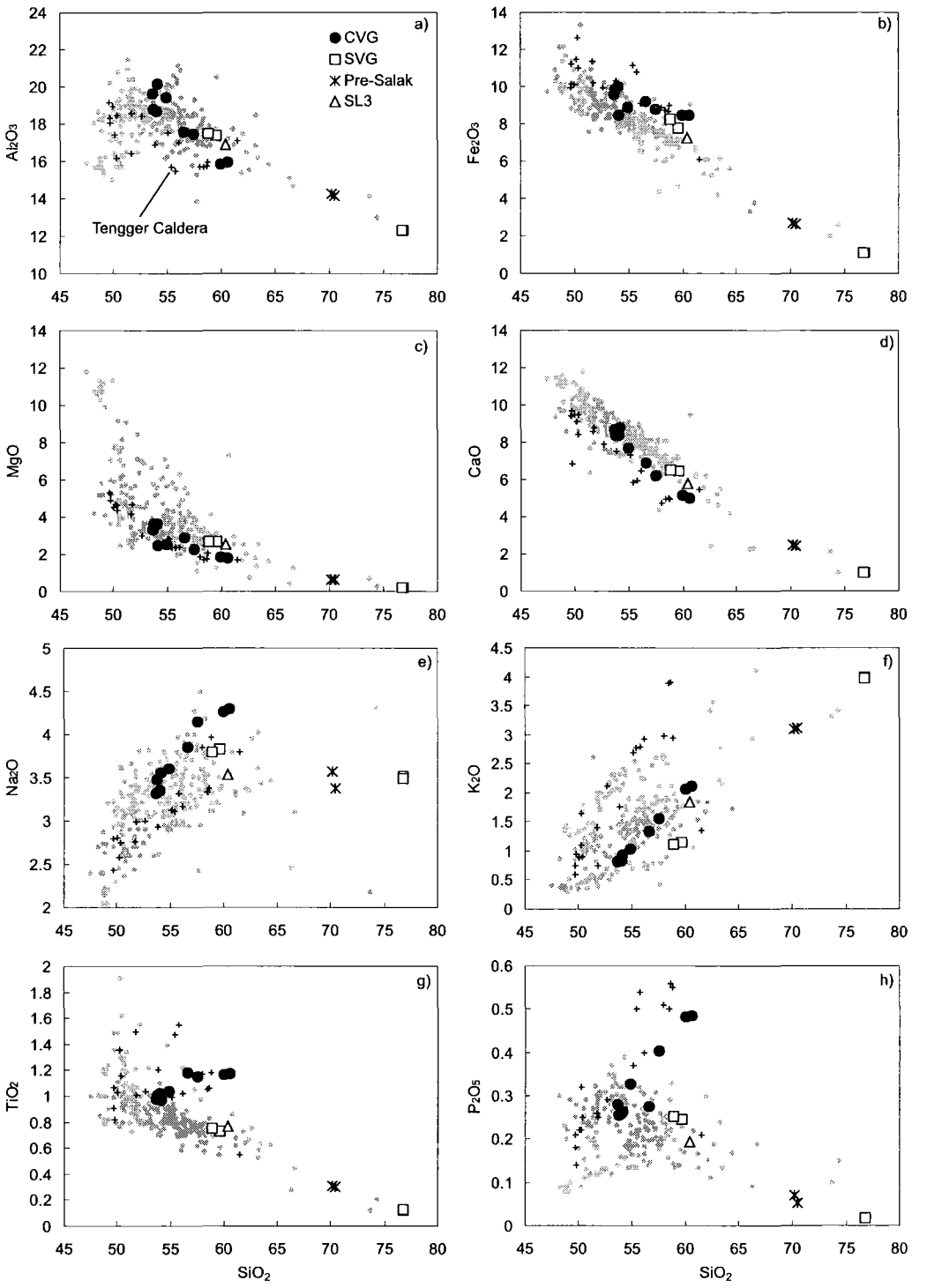

Fig. 3.4. Major element variation diagrams for Salak volcanic rocks. Tengger Caldera (black crosses) distinguished from the Java field to show it displays the unusual geochemical properties of the CVG rocks (data from van Gerven & Pichler, 1995). Java data (grey filled circles): Bayah Dome (Alves et al., 1999, Marcoux and Milesi, 1994); Galunggung (Gerbe et al., 1992; de Hoog et al., 2001); Guntur (Edwards, 1990; de Hoog et al., 2001); Slamet (Vukadinovic and Sutamidjaja, 1995; Reubi and Nicholls, 2002); Merapi (Gertisser and Keller, 2001); IVC and GVC (this study); Cereme (Edwards, 1990).

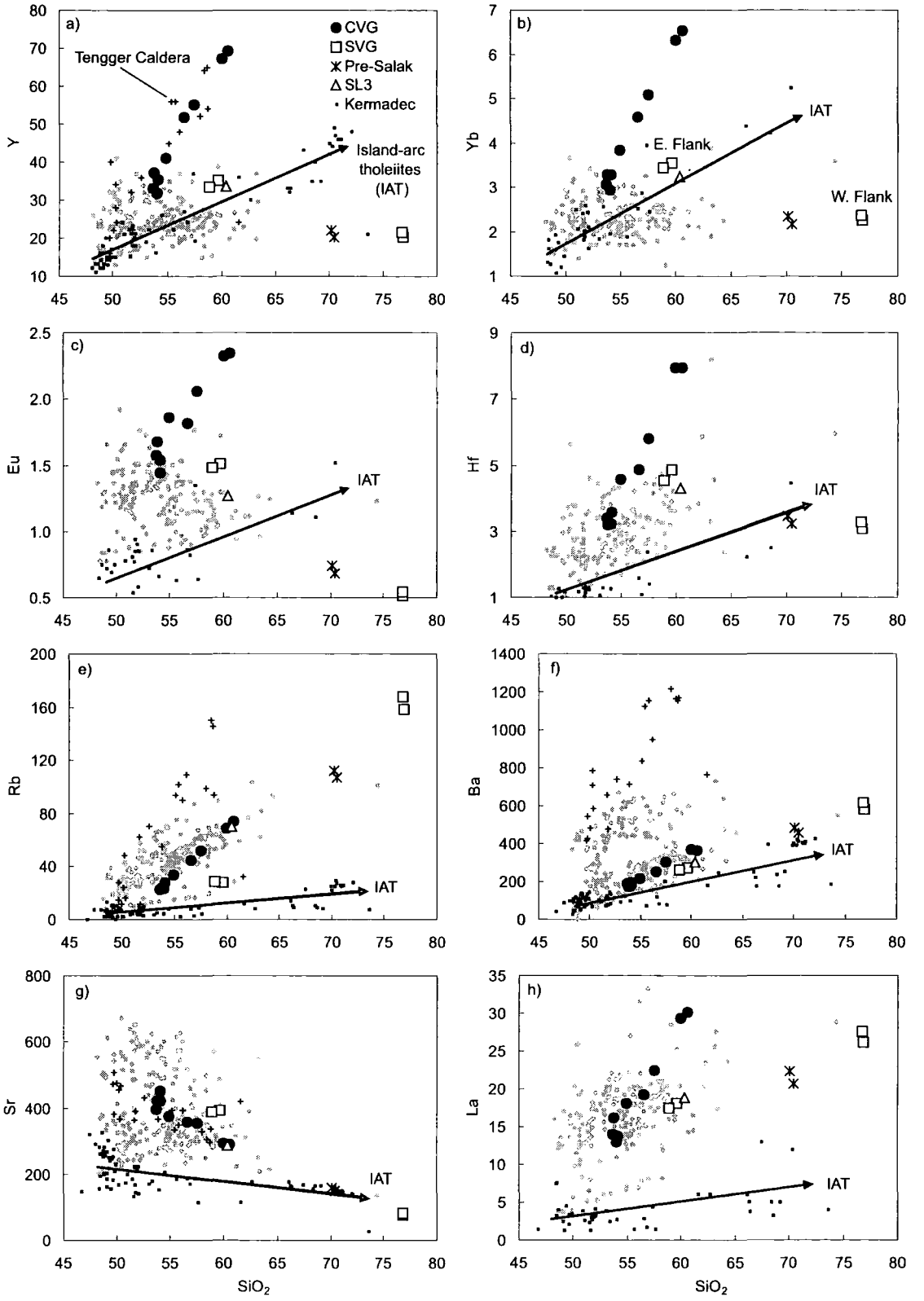

Fig. 3.5. Selected trace element variations with SiO_2 for Salak volcanic rocks. Java data sources as in Fig. 3.2. Typical differentiation trends of intra-oceanic lavas (IAT) are given by volcanic data from the Kermadec Arc (Turner et al., 1997; Gamble et al., 1993; Ewart et al., 1994 (and where available, Smith et al., 2003)). SVG samples erupted from eastern flank (E. Flank) and western flank (W. Flank) vents are indicated in b).

Caldera in East Java, and these samples have accordingly been distinguished in Figs. 3.4 & 3.5a. This unusual feature was not noted in the study of Tengger Caldera by van Gerven and Pichler (1995) and extensive comparisons of trace element variations between Tengger Caldera and Salak are restricted due to the limited data available for the former volcanic system. In contrast to the separate HSFE and REE variation trends displayed by the CVG and SVG at Salak, variations in large ion lithophile elements (LILE) are similar, displaying positive correlations with SiO_2 (Figs. 3.5e-g), with the exception of Sr, which generally decreases as SiO_2 increases (Fig. 3.5g). The SVG volcanic rocks containing around 60 wt% SiO_2 are slightly displaced below the main Salak trend in the majority of these diagrams with the exception of Sr, where they sit at slightly elevated values.

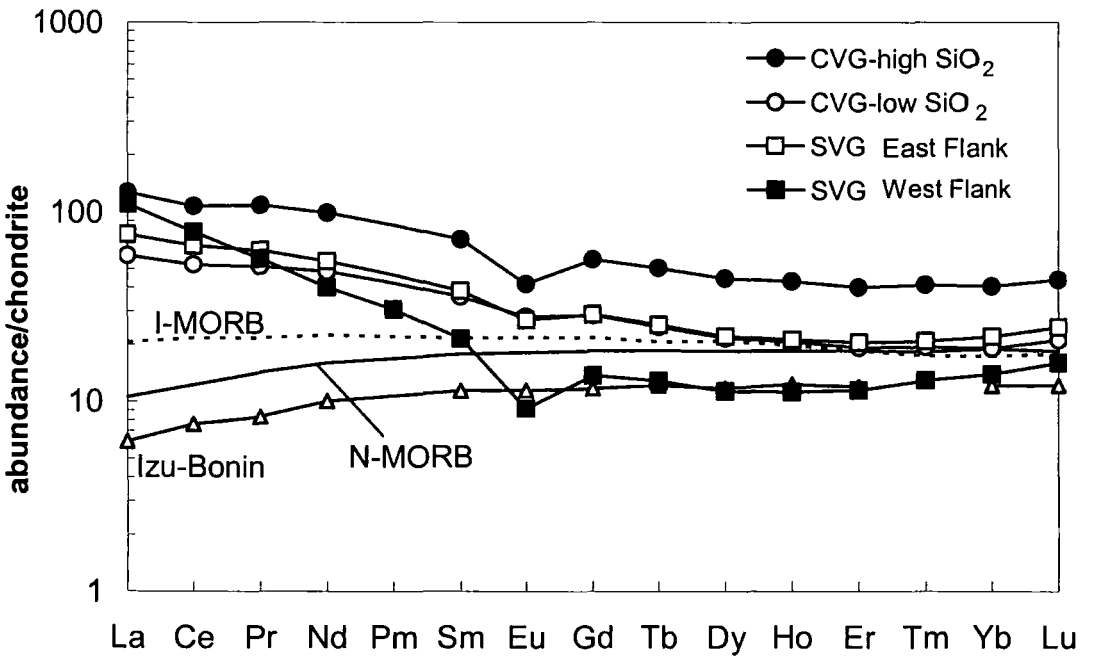

Fig. 3.6. Chondrite normalised rare earth element diagram of Salak rocks. Normalising factors and N-MORB values from Sun and McDonough (1989). Indian MORB (Chauvel and Blichert-Toft, 2001), and Izu-Bonin arc lava compositions (Taylor and Nesbitt, 1998) are shown for comparison.

Chondrite normalised REE patterns of selected Salak lavas are displayed in Fig. 3.6. Salak volcanic rocks are enriched in the light REE compared to mid-ocean ridge basalts (N-MORB and I-MORB) and other arc lavas, such as those from the Izu-Bonin arc. With the exception of the high silica rhyolite, the heavier REE show compositions more similar to MORB than those of the light REE, but are still enriched in heavy REE compared to Izu-Bonin lavas. The higher silica CVG andesite, is located parallel to, but at higher REE concentrations than the less evolved CVG rock. The enrichment of the REE in the evolved CVG sample is made obvious when compared to a SVG rock of comparable silica content (unfilled squares). Strong depletions are observed in the middle to heavy REE concentrations of the high SiO_2 (west flank) SVG rocks, compared to less evolved Salak rocks.

3.4.2. Radiogenic isotopes

Sr, Nd and Hf isotope data are presented in Appendix C, and shown in Figs. 3.7 and 3.8. $^{87}Sr/^{86}Sr$ and $^{143}Nd/^{144}Nd$ isotope ratios of Salak volcanic rocks define a negative array, lying within the field of previously published Java data. Salak exhibits a reasonably wide range in $^{87}Sr/^{86}Sr$ ratios, 0.704262 to 0.705051, although the majority of the lavas are more tightly constrained within the range 0.704569-0.705051. The two SVG samples, S102 and S103, erupted on the eastern flank of Salak are displaced from the rest of the Salak lavas, possessing significantly lower $^{87}Sr/^{86}Sr$ and higher $^{143}Nd/^{144}Nd$ ratios (Fig. 3.7 inset). In Hf-Nd isotope space (Fig. 3.8), Salak volcanic rocks also lie within the field defined by Java; possessing lower $^{143}Nd/^{144}Nd$ and $^{176}Hf/^{177}Hf$ isotope ratios than I- and N-MORB, and higher ratios than Indian Ocean sediments. SVG samples S102 and S103, again possess significantly more primitive $^{176}Hf/^{177}Hf$ isotope ratios compared to the other Salak samples (Fig. 3.8 inset).

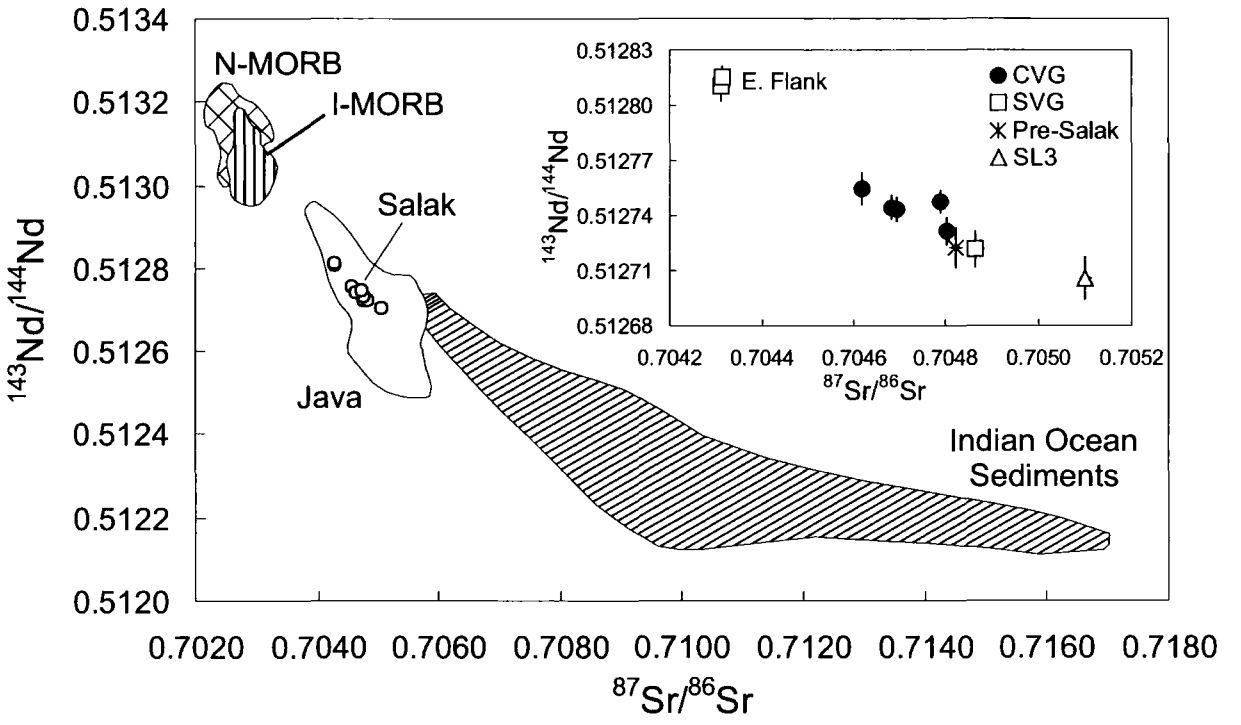

Fig. 3.7. Variation of $^{143}Nd/^{144}Nd$ with $^{87}Sr/^{86}Sr$ for Salak volcanic rocks. Data sources: I-MORB: Rehkämper and Hofmann, 1997; Ito et al., 1987; Price et al., 1986; Chauvel and Blichert-Toft, 2001; N-MORB: Ito et al., 1987; Chauvel and Blichert-Toft, 2001; Java: White and Patchett, 1984; Whitford et al, 1981; Edwards, 1990; Gertisser and Keller, 2003; Gerbe et al, 1992; plus this study; Indian ocean sediments: Ben Othman et al., 1989; Gasparon and Varne, 1998. Inset: Nd and Sr isotope ratio diagram separated by group. 2σ external errors shown for each analysis. E. Flank = eastern flank vent samples S102 and S103

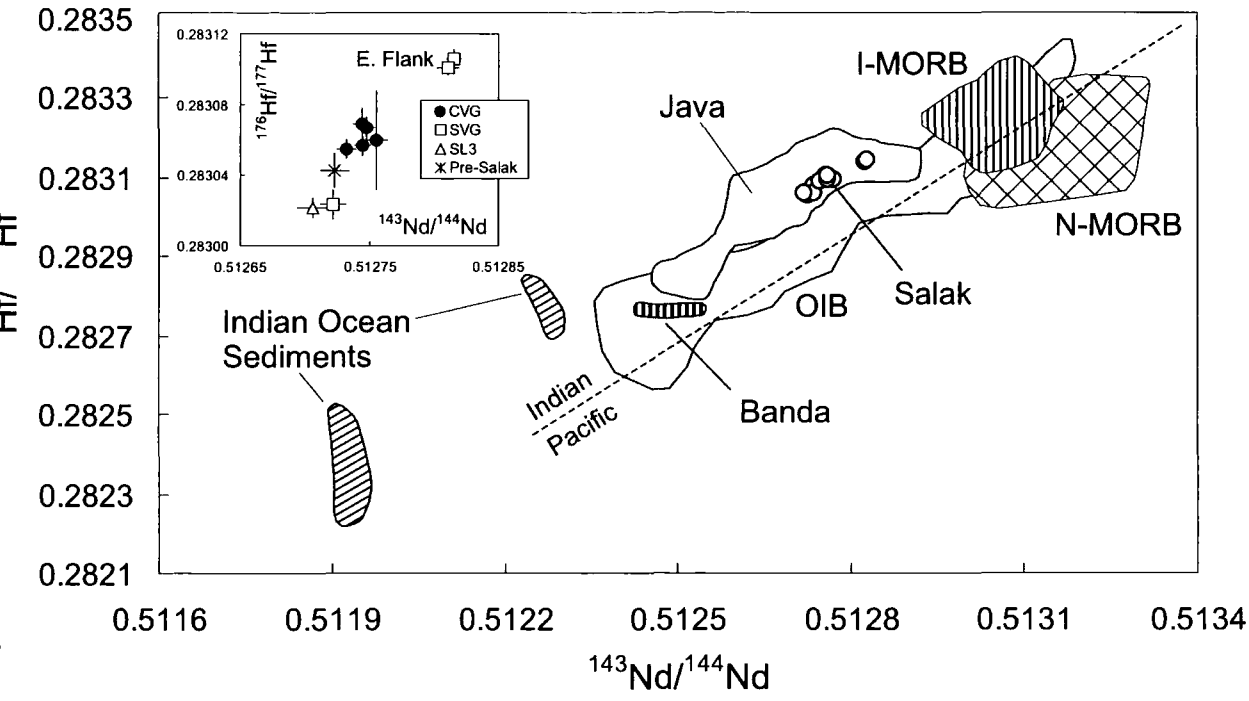

Fig. 3.8. $^{176}Hf/^{177}Hf$ - $^{143}Nd/^{144}Nd$ variation in Salak volcanic rocks. Data sources: I-MORB: Salters, 1996; Nowell et al., 1998; Chauvel and Blichert-Toft, 2001; N-MORB: I-MORB refs. and Salters and Hart, 1991; OIB: Salters and Hart, 1991; Salters and White, 1998; Nowell et al., 1998; Patchett and Tatsumoto, 1980; Patchett, 1983; Stille et al., 1986; Java: White and Patchett, 1984; Woodhead et al., 2001; Banda: White and Patchett, 1984; Indian ocean sediments: Ben Othman et al., 1989; White et al., 1986; Vervoort et al., 1999. Dividing line for Indian and Pacific MORB provenance from Pearce et al., 1999. Inset: Hf-Nd isotope diagram of Salak volcanic rocks separated by group. 2σ external errors shown for each analysis on the inset diagram. E. Flank = eastern flank vent samples S102 and S103.

3.4.3. Stable isotope data

Oxygen isotope data from mineral separates are presented in Appendix C. The restricted clinopyroxene and plagioclase analyses of Salak lavas have low $\delta^{18}O$ values ranging from +5.18 to +5.44‰ (n = 3) and +5.96 to +6.07‰ (n = 4), respectively. These values are similar to mantle $\delta^{18}O$ values reported by Mattey et al., 1994; Ionov et al., 1994 (+5.57 ± 0.32‰). Clinopyroxene $\delta^{18}O$ values from Salak are similar to or slightly lower than those reported from other volcanoes in Java (Galunggung, Harmon and Gerbe, 1992; IVC and GVC, Appendix C). Plagioclase $\delta^{18}O$ values of Salak are generally higher than those of Galunggung (+5.6 to +6.0‰, Harmon and Gerbe, 1992), but lower than those analysed in Merapi volcanics (+6.5 to +7.00‰, Gertisser and Keller, 2003). Differences in $\delta^{18}O$ values between coexisting plagioclase and clinopyroxene ($\Delta_{plag\text{-}cpx}$) are between 0.63 to 0.79‰, and suggest most of the mineral pairs record oxygen isotopic equilibrium at typical magmatic temperatures for andesite liquids. The limited number of analyses from Salak prohibits intra-group comparisons of $\delta^{18}O$ data; however the lowest $\delta^{18}O$ clinopyroxene value is measured in the sample with the most primitive radiogenic isotope ratios (SVG, S103).

3.5. Discussion

Minor and trace element variations at Salak are intriguing, and raise two important questions:

1. Why do the CVG display atypical differentiation trends and unusually high concentrations in minor and trace elements, in particular for the HREE, Y, P_2O_5 and TiO_2, compared to other Javan volcanoes?
2. Why are there separate differentiation trends in lavas from a single volcanic centre?

This discussion will focus initially on explaining the unusual geochemical variation in the CVG, thereby attempting to ascertain the relationship between the CVG and SVG rocks and then, in doing so, discover why some element variations in CVG rocks are remarkably different to the rest of Java.

Assuming that variations in silica content of volcanic rocks are generated as a result of differentiation of magma (Gill, 1981; Davidson et al., 2005), systematic increases of Y, Yb, TiO_2 and P_2O_5 with SiO_2 within the CVG (Figs. 3.5a & b, Figs. 3.4g & h, respectively) are compelling evidence for geochemical variation being imparted during differentiation in the crust. Processes of differentiation of arc magmas commonly invoked to explain element geochemistry in island arc petrogenesis include: 1. Magma mixing, 2. Fractional crystallisation, and 3. Combined assimilation and fractional crystallisation. The importance of these three main processes will now be evaluated in the discussion.

3.5.1. Differentiation in the Central Vent Group

3.5.1.1. Magma Mixing

Magma mixing is identified as an important composition-modifying process within the evolution of many arc magmas (e.g. George et al., 2004; Tepley et al., 2000) including some of the Sunda arc (Slamet, Reubi et al., 2003; Batur, Reubi and Nicholls, 2004). It is important to identify mixing processes in magmatic systems as they have the potential to influence eruptive style by altering the physical properties of magma such as gas content and viscosity, which may have serious implications in volcanic hazard prediction (Donoghue et al., 1995). Linear correlations displayed by the CVG rocks on bivariate element-silica diagrams (Figs. 3.4 and 3.5) suggest that chemical variation within this group may be explained by magma mixing. Direct evidence for the interaction of separate magmas can be found in hand specimens and thin sections e.g. banded volcanic rocks (Donoghue et al., 1995) and mineral

disequilibria in both composition (reverse/oscillatory zoning) and texture (reaction rims, resorbed cores) as noted by Troll and Schmincke (2002), Tepley et al. (2000) and Nakagawa et al. (2002).

CVG lavas show some petrographic evidence of magmatic disequilibrium; thin rims of clinopyroxene surround several orthopyroxene phenocrysts. This may indicate a change in magmatic composition: orthopyroxene may have been ingested by a more Ca-rich magma as a result of mixing, or orthopyroxene crystallising in magma may have no longer been a stable fractionating phase due to the influx of a more Ca-rich basic magma. However, mineralogically, clinopyroxene and orthopyroxene in one of the least evolved CVG rocks lack any compositional disequilibria; showing normal zoning towards more Fe-rich rims (S106B, Appendix D). Orthopyroxene and clinopyroxene compositions in the CVG andesite are homogeneous (Fig. 3.3a). High An contents of some plagioclase rims in CVG basaltic andesites, indicate that not all phenocrysts were in equilibrium with the host rock; groundmass plagioclase have much lower anorthite contents ($<An_{55}$). Disequilibrium textures in plagioclase phenocrysts (sieve textures, resorbed cores, oscillatory zoning etc.) are observed in all CVG samples suggesting that some phenocrysts have had complex histories. Phenocryst textures in CVG lavas therefore indicate that open system processes may have occurred at one or several points in the magmatic evolution of the CVG. However, messages from phenocryst compositions are mixed: within a number of rocks, minerals show normal evolution trends, and in others, disequilibrium. Therefore, we cannot conclude from petrographic and mineralogical data alone if mixing is responsible for the geochemical variation observed in the CVG.

A purely geochemical approach to evaluate mixing processes utilises element ratios (Vogel, 1982; Flood et al., 1989). Magma mixing should produce hyperbolic arrays in plots of a trace element ratio versus a concentration. Figs. 3.9a and b show that the CVG data

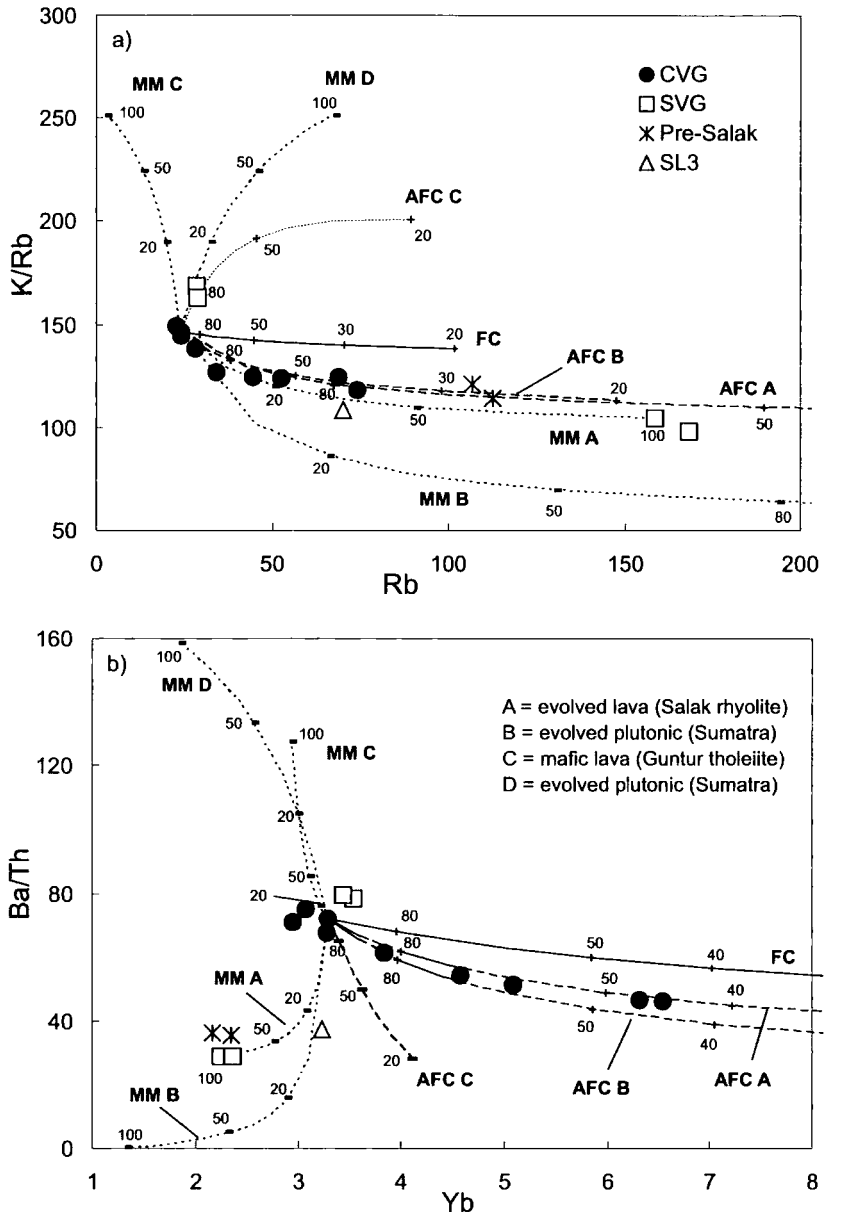

Fig. 3.9. a) K/Rb-Rb and b) Ba/Th-Y, showing fractional crystallisation (FC), combined assimilation and fractional crystallisation (AFC A, B and C), and bulk mixing (MM A, B, C and D) curves for models involving Salak basaltic andesite S106B and A: rhyolite (this study), B & D: Seputih granite plutonics 75415 and 75413 respectively (southern Sumatra, Gasparon, 1993) and C: Javan arc tholeiite from Guntur, GU1/T (Edwards, 1990). See Table 3.3 for end member compositions. Tick marks on FC and AFC curves indicate the percentage of liquid remaining. Tick marks on mixing curves represent the percentage of A, B, C or D mixed with the magma. FC and AFC calculations use the mineral proportions suggested by least squares major element modelling of CVG rocks S106B to S110B (Table 3.4, model 1): Plag = 0.7; Cpx = 0.1; Opx = 0.13; Oxide = 0.07. AFC curves calculated using DePaolo (1981). The rate ratio (r) of mass assimilated to mass crystallised in AFC model: A = 0.5, B = 0.05, C = 0.8.

largely define a curved array on some element-ratio diagrams. K/Rb and Ba/Th ratios were chosen, as these ratios correlate with SiO_2 and display a wide range in the CVG. The former ratio is also a potentially useful monitor of crust-magma interaction (Davidson, 1987, Hildreth & Moorbath, 1988) providing the melt and crust have distinctive values for the ratio. K/Rb and Ba/Th ratios are plotted against Rb and Yb respectively, which represent the degree of magma differentiation. The results of bulk-mixing calculations between one of the least evolved CVG samples and several end members are shown in Figs. 3.9a and b. S106B was chosen as the basic end member as it has one of the lowest SiO_2 contents (although clearly not representative of primary magma) and similar mineralogy to the other Salak basaltic andesites (cf. the slightly lower SiO_2 sample, S111, which contains no pyroxene). If element variation in the CVG is a result of simple mixing, the other end member must be more evolved (higher SiO_2) in composition. Granite xenoliths found within a deposit of cream tuff in the Perbakti-Gagak area adjacent to Salak provide evidence for the presence of evolved, granitic material (Stimac, 2003), in West Java. No data are available from this granite for use in modelling, therefore the more evolved end member magmas in mixing calculations are represented by a rhyolite from Salak (S107A) and by arc-related granites from some of the southern-most plutonics in Sumatra (i.e. close to West Java): monzodiorite (75413) and granodiorite (75415) (Gasparon, 1993). Mixing with a more basic end member (tholeiitic lava) from Guntur in West Java (Edwards, 1990) is also shown for comparison. End member compositions used in mixing calculations are given in Table 3.2.

Fig. 3.9a shows that mixing in K/Rb-Rb space between S106B and a granitic sample with a high K/Rb ratio (MM D) is unable to generate a mixing curve to fit the CVG data. Similar, unsatisfactory mixing trends would result from mixing with bulk upper-crustal material, which also has relatively high K/Rb (~250; Taylor, 1977). Mixing between S106B and granodiorite (MM B) or Javan tholeiite (MM C) also fail to fit the data, generating curves

Table 3.2. End member compositions used in modelling calculations

			Element Concentrations (ppm)				
	Sample	Type	K	Rb	Ba	Th	Yb
	S106B	Salak basaltic andesite	3470	24	176	2.4	3.29
A	107A	Salak rhyolite	16545	158	582	20.1	2.24
B	75415	Sumatran granitoid	14652	237	12	34.9	1.35
C	GU1/T	Javan tholeiite	1374	3.4	97	0.8	2.94
D	75413	Sumatran granitoid	17101	68	937	5.9	1.86

Sumatran granitoid data from Gasparon (1993); Javan tholeiite from Guntur (Edwards, 1990)

that have a large decrease and increase (respectively) in K/Rb ratio, with only a small change in Rb. The mixing curve produced using the Salak rhyolite (MM A) as the evolved end member, produces the best fit to the CVG data. Fig. 3.9b, Ba/Th-Yb, shows mixing curves generated between the same end members in Fig. 3.9a. Mixing in all cases is inadequate in explaining the Salak CVG data due to the low Yb content of the end members chosen. Low Yb contents of basic and evolved Javan lavas and evolved Sumatran plutonics, suggests that Yb contents of the CVG cannot be explained by simple mixing using the end members selected.

In the event that the appropriate end members have not been considered in the above modelling, a more easy to see test for mixing is to plot K/Rb and Ba/Th against the inverse of the denominator concentration (e.g. 1/Rb and 1/Th). Mixtures would be straight lines on diagrams of this type due to the fact that in ratio-element mixing, the denominators in the ratio control the curvature of the hyperbola (Vogel, 1982; Langmuir et al., 1978). Figs. 3.10a and b show that the CVG data display linearity on these diagrams. A strong correlation coefficient (R^2) of 0.99 on Ba/Th versus 1/Th (Fig. 3.10b) suggests that mixing is a strong possibility. R^2 of 0.93 for the CVG data on K/Rb versus 1/Rb (Fig. 3.10a) is reasonable, but not as convincing as Fig. 3.10b. The plots suggest that Ba/Th and K/Rb ratios in CVG rocks are consistent with mixing. One further check to test mixing, is to plot one of the original ratios i.e. Ba/Th against the ratio of the two denominators. If a mixing relationship is present,

then the CVG data should again plot as a linear array. Poor linearity on Fig. 3.10c suggests that even though good correlation coefficients were obtained on diagrams of A/B versus 1/B, the CVG data are not wholly consistent with mixing. We therefore need to evaluate the control of other differentiation processes on element evolution.

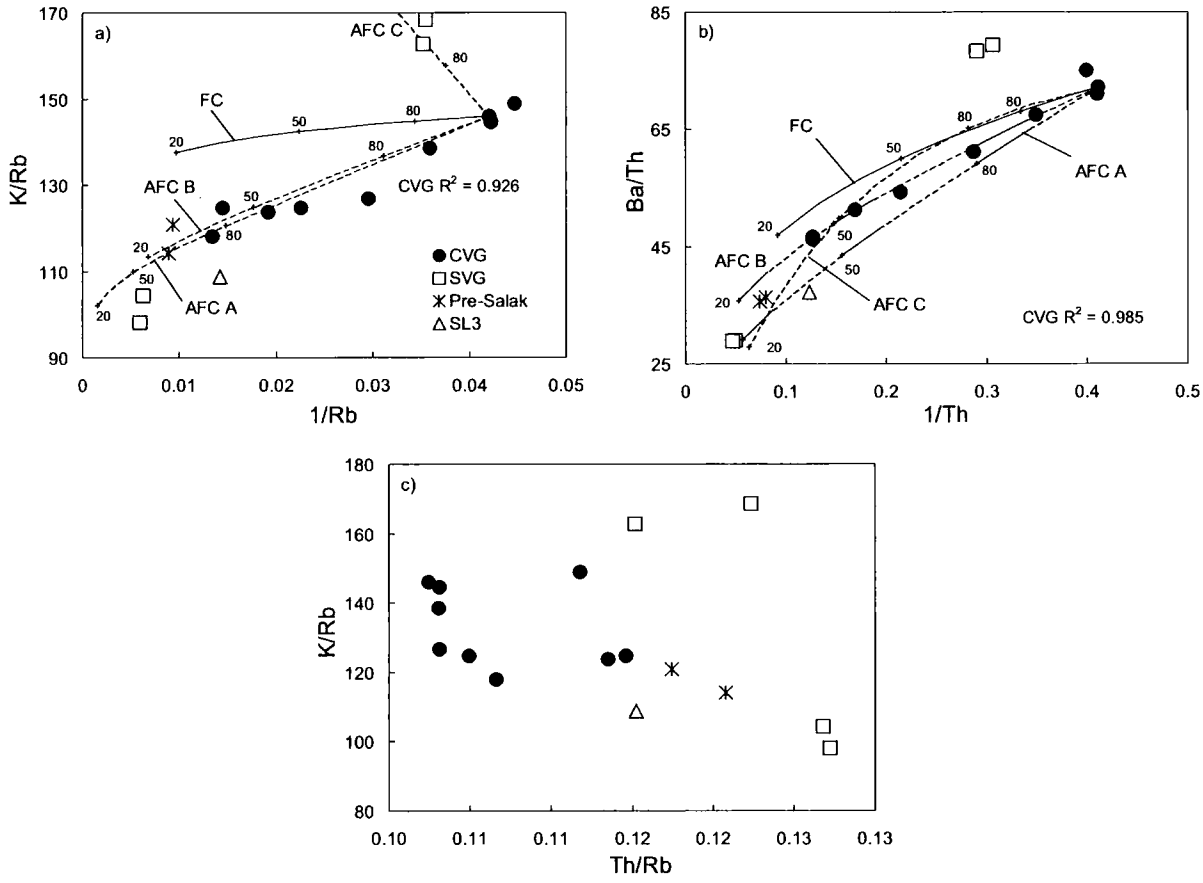

Fig. 3.10. a) K/Rb-1/Rb and b) Ba/Th-1/Th showing that linearity in the CVG data set (R^2 close to 1) is consistent with mixing, but is also consistent with other differentiation processes, such as AFC. FC and AFC curves are shown for the same models in Fig. 3.9 (see caption for calculation details). c) K/Rb-Th/Rb, showing that the Salak CVG data are not consistent with simple mixing.

3.5.1.2. Fractional crystallisation

Fractional crystallisation is commonly identified in studies of magmatic evolution as an important process controlling major and trace element compositions of arc lavas (Grove et al., 2005; Gerbe et al., 1992; Turner et al., 2003). Most major element trends at Salak (Figs. 3.4a-f), are similar to those displayed by other magmatic suites from Java (grey circles, Fig. 3.4), consistent with the removal of a typical Javan island-arc mineral assemblage of plagioclase, clinopyroxene, Fe-Ti oxide and olivine/orthopyroxene. This section will now test whether major and trace element variation in the CVG are best explained by fractional crystallisation. Least squares modelling using the XLFRAC programme (Stormer and Nicholls, 1978) has been carried out using major element data of the CVG. In this model, fractionating mineral phases are added to the most evolved rock (daughter) to try and reach the composition of the least evolved rock (parent). The mineral phases considered in modelling are limited to those observed as phenocrysts in either the parent or daughter rocks The success of the model is determined by the sum of the squares of the residuals (Σr^2) that are produced for every element; the closer Σr^2 is to zero, the more acceptable the model. In this study Σr^2 values of less than 0.1 are considered good. Summaries of least squares modelling results are shown in Table 3.3. The results suggest that the most evolved CVG lava

Table 3.3. Summary of least squares major element modelling calculations for CVG rocks

Model	Parent	Daughter	SiO_2 range (%)	Σr^2	% removed relative to initial magma					%C
					Plag	Cpx	Ol	Opx	Ox	
1	S106B	S110B	53.8-60.6	0.13	43.4	6.0	-	7.9	3.9	61
2	S106B	S108	53.8-57.5	0.13	32.9	5.7	-	6.1	3.0	48
3	S106B	S104	53.8-54.9	0.01	10.6	4.3	-	3.5	1.6	20
4	S106B	S104	53.8-54.9	0.01	8.2	4.5	2.7	-	0.8	16

%C = percentage of crystallisation (sum of phases removed)

can be produced by fractionation from the least evolved CVG lava by 61% crystallisation ($\Sigma r^2 = 0.13$; model 1). Smaller values of Σr^2 are obtained in models to less differentiated final lavas (models 2 & 3), regardless of whether orthopyroxene or olivine is included in the mineral assemblage (compare models 3 & 4). This suggests that like other lavas from Java, major element variation within the CVG can be explained by fractional crystallisation of a typical island arc mineral assemblage. However, can fractional crystallisation explain the unusual minor and trace element variation trends not seen in the majority of Javan lavas, using the same mineral assemblage?

Silica behaves incompatibly during differentiation, therefore, systematic increases of Y and Yb etc. with silica in the CVG may result if these elements also behave incompatibly during differentiation. Increasing TiO_2 content with increasing silica (Fig. 3.4g) is not normally observed in arc andesites, most probably due to the early fractionation of magnetite (Gill, 1981; Pearce, 1982). Y and the REE only usually behave as incompatible elements in primitive arc tholeiites, remaining constant or decreasing with fractionation in the calc-alkaline series, where they can be accommodated within amphibole, biotite and zircon (Pearce, 1982), as exemplified by the Java field in Figs. 3.4g, 3.5a and b. Differentiation trends of typical island-arc tholeiites (IAT) (Kermadec arc data) are indicated by the arrows in Fig. 3.5. Increases in HFSE and HREE with increase in SiO_2 are indeed shown by the arc-tholeiites, however increases in trace element concentrations are much lower, and over a broader range of silica than observed in the CVG rocks (e.g. Fig. 3.5b), further highlighting the extreme enrichment in HFSE and HREE within the CVG. To test whether fractional crystallisation can produce the large increase in Y and Yb etc. of the CVG, over a relatively narrow range in silica, simple calculations can be made using the Rayleigh fractionation equation, $C_l = C_o F^{(D-1)}$ where C_l is the concentration of an element in the liquid, C_o is the concentration of an element in the original liquid, F is the fraction of liquid remaining and D

Table 3.4. Results of trace element Rayleigh Fractionation modelling

Element	Yb	Ti	Y
normalised phase proportions			
Plag	70.97	70.97	70.97
Opx	12.84	12.84	12.84
Cpx	9.80	9.80	9.80
Fe-Ti Ox	6.40	6.40	6.40
Parent concentration (Co)	3.3	6605	37
Degree of fractionation (F)	0.39	0.39	0.39
D (bulk)	0.170	0.733	0.203
Calculated daughter comp. (Cl)	**7.2**	**8500**	**79**
Measured daughter comp. (Cl)	**6.5**	**7726**	**69**

Daughter (S110B) composition calculated by forward modelling of parent S106B using $C_l = C_o.F^{(D-1)}$. Phase proportions and degree of fractionation values used are those suggested by least squares modelling (Table 3.3, Model 1). Distribution coefficients are given in Appendix F

is the bulk distribution coefficient. The degree of fractionation (F) and the phase proportions used are those suggested by major element modelling (Table 3.3, model 1). The distribution coefficients used are given in Appendix F. Calculated Yb, Ti and Y compositions expected in the daughter rocks are displayed in Table 3.4. Results show that incompatible behaviour of HFSE and HREE during fractional crystallisation can account for the high concentrations of these elements in Salak rocks. In all three models, the concentrations predicted in the daughter rocks are higher than those actually measured. This contrasts with the results of mixing (Fig. 3.9b) between a basic CVG rock and the tholeiitic and more evolved volcanic and plutonic samples, which were unsuccessful in accounting for high Yb concentrations. Fractional crystallisation curves (FC) are shown on K/Rb-Rb and Ba/Th-Yb (Figs. 3.9a and b) for removal of the mineral assemblage suggested by least squares modelling (Table 3.3, model 1). It should be noted that an identical FC curve is produced if the modal mineral assemblage of S106B (Appendix A) is used instead. The Salak CVG data diverge from the calculated FC curve towards lower K/Rb and Ba/Th. The K/Rb ratio is relatively insensitive to crystal fractionation as both partition coefficients are close to zero for ferromagnesian

minerals (Appendix F; Davidson, 1987). Amphibole fractionation has the potential to decrease K/Rb ratios; however there is no evidence of significant amphibole fractionation in the petrography or REE patterns (Fig. 3.6) of CVG lavas, and increases of Y and Yb with silica are also inconsistent with fractionation of this phase. Plagioclase fractionation has the potential to fractionate K from Rb, though not by a large amount according to the distribution coefficient data in Appendix F. Calculation of a FC curve using the highest K (0.361, Philpotts and Schnetzler, 1970) and lowest Rb (0.008, Dun and Sen, 1994) distribution coefficient values reported for plagioclase in basaltic-dacitic systems in the GERM database produce K/Rb ratios similar to the more evolved CVG rocks. However it seems unreasonable to use such extremely fractionated distribution coefficients for plagioclase without good reason. Disequilibrium textures (see above) observed in the CVG lavas suggest that pure closed system fractional crystallisation is an unrealistic explanation of the data. Therefore, although FC can explain the unusually steep increases of HREE and HFSE with silica, compared to Javan and tholeiitic trends, the data diverge from calculated fractionation trends towards lower K/Rb and Ba/Th ratios. Combined assimilation and crystal fractionation may provide a better solution.

3.5.1.3. Assimilation and Fractional Crystallisation (AFC)

AFC processes are recognised in the evolution of magma in arc settings (Hildreth and Moorbath, 1988; Davidson et al., 1987; Davidson and Harmon, 1989) and have been suggested in the Sunda arc (Gasparon et al., 1994). Little is known about the nature and composition of the crust in West Java. The arc is thought to be built on continental material, as delimited by the Sundaland (the SE Asian continental parts of the Sunda block/Eurasian plate with pre-Tertiary basement) boundary (Hamilton, 1979; Hoffmann-Rothe et al., 2001, Fig. 1.2a, Chapter 1). Seismic velocities obtained at several locations along the Sunda arc

suggest that the crust in West Java is thicker than that at the eastern end of Java (Ben-Avraham and Emery, 1973; Curray et al., 1977; Kieckhefer et al., 1980). Large granite blocks found in a tuff deposit in the vicinity of Salak (Perbakti-Gagak area, Fig 3.1) show partially melted margins with adhering rhyolitic lava (Stimac, 2003). It is unknown when this granite was emplaced in the crust; however, it suggests that interaction and possible contamination of magma by evolved plutonic rocks may occur at Salak. AFC curves are shown on Figs. 3.9a and b for contamination of the most basic Salak magma, by evolved volcanic (AFC A) and plutonic (AFC B) rocks, possessing low K/Rb and Ba/Th ratios. These curves fit the array of Salak data well, even though the contaminants possess low Yb concentrations (cf. mixing) Assimilation of upper and bulk crust (e.g. Taylor, 1977; Sumatran granitoid 75413) would generate concave-down AFC curves, inconsistent with the CVG data. It was suggested by Hamilton (1979) that the crust in West Java is not truly silicic in character and may consist of older volcanic-arc rocks and ophiolite slivers. However, AFC models involving basic arc rocks (e.g. Fig. 3.9 AFC C) and a range of basic and ophiolite compositions (next section) are also inconsistent with the CVG array.

In summary, major and trace element modelling suggests that differentiation processes in the crust exert a strong control on major and trace element variation in the CVG. The unusual increases in HFSE and HREE with increasing SiO_2 are not consistent with magma mixing processes, and are most likely controlled by fractional crystallisation. However, closed system fractional crystallisation is incapable of explaining the systematic variation in K/Rb and Ba/Th ratios and not consistent with the multitude of disequilibrium textures observed in the rocks. Therefore, assimilation of a contaminant with low K/Rb and Ba/Th ratios during fractional crystallisation in the crust is proposed to explain these element variations in the CVG.

3.5.1.4. Isotopic constraints

Continental-type crustal rocks commonly have elevated $^{87}Sr/^{86}Sr$ isotope ratios compared to compared to Quaternary volcanics and mantle-derived magmas. Assimilation of continental crust during crystal fractionation (DePaolo, 1981) in arc magmas may therefore cause modification to the isotope ratios in resultant lavas. Consequently, a plot of Sr isotope ratio against an index of differentiation, e.g. SiO_2, can be used to detect AFC processes, in cases where the crust being assimilated is isotopically distinct. Even though the number of samples with isotope data is relatively limited and the variation in $^{87}Sr/^{86}Sr$ of the CVG is small, the more evolved CVG samples display generally higher $^{87}Sr/^{86}Sr$ ratios (Fig. 3.11), and the data patterns observed in this plot are identical (though the reverse) to those of Ba/Th with SiO_2 (see inset to Fig. 3.11). This suggests that Ba/Th, for which there is more data compared to $^{87}Sr/^{86}Sr$, might serve as a proxy for isotopic composition. Therefore, the roughly hyperbolic trend observed in Fig. 3.11, and variation in $^{87}Sr/^{86}Sr$ isotope ratio with SiO_2 in the CVG, suggests control by differentiation and, more specifically, AFC processes.

Fig. 3.12 shows that the five CVG data points define a, concave-down hyperbola on Ba/Th versus $^{87}Sr/^{86}Sr$. AFC curves are shown on Fig. 3.12 for the same AFC end members used in trace element modelling (see Fig. 3.9 caption for details). Neither models using evolved volcanic nor plutonic rocks produce hyperbolic curves to fit the CVG data. AFC curves for these models largely follow the same vertical trend shown by fractionation crystallisation (FC) alone (arrow, Fig. 3.12), and altering the rate ratio of mass assimilated to mass crystallised has little effect on the shape of the curve. The basic contaminant (see Fig. 3.9 and 3.11 captions for details) produces an AFC curve (C) with a much better fit to the CVG data, but suggests a large amount of contamination is required compared to crystallisation (mass assimilated:mass crystallised (r) of 0.8). Such high AFC r-values are not unreasonable, and have been proposed for differentiation of basalts at Jebel Marra volcano in

Sudan (Davidson and Wilson, 1989). However, the basic contaminant used here, and others listed in Table 3.5, do not produce acceptable AFC curves to fit the CVG data in K/Rb-Rb and Ba/Th-Yb space.

A contaminant with a significantly higher Sr content than that of the parental rock would be able to generate a hyperbola curving in the required direction from the parental composition of S106B and not require such a high *r*-value. Fig. 3.11 also indicates this;

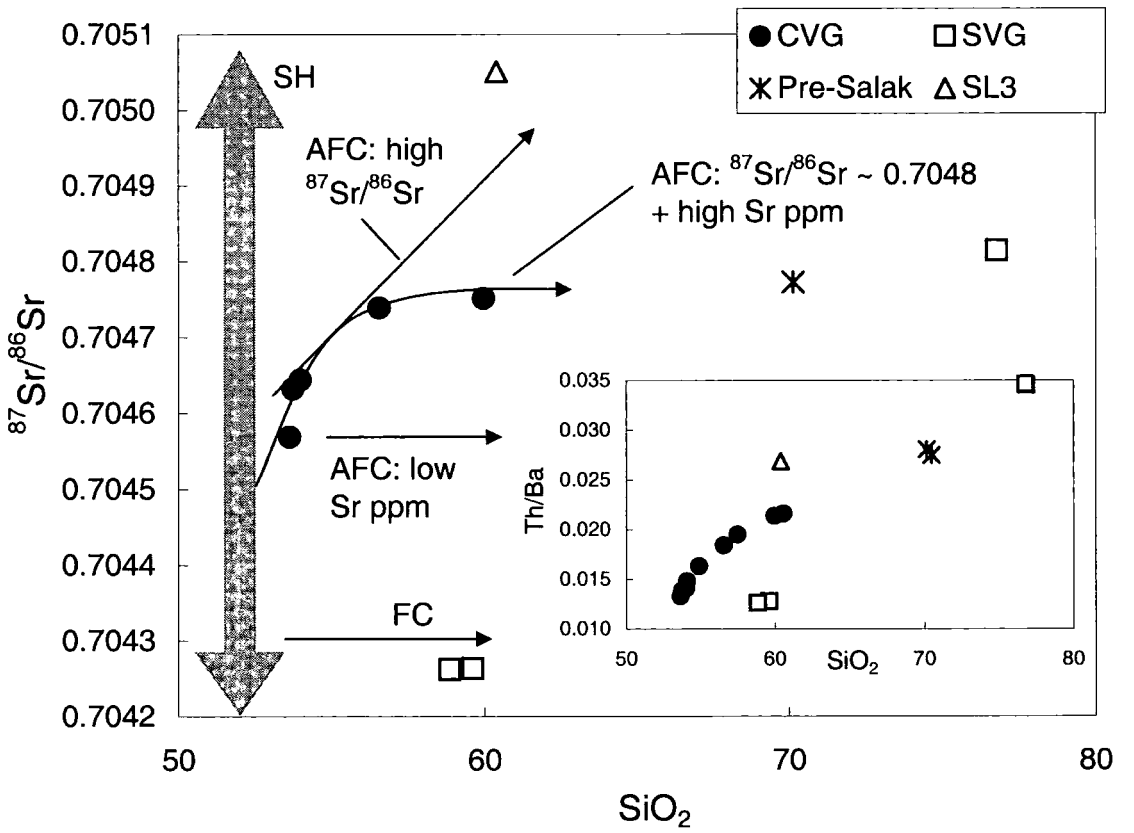

Fig. 3.11. Variation of $^{87}Sr/^{86}Sr$ isotope ratio versus SiO_2 for Salak volcanic rocks. Arrows labelled SH, AFC and FC indicate the hypothesised data trends related to: heterogeneity in the mantle source (SH), combined assimilation and fractional crystallisation (AFC) and fractional crystallisation (FC). Inset shows Th/Ba versus SiO_2 for Salak rocks, highlighting the similar differentiation patterns between Th/Ba and $^{87}Sr/^{86}Sr$ and suggesting the former, for which there is more data, might serve as a proxy for isotopic composition.

Table 3.5. Trace element and $^{87}Sr/^{86}Sr$ isotope compositions of potential crustal contaminants

	Sample no.	Rock Type	Sr (ppm)	$^{87}Sr/^{86}Sr$	K/Rb	Ba/Th
1	VM33-75	terrig.-bio. sediment	196	0.70925	106	16
2	VM33-79	terrigenous mud	160	0.70802	124	18
3	CS	calcareous-organogenic sediment	1258	~ 0.709	106	60
4	76100	S-Type granite	32	0.74036	185	0.2
5	ME99AL16	intrusive (51 wt % SiO_2)	609	0.706155	118	77
6	ME00AL42	intrusive (62 wt % SiO_2)	375	0.706600	126	53
7	H110x	intrusive (51 wt % SiO_2)	152	0.708561	139	292
8	J82x	intrusive (hbl spessarite)	173	0.705291	346	58
9	GU1/T	Javan tholeiitic lava	232	0.70393	404	127
10	TAF43/6	Tongan tholeiitic lava	118	0.70388	519	344
11	417D-418A	altered oceanic crust	118	0.704584	235	364
12	M22	basalt (ophiolitic)	143	-	416*	10
13	P-15	dolerite (ophiolitic)	171	-	4150	27
14	S-134	clinopyroxene gabbro (ophiolitic)	129	-	1245	70

Data sources: 1-4: Gasparon 1993; 1998; 5-8: Elburg, et al.,2005; 9: (Guntur tholeiite) Edwards, 1990; 10: Turner et al., 1997; 11: (average 417D-418A n = 7) Staudigel et al., 1996; 12-14 (Sulawesi ophiolite) Kadarusman et al., 2004.
* Rb concentration below detection limit, used Rb abundance of P-33 (0.5 ppm) from the same area

assimilation of a contaminant with low Sr concentration would produce a concave-up curve initially projecting in a horizontal direction away from the least evolved CVG sample. This is inconsistent with the concave-down data array in Fig. 3.11. The apparent plateau in $^{87}Sr/^{86}Sr$ isotope ratio in SiO_2-rich CVG rocks suggests that the $^{87}Sr/^{86}Sr$ ratio of the contaminant is asymptotic to the $^{87}Sr/^{86}Sr$ ratio of the more evolved CVG samples (i.e. ~0.7048). If the distribution coefficient for Sr in plagioclase is greater than one, then a magma crystallising this phase would become progressively more sensitive to Sr in the contaminant (which is assumed to be fixed). The more AFC a magma endures, the more isotopically sensitive to the contaminant it would become, therefore for a given shift in silica, the magma would obtain a larger shift in $^{87}Sr/^{86}Sr$ isotope ratio if the contaminant had a higher $^{87}Sr/^{86}Sr$ ratio. Therefore, it is argued that if the data are consistent with AFC, the contaminant has a high Sr concentration and Sr-isotope ratio ~0.7048 (curved arrow, Fig. 3.11); contamination by a high $^{87}Sr/^{86}Sr$ component would result in a data array with a steeper positive correlation on

Fig. 3.11 (diagonal arrow). An AFC calculation using S106B as the parent magma and the Sumatran granodiorite as the contaminant suggest that to produce a concave-down hyperbola to fit the data in Fig. 3.12 an extremely unrealistic Sr concentration in the contaminant of >7000 ppm is required. Evolved volcanic or plutonic contaminant end members are unlikely to possess higher Sr concentrations than the basaltic andesite S106B being contaminated as Sr content generally decreases with differentiation in arc-related igneous rocks due to plagioclase fractionation.

Table 3.5, shows trace element data and Sr-isotope ratios for a variety of rocks, which may represent the West Javan crust and may therefore be potential contaminants. Post-Miocene siliceous-clastic sediments (Table 3.5, lines 1 and 2) sampled in the vicinity of the

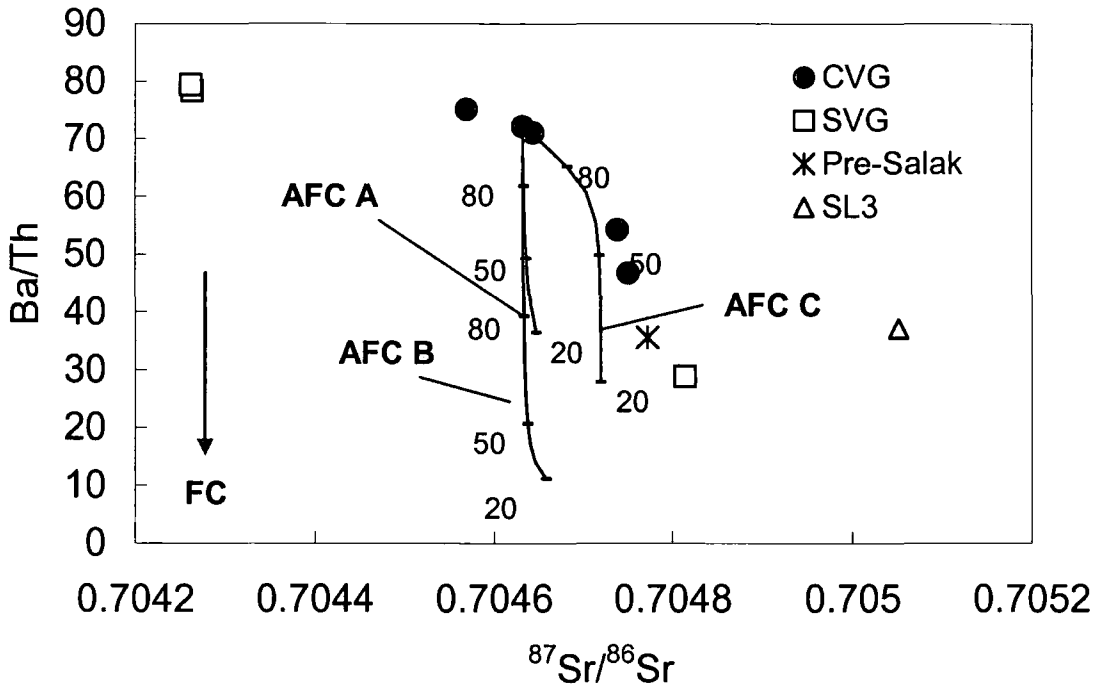

Fig. 3.12. Ba/Th against $^{87}Sr/^{86}Sr$ for Salak volcanic rocks. FC and AFC curves are shown for the same models (AFC A, B and C) in Fig. 3.9 (see caption for details). $^{87}Sr/^{86}Sr$ ratios used in model AFC C is that of GU2/C (Edwards, 1990). Arrow labelled FC indicates differentiation trend expected from fractional crystallisation alone. Tick marks on FC and AFC curves indicate the percentage of liquid remaining.

Sunda arc are largely thought to be derived from the arc itself and compositionally similar to typical average upper crust (Gasparon and Varne, 1998). These samples however, have Sr concentrations too low, and Sr-isotope ratios that are too high to be a likely contaminant. The North-eastern Indian Ocean, average calcareous-organogenic sample (line 3), has significantly higher Sr concentration (1258 ppm) but like the terrigenous sediments, has a $^{87}Sr/^{86}Sr$ isotope ratio considerably higher than ~0.7048. The $^{87}Sr/^{86}Sr$ isotope ratios of sedimentary-type granites from Sumatra are also too high, and their Sr contents are very low (e.g. line 4). Less evolved plutonic rocks and cumulates (lines 5-8) may possess greater Sr concentrations than granites and rhyolites, and have Sr-isotope ratios lower than sediments, however, diorites in the eastern Sunda arc (Elburg et al., 2005, Lytwyn et al., 2001) have Sr concentrations typically less than 620 ppm. Basic tholeiitic lavas, altered oceanic crust and ophiolitic rocks (lines 9-14) also do not fit the Sr concentration requirements of the contaminant envisaged and possess much higher K/Rb ratios than those sought. K/Rb and Ba/Th ratios of the majority of the end members in Table 3.5 are generally too high for the respective ratios of < ~110 and < ~45 hypothesised in the contaminant. If Sr-isotope variation in the CVG is controlled by AFC processes, as suggested by correlation with trace element ratios and SiO_2, then the contaminant is characterised by high Sr concentration, $^{87}Sr/^{86}Sr$ isotope ratio of around 0.7048 and low K/Rb and Ba/Th ratios. At present, a suitable contaminant to match these criteria is unidentified.

The low and homogeneous mantle-like oxygen isotope values of phenocryst separates from Salak lavas do not permit significant AFC of crustal material, unless either, 1) the rocks residing in the crust have undergone minimal interaction at low temperature with meteoric water, or 2) the contaminant possess low $\delta^{18}O$, such as those found in hydrothermally altered material and proposed to contaminate basic Galunggung magmas in West Java (Harmon and Gerbe, 1992). The lack of $\delta^{18}O$ data for the more evolved CVG rocks means that the

relationship between $\delta^{18}O$ and SiO_2 in the CVG rocks is largely unknown and therefore O-isotopes are not definitive in any case.

3.5.2. Relationship of the SVG to the CVG

If increases in HFSE and HREE with increasing silica in CVG rocks can be explained by highly incompatible behaviour during differentiation, then relatively low and decreasing HFSE and HREE concentrations in the SVG lavas may indicate relatively more compatible behaviour of these elements during differentiation of SVG magmas. A distinct difference in the type, or abundance of phases crystallising from the magma may therefore be expected. However, there is little difference between the mineralogies of the CVG and the lower silica, east flank SVG volcanic rocks. In contrast, the higher silica SVG samples from western flank vents have small amounts of amphibole in their modal mineralogies (Appendix A). Strong depletions in M-HREE of the western flank SVG samples, relative to those with lower silica content from the eastern flank of Salak (Fig. 3.6) suggests that fractionation of amphibole or accessory phases may explain the low relatively HREE and HFSE concentrations of the highly evolved samples. The similarly shaped REE profiles and modal mineralogies of the CVG and SVG lavas with < 70 wt % SiO_2 may preclude a similar explanation for the differences observed in the geochemistry of these samples.

In addition to mineralogical differences, isotopic differences also occur between the high SiO_2 (western flank) and low SiO_2 (eastern flank) SVG lavas. The lower silica samples, possess significantly higher $^{143}Nd/^{144}Nd$ and $^{176}Hf/^{177}Hf$ and lower $^{87}Sr/^{86}Sr$ isotope ratios than the SVG rhyolites and also the CVG rocks (Figs. 3.7 and 3.8 insets). The similar isotope ratios of CVG and SVG rocks suggests that the SVG volcanic rocks from the western flank vents may share a similar source and evolutionary history to the CVG lavas, but have undergone further fractionation prior to eruption. The notably more primitive radiogenic

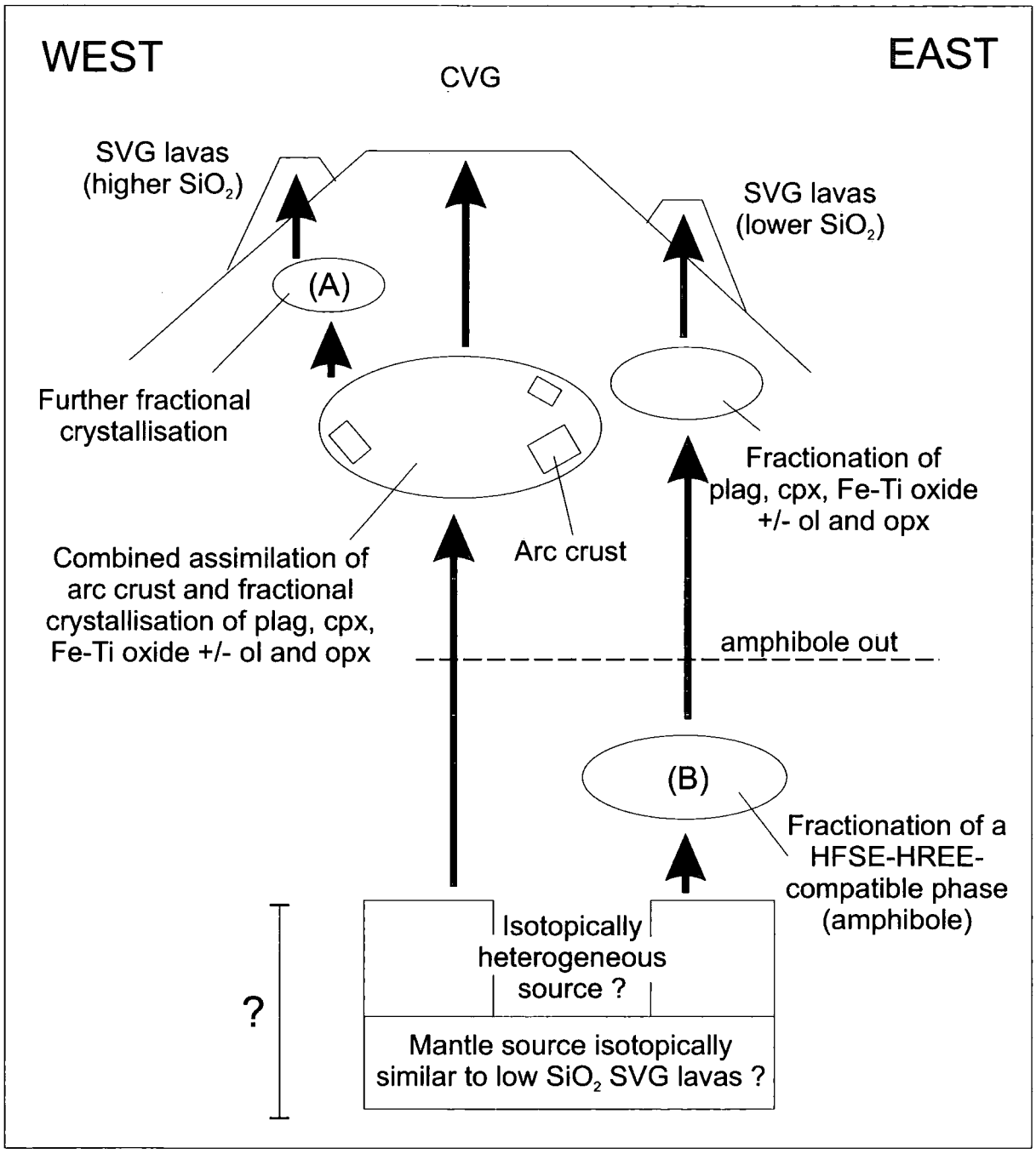

Fig. 3.13. Schematic representation of magmatic evolution, showing the multiple magma storage areas and pathways envisaged in petrogenesis at Salak. (A) and (B) relate to discussion in the text: (A) indicates further fractionation at shallow depth in petrogenesis of the higher SiO_2 SVG rocks (western flank), (B) indicates hypothesised fractionation of a HFSE-HREE compatible phase at depth in the evolution of SVG magma below the eastern flank vent.

isotope ratios of the lower SiO_2, east flank SVG lavas, suggest that they may have evolved from an isotopically distinct source, or may represent the least contaminated (either by arc crust or a subduction component) Salak lava. In the latter case, they reveal the best estimate of unmodified mantle wedge isotopic composition beneath Salak. The similar REE patterns of the lower SiO_2 SVG and lower SiO_2 CVG lavas (Fig. 3.6), suggests the magmatic source region of the two groups probably contained a comparable mineralogy and underwent similar degrees of melting.

Trace element ratios of HFSE and HREE (e.g. Zr/Nb, Y/Nb) are often used to investigate the source characteristics of magmas (McCulloch and Gamble, 1991; Woodhead et al., 1993; Reubi and Nichols., 2004). However, the limited number of samples from the SVG, combined with the reasonably differentiated nature of all Salak lavas and the uncertainty of HFSE/HREE concentrations in less differentiated samples (due to unusual increases of these elements in the CVG), hampers this approach at Salak, and limits the credibility of other studies using these ratios to identify source compositions without prior consideration of the effects of differentiation on the HFSE and HREE used.

A schematic diagram showing the proposed evolution of magma beneath Salak is displayed in Fig. 3.13. Petrographic and radiogenic isotope data suggest the high SiO_2 SVG rocks from the western flank vent, may be related to the CVG lavas, differentiating to lower HFSE and REE concentrations due to the fractionation of amphibole or accessory phases prior to eruption (A). However, the lower SiO_2 eastern SVG lavas are proposed to have taken a separate evolutionary pathway to the surface. Low concentrations of HFSE and HREE in these samples may be the result of fractionation of a HFSE-REE-compatible phase at depth (B), such as amphibole, which inhibits the increase of these elements during differentiation at shallower levels. A number of factors control amphibole fractionation from magma, these include the water content of the magma and also the pressure of crystallisation. Therefore, the

lack of deep-seated amphibole crystallisation in the CVG may imply that the water content was not as great in the parental magma, or CVG magmas were not stored at deeper levels in the arc crust. Other arc studies also support the proposal of multiple independent conduits and reservoirs in the crust beneath active volcanoes (Reubi and Nicholls, 2004; Grove et al., 2005).

3.6. Implications for differentiation of Javan volcanic rocks

Within andesite suites all REE concentrations commonly increase with silica (Gill, 1981). However, Javan within suite REE concentrations are typically constant (grey circles, Figs. 3.5b, c and h). Slight increases of HREE are observed within some intra-oceanic arcs, e.g. Mariana and Kermadec, but not to such extreme concentrations as those observed in the CVG at Salak (e.g. IAT trend Fig. 3.5). The only other volcanic rocks found to display steep positive correlations of Y, TiO_2 and P_2O_5 contents (and by inference other HFSE and HREE) are those erupted from Tengger Caldera Complex. Petrographically, lavas erupted from Tengger Caldera and Salak contain the typical Javan mineral assemblage of plagioclase, clinopyroxene, Fe-Ti oxide ± olivine or orthopyroxene. Hornblende is only found as a minor phase in the mineral assemblages of volcanic rocks of the Quaternary volcanic front in Java. This is surprising considering the generally low and flat differentiation trends of Y and Yb in Javan volcanic rocks, which are similar to the east flank SVG rocks at Salak (Figs. 3.5a and b), which do not display the incompatible behaviour expected with fractionation of a hornblende-free island arc mineral assemblage. It is suggested therefore that hornblende may also fractionate at depth below most Javan volcanoes and any entrained amphibole are dissolved in transit to surface. Although amphibole-bearing cumulate xenoliths have not been found in Salak lavas, plutonic blocks, often showing cumulate textures and containing

amphibole are commonly observed in basalts and basaltic-andesites of the Lesser Antilles arc, which are thought to be the products of fractional crystallisation (Smith et al., 1980).

3.7. Summary and Conclusions

Unusual HFSE and HREE variation trends (compared to most other volcanic rocks from Java) displayed by the CVG lavas of Salak are most likely produced during differentiation in the crust. Differentiation processes have been modelled to show that:

1) CVG element variation is not consistent with simple mixing, due to the low HFSE and HREE concentrations found in continental and oceanic crustal end members.
2) Evolution to high HFSE and HREE concentrations in the CVG can be explained by incompatible behaviour of these elements during fractional crystallisation.
3) K/Rb and Ba/Th ratios of the CVG are best explained by combined assimilation and fractional crystallisation processes.

AFC modelling and $\delta^{18}O$ suggests that typical continental-type upper-crustal contaminants are not likely to be involved in AFC processes at Salak (cf. the Andes and Lesser Antilles, Davidson et al., 2005 and references therein). Although at present a suitable end-member contaminant has not been identified, volcanic and plutonic (arc-related or ophiolitic) rocks are suggested as more probable contaminants of Salak magmas. This is consistent with Hamilton's (1979) suggestion the crust in western Java is composed of ophiolite slivers and older volcanic-arc rocks and also with evidence for the interaction between rhyolite magma and igneous plutonic rocks in the Perbakti-Gagak area adjacent to Salak (Stimac, 2003). However, if AFC processes also control Sr-isotope variation in the CVG, either the ratio of mass assimilated (of basic volcanic material) to mass crystallised must be relatively high, or the contaminant must be characterised by an extremely high Sr concentration. Other

characteristics envisaged for the contaminant include a $^{87}Sr/^{86}Sr$ isotope ratio ~0.7048 and relatively low K/Rb and Ba/Th ratios.

Volcanic rocks of the SVG display lower HFSE and HREE contents at comparable silica contents to the CVG which may be explained by amphibole fractionation in the higher silica (western flank) SVG samples, as these samples contain small phenocrysts of this phase. The lower silica (eastern flank) SVG samples do not contain amphibole but show some evidence for amphibole fractionation, forming part of a relatively coherent trend with the other SVG rocks. It is proposed therefore that amphibole is left at depth below the eastern flank vent at Salak and any amphibole entrained in the upward-migrating magmas are dissolved closer to the surface. Evolution to high HFSE and HREE concentrations in the CVG lavas suggests that magma beneath the central part of the volcano has bypassed the deep-level storage in the lower crust envisaged beneath the eastern flank vent.

The considerably more primitive radiogenic isotope ratios displayed by the eastern SVG rocks, suggest that either, these samples are the least affected by contamination at Salak and therefore best characterise the isotopic composition of the source, or, that the CVG and eastern SVG have evolved from isotopically distinct sources. The reasonably differentiated nature of the lavas (andesite-rhyolite) and limited number of SVG samples collected, prohibit detailed conclusions to be drawn regarding source composition and evolutionary history within this group.

HFSE and HREE variations in Salak lavas have drawn attention to the fact that Javan lavas do not show highly incompatible behaviour of these elements during differentiation (cf. island arc suites from the Kermadecs and Marianas). Y and Yb concentrations in eruptives from the volcanic front on Java display near-horizontal trends when plotted against silica. With little direct evidence of amphibole fractionation in these lavas, it is probable that cryptic amphibole fractionation occurs at depth beneath the majority of volcanoes on Java. Similar to

the CVG of Salak, Tengger Caldera, in East Java also displays abnormally steep, Y, P_2O_5 and TiO_2 differentiation trends, suggesting deep-fractionation of a HFSE-HREE-compatible phase does not take place at this volcano and further corroborates the idea that the cause is related to crustal-level processes, rather than isolated source contributions at single volcanic centres in both East and West Java.

Finally, the presence of a wide HFSE and HREE variation within a single volcanic centre, such as that at Salak, emphasises the importance of detailed geochemical study of individual volcanoes. It has implications for using high LREE/HFSE ratios to fundamentally characterise arc lavas. LREE/HFSE ratios in Salak lavas are relatively low in the CVG, even though LREE concentrations are relatively high, due to the high HSFE concentrations in these rocks. Therefore, caution should be employed when considering subduction enrichment in along-arc studies using LREE/HFSE ratios, as misleading interpretations may result where only a few samples have been analysed from each volcano.

Chapter 4

Characterising geochemical evolution and identifying 'crustal' contributions in petrogenesis at Gede Volcanic Complex

Characterising geochemical evolution and identifying 'crustal' contributions in petrogenesis at Gede Volcanic Complex.

4.1. Introduction

The wide variation in potential source components and processes involved in magma genesis and evolution at island-arc volcanoes precludes a single petrogenetic model for the formation of volcanic rocks in this setting. Many studies of arc lavas highlight the importance of differentiation processes in the geochemical evolution of primary arc magma. Among these processes, fractional crystallisation (Gerbe et al., 1992; Reubi and Nicholls, 2004), crustal contamination (Davidson et al., 1987; Hildreth and Moorbath, 1988; Davidson and Harmon, 1989; Macpherson et al., 1998) and magma mixing (Gamble et al., 1999; Tepley et al., 2000) are commonly called upon to explain geochemical variation in arc lavas. Constraints upon the relative importance of differentiation processes at individual volcanoes are essential before the characteristics of the source can be investigated.

Geochemical analysis of volcanic rocks from Salak (Chapter 3), slightly west of the Gede Volcanic Complex (GVC), suggest that assimilation of arc crust is important during magmatic evolution at this volcano. Further west still, in Sumatra, contamination of arc magmas by 'crustal' materials is implicated by He isotope studies (Gasparon et al., 1994) and correlations of Nd isotope ratios with SiO_2 (Turner and Foden, 2001). However, east of the GVC in Java, petrogenetic studies indicate negligible input of continental-type crust during magmatic evolution. The crustal component identified in magma genesis is thought to be provided by the subducting slab (Gertisser and Keller, 2003; Edwards, 1990; Gerbe et al., 1992; Turner and Foden, 2001). This conclusion was also reached for Ijen Volcanic Complex (East Java) in Chapter 2.

GVC has largely been ignored by geochemists studying petrogenesis of Sunda arc volcanoes. This is surprising considering the active Gede Volcano (from which the complex derives its name) is one of the most prominent in West Java and is located in close proximity (~70 km) to the densely populated capital, Jakarta. To the east of GVC researchers have argued that source contamination is important (Edwards, 1990; Turner and Foden, 2001; Gertisser and Keller, 2003), while to the west of GVC (admittedly different) researchers have called upon crustal contamination (Gasparon and Varne, 1998), therefore, GVC is in an ideal location to investigate contributions from the arc crust. Conclusions from this study will help elucidate the nature of the arc crust in West Java.

The aims of this chapter are therefore three-fold: first, to describe the petrography, mineralogy and geochemistry of GVC volcanic products; second, to use this information to characterise magmatic evolution and establish the role of the arc crust during differentiation; and third, to constrain the nature of the mantle source of GVC magmas.

4.2. Geological setting

The Quaternary GVC, in West Java (Fig. 4.1 inset), is dominated by the twin stratovolcanoes of Gede (2958 m), the only active volcano of the complex, and Pangrango (3019 m), an extinct volcano to the northwest (Fig. 4.1). Gede is divided morphologically and stratigraphically into Old and Young Gede. The remnant crater rim (50-200m high) of Old Gede is marked by Gunung Gumuruh (Fig. 4.1). This crater, now truncated by Young Gede in the north west, is the largest (~1600m in diameter) and oldest crater at Gede. The volcanic deposits of Old Gede are exposed on the south-eastern slope of Gede and form a deeply dissected morphology. Young Gede consists of several smaller craters (Sela, Ratu, Lanang, Wadon and Baru) contained within the 1km wide, steep-walled (200m) Gede crater. Most of the eruptive deposits of Young Gede are confined in relatively narrow belts, extending north

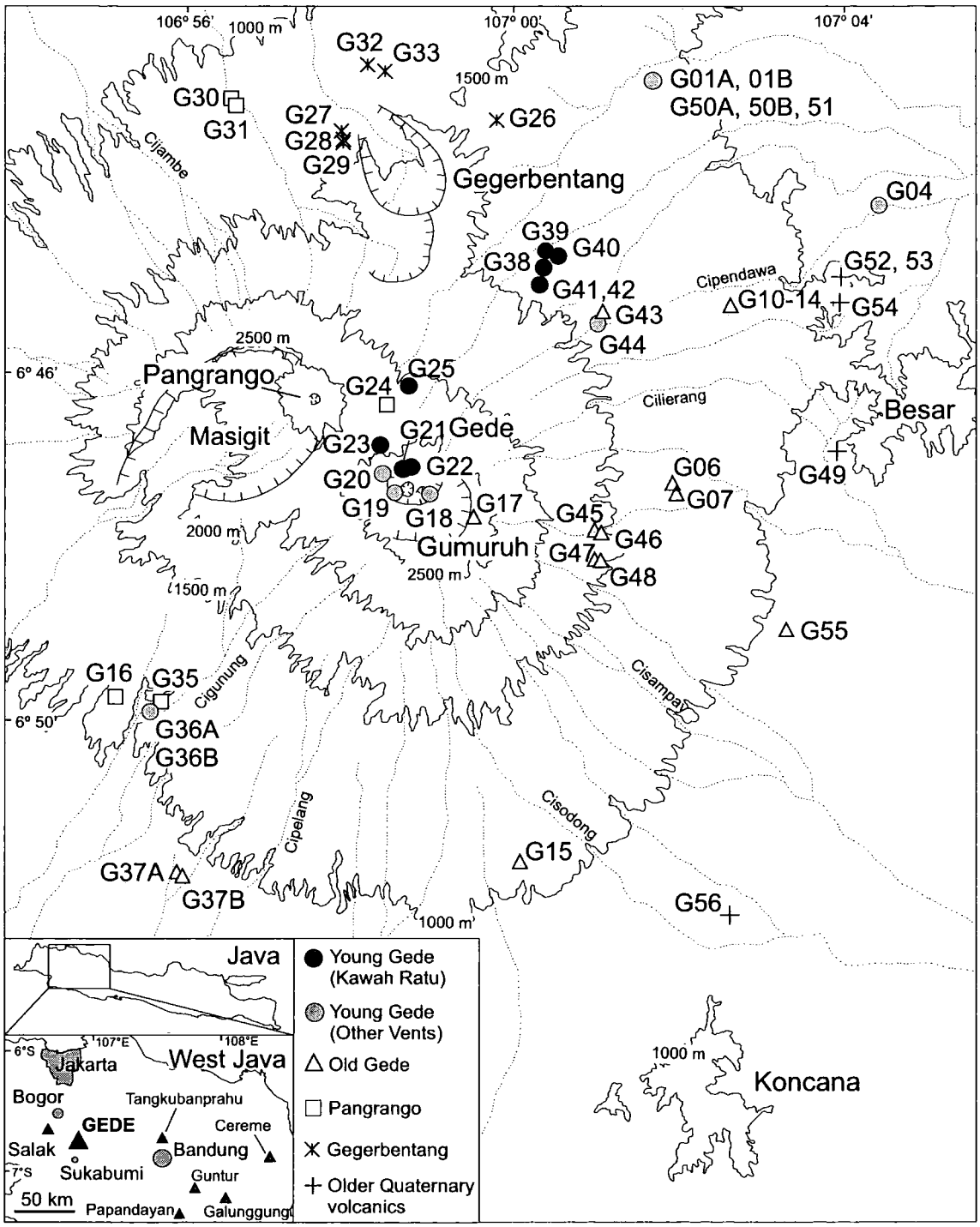

Fig. 4.1. Topographic sketch map of the Gede Volcanic Complex (GVC), showing the distribution of rock samples with corresponding data symbols used in subsequent figures (see inset for details). Selected rivers are shown by dashed lines. Solid lines with tick marks highlight volcanic craters and escarpments. Gumuruh is the remnant of the Old Gede Crater. Gede represents both Young Gede eruptive groups (Kawah Ratu and Other Vents). Inset diagram shows the location of Gede (large black triangle) in West Java, in relation to major centres of population (grey fill) and other Quaternary volcanoes (small black triangles).

east and south west of the summit due to the topographic highs of Pangrango-Masigit and Old Gede in the northwest and southeast respectively. The heavily forested Pangrango volcano is constructed on the north-east rim of a large caldera/collapse structure (Gunung Masigit, Fig. 4.1) which is open to the south-west. The Gegerbentang Complex consists of a series of eroded volcanoes situated to the north of Gede and is relatively older than both Gede and Pangrango. The oldest deposits of Quaternary volcanic material (Older Quaternary Volcanic group) are exposed to the east and south west of Gede (Besar and Koncana respectively, Fig. 4.1). Basement rocks of the complex and surrounding area are dominated by Tertiary volcanogenic and marine sediments (Effendi et al., 1998).

Around 20 eruptions have been reported from Gede volcano since the mid-18th century, which have generally been small explosive eruptions of short duration. The eruption in 1840 is the largest recorded and generated pyroclastic flows. More recently, a brief ash ejection occurred in 1957 (VSI). At the end of April 1991, a series of volcanic earthquake swarms were recorded (VSI), however no surface activity was observed. Kawah Lanang and Kawah Wadon are the most active craters at present, showing signs of hydrothermal activity (VSI).

4.3. Sample selection and grouping

The diverse range of volcanic rocks and volcanic related products from the GVC include: lavas and pyroclastic flow, air fall, debris flow and lahar deposits. Sample material collected for geochemical analysis was limited to fresh samples of lava flows and juvenile magmatic fragments from pyroclastic flow deposit units. The generally low LOI values for most samples (85% of rocks at <0.8 wt %) (Appendix B) and lack of visible alteration in rock samples and thin sections (except in a few specimens, Appendix A) confirm the samples are fresh. In this study the eruptive products of Young Gede are grouped into Young Gede

Kawah Ratu (those sourced from Kawah Ratu) and Young Gede Other Vents (sourced from the Gede crater in general) due to uncertainty in the provenance of some samples, and the distinction of these two groups on the geological map of the Gede Volcanic Complex (Situmorang and Hadisantono, 1992). In this study the term Pangrango refers to all units of the Pangrango-Masigit centres and likewise, Gegerbentang, refers to all volcanic units within the Gegerbentang complex.

4.4. Petrography and mineralogy

Compositions and textures of crystals in igneous rocks largely reflect the magmatic conditions controlling their growth. Petrographic information and mineralogical data of volcanic rocks can therefore provide evidence for the operation of magmatic processes, such as magma mixing, crystallisation and contamination. Volcanic rocks of GVC have not been previously described; therefore this section will focus on the petrography and mineralogy of each eruptive group, highlighting textural features which may contribute to the understanding of petrogenesis at GVC.

Basaltic andesite is the most common rock type erupted in the GVC; basalts are generally restricted to eruptives of Pangrango and Gegerbentang. The majority of GVC rocks contain similar mineral assemblages of plagioclase, clinopyroxene and Fe-Ti oxide ± orthopyroxene and olivine. In common with most arc rocks, plagioclase is the most abundant phenocryst phase and frequently displays evidence of disequilibrium, suggesting complex histories of these phenocrysts. Petrographic summaries of Gede lavas are given in Appendix A and mineral data are found in Appendix D.

4.4.1. General petrography

Volcanic rocks from the Kawah Ratu centre of Young Gede consist of basaltic andesites and andesites and contain a mineral assemblage of plagioclase, clinopyroxene, orthopyroxene and Ti-magnetite, set within a very fine-grained groundmass of plagioclase, Fe-Ti oxide and devitrified glass. The Kawah Ratu eruptives are dominantly seriate in texture and reasonably phenocryst rich, with modal phenocryst contents around 65% by volume.

Rocks erupted from the Other Vents group at Young Gede are dominated by basaltic andesites, with minor andesites and contain an identical mineral assemblage to the Kawah Ratu rocks, with the exception of olivine instead of orthopyroxene phenocrysts in a few basaltic andesite samples. Rocks of this group display mainly porphyritic textures, though glomeroporphyritic textures occur and are generally less phenocryst rich (Appendix A) than Kawah Ratu volcanic rocks. Many of the rocks sampled from this group are highly vesicular magmatic fragments of pyroclastic flow deposits, containing a very fine-grained groundmass of devitrified glass and plagioclase, or plagioclase, oxide and pyroxene. These samples commonly show evidence of magma mingling between dark, less evolved material and lighter more evolved material (described in more detail in section 4.4.4). Xenoliths of igneous origin are present in some Young Gede samples (section 4.4.3).

The basaltic andesites and andesites of Old Gede are dominantly porphyritic to seriate in texture. In the basaltic andesites, plagioclase, clinopyroxene and titanomagnetite are accompanied either by olivine, orthopyroxene or both; olivine is absent from the andesites. The volcanic products of Old Gede contain lower modal abundances of ferromagnesian minerals (Appendix A) compared to those of Young Gede. The very fine- to fine-grained groundmass contains plagioclase and oxide +/- pyroxene. Mingling of magma is also observed in magmatic fragments of pyroclastic flow deposits of this group (section 4.4.4).

Eruptives from Pangrango consist of basalts and basaltic andesites. Most of these lavas are strikingly porphyritic in hand specimen, containing large (up to ~1.2 cm), euhedral, clinopyroxene phenocrysts. The rocks are seriate in texture and mineral assemblages comprise plagioclase, clinopyroxene, Ti-magnetite with either olivine (in the basalts) or orthopyroxene (in the basaltic andesites). The phenocrysts are set in a fine-grained groundmass of plagioclase, clinopyroxene +/- olivine.

Most rocks from Gegerbentang display seriate textures of plagioclase, clinopyroxene, orthopyroxene, with minor Ti-magnetite and rare olivine, in a very fine-, to fine-grained groundmass of plagioclase and oxide +/- pyroxene.

It has proved difficult to obtain fresh samples from the Older Quaternary units; chlorite is commonly observed replacing ferromagnesian minerals in these rocks and LOI values are generally higher than those of other GVC rocks (0.35-0.91 wt%). The rocks contain the typical GVC mineral assemblage of plagioclase, clinopyroxene, orthopyroxene and Ti-magnetite. Minor hornblende is present within one sample, where it as been altered to biotite.

4.4.2. Mineral characteristics and compositions

4.4.2.1. Plagioclase

Subhedral to euhedral plagioclase dominates the modal phase assemblage of all GVC rocks. Oscillatory zoning, sieve textures and concentric bands of melt inclusions are observed in a large number of phenocrysts (e.g. Fig. 4.2a). In some Kawah Ratu samples, sieve-textured phenocryst cores are surrounded by clear rims of plagioclase. A large number of plagioclase phenocrysts in Young Gede and Old Gede rocks have irregular/patchy, pale brown, isotropic glass inclusions. Resorbed cores are present in occasional plagioclase phenocrysts from Pangrango and Kawah Ratu.

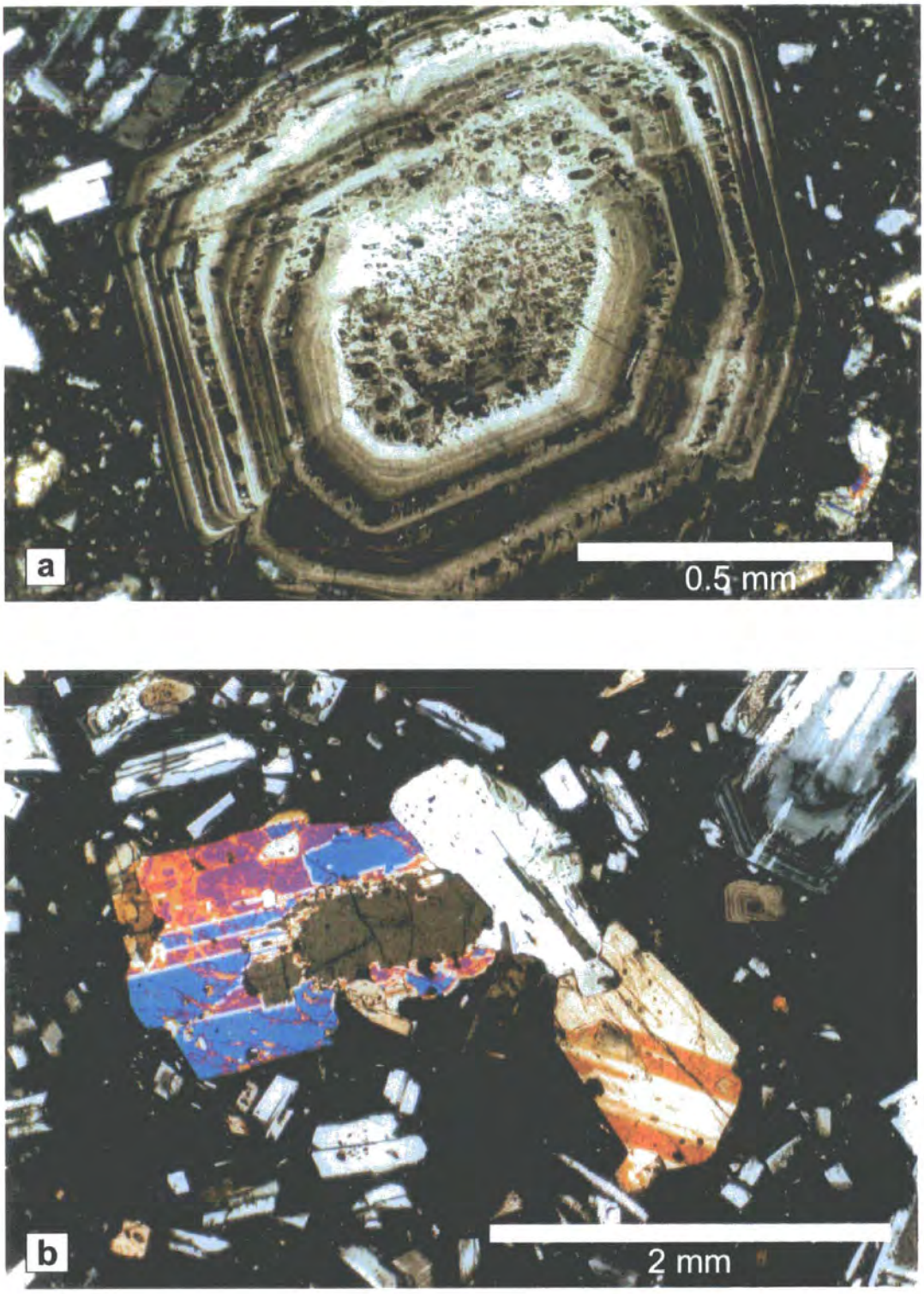

Fig. 4.2. Photomicrographs highlighting disequilibrium textures in GVC rocks. a) Sample G18: oscillatory zoning of a plagioclase phenocryst containing melt inclusions and displaying sieve-texture in the core. b) Sample G22: anhedral orthopyroxene mantled by clinopyroxene (left of centre). Oscillatory zoned plagioclase phenocrysts and microphenocrysts (top right).

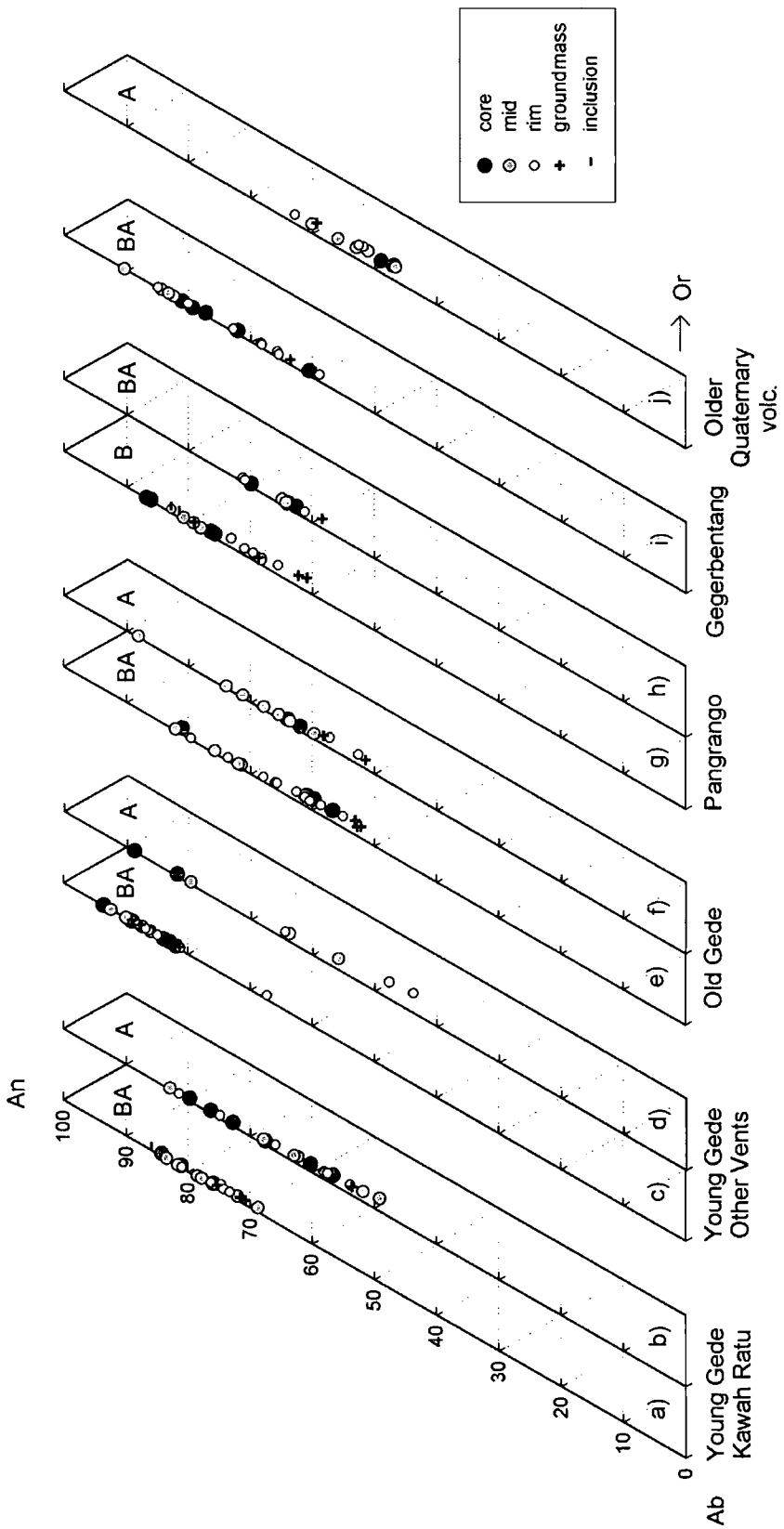

Fig. 4.3. Plagioclase analyses of volcanic rocks from the GVC separated by eruptive group and rock type (B = basalt, BA = basaltic andesite, A = andesite, based on total alkali versus silica classification of Le Bas et al., 1986).

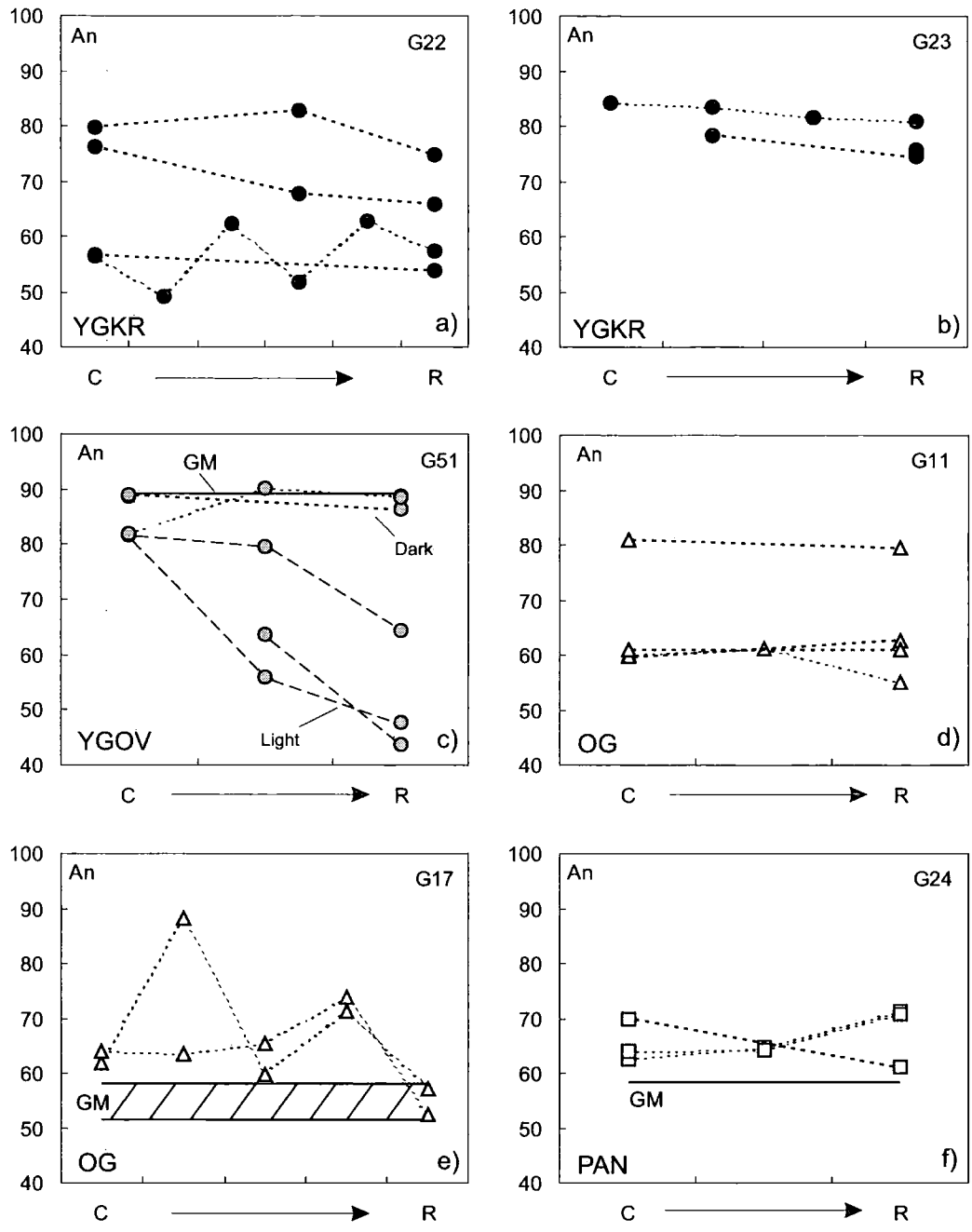

Fig. 4.4. Plagioclase compositions from core to rim of similar sized phenocrysts (~500-800 μm in diameter) of selected samples. Groundmass plagioclase compositions (GM) shown (where measured) by a horizontal line. Arrow on the x-axis indicates the direction of analyses from phenocryst core (C) to rim (R). Dashed lines connect analyses within the same phenocryst. Rock sample number is given in the top right corner. YGKR = Young Gede Kawah Ratu; YGOV = Young Gede Other Vents; OG = Old Gede; PAN = Pangrango. 'dark' and 'light' in Fig. 4.4c correspond to the layer from which they were analysed in the G51 mingled magmatic fragment.

Plagioclase phenocrysts of GVC rocks, display a broad range in composition from ~An_{45-95} (Fig. 4.3). In the Young Gede Kawah Ratu rocks, compositions are more restricted in the basaltic andesites (An_{68-86}) than in the andesites (An_{49-83}, Figs. 4.3a and b respectively), which display highly variable core, mid and rim anorthite contents. Plagioclase phenocrysts and groundmass An compositions in the basaltic andesites of the Young Gede Other Vents group are noticeably higher than those in other GVC groups (above 81% mol with the exception of one rim sample), including the basalts from Pangrango, and are extremely restricted in range (Fig. 4.3c). Plagioclase cores of the andesites lie within the range of basaltic andesite plagioclase cores of the Young Gede Other Vents group, however, mid and rim compositions extend to significantly lower Anorthite content (An_{44}). Plagioclase compositions cover a relatively broad range in both the basaltic andesite and andesites of Old Gede (Figs. 4.3e and f). Rim analyses of plagioclase in the basaltic andesites display a wide variation and extend to much higher An contents than groundmass analyses (An_{52-57}, Fig. 4.3e). Basaltic andesites of Pangrango possess relatively low anorthite contents compared to the basaltic andesites of Young Gede (both sub-groups). Analyses of phenocryst rims reveal that a small number have higher An contents than respective core analyses (Fig. 4.3h, Fig. 4.4f) while most are similar or lower in An content. Plagioclase compositions in rocks from Gegerbentang extend from moderate to high anorthite contents (An_{59-90}) with a reasonably wide range in core and rim composition when compared with mid sections of phenocrysts (Fig. 4.3i). In the Older Quaternary group, compositions are reasonably An poor (47-63% mol) and phenocryst cores possess some of the lowest An contents (47-49) of the GVC, with rim and mid sections displaying generally higher An contents (52-63 and 47-60% mol respectively, Fig. 4.3j).

Compositional variation from core to rim of individual plagioclase phenocrysts are shown in more detail for selected analyses in Fig. 4.4, and highlight the wide variation in An

content found within and across individual phenocrysts of GVC lavas. Oscillatory compositional zoning, normal zoning and variation in plagioclase core compositions are noted within the Kawah Ratu group (Figs. 4.4a and b). Normal zoning is also observed in phenocrysts of the light bands from a banded magmatic fragment (Young Gede Other Vent group), which contrasts with phenocrysts from the dark layers of the same magmatic fragment, where An content remains relatively constant or slightly increases towards the rim (Fig. 4.4c). Other examples of variable core compositions (Fig. 4.4d) and oscillatory compositional zoning (Fig. 4.4e) are displayed in phenocrysts of Old Gede rocks. Pangrango plagioclase phenocrysts display both normal and reverse compositional zoning (Fig. 4.4f).

4.4.2.2. Clinopyroxene

Clinopyroxene is the most abundant ferromagnesian mineral (by modal volume) in GVC rocks, found in all samples accompanied by either olivine or orthopyroxene and very occasionally both. Phenocrysts are typically subhedral to euhedral and most exhibit simple twining, although oscillatory zoning is observed in some crystals. Clinopyroxene phenocrysts display a broad range in size from microphenocryst to ~1.2 cm. Large (0.5-1.2cm) phenocrysts are characteristic of the Pangrango basalts, and this phase therefore accounts for a significant proportion of the modal rock volume (9-22%, Appendix A) within this eruptive group. Clinopyroxene phenocrysts of slightly smaller dimensions are featured in the volcanic products of Gegerbentang. Several clinopyroxene phenocrysts of the Young Gede Other Vent group contain anhedral glass inclusions, similar to those seen in plagioclase phenocrysts of the same group. Some clinopyroxenes in the Older Quaternary group lavas display minor alteration.

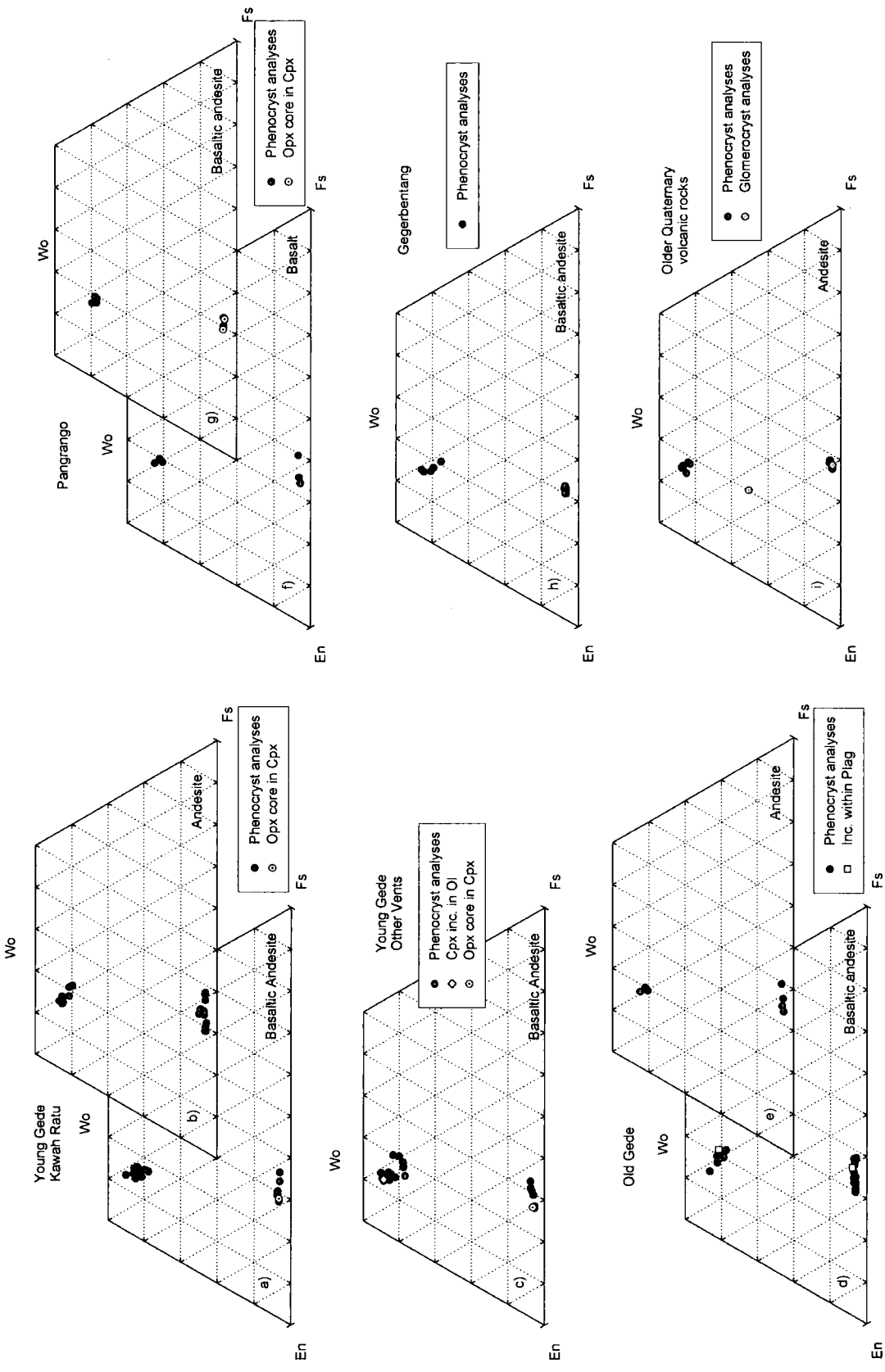

Fig. 4.5. Analyses of pyroxene phenocrysts in GVC lavas and magmatic fragments. Dashed lines represent 10% increments.

All clinopyroxene phenocrysts of GVC rocks are augites and most of the eruptive groups display a fairly restricted range in composition (Figs. 4.5a-i). Clinopyroxene compositions in the basaltic andesites of the Young Gede Other Vent group display the greatest within-group variation ($En_{38-45}Wo_{38-45}Fs_{12-20}$, Fig. 4.5c), and contrast with the highly restricted range in plagioclase composition observed in this group (Fig. 4.3c). Within each eruptive series, clinopyroxene phenocrysts in the andesites display generally more Fe-rich compositions than the respective basaltic andesites. The Pangrango basalts do not possess the most Ca-rich or Fe-poor clinopyroxene compositions, as might be expected in the least evolved (lowest SiO_2) rocks analysed from GVC (Fig. 4.5f). Pigeonite ($En_{55}Wo_{25}Fs_{20}$) was discovered in a 4 mm glomerocryst/cumulate xenolith in an Older Quaternary Volcanic group lava (Fig. 4.5i).

4.4.2.3. Orthopyroxene

Orthopyroxene phenocrysts are less abundant than clinopyroxene in GVC rocks, and generally smaller in size. They are usually subhedral to euhedral, except when mantled by clinopyroxene, where they are typically andhedral to subhedral. Mantling of orthopyroxene is commonly observed in GVC rocks, especially in some of the basaltic andesites and all of the andesites of the Young Gede Kawah Ratu group (Fig. 4.2b). Clinopyroxene overgrowths on orthopyroxenes are less frequently observed (cf. Kawah Ratu rocks) in Old Gede lavas, except in one sample (G46). Orthopyroxene is rarely found within basalts of Pangrango, but where present is observed as subhedral-euhedral cores within clinopyroxene phenocrysts and as occasional overgrowths on olivine phenocrysts. In Gegerbentang rocks, orthopyroxene is sometimes surrounded by a thin rim of clinopyroxene or completely enclosed within it. Mantling of orthopyroxene by clinopyroxene is relatively common in arc lavas, and is observed in volcanic products of other volcanoes from Java: Slamet (Vukadinovic and

Sutawidjaja, 1995; Reubi et al., 2003), Lamongan (Carn and Pyle, 2001), Ijen (Sitorus, 1990) and also in lavas from other arcs e.g. Ruapehu (Donoghue et al., 1995).

There is little distinction between orthopyroxene compositions in the basaltic andesites and andesites within most eruptive series. Orthopyroxene enclosed within clinopyroxene in the basaltic andesites of the Young Gede Kawah Ratu and Other Vents groups (Figs. 4.5a and c) lie among the higher Mg orthopyroxene compositions (En_{68} and En_{70} respectively) of both groups (En_{62-69} and En_{64-71}). Orthopyroxene mantled by clinopyroxene in the basaltic andesites of Pangrango possess identical compositions to those not shrouded by clinopyroxene (Fig. 4.5g). Orthopyroxene compositions in the Old Gede group (Figs. 4.5d and e) are comparable to those measured in similarly evolved rocks of Young Gede. Fe contents in orthopyroxene phenocrysts of the Older Quaternary units (Fs_{37-39}) lie towards the higher end of the range measured in the rest of Gede Complex rocks (Fs_{27-40}).

4.4.2.4. Olivine

Olivine displays a limited presence in GVC volcanic rocks, restricted to a smaller number of basalts and basaltic andesites. The anhedral and occasionally embayed olivine phenocrysts are typically smaller than pyroxene and plagioclase phenocrysts within the same samples from the Young Gede Other Vents group. In one sample from Old Gede (G07), olivine is the dominant ferromagnesian phase (Appendix A) and occurs as large subhedral crystals. In other Old Gede samples olivine phenocrysts are small, anhedral and co-exist with orthopyroxene. A small number of anhedral to subhedral olivine phenocrysts in Old Gede basaltic andesites show alteration to iddingsite, others are present as inclusions within clinopyroxene phenocrysts. Olivine is a major component of the ferromagnesian mineral assemblage in basalts from Pangrango, constituting ~8-12 % of the modal rock volume. Most crystals are

Fig. 4.6. Analyses of olivine phenocrysts in basalt from Pangrango and basaltic andesites of Young Gede (Kawah Ratu and Other Vents) and Gegerbentang.

small, commonly with rounded edges, and sometimes occur as inclusions within clinopyroxene. Olivine is only observed in one sample from Gegerbentang, characterised by small, anhedral phenocrysts, some showing evidence of resorption.

Olivine compositions are displayed in Fig. 4.6. Forsterite (Fo) contents of olivines in basaltic andesites of the Young Gede Other Vent group, Fo_{70-72}, are higher than Fo contents in any other GVC group; consistent with the high (most primitive) An contents of plagioclase phenocrysts (Fig. 4.3c) in this group. Fo contents of the Pangrango basalts are less magnesium-rich than those in the more evolved rocks of Young Gede, and generally more magnesium-rich than those of Gegerbentang, with the exception of one phenocryst.

4.4.2.5. Fe-Ti oxide

Fe-Ti oxide (titanomagnetite) occurs as phenocrysts, inclusions within ferromagnesian minerals (dominantly clinopyroxene) and as a groundmass phase in most GVC rocks. Titanomagnetite is typically subhedral and constitutes a small percentage of the modal rock volume (~1-3%). Subhedral titanomagnetite phenocrysts are relatively more abundant in the Older Quaternary Volcanic group, compared with the majority of GVC rocks (Appendix A), and have higher than average Ti contents. Relatively high Ti contents are also observed in titanomagnetite phenocrysts in Pangrango lavas (Appendix D).

4.4.3. Xenoliths

Xenoliths are uncommon in GVC rocks. Angular clasts of igneous material ~1mm to 2cm in size are observed within the Young Gede Other Vents group, particularly within primary magmatic fragments of pyroclastic flow deposits (e.g. G51, G01A). The most abundant type consists of large plagioclase and orthopyroxene phenocrysts, within a fine- to medium-grained groundmass of plagioclase, orthopyroxene and oxide. The holocrystalline clasts, display sharp contacts with the host rock and can be removed relatively efficiently from the host matrix.

A different type of igneous xenolith, dominated by tabular, plagioclase (with melt-inclusions), amphibole and elongate pyroxene was found in G18 (Old Gede). The amphibole is heavily altered, especially at crystal edges, where a thick rim of opaque oxide has formed. The contact between the host and the (0.5 x 0.8cm) xenolith is irregular and slightly diffuse.

A cumulate xenolith was found within Pangrango sample G16. The oval-shaped cumulate is ~0.5cm in diameter and composed of relatively large, generally interlocking plagioclase and pyroxene (orthopyroxene with minor clinopyroxene) crystals, with minor interstitial pyroxene. There is no obvious reaction rim at the contact between the cumulate xenolith and the host lava.

4.4.4. Magma mingling in GVC rocks

Several primary magmatic fragments in pyroclastic flow deposit units of Young Gede (Kawah Ratu and Other Vents) and Old Gede show evidence for the mingling of distinct magmas. The vesicular magmatic fragments are composed of dark grey/black material, with irregularly shaped lenses or bands, of lighter, pale-grey material. The majority of magmatic fragments from Young Gede are composed of the dark component (Fig. 4.7a$_i$, G36B & G51), while the samples from Old Gede are variably banded with more equal shares of both light

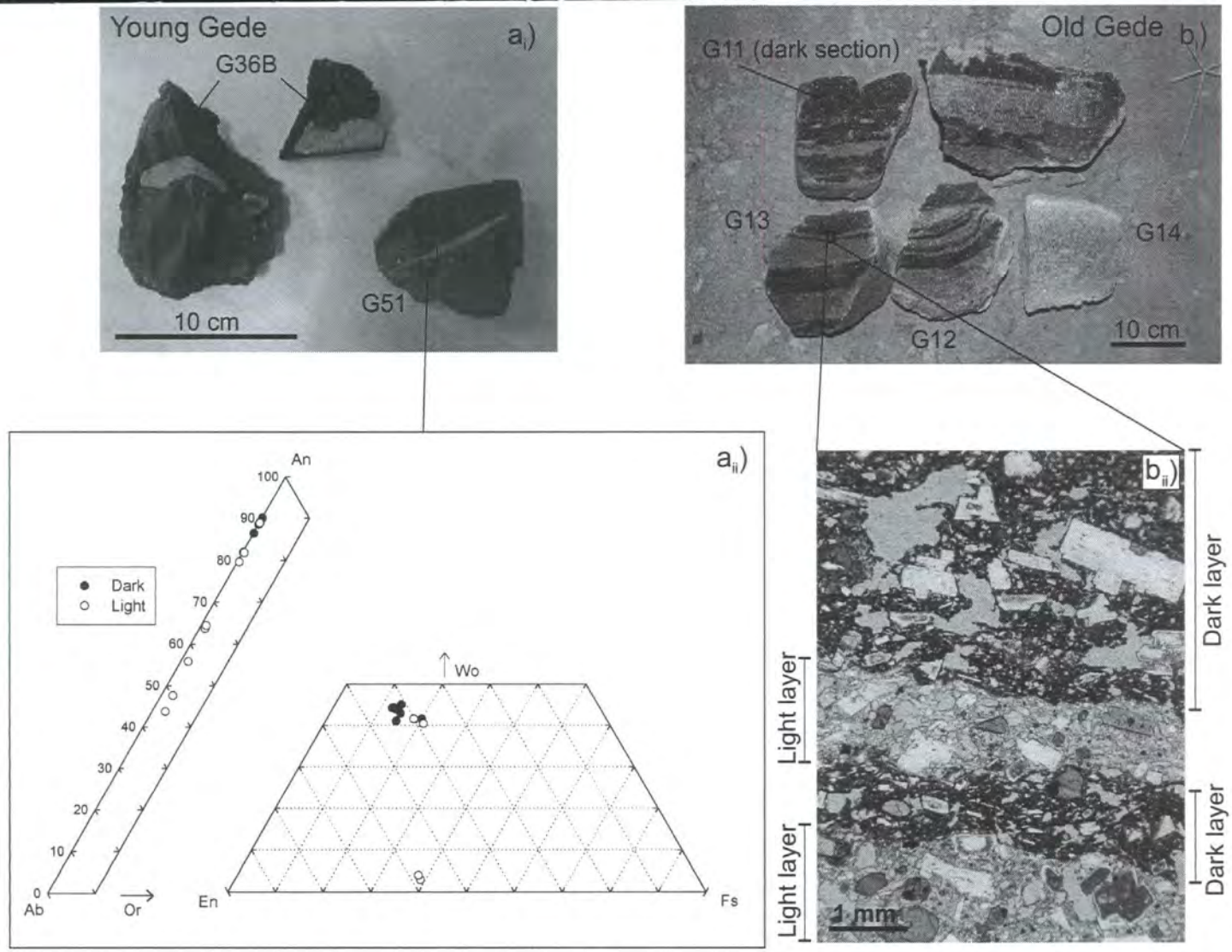

Fig. 4.7. Photographs of magma mingling in magmatic fragments from pyroclastic flows of a_i) Young Gede Other Vents and b_i) Old Gede. a_{ii}) Plagioclase and pyroxene analyses in mingled magmatic fragment G51. b_{ii}) Micrograph showing detail of the contact between the light and dark layers in mingled magmatic fragment G13.

and dark layers (Fig. 4.7b_i, G13). The dark bands contain phenocrysts of sub- to euhedral plagioclase, clinopyroxene and titanomagnetite and anhedral to subhedral olivine. The lighter layers contain the same mineral assemblage but with orthopyroxene substituted for olivine. Both layers display porphyritic textures (Fig. 4.7b_{ii}), and oscillatory zoning and sieve textures in plagioclase phenocrysts. The contact between the two layers is always irregular in detail (Fig. 4.7b_{ii}) and ranges from sharp to diffuse, indicating that mixing may have occurred in some samples. The Young Gede magmatic fragments (G36B and G51) possess small, angular xenolith clasts (described above) that display sharp contacts with the host rock.

Compositions of plagioclase and pyroxene phenocryst in the light and dark layers of sample G51 are plotted in Fig. 4.7a_{ii}. Anorthite contents of plagioclase in the dark layer are high and restricted between An_{80-90}. Plagioclase compositions in the light layer, overlap with those in the dark layer, but extend to much lower An contents (~An_{45-90}). Variations of An content within individual phenocrysts (Fig. 4.4), show that there is a significant drop in An content from the core to the rim in plagioclase phenocrysts from the light-coloured layer of G51 (Fig. 4.4c). The An content of plagioclase phenocrysts from the dark layer remains fairly constant, around An_{90}, and is very similar to An content of plagioclase in the dark layer groundmass. Plagioclase core compositions in G11 (a dark magmatic fragment from the same locality as G13) display high and low An contents, with comparably high and low An content in the respective rims (Fig. 4.4d). Clinopyroxene compositions in the light layer of G51 (Fig. 4.7a_{ii}) are relatively Fe-rich compared to those measured in the dark layer, with the exception of one phenocryst, which plots between the light layer data points.

4.5. Geochemical data

4.5.1. Major element geochemistry

Major element data are listed in Appendix B. GVC rocks possess intermediate silica contents (~51-63 wt%), with a predominance of basaltic andesite and andesite rock types. Basalts are fairly rare, and generally restricted to eruptives of the older Pangrango and Gegerbentang units. Low MgO contents in the basalts (~4-5 wt%) suggest that even these samples are relatively fractionated and do not represent primary basalts. Major element trends are similar for most of the Gede Complex groups (Figs. 4.8a-h); negative correlations against silica are displayed for Fe_2O_3, MgO, CaO and TiO_2, and positive correlations are generally observed for K_2O and Na_2O. Al_2O_3 and P_2O_5 data show more scatter. Volcanic rocks of Young Gede (both groups) display the greatest range in silica content (52-62 wt%), although the majority of these samples cluster at ~55 wt% SiO_2. The Pangrango lavas are among the least evolved samples collected from the complex and possess the highest TiO_2 contents, up to ~1.2 wt% (Fig. 4.8g). Eruptives of Gegerbentang cluster towards the lower silica end of the GVC array and possess slighter higher P_2O_5 content compared to other GVC rocks of comparable silica content (e.g. Pangrango, Fig. 4.8h).

4.5.2. Trace element geochemistry

Variations of selected trace elements with SiO_2 are displayed in Fig. 4.9. In common with orogenic andesites (Gill, 1981), GVC rocks display systematic increases with increasing silica of most LILE (e.g. Ba, Rb, and here including Th and U, Fig. 4.9a), LREE (e.g. La, Fig. 4.9b), and some HFSE (Zr, Hf, and to a lesser extent Nb, Figs. 4.9c and d). Elements that behave compatibly in most arc magmas, such as vanadium (Fig. 4.9e), also display strong negative correlations with SiO_2 in GVC rocks. Y, Yb, Sr, Pb and Eu remain relatively constant over the range in silica content (Figs. 4.9f-h). There is little distinction in trace

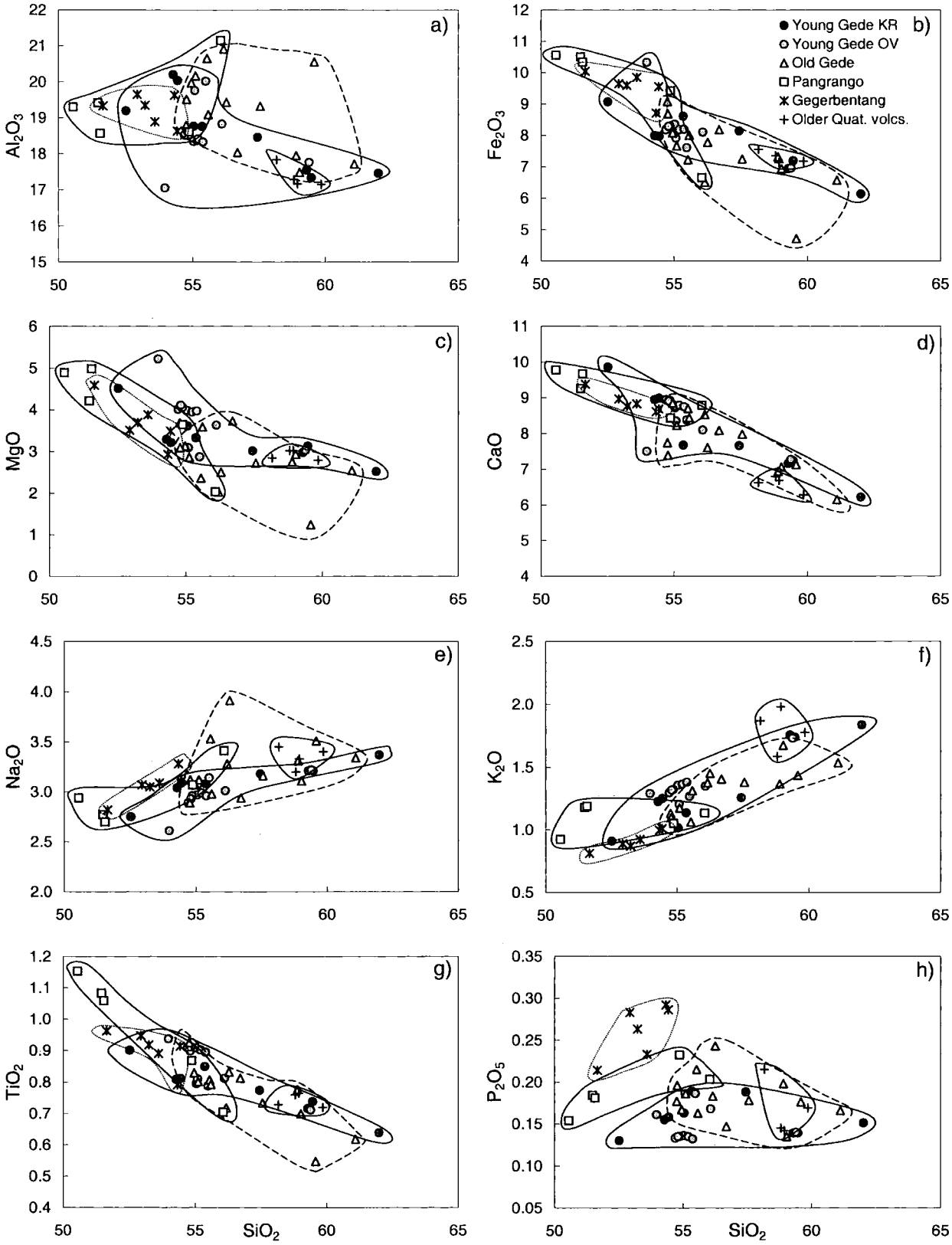

Fig. 4.8. Major element variation diagrams for GVC rocks.

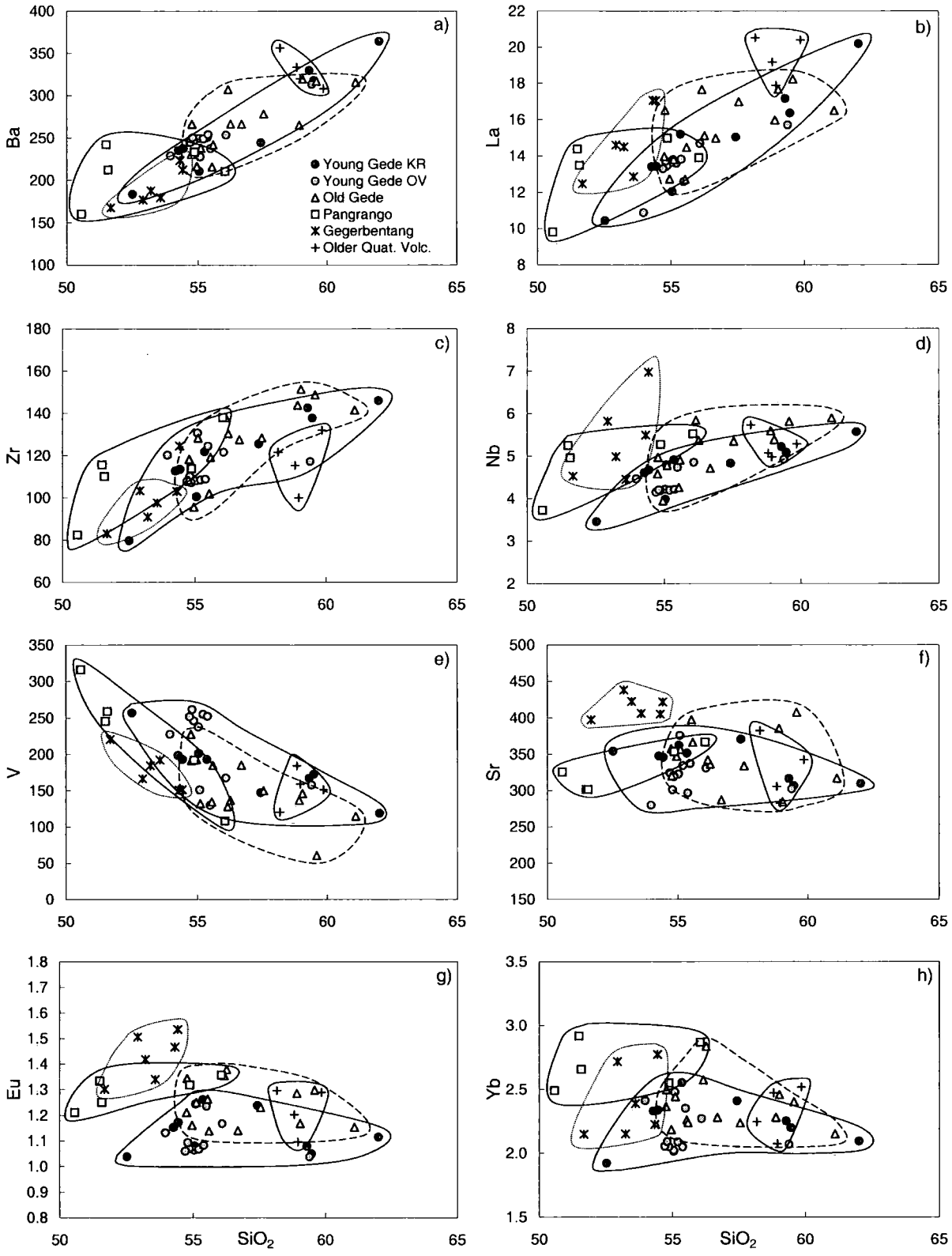

Fig. 4.9. Selected trace element variations with SiO_2 for GVC rocks.

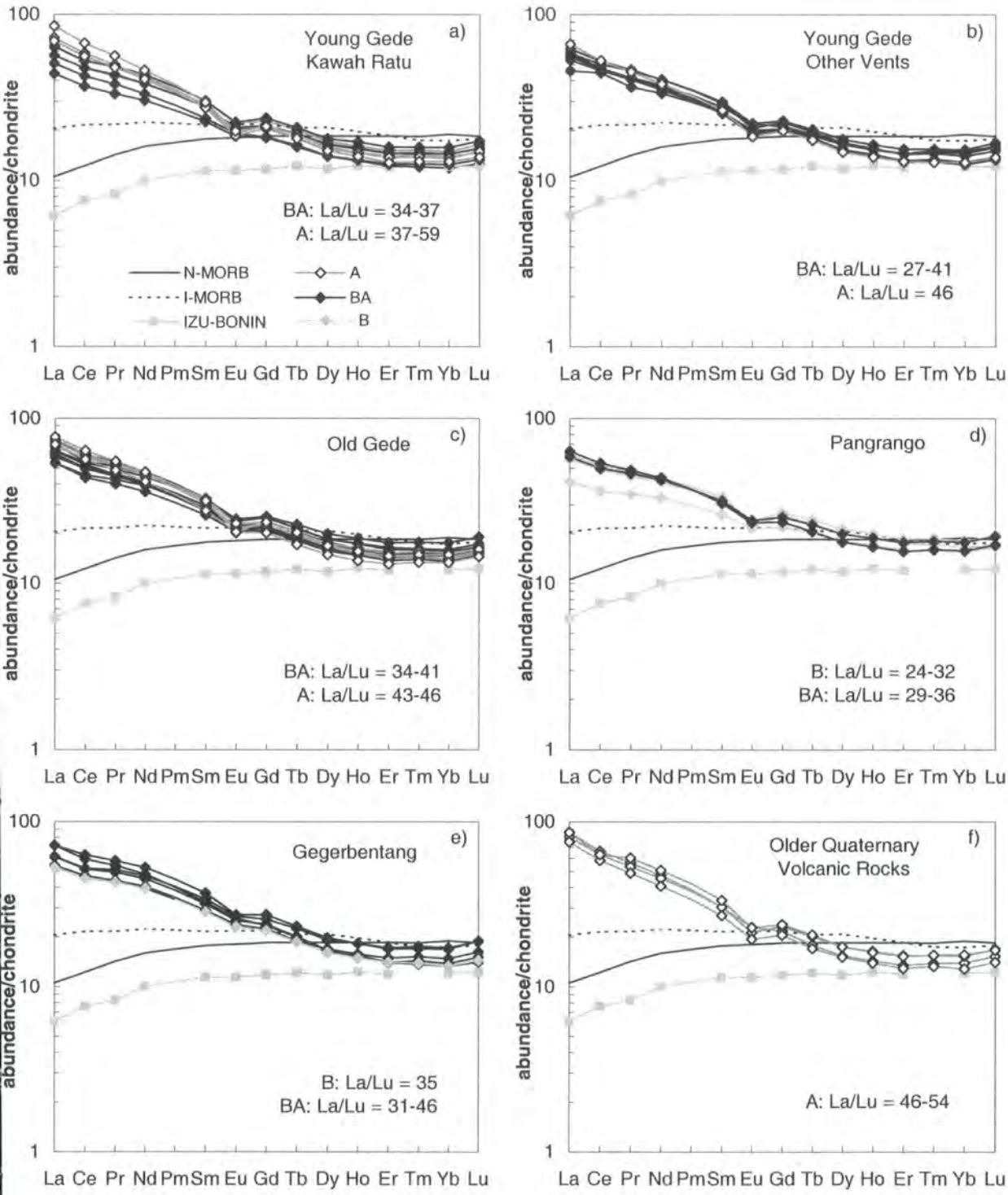

Fig. 4.10. Chondrite normalised rare earth element diagram of GVC rocks. Normalising factors and N-MORB values from Sun and McDonough (1989). Indian MORB (Chauvel and Blichert-Toft, 2001), and Izu-Bonin arc lava compositions (Taylor and Nesbitt, 1998) are shown for comparison.

element variations of the separate eruptive groups, variation appears to be largely dependant on silica content, rather than the eruptive group to which the rocks belong.

Chondrite-normalised REE patterns of GVC lavas are enriched in LREE relative to MORB (N-MORB and I-MORB) (Figs. 4.10a-f), typical of other Javan volcanic rocks e.g. Slamet (Vukadinovic and Sutawidjaja, 1995), Merapi (Gertisser and Keller, 2003) and Cereme (Edwards, 1990) and lavas from oceanic island arcs associated with back-arc spreading (e.g. Izu-Bonin). HREE in GVC rocks are similar to, or slightly more depleted than N-MORB, I-MORB and Izu-Bonin lava HREE compositions. Negative europium anomalies are present in the majority of volcanic rocks from all groups. LREE-MREE (La-Nd) concentrations of most GVC rocks lie parallel to each other on chondrite normalised REE diagrams within each eruptive group. La/Lu ratios display a fairly wide range 24-59, but are similar for samples of comparable silica content: the basalts and basaltic andesites, generally possess lower La/Lu ratios, i.e. flatter REE patterns than more evolved samples of respective volcanic centres. The largest within-group variation of La/Lu (34-59), and REE variation in general, is seen within the Kawah Ratu group of Young Gede (Fig. 4.10a); the LREE show large variability in abundance within this group, but display fairly parallel LREE patterns.

4.5.3. Isotope geochemistry

4.5.3.1. Radiogenic isotopes

Sr, Nd and Hf isotope data are listed in Appendix C and displayed in Figs. 4.11 and 4.12. $^{87}Sr/^{86}Sr$ and $^{143}Nd/^{144}Nd$ isotope ratios of volcanic rocks from the Gede Volcanic Complex span a fairly wide range (0.704502-0.705513 and 0.512629-0.512737 respectively) but form a tight negative array within the centre of the Java domain in Fig. 4.11, defined by previously published data. GVC data generally plot between the fields of MORB (I-MORB and N-MORB) and Indian Ocean sediments. The inset diagram of Fig. 4.11, shows the $^{87}Sr/^{86}Sr$ and

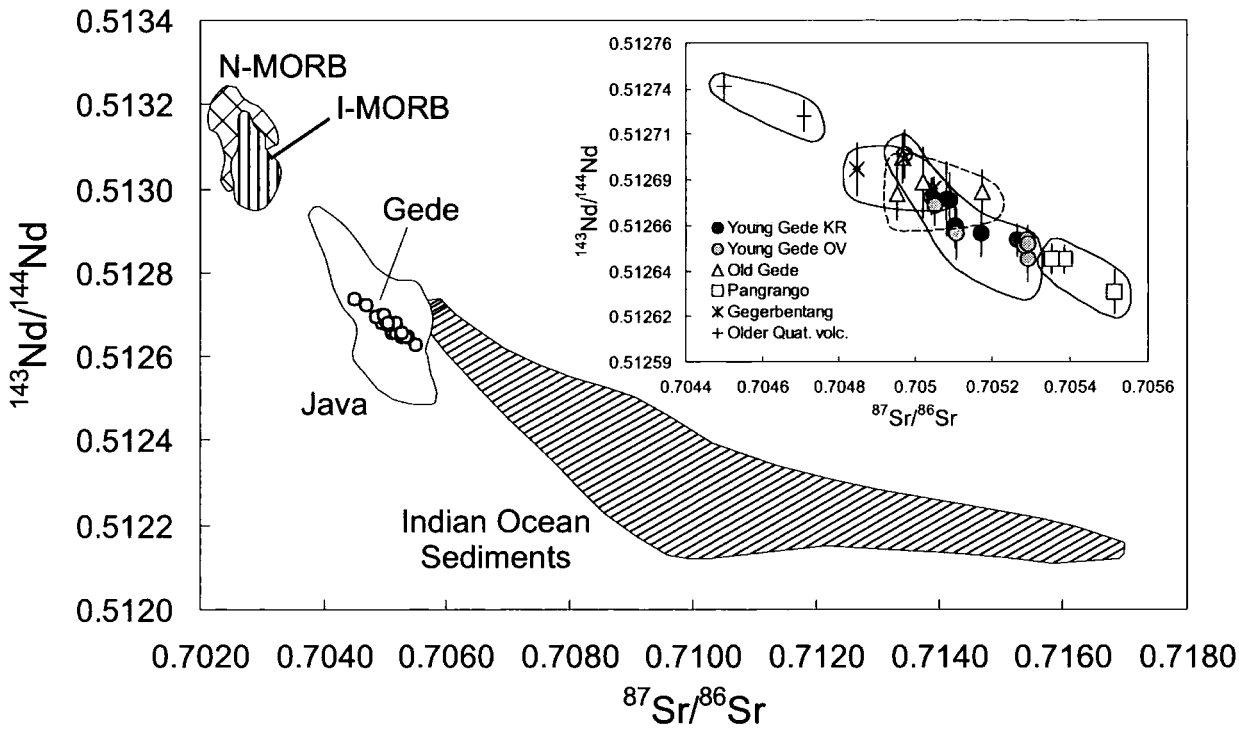

Fig. 4.11. Variation of $^{143}Nd/^{144}Nd$ with $^{87}Sr/^{86}Sr$ for GVC. Data sources: I-MORB: Rehkämper and Hofmann, 1997; Ito et al., 1987; Price et al., 1986; Chauvel and Blichert-Toft, 2001; N-MORB: Ito et al., 1987; Chauvel and Blichert-Toft, 2001; Java: White and Patchett, 1984; Whitford et al, 1981; Edwards, 1990; Gertisser and Keller, 2003; Gerbe et al, 1992; Ijen and Salak, this study; Indian ocean sediments: Ben Othman et al., 1989; Gasparon and Varne, 1998. Inset: Nd and Sr isotope ratio diagram separated by group. Errors shown are 2σ external errors of each analysis.

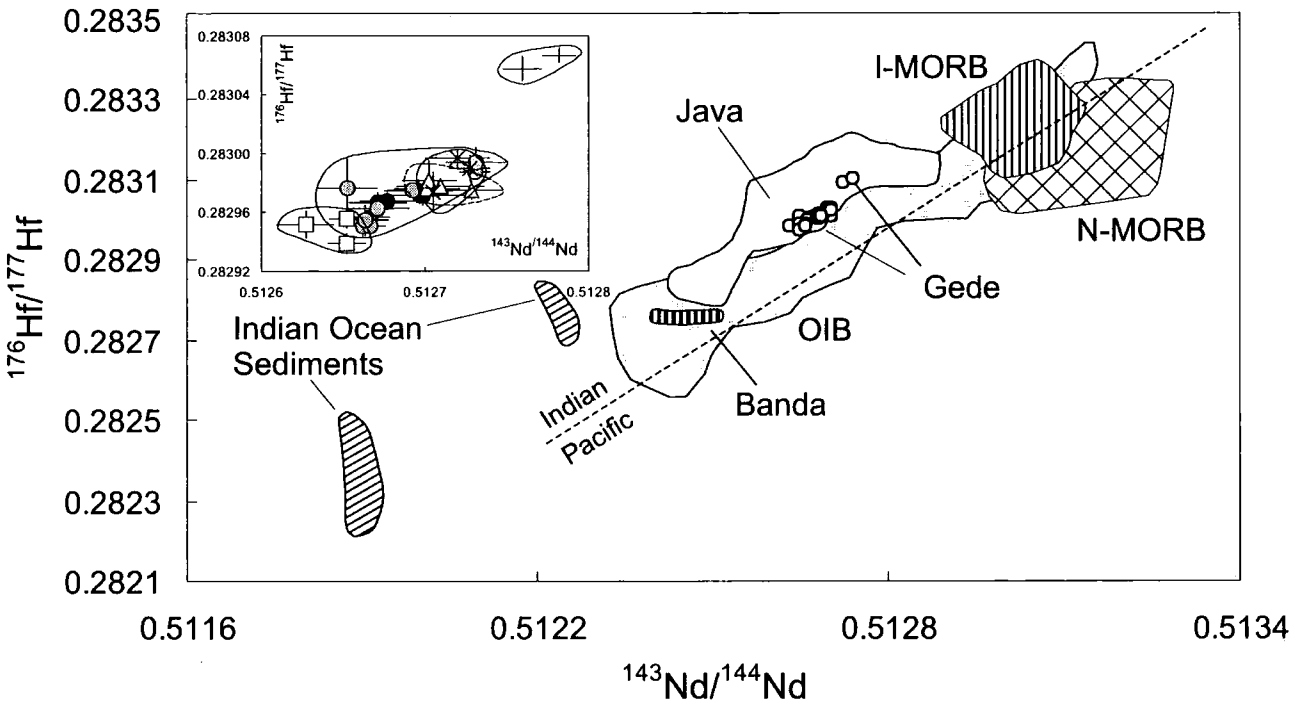

Fig. 4.12. $^{176}Hf/^{177}Hf$ - $^{143}Nd/^{144}Nd$ variation of GVC rocks. Data sources: I-MORB: Salters, 1996; Nowell et al., 1998; Chauvel and Blichert-Toft, 2001; N-MORB: I-MORB references plus Salters and Hart, 1991; OIB: Salters and Hart, 1991; Salters and White, 1998; Nowell et al., 1998; Patchett and Tatsumoto, 1980; Patchett, 1983; Stille et al., 1986; Java volcanics: White and Patchett, 1984; Woodhead et al., 2001; Ijen and Salak, this study; Banda arc: White & Patchet, 1984; Indian ocean sediments: Ben Othman et al., 1989; White et al., 1986; Vervoort et al., 1999. Dividing line for Indian and Pacific MORB provenance from Pearce et al., 1999. Inset: $^{176}Hf/^{177}Hf$ with $^{143}Nd/^{144}Nd$ diagram of GVC rocks separated by eruptive group. 2σ external errors of each sample are shown on the inset diagram top left.

$^{143}Nd/^{144}Nd$ variation of each eruptive centre. The Older Quaternary samples possess the most primitive Sr-Nd isotope ratios. The opposite is observed for Pangrango rocks, which possess the highest $^{87}Sr/^{86}Sr$ and lowest $^{143}Nd/^{144}Nd$ ratios of GVC. Sr-Nd isotope ratios of rocks from Young and Old Gede and Gegerbentang generally overlap and form a relatively linear array between Pangrango and the Older Quaternary volcanic rocks.

GVC rocks display a moderate range in $^{176}Hf/^{177}Hf$ isotope ratios (0.282977-0.283067). Fig. 4.12 shows that GVC rocks also lie within the field of previously published Java data in $^{176}Hf/^{177}Hf$-$^{143}Nd/^{144}Nd$-isotope space, between I-MORB, N-MORB and the Indian Ocean sediment fields. It also shows that samples with the most and least primitive Sr-Nd isotope signatures (Older Quaternary and Pangrango respectively) also possess the most and least primitive Hf isotope values respectively. The Young Gede Other Vents group display the widest variation overall in Sr-Nd-Hf isotope ratios.

4.5.3.2. Oxygen isotope data

Oxygen isotope data are listed in Appendix C. Mineral separates of olivine, clinopyroxene and plagioclase from Gede Complex lavas possess relatively restricted $\delta^{18}O$ values ranging from +5.32 to +5.42 ‰ (n = 3), +5.52 to +5.94‰ (n = 12) and +6.07‰ (n = 1), respectively. The majority of the GVC data lie within error of $\delta^{18}O$ values measured in mantle olivine and clinopyroxene (+5.18 ±0.28‰, n = 76 and +5.57 ±0.32‰, n = 57, 2SD respectively, Mattey et al., 1994; Ionov et al., 1994; Fig. 4.13). Differences in $\delta^{18}O$ values between coexisting clinopyroxene and olivine ($\Delta_{cpx\text{-}ol}$) and plagioclase and clinopyroxene ($\Delta_{plag\text{-}cpx}$) at GVC are 0.30-0.44‰ and 0.44‰ respectively, suggesting isotopic equilibrium at typical magmatic temperatures for andesite liquids. (Macpherson and Mattey, 1998; Macpherson et al., 1998).

Clinopyroxene $\delta^{18}O$ values from the GVC are slightly higher than those of Galunggung lavas (+5.3 to +5.6‰) from West Java (Harmon and Gerbe, 1992, Fig. 4.13) but

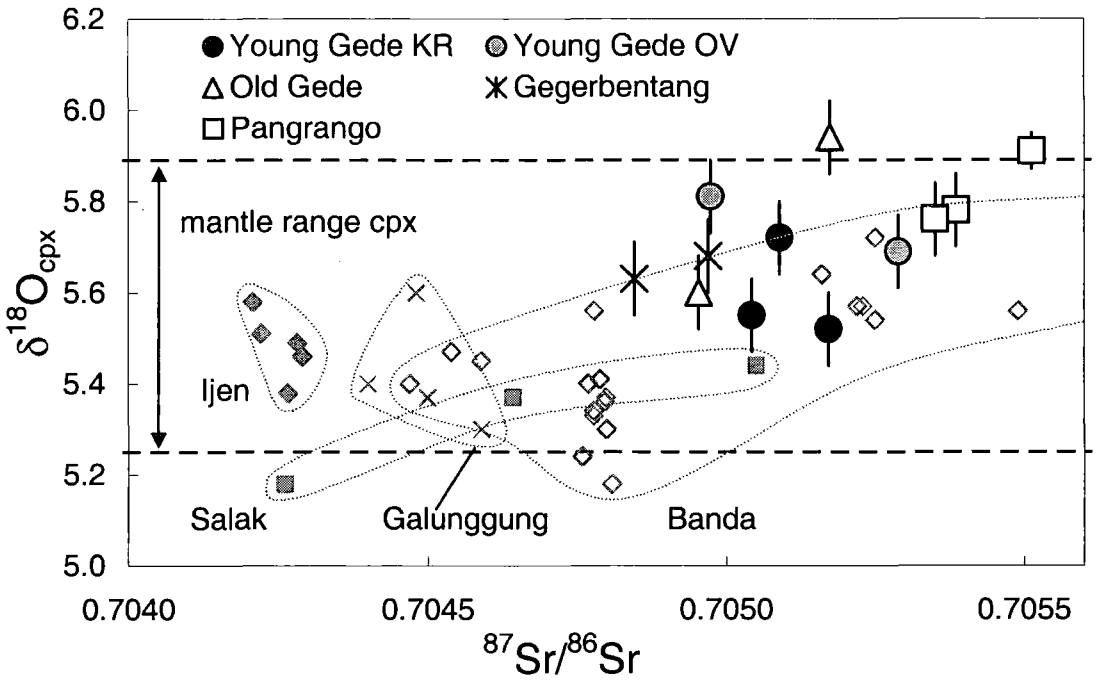

Fig. 4.13. $\delta^{18}O$ (clinopyroxene) versus $^{87}Sr/^{86}Sr$ (whole rock) for GVC lavas. Error bars are ± 1σ of replicate analysis or ±0.09‰ where replicate analyses were not carried out. External error (2σ) of $^{87}Sr/^{86}Sr$ analyses are smaller than the symbol size. Mantle range of clinopyroxene (5.57 ± 0.32 ‰) from Mattey et al. (1994) and Ionov et al. (1994). Java clinopyroxene $\delta^{18}O$ data: Galunggung (Harmon and Gerbe, 1992); Banda arc (Vroon et al., 2001); IVC and Salak (this study).

lie within the range of both clinopyroxene and olivine $\delta^{18}O$ values reported for the Banda arc (+5.18 to +7.04‰ and +4.92 to +5.59‰ respectively, Vroon et al., 2001). Plagioclase $\delta^{18}O$ values of Gede are generally higher than those of Galunggung (+5.6 to +6.0‰, Harmon and Gerbe, 1992), but lower than those analysed in Merapi volcanics (+6.5 to +7.0‰, Gertisser and Keller, 2003). $\delta^{18}O$ values do not appear to show significant distinctions between different eruptive centres.

4.6. Discussion

4.6.1. Differentiation of magma

Very few arc magmas ascend the arc lithosphere and escape some degree of chemical modification via processes of differentiation (Davidson, 1996; Davidson et al., 2005). The importance of differentiation processes in controlling geochemical trends, has been highlighted in many studies of arc volcanoes worldwide: New Zealand (Gamble et al., 1999; Price et al., 1999; Donoghue et al., 1995), The Andes (Davidson et al., 1987; Hildreth and Moorbath, 1988; Davidson and Harmon, 1989), North and Central America (Tepley et al., 1999; Tepley et al., 2000), Lesser Antilles (Defant et al., 2001) and also in magmatic evolution at the Sunda arc (Gerbe et al., 1992; Vukadinovic and Sutaidjaja, 1995; Turner et al., 2003; Reubi and Nicholls, 2004). Therefore elucidating composition-modifying processes in arc lavas is an essential step, before the nature, composition and components of the source can be determined. Among the variety of processes capable of obscuring compositions of primary magmas, fractional crystallisation, magma mixing and crustal contamination and are commonly identified in arc lavas.

The predominance of basaltic andesites and low MgO contents in basalts of the GVC indicate that lavas erupted within the complex are highly differentiated. Correlations of various major and trace elements with indices of differentiation in GVC lavas (Figs. 4.8 and 4.9), suggest that shallow level differentiation processes may control the concentrations of some elements.

4.6.1.1. Fractional crystallisation

Fractional crystallisation is commonly identified in arc studies as an important process controlling major and trace element compositions of arc lavas (Grove et al., 2005; Gerbe et al., 1992; Turner et al., 2003). Most major element trends at GVC (Figs. 4.8a-f), are similar to

those displayed by other magmatic suites from Java, consistent with the removal of a typical island-arc mineral assemblage of plagioclase, clinopyroxene, Fe-Ti oxide and olivine/orthopyroxene, consequently indicating that fractional crystallisation may be responsible for the element variations observed in CVG rocks. These qualitative observations will now be tested quantitatively by major and trace element modelling. GVC includes several large volcanic centres, therefore the aims of modelling are 2 fold:

1. To determine whether fractional crystallisation can explain major element variation within each eruptive series.
2. To establish whether the eruptive series of Gede volcano (Young Gede Kawah Ratu, Young Gede Other Vents and Old Gede) may be related by the process of fractional crystallisation and therefore be linked genetically.

Least squares modelling of GVC major element data utilises the XLFRAC programme of Stormer and Nicholls (1978). This technique, the mineral phase considerations made and parameters on model success are the same as those outlined in Chapters 2 and 3. Summaries of least squares modelling results are given in Table 4.1.

Models 1-11 in Table 4.1 show that fractionation modelling between the least evolved (lowest SiO_2) and most evolved (highest SiO_2) rocks within each eruptive group yield good to excellent results, with Σr^2 values less than or equal to 0.1. Modelling suggests that within-group major element variation can be explained by the fractional crystallisation of plagioclase, clinopyroxene, Fe-Ti oxide, plus olivine or orthopyroxene from the most basic end-members in each eruptive group with a maximum degree of crystallisation of 50% (model 10). However, model 9, between basic and evolved members of the Young Gede Other Centres group, indicates the addition of ~8.5% plagioclase is required along with fractionation of clinopyroxene, orthopyroxene and oxide.

Table 4.1. Results of least squares major element modelling

Model	Parent		Daughter		SiO_2 range	Σr^2	Plag	Cpx	Ol	Opx	Ox	%C
1	G29	GEG	G28	GEG	52-54	0.07	26.1	1.51		9	2.23	39
2	G29	GEG	G32	GEG	52-54	0.09	23.8	3.46		9.2	2.45	39
3	G35	PAN	G31	PAN	51-56	0.07	26	7.79	8.05		3.61	45
4	G35	PAN	G24	PAN	51-55	0.10	31.7	5.42	6.47		2.95	47
5	G48	OG	G17	OG	55-61	0.09	25.9	0.57		8.34	3.34	38
6	G48	OG	G15	OG	55-60	0.05	14.9	2.96		9.89	3.54	31
7	G20	YGOV	G18	YGOV	54-59	0.03	8.79	1.27		6.74	3.01	20
8	G36A	YGOV	G18	YGOV	55-59	0.06	15.7	4.2		2.83	1.94	25
9	G20	YGOV	G19	YGOV	54-55	0.10	**8.56**	3.37		5.17	1.15	1
10	G23	YGKR	G39	YGKR	53-62	0.08	33.3	8.1	5.16		3.89	50
11	G23	YGKR	G22	YGKR	53-60	0.06	29.7	5.8	4.75		3.12	43
12	G48	OG	G39	YGKR	55-62	0.03	27.6	**0.47**		9.15	3.66	40
13	G48	OG	G18	YGOV	55-59	0.03	20.3	**2.63**		7.73	2.89	28
14	G23	YGKR	G15	OG	53-60	0.06	22.6	11.1	5.4		3.95	43

SiO_2 range in wt %
C% = degree of crystallisation
Plag, plagioclase; Cpx, clinopyroxene; Ol, olivine; Opx, orthopyroxene; Ox, Fe-Ti oxide.
GEG, Gegerbentang; PAN, Pangrango; OG, Old Gede; YGO, Young Gede Other Vents; YGKR, Young Gede Kawah Ratu
Bold font indicates the addition rather than removal of a particular phase

The second objective of least squares modelling is to find out if major element variation between Gede sub-units may be explained through crystal fractionation. Models 12-14 show that excellent Σr^2 values of <0.06 are obtained, especially in models using the most basic Old Gede sample as parent to the most evolved Young Gede Kawah Ratu and Other Centre lavas (models 12 & 13, Σr^2 = 0.03). However, both of these models require the addition, rather than removal, of a small percentage of clinopyroxene.

The concentrations of many trace elements e.g. Ba, La, Zr, Nb in GVC rocks also correlate with SiO_2 (Fig. 4.9), further suggesting that variations of these elements may be controlled by fractional crystallisation. Utilising the phase proportions and degree of crystallisation predicted from major element modelling (Table 4.1) it is possible to test the conclusions of least squares analysis through forward modelling of trace element

concentrations. If data variations are consistent with a model of fractional crystallisation, trace element modelling should be able to produce calculated values comparable to the trace element concentrations observed in the daughter rocks. The Rayleigh fractionation equation, $C_l = C_o F^{(D-1)}$, has been employed to address this: where C_l and C_o represent the concentration of an element in the daughter and parental liquids respectively, F is the fraction of liquid remaining and D is the bulk distribution coefficient. The distribution coefficients used in modelling are given in Appendix F. The results of selected trace element models are shown in Table 4.2 and the difference between calculated and measured concentrations are plotted in Fig. 4.14. If the degree of crystallisation and the phase proportions determined by major element modelling are accurate, the data will have normalised values close to 1. The majority

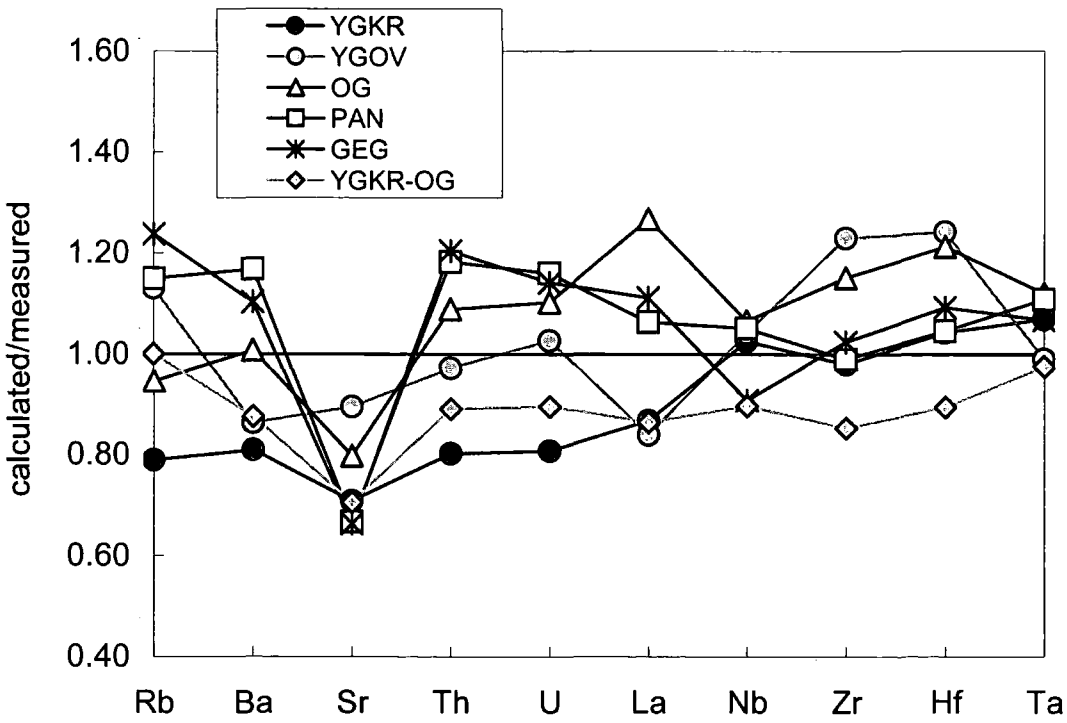

Fig. 4.14. Comparison of trace element concentrations determined by forward modelling (using the Rayleigh fractionation equation, $C_l = C_o F^{(D-1)}$) with those measured in the rocks. Mineral phases, abundances and degree of crystallisation used in modelling are those predicted by major element least squares modelling (Table 4.1). The closer the data lie to 1 the smaller the discrepancy between modelled and measured compositions. For acronym definitions see Table 4.1.

Table 4.2. Results of trace element fractional crystallisation modelling

Model no.	1	3	5	7	10	14
Parent	G29	G35	G48	G20	G23	G23
Daughter	G28	G31	G17	G18	G39	G15
centre model	GEG	PAN	OG	YGOV	YGKR	YGKR-OG
Σr^2	0.07	0.07	0.09	0.03	0.08	0.06
F=	61.21	54.55	61.86	80.19	49.59	56.89
			Calculated concentrations (ppm)			
Rb	48	52	55	70	61	54
Ba	234	246	318	270	295	278
Sr	280	245	253	270	219	288
Th	4.99	5.48	6.79	6.42	6.49	5.75
U	1.16	1.26	1.53	1.54	1.47	1.31
La	19	15	21	13	18	16
Nb	6.34	5.81	6.29	5.13	5.71	5.22
Zr	128	137	163	144	143	127
Hf	3.58	3.85	4.50	3.98	4.00	3.50
Ta	0.46	0.44	0.49	0.40	0.48	0.42
			Measured concentrations (ppm)			
Rb	39	45	59	62	77	54
Ba	212	210	315	313	364	317
Sr	422	367	317	302	309	407
Th	4.14	4.64	6.24	6.61	8.10	6.46
U	1.01	1.09	1.39	1.50	1.82	1.46
La	17	14	17	16	20	18
Nb	6.98	5.52	5.90	4.92	5.57	5.82
Zr	125	138	142	117	146	149
Hf	3.28	3.68	3.71	3.21	3.84	3.91
Ta	0.43	0.40	0.44	0.40	0.45	0.43

Daughter compositions calculated by forward modelling of parent using $C_l = C_o.F^{(D-1)}$. Σr^2, phase proportions and degree of fractionation (F) are those suggested by least squares modelling (Table 4.1).
Model no. refers to Least Squares Models (Table 4.1).

of calculated GVC trace element concentrations lie within ~20% of the measured concentrations in daughter samples. Calculated Sr concentrations are consistently lower in all models than those actually measured, leading to calculated/measured values of less than one (Fig. 4.14). This suggests that the (basaltic-dacitic system) distribution coefficient used for Sr (2.5) may be too high, or the calculated values are too low possibly due to accumulation in the daughter samples of a Sr bearing phase, e.g. plagioclase. Both of these suggestions are

plausible: using a lower Sr distribution coefficient value of 1.83 (reported for basalts-basaltic andesites rather than basalts-dacties, Rollinson, 1993) the calculated values lie within 5-12% of the measured Sr concentrations (calculated/measured = 0.88-1.05). In addition, least squares modelling suggests that CaO and Al_2O_3 variations between parent and daughter rocks are consistent with the removal of a fractionating mineral assemblage containing plagioclase. However, magmatic disequilibrium is suggested by the textures observed in plagioclase phenocrysts within all GVC rocks (section 4.4.2.1, e.g. Fig. 4.2a) and by the range in plagioclase core compositions of similarly sized phenocrysts in some samples (Fig. 4.4), e.g. mixing, therefore it is not possible to discount this on the basis of least squares modelling.

In summary, GVC major and trace element data are largely consistent with magmatic evolution by fractional crystallisation within each eruptive group. Fractionation models between Old and Young Gede samples, require the addition rather than removal of clinopyroxene to produce acceptable Σr^2 values, suggesting that the volcanic products of the two centres may not be genetically related through simple crystal fractionation. This is also suggested by the abundant evidence for magmatic disequilibrium and mingling in the petrography and mineralogy of these rocks (section 4.4). Therefore, we will now investigate whether mixing may better explain element variation in GVC rocks, and the Gede volcano groups in particular.

4.6.1.2. Magma mixing

Petrographic features in GVC rocks, such as oscillatory zoning, sieve textured and resorbed cores in plagioclase phenocrysts and mantling of orthopyroxene by clinopyroxene, along with evidence of magma mingling in magmatic fragments, indicates that closed system crystal fractionation may be an over-simplistic model for magmatic evolution at GVC. Correlations of major and trace elements with silica may also be explained by mixing. Mixing processes

are important in the evolution of many arc magmas (e.g. George et al., 2004; Tepley et al., 2000), in magmatic evolution at volcanoes of the Sunda arc (Slamet, Reubi et al., 2003; Batur, Reubi and Nicholls, 2004; Krakatau, Mandeville et al., 1996; Merapi, Camus et al., 2000) and in the adjacent Banda arc (Vroon, 1992). There is unequivocal evidence for the interaction of distinct magmas at GVC (Fig. 4.7) and therefore a distinct possibility that magma mixing processes may play a role in controlling the geochemistry of GVC rocks, particularly in the formation of Young Gede and Old Gede volcanic rocks, which contain the most evidence for magmatic mingling and disequilibrium (section 4.4.4). The question then arises whether or not magma mixing can impart a recognisable influence upon element concentrations in GVC lavas?

Sr concentrations predicted by Rayleigh fractionation models (Table 4.2) are consistently lower than those measured in the actual rocks (Fig. 4.14). One explanation for this involves plagioclase accumulation, which may have occurred as a result of mixing. To test whether variations in Sr concentration of GVC rocks are consistent with mixing, $^{87}Sr/^{86}Sr$ isotope ratios of GVC rocks are plotted against 1/Sr (Fig. 4.15a). Mixing is controlled by the concentration of the denominator in the ratio (i.e. Sr concentration), therefore plots of this type (A/B versus 1/B) provide a simple check to see if data are consistent with binary mixing, as data should form a linear array (Vogel, 1982; Langmuir et al., 1978), cf. plots of element versus ratio (A/B versus B) in which mixing would generate hyperbolic data arrays. Fig. 4.15a shows that the GVC data are generally scattered and therefore largely inconsistent with simple mixing processes. The low Sr concentrations predicted by fractional crystallisation modelling may therefore be a consequence of the slightly high basalt-andesite distribution coefficient used (2.5) and in which case the basalt-basaltic andesite coefficient of ~1.8 (above) may be more appropriate.

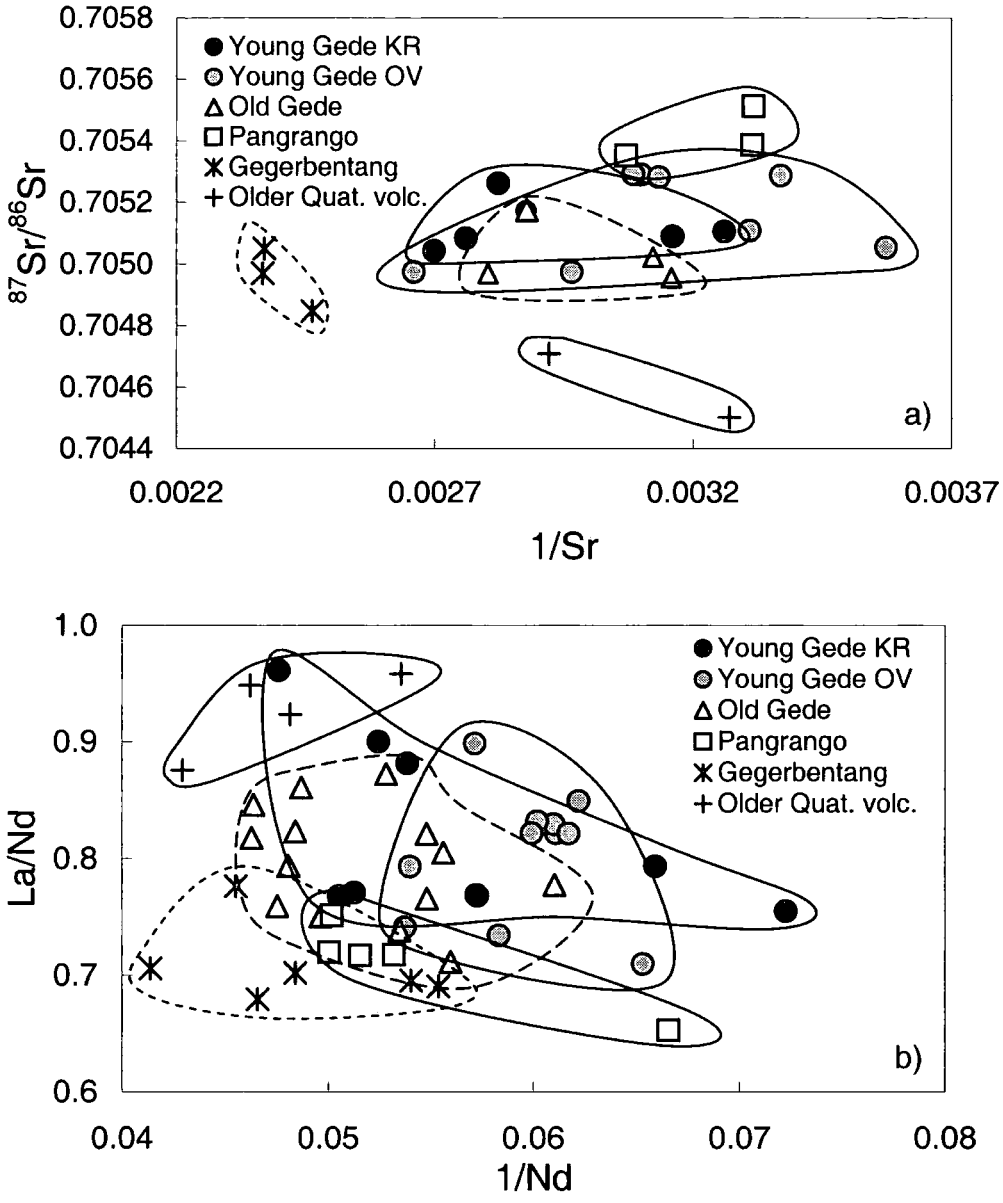

Fig. 4.15. a) $^{87}Sr/^{86}Sr$ -1/Sr and b) La/Nd-1/Nd showing that the GVC data are not consistent with simple binary mixing.

It was noted earlier that the LREE-MREE (La-Nd) concentrations of most GVC rocks lie parallel to each other on chondrite normalised REE diagrams within each eruptive group (Fig. 4.10), and this is especially notable in the Young Gede Kawah Ratu group (Fig. 4.10a). Parallel REE patterns are more consistent with evolution through fractional crystallisation or magma mixing as opposed to variation in the melting regime of the source region within each GVC group. La and Nd concentrations increase with differentiation therefore, using the

approach above, a plot of La/Nd versus 1/Nd should indicate whether or not the systematic variation in LREE-MREE is consistent with mixing (in which case data should lie on a straight line). Fig. 4.15b shows poor linearity within each eruptive group and within the GVC as a whole, and therefore LREE-MREE variations with silica are unlikely to be created a result of simple binary mixing.

The relatively evolved compositions of both the light and dark layers in banded magmatic fragments (56 wt% and 59 wt% SiO_2 respectively) also suggest that simple binary mixing, at least of these components, is an unrealistic model for explaining the geochemical variation observed within each group. Mixing between these two components would be unable to account for rock compositions with SiO_2 contents <56 or >59 wt%. Furthermore, distinct plagioclase core compositions (Fig 4d) are observed in similar sized phenocrysts within the dark, more basic component (G11) of the mingled rocks, indicating that the parental magma to the basic lava may have experienced mingling and mixing with other magma prior to the clear evidence for magma mingling observed in G13.

In summary, correlations of major and trace elements with indices of differentiation (e.g. SiO_2) are not consistent with simple magma mixing processes, and are most likely controlled by fractional crystallisation. However, petrographic analysis of the rocks suggests that simple closed-system fractional crystallisation is also unrealistic and not consistent with the multitude of disequilibrium textures observed in the rocks. It is, therefore, proposed that fractional crystallisation provides the principle control on major and trace element variations in GVC rocks, however magma mixing and mingling processes may play a minor role during magmatic evolution. This conclusion is similar to that reached by Gerbe et al. (1992) for magmatic differentiation at Galunggung Volcano in West Java.

4.6.1.3. Crustal contamination

There is widespread evidence from island arcs (Thirlwall and Graham, 1984; Davidson et al. 1987; Ellam and Harmon, 1990; Thirlwall et al., 1996; Macpherson et al., 1998) for the contamination of primary magmas by the arc crust. Contamination is also thought to be an important process in the western Sunda arc (Gasparon et al., 1994; Gasparon and Varne, 1998), and responsible for modifying isotope ratios of lavas at Sangeang Api volcano in the east Sunda arc (Turner et al., 2003). The relatively wide range in radiogenic isotope ratios of volcanic rocks from the GVC suggests that this variation could be the result of the assimilation of arc crust. Therefore, prior to characterising source components in GVC rocks it is important to assess the role, if any, of crustal contamination.

Differentiation of magma to intermediate and silicic compositions takes place primarily in the crust (Davidson et. al., 2005). Incorporation of crustal material during crustal differentiation may generate correlations of isotope ratios with indices of differentiation (e.g. SiO_2, Rb). Investigations and discussions of the contamination of arc lavas by crustal material commonly consider such correlations (Gertisser and Keller, 2003; Elburg et al., 2002, 2005; Peccerillo et al., 2004; Gamble et al. 1999; Davidson et al., 1991, 2005; Graham and Hackett, 1987). However this approach assumes that a contaminant will have an isotopic composition distinct from that of the magmas ascending from the mantle. Relatively little is known about the composition of the arc crust in West Java. It is hypothesised that West Java (Figs. 1.1a and 1.2, Chapter 1) is built upon pre-Tertiary, continental-type basement (Hutchinson, 1989; Metcalfe, 1996; Soeria-Atmadja et al., 1998; Hoffmann-Rothe et al., 2001). Hamilton (1979) suggests that the crust in West Java may consist of relatively immature continental crust, ophiolite slivers, and older volcanic rocks, and therefore, crustal contamination involving these materials may be more difficult to detect. Continental-type crustal xenoliths have not been discovered in any GVC units, only clasts of igneous origin are observed (section 4.4.3),

further confirming the difficulty of identifying 'crustal' contributions in some arc lavas. Figs. 4.16a-d, show that there are no clear correlations between Sr, Nd, Hf and O isotope ratios and SiO_2 within the individual eruptive groups. The Young Gede Other Vent samples, display a broad range in Sr isotope ratios over a fairly small range (~2%) in silica. There is a slight correlation observed in the data set as a whole: the most evolved samples (Older Quaternary) possess the most primitive radiogenic isotope compositions (no $\delta^{18}O$ data available), and the least evolved rocks (Pangrango) display the least primitive isotopic compositions (Figs. 4.16a-c), although $\delta^{18}O$ values of Pangrango rocks are not particularly elevated compared to the rest of the GVC lavas (Fig. 4.16d). The weak correlations are the reverse trends of those expected by the assimilation of continental crust during fractional crystallisation (AFC, DePaolo 1981), which typically generate positive correlations between $^{87}Sr/^{86}Sr$ ratios and SiO_2, like those observed in the Lesser Antilles (Davidson, 1987). It is similar however, to the trend observed in Alicudi lavas in Italy (Peccerillo et al., 2004) where the most mafic magmas display the most 'contaminated' isotope signatures due to the higher temperature and lower viscosity of basalts, relative to differentiates, which are therefore capable of assimilating more crust. The isotopic variation observed could also, however, be a result of isotopic heterogeneity of the source. To help address the issue of crustal versus source contamination $\delta^{18}O$ and $^{87}Sr/^{86}Sr$ isotope data can be utilised.

A large contrast exists between the low $\delta^{18}O$ values of the mantle (+5.57 ± 0.32‰, Mattey et al., 1994; Ionov et al., 1994) and the generally high and variable $\delta^{18}O$ values (often > +10‰, Davidson, 1989) of upper crustal materials, due to low temperature interaction with H_2O in the latter. Therefore, the combination of oxygen and radiogenic isotope ratios e.g. $^{87}Sr/^{86}Sr$, can help diagnose involvement of the crust in magma genesis (James, 1981; Davidson et. al, 2005). The inset diagram of Fig. 4.17a shows the different curvatures expected for crustal contamination (mixing crust with basalt during magma evolution) and

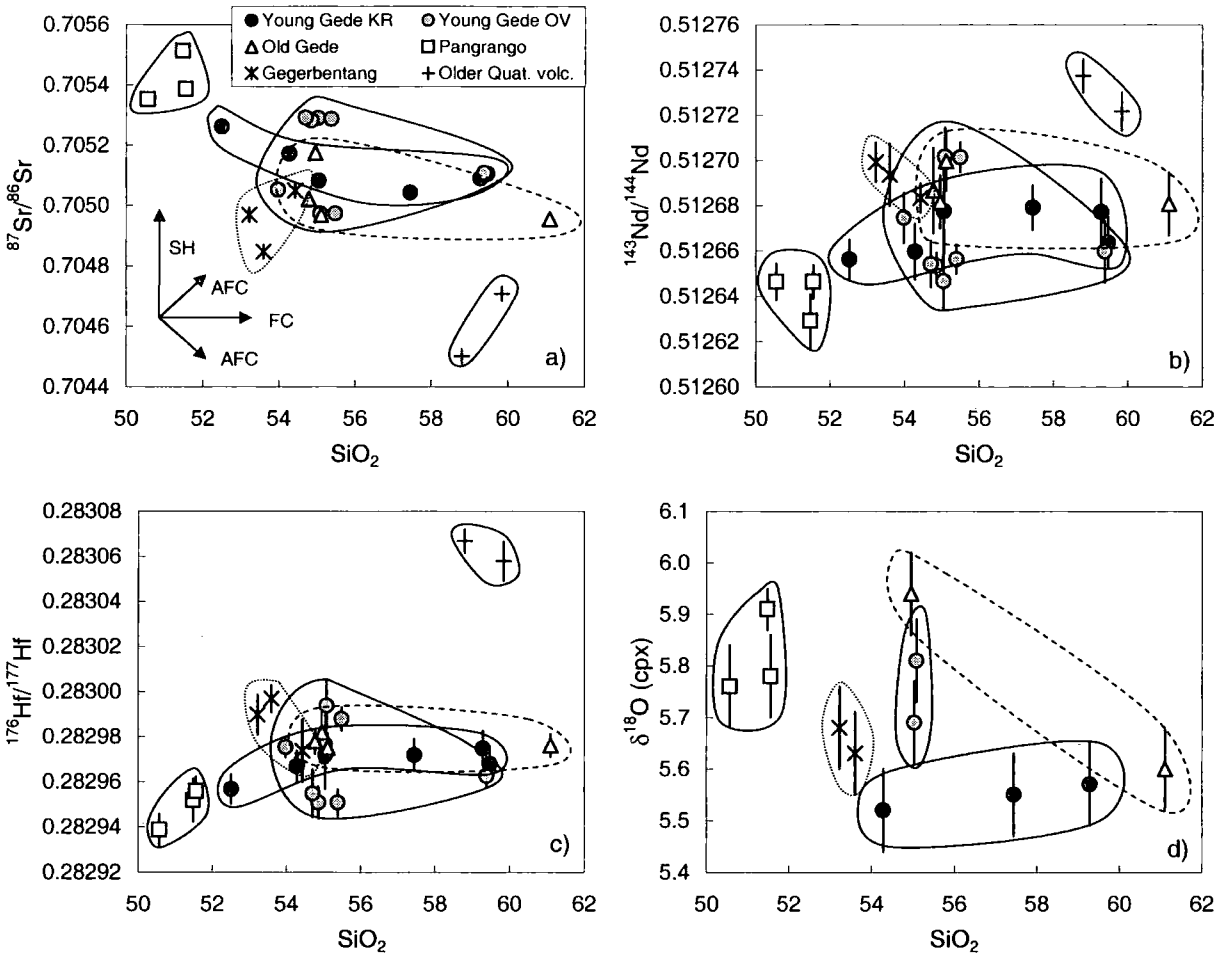

Fig. 4.16. Variation of Sr-Nd-Hf-O isotope ratios (a-d respectively) with SiO_2 for GVC rocks. Arrows labelled SH, AFC and FC indicate the hypothesised data trends related to: heterogeneity in the mantle source (SH), combined assimilation and fractional crystallisation (AFC) and fractional crystallisation (FC). 2σ (a-c) and 1σ(d) error bars plotted as in Figs. 4.11, 4.12 and 4.13.

source contamination (mixing sediment into a mantle source prior to production of primary basalt, Davidson et al., 2005) that result from the significant difference in Sr/O ratios of mantle and mantle-derived basalt. The GVC data are displaced from mantle values towards higher $^{87}Sr/^{86}Sr$ isotope ratios, but clinopyroxene $\delta^{18}O$ values of GVC lavas are relatively homogeneous (+5.52 to +5.94‰), and low, lying in the region of mantle values (Fig. 4.17b). The GVC data generally lie along a mixing curve representing contamination of the mantle source by a high $\delta^{18}O$, high $^{87}Sr/^{86}Sr$ component, in this case sediment (see figure caption for

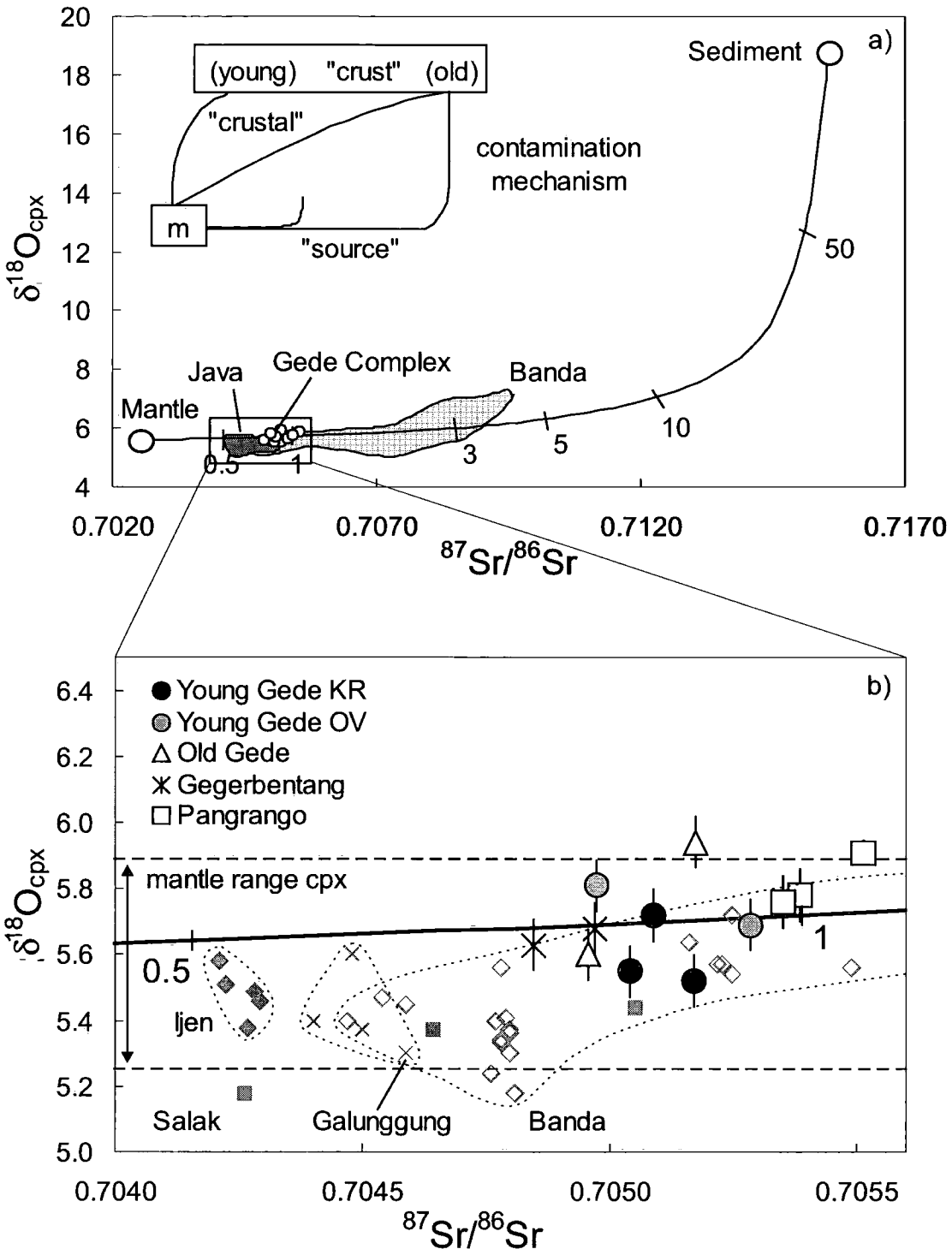

Fig. 4.17. a) Plot of $\delta^{18}O$ (clinopyroxene) versus $^{87}Sr/^{86}Sr$ (bulk rock) for GVC lavas. A simple mixing curve is plotted between sediment and depleted mantle source to illustrate that GVC lavas are consistent with 'source contamination' (fractionation between magma and clinopyroxene is insignificant on this scale). Tick marks indicate the amount of sediment added to the mantle source. Data used in mixing calculation: Bulk sediment Sr = 450 ppm; O = 50.2 wt %, $^{87}Sr/^{86}Sr = 0.7156$; $\delta^{18}O = 18.7‰$ (Vroon et al., 2001). Depleted mantle source: Sr = 12.94 ppm; O = 43.8 wt %, $^{87}Sr/^{86}Sr = 0.7026$ (Vroon et al., 2001 and references therein); $\delta^{18}O = 5.57‰$ (Mattey et al., 1994; Ionov et al., 1994). For Java and Banda data

sources see below. Inset diagram shows the expected data trends for 'crustal' versus 'source' contamination. b) Enlargement of boxed section in a), showing within-group $\delta^{18}O$ and $^{87}Sr/^{86}Sr$ relationships. GVC data are consistent with a small percentage of sediment addition in the mantle source (solid black line). Mantle range of clinopyroxene (dashed black lines, 5.57 ± 0.32 ‰) from Mattey et al. (1994) and Ionov et al. (1994). Java clinopyroxene $\delta^{18}O$ data: Galunggung (Harmon and Gerbe, 1992); Banda arc (Vroon et al., 2001); Ijen and Salak (this study). Error bars are ± 1σ of replicate analysis or ±0.04‰ and ±0.09‰ for olivine and clinopyroxene respectively where replicate analyses were not carried out. 2σ $^{87}Sr/^{86}Sr$ external error bars are plotted; in most cases they are smaller than the symbol size.

end member compositions). It is therefore unlikely that the lavas have been contaminated by upper crustal, continental material. Ophiolite material, i.e. oceanic crust, displays a wide range in oxygen isotope ratios due to interaction between basaltic rocks and seawater over a wide range of temperatures (Muehlenbachs, 1986). Therefore, if interaction with oceanic basement had been a significant process at GVC we may predict greater scatter in $\delta^{18}O$ values. Similarly, a wide range of oxygen isotope ratios may develop in the mafic to intermediate edifices and roots of Sunda arc magmatism that pre-dates GVC.

In summary, mantle-like clinopyroxene $\delta^{18}O$ values of GVC lavas suggest negligible input of high $\delta^{18}O$ crustal rocks during differentiation. This conclusion is similar to those reached in studies of other Sunda arc volcanoes (Elburg et al., 2002; Gerbe et al., 1992; Gertisser and Keller, 2003). Therefore fractional crystallisation is thought to be the most important differentiation process responsible for modifications to primary magmatic geochemical composition. Magma mingling and mixing processes are evident in the volcanic rocks, however these processes are thought to play a minor role in geochemical modification of differentiating magma. Most variation in radiogenic isotope ratios of GVC lavas are therefore proposed to arise from variations in source compositions/components.

4.6.2. Source compositions

The discussion above concludes that involvement of the arc lithosphere in magma genesis at GVC has little, if any, impact on the chemical composition of lavas erupted and presents a case for the contribution of a crustal component to the source region (mantle wedge), most likely as a contribution from the subducting slab. Source contamination is envisaged in the petrogenesis of many other arc lavas worldwide (Ellam and Hawkesworth, 1988; Thirlwall et al., 1996; Elliot et al., 1997) and specifically at the Sunda arc (Stolz et al., 1990; Turner and Foden, 2001; Gertisser and Keller, 2003). The following discussion will focus on elucidating the nature of this component. However, it is first necessary to characterise the nature of the GVC mantle source, in order to obtain a geochemical baseline upon which the impact from addition of such a component can be identified.

4.6.2.1. Pre-subduction composition of the mantle wedge

The majority of island arc magmas are thought to originate in the mantle wedge (Ringwood, 1974; Ellam and Hawkesworth, 1988; McCulloch and Gamble, 1991), which is inferred by several authors to be similar to the source of MORB (Gamble et al., 1996; Woodhead et al., 1993; Davidson, 1987; Turner et al., 2003). It has been proposed that there may be contribution from an enriched mantle component (OIB source) in some Sunda arc lavas (Wheller et al., 1987; Edwards et al., 1991, 1993; Van Bergen et al., 1992), although a MORB-like mantle source is advocated for the Sunda arc by others (e.g. White and Patchett, 1984; Turner and Foden, 2001; Elburg et al., 2002). Helium isotope values of olivine crystals in mantle xenoliths and island arc volcanics have also implicated a MORB-like mantle source in the western Sunda arc (Gasparon et al., 1994; Hilton and Craig, 1989).

Based primarily on HREE and HFSE data, and further discussion, it was proposed that mantle wedge composition is best represented by an Indian MORB source beneath Ijen Volcanic Complex in East Java (Chapter 2). Fig. 4.18 shows variation of HFSE (Zr/Nb and Ta/Nb) and HREE (Dy/Yb) ratios with SiO_2 in the GVC. These elements are thought to remain relatively immobile during slab dehydration compared to LILE and LREE (You et al., 1996; Tatsumi et al., 1986; Brenan et al., 1995; Kessel et al., 2005). The HFSE and the HREE in particular (Kessel et al., 2005), may therefore help ascertain the pre-subduction composition of the mantle wedge and indicate the degree of homogeneity of the source of GVC magmatism. If eruptive units share the same source then they should possess similar ratios of the relatively immobile trace elements. Zr/Nb, Ta/Nb and Dy/Yb ratios of GVC rocks vary little with differentiation and are relatively homogeneous, with the exception of Gegerbentang (Figs. 4.18a and b). These ratios closely resemble those of I-MORB rather than N-MORB. Zr/Nb and Dy/Yb of GVC rocks are significantly higher and lower than the respective ratios of OIB (Figs. 18a and c). Gegerbentang volcanic rocks display somewhat lower Zr/Nb and Ta/Nb compared to the other GVC groups, although Dy/Yb ratios are indistinguishable. Recent experimental work by Kessel et al. (2005) suggests that the HREE elements, Y and Sc are the least mobile in either fluids or melts generated from the slab (eclogite) at temperatures (700-1200°C) and pressures (4-6GPa) equivalent to 120-180 km depth. Therefore, identical Dy/Yb (HREE) ratios, similar REE patterns (Fig. 4.10) and overlapping radiogenic isotope ratios (Fig. 4.16) of Gegerbentang rocks compared to other GVC rocks, suggests that the magmatic source of Gegerbentang lavas is comparable to the source of other GVC lavas, which are relatively homogeneous indicated by HFSE and HREE ratios.

HFSE and HREE concentrations and ratios of GVC lavas also indicate that the mantle wedge is not significantly depleted beneath GVC, in contrast to volcanoes of other arcs such

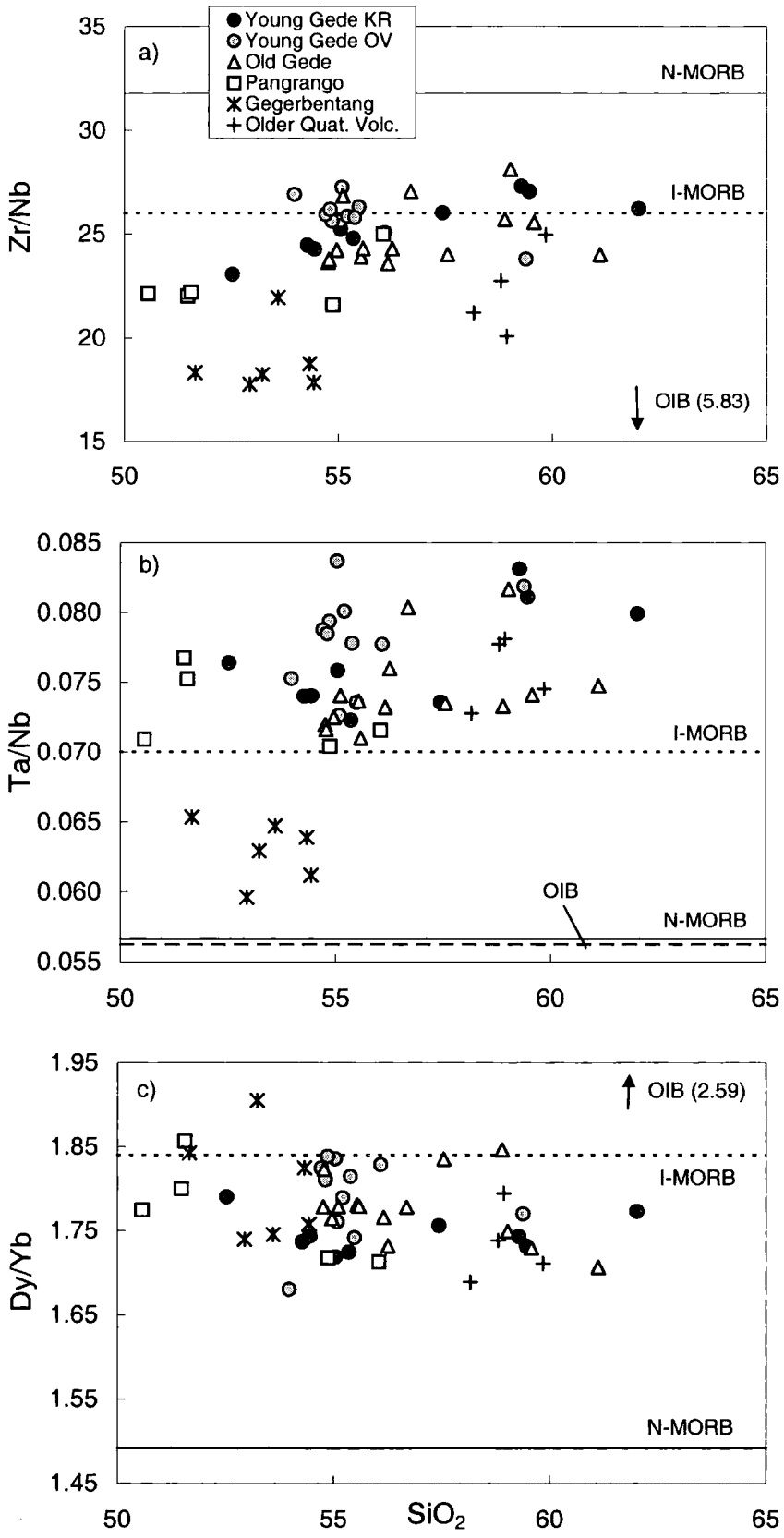

Fig. 4.18. a) Zr/Nb, b) Ta/Nb and c) Dy/Yb variation with SiO_2 for GVC rocks. N-MORB and OIB data from Sun and McDonough (1989). Indian MORB from Chauvel and Blichert-Toft, 2001.

as the Izu-Bonin and Marianas (Fig. 4.10), where mantle sources are thought to have experienced melt extraction prior to involvement in arc petrogenesis (Taylor and Nesbitt, 1998; Elliot et al., 1997; Woodhead et al., 1993).

It is proposed therefore, that the mantle wedge beneath GVC in West Java is similar to the source of I-MORB; comparable with conclusions reached for IVC in East Java (Chapter 2), and concurs with other petrogenetic studies of Javan volcanic rocks utilising Pb isotopic and trace element ratios in SE Asia throughout the Cenozoic (Taylor et al. 1994; Hickey-Vargas, 1998; Macpherson and Hall, 2001 & 2002; Elburg, et al., 2002; Macpherson et al. 2003).

4.6.2.2. Sediment contribution to the source

Contributions of subducted sediment to the mantle source of island arc volcanic rocks is implicated in many arc petrogenetic studies, based on displacement of lava Sr-Nd-Hf isotope ratios from depleted mantle fields (i.e. MORB) and elevations of some trace element ratios (e.g. Th/Ce, Ce/Pb, Th/Nb) in arc lavas compared to MORB (White and Patchett, 1984; White and Dupré, 1986; Ben Othman et al., 1989; Vroon, 1992; Elliot et al., 1997; Hawkesworth et al., 1997; Gertisser and Keller, 2003). Unequivocal evidence for sediment contribution in arc sources is provided by ^{10}Be studies (Tera, et al., 1986; Leeman et al., 1994). Low Ce/Pb and high Th/Nb and Th/Ce average ratios (Ce/Pb = 3.3, Th/Nb = 1.1, Th/Ce = 0.17) in GVC rocks relative to I-MORB (Ce/Pb = 15, Th/Nb = 0.08, Th/Ce = 0.03; Chauvel and Blichert-Toft, 2001) provide evidence for the introduction of sedimentary material into the mantle source of GVC magmas. However, the importance of fluids created during dehydration of the down-going altered oceanic crust is also highlighted by several authors e.g. Tatsumi et al. (1986); Turner et al. (1997), and for Ijen Volcanic Complex (Chapter 2), in contributing to the shift of arc rock radiogenic isotopes from the depleted

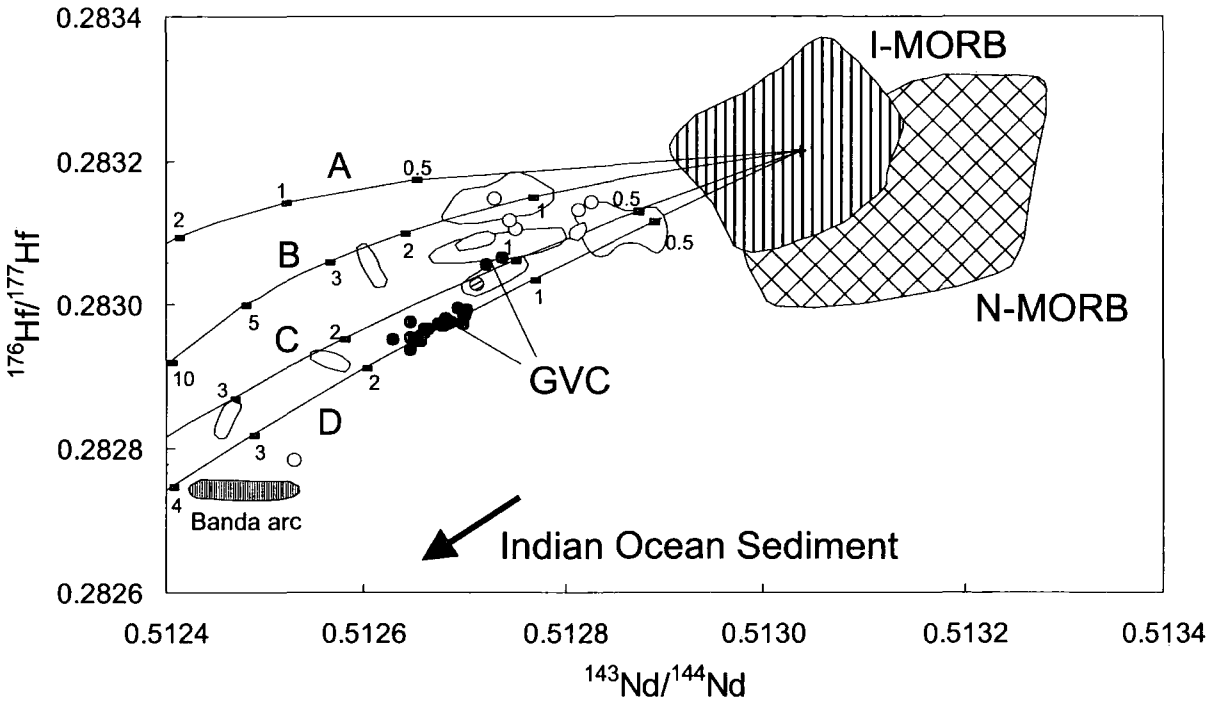

Fig. 4.19. $^{176}Hf/^{177}Hf$-$^{143}Nd/^{144}Nd$ plot showing bulk mixing models between I-MORB source and Indian Ocean sediments: A = Mn nodule (V34-62, White et al., 1986; Ben Othman et al., 1989), B = pelagic sediment (V34-45 White et al., 1986; Ben Othman et al., 1989) C and D = terrigenous sediments V28-357-M (CA30-M) and V28-357-M (CA30-S) respectively (Vervoort et al., 1999). Data sources as in Fig. 4.12. Open fields = Javan volcanoes, as identified in Fig. 2.15b, Chapter 2. End member compositions given in Table 4.3.

Table 4.3. End-member compositions used in $^{143}Nd/^{144}Nd$ and $^{176}Hf/^{177}Hf$ mixing calculations

	Nd (ppm)	Hf (ppm)	$^{143}Nd/^{144}Nd$	$^{176}Hf/^{177}Hf$
I-MORB Source	0.97	0.25	0.513042	0.283211
Sediment A	187.9	5.73	0.512236	0.282828
Sediment B	55.26	3.67	0.512278	0.282712
Sediment C	35	5.09	0.51193	0.282311
Sediment D	31.3	5.58	0.51191	0.28223

Mantle wedge represented by I-MORB source (I-MORB/10 assuming 10% melting) I-MORB data from Chauvel and Blichert-Toft (2001).
Sediments: A = Mn nodule and B = pelagic clay, V34-45 (Nd conc. and isotope composition from Ben Othman et al., 1989; Hf conc. and isotope composition from White et al., 1984); C = deep sea turbidite, V28-357-M (CA30-M) and D = deep sea turbidite, V28-357-M (CA30-S) (Vervoort et al., 1999).

mantle domain. It is suggested in Chapter 2 that contamination of the mantle source by a fluid created during dehydration of the altered oceanic crust would largely be undetectable on plots of $^{143}Nd/^{144}Nd$ versus $^{176}Hf/^{177}Hf$. Displacement of GVC lavas from I-MORB $^{143}Nd/^{144}Nd$ and $^{176}Hf/^{177}Hf$ ratios can therefore, be quantatively modelled, to determine the sedimentary contribution to the mantle source from the subducting slab. Fig. 4.19. shows that bulk addition of between 1-2 % of local terrigenous Indian Ocean sediment (mixing curves C and D) to an I-MORB source (mixing end member compositions in Table 4.3) can explain the shift in Hf and Nd isotope ratios of GVC rocks from average I-MORB. Relatively less subducted sediment input is required to explain the isotopic characteristics of the Older Quaternary Volcanic rocks than the rest of GVC lavas.

Several geochemical studies of arc lavas conclude that sediment contributions from the slab are incorporated into the source region as a partial melt rather than through bulk sediment addition (e.g. Elliot et al., 1997; Vroon et al., 2001). Experimental determinations by Kessel et al. (2005) of trace element partitioning in hydrous melts from the slab (eclogite) at 1,000°C and 4GPa suggest that Hf and Nd partition coefficients are identical (~3) under these conditions. The authors suggest that their data can be equally applied to hydrous melts of pelitic and clastic metasediments. If Hf and Nd partition equally into partial melts of sediment, the elemental ratio of Hf and Nd will be almost the same as that in the bulk sediment composition and therefore mixing curves will be identical, although the calculated proportion of subducted sediment required would be slightly less. Therefore, 2% sediment addition to the mantle source of GVC lavas is proposed to represent the maximum amount of subducted sedimentary material involved.

Bulk mixing of sediment to an I-MORB source in $^{87}Sr/^{86}Sr$-$^{143}Nd/^{144}Nd$ isotope space (Fig. 4.20), is also consistent with addition of a similar amount (1-2.5%) of local Indian Ocean Sediment (see Table 4.4 for sediment compositions). The curvature of the GVC data is

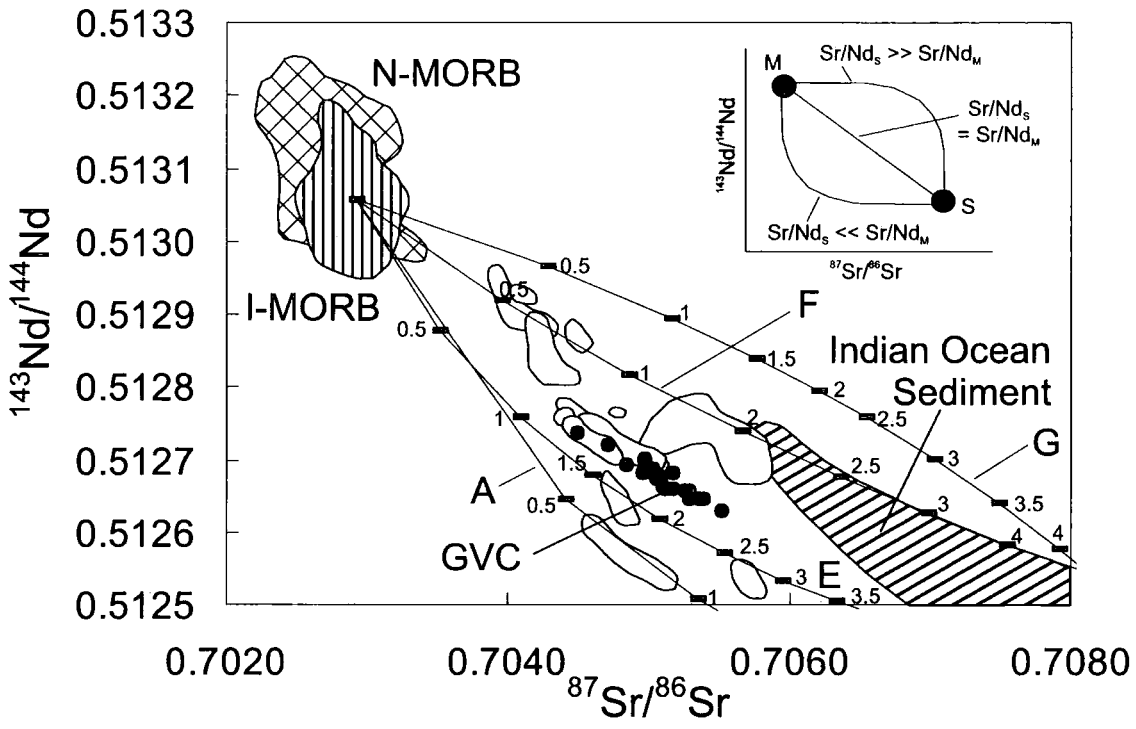

Fig. 4.20. $^{143}Nd/^{144}Nd$-$^{87}Sr/^{86}Sr$ diagram showing bulk mixing between I-MORB source (I-MORB*0.1, assuming 10% melting) and bulk sediment. Data sources of I-MORB, N-MORB and Indian Ocean sediment see Fig. 4.11. Sediment mixing curves: A = Mn nodule (Ben Othman et al., 1989); E = nanno ooze, DSDP site 211 (Gasparon and Varne, 1998); F = average Java sediment (Plank and Langmuir, 1998); G = terrigenous-biogenic, average of V33-75, -77, -79 (Gasparon and Varne, 1998; Ben Othman et al., 1989). Ticks along the mixing curves show the percent of sediment in the mixture. Open symbols = Javan volcanoes, as identified in Fig. 2.15a, Chapter 2. End member compositions used in the calculations are given in Table 4.4.

Table 4.4. End-member compositions used in $^{87}Sr/^{86}Sr$ and $^{143}Nd/^{144}Nd$ mixing calculations

	Sr (ppm)	Nd (ppm)	$^{87}Sr/^{86}Sr$	$^{143}Nd/^{144}Nd$
I-MORB Source	13.5	0.97	0.702915	0.513042
Sediment A	857	187.9	0.709117	0.512236
Sediment E	126	51.9	0.71643	0.512228
Sediment F	218	33.95	0.71682	0.51216
Sediment G	398.25	15.36	0.708875	0.512411

Mantle wedge represented by I-MORB source (I-MORB/10, assuming 10% melting). Data: I-MORB average Sr concentration from Price et al., 1986; Chauvel and Blichert-Toft, 2001; Rekhamper & Hofmann, 1997; I-MORB Nd concentration, Sr and Nd isotope data from Chauvel and Blichert-Toft, 2001. Sediments: A = Mn nodule (Ben Othman et al., 1989) E = nanno ooze (Gasparon and Varne, 1998) F = bulk Java sediment (Plank and Langmuir, 1998); D = terrigenous-biogenic average value of V33-75, -77, -79 (Ben Othman et al., 1989).

consistent with relatively low Sr/Nd ratios (inset Fig. 4.20), and therefore largely inconsistent with a major role of sediment-generated fluid (which would generate a convex-up curve that would not fit the data), further supporting the addition of sediment addition to the mantle wedge in the form of a partial melt or bulk contribution. However, this does not imply that slab fluids did not play any role in the formation of GVC arc magmas, just that they have a limited influence on isotopic signatures of the volcanic rocks (cf. IVC, Chapter 2). The calculated proportions of subducted sediment involved in magma genesis at GVC are similar to those proposed in other studies of Sunda arc volcanic rocks (Turner and Foden, 2001; Gertisser and Keller, 2003) and also at other arcs: Banda (Vroon, 1992), Izu-Bonin (Taylor and Nesbit, 1998), Lesser Antilles (White and Dupré, 1986) and Aleutian (McCulloch and Perfit, 1981).

4.7. Summary and conclusion

Open and closed system processes operate during magmatic evolution at GVC. Despite strong evidence for the interaction of distinct magmas at GVC (banded magmatic fragments, disequilibrium in plagioclase and pyroxene textures and compositions), particularly within volcanic rocks from Young and Old Gede units, evolution of whole rock major and trace element geochemistry within each eruptive series is generally consistent with fractional crystallisation of plagioclase, clinopyroxene, titanomagnetite accompanied by either olivine or orthopyroxene. Mingling and mixing processes may be an important eruption triggering mechanism at GVC but do not significantly modify bulk rock compositions.

Low, mantle-like clinopyroxene $\delta^{18}O$ values of GVC lavas suggest negligible input of high $\delta^{18}O$ crustal materials during magmatic differentiation. Poor correlations of radiogenic isotopes and indices of differentiation of GVC rocks preclude significant assimilation of continental-type crust beneath GVC. In contrast therefore, to conclusions reached by

Gasparon et al. (1994) for the western Sunda arc, it is not proposed for GVC that the Javan upper-crust is the dominant source responsible for the 'crustal' geochemical and isotopic signatures observed in GVC lavas. Instead, stable and radiogenic isotopes indicate that 'crustal' geochemical and isotopic characteristics arise in GVC rocks as a result of contamination of the mantle source. Mantle wedge contamination has also been proposed in studies of other Sunda arc volcanoes (Elburg et al., 2002; Gerbe et al., 1992; Gertisser and Keller, 2003).

The mantle wedge source for all GVC eruptive centres is relatively homogeneous, fertile (compared to arcs with associated back-arc spreading systems), and similar in composition to the source of I-MORB. Displacement of GVC radiogenic isotope ratios from the I-MORB domain towards less primitive ratios, combined with low Ce/Pb and high Th/Nb and Th/Ce average ratios in GVC rocks relative to I-MORB are consistent with the addition of a subducted sedimentary component. Less than 2.5% of subducted Indian-Ocean sediment (bulk or melt thereof) is required to shift Hf-Nd-Sr isotopic compositions from the I-MORB source to those exhibited in GVC volcanic rocks. The proposed magnitude of sediment contribution (a few percent) is similar to that suggested in other studies of Sunda arc volcanic rocks (Turner and Foden, 2001; Gertisser and Keller, 2003).

In conclusion, the geochemical analysis of volcanic rocks from GVC, provide no substantial evidence for the interaction of mature continental-type crust with magma beneath the complex. This implies that the relatively thick (compared to East Java) West Javan arc crust has not attained truly continental character yet and any deep-seated (shallow contamination is not consistent with O-isotope data) crustal contamination evades detection probably due to the similar geochemical characteristics shared by the crust and ascending magma. These conclusions are consistent with the geochemical characteristics of the crustal contaminant acting in AFC at neighbouring Salak (Chapter 3). However, this does not truly

rule out the possibility that continental-type material constitutes part of the crust beneath all of West Java, just that it is not required to explain the geochemical variation observed in GVC lavas, and volcanic rocks of other West Javan arc-front volcanoes.

Chapter 5

Geochemical and Sr-Nd-Hf-O isotopic constraints on the genesis of Sunda arc lavas: evidence for along-arc subduction input heterogeneity and structural transition in the arc crust

Geochemical and Sr-Nd-Hf-O isotopic constraints on the genesis of Sunda arc lavas: evidence for along-arc subduction input heterogeneity and structural transition in the arc crust

5.1. Extricating crustal from slab contributions in Sunda arc lavas: an introduction to the problem

Understanding the genesis of volcanic rocks in subduction zone settings is complicated due to the multitude of differentiation processes and source components that exert control on lava geochemistry. Enrichment in LILE and LREE cf. HFSE and HREE (Hildreth and Moorbath, 1988; Plank and Langmuir, 1998, Gasparon and Varne, 1998), which is characteristic of arc lavas, relative to a MORB-like mantle source, may be consistent with either sediment subduction or assimilation of arc crust. Previous workers have highlighted the importance of both a subducted component (Tera, et al., 1986; Plank and Langmuir, 1993, 1998; Vroon, 1992) and crustal level incorporation (Davidson et al., 1987; Hildreth and Moorbath, 1988; Davidson and Harmon, 1989) of continental material in the petrogenesis of arc lavas. Furthermore, within-arc variations in crustal architecture and the nature (age and composition) of the subducting slab and its associated sediments augment the difficulty of disentangling differentiation effects on primary magmas from source characteristics.

Initial geochemical study of Sunda arc lavas noted a general decrease in Sr isotope ratios from West Java to Bali (Whitford, 1975) and it is suggested that the decrease may arise due to diminishing crustal contamination as a result of eastward arc-crustal thinning (Hamilton, 1979). Gasparon and Varne (1998) have more recently argued that crustal assimilation can account for the elevated Sr and lower Nd isotope ratios in Sunda arc volcanic rocks relative to MORB. However, it is also possible that Sr-isotopic variation may

arise due to differences in the type and amount of sediment deposited on the down-going Indian Ocean Plate (Hamilton, 1979; Moore et al., 1980; Plank and Langmuir, 1998, Gasparon and Varne, 1998, see section 1.2.2.2, Chapter 1) that is then incorporated into the mantle source through subduction. The addition of a subducted sedimentary component to the Sunda arc mantle wedge is advocated by several authors (e.g. Edwards, 1990; Turner and Foden, 2001; Gertisser and Keller, 2003). Constraining the relative contributions in Sunda arc lavas from subducted components and material assimilated as melts pass through the crustal basement is complicated by the variable nature of the upper Eurasian and lower Indian Ocean plates highlighted in Chapter 1. Previous chapters in this study have both highlighted evidence for crustal contamination (via AFC processes at Salak, Chapter 3) and slab component contributions to the mantle wedge (IVC and GVC, Chapters 2 & 4 respectively).

The aims of this chapter are therefore 3-fold:

1. To compare and contrast the geochemistry of lavas from Salak and GVC in West Java with those from IVC in East Java, in order to establish contrasting East-West geochemical traits.
2. Use any key elements/ratios resultant from addressing the above aim to ascertain along-arc Javan geochemical trends. Data in this study will be complemented with the growing geochemical data set available for Javan lavas (cf. 1970s) and include new Hf-isotope data for Guntur and Merapi (Appendix C).
3. Establish whether variable contributions from the subducting slab, or a change in crustal architecture of the overriding plate, best explain along-arc variations in isotope ratios and trace element characteristics of Javan volcanic rocks.

This information will help elucidate the nature of the transition between the continental and oceanic basement to the arc, which is expected to lie between Sumatra and East Java (Fig. 1.4, Chapter 1). The location of this boundary is particularly important in understanding the tectonic history of southern Indonesia and the distribution of different types of volcanoes.

5.2. Comparing and contrasting volcanic rocks from West and East Java

5.2.1. Petrography, major and trace elements

Petrographically, IVC (East Java), GVC and Salak (West Java) lavas are very similar (Appendix A) and are characteristically seriate-porphyritic in texture and dominated by sub-euhedral, variably zoned plagioclase phenocrysts. Clinopyroxene is the most common mafic phase in the lavas, accompanied by subordinate olivine or orthopyroxene (or both in a few samples) and a smaller relative abundance of titanomagnetite phenocrysts. In comparison with most other Javan volcanic rocks, hornblende phenocrysts are absent in almost all IVC, GVC and Salak lavas with the exception of the highest SiO_2 (> 65 wt %) volcanic rocks of Salak.

The majority of IVC, GVC and Salak lavas display a similar range in SiO_2 content, and are dominated by basaltic-andesites and andesites. Basalts (< 52 wt% SiO_2) are limited to a small number of IVC and GVC rocks and dacites and rhyolites have only been sampled at Salak. Fe_2O_3, MgO and CaO display identical, overlapping, well-correlated negative trends for the three volcanic centres (Figs. 5.1a-c). The rocks display less well-correlated negative trends on Al_2O_3 against SiO_2 (Fig. 5.1d). Most of the lavas from all three volcanic centres display a broad increase in K_2O and Na_2O contents with increasing SiO_2 (Figs. 5.1e and f), but K_2O contents of IVC lavas are slightly higher than those from GVC and Salak (e.g. Fig. 5.1e) at comparable SiO_2 content. The contrasting intra-volcano differentiation trends exhibited by Salak are evident in the plot of Na_2O against SiO_2 (Fig. 5.1f), and even more

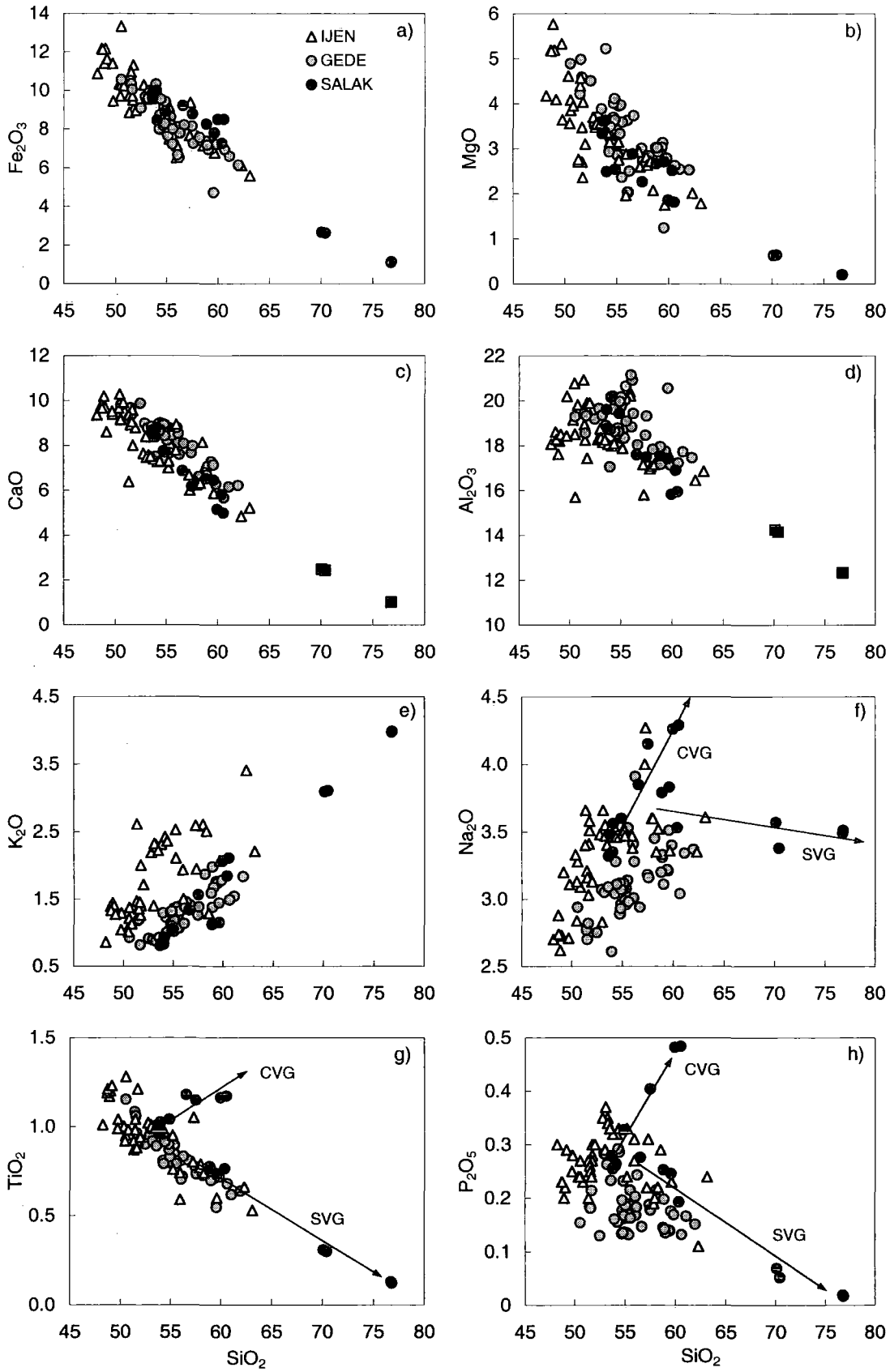

Fig. 5.1. Major element variation diagrams for IVC, GVC and Salak volcanic rocks. Major element data of IVC rocks from Sitorus (1990). Arrows indicate the different differentiation trends of the CVG and SVG of Salak.

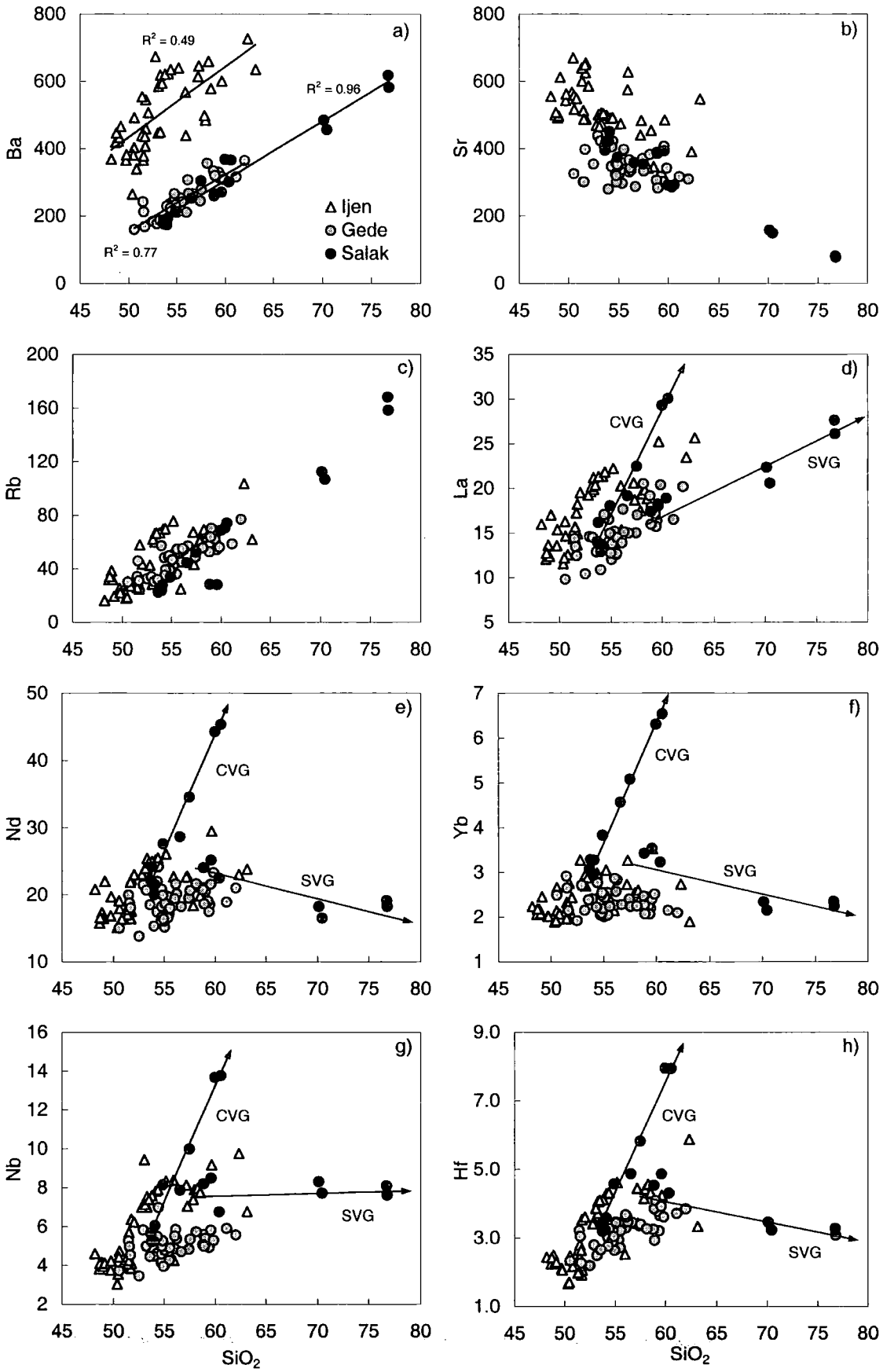

Fig. 5.2. SiO_2 variation diagrams for selected trace elements of IVC, GVC and Salak volcanic rocks. Arrows indicate the different differentiation trends of the CVG and SVG of Salak.

pronounced on the plots of TiO_2 and P_2O_5 against SiO_2 (Figs. 5.1g and h respectively; discussed in Chapter 3); where the differentiation trends of rocks erupted from the Central Vent Group (CVG) of Salak diverge markedly from both the Side Vent Group (SVG) of Salak and the generally negative correlations displayed by the other East and West Javan volcanic rocks.

LILE variations in IVC, GVC and Salak lavas display similar trends i.e. largely positive correlations against silica, with the exception of Sr, which broadly decreases with increasing silica (Figs. 5.2a-c). The abundance of Ba (Fig. 5.2a) is significantly higher in IVC rocks compared to those of GVC and Salak at similar degrees of differentiation. This is also shown to a lesser extent in Sr variation (Fig. 5.2b), but contrasts with Rb concentrations, which exhibit near-identical abundances at comparable SiO_2 contents. REE variation with SiO_2 is similar for IVC and GVC. The rocks from these volcanic complexes display generally well-correlated LREE (Fig. 5.2d), less well-correlated MREE (Fig. 5.2e) and poorly correlated (generally constant with varying SiO_2) HREE (Fig. 5.2f) trends against SiO_2. The bi-variant Salak differentiation trend and unusual positive correlation shown by the CVG between M-HREE and SiO_2 was noted and discussed in Chapter 3. The HFSE (e.g. Nb, Hf and Zr) generally increase with increasing SiO_2 (Figs. 5.2g and h), with the exception the SVG samples of Salak.

5.2.2. Radiogenic and stable isotope data

Whole rock Sr-Nd-Hf isotope data from GVC, Salak and IVC are displayed in Figs. 5.3a and b. IVC rocks display more primitive Sr-Nd-Hf isotope ratios, located closer to MORB Sr-Nd-Hf ratios, and, in contrast to the strong positive correlation in Nd-Hf isotope space displayed by both GVC and Salak lavas, IVC lavas define a generally horizontal array. IVC lavas also

display a steeper negative correlation than GVC and Salak rocks in Sr-Nd isotope space (cf. Fig. 2.15a, Chapter 2).

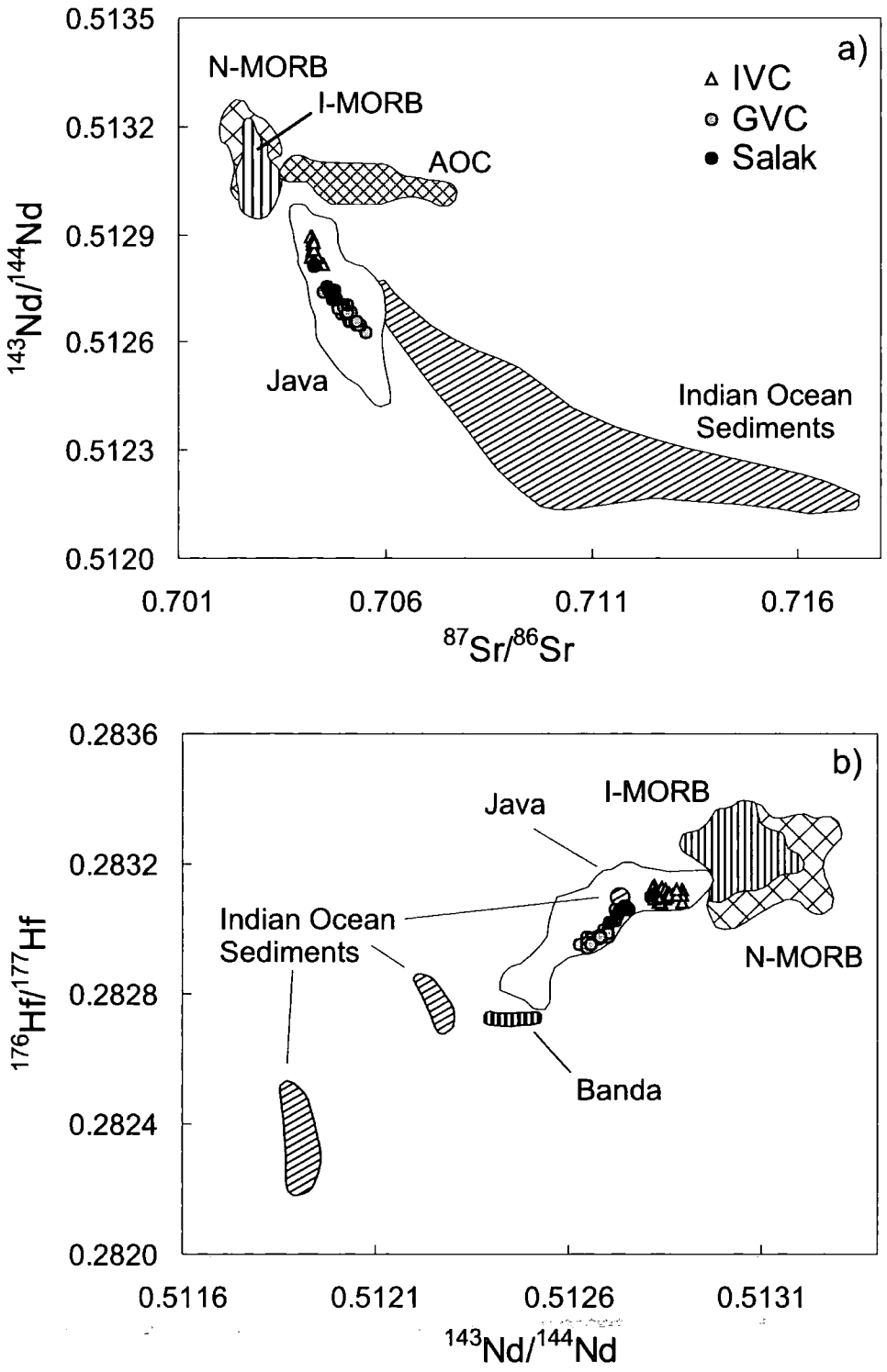

Fig. 5.3. a) Variation of $^{143}Nd/^{144}Nd$ with $^{87}Sr/^{86}Sr$ for IVC, GVC and Salak volcanic rocks. Data sources: I-MORB: Rehkämper and Hofmann, 1997; Ito et al., 1987; Price et al., 1986; Chauvel and Blichert-Toft, 2001; N-MORB: Ito et al., 1987; Chauvel and Blichert-Toft, 2001; Altered oceanic crust (AOC): Staudigel et al., 1995; Java volcanic rocks: White and Patchett, 1984; Whitford et al, 1981; Edwards, 1990; Gertisser and Keller, 2003; Gerbe et al, 1992; Woodhead et al., 2001; Indian ocean sediments: Ben Othman et al., 1989; Gasparon and Varne, 1998. 2σ external errors are smaller than symbol size. b). Variation of $^{176}Hf/^{177}Hf$ with $^{143}Nd/^{144}Nd$ for IVC, GVC and Salak volcanic rocks. Data sources: I-MORB: Salters, 1996; Nowell et al., 1998; Chauvel and Blichert-Toft, 2001; N-MORB: I-MORB references above plus Salters and Hart, 1991; OIB: Salters and Hart, 1991; Salters and White, 1998; Nowell et al., 1998; Patchett and Tatsumoto, 1982; Patchett, 1983; Stille et al., 1986; Java volcanic rocks: White and Patchett, 1984; Woodhead et al., 2001; Indian ocean sediments: Ben Othman et al., 1989; White et al., 1984; Vervoort et al., 1999. 2σ external errors are smaller than symbol size.

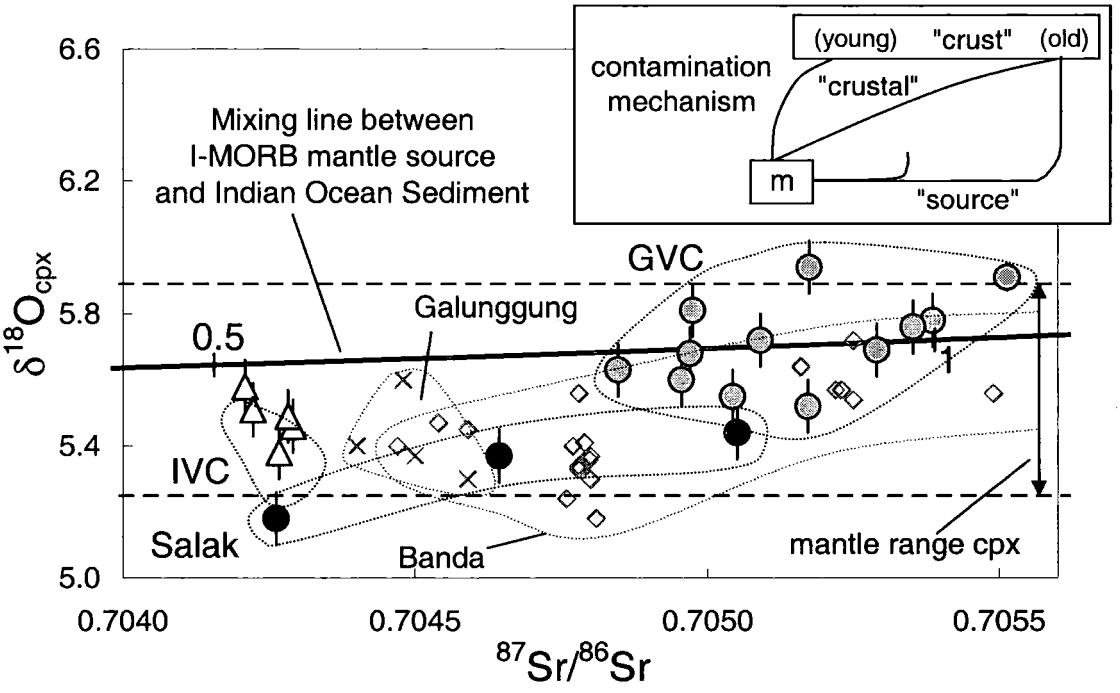

Fig. 5.4. Plot of $\delta^{18}O$ versus $^{87}Sr/^{86}Sr$ for clinopyroxene in IVC, GVC and Salak lavas. Mantle range of clinopyroxene (dashed black lines, 5.57 ± 0.32 ‰) from Mattey et al. (1994) and Ionov et al. (1994). Java (Galunggung) clinopyroxene $\delta^{18}O$ data from Harmon and Gerbe (1992); Banda arc data from Vroon et al. (2001). Error bars are ± 1σ of replicate analysis or ±0.09‰ for clinopyroxene where replicate analyses were not carried out. 2SD $^{87}Sr/^{86}Sr$ error bars are smaller than the symbol size. A simple mixing curve is plotted between sediment and depleted mantle source to illustrate that Javan lavas are generally consistent with 'source contamination'. Tick marks (0.5 and 1) indicate the amount of sediment added to the mantle source. Data used in mixing calculation: Bulk sediment Sr = 450 ppm; O = 50.2 wt %, $^{87}Sr/^{86}Sr$ = 0.7156; $\delta^{18}O$ = 18.7‰ (Vroon et al., 2001). Depleted mantle source: Sr = 12.94 ppm; O = 43.8 wt %, $^{87}Sr/^{86}Sr$ = 0.7026 (Vroon et al., 2001 and references therein); $\delta^{18}O$ = 5.57‰ (Mattey et al., 1994; Ionov et al., 1994). Inset box shows the expected data trends for 'crustal' versus 'source' contamination, m = mantle source.

Clinopyroxene $\delta^{18}O$ values for IVC, GVC and Salak are relatively restricted (+5.18 to +5.94‰, n = 20) and lie within error of $\delta^{18}O$ values measured in mantle olivine and clinopyroxene (+5.18 ±0.28‰, n = 76 and +5.57 ±0.32‰, n = 57, 2sd respectively, Mattey et al., 1994; Ionov et al., 1994; Fig. 5.4). There is no distinction in oxygen isotope composition between volcanic rocks situated in East and West Java. Salak clinopyroxene $\delta^{18}O$ values are lower than those of IVC, GVC and other Sunda arc $\delta^{18}O$ clinopyroxene analyses and GVC clinopyroxenes display the highest $\delta^{18}O$ values (Fig. 5.4).

In Summary, IVC, GVC and Salak lavas display similar overall trends in the majority of major and trace element variation diagrams. Nevertheless (excluding the unusual differentiation trends exhibited by a subgroup of Salak samples compared to the rest of Java), some notable differences are observed between volcanic rocks from IVC in the east and GVC and Salak in the west:

1. Relative enrichments of Ba, K and to a lesser extent Na, Sr and La in the most basic IVC lavas compared to GVC and Salak rocks of comparable SiO_2 content.
2. IVC volcanic rocks display a different trajectory on Sr-Nd-Hf isotope diagrams compared to GVC and Salak rocks.

LILE/alkaline element enrichments in arc lavas, relative to MORB, are commonly attributed to contributions from the subducting slab and/or assimilation of crustal material during island-arc petrogenesis. The contrasting variation in these elements in East and West Javan lavas can therefore help constrain the relative importance of subducted slab and arc crust components in the petrogenesis of Javan arc lavas and potentially illuminate any along-arc variations in the upper and lower plate contributions. To investigate whether the spatial geochemical variation identified in lavas from the opposite ends of Java (in this study) reflect progressive along-arc patterns or just represent isolated differences, IVC, GVC and Salak data will now be compared with previously published data of other Javan volcanoes, focusing

on the elements and isotope ratios that have shown the greatest contrast between East and West Java. However, in order to compare data from different volcanoes, a few considerations need to be taken into account.

5.3. Sample selection

Data presented for IVC, GVC and Salak is supplemented in an along-arc comparison with data from other Javan volcanoes. In order to most accurately recognise and correct for differentiation effects an emphasis is placed on including volcanoes with comprehensive data sets available e.g. Guntur, Galunggung and Cereme in West Java and Slamet and Merapi in Central Java. Excluding IVC, only limited elemental and isotopic geochemical data are available for East Javan volcanoes, therefore single sample analyses and limited data sets from some East Javan volcanoes are included. New Hf isotope data for Merapi and Guntur (Appendix C) are also presented.

Across-arc changes in chemistry are widely recognised at the Sunda arc (Rittman, 1953; Whitford and Nicholls, 1976; Hutchinson, 1976; Edwards, 1990), therefore, only volcanoes situated in the volcanic front, 100-200 km above the Wadati-Benioff zone (WBZ) are considered. Muriah (370 km above the WBZ in Central Java) and Ringit Besar (210 km above the WBZ in East Java) volcanoes are excluded on this basis. The distance from volcano to the underlying WBZ is taken from Hutchinson (1982). However, the depth to the underlying WBZ is not given for GVC and so 125 km is used for GVC, sourced from the Volcanic Survey of Indonesia (http://www.vsi.esdm.go.id/volcanoes/gede/geology.html). The island of Java and the strike of subduction, as indicated by the Java Trench south of Java, are oriented generally East-West, therefore the longitude of the volcano is used to represent volcano position along the arc. To ease the of recognition of general along-arc contrasts in the large Javan dataset (particularly on bivariate diagrams), volcanoes are grouped into East,

Central and West Javan provenance based on geographic boundaries. The boundary for Central Java passes between Cereme and Slamet volcanoes in the West and Wilis and Kelut volcanoes in the East (Fig. 1.2b, Chapter 1). Krakatau, in the Sunda Strait (west of Java) is included, accordingly, within the West Java group.

Indian Ocean sediments used in geochemical comparisons and modelling, have been broadly divided into pelagic and terrigenous groups. The terms 'pelagic' and 'terrigenous' are employed to distinguish between samples with a high abundance of detrital phases (e.g. turbidites) from those rich in biogenic (carbonate and silica) phases (e.g. nanno ooze) as these proportions are a first order control on many element ratios (Plank and Langmuir, 1998). It is acknowledged that there is a wide variation in chemistry for some elements within each group. However, for most elements, there are strong links between sediment geochemistry and lithology. For example, biogenic oozes will be poor in REE and HFSE but generally rich in Sr and Ba compared to turbidites (Plank and Langmuir, 1998).

5.4. Discussion

5.4.1. Nature and influence of Javan arc crust

5.4.1.1. Previous evidence for crustal contamination at the Sunda arc

The most frequently quoted along-arc change in geochemistry of the Sunda arc is the progressive eastward decrease in $^{87}Sr/^{86}Sr$ isotope ratios (Whitford, 1975; Hamilton, 1979; 1988; Hutchinson, 1982; Turner and Foden, 2001). $^{87}Sr/^{86}Sr$ isotope studies by Whitford (1975) show that $^{87}Sr/^{86}Sr$ isotope ratios in normal calc-alkaline rocks increase from Krakatau to the Dieng volcanic complex, ~500 km to the east (Fig. 1.2b), then decrease eastwards along the rest of Java to the eastern side of Bali. Correlation of $^{87}Sr/^{86}Sr$ with distance to the underlying WBZ was thought by Whitford (1975) to account for the increase from Krakatau to the Dieng complex. After removal of the possible effects of WBZ depth on $^{87}Sr/^{86}Sr$ lava

ratios, Whitford suggested an apparent eastward decrease in $^{87}Sr/^{86}Sr$ from West Java to Bali. The general eastward decrease in $^{87}Sr/^{86}Sr$ from Java to Bali was taken to suggest a transition from continental Sunda shelf to oceanic arc basement (Hutchinson, 1982), i.e. eastward thinning of the crust and a consequential decrease in the importance of crustal contamination of magma (Hamilton, 1979). The more silicic nature of the young volcanogenic sediments in the west, relative to the east, was also taken as an indication of thicker crust in the west (Hamilton, 1979). More recently, Gasparon and Varne (1998) also advocate a major role for the arc crust in the genesis of west Sunda arc volcanic rocks. They argue that assimilation during magmatic fractionation has overprinted Sr and Nd isotopic signatures of source contamination and is primarily responsible for the range observed in the rocks.

This study has highlighted the importance of crustal contamination in the magmatic evolution of the CVG group at Salak Volcano (Chapter 3). Field evidence for direct interaction between rhyolitic lava and granite blocks in the Perbakti-Gagak area, adjacent to Salak, has been recorded by Stimac (2003), and field evidence for the existence of crustal anatectic melts is widespread in Sumatra and West Java (Gasparon and Varne, 1998; Hamilton, 1979). Therefore, before addressing the question of variable source inputs along Java, it is imperative to ascertain the geochemical influence of the Javan arc crust on trace element and isotope ratios of the volcanic rocks, which will: 1) obscure slab component signatures in the source, and 2) shed light on the nature of the volcanic basement in Java.

5.4.1.2. Sr isotope constraints

Since the preliminary along-arc geochemical studies of Java in the 1970s, there has been a substantial increase in $^{87}Sr/^{86}Sr$ isotope data available for Javan volcanoes (e.g. this study alone has contributed 59 $^{87}Sr/^{86}Sr$ analyses). It is therefore necessary, first of all, to establish whether the along-arc trends previously identified, still prevail in the expanded dataset.

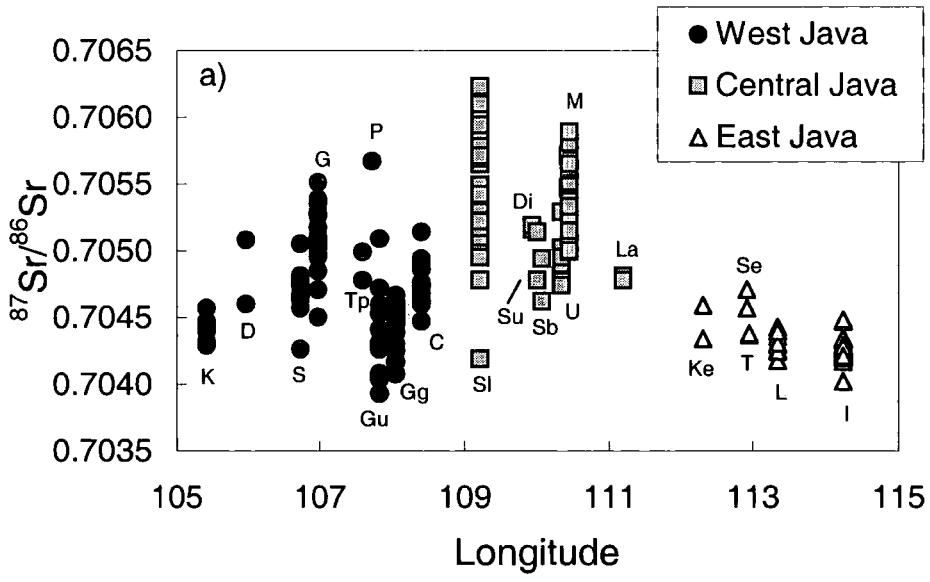
a)
West Java
Central Java
East Java
$^{87}Sr/^{86}Sr$
0.7065
0.7060
0.7055
0.7050
0.7045
0.7040
0.7035
105
107
109
111
113
115
Longitude
K
D
S
G
P
Tp
Gu
Gg
C
Sl
Di
M
Su
Sb
U
La
Ke
Se
T
L
I

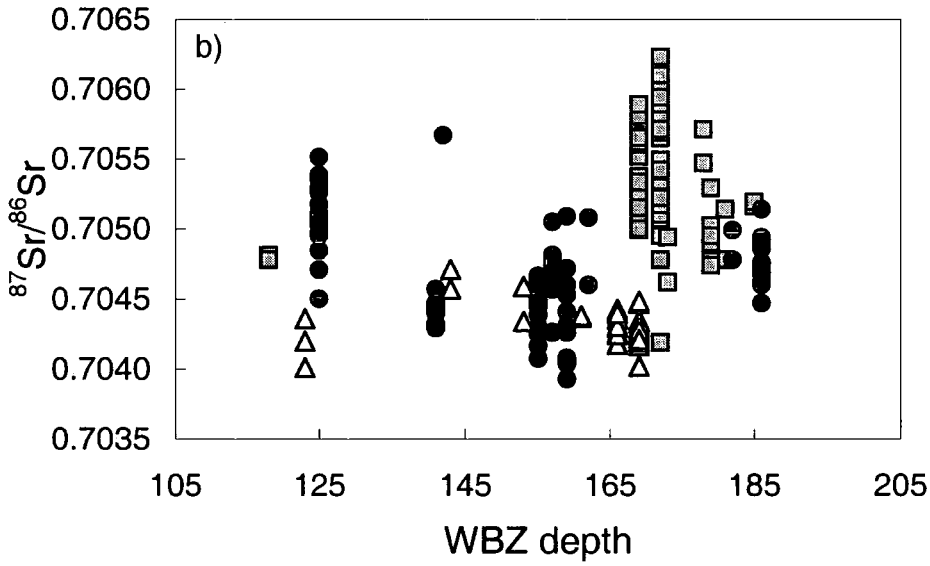
b)
$^{87}Sr/^{86}Sr$
0.7065
0.7060
0.7055
0.7050
0.7045
0.7040
0.7035
105
125
145
165
185
205
WBZ depth

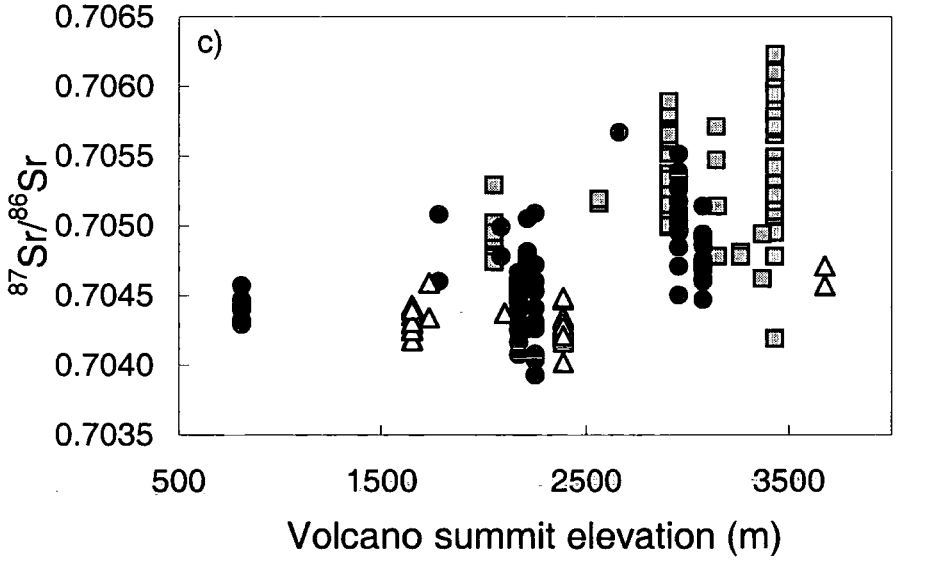
c)
$^{87}Sr/^{86}Sr$
0.7065
0.7060
0.7055
0.7050
0.7045
0.7040
0.7035
500
1500
2500
3500
Volcano summit elevation (m)

Fig. 5.5. $^{87}Sr/^{86}Sr$ versus a) Longitude, b) WBZ depth and c) volcano summit elevation (used as a function of crustal thickness - cf. Hildreth and Moorbath, 1988, and see text) for Javan volcanic rocks, separated by geographical regions. West Java: K = Krakatau (Anak) (Turner and Foden, 2001; Whitford, 1975; Woodhead et al., 2001), D = Danau Complex (Whitford, 1975), S = Salak (this study), G = GVC (this study), Tp = Tangkuban Prahu (Whitford, 1975), P = Papandayan (Whitford, 1975; Woodhead et al., 2001), Gu = Guntur, Whitford, 1975; Edwards, 1990), Gg = Galunggung (Gerbe et al., 1992; Whitford, 1975; Woodhead et al., 2001, Turner and Foden, 2001); C = Cereme (Whitford, 1975; Edwards, 1990); Central Java: Sl = Slamet (Whitford, 1975; Vukadinovic and Sutawidjaja, 1995), Di = Dieng (Whitford, 1975), Su = Sundoro (Whitford, 1975), Sb = Sumbing (Whitford, 1975), U = Ungaran (Whitford, 1975), M = Merapi (Turner and Foden, 2001; Gertisser and Keller, 2003; Whitford, 1975), La = Lawu (Whitford, 1975); East Java: Ke = Kelud, (Whitford, 1975), Se = Semaru (Whitford, 1975, Woodhead et al., 2001), T = Tengger Caldera (Whitford, 1975), L = Lamongan (Whitford, 1975; Carn and Pyle, 2001; Woodhead et al., 2001), I = IVC (this study). Location of volcanoes shown in Fig. 1.2b. Depth to the Wadati-Benioff zone below the volcanoes taken from Hutchinson, 1982, except for GVC (Volcanic Survey of Indonesia, http://www.vsi.esdm.go.id/volcanoes/gede/geology.html).

$^{87}Sr/^{86}Sr$ variation plotted against volcano longitude (Fig. 5.5a) shows that West and Central Javan volcanoes (Krakatau to Merapi), possess a much wider range and broad increase in $^{87}Sr/^{86}Sr$ isotope ratios, compared to East Javan volcanoes, where ratios are significantly lower and relatively constant. Although a greater number of analyses are available for West Java, the more primitive and homogenous nature (in a comparable number of single volcanic analyses) of East Javan lavas than West Javan lavas was highlighted for IVC in Chapter 2. Whitford (1975) discounted an eastward increase in $^{87}Sr/^{86}Sr$ along West and Central Java due to correlations between WBZ depth and $^{87}Sr/^{86}Sr$ isotope ratios. However, Fig. 5.5b reveals that Sr isotope ratios of West and Central Javan volcanic rocks show little correlation with the depth of the WBZ below the volcanoes. It is proposed, therefore, that the eastward increase in $^{87}Sr/^{86}Sr$ isotope ratios through West and Central Java is not related to the distance between the volcano and the subducting slab as previously suggested.

It is interesting to note that the volcanoes in West Java with the lowest Sr isotope ratios are those from Guntur (Gu) and Galunggung (Gg) (Fig. 5.5a). These volcanoes are both situated towards the northern edge of an extensional tectonic triangle (Fig. 1.2b, Chapter 1)

where the crust may be thinner and decompression-melting important in magma genesis (e.g. Sissons and Bronto, 1998). There is little detailed information available on crustal thickness beneath the volcanic-front along Java, so in order to investigate the relationship between crustal thickness and $^{87}Sr/^{86}Sr$ isotope ratios along Java, volcano edifice elevation is used to denote crustal thickness; on the basis that thicker crust can isostatically support a greater volcanic mass and therefore volcano elevation will be higher. A similar approach was taken by Hildreth and Moorbath (1988) investigating crustal contributions in Andean lavas. They noted a correlation between volcano elevation (basal and summit height) of Quaternary volcanic centres and Bouguer gravity anomaly profile with latitude (along the arc), and suggested that volcanic edifice elevation can act as a general indicator of subjacent crustal thickness. Therefore, as there are no along-arc gravity profiles available for the Sunda arc, volcano summit elevation (relative to sea level) is used as an expression of crustal thickness along Java. Fig. 5.5c reveals that West and Central Javan volcanoes show a general correlation between elevation and maximum $^{87}Sr/^{86}Sr$ isotope ratio of volcanic rocks. The summits of central Javan volcanoes are generally at greater elevations than West or East Javan volcanoes. The latter volcanoes largely display constant Sr isotope ratios over a sizeable range in volcano elevation. The suggestion that higher $^{87}Sr/^{86}Sr$ isotope ratios are found in lavas from Javan volcanoes situated on (inferred) thicker arc crust might imply that these volcanoes have either undergone more crustal contamination by mass (as the magmas have had to ascend through more crust), or, been contaminated by more 'continental' type material. Incorporation of crustal material during crustal differentiation (Davidson et. al., 2005) of Javan magmas may be expected to generate correlations between Sr isotope ratios and indices of differentiation (e.g. SiO_2) for each magmatic series (AFC labelled arrows Fig. 5.6). Nevertheless, convincing relationships are absent within individual magmatic series (Fig. 5.6a-d), which display generally horizontal trends. Even for Salak, it is difficult to

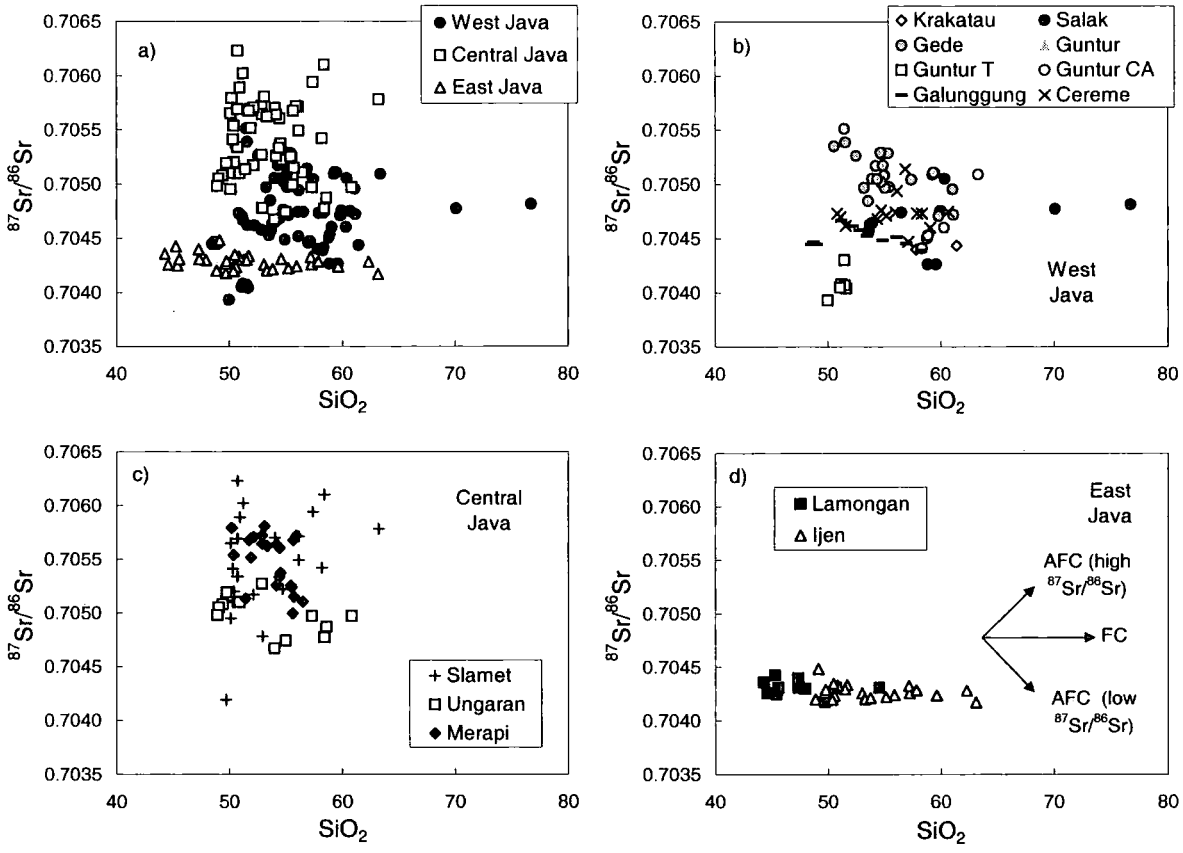

Fig. 5.6. $^{87}Sr/^{86}Sr$ versus SiO_2 for a) all Java, b) West Java, c) Central Java and d) East Java, highlighting the general lack of correlation between isotope ratios and indices of differentiation both in the data set as a whole and at individual volcanic centres. Data sources as in Fig. 5.5. Arrows labelled AFC and FC in d) indicate the differentiation trends expected from assimilation and fractional crystallisation of high $^{87}Sr/^{86}Sr$ material (e.g. radiogenic continental crust) and low $^{87}Sr/^{86}Sr$ material (e.g. low Sr-isotope oceanic basement) and fractional crystallisation respectively.

recognise any significant correlation between $^{87}Sr/^{86}Sr$ isotope ratio and SiO_2 on this scale (cf. Fig. 3.11, Chapter 3). However, this approach assumes that a contaminant will have an isotopic composition distinct from that of the island arc lavas being investigated. Modelling AFC for the CVG of Salak Volcano (Chapter 3) suggested that the crustal contaminant involved has a $^{87}Sr/^{86}Sr$ isotope ratio ~0.7048, arguing against significant contamination by typical 'continental' material, and suggesting probable contamination by older, arc-related,

volcanic rocks. Crustal contamination involving these materials may be more difficult to detect, and implies that the hypothesised decrease in crustal thickness between Central and East Java, may not necessarily be accompanied by a significant change in crustal composition. An additional line of evidence against significant contamination by continental-type crust is that xenoliths of this type have not been discovered in any volcanic rocks at IVC, GVC or Salak; only clasts of igneous origin have been observed (Sections 2.5.1.2, 3.3 and 4.4.3 in Chapters 2, 3 and 4, respectively), further highlighting the potential difficulty of identifying 'crustal' contributions in arc lavas. However, at Merapi in Central Java, where the crust is proposed to be thickest and Sr isotope ratios are high compared to other Javan lavas, calc-silicate xenoliths are evident in the lavas (J. Chadwick, pers. comm.).

Alternatively, higher (maximum) Sr isotope ratios in lavas of volcanoes situated on relatively thicker crust compared to those on relatively thinner crust in Java may be a result of the available length (and therefore volume) of the mantle melting column beneath the volcanoes. For example, it was highlighted above that Galunggung and Guntur in West Java display relatively low Sr isotope ratios compared to their neighbours (Figs. 5.5a and 5.7) for which an equally large dataset is available (i.e. GVC and Cereme). The lower summit elevations of Galunggung and Guntur (cf. GVC and Cereme) and location within an extensional tectonic triangle suggests that the arc lithosphere is thinner in this region (Fig. 5.7). Assuming a relatively constant quantity of slab-derived input to the mantle wedge in West Java (and similar depths for the base of the mantle column), the inferred longer melting columns present beneath Galunggung and Guntur (Fig. 5.7) may effectively dilute the subduction component more than in the relatively shorter melting columns available beneath other volcanoes in West Java situated on relatively thicker crust (e.g. GVC and Cereme, Fig. 5.7). On a larger scale, a similar reasoning can be used to explain the noticeably higher Sr isotope ratios in West Java compared to East Java. This explanation is consistent with the

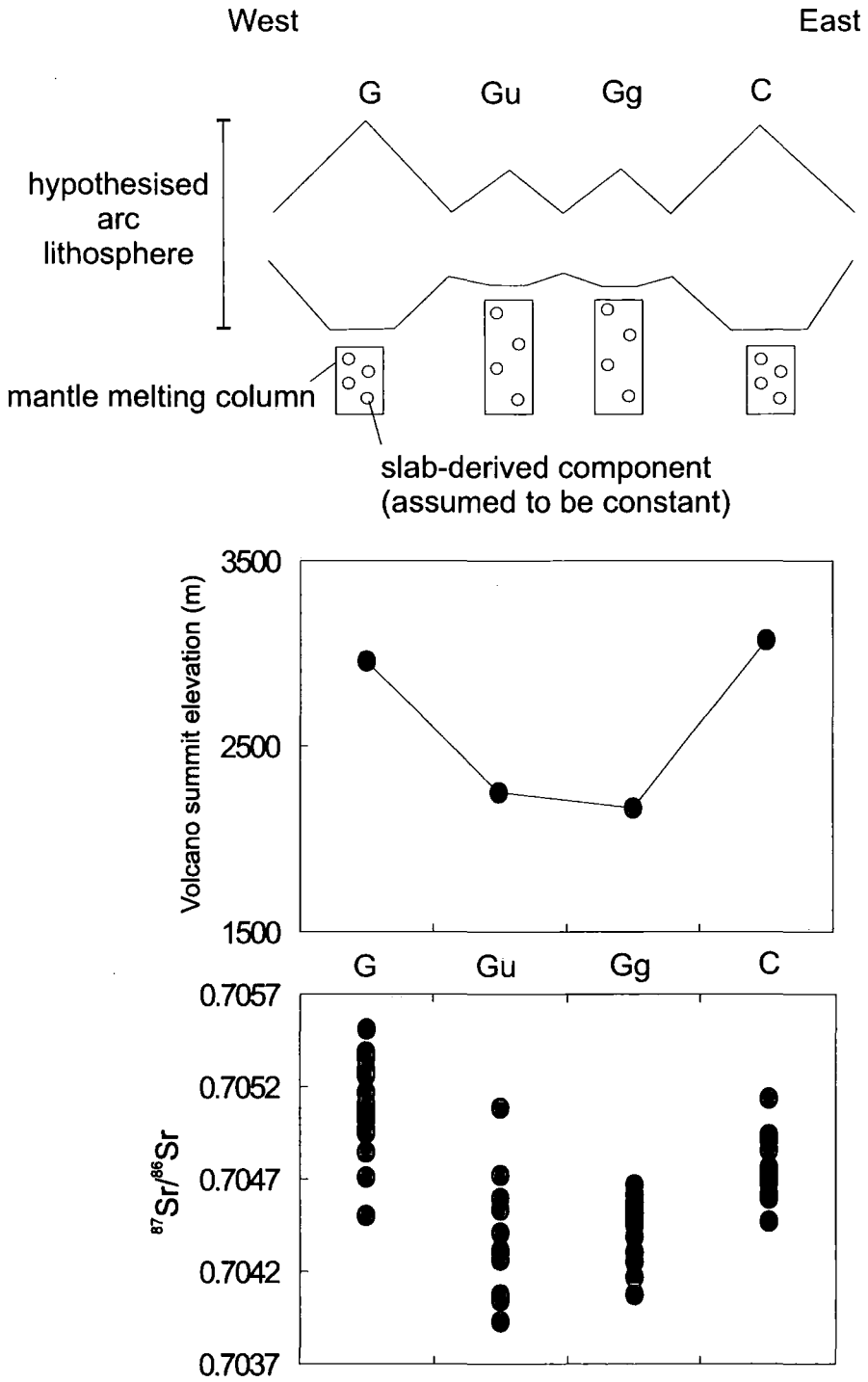

Fig. 5.7. Schematic diagram highlighting the relationship between volcano summit elevation and $^{87}Sr/^{86}Sr$ isotope ratio, as exemplified by volcanoes in West Java (names of volcanoes given in Fig. 5.5). Longer melting columns beneath volcanoes with inferred thinner arc lithosphere (Gu and Gg) are proposed to explain the lower $^{87}Sr/^{86}Sr$ isotope ratios in volcanic rocks of these volcanoes.

slightly higher percentage of slab-derived sedimentary material modelled for GVC (< 2.5%) in West Java than IVC (< 1%) in East Java and obviates the need for deep-level crustal contamination to explain Sr isotope variations, consistent with the general conclusions that assimilation of crustal material at GVC (Chapter 4), and other volcanoes in West and Central Java such as Cereme (Edwards, 1990) and Merapi (Gertisser and Keller, 2003) has negligible impact on the chemistry of lavas.

5.4.1.3. O isotope constraints

$\delta^{18}O$ values of Javan volcanic rocks also preclude significant contaminant by typical upper crustal 'continental' type material: all clinopyroxene data available for Javan volcanic rocks report low, mantle like $\delta^{18}O$ values (Fig. 5.4). The Java data generally lie along a mixing curve (solid line Fig. 5.4) consistent with sediment contamination of the mantle source, as opposed to mixing continental crust with basalt during magmatic evolution (see Chapter 4, section 4.6.1.3 for discussion on using radiogenic and stable isotope ratios to diagnose 'crustal' contamination mechanisms). Salak lavas, possess the least 'upper crustal' (lowest) $\delta^{18}O$ values, even though crustal contamination processes are implicated at Salak Volcano, which may suggest that contamination occurs relatively deep in the crust. On the other hand, the contaminant may possess lower than average mantle $\delta^{18}O$ values, such as altered oceanic crust, which is known to have variable, including low, $\delta^{18}O$ values (McCulloch et al., 1980; Alt et al., 1986; Muehlenbachs, 1986). Introduction of an ^{18}O-depleted meteoric fluid is suggested for some volcanic rocks of Galunggung (West Java, Harmon and Gerbe, 1992). These conclusions are consistent with Hamilton's (1979) suggestion that the crust in western Java is not typically continental in character, and may consist of ophiolite slivers, and older volcanic rocks.

5.4.1.4. Summary: the nature of the Javan crust and its role in magmatic differentiation

The progressive eastward increase in Sr isotope ratio across West and Central Java, which broadly correlates with inferred crustal thickness, suggests that crustal contamination may have played a role in the $^{87}Sr/^{86}Sr$ isotopic evolution in of West and Central Javan magmas. The lack of correlation between $^{87}Sr/^{86}Sr$ and indices of differentiation, implies that contamination of West and Central Javan magmas (to produce higher $^{87}Sr/^{86}Sr$ ratios cf. East Javan lavas) is likely to have occurred before significant magmatic differentiation (or during an earlier phase of it), i.e. relatively deep in the crust. However, the isotopic data are more consistent with source contamination rather than assimilation of continental crust. $^{87}Sr/^{86}Sr$ of the volcanic rocks is therefore proposed to be controlled to some extent by the length of the mantle melting column beneath the volcanoes, which is largely dependant on the thickness of the arc crust.

From the evidence above, it is proposed therefore, that there may be a significant change in Javan crustal architecture (mainly thickness) located between Merapi (Central Java) and Kelud (East Java). It is curious that this portion of Java is regarded as volcanologically 'extinct' (Wheller et al., 1987); Wilis and Lawu are the only significant volcanoes within this sector and both show only solfataric activity (Wheller et al., 1987). The general topography of Java also suggests some type of crustal transition at this point (Fig. 1.2b, Chapter 1): the deeply-dissected mountainous and more rugged topography of the volcanic front in West and Central Java contrasts with the relatively flat East Javan topography, punctuated by conical volcanoes with relatively smooth volcanic slopes. However, it is noted that rugged topography is present in slivers, south of the active volcanic front in East Java.

The along-arc transition in crustal architecture suggested may represent the south-eastern boundary of Sundaland (pre-Tertiary basement) suggested to be located somewhere between Sumatra and East Java, but commonly placed transversely within West Java (Hamilton, 1979; Hutchinson, 1982; Hutchinson, 1989; Susilohadi et al., 2005; Hoffmann-Rothe et al., 2001, Fig. 1.2a, Chapter 1). The more rugged, eroded topography in West and Central Java, compared to East Java, may too reflect the older nature of the crust in the central and western parts. The extremely limited $^{87}Sr/^{86}Sr$ isotopic data available for volcanoes located between Merapi and Kelud (Lawu and Wilis) precludes ascertaining the exact nature of the proposed boundary (i.e. relatively sharp or gradual).

Recent study of zircons from sedimentary rocks and older volcanic rocks (relative to the products of the active volcanoes) in East and Central Java, south of the present volcanic axis, also suggest a significant transition in the arc crust between Central and East Java: zircons of Cretaceous (i.e. pre-Tertiary) age have been found in Central Javan deposits, while no Cretaceous ages have been measured in zircons further east (H. Smyth, pers. comm.). This evidence provides support for a model in which a general boundary between pre- and post-Tertiary age crust is positioned between Central and East Java. However, south of the volcanic axis in East Java ages of 550-3200 Ma are measured in zircons implicating the presence of continental basement at depth. It is important to note that the 'old' zircon ages are recorded in rocks sampled from the aforementioned slivers of rugged topography in southern East Java. It may therefore, be tentatively hypothesised that, another crustal boundary exists in East Java, oriented roughly east-west between the present volcanic axis and rugged southern mountains (see later Figs. 5.13 and 6.1, Chapter 6). It is unknown at present whether magma beneath the present volcanic axis in East Java is traversing such continental arc basement, but nevertheless, it highlights the complexity of the Javan arc crust and places

limitations on simplistic assumptions of smooth, west-east transitions in the nature of the Javan arc crust.

In summary, contrasting with the conclusions of Gasparon and Varne (1998), the lack of correlation between Sr isotope ratios and indices of differentiation, Sr-O isotope mixing calculations and constraints placed on the $^{87}Sr/^{86}Sr$ isotope ratio of the contaminant at Salak (Chapter 3), suggest that typical upper-crustal contamination cannot explain Sr isotope variations in Javan volcanic rocks. Furthermore, enrichment of LILE (e.g. Ba, Sr, K) in IVC lavas relative to GVC and Salak is the opposite of that which may be expected, considering the Javan crustal structure (relatively thicker in the west than the east). The lowest $^{87}Sr/^{86}Sr$ isotope ratios measured in volcanic rocks of most Javan volcanoes are appreciably more radiogenic than that of an inferred I-MORB source (Fig. 5.3). Elevations of Sr isotope ratios, relative to I-MORB, have been attributed to subducted material in magma genesis at the Sunda arc (Edwards, 1990; Turner and Foden, 2001; Gertisser and Keller, 2003) and so source contributions from the down-going plate will now be investigated. However, in order to ascertain any potential source component variations in Javan lavas, it is first necessary to try and remove trend-obscuring effects created by subsequent magmatic differentiation.

5.4.2. Differentiation-correction method

Basalts erupted at Javan volcanoes are clearly differentiated (the majority contain less than 7 wt% MgO) and have, therefore, experienced some degree of composition-modifying processes. Crystal fractionation, magma mixing and crustal contamination are all thought to play a part in producing the geochemical diversity of Sunda arc volcanic rocks (Gerbe et al., 1992; Vukadinovic and Sutaidjaja, 1995; Turner et al., 2003; Gertisser and Keller, 2003; Reubi and Nicholls, 2004). Therefore in order to investigate along-arc variations in source

components, it is important to minimise the effects of crustal processes and to compare inter-volcanic rocks of Java at similar degrees of evolution.

An intra-arc comparison approach using the least evolved rocks (lowest SiO_2 or highest MgO) from each volcano is unsuitable due to a wide variation in SiO_2 content of the least evolved lavas produced at each volcano. Previous workers have, therefore, calculated regression lines for each individual magmatic series within an arc and then chosen an 'appropriate' MgO or SiO_2 (x) value e.g. 6 wt % MgO (Plank and Langmuir, 1988; 1998) or 57.5 wt % SiO_2 (Hildreth and Moorbath, 1988) to intercept the calculated regression lines and obtain a comparable set of element/ratios values of individual volcanoes/whole arc suites. However, there are inherent problems in adopting this approach where volcanic suites do not display parallel differentiation trends relative to one another. Magmatic suites that display variably-sloped element/ratio correlations with indices of differentiation to one another, will produce values of y (element abundance/ratio value of interest), which are partly dependent

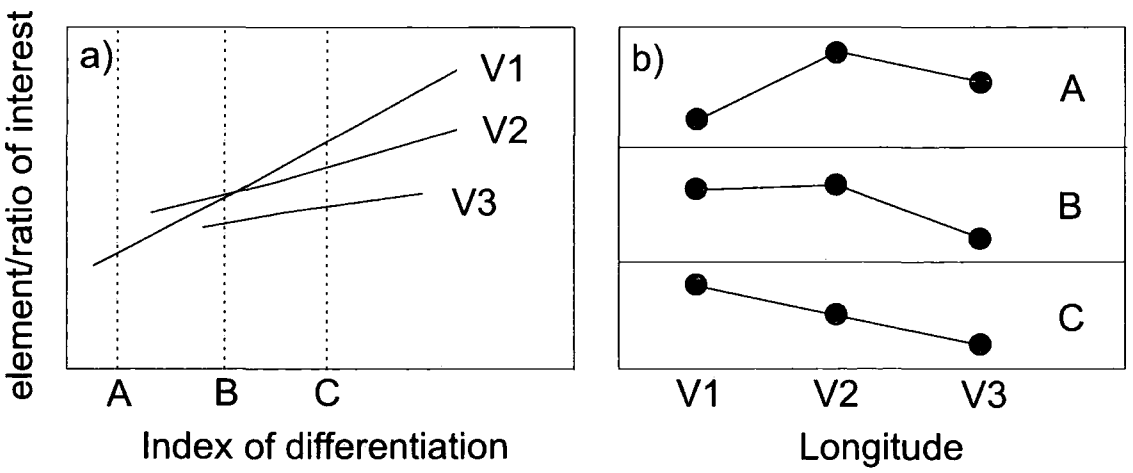

Fig. 5.8. Schematic diagram illustrating the potential dependency of apparent along-arc geochemical trends on choice of differentiation intercept. a). Solid lines represent differentiation trends for 3 volcanoes (V1, V2, V3) along the arc; dashed vertical lines represent the intercept chosen in order to compare the volcanoes at comparable degrees of differentiation (A, B and C). b) displays the relative along-arc (V1-V3) volcano data trends for each of the differentiation intercepts in a).

on the differentiation (MgO or SiO_2) value chosen to intercept the data regression. This is schematically illustrated in Fig. 5.8. The three different differentiation intercept values (A, B and C, Fig. 5.8a) produce notably different along-arc patterns for volcanoes 1, 2 and 3 (Fig. 5.8b), depending on the intercept value of x chosen. This illustration raises the question of what is the most appropriate intercept value for an along-arc comparison of Javan lavas? In Fig. 5.9a, Ba/La has been differentiaion-corrected at a range of differentiation intercepts (for both SiO_2 and MgO) for the data available of Javan volcanoes. Where volcanoes possess horizontal Ba/La variation trends there is little variation in the Ba/La value regardless of the normalisation value chosen, i.e. at 45, 50 or 55 wt% SiO_2, or 5 or 6 wt% MgO (e.g. IVC (I) in Figs. 5.9a and b). However where either a positive or negative correlation is observed between Ba/La and SiO_2 e.g. Merapi (M) and Salak (S), then a range of Ba/La values are produced depending on the intercept chosen (e.g. Salak in Figs. 5.9a and b). Two important points are noted from Fig. 5.9a:

1. The overall along-arc pattern in Ba/La remains the same regardless of choice of intercept of the regression line.
2. There is very little difference between the Ba/La volcano values obtained at intercepts of 5 wt % MgO (Mg5) and 50 wt % SiO_2 (Si50).

In this study the intercept of the regression line at 50 wt% SiO_2 is used as the differentiation-corrected index of the volcano's composition. An intercept value lower than 50 wt% SiO_2, while arguably closer to putative primary magma values, would increase the extent of linear extrapolation and therefore increase uncertainty in the method (e.g. Si45 compared to Si50 for Salak in Fig. 5.9b).

Variations in the degree of melting beneath each volcano may also influence the absolute abundances of some elements. To take this effect into account Plank and Langmuir (1998) normalise the differentiation-corrected element of interest to Na, also corrected for

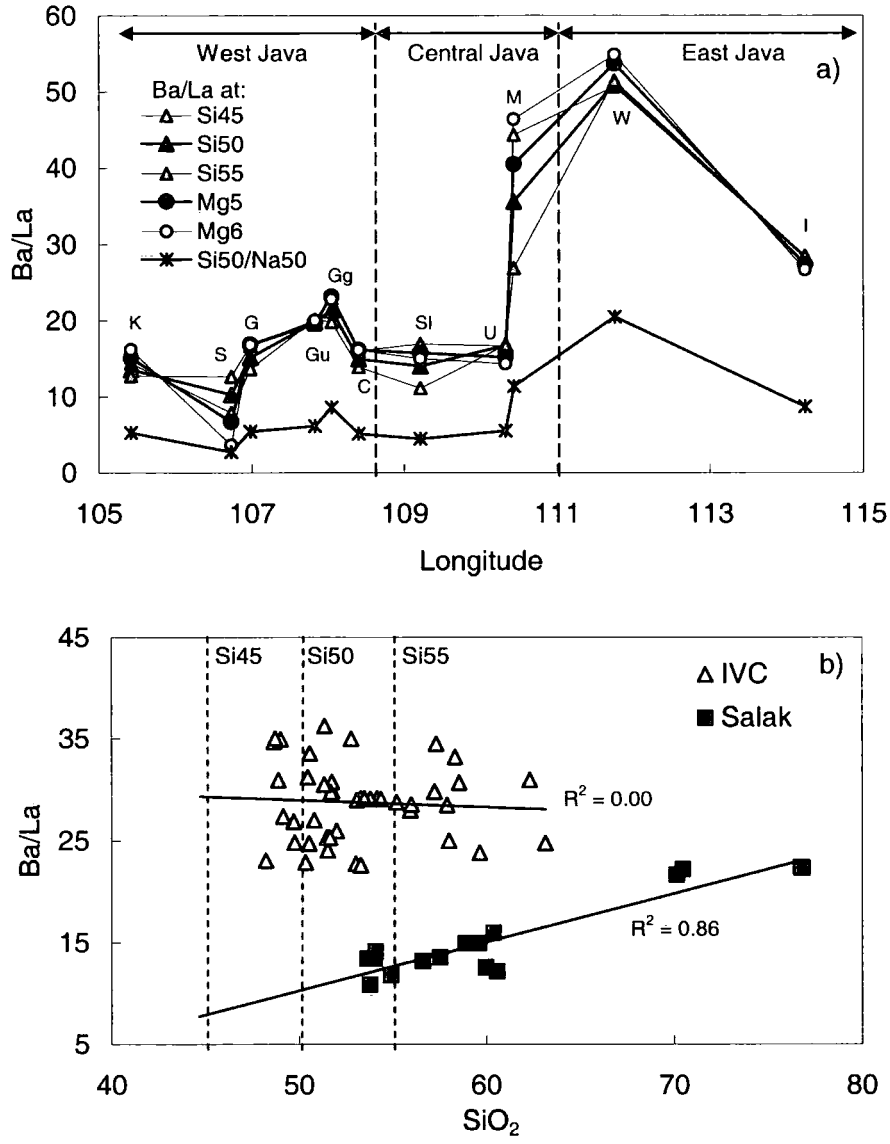

Fig. 5.9. a) Differentiation-corrected Ba/La ratios of Javan volcanoes showing along-arc variation in Ba/La. Dashed lines separate volcanoes in West, Central and East Java as shown by the double-headed arrows. Data sources of Javan volcanic rocks as in Fig. 5.5 (where Ba/La data are available) plus Mandeville et al. (1996) and Camus et al. (1987) for Krakatau, Claproth (1988) for Ungaran, and Hartono (1996) for Wilis. For volcano names see caption to Fig. 5.5. Ba/La ratios of volcanoes were calculated by linear regression, and differentiation intercepts were chosen for a variety of MgO (5 and 6 wt%, Mg5 and Mg6 respectively) and SiO_2 (45, 50 and 55 wt%, Si45, Si50 and Si55 respectively) contents. Ba/La ratio is also plotted for Si50 normalised to Na50 (Na_2O content at Si50) to account for differential melting effects at each volcano (see Plank and Langmuir, 1993). Note that along-arc geochemical trends in Ba/La ratios are relatively unaffected by the differentiation intercept chosen. b) Ba/La versus SiO_2 for IVC and Salak volcanic rocks. Dashed vertical lines represent the different intercept values discussed in the text. R^2 = correlation coefficient.

differentiation using the same intercept value (e.g. at 6 wt% MgO). This is based on the fact that Na shows the strongest correlation with lithospheric thickness, which they infer to control the degree of mantle melting. Application of this method (normalising Ba/La at 50 wt% SiO_2 to Na at 50 wt% SiO_2) to Javan volcanic rocks (Fig. 5.9, Ba/La at Si50/Na50) shows that this does not alter the general trend of increasing Ba/La from Merapi eastwards. This trend in Ba/La therefore appears to be robust even after the effects of melting and differentiation have been taken into account and Ba/La variation may therefore arise due to source variations throughout Java; this will now be investigated.

5.4.3. Variable slab contributions in magma genesis along the Sunda arc

Is it not clear whether there is any change in the nature of the subduction component along the Sunda arc. Edwards et al. (1993) propose a homogeneous slab contribution along the Sunda arc, while Turner et al. (2001) identify along-arc heterogeneity in this component. Assuming an I-MORB mantle wedge source, which has been suggested across Java in this study (section 2.5.2.1, Chapter 2 and 4.6.2.1, Chapter 4) and also by Gasparon and Varne (1998) and other petrogenetic studies of Javan volcanic rocks utilising Pb isotopic and trace element ratios in SE Asia throughout the Cenozoic (Taylor et al. 1994; Hickey-Vargas, 1998; Macpherson and Hall, 2001, 2002; Elburg, et al., 2002; Macpherson et al. 2003), along-arc variation in the slab contribution may therefore explain the observed eastward elevation of Ba/La identified above.

It was outlined in Chapter 1, that both sediment type and mass deposited on the down-going plate change along the arc. The thicker sedimentary deposits present at the site of subduction in West Java, than East Java, are a result of the closer proximity of West Java to turbiditic material sourced from the Himalayan collision zone and deep-sea fans surrounding India in the west (Plank and Langmuir, 1998). However, although unequivocal evidence for

sedimentary incorporation in other arcs, comes from studies of the cosmogenic isotope ^{10}Be (Tera et al., 1986; Morris et al., 1990) it is uncertain whether trench sediments are largely subducted or accreted at the Java Trench. ^{10}Be data of Sunda arc lavas cannot confirm sediment input to the mantle wedge (Edwards et al., 1993), but does also not preclude it. The presence of an accretionary prism in the fore-arc region of the Sunda arc at Java (Kop et al., 2001) suggests that off-scraping of some proportion of trench sediments clearly occurs. Nevertheless, even where large accretionary prisms are formed at convergent margins, some portion of the sedimentary pile is still thought to be subducted (Westbrook et al., 1988; von Huene and Scholl, 1991). von Huene and Scholl (1991) assume that 70-80% of the trench sediment is subducted at accretionary margins; 200-300m of subducted sediment is proposed to be subducted beneath Java by Plank and Langmuir (1998). The large contrast between some element concentrations in sediments and the mantle, suggests that even small amounts of subducted sediment may result in large differences in the compositions of arc lavas produced from the subduction-modified mantle (Plank and Langmuir, 1998). Identification of such contrasts in geochemistry between the mantle and lavas, which are not a result of magmatic differentiation, are key to answering the question of heterogeneity in the subducted component along Java.

5.4.3.2. Trace element constraints

It was highlighted above that Ba concentrations in IVC lavas are substantially higher than those in Salak and GVC rocks for a given SiO_2 content (Fig. 5.2a). Linear regression of the data shows that differentiation trends for the three volcanic suites lay parallel to each other and do not converge (when projected back to less evolved SiO_2 contents) upon a common parental composition, thus suggesting that the differences in Ba concentrations of the Javan rocks result from heterogeneity in the source region. Ba variations of Salak lavas, largely

define a single differentiation trend, suggesting that the crustal contamination process proposed at Salak does not influence Ba concentrations to a significant extent.

Amphibole has the potential to fractionate Ba from the melt in basaltic systems (D ~0.4) (Rollinson, 1993; Matsui et al. 1977). Therefore, variable Ba abundance in the rocks may be controlled by differential amounts of deep-seated amphibole fractionation. Amphibole fractionation at depth (~ base of the crust) is envisaged beneath the majority of Javan volcanoes, including IVC and GVC (but not from CVG magmas at Salak) and an amphibole-bearing xenolith has been observed in a GVC lava (section 4.4.3, Chapter 4). However, as amphibole fractionation is proposed at both GVC and IVC, it is unlikely that this process is responsible for the contrasting low and high Ba abundances of the respective centres. Furthermore, if the amount of amphibole fractionated at depth differed beneath GVC and IVC, then one might expect there to be noticeable effects (similar to that observed in Ba) on other amphibole-compatible elements, possessing similar or slightly higher distribution coefficients to Ba, such as Yb (D ~ 0.5-0.6) (Rollinson, 1993; McKenzie & O'Nions 1991). Fig. 5.2f shows that Yb concentrations in GVC and IVC lavas are largely indistinguishable from one another and do not show the dramatic division witnessed between the two volcanic complexes for Ba (Fig. 5.2a).

Differentiation-corrected Ba/La ratios of Javan lavas (Fig. 5.9a) highlight a general increase in Ba/La east of Merapi volcano. Along Java, a stepped eastward increase in Ba/La is observed when the ranges of Ba/La in Javan volcanic rocks are plotted (Fig. 5.10a). Ba/La ratios in rocks of Central and East Javan volcanoes are elevated compared to West Java, largely a result of the higher Ba concentrations observed in Central and East Javan rocks, e.g. IVC Fig. 5.2a. The fact that La concentrations are also higher in East Javan IVC rocks than West Javan rocks (Fig. 5.2d), makes the high Ba/La ratios highly significant. The Central and East Javan rocks possess similar Ba/La ratios to average oceanic island-arc lavas (OIAV, Fig.

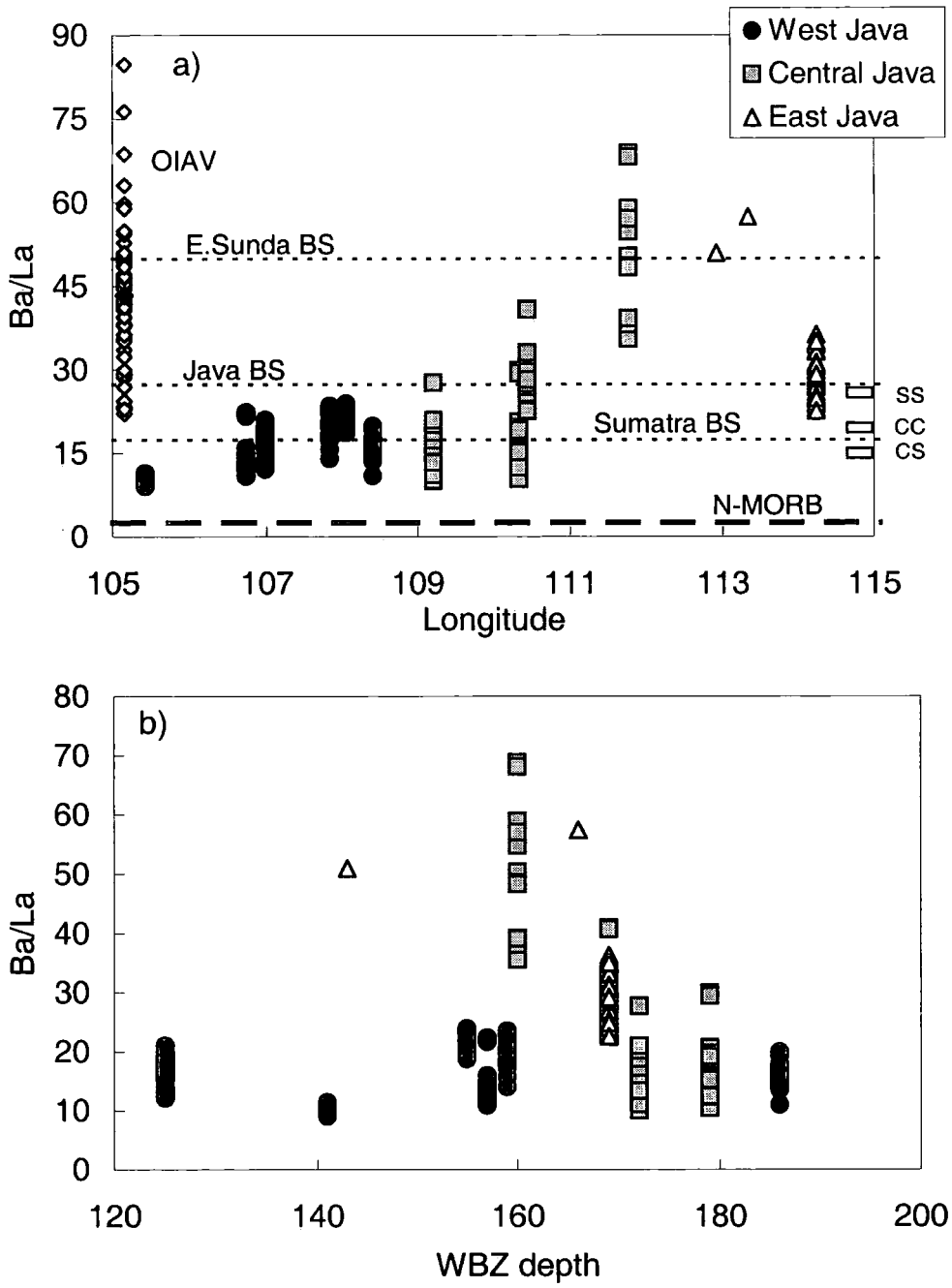

Fig. 5.10. a) Overall along-arc variation in Ba/La ratios of Javan volcanic rocks compared to: N-MORB (thick-dashed line, Sun and McDonough, 1989); Sumatra, Java and East Sunda bulk subducting sediment (BS, thin-dashed lines, Plank and Langmuir, 1998); oceanic island arc volcanic rocks (OIAV, open diamond symbols) represented by Kermadec (Turner et al., 1997; Ewart et al., 1998) and Mariana (Elliot et al., 1997) lavas (filled diamond symbol = average OIAV); average continental crust (CC, Taylor and McLennan 1985); silicic sediments (SS) and carbonatic sediments (CS) (Gasparon and Varne, 1998). Data sources of Javan volcanic rocks as in Figs. 5.5 and 5.8. b) Ba/La versus WBZ depth for volcanic rocks of Java.

5.10a). Whitford et al. (1979) suggested that Ba concentrations correlate with depth to the underlying WBZ in Sunda arc lavas. It is important, therefore, to establish whether Ba/La ratios are also controlled by WBZ depth. Fig. 5.10b shows that there is generally no correlation between Ba/La of the volcanic rocks and WBZ depth beneath the volcano. Consequently, the general along-arc increase in Ba/La is proposed to be a result of heterogeneity in the (subduction-modified) mantle source region along Java. The nature of this component will now be investigated to establish whether it is sourced from the subducted basaltic oceanic crust or the accompanying down-going sediments.

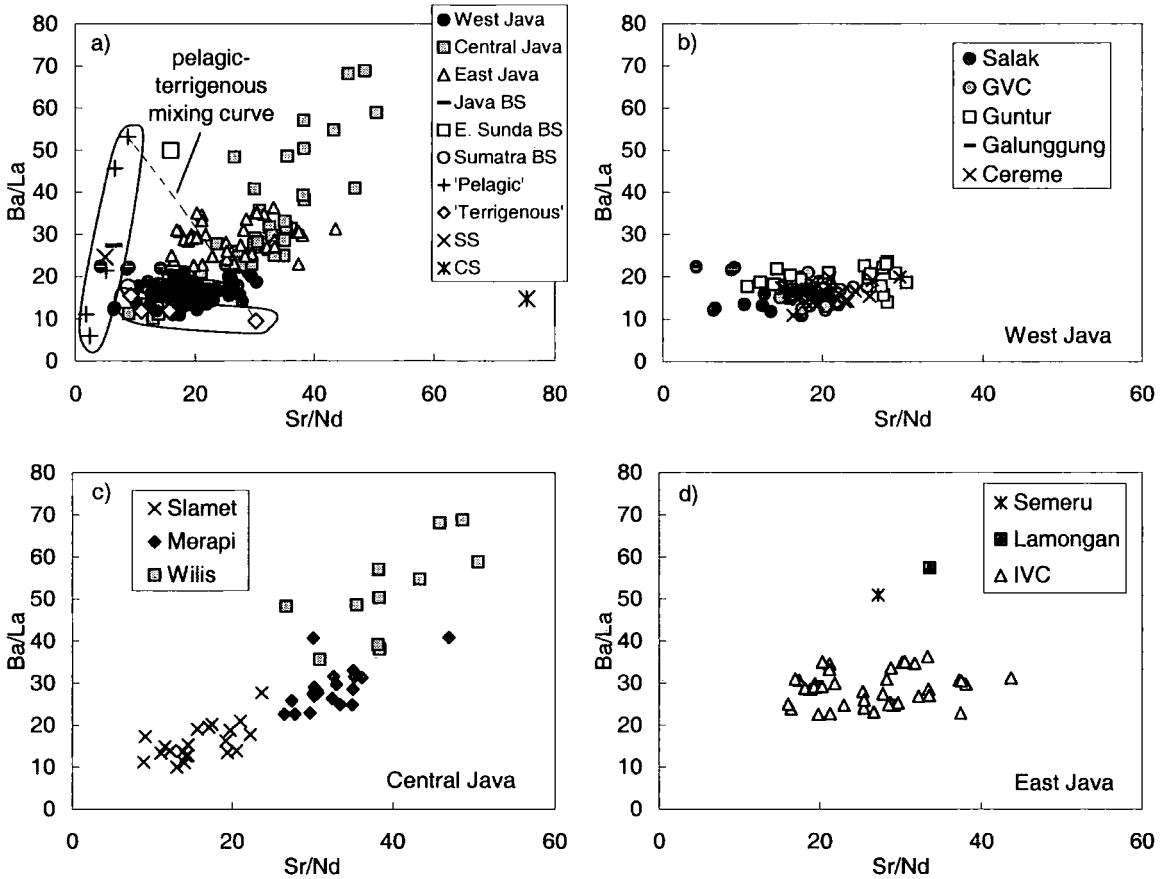

Fig. 5.11. Ba/La versus Sr/Nd for volcanic rocks from a) Java (whole data set), b) West Java, c) Central Java, and d) East Java, highlighting the relative enrichment in Ba/La and Sr/Nd of Central and East Javan volcanoes relative to West Javan volcanoes. Individual 'Pelagic' and 'Terrigenous' Indian Ocean sediment data samples in a) from Gasparon and Varne (1998) and Plank and Langmuir (1998), and Ben Othman et al. (1989) and Plank and Langmuir (1998) respectively. For data sources of bulk Indian Ocean sediments and Javan volcanic rocks in a) (where available) see Figs. 5.5 and 5.9. Bulk mixing between high Ba/La pelagic sediment (Pel. Clay, 261; Gasparon and Varne, 1998) and high Sr/Nd terrigenous sediment is shown by the dashed curve in a).

Elevations of LILE/LREE ratios such as Ba/La and Sr/Nd in arc lavas compared to MORB are frequently attributed to fluid addition to the mantle wedge from the dehydration of the subducting slab (Ben Othman et al., 1989; Elliot et al., 1997). Central (Fig. 5.11c) and East (Fig. 5.11d) Javan volcanic rocks display elevations in both of these fluid-flux indicators compared to West Javan rocks (Fig. 5.11b), which display limited variation in Ba/La over a moderate range in Sr/Nd. Therefore, it may be hypothesised that there is a stronger fluid contribution from the slab (AOC) to the mantle source in Central and East Java than west Java. However, the majority of Central and East Javan volcanic rocks possess lower Ba/La ratios than those of Kermadec and Mariana arc rocks (Fig. 5.10a), where the dominant slab input is thought to be a hydrous fluid (Woodhead et al., 2001). In addition to hydrous fluid, high Ba/La ratios are found in pelagic sediments from the Indian Ocean (Fig. 5.11a). The distribution of Ba in deep-sea sediments is variable and complex, but some Javan diatom and radiolarian oozes are very rich in Ba (Plank and Langmuir, 1998). Likewise, Sr substitution for Ca in calcium carbonate can result in high Sr concentrations in nannofossil and foraminiferal oozes on the sea floor (Plank and Langmuir, 1998). High Ba/La and Sr/Nd in Central and East Javan lavas may, therefore, be a result of a dominant pelagic contribution to the source from the subducting sediment. Conversely, moderate Sr/Nd and low Ba/La in West Javan volcanoes may be explained by less input from a pelagic sedimentary component, and greater terrigenous sediment contribution to the magmatic source region. This hypothesis is consistent with the eastward thinning of terrigenous (turbiditic) sediment deposition on the down-going plate from the Himalayan and Ganges delta source in the west (Susilohadi et al., 2005; Plank and Langmuir, 1998; Gasparon and Varne, 1998). Therefore it is possible that the along arc changes in trace element ratios from West to East Java may reflect:

1. An increasing fluid contribution sourced from the altered oceanic crust, and/or

2. Transition from a 'terrigenous' to 'pelagic' dominated subducted sedimentary component.

A mixing curve between the pelagic sediment with the highest Ba/La (Pel. clay, 261; Plank and Langmuir, 1998) and terrigenous sediment with the highest Sr/Nd (V33-77; Ben Othman et al., 1989) of 5.10a is plotted to show the potential extent of bulk sediment source input control on the trace element ratios of the lavas. The positive correlation observed between Ba/La and Sr/Nd for Central Javan volcanic rocks extends beyond the field of bulk sediment control constrained by the mixing curve. This suggests that 1) the sedimentary component is more likely added to the mantle wedge as a fluid rather than by bulk addition, 2) that a slab fluid (with characteristically high Ba/La and Sr/Nd) exerts the major control on Ba/La and Sr/Nd ratios of the lavas, or 3) both of the above. However, the fields for pelagic and terrigenous sediments outlined here are defined by only a handful of samples. It is possible that Indian Ocean sediments possess a wider range in these ratios than currently observed. It is stated above that pelagic sediments can have high Sr concentrations, but the Indian Ocean pelagic sediments plotted only display relatively low Sr/Nd. Based on chemical composition, Gasparon and Varne (1998) (and see earlier work by Cook, 1974) identified two Indian Ocean sediment end members: SS (siliceous-clastic) and CS (calcareous-organogenic). The latter type (asterisk Fig. 5.11a) possesses a significantly higher Sr/Nd ratio than any of the individual Indian Ocean sediment samples and all of the Javan volcanic rocks plotted in Fig. 5.11a. Other, calculated average sedimentary compositions also lie outside the space defined by the pelagic-terrigenous mixing, for example, the bulk sediment calculated by Plank and Langmuir (1998) for East Sunda (open square, Fig. 5.11a). In conclusion Ba/La and Sr/Nd characteristics of Javan arc lavas implicate a variable contribution from the subducting plate. However, these ratios prevent precise identification of this component (altered oceanic crust fluid or sediment, or both).

Woodhead et al. (2001) use a plot of Ba/La versus Th/Yb to distinguish oceanic arcs dominated by slab-derived fluids from those dominated by sediment/sedimentary melts (similar discriminatory diagrams in Hawkesworth et al., 1997): volcanic rocks strongly influenced by the former, trend to high Ba/La, while the later, towards high Th/Yb. The authors show that Sunda arc samples gather around the apex of the two trends suggesting that both fluid and sedimentary components are involved in petrogenesis of Sunda arc lavas. Th and Yb concentrations in Salak volcanic rocks (Fig. 3.5, Chapter 3) both increase with increasing magmatic differentiation (note Yb concentrations do not usually vary with differentiation in Javan volcanic rocks). As a result Th/Yb of Salak lavas appear relatively low compared to other Javan lavas despite similar Th concentrations in Salak basaltic-andesites and andesites (2-8 ppm) to basalts-andesites of GVC and IVC (3-9 ppm and 2-11 ppm respectively), which may therefore lead to misinterpretations of source inputs. However, in agreement with the general suggestion by Woodhead et al. (2001), geochemical modelling of East Javan IVC lavas (Chapter 2) suggested that both a slab fluid and sedimentary contribution are required in magma petrogenesis.

5.4.3.3. Nd-Hf isotope constraints on subducted sediment type

It was proposed in Chapter 2, that contamination of the mantle source by a fluid created during dehydration of the AOC would largely be undetectable on plots of $^{143}Nd/^{144}Nd$ versus $^{176}Hf/^{177}Hf$, and therefore a plot of this type may be more useful for identifying whether along arc geochemical variation of lavas from Java are consistent with spatial variations in the composition of subducting sediment. A plot of this nature is transparent to fluid addition due to the fact that Nd isotope ratios remain relatively constant during hydrothermal and low temperature seawater alteration of MORB, and by inference (White and Patchett, 1984), that Hf isotope ratios will be equally unaffected by such alteration, due to the low concentrations

of both Nd and Hf in seawater. Mantle source modification by an AOC fluid would also have limited effect on $^{143}Nd/^{144}Nd$ and $^{176}Hf/^{177}Hf$ isotope ratios, due to the geochemical similarity of the down-going plate and mantle source proposed in Javan magma genesis (both I-MORB in composition). Furthermore, experimental investigations (You et al., 1996; Tatsumi et al., 1986; Brenan et al., 1995; Kessel et al., 2005) and conclusions from other arc studies (McCulloch and Gamble, 1991: Pearce and Peate, 1995; Münker et al., 2004) suggest that Nd and Hf are relatively fluid immobile elements (e.g. compared to Sr). Finally, AOC has characteristically high $^{87}Sr/^{86}Sr$ isotope ratios (due to interaction with seawater), therefore an increasing level of incorporation of fluid sourced from the AOC towards East Java would be predicted to create an increase in $^{87}Sr/^{86}Sr$ isotope ratio from Central to East Java, i.e. correlate with Ba/La. This trend is not observed in along-arc Sr isotopes (Fig. 5.5a). However, this does not preclude a role for slab-fluid sourced from the AOC, which is clearly important in the magma genesis of IVC lavas (Chapter 2), where a two-stage source contamination process has been proposed, it emphasises that another source component is required to explain along-arc geochemical variations.

Incorporation of a subducted component in the mantle source dominated by either pelagic or terrigenous sediment will produce very different mixing trends in Nd-Hf isotope space due to the contrasting Nd/Hf ratios of the sediments (Patchett et al., 1984): pelagic sediments have variable and relatively high Nd/Hf (6-42, n = 9, Plank and Langmuir, 1998; Ben Othman et al., 1989; Gasparon and Varne, 1998) resulting in convex-up mixing trends, whereas terrigenous sediments tend to have relatively low Nd/Hf (4-7, n = 6, Ben Othman et al., 1988; Vervoort et al., 1999; Gasparon and Varne, 1998) producing relatively straight mantle source-sediment mixing curves (Fig. 5.12 inset). Therefore, in contrast to Ba/La and Sr/Nd element ratios, Nd-Hf isotope ratios of Javan lavas may be able to address whether along-arc variations in geochemistry reflect changes in the subducted component outlined

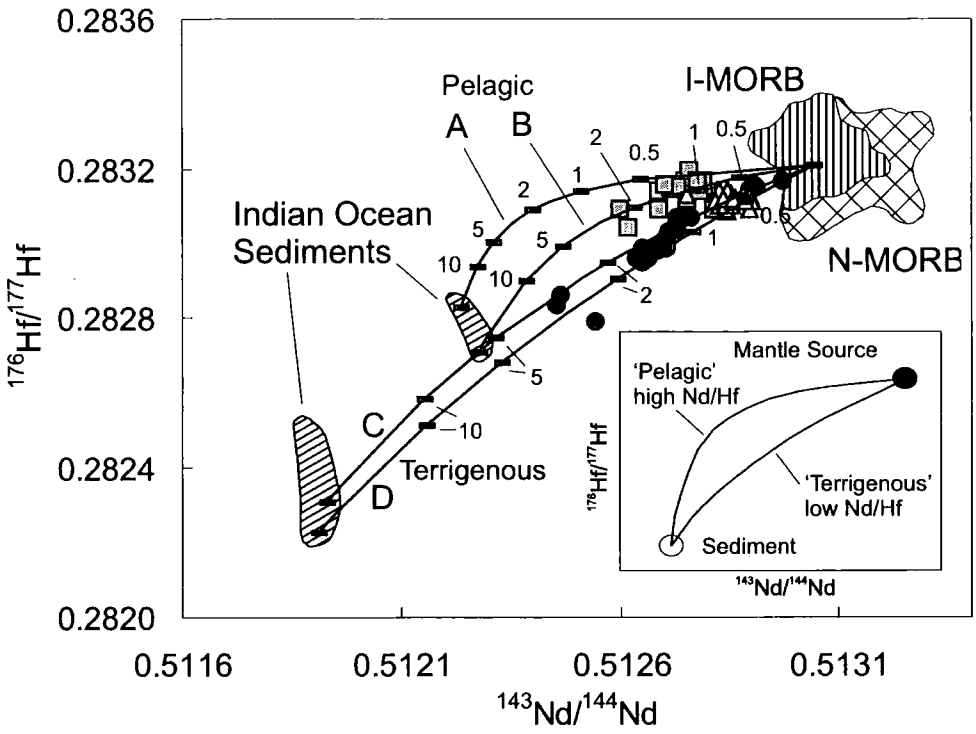

Fig. 5.12. $^{176}Hf/^{177}Hf$-$^{143}Nd/^{144}Nd$ plot showing bulk mixing models between I-MORB source and Indian Ocean sediments, highlighting the different curvatures produced from mixing mantle and 'pelagic' high Nd/Hf (15-33) sediment (curves A & B), or with 'terrigenous' low Nd/Hf (6-7) sediment (curves, C and D). A = Mn nodule (V34-62, White et al., 1986; Ben Othman et al., 1989), B = pelagic clay (V34-45 White et al., 1986; Ben Othman et al., 1989) C and D = terrigenous sediments V28-357-M (CA30-M) and V28-357-M (CA30-S) respectively (Vervoort et al., 1999). End member compositions given in Chapter 4, Table 4. Java data distinguished by geographical region, data sources as in Fig. 5.3b and data symbols as in Fig. 5.5. Inset: schematic illustration of mixing curves produced from mixing low and high Nd/Hf sediments with a MORB-like mantle source.

and hypothesised above. Fig. 5.12 shows that West, Central and East Javan volcanic rocks generally define arrays with slightly different trajectories: West Java, for which there is the most data available, displays a positively correlated trend in $^{143}Nd/^{144}Nd$-$^{176}Hf/^{177}Hf$ isotope space, while Central, and particularly East Javan rocks, define generally horizontal arrays. Simple bulk mixing calculations between I-MORB mantle source and pelagic (curves A and B) and terrigenous (curves C and D) sediments suggest that displacement of Javan arc lavas from I-MORB $^{143}Nd/^{144}Nd$ and $^{176}Hf/^{177}Hf$ ratios and domain trajectories can be explained by

addition of a small amount (generally < 5 %) of terrigenous low Nd/Hf sedimentary material to the mantle source of West Javan lavas, and addition of similar-sized, sedimentary component dominated by pelagic, high Nd/Hf material to the mantle source of Central and East Javan lavas (noting the lower than average I-MORB Hf isotope ratio of the East Javan mantle source discussed in Chapter 2). This interpretation is consistent with greater amount of turbidite sediments on the down-going plate in West Java than Central and East Java due to the closer proximity of West Java to the Himalayan/Ganges turbidite source, and suggests that the higher Ba/La and Sr/Nd ratios found in Central and East Javan volcanic rocks may too reflect subducted sediment rather than slab-fluid control. In summary, several geochemical characteristics of Javan arc lavas can be attributed to incorporation of subducted sediment, the composition of which is controlled by spatial variations in the sediments deposited on the down-going Indian Ocean plate.

5.5. Summary and Conclusions

IVC (East Java), GVC and Salak (West Java) volcanic rocks possess largely identical mineral assemblages and display similar trends in the majority of major and trace element variation diagrams. Excluding the unusual (compared to the rest of Javan lavas) differentiation trends exhibited by some Salak samples, there are notable geochemical differences in lavas from East and West Java: relative enrichments of Ba, K and to a lesser extent Na, Sr and La are observed the most basic IVC lavas compared to GVC and Salak rocks of similar SiO_2 content. Also, different trajectories are defined by IVC data on Sr-Nd-Hf isotope diagrams compared to data from GVC and Salak.

Comparison of IVC, GVC and Salak lava geochemistry, new Hf-isotope data for Merapi and Guntur, and data from other volcanoes of Java located along the volcanic front, has revealed significant spatial geochemical variations along Java. Contrary to the frequently

quoted generalisation of decreasing $^{87}Sr/^{86}Sr$ isotope ratio eastwards along Java, $^{87}Sr/^{86}Sr$ is shown to broadly increase in volcanic rocks from Krakatau (west of Java), to ~Merapi Volcano (eastern Central Java). Further east of this point, $^{87}Sr/^{86}Sr$ isotope ratios of Javan volcanic rocks are much lower and relatively constant. Correlation of maximum $^{87}Sr/^{86}Sr$ isotope ratio with volcanic edifice summit elevation in West and Central Javan volcanoes and not with WBZ depth (as previously suggested) indicates that some of the isotopic variation is related to lithospheric thickness. The lack of correlation between Sr isotope ratios and indices of differentiation, Sr-O isotope mixing calculations and constraints placed on the $^{87}Sr/^{86}Sr$ isotope ratio of the contaminant at Salak (Chapter 3), suggest that typical upper-crustal contamination cannot explain Sr isotope variations in Javan volcanic rocks as previously hypothesised (Whitford, 1975; Hamilton, 1979) and concluded (Gasparon and Varne, 1998). Therefore it is proposed, that longer melting columns are present beneath volcanoes situated on relatively thinner arc lithosphere in eastern Java (and Galunggung and Guntur in West Java), which effectively dilute the subduction component and reduce the impact of isotopic modification of the magmas produced, resulting in relatively lower $^{87}Sr/^{86}Sr$ isotope ratios in volcanic rocks of these volcanoes. $^{87}Sr/^{86}Sr$ ratios of lavas may also be partly controlled by heterogeneity in the sedimentary input along the arc). A transition in the architecture of the crust between Central and East Java is consequently proposed (Fig. 5.13), which may correspond to the south-eastern limit of the pre-Tertiary 'continental' Sundaland boundary. However, zircon data highlights complexity in the nature of the Javan arc crust and precludes the simplistic assumption of a smooth lateral transition from thicker 'continental' to thinner 'oceanic' arc crust in Java (Fig. 5.13). Mantle-like $\delta^{18}O$ values of clinopyroxene phenocrysts in Javan lavas and contaminant constraints from AFC modelling of Salak lavas, suggest that although the crust is thicker beneath the main volcanic axis in West and Central Java (Fig. 5.13) it is not typically 'continental' in character, but consistent with the proposal by

Hamilton (1979) that the crust in this region may consist of melange, and older volcanic rocks.

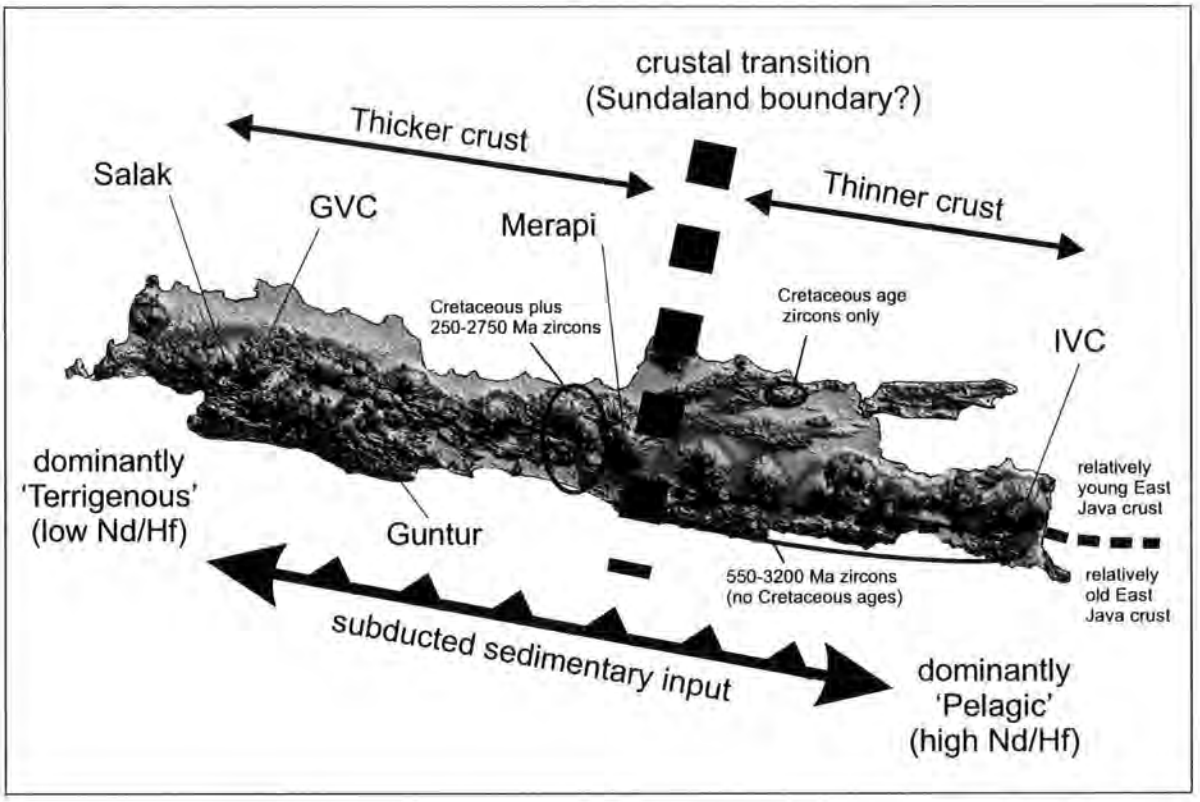

Fig. 5.13. Schematic diagram showing the hypothesised transition in the Javan crust based on Sr isotope data (dashed line, see text). Double-headed arrow represents heterogeneity in the subducted sediment component along the arc: from terrigenous in West Java to pelagic in Central and East Java. The main volcanoes of this study (Salak, GVC and IVC) are marked, along with other volcanoes for which new Hf data has been presented (Guntur and Merapi, Table C.2. Appendix C). The general fields of inherited zircon ages (U-Pb dating) are shown for Central and East Java (H. Smyth, pers. comm.). The hypothesised arc-parallel crustal boundary in East Java between relatively old and young crust, constrained by zircon ages and nature of the topography is also shown (thin black dash). Elevation Model of Java from SRTM data (Shuttle Radar Topography Mission, NASA data).

Along-arc increases in Ba/La and Sr/Nd in Javan volcanic rocks, combined with different trajectories of the Javan domains in Nd-Hf isotope space can be attributed to incorporation of a heterogeneous subduction component, which largely reflects spatial variations in sediment types deposited on the down-going plate along the Java Trench (Fig.

5.13). Relatively low Ba/La, moderate Sr/Nd and a positive correlation in Nd-Hf isotope space for West Javan volcanic rocks is consistent with the incorporation of a dominantly terrigenous sedimentary component, whereas, relatively high Ba/La, Sr/Nd and horizontal arrays of volcanic data in Nd-Hf isotope space for Central and particularly East Javan volcanoes is consistent with a more pelagic subducted sedimentary component and possibly stronger slab-fluid imprint (e.g. as concluded for IVC, Chapter 2). The along arc variation in sediment type involved in magma genesis is consistent with the decreasing thickness of turbidite deposits on the down-going slab from Sumatra to East Java and in agreement with previous petrogenetic studies of Sunda arc lavas (Edwards, 1990; Hoogewerff et al., 1997; de Hoog et al., 2001; Turner and Foden, 2001; Gertisser and Keller, 2003) that propose subducted sediments play a major role in determining many geochemical characteristics of arc lavas.

Chapter 6

Summary and conclusions: petrogenesis of Salak, GVC and IVC lavas and along-arc variation in source contributions in Sunda arc magma genesis

Summary and conclusions: petrogenesis of Salak, GVC and IVC lavas and along-arc variation in source contributions in Sunda arc magma genesis

6.1. Differentiation of Magma

Differentiation processes e.g. magma mixing, fractional crystallisation and AFC play a major role in modifying the geochemical composition of Salak, GVC and IVC primary magmas. However, the relative importance and traceable impact of the different processes varies at each volcanic centre.

Banded primary magmatic fragments in pyroclastic flow deposits at GVC provide direct evidence for the physical mingling and mixing of magmas of more evolved and less evolved compositions. Plagioclase and pyroxene textures and compositions in Salak, GVC and IVC volcanic rocks also suggest magmatic disequilibrium. Magma mixing may provide an important eruption triggering mechanism but it is incapable of explaining the overall major and trace element variation displayed by GVC, Salak and IVC lavas. Similar to conclusions reached in other arc studies (e.g. Grove et al., 2005; Turner et al., 2003) fractional crystallisation exerts the largest control on major and trace element composition of the volcanic rocks. The more evolved rocks can be produced by fractionation of a typical Javan island arc mineral assemblage of plagioclase, clinopyroxene, Fe-Ti oxide ± olivine and orthopyroxene from the less evolved members of each magmatic suite.

IVC and Salak volcanic rocks display distinct intra-volcanic complex differentiation trends that are explained by independent conduits and multiple magma reservoirs at different depths in the crust. Spatial variations in chemistry at IVC are clearly linked to sub-volcanic structure. Magmatic differentiation occurs deeper in the crust beneath volcanoes situated around the caldera rim compared to relatively shallow-level fractionation beneath volcanoes located inside the caldera. Storage of magma at greater depth beneath the caldera-rim

volcanoes results in the suppression of plagioclase fractionation, which is reflected in the chemistry of the volcanic rocks. Separate magmatic pathways and storage depths in the crust are also advocated at Salak. Significantly lower HFSE and HREE contents at comparable silica contents in SVG rocks compared to CVG rocks suggest that amphibole fractionation occurs at depth below the eastern flank vent and that any entrained amphibole cargo is dissolved closer to the surface. By inference, deep fractionation of amphibole is suggested at the majority Javan volcanoes, which also display negligible HREE variation with SiO_2. Evolution to high HFSE and HREE concentration in the CVG lavas suggests that magma beneath the central part of the volcano has by-passed the deep-level crustal storage envisaged beneath the eastern flank vent. Increases in HFSE and HREE with increasing SiO_2 are most likely controlled by incompatible behaviour during progressive fractional crystallisation. However, closed system fractionation is incapable of explaining the systematic variation in some trace element ratios and therefore, assimilation of a low K/Rb and Ba/Th crustal component is required during fractionation to explain element variations in CVG lavas of Salak.

GVC, IVC and Salak clinopyroxenes present low, mantle-like $\delta^{18}O$ values and the volcanic rocks do not display significant correlations of radiogenic isotope ratios or $\delta^{18}O$ values with indices of differentiation, implying that shallow level contamination by upper-crustal continental material is inconsequential during magmatic differentiation (cf. the Andes and Lesser Antilles, see Davidson et al., 2005 and references therein). However, careful investigation of the CVG lavas of Salak, reveals a small but notable correlation between Sr isotopic ratios and SiO_2 and suggests that AFC processes are operating beneath Salak. The contaminant involved is largely similar in geochemical and isotopic composition to the lavas themselves and is characterised by $^{87}Sr/^{86}Sr \sim 0.7048$, relatively low K/Rb, Ba/Th and $\delta^{18}O$ and relatively high Sr concentration. This suggests that the composition of the crust in West

Java beneath Salak is relatively primitive compared that of mature continental crust. Any interaction of IVC and GVC magmas with the upper arc crust during differentiation has had negligible impact on their geochemistry, but assimilation of isotopically indistinct material (i.e. older volcanic crust) cannot be discounted.

6.2. Source Characteristics

In agreement with most models of subduction zone petrogenesis (e.g. Ellam and Hawkesworth, 1988; McCulloch and Gamble, 1991; Pearce and Peate, 1995) the mantle wedge and subducting slab are important for the formation of Sunda arc magmas. HREE of Salak, GVC and IVC rocks generally display relatively flat profiles suggesting that garnet is not an important residual mineral in the source region and implying that magmas are derived from a relatively shallow mantle, above the garnet/spinel transistion for wet peridotite. Contrary to some suggestions of an enriched mantle component (Edwards et al., 1991, 1993; Wheller et al., 1987) in the source region, this study agrees with the majority of Sunda arc petrogenetic studies (e.g. White and Patchett, 1984; Stolz et al., 1990; Turner and Foden, 2001; Elburg et al., 2002), which advocate a MORB-like source for Sunda arc lavas. Similarity of HFSE and HREE concentrations in IVC and GVC basalts to those of I-MORB (compared to N-MORB) suggest the mantle source composition is best represented by I-MORB. Isotopic heterogeneity is proposed in the I-MORB source component. Data trajectories suggest that I-MORB with lower than average $^{176}Hf/^{177}Hf$ isotope ratios exists beneath IVC in East Java. Intra-volcano HFSE/HREE ratios of IVC and GVC lavas are fairly homogenous and indicate that the mantle wedge is not significantly depleted beneath Java, compared to that at other arcs such as the Izu-Bonin and Marianas, where melt extraction prior to involvement in arc petrogenesis is implicated – most likely by back-arc processes

which do not operate at Java (Taylor and Nesbit, 1998; Elliot et al., 1997; Woodhead et al., 1993).

Higher Sr and lower Nd and Hf isotope ratios in IVC, Salak and GVC lavas than I-MORB largely arise from contamination of the mantle source by subducting slab components. Radiogenic and trace element data of IVC suggest a 3-component, 2-stage source contamination model is applicable at IVC. In this model I-MORB mantle is metasomatised by slab fluid, sourced from the AOC, prior to addition of subducted sediment. 3-component models have been suggested for other arcs e.g. Mariana and Tonga-Kermadec (Ellam and Hawkesworth, 1988; Taylor and Nesbit, 1998; Elliot et al., 1997, Turner et al., 1997), although the order in which the components are introduced to the mantle wedge in East Java (fluid first, then sediment) differs from that in some of the models proposed. At GVC (and Salak), 2-component mixing between I-MORB mantle source and Indian Ocean sediment can explain the displacement of lava isotopic ratios from the I-MORB domain. The percentage of Indian Ocean sediment involved in magma genesis at GVC (< 2.5%) and IVC (< 1%) are comparably small but is slightly less at IVC. The percentages of subducted sediment required are similar to those proposed in the petrogenesis of other Sunda arc lavas. e.g. 2.5% subducted Sunda sediment at Sangeang Api, East Sunda (Turner et al., 2003) and 1-2% Indian Ocean sediment at Merapi (Gertisser and Keller, 2003).

6.3. Along-arc geochemical variations

Notable differences are observed in the geochemistry of volcanic rocks between IVC in East Java and GVC and Salak in West Java. These include relative enrichments of Ba, K and to a lesser extent Na, Sr and La in IVC samples compared to GVC and Salak samples. IVC volcanic rocks also display a different trajectory on Sr-Nd-Hf isotope diagrams compared to GVC and Salak rocks. Contrary to the previously noted eastward decrease in $^{87}Sr/^{86}Sr$ along

Java (Whitford, 1975) a progressive eastward increase in Sr isotope ratio across West and Central Java is recognised in this study, which broadly correlates with inferred crustal/lithospheric thickness. East Javan lavas display relatively low and homogenous Sr isotope ratios and do not show any correlation with inferred crustal thickness. Higher Sr isotope ratios in volcanic rocks erupted through relatively thicker crust appears to suggest probable assimilation of crustal material. However, the general absence of correlation between $^{87}Sr/^{86}Sr$ and indices of differentiation, plus low $\delta^{18}O$ clinopyroxene values imply that contamination of West and Central Javan magmas by isotopically-distinct material is negligible. $^{87}Sr/^{86}Sr$ of volcanic rocks are more likely controlled by the length of the mantle melting column beneath the volcanoes, which is largely dependant on the thickness of the arc crust. It is proposed that there is a significant change in crustal thickness between Central Java (Merapi) and East Java (Kelud) (Fig. 6.1), and that this transition may represent the south-eastern boundary of Sundaland (pre-Tertiary basement) previously suggested to be located somewhere between Sumatra and East Java.

Elevation of Ba/La and Sr/Nd in volcanic rocks of eastern Java compared to western Java, along with different trajectories of Javan domains in Nd-Hf isotope space, can be attributed to incorporation of a heterogeneous subduction component, which largely reflects spatial variations in sediment compositions on the down-going plate along the Java Trench (Fig. 6.1). Relatively low Ba/La, moderate Sr/Nd and a positive correlation in Nd-Hf isotope space for West Javan volcanic rocks is consistent with the incorporation of a dominantly terrigenous sedimentary component, whereas, relatively high Ba/La, Sr/Nd and horizontal arrays of volcanic data in Nd-Hf isotope space for Central and particularly East Javan volcanoes is consistent with a more pelagic subducted sedimentary component and possibly stronger slab-fluid imprint (as suggested by geochemical modelling IVC lavas) (Fig. 6.1). Transition from a terrigenous to pelagic dominated subduction component eastwards from

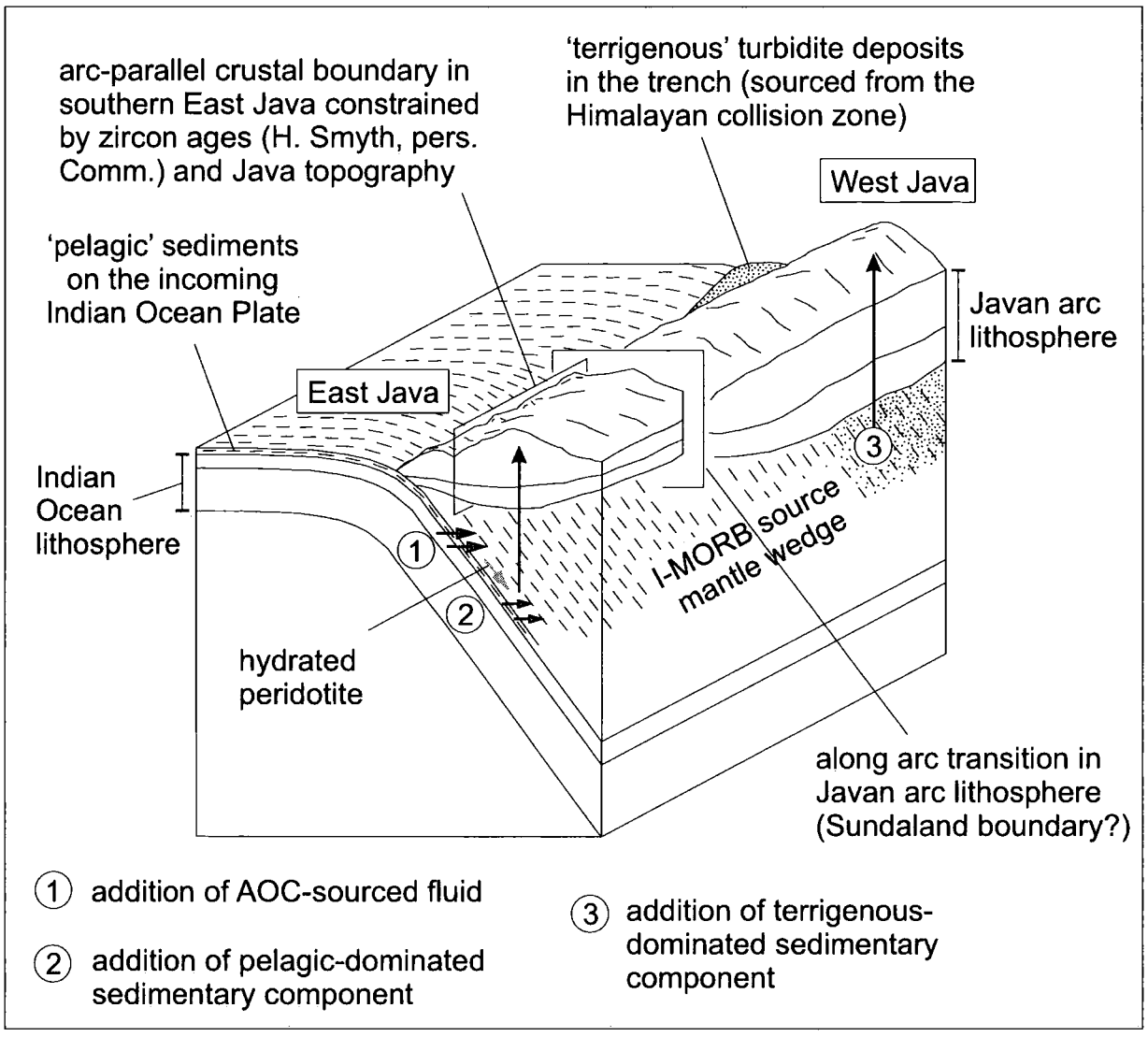

Fig. 6.1. Schematic diagram of the Javan subduction zone system illustrating the along arc variability in upper plate lithospheric thickness and heterogeneity in the subducted sedimentary component from West to East Java, as discussed in the text. The E-W arc parallel lithospheric boundary, south of the present volcanic axis in East Java, separates 'old' arc lithosphere in the south from relatively younger lithosphere to the north, based on zircon studies by H. Smyth (pers. comm.) and the more rugged topography of southern East Java than that further to the north.

West Java is consistent with the variation in composition of sediment presently deposited on the down-going plate at the Java trench and concurs with previous petrogenetic studies that advocate a major role for subducted sedimentary material in the petrogenesis of Sunda arc lavas (Edwards, 1990; Hoogewerff et al., 1997; de Hoog et al., 2001; Turner and Foden, 2001; Gertisser and Keller, 2003).

6.4. Implications and considerations for arc-wide geochemical studies

The intra-volcanic complex variations in lava geochemistry identified at Salak and IVC emphasise the need for detailed investigation of individual volcanic studies prior to inclusion of selected samples in along arc studies. Magmatic differentiation has created a wide range in Javan lava compositions and complicates source component characterisation. Prior to investigation of along-arc variations in source composition, it is therefore imperative that the geochemical impacts of composition-modifying processes are established.

Arc lavas are generally characterised by high LREE/HFSE ratios, attributed to involvement of a subducted component. LREE/HFSE ratios in Salak lavas are relatively low in the CVG, even though LREE concentrations are relatively high. This results from high HSFE concentrations and positive correlations of both LREE and HFSE with SiO_2 in the CVG rocks. Therefore, caution should be employed when considering subduction enrichment in along-arc studies using LREE/HFSE ratios, as misleading interpretations may result where only a few samples have been analysed from each volcano. It also has implications for using high LREE/HFSE ratios to fundamentally characterise arc lava sources. Furthermore, detailed volcano-scale study is essential prior to along arc comparisons of volcanic data, as subtle evidence for particular processes may be difficult to discern on a larger scale. For example, the contamination of CVG magmas at Salak during fractional crystallisation is largely undetectable when comparing the Salak data set as a whole with other Javan data.

This study has shown that arc magmatic suites of a single arc can display variably sloped element/ratio correlations with indices of differentiation, which will produce values of y (element abundance/ratio value of interest) that are partly dependent on the differentiation (MgO or SiO_2) value chosen to intercept the data regression. Consequently, along-arc petrogenetic studies must assess and take into account: 1) variation in differentiation trends between magmatic suites, and 2) the dependency of apparent along-arc geochemical trends

on the differentiation intercept (i.e. wt% MgO or SiO_2) chosen to obtain a comparable set of elements/ratios of individual volcanoes/whole arc suites.

Finally, it is shown that isotope ratios and trace element characteristics of Javan arc lavas are strongly influenced by the composition of the local subducting sediment and local nature of the arc crust. Along-arc variations in the character and composition of both the overriding and down-going plates must therefore be considered in any assessment of lateral variations in the geochemistry of arc lavas.

6.5. Areas for future research

Assessment of temporal geochemical evolution at volcanoes in this study, in particular Salak and GVC, is severely impeded due to the lack (and even complete absence) of accurately dated samples. This has led to reliance on basic geological maps and relative stratigraphic relationships to establish broad volcanic stratigraphy in this study (i.e. on a volcanic centre-scale). The separate intra-volcanic differentiation trends highlighted above (e.g. within IVC and Salak) suggest that multiple independent conduits and reservoirs exist beneath the volcanoes. Better constraints on sub-volcanic architecture and rates of differentiation processes during crystallisation could be obtained by a more detailed stratigraphically controlled study of GVC, Salak and IVC lavas, such as that carried out by Price et al. (1999) and Gamble et al. (1999) on volcanic rocks from New Zealand.

Recent work by Blundy and Cashman (2005), has shown that disequilibrium textures in arc lavas, such as oscillatory zoning in plagioclase (accompanied by changes in anorthite content) that are commonly attributed to open system magmatic processes, e.g. mixing, can result from the interplay of magma decompression and cooling alone. There is much evidence for apparent magmatic disequilibrium from plagiolcase and pyroxene textures in GVC, Salak and IVC rocks, therefore mineral scale isotopic profiling (e.g. Davidson and Tepley, 1997)

would be invaluable for determining whether disequilibrium in crystal growth arises due to changes in pressure, temperature or volatile content during closed system magmatic evolution or as a result of open system processes (e.g. mixing or contamination). Analysis of water/volatile contents of melt inclusions could yield potential information as to whether the deep-seated fractionation of amphibole beneath the east flank SVG of Salak (and by inference the majority of Javan volcanoes) arises due to differences in the water/volatile contents of these magmas compared to those rising beneath the central vent at Salak.

On a larger scale, comparative evaluation of specific source component inputs in Javan magma genesis between different isotopic systems e.g. Sr-Nd and Nd-Hf is severely restricted due to the lack of complete isotopic data sets available for Indian Ocean sediment samples, which is mainly a result of limited Hf isotope measurements. Furthermore, an assumption on the Hf isotopic ratio of altered oceanic crust has had to be made in this study. Hf isotope analysis of Indian Ocean sediments and altered oceanic crust which have already undergone Sr and Nd isotopic analysis would, therefore, circumvent assumptions on input component compositions and allow better testing of source input conclusions gained from geochemical modelling.

A 2-stage source contamination model is proposed in the petrogenesis of IVC volcanic rocks. However, only limited constraints on the order of input addition can be placed. Detailed U-series analysis of IVC lavas may provide unique insights on the rates and timing of the fluid and sediment inputs. Enlargement of the U-series database for Javan volcanic rocks would provide important information on mantle wedge dynamics at the Sunda arc and help ascertain whether there is a stronger fluid contribution to the mantle wedge in East Java compared to West Java, as hypothesised in this study.

References

References

Alt, J.C., Muehlenbachs, K., Honnorez, J. (1986). An oxygen isotopic profile through the upper kilometre of the oceanic crust, DSDP Hole 504B. Earth Planet. Sci. Lett., 80 (3-4): 217-229.

Alves, S., Schiano, P., Allegre, C.J. (1999). Rhenium-osmium isotopic investigation of Java subduction zone lavas. Earth Planet. Sci. Lett., 168: 65-67.

Andreastuti, S.D. (1999). Stratigraphy and geochemistry of Merapi Volcano, Central Java, Indonesia: implication for assessment of volcanic hazards. Ph.D. thesis, University of Auckland, New Zealand.

Anikouchine, W.A., Ling, Hsin-yi. (1967). Evidence for turbidite accumulation in trenches in the Indo-Pacific region. Marine Geology, 5: 141-154.

Barth, M.G., McDonough, W.F., Rudnick, R.L. (2000). Tracking the budget of Nb and Ta in the continental crust. Chemical Geology, 165: 197-213.

Ben-Avraham, Z., Emery, K.O. (1973). Structural framework of Suna Shelf. Bull. Amer. Assoc. Pet. Geol., 57: 2323-2366.

Ben Othman, D.B., White, W.M., Patchett, J. (1989). The geochemistry of marine sediments, island arc magma genesis, and crust-mantle recycling. Earth Planet. Sci. Lett., 94: 1-21.

Berlo, K. (2001). The magmatic evolution of the Ijen Caldera, East Java, Indonesia. Thesis, University of Utrecht, The Netherlands.

Blundy, J., Cashman, K. (2005). Rapid decompression-driven crystallisation recorded by melt inclusions from Mount St. Helens Volcano. Geology, 33(10): 793-796.

Brennan, J., Shaw, H.F., Phinney, D.L., Ryerson, J.F. (1995). Mineral-aqueous fluid partitioning of trace elements at 900°C and 2.0 Gpa: Constraints on the trace element geochemistry of mantle and deep crustal fluids. Geochim. Cosmochim. Acta, 59: 3331-3350.

Camus, G., Gourgaud, A., Mossand-Berthommier, P., Vincent, P.M. (2000). Merapi (Central Java, Indonesia): an outline of the structural and magmatological evolution with a special emphasis to the major pyroclastic events. J. Volcanol. Geotherm. Res., 100: 139-163.

Cardwell, R.K., Isacks, B.L. (1978). Geometry of the subducted lithosphere beneath the Banda Sea in eastern Indonesia from seismicity and fault plane solutions. J. Geophys. Res., 83: 2825-2838.

Carn, S.A., Pyle, D.M. (2001). Petrology and geochemistry of the Lamongan Volcanic Field, East Java, Indonesia: Primitive Sunda Arc magmas in an extensional tectonic setting? Journal of Petrology, 42(9): 1643-1683.

Chase, C.G. (1978). Plate kinematics: the Americas, East Africa, and the rest of the world. Earth Planet. Sci. Lett., 37(3): 355-368.

Charlier et al. (in press 2006). Chemical Geology.

Chauvel, C., Blichert-Toft, J. (2001). A hafnium isotope and trace element perspective on melting of the depleted mantle. Earth Planet. Sci. Lett., 190: 137-151.

Class, C., Miller, D.M., Goldstein, S.L. Langmuir, C.H. (2000). Distinguishing melt and fluid subduction and components in Umnak volcanics, Aleutian Arc. Geochemisty, Geophysics, Geosystems 1, no.6 (20000601)

Cook, P.J. (1974). Major and trace element geochemistry of sediments from DSDP leg 27, sites 259-263, Eastern Indian Ocean. In: Robinson, P.T. et al. (eds) Inital Reports of the Deep Sea Drilling Project, 27: 481-497.

Curray, J.R., Shor Jr, G.G., Raitt, R.W., Henry, M. (1977). Seismic refractiona nd reflection studies of crustal structure of the eastern Sunda and western Banda arcs. J. Geophys. Res., 82: 2479-2489.

Davidson, J.P. (1987). Crustal contamination versus subduction zone enrichment: Examples from the Lesser Antilles and implications for mantle source compositions of island arc volcanic rocks. Geochim. Cosmochim. Acta, 51: 2185-2198.

Davidson, J.P. (1996). Deciphering mantle and crustal signatures in subduction zone magmatism. Subduction: Top to Bottom, Am.Geophys. Union. Monogr. 95: 251-262.

Davidson, J.P., Dungan, M.A., Ferguson, K.M., Colucci, M.T. (1987). Crust-magma interactions and the evolution of arc magmas: The San Pedro-Pellado volcanic complex, southern Chilean Andes. Geology, 15: 443-446.

Davidson, J.P., Harmon, R.S. (1989). Oxygen isotope constraints on the petrogenesis of volcanic arc magmas from Martinique, Lesser Antilles. Earth Planet. Sci. Lett., 95: 255-270.

Davidson, J.P., Harmon, R.S., Woerner, G. (1991). The source of Central Andean magmas: some considerations. Geol. Soc. Am. Spec. Paper, 265: 233-243

Davidson, J.P., Hora, J.M., Garrison, J.M., Dungan, M.A. (2005). Crustal forensics in arc magmas. J. Volcanol. Geotherm. Res., 140: 157-170.

Davidson, J.P., Wilson, I.R. (1989). Evolution of an alkali basalt-trachyte suite from Jebel Marra volcano, Sudan, through assimilation and fractional crystallization. Earth Planet. Sci. Lett., 95: 141-160.

Defant, M.J., Drummond, M.S. (1990). Derivation of some modern arc magmas by melting of young subducted lithosphere. Nature, 347: 662-665.

Defant, M.J., Sherman, S., Maury, R.C., Bellon, H., de Boer, J., Davidson, J., Kepezhinskas, P. (2001). The geology, petrology, and petrogenesis of Saba Island, Lesser Antilles. J. Volcanol. Geotherm. Res., 107: 87-111.

de Hoog, J.C.M., Taylor, B.E., van Bergen, M.J. (2001). Sulfur isotope systematics of basaltic lavas from Indonesia: implications for the sulfur cycle in subduction zones. Earth Planet. Sci. Lett., 189: 237-252.

DeMets, C., Gordon, R.G., Argus, D.F., Stein, S. (1990). Current plate motions. Geophysical Journal International, 101(2): 425-478.

DePaolo, D.J. (1981). Trace element and isotopic effects of combined wallrock assimilation and fractional crystallization. Earth Planet. Sci. Lett., 53: 189-202.

Donoghue, S.L., Gamble, J.A., Palmer, A.S., Stewart, R.B. (1995). Magma mingling in an andesite pyroclastic flow of the Pourahu Member, Ruapehu volcano, New Zealand. J. Volcanol. Geotherm. Res., 68: 177-191.

Dowall, D.P, Nowell, G.M., Pearson, D.G. (2003). Chemical pre-concentration procedures for high-precision analysis of Hf-Nd-Sr isotopes in geological materials by plasma ionisation multi-collector mass spectrometry (PIMMS) techniques. Plasma Source Mass Spectrometry. Spec. Pub. Royal Society of Chemistry 321-337.

Dunn, T., Sen, C. (1994). Mineral/matrix partition coefficients for orthopyroxene, plagioclase and olivine in basaltic to andesitic systems: A combined analytical and experimental study. Geochim. Cosmochim. Acta, 58(2): 717-733.

Edwards, C.M.H. (1990). Petrogenesis of tholeiitic, calc-alkaline and alkaline volcanic rocks, Sunda arc, Indonesia. Ph.D. Thesis, Royal Holloway, University of London.

Edwards, C.M.H., Menzies, M.A., Thirlwall, M.F. (1991). Evidence from Muriah, Indonesia, for the interplay of supra-subduction zone and intraplate processes in the genesis of potassic alkaline magmas. Journal of Petrology, 32: 555-592.

Edwards, C.M.H., Morris, J.D., Thirlwall, M.F. (1993). Separating mantle from slab signatures in arc lavas using B/Be and radiogenic isotope systematics. Nature, 362: 530-533.

Effendi, A.C., Kusnama, Hermanto, B. (1998). Geological map of the Bogor quadrangle, Java. Volcanological Survey of Indonesia.

Eiler, J.M., Crawford, A.J., Elliot, T.R., Farley, K.A., Valley, J.W., Stopler, E.M. (2000). Oxygen isotope geochemistry of oceanic-arc lavas. Journal of Petrology, 41(2): 229-256.

Eiler, J.M., Farley, K.A., Valley, J.W., Hauri, E., Craig, H., Hart, S.R., Stolper, E.M., 1997. Oxygen isotope variations in ocean island basalt phenocrysts. Geochimica et Cosmochimica Acta, 61(11): 2281-2293.

Elburg, M., Foden, J., van Bergen, M.J, Zulkarnain, I. (2005). Australia and Indonesia in collision: geochemical sources of magmatism. J. Volcanol. Geotherm. Res., 140: 25-47.

Elburg, M., van Bergen, M., Hoogewerff, J., Foden, J., Vroon, P., Zulkarnain, I., Nasution, A. (2002). Geochemical trends across an arc-continent collision zone: magma sources and slab-wedge transfer processes below the Pantar Strait volcanoes, Indonesia. Geochim. Cosmochim. Acta, 66(15): 2771-2789.

Ellam, R.M., Harmon, R.S. (1990). Oxygen isotope constraints on the crustal contribution to the subduction-related magmatism of the Aeolian Islands, southern Italy. J. Volcanol. and Geotherm. Res., 44: 105-122.

Ellam, R.M., Hawkesworth, C.J. (1988). Elemental and isotopic variations in subduction related basalts: evidence for a three component model. Contrib. Mineral. Petrol., 98: 72-80.

Elliott, T., Plank, T., Zindler, A., White, W. Bourdon, B. (1997). Element transport from slab to volcanic front at the Mariana Arc. J. Geophys. Res., 102: 14,991-15,019.

Ewart, A., Bryan, W. B., Chappell, B. W., Rudnick, R. L. (1994). Regional geochemistry of the Lau-Tonga arc and back-arc systems. Proc. Ocean Drilling Program, Scientific Results, 135: 385-425.

Fitch, T.J. (1970). Earthquake mechanisms and island arc tectonics in the Indonesian-Philippine region. Bull. Seismol. Soc. Am., 60: 565-591.

Flood, T.P., Schuraytz, B.C., Vogel, T.A. (1989) Magma mixing due to disruption of a layered magma body. J. Volcanol. Geotherm. Res. 36(4): 241-255

Fryer, P. (1992). A synthesis of Leg 125 drilling of serpentine seamounts on the Mariana and Izu-Bonin forearcs. Proc. Ocean Drilling Program, Scientific Results, 125: 593-614.

Gamble, J.A., Smith, I.E.M., McCulloch, M.T., Graham, I.J., Kokelaar, B.P. (1993). The geochemistry and petrogenesis of basalts from the Taupo volcanic zone and Kermadec island arc, S.W. Pacific. J. Volcanol. Geotherm. Res. 54(3-4): 265-290

Gamble, J.A., Wood, C.P., Price, R.C., Smith, I.E.M., Stewart, R.B., Waight, T. (1999). A fifty year perspective of magmatic evolution on Ruapehu Volcano, New Zealand: verification of open system behaviour in an arc volcano. Earth Planet. Sci. Lett., 170: 301-314.

Gamble, J., Woodhead, J., Wright, I., Smith, I. (1996). Basalt and sediment geochemistry and magma petrogenesis in a transect from oceanic island arc to rifted continental margin arc: the Kermadec-Hikurangi Margin, SW Pacific. Journal of Petrology, 37(6): 1523-1546.

Garrison, J.M., Davidson, J.P. (2003). Dubious cases for slab melting in the Northern volcanic zones of the Andes. Geology, 31 (6): 565-568.

Gasparon, M. (1993). Origin and evolution of mafic volcanics of Sumatra (Indonesia): their mantle sources, and roles of subducted oceanic sediments and crustal contamination. Ph.D. Thesis, Univ. Tasmania.

Gasparon, M., Hilton, D. R., Varne, R. (1994). Crustal contamination processes traced by helium isotopes: Examples from the Sunda arc, Indonesia. Earth Planet. Sci. Lett., 126: 15-22.

Gasparon, M., Varne, R. (1998). Crustal assimilation versus subducted sediment input in west Sunda arc volcanics: an evaluation. Mineralogy and Petrology, 64: 89-117.

George, R., Turner, S., Hawkesworth, C., Bacon, C.R., Nye, C., Stelling, P., Dreher, S. (2004). Chemical versus temporal controls on the evolution of tholeiitic and calc-alkaline magmas at two volcanoes in the Alaska-Aleutian Arc. Journal of Petrology, 45: 203-219.

Gertisser, R., Keller, J. (2003). Trace element and Sr, Nd, Pb and O isotope variations in medium-K and high-K volcanic rocks from Merapi Volcano, Central Java, Indonesia: evidence for the involvement of subducted sediments in Sunda Arc magma genesis. Journal of Petrology, 44(3): 457-489.

Gerbe, M.-C., Gouraud, A., Sigmarsson, O., Harmon, R.S., Joron, J-L., Provost, A. (1992). Mineralogical and geochemical evolution of the 1982-1983 Galunggung eruption (Indonesia). Bulletin of Volcanology, 54: 284-298.

GERM: http://earthref.org/GERM/index.html

Giannetti, B. (2001). Origin of the calderas and evolution of Roccamonfina volcano (Roman Region, Italy). J. Volcanol. Geotherm. Res., 106: 301-319.

Gill, J.B. (1981). Orogenic Andesites and Plate Tectonics. Springer, Berlin.

Graham, I.J., Hackett, W.R. (1987) Petrology of calcalkaline lavas from Ruapehu Volcano and related vents, Taupo Volcanic Zone, New Zealand. Journal of Petrology, 28: 531-567.

Grove, T.L., Baker, M.B., Price, R.C., Parman, S.W., Elkins-Tanton, L.T., Chatterjee, N., Muntener, O. (2005). Magnesian andesite and dacite lavas from Mt. Shasta, northern California: products of fractional crystallisation of H2O-rich mantle melts. Contrib. Mineral. Petrol., 148: 542-565.

Grove, T.L., Elkins-Tanton, L.T., Parman, S.W., Chatterjee, N., Muntener, O., Gaetani, G.A. (2003). Fractional crystallization and mantle-melting controls on calc-alkaline differentiation trends. Contrib. Mineral. Petrol., 145: 515-533.

Hamilton, W.B. (1979). Tectonics of the Indonesian region. U.S. Geological Survey Professional Paper reprinted with corrections, 1981 and 1985, 1078: 345.

Hamilton, W.B. (1988). Plate tectonics and island arcs. Geological Society of America Bulletin, 100: 1503-1527.

Harmon, R.S., Gerbe, M.C. (1992). The 1982-83 eruption at Galunggung volcano, Java (Indonesia): oxygen isotope geochemistry of a zoned magma chamber. Journal of Petrology, 33: 585-609.

Hart, S.R., Erlank, A.J., Kable, E.J.D. (1974). Sea Floor Basalt Alteration: some chemical and Sr isotopic effects. Contrib. Mineral. Petrol., 44(3): 219-230.

Hawkesworth, C.J., Hergt, J.M., Ellam, R.M., McDermott, F. (1991). Element fluxes associated with subduction related magmatism. Philos. Trans. R. Soc. Lond. A., 335: 393-405.

Hawkesworth, C.J., O'Nions, R.K., Arculus, R.J. (1979). Nd and Sr isotope geochemistry of island arc volcanics, Grenada, Lesser Antilles. Earth Planet. Sci. Lett., 45(2): 237-248.

Hawkesworth, C.J., Turner, S.P., McDermott, F., Peate, D.W., van Calsteren, P.J. (1997). U-Th isotopes in arc magmas: Implications for element transfer from the subducted slab. Science, 276: 551-555.

Hickey-Vargas, R. (1998). Origin of the Indian Ocean-type isotopic signature in basalts form the Philippine Sea plate spreading centres: an assessment of local versus large-scale processes. J. Geophys. Res. 103(B9): 20,963-20979.

Hildreth, W., Moorbath, S. (1988). Crustal contributions to arc magmatism in the Andes of Central Chile. Contrib. Mineral. Petrol., 98: 455-489.

Hilton, D.R., Craig, H. (1989). A helium isotope transect along the Indonesian archipelago. Nature, 342: 906-908.

Hoffmann-Rothe, A., Ritter, O., Haak, V. (2001). Magnetotelluric and geomagnetic modelling reveals zones of very high electrical conductivity in the upper crust of Central Java. Physics of The Earth and Planetary Interiors, 124(3-4): 131-151.

Hoogewerff, J.A., van Bergen, M.J., Vroon, P.Z., Hertogen, J., Wordel, R., Sneyers, A., Nasution, A., Varekamp, J.C., Moens, H.L.E., Mouchel, D. (1997). U-series, Sr-Nd-Pb isotope and trace element systematics across an active island arc-continent collision zone: Implications for element transfer at the slab-wedge interface. Geochim. Cosmochim. Acta, 61(5): 1057-1072.

Hutchinson, C.S. (1976). Indonesian active volcanic arc: K, Sr and Rb variation with depth to the Benioff zone. Geology, 4: 407-408.

Hutchinson, C.S. (1982). Indonesia. Andesites: Orogenic Andesites and Related Rocks: 207-224.

Hutchinson, C.S. (1989). Geological evolution of South-east Asia. Oxford Monographs on Geology and Geophysics, 13: pp. 368.

Ionov, D.A., Harmon, R.S., France-Lanord, C., Greenwood, B., Ashchepkov, I.V. (1994). Oxygen isotope composition of garnet and spinel peridotites in the continental mantle: Evidence from the Vitim xenolith suite, southern Siberia. Geochim. Cosmochim. Acta, 58(5): 1463-1470.

Ito, E., White, W.M., Gopel, C. (1987). The O, Sr, Nd and Pb isotope geochemistry of MORB. Chemical Geology, 62: 157-176.

James, D.E. (1981). The combined use of oxygen and radiogenic isotopes as indicators of crustal contamination. Ann. Rev. Earth and Planet. Sci., 9: 311-344.

Jarrard, R.D. (1986). Relations among subduction parameters. Rev. Geophys., 24: 217-284.

Johnson, M.C., Plank, T. (1999). Dehydration and melting experiments constrain the fate of subducted sediments. Geochem. Geophys. Geosyst., 1(1): paper no 1999GC000014.

Kadarusman, A., Miyashita, S., Maruyama, S., Parkinson, C.D., Ishikawa, A. (2004). Petrology, geochemistry and paleogeographic reconstruction of the East Sulawesi Ophiolite, Indonesia. Tectonophysics, 392: 55-83.

Katili, J.A. (1975). Volcanism and plate tectonics in the Indonesian island arcs. Tectonophysics, 26: 165-188.

Kay, R.W. (1980). Volcanic arc magmas: implications of a melting-mixing model for element recycling in the crust-upper mantle system. Journal of Geology, 88: 497-522.

Kemmerling, G.L.L. (1921). Het Idjen Hoogland de geologie en geomorphologie van den Idjen. Batavia. H. Woudstra, Analyse van merkwaardige watersoorten op het Idjen-Hoogland.

Keppler, H. (1996). Constraints from partitioning experiments on the composition of subduction zone fluids. Nature, 380: 237-240.

Kessel, R., Schmidt, M.W., Ulmer, P., Pettke, T. (2005). Trace element signature of subduction-zone fluids, melts and supercritical liquids at 120-180 km depth. Nature, 437: 724-727.

Kieckhefer, R.M., Shor Jr, G.G., Curray, J.R. (1980). Seismic refraction studies of the Sunda trench and forearc basin. J. Geophys. Res., 85: 863-889.

Kirby, S.H., Stein, S., Okal, E.A., Rubie, D.C., (1996). Metastable mantle phase transformations and deep earthquakes in subducting oceanic lithoshphere. Rev. Geophys., 34(2): 261-306.

Kop, H., Flueh, E.R., Klaeshen, D., Bialas, J., Reichert, C. (2001). Crustal structure of the Sunda margin at the onset of oblique subduction. Geophys. J. Int., 147: 449-474.

Langmuir, C.H., Voche, R.D., Hanson, G.N., Hart, S.R. (1978). A general mixing equation with applications to Icelandic basalts. Earth Planet. Sci. Lett., 37: 380-392.

Leeman, W.P., Carr, M.J., Morris, J.D. (1994). Boron geochemistry of the Central American Volcanic Arc: constraints on the genesis of subduction-related magmas. Geochim. Cosmochim. Acta, 58: 149-168.

Le Bas, M.J., Le Maitre, R.W., Streckeisen, A., Zanettin, B. (1986). A chemical classification of volcanic rocks based on the total alkali-silica diagram. Journal of Petrology, 27(3) : 745-750.

Le Pichon, X. (1968). Sea-floor spreading and continental drfit. J. Geophys. Res., 73(12): 3661-3697.

Lytwyn, J., Rutherford, E., Burke, K., Xia, C. (2001). The geochemistry of volcanic, plutonic and turbiditic rocks from Sumba, Indonesia. Journal of Asian Earth Sciences, 19: 481-500.

Malod, J.A., Komar Karta, Beslier, M.O., Zen Jr., M. T. (1995). From normal to oblique subduction: Tectonic relationships between Java and Sumatra. Journal of Southeast Asian Earth Sciences, 12(1-2): 85-93.

Mandeville, C.W., Carey, S., Sigurdsson, H. (1996). Magma mixing, fractional crystallization and volatile degassing during the eruption of Krakatau volcano, Indonesia. J. Volcanol. Geotherm. Res., 74: 243-274.

Macpherson, C.G., Dreher, S.T., Thirlwall, M.F. (in press). Adakites without slab melting: High pressure differentiation of island arc magma, Mindanao, the Philippines. Earth Planet. Sci. Lett.

Macpherson, C.G., Forde, E.J., Hall, R., Thirlwall, M.F. (2003). Geochemical evolution of magmatism in an arc-arc collision; the Halmahera and Sangihe Arcs, eastern Indonesia. Geol. Soc. Spec. Pub. 219: 207-220.

Macpherson, C.G., Gamble, J.A., Mattey, D.P. (1998). Oxygen isotope geochemistry of lavas from an oceanic to continental arc transition, Kermadec-Hikurangi margin, SW Pacific. Earth Planet. Sci. Lett., 160: 609-621.

Macpherson, C.G., Hall, R. (2001). Tectonic setting of Eocene boninite magmatism in the Izu-Bonin-Mariana forearc. Earth Planet. Sci. Lett., 186(2): 215-230.

Macpherson, C.G., Hall, R. (2002). Timing and tectonic controls in the evolving orogen of SE Asia and the western Pacific and some implications for ore generation. Geol. Soc. Spec. Pub. 204: 49-67.

Macpherson, C.G., Hilton, D.R., Mattey, D.P., Sinton, J.M. (2000). Evidence for an ^{18}O-depleted mantle plume from contrasting $^{18}O/^{16}O$ ratios of back-arc lavas from the Manus Basin and Mariana Trough. Earth Planet. Sci. Lett., 176(2): 171-183.

Macpherson, C.G., Mattey, D.P. (1998). Oxygen isotope variations in Lau Basin lavas. Chemical Geology, 144: 177-194.

Marcoux, E., Milesi, J-P. (1994). Epithermal gold deposits in West Java, Indonesia: geology, age and crustal source. Journal of Geochemical Exploration, 50(1-3): 393-408.

Matsui, Y., Onuma, N., Nagasawa, H., Higuchi, H. and Banno, S. (1977). Crystal structure control in trace element partition between crystal and magma. Tectonics, 100: 315-324.

Mattey, D., Lowry, D., Macpherson, C. (1994). Oxygen isotope composition of mantle peridotite. Earth Planet. Sci. Lett., 128(3-4): 231-241.

McCaffrey, R. (1991). Slip vectors and stretching of the Sumatran fore arc. Geology, 19: 881-884.

McCulloch, M.T., Gamble J.A. (1991). Geochemical and geodynamical constraints on subduction zone magmatism. Earth Planet. Sci. Lett., 102: 358-374.

McCulloch, M.T., Gregory, R.T., Wasserburg, G.J., Taylor, H.P., Jr. (1980). A neodymium, strontium and oxygen isotopic study of the Cretaceous Samail Ophiolite and implications for the petrogenesis and seawater-hydrothermal alteration of oceanic crust. Earth Planet. Sci. Lett., 46(2): 201-211.

McCulloch, M.T., Perfit, M.R. (1981). $^{143}Nd/^{144}Nd$, $^{87}Sr/^{86}Sr$ and trace element constraints on the petrogenesis of Aleutian island arc magmas. Earth Planet. Sci. Lett., 56: 167-179.

McKenzie, D., O'Nions, R.K. (1991). Partial melt distributions from inversion of rare earth element concentrations. Journal of Petrology, 32(5): 1021-1091.

Metcalfe, I. (1996). Pre-Cretaceous evolution of SE Asian terranes. Geol. Soc. Spec. Pub., 106: 97-122.

Moore, G.F., Curray, J.R., Moore, D.G., Karig, D.E. (1980). Variations in geologic structure along the Sunda fore arc, northeastern Indian Ocean. In: Hayes, D.E. (ed) The tectonic and geological evolution of Southeast Asian seas and islands. Am. Geophys. Union, Washington, pp. 145-160.

Morris, J.D., Leeman, W.P., Tera, F. (1990). The subducted component in island arc lavas: constraints from Be isotopes and B-Be systematics. Nature, 344: 31-36.

Muehlenbachs, K. (1986). Alteration of the oceanic crust and the ^{18}O history of seawater. Reviews in Mineralogy, 16: 425-444.

Münker, C., Worner, G., Yogodzinski, G., Churikova, T. (2004). Behaviour of high field strength elements in subduction zones: constraints from Kamchatka-Aleutian arc lavas. Earth Planet. Sci. Lett., 224: 275-293.

Nakagawa, M., Wada, K., Wood, P.C. (2002). Mixed magmas, mush chambers and eruption triggers; evidence from zoned clinopyroxene phenocrysts in andesitic scoria from the 1995 eruptions of Ruapehu Volcano, New Zealand. Journal of Petrology, 43(12): 2279-2303.

Nowell, G.M., Kempton, P.D., Noble, S.R., Fitton, J.G., Saunders, A.D., Mahoney, J.J., Taylor, R.N. (1998). High precision Hf isotope measurements of MORB and OIB by thermal ionisation mass spectrometry: insights into the depleted mantle. Chemical Geology, 149: 211-233.

Nowell, G.M., Parrish, R.R. (2002). Simultaneous acquisition of isotope compositions and parent/daughter ratios by non-isotope dilution solution-mode Plasma ionisation Multi-collector Mass Spectrometry (PIMMS). Plasma Source Mass Spectrometry The New Millenium, 298-310.

Nowell, G.M, Pearson, D.G, Ottley, C.J., Schweiters, J. (2003). Long-term performance characteristics of a plasma ionisation multi-collector mass spectrometer (PIMMS): the ThermoFinnigan Neptune. Plasma Source Mass Spectrometry. Spec. Pub. Royal Society of Chemistry, 307-320.

Ottley, C.J, Pearson, D.G., Irvine, G.J (2003). A routine method for the dissolution of geological samples for the analysis of REE and trace elements via ICP-MS. Plasma Source Mass Spectrometry. Spec. Pub. Royal Society of Chemistry, 221-230.

Patchett, P.J. (1983). Hafnium isotope results from mid-ocean ridges and Kerguelen. Lithos, 16: 47-51.

Patchett, P.J., Tatsumoto, M. (1980). Hafnium isotope variations in oceanic basalts. Geophys. Res. Lett. 7(12): 1077-1080.

Patchett, P.J., White, W.M., Feldmann, W.H., Kielinczuk, Hofmann, A.W. (1984). Hafnium/rare earth element fractionation in the sedimentary system and crustal recycling into the Earth's mantle. Earth Planet. Sci. Lett., 69: 365-378.

Peacock, S.M. (1991). Numerical simulation of subduction zone pressure-temperature-time paths: constraints on fluid production and arc magmatism. Philos. Trans. R. Soc. Lond. A., 335: 341-353.

Pearce, J.A. (1982). Trace element characteristics of lavas from destructive plate boundaries. Andesites: Orogenic Andesites and Related Rocks. John Wiley & Sons, Chichester, UK: 525-548.

Pearce, J.A., Kempton, P.D., Nowell, G.M., Noble, S.R. (1999). Hf-Nd Element and Isotope Perspective on the Nature and Provenance of Mantle and Sunduction Components in Western Pacific Arc-Basin Systems. Journal of Petrology, 40(11): 1579-1611.

Pearce, J.A., Peate, D.W. (1995). Tectonic implications of the composition of volcanic arc magmas. Annu. Rev. Earth Planet. Sci., 24: 251–285.

Pearson, D.G & Nowell, G.M 2005. Accuracy and precision in plasma ionisation multi-collector mass spectrometry: Constraints from neodymium and hafnium isotope measurements. Plasma Source Mass Spectrometry, Current Trends and Future Developments 284-314.

Peccerillo, A., Dallai, L., Frezzotti, M.L., Kempton, P.D. (2004). Sr-Nd-Pb-O isotopic evidence for decreasing crustal contamination with ongoing magma evolution at Alicudi volcano (Aeolian arc, Italy): implications for style of magma-crust interaction and for mantle source compositions. Lithos, 78: 217-233.

Philpotts, J.A., Schnetzler, C.C. (1970). Phenocryst-matrix partition coefficients for K, Rb, Sr and Ba, with applications to anorthosite and basalt genesis. Geochim. Cosmochim. Acta, 34: 307-322.

Plank, T., Langmuir, C.H. (1988). An evaluation of the global variations in the major element chemistry of arc basalts. Earth Planet. Sci. Lett., 90: 349-370.

Plank, T., Langmuir, C.H. (1993). Tracing trace elements from sediment input to volcanic output at subduction zones. Nature, 362: 739-743.

Plank, T., Langmuir, C.H. (1998). The chemical composition of subducting sediment and its consequences for the crust and mantle. Chemical Geology, 145: 325-394.

Potts, P.J., Tindle, A.G. Webb, P.C. (1992). Geochemical reference material compositions: rocks, minerals, sediments, soils, carbonates, refractories and ores used in research and industry. Whittles Publishing, Caithness, U.K.

Price, R.C., Kennedy, A.K., Riggs-Sneeringer, M., Frey, F.A. (1986). Geochemistry of basalts from the Indian Ocean triple junction: implications for the generation and evolution of Indian Ocean ridge basalts. Earth Planet. Sci. Lett., 78: 379-396.

Price, R.C., Stewart, R.B., Woodhead, J.D., Smith, I.E.M. (1999). Petrogenesis of high-K arc magmas: evidence from Egmont Volcano, North Island, New Zealand. Journal of Petrology, 40: 167-197.

Rehkämper, M., Hofmann, A.W. (1997). Recycled ocean crust and sediment in Indian Ocean MORB. Earth Planet. Sci. Lett., 147: 93-106.

Reubi, O., Nicholls, I.A. (2004). Magmatic evolution at Batur volcanic field, Bali, Indonesia: petrological evidence for polybaric fractional crystallisation and implications for caldera-forming eruptions. J. Volcanol. Geotherm. Res., 138: 345-369.

Reubi, O., Nicholls, I.A., Kamenetsky, V.S. (2003). Early mixing and mingling in the evolution of basaltic magmas: evidence from phenocryst assemblages, Slamet Volcano, Java, Indonesia. J. Volcanol. Geotherm. Res., 119: 255-274.

Ringwood, A.E., 1974. The petrological evolution of island arc systems. J. Geol. Soc. London, 130: 183-204.

Rittman, A. (1953). Magmatic character and tectonic position of the Indonesian volcanoes. Bull. Volcanol., 14: 45-58.

Rollinson, H.R. (1993). Using geochemical data: evaluation, presentation, interpretation. Longman, UK.

Rotolo, S.G., Castorina, F. (1998). Transition from mildly-tholeiitic to calc-alkaline suite: the case of Chichontepec volcanic centre. El Salvador, Central America. J. Volcanol. Geotherm. Res., 86: 117-136.

Royse, K., Kempton, P.D., Darbyshire, D.P.F. (1998). NERC Isotope Geosciences Laboratory Report Series, 121.

Rudnick, R.L. (1995). Making continental crust. Nature, 378: 571-578.

Salters, V.J.M. (1996). The generation of mid-ocean ridge basalts from the Hf and Nd isotope perspective. Earth Planet. Sci. Lett., 141: 109-123.

Salters, V.J.M., Hart, S.R. (1991). The mantle sources of ocean islands and arc basalts: the Hf isotope connection. Earth Planet. Sci. Lett., 104: 364-380.

Salters, V.J.M., White, W.M. (1998). Hf isotope constraints on mantle evolution. Chemical Geology, 145: 447-460.

SEATAR (1981): http://www.ngdc.noaa.gov/mgg/geology/seatar.html

Sissons, T.W., Bronto, S. (1998). Evidence for pressure-release melting beneath magmatic arcs from basalt at Galunggung, Indonesia. Nature, 391: 883-886.

Sitorus, K. (1990). Volcanic stratigraphy and geochemistry of the Idjen Caldera Complex, East Java, Indonesia, MSc thesis, University of Wellington, New Zealand.

Situmorang, T., Hadisantono, R.D. (1992). Geological map of Gede Volcano, Cianjur, West Java. Volcanic Survey of Indonesia.

Smith, A.L., Roobol, M.J., Gunn, B.M. (1980). The Lesser Antilles - a discussion of the island arc magmatism. Bulletin Volcanologique, 43(2): 287-302.

Smith, I.E.M., Stewart, R.B., Price, R.C. (2003). The petrology of a large intra-oceanic silicic eruption: the Sandy Bay Tephra, Kermadec arc, southwest Pacific. J. Volcanol. Geotherm. Res., 124: 173-194.

Smith, T.E., Thirlwall, M.F., Macpherson, C. (1996). Trace element and isotope geochemistry of the volcanic rocks of Bequia, Grenadine Islands, Lesser Antilles Arc; a study of subduction enrichment and intra-crustal contamination. Journal of Petrology, 37(1): 117-143.

Soeria-Atmadja, R., Suparka, S., Abdullah, C., Noeradi, D., Sutanto (1998). Magmatism in western Indonesia, the trapping of the Sumba Block and the gateways to the east of Sundaland. Journal of Asian Earth Sciences, 16 (1): 1-12.

Staudigel, H., Davies, G.R., Hart, S.R., Marchant, K.M., Smith, B.M. (1995). Large scale isotopic Sr, Nd and O isotopic anatomy of altered oceanic crust: DSDP/ODP sites 417/418. Earth Planet. Sci. Lett., 130: 169-185.

Staudigel, H., Plank, T., White, B., Schimincke,H-U. (1996). Geochemical fluxes during seafloor alteration of the basaltic upper oceanic crust: DSDP Sites 417 and 418, Subduction: Top to Bottom. Geophysical Monograph 96, pp. 19-36.

Stille, P., Unruh, D.M., Tatsumoto, M. (1986). Pb, Sr, Nd, and Hf isotopic constraints on the origin of Hawaiian basalts and evidence for a unique mantle source. Geochim. Cosmochim. Acta, 50(10): 2303-2319.

Stimac, J. (2003). Surface geology of the Awibengkok geothermal development area, Java, Indonesia. Unocal report, Philippines.

Stolz, A.J., Varne, R., Davies, G.R., Wheller, G.E., Foden, J.D. (1990). Magma source components in an arc-continent collision zone: the Flores-Lembata sector, Sunda arc, Indonesia. Contrib. Mineral. Petrol., 105: 585-601.

Stormer, J. C., Jr., Nicholls, J. (1978). XLFRAC; a program for the interactive testing of magmatic differentiation models. Computers & Geosciences, 4 (2): 143-159.

STRM: http://srtm.usgs.gov/

Sun, S., McDonough, W.F. (1989). Chemical and isotopic systematics of oceanic basalts: implications for mantle composition and processes. In: A.D. Saunders, Norry, M.J. (Editor), Magmatism in the Ocean Basins. Geological Society Special Publication, 313-345.

Susilohadi, S., Gaedicke, C., Ehrhardt, A. (2005). Neogene structures and sedimentation history along the Sunda forearc basins off southwest Sumatra and Southwest Java. Marine Geology, 219: 133-154.

Tatsumi, Y., Hamilton, D.L., Nesbitt, R.W. (1986). Chemical characteristics of fluid phase released from a subducted lithosphere and origin of arc magmas: evidence from high-pressure experiments and natural rocks. J. Volcanol. Geotherm. Res., 29: 293-309.

Taylor, S.R. (1977). Island arc models and the composition of the continental crust, in Talwani, M., Pitman, W., eds., Island arcs, deep sea trenches and back arc basins: American Geophysical Union, Maurice Ewing Series (1): 325-335.

Taylor, S.R., McLennan, S.M. (1985). The continental crust; its composition and evolution. Blackwell Scientific Publications, Oxford, England, 312 pp.

Taylor, R.N., Nesbitt, R.W. (1998). Isotopic characteristics of subduction fluids in an intra-oceanic setting, Izu-Bonin Arc, Japan. Earth Planet. Sci. Lett., 164: 79-98.

Taylor, R.N., Nesbitt, R.W., Vidal, P., Harmon, R.S., Auvray, B., Croudace, I.W. (1994). Mineralogy, chemistry, and genesis of the boninite series volcanics, Chichijima, Bonin Islands, Japan. Journal of Petrology, 35(3): 577-617.

Tepley, F.J., III, Davidson, J.P., Clynne, M.A. (1999). Magmatic interactions as recorded in plagioclase phenocrysts of Chaos Crags, Lassen Volcanic Center, California. Journal of Petrology, 40: 787-806.

Tepley, F.J., III, Davidson, J.P., Tilling, R.I., Arth, J.G. (2000). Magma mixing, recharge and eruption histories recorded in plagioclase phenocrysts from El Chichon, Mexico. Journal of Petrology, 41: 1397-1411.

Tera, F., Brown, L., Morris, J., Sacks, I.S., Klein, J., Middleton, R. (1986). Sediment incorporation in island-arc magmas: inferences from ^{10}Be. Geochim. Cosmochim. Acta, 50: 535-550.

Thirlwall, M.F. (1991). Long-term reproducibility of multicollector Sr and Nd isotope ratio analysis. Chemical Geology; Isotope Geoscience Section, 94 (2): 85-104.

Thirlwall, M.F., Graham, A.M. (1984). Evolution of high-Ca, high-Sr C-series basalts from Grenada, Lesser Antilles: the effects of intra-crustal contamination. J. Geol. Soc. London, 141: 427-445.

Thirlwall, M.F., Graham, A.M., Arculus, R.J., Harmon, R.S., Macpherson, C.G. (1996). Resolution of the effects of crustal assimilation, sediment subduction, and fluid

transport in island arc magmas: Pb-Sr-Nd-O isotope geochemistry of Grenada, Lesser Antilles. Geochim. Cosmochim. Acta, 60(23): 4785-4810.

Tregoning, P., Brunner, F.K., Bock, Y., Puntodewo, S.S.O., McCaffrey, R., Genrich, J.F., Calais, E., Rais, J., Subarya, C. (1994). First geodetic measurement of convergence across the Java Trench. Geophys. Res. Lett. 21(19): 2135-2138.

Troll, V.R, Schmincke, H-U. (2002). Magma mixing and crustal recycling recorded in ternary feldspar from compositionally zoned peralkaline ignimbrite "A", Gran Canaria, Canary Islands. Journal of Petrology, 43 (2): 243-270.

Turner, S., Foden. J. (2001). U, Th and Ra disequilibria, Sr, Nd and Pb isotope and trace element variations in Sunda arc lavas: predominance of a subducted sediment component. Contrib. Mineral. Petrol., 142: 43-57.

Turner, S., Foden. J, George, R., Evans, P., Varne, R., Elburg, M., Jenner, G. (2003). Rates and processes of potassic magma evolution beneath Sangeang Api volcano, East Sunda Arc, Indonesia. Journal of Petrology, 44(3): 491-515.

Turner, S., Hawkesworth, C. (1997). Constraints on flux rates and mantle dynamics beneath island arcs from Tonga-Kermadec lava geochemistry. Nature, 389: 568-573.

Turner, S., Hawkesworth, C., Rogers, N., Bartlett, J., Worthington, T., Hergt, J., Pearce, J., Smith, I. (1997). ^{238}U-^{230}Th disequilibria, magma petrogenesis and flux rates beneath the depleted Tonga-Kermadec island arc. Geochim. Cosmochim. Acta, 61: 4855-4884.

van Bemmelen, R.W. (1949). The geology of Indonesia. Vol 1A. Government Printing Office, The Hague, 732pp.

van Bergen, M.J., Vroon, P.Z., Varekamp, J.C., Poorter, R.P.E. (1992). The origin of the potassic rock suite from Batu Tara Volcano (East Sunda Arc, Indonesia). Lithos, 28: 261-282.

van Gerven, M., Pichler, H. (1995). Some aspects of the volcanology and geochemistry of the Tengger Caldera, Java, Indonesia: eruption of a K-rich tholeiitic series. Journal of Southeast Asian Earth Sciences, 11(2): 125-133.

Vervoort, J.D., Patchett, P.J., Blichert-Toft, J., Albarede, F. (1999). Relationships between Lu-Hf and Sm-Nd isotopic systems in the global sedimentary system. Earth Planet. Sci. Lett., 168: 79-99.

Vogel, T.A. (1982). Magma mixing in the acidic-basic complex of Ardnamurchan; implications on the evolution of shallow magma chambers. Contrib. Mineral. Petrol., 79(4): 411-423.

von Huene, R., Scholl. D.W. (1991). Observations at convergent margins concerning sediment subduction, subduction erosion, and the growth of continental crust. Rev. Geophys., 29: 279-316.

Vroon P. Z. (1992). Subduction of continental material in the Banda Arc, Eastern Indonesia: Sr-Nd-Pb isotope and trace-element evidence from volcanics and sediments. Ph.D. thesis University of Utrecht.

Vroon, P.Z., Lowry, D., van Bergen, M. J., Boyce, A.J., Mattey, D.P. (2001). Oxygen isotope systematics of the Banda arc: Low $\delta^{18}O$ despite involvement of subducted continental material in magma genesis. Geochim. Cosmochim. Acta, 65(4): 589-609.

Vroon, P.Z., van Bergen, M. J., Klaver, G. J., White, W. M. (1995). Strontium, neodymium, and lead isotopic and trace-element signatures of the East Indonesian sediments: Provenance and implications for Banda Arc magma genesis. Geochim. Cosmochim. Acta, 59(12): 2573-2598.

VSI: http://www.vsi.esdm.go.id/volcanoes/

Vukadinovic, D., Sutawidjaja, I. (1995). Geology, mineralogy and magma evolution of Gunung Slamet Volcano, Java, Indonesia. Journal of Southeast Asian Earth Sciences, 11(2): 135-164.

Westbrook, G.K., Ladd, J.W., Buhl, P., Bangs, N., Tiley, G.J. (1988). Cross section of an accretionary wedge; Barbados Ridge Complex. Geology, 16(7): 631-635.

Wheller, G.E., Varne, R., Foden, J.D., Abbott, M.J. (1987). Geochemistry of Quaternary volcanism in the Sunda-Banda Arc, Indonesia, and three-component genesis of island arc basaltic magmas. J. Volcanol. and Geotherm. Res., 32: 137-160.

White, W.M., Dupré, B. (1986). Sediment subduction and magma genesis in the Lesser Antilles: isotopic and trace element constraints. J. Geophys. Res., 91: 5927-5941.

White, W.M., Patchett, J. (1984). Hf-Nd-Sr isotopes and incompatible element abundances in island arcs: implications for magma origins and crustal-mantle evolution. Earth Planet. Sci. Lett., 67: 167-185.

White, W.M., Patchett, J., BenOthman, D. (1986). Hf isotope ratios of marine sediments and Mn nodules; evidence for a mantle source of Hf in seawater. Earth Planet. Sci. Lett., 79(1-2): 46-54.

Whitford, D.J. (1975). Strontium isotopic studies of the volcanic rocks of the Sunda arc, Indonesia, and their petrogenesis. Geochim. Cosmochim. Acta, 39: 1287-1302.

Whitford, D.J., Nicholls, I.A. (1976). Potassium variations in lavas across the Sunda arc in Java and Bali. In: R.W.Johnson (Editor), Volcanism in Australasia. Elsevier, Amsterdam, pp. 63-75.

Whitford, D.J., Nicholls, I.A., Taylor, S.R. (1979). Spatial variations in the geochemistry of Quaternary lavas across the Sunda arc in Java and Bali. Contrib. Mineral. Petrol., 70: 341-356.

Whitford, D.J., White, W.M., Jezek, P.A. (1981). Neodymium isotopic composition of Quaternary island arc lavas from Indonesia. Geochim. Cosmochim. Acta, 45: 989-995.

Widiyantoro, S., van der Hilst, R. (1996). Structure and evolution of lithospheric slab beneath the Sunda Arc, Indonesia. Science, 271: 1566-1570.

Woodhead, J.D., Eggins, S.M., Gamble, J. (1993). High field strength and transition element systematics in island arc and back-arc basin basalts: evidence for multi-phase melt extraction and depleted mantle wedge. Earth Planet. Sci. Lett., 114: 491-504.

Wortel, M.R.J., Vlaar, N.J. (1988). Subduction zone seismicity and the thermo-mechanical evolution of the downgoing lithosphere. Pure Appl. Geophys., 128: 625-659.

You, C.-F., Castillo, P.R., Gieskes, J.M., Chan. L.H., Spivack, A.J. (1996). Trace element behaviour in hydrothermal experiments: Implications for fluid processes at shallow depths in subduction zones. Earth Planet. Sci. Lett., 140: 41-52.

Zaenudin, A., Sutawidjaja, I.S., Aswin, D. (1993). Geological map of Salak Volcano, West Java. Volcanic Survey of Indonesia.

Appendices

Appendices

Data presented in this study are provided on a CD located inside the back cover of this thesis

Appendix A. Sample locations and descriptions.

Appendix B. Whole-rock major and trace element data

Appendix C: Whole-rock isotopic data

Appendix D: Mineral data

Appendix E. Analytical techniques

Appendix F: Distribution coefficients used in modelling

Table A.1. GVC sample locality details

Sample No.	Grid Reference S	Grid Reference E	Elevation (m)	Elevation error +/- (m)	Locality Details	Deposit	Group	Comments
G01A	06 42 16.9	107 01 39.6	1088	17	Tegallega Quarry near Cikundul River	MF	YGOV	
G1B	06 42 16.9	107 01 39.6	1088	17	Tegallega Quarry near Cikundul River	MF	YGOV	abundant small xenoliths
G02	06 42 16.9	107 01 39.6	1088	17	Tegallega Quarry near Cikundul River	charcoal in PFD	YGOV	
G03	06 42 16.9	107 01 39.6	1088	17	Tegallega Quarry near Cikundul River	MF w xenolith	YGOV	highly vesicular
G04	06 43 43.0	107 04 21.2	849	7	Large Quarry near Pataruman	MF	YGOV	slight alteration
G05	06 43 43.0	107 04 21.2	849	7	Large Quarry near Pataruman	charcoal in PFD	YGOV	
G06	06 47 12.4	107 01 51.4	854	47	Batu Lempar river valley	lava	OG	
G07	06 47 16.0	107 01 51.0	854	64	Batu Lempar river valley	MF	OG	
G08	06 50 51.3	107 08 00.9	496	7	Pasirayam Quarry ~3km SW of Cianjur	debris flow deposit	PAN	
G09	06 50 51.3	107 08 00.9	496	7	Pasirayam Quarry ~3km SW of Cianjur	debris flow deposit	PAN	slightly vesicular, large cpx
G10	06 44 51.5	107 02 28.3	1160	7	Quarry next to Cipandawa River near Patjet 1/2km south of Pasirkampung	MF	OG	vesicular, very fine grained
G11	06 44 51.5	107 02 28.3	1160	7	Quarry next to Cipandawa River near Patjet 1/2km south of Pasirkampung	MF	OG	contains lenses of lighter rock
G12	06 44 51.5	107 02 28.3	1160	7	Quarry next to Cipandawa River near Patjet 1/2km south of Pasirkampung	MF	OG	banded
G13	06 44 51.5	107 02 28.3	1160	7	Quarry next to Cipandawa River near Patjet 1/2km south of Pasirkampung	MF	OG	banded
G14	06 44 51.5	107 02 28.3	1160	7	Quarry next to Cipandawa River near Patjet 1/2km south of Pasirkampung	MF	OG	
G15	06 51 43.4	107 00 18.7	1161	9	Pasir Pogor hill	nose of lava flow	OG	
G16	06 49 47.6	106 55 35.3		40	Small waterfall at Situ Gunung	lava	PAN	
G17	06 47 27.7	106 59 40.6	2801	8	Eastern side of Gumuruh Crater ridge	lava	OG	
G18	06 47 23.5	106 58 59.8	2985	6	Gede Crater top	lava bomb	YGOV	
G19	06 47 12.7	106 58 43.1	2874	6	Gede Crater 2nd lava from top	lava	YGOV	slight alteration
G20	06 47 03.1	106 58 30.6	2655	18	lower Gede lava	lava (rubbly nose)	YGOV	
G21	06 46 59.8	106 58 44.8	2655	40	near Kawah Wadon	lava (boulder)	YGKR	
G22	-	-	-	-	Kawah Wadon	lava (blocky)	YGKR	
G23	06 46 40.5	106 58 31.7	2654	11	Path crossroads to Gede,Pangrango,Kawah Wadon and Cibodas	MF	YGKR	contains xenoliths
G24	-	-	-	-	Pangrango contact with Gede	lava	PAN	
G25	06 46 03.0	106 58 49.1	2139	22	Cipanas, path cutting hot spring	lava	YGKR	
G26	-	-	-	-	Just down path from Gede observatory	lava (nose of flow)	GEG	
G27	06 43 00.6	106 57 58.1	1247	7	stream cutting on tea plantation	lava	GEG	slight alteration
G28	06 43 05.6	106 57 54.4	1266	7	next river valley to loc 20	lava (boulder)	GEG	contains large euhedral cpx
G29	06 43 05.6	106 57 54.4	1266	7	next river valley to loc 20	lava (boulder)	GEG	contains large euhedral cpx
G30	06 42 36.5	106 56 47.2	1063	11	wide river at safari park enterance ~400m due south of Paragadjen village	lava (huge block)	PAN	contains large euhedral cpx
G31	06 42 36.5	106 56 47.2	1063	11	wide river at safari park enterance ~400m due south of Paragadjen village	lava (huge block)	PAN	heavily porphyritic
G32	06 42 15.9	106 58 22.6	1078	8	river valley by roadside in tea plantation, west of Gunung Mas	lava (block)	GEG	
G33	06 42 20.4	106 58 35.8	1215	9	lava ridge along top of tea plantation, west of Gunung Mas	lava	GEG	contains large euhedral cpx
G34	06 49 48.6	106 55 58.7	829	52	large waterfall Situ Gunung	MF?	PAN	
G35	06 49 48.6	106 55 58.7	829	52	large waterfall Situ Gunung	lava	PAN	
G36A	~40m from above location				on the path at the side of the large waterfall at Situ Gunung	MF	YGOV	
G36B	~40m from above location				on the path at the side of the large waterfall at Situ Gunung	MF	YGOV	contains xenoliths
G37A	06 51 23.7	106 56 12.7	~900	10	near Pamubutan village ~6km north of Sukabumi	MF	OG	slight alteration
G37B	06 51 23.7	106 56 12.7			near Pamubutan village ~6km north of Sukabumi	Lithic in PFD	OG	slight alteration

PFD, pyroclastic flow deposit; MF; primary magmatic fragment in pyroclastic flow deposit
YGKR, Young Gede Kawah Ratu; YGOV, Young Gede Other Vents; OG, Old Gede; PAN, Pangrango; GEG, Gegerbentang; OQV, Older Quaternary Volcanic rocks

Table A.1 (continued). GVC and Salak sample locality details

Sample No.	Grid Reference S	Grid Reference E	Elevation (m)	Elevation error +/- (m)	Locality Details	Deposit	Group	Comments
G38	06 44 33.2	107 00 20.8		15	long, m high exposure inside GPNP at Cibodas	MF	YGKR	
G39	06 44 18.6	107 00 23.6	1370	12	ridge of lava blocks at Cibodas Gardens	lava (blocky ridge)	YGKR	some alteration of plagioclase
G40	06 44 20.9	107 00 30.6	1336	15	waterfall with outcrop part covered in concrete	lava	YGKR	
G41	06 44 51.5	107 00 20.6	1273	41	waterfall	lava	YGKR	
G42	06 44 51.5	107 00 20.6	1273	41	waterfall	lava	YGKR	
G43	06 45 11.1	107 01 03.0	1458	10	Gunung Putri	lava	OG	slight alteration
G44	06 45 19.1	107 01 04.4	1454	13	Gunung Putri, close to Cipandawa river	MF	YGOV	
G45	06 47 42.6	107 01 09.1	1601	22	higher part of flow in valley cutting nr virgin forest	lava	OG	
G46	06 47 42.6	107 01 09.1	1601	22	lower part of flow in valley cutting nr virgin forest	lava	OG	
G47	06 48 03.9	107 01 18.9	1598	53	dried up waterfall lower lava	lava	OG	
G48	06 48 03.9	107 01 18.9	1598	53	dried up waterfall higher lava	lava	OG	
G49	06 46 41.2	107 03 50.7	949	15	where Tsv unit at Tjiherang Gunung Balukbuk meets road, and river	lava	OQV	contains xenoliths
G50A	06 42 16.9	107 01 39.6	1088	17	Tegallega Quarry near Cikundul River	lithic in PFD	YGOV	
G50B	06 42 16.9	107 01 39.6	1088	17	Tegallega Quarry near Cikundul River	lithic in PFD	YGOV	
G51	06 42 16.9	107 01 39.6	1088	17	Tegallega Quarry near Cikundul River	MF	YGOV	contains irregular patches of lighter rock
G52	06 44 32.7	107 03 55.3	1078	6	Quarry on small hill with hydrothermal deposits, west of Tjikanjere	lava	OQV	slight alteration
G53	06 44 32.7	107 03 55.3	1078	6	Quarry on small hill with hydrothermal deposits, west of Tjikanjere	lava	OQV	slight alteration
G54	06 44 52.7	107 03 52.9	1058	6	Quarry on small hill with hydrothermal deposits nr Patjet-K, west of Tjikanjere	lava	OQV	some alteration of plagioclase
G55	06 48 46.7	107 03 28.0	941	11	Roadside outcrop	MF	OG	
G56	06 52 13.0	107 02 43.3	849	8	Hillside exposure/small quarry	lava/instrusion	OQV	
G57	06 55 23.9	106 59 50.9	737	7	Huge quarry face	lava	TSV	altered (pale green appearance)
G58	06 55 23.9	106 59 50.9	737	7	Huge quarry face	lava	TSV	altered (greeny-blue appearance)
S100	06 45 09.4	106 46 29.1	656	15	1st Quarry along road heading N/NE from salak observatory	AFD	Pre-Salak	pumice, fibreous texture
S101	06 43 16.7	106 46 52.1	704	8	1st Quarry along road heading N/NE from salak observatory	AFD	Pre-Salak	pumice, fibreous texture
S102	06 42 43.0	106 45 35.3	706	36	up mountain beyond campsite upper Cibadak River, Pasirdalem lava flow	lava (boulder)	SVG	contains xenoliths
S103	06 42 43.0	106 45 35.3	706	36	up mountain beyond campsite upper Cibadak River, Pasirdalem lava flow	lava	SVG	
S104	06 40 16.2	106 46 43.3	716	10	Tjidjulang by the Tji Leungsir River	lava	CVG	
S105	06 40 17.5	106 43 37.2	739	18	country park at Nangka River, waterfall	lava	CVG	slightly weathered
S106A	06 40 07.5	106 43 37.2	739	18	country park at Nangka River, fenced waterfall	lava	CVG	
S106B	06 40 17.5	106 43 37.2	739	18	country park at Nangka River, hillside crag	lava	CVG	
S107A	06 43 08.9	106 42 45.9	1404	7	along path west of Salak crater	lava	SVG	glass, banded in places
S107B	06 43 08.9	106 42 45.9	1404	7	along path west of Salak crater	lava	SVG	glass, banded in places
S108	06 43 08.9	106 42 45.9	1404	7	along path south of Salak crater	lava	CVG	
S109	06 45 16.0	106 43 20.3	954	16	salak park enterance, path to waterfall	lava	CVG	streaks of alteration
S110A	06 45 58.4	106 43 40.0	954	11	well-exposed cross-section of a lava flow in quarry, higher in flow	lava	CVG	
S110B	06 45 58.4	106 43 40.0	954	11	well-exposed cross-section of a lava flow in quarry, lower in flow	lava	CVG	dusty appearance of plagioclase
S111	06 39 37.7	106 42 21.3	570	19	Cucung waterfall	lava	CVG	slight alteration
S112	06 40 20.4	106 41 17.3	777	7	roadside outcrop	lava	SL3	slight alteration

PFD, pyroclastic flow deposit; MF; primary magmatic fragment in pyroclastic flow deposit; AFD, air fall deposit
YGKR, Young Gede Kawah Ratu; YGOV, Young Gede Other Vents; OG, Old Gede; PAN, Pangrango; GEG, Gegerbentang; OQV, Older Quaternary Volcanic rocks; SVG, side vent group, CVG, central vent group; SL3, Salak lava flow 3 (VSI)

Table A.2. Modal proportions of mineral phases in GVC volcanic rocks

% vol.	G01A	G01B	G04	G06	G07	G08	G09	G10
Ol	3.2	4.1	-	1.2	8.5	11.8	11.1	-
Opx	-	-	5.2	3.1	-	-	-	1.1
Cpx	8.3	9.8	10.7	6.9	3.2	3.1	7.3	4.9
Plag	26.5	31.2	44.3	57.3	64.8	31.7	57.7	31.3
Ox	1.5	-	0.8	3.1	1.2	1.5	1.9	0.8
Hbl	-	-	-	-	-	-	-	-
Bio	-	-	-	-	-	-	-	-
GM	60.5	54.9	39.0	28.4	22.3	51.9	22.0	61.9
% vol.	G13(light)	G13(dark)	G15	G16	G17	G18	G19	G20
Ol	-	3.9	-	8.8	-	-	-	-
Opx	3.8	3.2	4.3	1.1	12.1	8.2	4.5	3.2
Cpx	10.8	8.7	2.8	13.3	6.3	10.6	7.2	16.2
Plag	38.4	41.3	53.9	53.8	39.5	42.3	30.4	27.6
Ox	2.4	1.8	1.8	2.2	2.8	2.8	1.1	2.7
Hbl	-	-	-	-	-	-	-	-
Bio	-	-	-	-	-	-	-	-
GM	44.6	41.1	37.2	20.8	39.3	36.1	56.8	50.3
% vol.	G21	G22	G24	G25	G26	G27	G28	G29
Ol	-	-	-	-	3.7	-	-	10.9
Opx	3.4	5.3	7.2	9.2	2.1	6.2	5.3	-
Cpx	13.6	11.0	19.5	11.2	19.7	8.5	15.6	14.1
Plag	52.8	48.4	37.1	41.5	31.7	41.4	29.7	50.4
Ox	1.5	3.2	4.0	2.2	3.8	3.7	2.1	1.3
Hbl	-	-	-	-	-	-	-	-
Bio	-	-	-	-	-	-	-	-
GM	28.7	32.1	32.2	35.9	39.0	40.2	47.3	23.3
% vol.	G30	G31	G32	G33	G35	G36A	G36B	G37A
Ol	8.3	-	-	-	12.2	10.4	7.6	-
Opx	-	3.2	3.1	7.2	-	-	-	3.1
Cpx	22.4	14.3	14.8	10.5	9.1	19.2	17.1	5.4
Plag	34.9	35.3	35.3	41.3	34.4	27.7	21.7	31.3
Ox	2.1	3.1	2.8	2.4	1.3	1.4	1.3	1.9
Hbl	-	-	-	-	-	-	-	-
Bio	-	-	-	-	-	-	-	-
GM	32.3	44.1	44.0	38.6	43.0	41.3	52.3	58.3
% vol.	G37B	G38	G39	G40	G41	G42	G43	G44
Ol	-	-	-	-	-	-	-	-
Opx	3.2	6.3	12.4	18.2	10.4	20.2	4.9	10.0
Cpx	7.3	11.0	9.0	10.2	7.3	5.7	17.0	6.1
Plag	39.5	32.3	45.2	34.1	46.3	39.5	37.3	25.7
Ox	0.9	1.2	2.7	2.7	0.5	1.3	1.2	1.1
Hbl	-	-	-	-	-	-	-	-
Bio	-	-	-	-	-	-	-	-
GM	49.1	49.2	30.7	34.8	35.5	33.3	39.6	57.1

Modal phase volume established from point-counting between 200-300 points per sample. Ol, olivine; Opx, orthopyroxene; Cpx, clinopyroxene; Plag, plagioclase; Ox, Fe-Ti oxide; Hbl, hornblende; Bio, biotite; GM, groundmass; XEN, xenolith.

Table A.2. Modal proportions of mineral phases in GVC and Salak volcanic rocks

% vol.	G45	G46	G47	G48	G49	G50A	G51(dark)	G51(light)
Ol	-	-	-	3.2	-	-	3.2	-
Opx	0.8	0.5	3.1	2.1	4.2	4.9	-	0.5
Cpx	4.2	5.3	3.5	4.8	6.2	2.3	17.1	1.1
Plag	44.6	38.5	44.2	34.7	42.7	37.4	30.6	11.8
Ox	2.3	3.2	1.6	1.1	3.2	1.2	3.0	0.5
Hbl	-	-	-	-	-	-	-	-
Bio	-	-	-	-	-	-	-	-
GM	48.1	52.5	47.6	54.1	43.7	54.2	46.1	86.1

% vol.	G52	G53	G54	G55	G56	G57	G58
Ol	-	-	-	0.5	0.5	-	-
Opx	2.1	3.2	2.1	0.9	6.1	12.1	7.2
Cpx	8.7	6.9	13.4	2.1	3.2	4.0	16.8
Plag	63	42.6	48.2	17.5	51.7	59.6	45.7
Ox	2	3.1	4.3	2.3	4.1	1.1	1.0
Hbl	0.5	-	-	-	-	-	-
Bio	-	-	-	0.4	-	-	-
GM	23.7	44.2	32.0	76.3	34.4	23.2	29.3

% vol.	S101	S102	S103	S104	S105	S106A	S106B	S107B
Ol	-	-	-	2.1	4.2	3.3	3.2	-
Opx	1.5	6.2	10.8	1	0.8	7.2	5.9	-
Cpx	0.25	5.1	9	0.3	0.4	2.1	3.8	0.1
Plag	8.2	34.3	35.4	26.4	32.8	31.2	32.3	4.3
Ox	-	2.9	3.9	1.1	1.8	2	2	0.5
Hbl	0.25	-	-	-	-	-	-	0.25
Bio	-	-	-	-	-	-	-	0.25
Qtz	0.5	-	-	-	-	-	-	1.5
GM	89.3	51.5	40.9	69.1	60	54.2	52.8	93.1

% vol.	S108	S109	S110A	S110B	S111	S112	S102XEN
Ol	-	1.9	-	-	9.1	-	-
Opx	2.3	3.2	4.2	3.2	-	7.4	2.7
Cpx	1.4	7.1	4.3	2.1	-	10.2	4.6
Plag	15.5	28.6	14.3	12.7	31.5	41.1	10.3
Ox	1.9	2	2.1	1.5	2.1	4	1.7
Hbl	-	-	-	-	-	-	-
Bio	-	-	-	-	-	-	-
Qtz	-	-	-	-	-	-	-
GM	78.9	57.2	75.1	80.5	57.3	37.3	80.7

Modal phase volume established from point-counting between 200-300 points per sample. Ol, olivine; Opx, orthopyroxene; Cpx, clinopyroxene; Plag, plagioclase; Ox, Fe-Ti oxide; Hbl, hornblende; Bio, biotite; Qtz, quartz; GM, groundmass; XEN, xenolith.

Table B.1. Major and trace element data of GVC volcanic rocks

Sample	G01A	G01B	G03	G04	G06	G07	G10	G11	G14
SiO_2	55.04	54.86	55.21	56.10	55.54	56.27	55.11	56.70	59.03
Al_2O_3	18.34	18.53	18.41	18.83	20.65	19.43	20.17	18.04	17.49
Fe_2O_3	8.35	8.30	8.18	8.10	7.22	7.78	7.66	8.19	6.93
MgO	3.98	4.06	3.95	3.63	2.36	2.50	2.86	3.73	2.93
CaO	8.78	8.92	8.79	8.10	8.70	7.60	8.23	8.08	7.06
Na_2O	2.97	2.96	2.99	3.01	3.53	3.91	3.12	2.94	3.11
K_2O	1.36	1.32	1.37	1.35	1.06	1.45	1.18	1.41	1.67
TiO_2	0.91	0.91	0.90	0.81	0.81	0.83	0.80	0.81	0.70
MnO	0.15	0.15	0.15	0.14	0.14	0.16	0.15	0.15	0.14
P_2O_5	0.14	0.14	0.14	0.17	0.22	0.24	0.19	0.15	0.14
LOI	0.09	0.15	0.16	0.05	-0.07	-0.02	0.80	0.04	0.89
Total	100.10	100.29	100.24	100.29	100.16	100.16	100.26	100.24	100.08
Sc	30	30	31	20	18	18	17	21	17
Ti	5467	5556	5898	4909	5017	5455	4939	4406	3878
V	238	246	255	167	135	137	132	185	146
Cr	17.4	18.2	17.4	9.9	4.0	3.2	8.8	14.0	11.4
Mn	1185	1185	1046	1154	1154	1162	1216	1224	1115
Co	24	25	26	22	17	19	19	23	19
Ni	15.6	13.0	7.4	11.2	5.5	1.3	7.6	9.8	7.5
Cu	12	15	16	54	52	63	48	25	38
Zn	76	76	70	77	77	85	67	77	71
Ga	18	19	19	19	20	21	19	18	18
Rb	49.6	49.0	50.4	53.4	36.0	54.3	46.7	57.0	70.2
Sr	323	319	334	331	397	336	357	287	285
Y	22	22	23	25	24	31	26	25	26
Zr	108	107	108	122	102	130	128	128	151
Nb	4.22	4.18	4.20	4.85	4.26	5.37	4.78	4.72	5.39
Cs	3.33	3.31	3.24	2.59	1.68	3.89	3.44	3.91	4.77
Ba	250	247	249	254	216	267	238	266	320
La	13.6	13.4	13.6	14.7	12.7	15.1	13.8	15.0	17.7
Ce	28.6	28.5	28.7	32.1	27.8	33.0	30.8	32.1	37.4
Pr	3.78	3.76	3.78	4.31	3.94	4.55	4.26	4.24	4.89
Nd	16.1	16.4	16.4	18.5	17.9	20.2	18.7	18.2	20.5
Sm	3.76	3.80	3.79	4.32	4.19	4.78	4.37	4.16	4.60
Eu	1.06	1.07	1.07	1.17	1.26	1.38	1.25	1.14	1.17
Gd	3.98	4.09	3.99	4.48	4.36	5.06	4.68	4.39	4.69
Tb	0.63	0.63	0.63	0.71	0.69	0.82	0.74	0.69	0.73
Dy	3.71	3.77	3.74	4.15	4.03	4.91	4.34	4.05	4.30
Ho	0.77	0.78	0.77	0.86	0.83	1.03	0.89	0.85	0.89
Er	2.07	2.11	2.12	2.30	2.27	2.82	2.45	2.29	2.43
Tm	0.32	0.33	0.33	0.36	0.36	0.44	0.38	0.35	0.39
Yb	2.02	2.05	2.09	2.27	2.26	2.84	2.44	2.28	2.46
Lu	0.33	0.34	0.34	0.37	0.37	0.47	0.41	0.38	0.40
Hf	2.90	2.92	2.94	3.29	2.72	3.46	3.43	3.45	4.08
Ta	0.35	0.33	0.34	0.38	0.31	0.41	0.35	0.38	0.44
Pb (total)	10.5	10.3	10.4	11.4	7.2	13.0	6.6	12.8	14.2
Th	5.48	5.47	5.53	5.78	3.73	5.46	5.40	6.21	7.68
U	1.22	1.20	1.23	1.33	0.88	1.32	1.22	1.41	1.75

Table B.1. Major and trace element data of GVC volcanic rocks continued

Sample	G15	G16	G17	G18	G19	G20	G21	G22	G23
SiO_2	59.58	51.48	61.11	59.39	55.49	53.98	55.05	59.47	52.52
Al_2O_3	20.55	19.41	17.72	17.76	20.02	17.05	18.77	17.34	19.19
Fe_2O_3	4.71	10.50	6.57	6.96	7.61	10.33	8.22	7.19	9.07
MgO	1.24	4.21	2.54	3.03	2.87	5.22	3.61	3.13	4.51
CaO	7.13	9.26	6.15	7.27	8.38	7.50	8.72	7.23	9.86
Na_2O	3.51	2.77	3.34	3.22	3.14	2.61	3.07	3.21	2.75
K_2O	1.44	1.18	1.53	1.73	1.27	1.29	1.02	1.74	0.91
TiO_2	0.55	1.08	0.62	0.71	0.79	0.94	0.80	0.74	0.90
MnO	0.11	0.20	0.14	0.14	0.15	0.19	0.16	0.14	0.17
P_2O_5	0.18	0.18	0.17	0.14	0.19	0.16	0.16	0.14	0.13
LOI	0.95	-0.15	0.32	-0.20	0.18	0.89	0.47	0.00	0.07
Total	99.94	100.12	100.21	100.15	100.08	100.16	100.05	100.32	100.08
Sc	9	29	13	19	16	27	22	20	30
Ti	3518	6683	3465	4256	4316	5814	4957	4621	5712
V	61	245	115	158	130	228	201	173	257
Cr	2.2	6.2	3.7	6.2	14.6	26.5	5.1	8.4	8.3
Mn	751	1603	1162	1076	1208	1557	1324	1162	1371
Co	8	29	15	19	18	31	22	19	29
Ni	2.2	6.1	4.2	5.2	8.9	17.0	6.1	4.9	8.0
Cu	11	72	17	21	49	50	21	23	48
Zn	56	95	68	69	70	88	82	75	81
Ga	19	21	18	18	19	18	19	18	19
Rb	54.2	34.1	58.5	62.1	50.7	57.3	37.0	66.2	32.4
Sr	407	301	317	302	337	280	362	307	354
Y	26	32	22	23	25	24	21	24	21
Zr	149	116	142	117	124	120	100	138	80
Nb	5.82	5.25	5.90	4.92	4.73	4.47	3.98	5.09	3.46
Cs	3.88	2.55	1.99	2.11	2.59	4.19	2.39	4.41	2.28
Ba	317	242	315	313	237	229	211	318	183
La	18.2	14.4	16.5	15.7	12.6	10.9	12.0	16.4	10.4
Ce	39.1	31.5	34.5	32.4	28.1	27.2	26.0	34.3	22.6
Pr	5.10	4.40	4.49	4.19	3.87	3.39	3.52	4.44	3.07
Nd	21.6	20.0	18.9	17.5	17.1	15.3	15.2	18.6	13.8
Sm	4.67	4.96	4.08	3.92	4.09	3.82	3.50	4.05	3.34
Eu	1.30	1.33	1.15	1.04	1.24	1.13	1.08	1.05	1.04
Gd	4.67	5.35	4.03	3.98	4.23	4.07	3.64	4.10	3.60
Tb	0.73	0.88	0.62	0.64	0.69	0.68	0.59	0.65	0.58
Dy	4.15	5.25	3.67	3.66	4.10	4.05	3.46	3.81	3.44
Ho	0.85	1.09	0.75	0.76	0.84	0.84	0.73	0.80	0.72
Er	2.34	2.99	2.10	2.09	2.33	2.33	2.01	2.19	1.96
Tm	0.37	0.46	0.33	0.32	0.37	0.38	0.31	0.34	0.30
Yb	2.40	2.92	2.15	2.07	2.35	2.41	2.01	2.20	1.92
Lu	0.40	0.48	0.36	0.34	0.39	0.40	0.33	0.37	0.31
Hf	3.91	3.22	3.71	3.21	3.38	3.27	2.66	3.64	2.20
Ta	0.43	0.40	0.44	0.40	0.35	0.34	0.30	0.41	0.26
Pb (total)	13.6	11.7	11.3	9.5	10.4	7.5	8.8	12.6	8.3
Th	6.46	5.50	6.24	6.61	5.30	5.23	4.10	7.15	3.45
U	1.46	1.16	1.39	1.50	1.23	1.25	0.92	1.63	0.78

Table B.1. Major and trace element data of GVC volcanic rocks continued

Sample	G24	G25	G26	G27	G28	G29	G30	G31	G32
SiO_2	54.87	59.29	53.60	52.93	54.43	51.66	51.56	56.06	54.33
Al_2O_3	18.61	17.55	18.89	19.65	18.63	19.33	18.56	21.15	19.63
Fe_2O_3	9.42	6.94	9.85	9.65	9.55	10.04	10.34	6.65	8.71
MgO	3.64	2.97	3.88	3.51	3.49	4.59	4.98	2.03	2.93
CaO	8.43	7.16	8.83	8.97	8.69	9.38	9.67	8.79	8.61
Na_2O	3.07	3.21	3.09	3.07	3.11	2.82	2.70	3.41	3.28
K_2O	1.05	1.76	0.93	0.89	1.01	0.81	1.19	1.13	1.00
TiO_2	0.87	0.72	0.89	0.95	0.91	0.96	1.06	0.70	0.79
MnO	0.19	0.14	0.20	0.19	0.20	0.18	0.18	0.14	0.19
P_2O_5	0.23	0.14	0.23	0.28	0.29	0.21	0.18	0.20	0.29
LOI	-0.17	-0.08	-0.23	-0.05	-0.21	-0.13	-0.40	-0.11	0.02
Total	100.21	99.79	100.16	100.04	100.10	99.86	100.02	100.16	99.78
Sc	21	19	20	19	19	26	32	13	13
Ti	5496	4567	5898	6132	5682	6156	6713	4633	4501
V	192	167	192	166	152	221	259	108	151
Cr	2.6	6.6	5.6	10.2	4.6	12.6	10.9	1.5	2.6
Mn	1557	1146	1820	1781	1619	1541	1518	1022	1549
Co	24	19	25	22	21	28	32	15	20
Ni	4.8	4.1	5.6	5.4	3.6	9.3	9.6	0.8	3.9
Cu	42	25	39	24	80	36	104	35	41
Zn	89	74	79	79	88	87	96	77	89
Ga	20	19	20	20	20	20	20	21	21
Rb	38.7	68.8	31.9	34.0	39.1	30.9	45.8	45.0	35.1
Sr	353	316	406	438	422	397	302	367	405
Y	27	24	26	30	30	24	30	31	26
Zr	114	143	98	103	125	83	110	138	103
Nb	5.27	5.22	4.45	5.82	6.98	4.53	4.96	5.52	5.49
Cs	1.44	4.55	0.91	1.52	1.11	1.78	1.01	2.31	1.61
Ba	233	330	179	177	212	168	212	210	223
La	15.0	17.2	12.9	14.6	17.1	12.5	13.5	13.9	17.1
Ce	32.8	35.9	28.8	32.0	38.6	27.7	29.9	30.5	36.3
Pr	4.51	4.61	4.09	4.74	5.38	3.98	4.17	4.31	5.05
Nd	19.9	19.1	18.5	21.5	24.2	18.1	18.8	19.4	22.0
Sm	4.53	4.22	4.30	5.04	5.47	4.21	4.72	4.70	4.80
Eu	1.32	1.08	1.34	1.51	1.54	1.30	1.25	1.36	1.47
Gd	4.69	4.28	4.46	5.11	5.44	4.37	5.16	5.02	4.69
Tb	0.75	0.68	0.68	0.81	0.84	0.68	0.83	0.82	0.72
Dy	4.38	3.93	4.17	4.73	4.87	3.96	4.93	4.91	4.06
Ho	0.91	0.81	0.86	1.00	1.00	0.82	1.02	1.03	0.83
Er	2.50	2.24	2.39	2.71	2.76	2.24	2.78	2.85	2.24
Tm	0.40	0.35	0.38	0.42	0.43	0.34	0.43	0.45	0.35
Yb	2.55	2.25	2.39	2.72	2.77	2.15	2.66	2.87	2.23
Lu	0.42	0.36	0.40	0.47	0.46	0.36	0.43	0.47	0.37
Hf	3.04	3.77	2.65	2.79	3.28	2.27	3.04	3.68	2.76
Ta	0.37	0.43	0.29	0.35	0.43	0.30	0.37	0.40	0.35
Pb (total)	18.1	12.9	5.1	6.7	12.2	8.2	14.4	9.9	7.7
Th	4.50	7.43	3.73	3.32	4.14	3.14	5.16	4.64	4.32
U	1.06	1.70	0.86	0.80	1.01	0.74	1.17	1.09	1.00

Table B.1. Major and trace element data of GVC volcanic rocks continued

Sample	G33	G35	G36A	G36B	G37A	G38	G39	G40	G41
SiO_2	53.23	50.56	54.71	54.81	56.17	55.36	62.01	57.45	54.45
Al_2O_3	19.35	19.29	18.52	18.63	20.91	18.76	17.46	18.46	20.04
Fe_2O_3	9.59	10.56	8.18	8.29	6.51	8.61	6.13	8.14	7.97
MgO	3.70	4.89	4.01	4.11	2.03	3.33	2.52	3.01	3.21
CaO	8.76	9.78	8.95	8.91	8.53	7.67	6.22	7.66	8.99
Na_2O	3.05	2.94	2.89	2.93	3.28	3.08	3.37	3.18	3.09
K_2O	0.87	0.92	1.30	1.32	1.38	1.14	1.84	1.26	1.25
TiO_2	0.92	1.15	0.91	0.90	0.72	0.85	0.64	0.77	0.81
MnO	0.19	0.18	0.14	0.15	0.13	0.17	0.13	0.17	0.15
P_2O_5	0.26	0.15	0.13	0.14	0.18	0.19	0.15	0.19	0.16
LOI	0.20	-0.43	0.22	0.05	0.51	0.97	-0.19	-0.14	0.17
Total	100.12	100.00	99.96	100.23	100.35	100.12	100.27	100.14	100.29
Sc	19	36	30	30	14	20	13	17	20
Ti	5706	7636	5688	5113	4160	5556	3554	5065	5353
V	184	316	252	262	128	193	119	147	193
Cr	10.4	15.6	17.3	17.9	1.2	4.6	10.9	2.5	3.0
Mn	1541	1688	1200	1200	1092	1200	1053	1216	1076
Co	24	33	26	26	16	22	15	18	23
Ni	7.3	8.6	7.9	9.1	2.7	2.6	7.7	1.9	4.3
Cu	42	73	14	15	40	36	41	28	50
Zn	88	84	77	77	71	79	60	65	70
Ga	20	21	19	19	21	20	17	18	20
Rb	30.4	30.0	48.8	49.8	55.0	43.4	77.0	48.6	48.4
Sr	423	326	324	301	342	351	309	370	346
Y	24	27	22	23	29	27	23	26	26
Zr	91	82	108	110	138	122	146	126	113
Nb	4.99	3.72	4.15	4.21	5.85	4.91	5.57	4.83	4.67
Cs	1.27	0.84	3.27	3.29	4.24	3.26	2.69	2.08	3.51
Ba	188	160	245	250	307	251	364	245	238
La	14.5	9.8	13.3	13.7	17.7	15.2	20.2	15.0	13.4
Ce	31.7	22.2	28.2	29.1	36.9	32.1	41.1	32.0	29.1
Pr	4.59	3.22	3.76	3.86	5.04	4.52	5.22	4.44	4.01
Nd	20.7	15.0	16.2	16.7	21.6	19.8	21.0	19.5	17.5
Sm	4.70	3.89	3.80	3.86	4.84	4.47	4.38	4.47	4.10
Eu	1.42	1.21	1.06	1.09	1.35	1.26	1.12	1.24	1.17
Gd	4.76	4.35	4.00	4.08	5.06	4.72	4.21	4.55	4.25
Tb	0.73	0.73	0.64	0.65	0.78	0.75	0.65	0.73	0.69
Dy	4.10	4.42	3.75	3.78	4.54	4.40	3.71	4.23	4.07
Ho	0.85	0.93	0.77	0.79	0.96	0.93	0.76	0.88	0.86
Er	2.25	2.56	2.09	2.12	2.63	2.55	2.05	2.43	2.33
Tm	0.34	0.39	0.32	0.33	0.40	0.39	0.32	0.38	0.36
Yb	2.15	2.49	2.05	2.09	2.57	2.55	2.09	2.41	2.34
Lu	0.35	0.41	0.33	0.34	0.43	0.43	0.34	0.41	0.38
Hf	2.49	2.33	2.91	2.96	3.62	3.25	3.84	3.35	3.07
Ta	0.31	0.26	0.33	0.33	0.43	0.36	0.45	0.36	0.35
Pb (total)	8.9	5.1	10.4	10.7	13.9	9.9	11.9	8.6	11.1
Th	3.41	3.21	5.34	5.51	6.06	4.82	8.10	5.08	4.82
U	0.82	0.73	1.18	1.24	1.44	1.12	1.82	1.19	1.15

Table B.1. Major and trace element data of GVC volcanic rocks continued

Sample	G42	G43	G44	G45	G46	G47	G48	G49	G51
SiO_2	54.28	55.59	55.09	57.56	54.96	58.90	54.76	59.85	55.39
Al_2O_3	20.20	19.09	19.76	19.32	19.97	17.95	18.79	17.15	18.33
Fe_2O_3	7.99	8.01	7.91	7.25	8.09	7.32	9.08	7.18	8.20
MgO	3.29	3.59	3.09	2.72	3.13	2.75	3.69	2.79	3.97
CaO	8.95	8.44	8.35	7.98	8.85	6.94	7.74	6.28	8.75
Na_2O	3.04	2.98	3.08	3.16	3.07	3.31	2.89	3.40	2.96
K_2O	1.23	1.31	1.20	1.38	1.06	1.37	1.13	1.78	1.38
TiO_2	0.81	0.79	0.81	0.73	0.83	0.78	0.91	0.72	0.90
MnO	0.15	0.15	0.16	0.14	0.15	0.14	0.17	0.14	0.15
P_2O_5	0.16	0.16	0.19	0.18	0.17	0.20	0.18	0.17	0.13
LOI	0.19	-0.15	0.48	-0.09	0.07	0.18	0.78	0.35	0.23
Total	100.27	99.97	100.12	100.33	100.34	99.83	100.12	99.80	100.38
Sc	21	21	18	15	21	16	24	17	29
Ti	5401	5425	5443	4070	5257	5149	5976	4645	5011
V	198	185	151	150	193	137	228	151	252
Cr	3.3	10.1	11.0	2.8	3.1	10.4	5.3	13.1	16.1
Mn	1076	1115	1169	1146	1247	1053	1200	1169	1185
Co	23	24	22	17	21	17	25	18	25
Ni	3.0	7.0	6.7	3.8	4.4	5.5	3.0	7.3	8.6
Cu	49	49	59	34	45	22	40	43	14
Zn	72	75	67	72	77	62	86	70	74
Ga	21	20	20	19	20	19	20	18	18
Rb	48.3	54.6	50.1	52.6	38.7	52.7	35.9	56.1	51.5
Sr	347	366	376	334	347	386	358	342	297
Y	25	26	27	25	24	26	26	26	23
Zr	113	119	131	128	96	144	108	132	109
Nb	4.61	4.90	4.79	5.35	3.95	5.60	4.59	5.29	4.22
Cs	3.48	1.87	3.45	2.27	2.23	1.79	1.84	1.54	3.34
Ba	235	242	228	279	217	265	231	308	254
La	13.4	14.5	13.8	17.0	12.7	16.0	14.0	20.4	13.8
Ce	29.1	30.5	30.8	36.3	26.8	35.3	30.3	38.8	29.2
Pr	3.97	4.17	4.25	4.82	3.71	4.83	4.12	5.60	3.84
Nd	17.5	18.0	18.6	20.7	16.4	21.0	18.2	23.3	16.6
Sm	4.13	4.07	4.40	4.53	3.83	4.84	4.19	4.94	3.84
Eu	1.15	1.14	1.24	1.23	1.16	1.29	1.21	1.29	1.08
Gd	4.24	4.20	4.55	4.49	4.14	4.66	4.34	4.74	3.99
Tb	0.69	0.68	0.73	0.71	0.65	0.74	0.71	0.75	0.63
Dy	4.05	3.98	4.36	4.10	3.85	4.21	4.20	4.31	3.72
Ho	0.85	0.83	0.90	0.83	0.81	0.85	0.87	0.88	0.77
Er	2.33	2.29	2.48	2.26	2.20	2.25	2.40	2.45	2.10
Tm	0.36	0.35	0.38	0.36	0.35	0.35	0.37	0.39	0.33
Yb	2.33	2.24	2.48	2.24	2.18	2.28	2.36	2.52	2.05
Lu	0.39	0.38	0.42	0.37	0.36	0.37	0.39	0.41	0.34
Hf	3.02	3.21	3.46	3.39	2.64	3.85	2.90	3.61	2.94
Ta	0.34	0.35	0.35	0.39	0.29	0.41	0.33	0.39	0.33
Pb (total)	11.0	10.3	10.7	10.1	9.7	12.3	10.1	8.8	10.5
Th	4.78	5.47	5.29	5.61	3.96	5.46	4.36	7.43	5.60
U	1.13	1.26	1.25	1.29	0.93	1.28	0.99	1.54	1.27

Table B.1. Major and trace element data of GVC volcanic rocks

Sample	G52	G53	G54	G55	G57	G58
SiO_2	58.81	58.94	58.17	54.78	60.77	60.69
Al_2O_3	17.29	17.17	17.84	19.51	17.30	17.11
Fe_2O_3	7.36	7.14	7.55	8.69	6.60	6.45
MgO	3.02	3.02	2.84	3.09	2.41	2.71
CaO	6.79	6.68	6.62	7.39	6.82	6.52
Na_2O	3.20	3.33	3.45	3.12	2.64	2.54
K_2O	1.59	1.98	1.87	1.10	1.35	1.33
TiO_2	0.76	0.76	0.73	0.93	0.79	0.80
MnO	0.13	0.15	0.15	0.16	0.13	0.09
P_2O_5	0.15	0.14	0.22	0.20	0.13	0.13
LOI	0.91	0.50	0.65	1.21	1.40	1.64
Total	100.00	99.81	100.08	100.17	100.34	100.01
Sc	20	15	10	17	22	18
Ti	4382	3812	3710	4873	5221	4124
V	184	159	120	191	118	107
Cr	13.3	11.8	3.9	1.9	21.9	23.8
Mn	1131	1100	1107	1239	945	666
Co	20	18	17	21	16	15
Ni	7.8	7.1	5.6	2.8	5.6	7.4
Cu	35	32	8	49	16	16
Zn	85	59	52	79	64	64
Ga	18	16	16	20	17	16
Rb	52.8	63.9	55.6	40.0	47.6	43.8
Sr	306	283	382	320	221	199
Y	27	22	23	28	27	25
Zr	115	100	122	118	22	19
Nb	5.07	4.98	5.73	4.97	7.64	7.54
Cs	3.18	1.52	1.20	3.35	1.85	1.97
Ba	334	320	356	266	250	250
La	19.2	17.9	20.5	16.5	19.0	19.1
Ce	38.6	35.8	40.8	33.5	39.2	39.2
Pr	4.96	4.54	5.26	4.76	4.97	4.89
Nd	20.8	18.7	21.6	20.8	20.5	20.1
Sm	4.52	4.01	4.52	4.71	4.37	4.31
Eu	1.20	1.10	1.30	1.34	1.14	1.12
Gd	4.63	4.11	4.33	4.97	4.56	4.65
Tb	0.73	0.62	0.65	0.78	0.77	0.76
Dy	4.30	3.72	3.79	4.55	4.56	4.40
Ho	0.90	0.76	0.79	0.95	0.94	0.88
Er	2.48	2.07	2.16	2.57	2.46	2.31
Tm	0.38	0.33	0.34	0.39	0.38	0.36
Yb	2.47	2.07	2.25	2.50	2.38	2.21
Lu	0.42	0.35	0.38	0.41	0.39	0.36
Hf	3.25	2.93	3.27	3.22	0.75	0.69
Ta	0.39	0.39	0.42	0.36	0.63	0.60
Pb (total)	8.4	7.1	5.8	12.3	9.4	8.8
Th	9.34	8.93	8.77	4.99	6.28	5.56
U	1.83	1.76	1.75	1.15	0.60	0.51

Table B.2. Major and trace element data of Salak volcanic rocks

Sample	S100	S101	S102	S103	S104	S105	S106A	S106B	S107A
SiO_2	70.12	70.44	59.61	58.87	54.90	54.09	54.01	53.77	76.82
Al_2O_3	14.24	14.15	17.42	17.54	19.43	20.16	18.71	18.78	12.34
Fe_2O_3	2.66	2.62	7.77	8.24	8.89	8.45	9.99	9.85	1.13
MgO	0.63	0.64	2.71	2.67	2.54	2.49	3.63	3.61	0.20
CaO	2.47	2.43	6.45	6.52	7.70	8.79	8.38	8.39	1.02
Na_2O	3.57	3.38	3.83	3.79	3.60	3.56	3.35	3.48	3.51
K_2O	3.09	3.11	1.15	1.11	1.03	0.93	0.83	0.84	3.99
TiO_2	0.31	0.30	0.73	0.75	1.04	0.97	1.02	1.01	0.12
MnO	0.07	0.07	0.18	0.18	0.17	0.17	0.19	0.19	0.04
P_2O_5	0.07	0.05	0.25	0.25	0.33	0.26	0.26	0.26	0.02
LOI	2.88	3.03	0.14	0.07	0.48	-0.13	-0.05	0.05	1.06
Total	100.11	100.22	100.23	100.00	100.12	99.74	100.32	100.22	100.24
Sc	2	2	16	16	23	20	23	23	0
Ti	1558	1463	4765	4717	6851	6683	6671	6605	653
V	23	24	103	103	160	143	178	177	2
Cr	0.1	1.2	2.9	1.9	2.2	1.1	2.4	4.3	0.1
Mn	472	449	1348	1340	1262	1239	1727	1743	271
Co	3	3	16	16	19	18	22	22	1
Ni	0.4	0.4	2.8	2.1	4.7	1.5	4.3	4.2	0.0
Cu	7	6	19	19	52	26	38	36	2
Zn	35	33	72	68	72	58	70	74	23
Ga	13	12	18	17	20	19	19	19	11
Rb	112.4	106.8	28.2	28.4	33.8	27.8	23.7	23.8	158.3
Sr	158	149	394	388	374	451	422	422	77
Y	22	20	35	33	41	35	32	37	20
Zr	115	109	195	180	188	140	125	125	85
Nb	8.31	7.71	8.49	8.21	8.15	6.04	5.25	5.21	7.62
Cs	6.90	6.76	1.63	1.27	2.27	0.99	0.75	0.95	9.87
Ba	484	456	270	260	214	194	173	176	582
La	22.4	20.6	18.1	17.4	18.1	13.7	12.9	16.2	26.1
Ce	42.5	39.0	40.9	39.7	41.6	31.9	29.2	29.8	48.2
Pr	4.94	4.49	5.83	5.55	6.07	4.68	4.32	5.20	5.28
Nd	18.2	16.5	25.2	24.1	27.6	21.6	20.0	24.2	18.2
Sm	3.45	3.15	5.68	5.43	6.48	5.20	4.84	5.67	3.17
Eu	0.75	0.69	1.51	1.48	1.86	1.54	1.44	1.68	0.52
Gd	3.27	2.95	5.75	5.54	6.79	5.70	5.25	6.19	2.74
Tb	0.53	0.49	0.92	0.90	1.08	0.91	0.83	0.98	0.46
Dy	3.25	2.97	5.44	5.33	6.52	5.50	4.96	5.83	2.80
Ho	0.69	0.63	1.16	1.13	1.36	1.17	1.05	1.22	0.61
Er	2.05	1.88	3.29	3.20	3.77	3.24	2.90	3.36	1.84
Tm	0.34	0.32	0.52	0.51	0.60	0.51	0.46	0.51	0.32
Yb	2.34	2.16	3.54	3.43	3.84	3.28	2.94	3.29	2.24
Lu	0.41	0.37	0.61	0.59	0.64	0.54	0.49	0.55	0.40
Hf	3.45	3.22	4.86	4.53	4.58	3.58	3.23	3.19	3.07
Ta	0.75	0.71	0.50	0.49	0.47	0.34	0.30	0.31	0.84
Pb (total)	16.4	15.4	7.7	6.0	7.0	6.3	4.7	6.8	21.1
Th	13.58	12.54	3.45	3.27	3.49	2.87	2.44	2.43	20.08
U	2.88	2.68	0.74	0.74	0.81	0.64	0.56	0.56	4.10

Table B.2. Major and trace element data of Salak volcanic rocks continued

Sample	S107B	S108	S109	S110A	S110B	S111	S112
SiO_2	76.76	57.50	56.58	59.97	60.57	53.66	60.38
Al_2O_3	12.32	17.49	17.60	15.83	15.94	19.61	16.90
Fe_2O_3	1.10	8.78	9.21	8.50	8.50	9.60	7.24
MgO	0.20	2.26	2.88	1.86	1.81	3.33	2.51
CaO	1.00	6.20	6.89	5.14	4.98	8.67	5.81
Na_2O	3.49	4.15	3.85	4.26	4.29	3.32	3.53
K_2O	3.98	1.56	1.34	2.07	2.11	0.80	1.84
TiO_2	0.13	1.15	1.18	1.16	1.17	0.98	0.76
MnO	0.04	0.21	0.20	0.19	0.16	0.18	0.15
P_2O_5	0.02	0.40	0.28	0.48	0.48	0.28	0.19
LOI	1.04	0.16	0.01	0.08	0.15	-0.08	0.73
Total	100.07	99.86	100.01	99.54	100.17	100.36	100.05
Sc	0	24	27	24	23	20	17
Ti	695	7618	7876	7750	7726	5568	5137
V	1	99	161	75	74	164	125
Cr	0.5	0.4	0.5	0.3	0.9	7.7	1.0
Mn	287	1928	1835	1750	1193	1495	1100
Co	1	14	17	13	10	21	15
Ni	0.0	0.8	1.1	1.1	0.9	8.1	2.0
Cu	2	38	35	54	41	18	23
Zn	24	87	73	81	76	70	59
Ga	12	19	19	19	19	19	17
Rb	168.1	52.3	44.4	68.8	74.1	22.4	70.3
Sr	81	354	358	292	291	395	287
Y	21	55	52	67	69	33	34
Zr	89	226	189	311	310	133	160
Nb	8.09	9.99	7.87	13.67	13.76	5.65	6.75
Cs	10.54	2.80	2.31	3.83	4.13	0.78	4.49
Ba	618	304	253	368	366	188	301
La	27.6	22.5	19.2	29.3	30.1	14.0	18.9
Ce	50.9	52.1	41.7	68.2	65.9	32.4	39.1
Pr	5.61	7.56	6.29	9.76	10.09	4.79	5.26
Nd	19.1	34.5	28.7	44.2	45.3	22.2	22.5
Sm	3.35	8.33	6.95	10.43	10.65	5.28	5.07
Eu	0.54	2.06	1.82	2.33	2.35	1.58	1.27
Gd	2.90	8.93	7.50	11.03	11.24	5.68	5.26
Tb	0.49	1.45	1.24	1.77	1.83	0.90	0.84
Dy	2.98	8.69	7.55	10.67	10.99	5.33	5.19
Ho	0.64	1.83	1.63	2.25	2.35	1.13	1.08
Er	1.94	5.06	4.56	6.27	6.42	3.09	3.12
Tm	0.34	0.79	0.71	0.97	1.02	0.48	0.49
Yb	2.36	5.08	4.57	6.31	6.54	3.07	3.23
Lu	0.42	0.85	0.77	1.07	1.08	0.52	0.54
Hf	3.27	5.82	4.87	7.94	7.93	3.41	4.30
Ta	0.90	0.60	0.47	0.81	0.87	0.33	0.51
Pb (total)	22.7	13.8	9.2	16.1	22.6	5.3	12.4
Th	21.39	5.94	4.66	7.88	7.90	2.51	8.10
U	4.34	1.32	1.02	1.72	1.74	0.58	1.70

Table B.3. Trace element data of IVC volcanic rocks

Sample	KI 11	KI 18	KI 26A	KI 26B	KI 28	KI 29B	KI 29D	KI 31D	KI 34	KI 35	KI 36	KI 39
Sc	32	20	19	19	16	21	18	23	21	15	21	22
Ti	6384	5694	5694	5005	4094	5754	4424	5796	6258	4274	5496	6294
V	381	222	217	217	171	234	182	287	197	127	201	207
Cr	4.5	0.2	0.0	0.3	6.6	1.0	7.0	3.7	2.3	4.3	3.4	2.0
Mn	1510	1936	2014	1851	1115	1781	1193	1262	1456	999	1417	1626
Co	46	35	32	37	30	40	29	79	34	33	61	49
Ni	23.3	4.5	4.8	4.0	8.0	6.8	8.0	11.9	7.2	5.3	14.0	8.2
Cu	198	113	125	123	45	136	53	105	75	25	64	71
Zn	86	75	77	73	62	74	63	81	87	60	76	88
Ga	19	18	18	18	16	19	16	19	20	18	18	19
Rb	31.9	27.2	27.0	25.0	60.7	18.7	63.8	22.0	75.7	103.6	59.9	66.3
Sr	500	640	654	626	346	670	346	562	474	391	473	506
Y	23	23	23	21	23	21	25	23	32	27	29	31
Zr	82	72	73	69	158	61	167	74	177	223	144	157
Nb	3.83	4.08	4.11	3.86	7.39	3.54	7.75	4.23	8.34	9.75	7.01	7.53
Cs	1.21	1.10	1.10	0.98	2.71	0.59	2.75	0.70	3.12	4.44	2.26	2.69
Ba	419	439	459	407	498	381	578	382	639	727	449	618
La	12.1	14.4	14.9	13.7	17.5	12.2	18.8	15.4	22.2	23.5	19.9	21.2
Ce	25.3	28.9	29.9	28.3	36.4	25.2	37.8	33.1	45.5	46.3	41.2	43.8
Pr	3.55	3.89	3.98	3.75	4.54	3.39	4.92	4.52	6.10	5.81	5.60	5.89
Nd	15.8	17.1	17.6	16.4	18.4	15.3	19.9	19.7	26.1	23.0	23.9	25.4
Sm	3.86	4.06	4.18	3.81	4.00	3.60	4.32	4.41	5.81	4.79	5.35	5.69
Eu	1.19	1.34	1.37	1.26	1.01	1.26	1.09	1.37	1.50	1.11	1.40	1.52
Gd	4.23	4.21	4.30	3.98	3.95	3.86	4.24	4.52	5.95	4.64	5.37	5.84
Tb	0.66	0.64	0.66	0.61	0.62	0.59	0.68	0.68	0.91	0.72	0.83	0.89
Dy	3.85	3.77	3.87	3.60	3.71	3.46	4.02	3.93	5.24	4.22	4.83	5.20
Ho	0.79	0.79	0.81	0.74	0.76	0.72	0.84	0.80	1.07	0.88	0.99	1.08
Er	2.10	2.12	2.20	1.99	2.15	1.96	2.35	2.10	2.96	2.46	2.70	2.97
Tm	0.35	0.35	0.35	0.34	0.37	0.31	0.40	0.35	0.51	0.43	0.45	0.49
Yb	2.06	2.11	2.16	1.98	2.31	1.92	2.46	2.02	3.05	2.74	2.70	2.96
Lu	0.33	0.35	0.37	0.33	0.38	0.32	0.41	0.33	0.50	0.45	0.44	0.48
Hf	2.25	1.98	2.06	1.92	4.15	1.71	4.31	2.06	4.61	5.87	3.71	4.05
Ta	0.33	0.37	0.40	0.43	0.68	0.39	0.70	0.39	0.71	0.91	0.73	0.81
Pb (total)	5.7	6.0	6.9	6.3	10.3	5.0	10.7	5.7	11.2	17.1	9.3	10.2
Th	3.09	3.10	3.17	2.83	6.54	2.39	6.98	2.73	7.81	11.47	6.18	6.93
U	0.86	0.72	0.78	0.71	1.69	0.55	1.77	0.66	2.01	2.79	1.63	1.83

Sample	KI 52	KI 57	KI 63	KI 69	KI 75	KI 79	KI 85	KI 89	KI 90	KI 92	KI 105	KI 106
Sc	37	26	34	38	20	37	24	21	22	22	29	27
Ti	7079	6342	6617	7768	5844	8260	6911	6114	6474	6485	6174	5736
V	333	226	314	418	187	462	176	199	162	210	281	285
Cr	8.6	1.9	18.5	59.4	0.2	0.0	1.1	1.8	0.2	1.8	7.6	9.4
Mn	1983	1456	1650	1572	1998	2192	2378	1704	2246	1541	1471	1572
Co	46	35	51	55	43	58	51	33	54	37	46	78
Ni	17.3	9.8	28.4	37.8	4.1	8.3	10.7	6.8	2.5	8.0	17.4	39.8
Cu	90	99	147	175	63	233	43	75	33	79	133	97
Zn	97	94	93	85	93	111	115	85	109	90	85	79
Ga	22	21	21	19	21	20	21	19	19	20	20	19
Rb	33.0	43.3	25.4	38.5	33.0	27.4	43.1	69.9	42.6	66.5	30.3	16.1
Sr	487	586	543	491	649	517	484	492	469	504	558	555
Y	25	27	22	25	25	30	35	32	34	31	24	26
Zr	107	138	78	93	97	85	125	167	123	157	92	92
Nb	5.70	6.22	3.76	4.15	4.74	4.73	7.04	7.89	7.00	7.39	4.43	4.60
Cs	0.86	1.60	0.99	1.23	1.07	0.38	1.83	2.87	1.75	2.66	1.23	0.62
Ba	378	507	365	422	436	492	646	635	673	594	403	368
La	15.7	19.5	13.6	13.6	17.3	14.7	18.7	21.8	19.2	20.4	16.3	16.0
Ce	32.5	40.0	28.0	28.4	36.0	28.6	37.8	44.7	38.8	42.4	32.7	33.8
Pr	4.43	5.45	3.84	3.96	4.98	4.01	5.23	5.99	5.20	5.78	4.41	4.75
Nd	19.1	23.0	16.9	17.4	21.9	18.0	22.8	25.5	23.1	24.9	19.1	20.8
Sm	4.47	5.15	3.94	4.29	4.89	4.44	5.50	5.74	5.53	5.58	4.33	4.73
Eu	1.37	1.51	1.27	1.30	1.51	1.47	1.77	1.49	1.73	1.53	1.33	1.37
Gd	4.69	5.16	4.04	4.47	4.86	4.97	6.01	5.80	5.96	5.80	4.37	4.76
Tb	0.72	0.77	0.63	0.71	0.73	0.81	0.96	0.88	0.94	0.88	0.68	0.71
Dy	4.19	4.42	3.66	4.12	4.19	4.75	5.68	5.14	5.60	5.08	3.85	4.14
Ho	0.87	0.90	0.75	0.85	0.86	0.99	1.18	1.07	1.17	1.05	0.80	0.85
Er	2.34	2.44	2.00	2.24	2.29	2.67	3.25	2.94	3.22	2.87	2.14	2.32
Tm	0.39	0.41	0.34	0.36	0.39	0.44	0.55	0.49	0.55	0.49	0.36	0.38
Yb	2.34	2.44	2.02	2.17	2.29	2.66	3.27	2.99	3.28	2.88	2.14	2.24
Lu	0.39	0.41	0.34	0.35	0.39	0.44	0.54	0.50	0.55	0.48	0.36	0.37
Hf	2.79	3.61	2.11	2.49	2.64	2.36	3.43	4.31	3.41	4.09	2.47	2.44
Ta	0.44	0.51	0.34	0.43	0.55	0.34	0.73	0.64	0.77	0.63	0.38	0.32
Pb (total)	7.2	9.0	6.7	6.1	7.6	6.3	10.1	10.6	10.2	9.8	6.9	5.9
Th	3.90	4.85	2.90	3.68	3.50	3.38	4.50	7.41	4.59	6.68	3.65	2.96
U	0.90	1.12	0.65	1.07	0.78	0.63	1.11	1.91	1.14	1.77	0.83	0.69

Table B.3. Trace element data of IVC volcanic rocks

Sample	KI 108	KI 114	KI 116	KI 136	KI 137	KI 139	KI 140	KI 142	KI 143	KI 145	KI 162	KI 164
Sc	31	12	27	10	18	20	21	22	34	34	18	11
Ti	8134	4585	5496	3830	6114	5934	6054	6174	7373	6689	4975	3219
V	333	95	264	89	199	192	197	204	389	397	172	85
Cr	0.9	0.4	12.2	1.4	1.1	2.2	1.7	1.1	4.1	4.7	3.3	0.8
Mn	1990	1177	1402	1069	1781	1394	1549	1704	1859	1580	1340	1177
Co	207	31	48	24	35	48	40	41	47	52	29	27
Ni	10.8	2.6	22.2	2.7	7.1	7.5	8.4	6.3	24.4	24.9	7.9	3.1
Cu	181	42	68	24	34	70	66	74	192	194	49	35
Zn	101	73	79	89	106	82	87	86	111	85	79	75
Ga	21	20	19	19	20	18	19	19	20	20	19	18
Rb	57.7	45.1	25.9	60.3	28.4	62.1	69.5	66.7	33.9	31.8	69.2	25.0
Sr	487	575	513	485	501	466	490	499	507	497	455	628
Y	31	28	21	39	30	30	32	31	24	23	27	23
Zr	136	146	92	166	135	149	166	159	88	84	176	97
Nb	6.37	8.38	4.25	9.17	9.43	7.13	7.82	7.59	4.09	3.94	7.96	4.26
Cs	2.22	1.52	0.65	1.35	0.76	2.56	2.86	2.70	1.24	1.21	2.39	0.77
Ba	545	568	365	601	446	585	622	621	446	433	659	438
La	18.2	20.3	14.4	25.2	19.6	20.2	21.4	21.3	12.7	12.4	19.8	15.4
Ce	37.8	40.7	30.5	45.9	40.3	41.6	44.0	43.8	26.8	26.0	39.7	29.9
Pr	5.15	5.42	4.15	6.89	5.41	5.59	5.88	5.85	3.70	3.65	5.18	4.32
Nd	22.3	22.7	17.8	29.5	23.5	24.0	25.2	25.0	16.6	16.5	21.5	18.8
Sm	5.24	4.94	3.95	6.37	5.28	5.49	5.61	5.73	4.12	3.99	4.57	4.06
Eu	1.50	1.54	1.21	1.73	1.63	1.44	1.48	1.51	1.29	1.22	1.24	1.28
Gd	5.48	4.90	3.98	6.54	5.52	5.50	5.72	5.72	4.47	4.35	4.63	4.17
Tb	0.85	0.76	0.62	0.98	0.85	0.84	0.87	0.88	0.70	0.67	0.74	0.63
Dy	4.99	4.43	3.53	5.72	4.98	4.88	5.09	5.14	4.05	3.92	4.26	3.67
Ho	1.02	0.92	0.72	1.21	1.04	1.01	1.06	1.06	0.83	0.80	0.89	0.77
Er	2.72	2.47	1.98	3.35	2.84	2.80	2.91	2.92	2.26	2.16	2.49	2.09
Tm	0.46	0.43	0.32	0.58	0.48	0.45	0.49	0.47	0.37	0.35	0.43	0.36
Yb	2.76	2.61	1.96	3.53	2.84	2.73	2.93	2.92	2.18	2.08	2.60	2.15
Lu	0.46	0.43	0.33	0.61	0.47	0.46	0.48	0.48	0.36	0.34	0.45	0.36
Hf	3.53	3.67	2.43	4.24	3.43	3.86	4.29	4.12	2.42	2.26	4.56	2.52
Ta	0.85	0.74	0.37	0.67	0.74	0.71	0.75	0.69	0.43	0.40	0.69	0.37
Pb (total)	8.5	8.3	6.7	10.0	6.3	9.6	10.5	9.8	6.3	5.5	10.8	7.3
Th	5.64	4.87	3.08	6.00	4.25	6.57	7.31	7.02	3.42	3.17	7.22	2.47
U	1.52	1.15	0.73	1.45	1.00	1.72	1.90	1.83	0.91	0.89	1.80	0.64

Sample	KI 165	KI 176	KI 178	KI 182	KI 190	KI 194	KI 202
Sc	18	27	25	11	28	21	17
Ti	5395	5359	8014	3291	6533	5257	4484
V	198	279	241	95	306	197	179
Cr	0.1	18.2	1.3	4.3	4.9	5.8	2.6
Mn	1471	1417	2416	1092	1518	1293	1177
Co	42	33	36	32	49	33	37
Ni	6.9	14.6	4.3	3.8	12.5	6.9	4.7
Cu	88	74	52	24	107	21	38
Zn	72	74	98	62	86	72	62
Ga	20	18	19	17	22	18	17
Rb	32.9	17.8	19.4	61.9	26.9	67.4	62.8
Sr	600	567	612	547	549	440	342
Y	23	20	28	20	22	28	26
Zr	100	60	81	131	81	170	168
Nb	4.44	3.03	4.11	6.78	3.90	8.13	7.90
Cs	1.28	0.58	0.26	1.50	0.56	2.84	2.88
Ba	554	265	466	635	339	614	484
La	15.3	11.6	17.0	25.7	12.6	20.6	19.4
Ce	31.1	24.2	34.3	45.2	26.4	41.8	39.9
Pr	4.19	3.42	4.93	6.14	3.69	5.50	5.20
Nd	18.0	15.1	22.0	23.8	16.4	22.7	21.2
Sm	4.12	3.54	5.20	4.49	3.86	4.97	4.57
Eu	1.30	1.18	1.66	1.26	1.25	1.29	1.14
Gd	4.19	3.80	5.33	4.00	4.00	5.02	4.44
Tb	0.65	0.57	0.80	0.58	0.63	0.76	0.70
Dy	3.77	3.36	4.67	3.28	3.68	4.51	4.12
Ho	0.77	0.70	0.95	0.66	0.74	0.95	0.86
Er	2.12	1.88	2.51	1.77	2.03	2.61	2.42
Tm	0.34	0.31	0.41	0.31	0.34	0.46	0.42
Yb	2.12	1.90	2.46	1.90	2.08	2.73	2.55
Lu	0.36	0.31	0.40	0.32	0.34	0.47	0.42
Hf	2.64	1.66	2.29	3.33	2.18	4.44	4.41
Ta	0.37	0.25	0.28	0.67	0.38	0.65	0.77
Pb (total)	7.5	3.3	5.6	11.4	5.5	9.8	10.4
Th	3.77	2.02	3.41	6.19	3.01	7.44	7.33
U	0.93	0.46	0.55	1.67	0.71	1.79	1.78

Table C.1. Whole rock Sr-Nd-Hf isotope data for GVC, Salak and IVC volcanic rocks

Sample	$^{87}Sr/^{86}Sr_m$	2SE	$^{143}Nd/^{144}Nd_m$	2SE	$^{176}Hf/^{177}Hf_m$	2SE	Sample	$^{87}Sr/^{86}Sr_m$	2SE	$^{143}Nd/^{144}Nd_m$	2SE	$^{176}Hf/^{177}Hf_m$	2SE
G01A	0.705325[b]	0.000009	0.512649[b]	0.000013	0.282971[f]	0.000020	KI 11			0.512848[a]	0.000005	0.283103[a]	0.000008
G01B	0.705288[c]	0.000009	0.512647[e]	0.000006	0.282934[d]	0.000007	KI 26B	0.704353[d]	0.000011	0.512827[a]	0.000007	0.283128[a]	0.000007
G10	0.705004[b]	0.000010	0.512702[b]	0.000013	0.282960[b]	0.000006	KI 28	0.704304[d]	0.000009	0.512857[f]	0.000006	0.283097[f]	0.000004
G16	0.705540[a]	0.000012	0.512634[c]	0.000012	0.282938[c]	0.000010	KI 29B	0.704382[b]	0.000008	0.512825[b]	0.000010	0.283118[b]	0.000007
G17	0.704990[b]	0.000009	0.512683[b]	0.000014	0.282970[f]	0.000005	KI 31D	0.704310[d]	0.000009	0.512803[a]	0.000004	0.283104[a]	0.000008
G18	0.705143[b]	0.000009	0.512662[b]	0.000014	0.282957[f]	0.000004	KI 34	0.704257[b]	0.000010	0.512837[b]	0.000008	0.283078[b]	0.000005
G19	0.704980[c]	0.000013	0.512695[e]	0.000007	0.282971[d]	0.000005	KI 35	0.704317[b]	0.000009	0.512835[b]	0.000010	0.283095[b]	0.000005
G20	0.705088[b]	0.000011	0.512677[b]	0.000011	0.282969[f]	0.000005	KI 36	0.704227[d]	0.000010	0.512843[a]	0.000006	0.283101[a]	0.000006
G21	0.705118[b]	0.000008	0.512680[b]	0.000020	0.282958[c]	0.000006	KI 39	0.704221[d]	0.000008	0.512854[f]	0.000006	0.283105[f]	0.000005
G22	0.705140[b]	0.000011	0.512666[b]	0.000012	0.282954[c]	0.000006	KI 63	0.704286[d]	0.000009	0.512855[f]	0.000006	0.283101[f]	0.000006
G23	0.705268[c]	0.000011	0.512650[e]	0.000009	0.282940[d]	0.000006	KI 69	0.704219[d]	0.000006	0.512859[a]	0.000005	0.283102[a]	0.000010
G25	0.705117[a]	0.000010	0.512682[c]	0.000015	0.282961[c]	0.000008	KI 79	0.704252[d]	0.000009	0.512890[f]	0.000006	0.283113[f]	0.000005
G26	0.704882[b]	0.000011	0.512696[b]	0.000014	0.282983[c]	0.000006	KI 85	0.704275[d]	0.000008	0.512875[f]	0.000007	0.283114[f]	0.000004
G28	0.705056[c]	0.000011	0.512677[e]	0.000006	0.282957[d]	0.000014	KI 106			0.512821[a]	0.000004	0.283097[a]	0.000008
G30	0.705393[c]	0.000013	0.512640[e]	0.000008	0.282939[d]	0.000007	KI 108			0.512839[a]	0.000005	0.283121[a]	0.000006
G33	0.704997[a]	0.000008	0.512704[c]	0.000009	0.282976[c]	0.000009	KI 114	0.704257[d]	0.000013	0.512891[f]	0.000011	0.283075[f]	0.000006
G35	0.705358[c]	0.000009	0.512640[e]	0.000008	0.282922[d]	0.000007	KI 116	0.704316[d]	0.000012	0.512808[a]	0.000005	0.283101[a]	0.000007
G36A	0.705318[a]	0.000012	0.512659[c]	0.000010	0.282941[c]	0.000011	KI 136	0.704272[b]	0.000008	0.512850[b]	0.000010	0.283079[b]	0.000005
G40	0.705070[a]	0.000010	0.512684[c]	0.000010	0.282958[c]	0.000007	KI 137	0.704292[b]	0.000008	0.512842[b]	0.000008	0.283063[b]	0.000006
G42	0.705207[b]	0.000009	0.512662[b]	0.000012	0.282953[c]	0.000007	KI 142	0.704231[d]	0.000009	0.512879[f]	0.000009	0.283099[f]	0.000007
G44	0.705001[a]	0.000009	0.512693[d]	0.000013	0.282980[c]	0.000011	KI 145			0.512847[a]	0.000005	0.283108[a]	0.000008
G46	0.705201[a]	0.000012	0.512673[d]	0.000012	0.282968[c]	0.000014	KI 176	0.704231[b]	0.000010	0.512839[b]	0.000014	0.283064[b]	0.000060
G49	0.704735[a]	0.000008	0.512713[d]	0.000009	0.283044[c]	0.000009	KI 178	0.704518[b]	0.000009	0.512785[b]	0.000009	0.283109[b]	0.000006
G51	0.705294[c]	0.000012	0.512650[e]	0.000006	0.282934[d]	0.000006	KI 182	0.704188[d]	0.000006	0.512893[f]	0.000010	0.283097[f]	0.000016
G52	0.704508[c]	0.000009	0.512731[e]	0.000007	0.283050[d]	0.000005	KI 190	0.704366[b]	0.000008	0.512825[b]	0.000013	0.283094[a]	0.000010
G55	0.705057[b]	0.000009	0.512689[b]	0.000019	0.282964[c]	0.000005	KI 194	0.704361[b]	0.000010	0.512824[b]	0.000010	0.283092[b]	0.000006
							KI 202			0.512839[a]	0.000007	0.283104[a]	0.000005
S100	0.704799[a]	0.000014	0.512714[d]	0.000011	0.283029[c]	0.000010							
S102	0.704270[c]	0.000010	0.512809[e]	0.000006	0.283089[d]	0.000005							
S103	0.704289[a]	0.000010	0.512802[d]	0.000009	0.283087[c]	0.000004							
S106A	0.704671[a]	0.000009	0.512735[d]	0.000007	0.283055[c]	0.000009							
S106B	0.704639[c]	0.000009	0.512738[e]	0.000006	0.283040[d]	0.000006							
S107B	0.704841[a]	0.000018	0.512713[d]	0.000010	0.283010[c]	0.000009							
S109	0.704745[c]	0.000009	0.512741[e]	0.000006	0.283050[d]	0.000006							
S110A	0.704778[a]	0.000010	0.512723[d]	0.000008	0.283041[c]	0.000006							
S111	0.704596[a]	0.000010	0.512746[d]	0.000009	0.283046[c]	0.000028							
S112	0.705070[a]	0.000013	0.512697[d]	0.000012	0.283008[c]	0.000006							

Superscript font refers to the respective analytical session for which standard data is presented in Table E.8, Appendix E
m = measured, 2SE = 2 x standard internal error
G# = GVC samples, S# = Salak samples, KI# = IVC samples

Table C.2. Whole rock Sr-Nd-Hf isotope data for Merapi and Guntur volcanic rocks

Sample	$^{176}Hf/^{177}Hf_m$	2SE	Sample	$^{176}Hf/^{177}Hf_m$	2SE
M95-26	0.283132[c]	0.000009	M98-031	0.283124[d]	0.000005
M95-028	0.283129[e]	0.000013	M98-047	0.283127[d]	0.000011
M96-50	0.283143[d]	0.000007	M98-0532	0.283143[d]	0.000012
M96-056	0.283125[f]	0.000007	M98-096	0.283130[e]	0.000009
M96-073	0.283140[d]	0.000015	M98-107	0.283127[d]	0.000009
M96-137	0.283134[c]	0.000011	GU 1	0.283151[f]	0.000007
M96-142	0.283114[c]	0.000011	GU 5	0.283141[f]	0.000001
M96-175	0.283168[e]	0.000016	GU 7	0.283128[f]	0.000006
M97-021	0.283124[c]	0.000009	GU 9	0.283136[f]	0.000011
M97-0392	0.283120[e]	0.000010	GU 15	0.283132[f]	0.000005
M97-068	0.283111[e]	0.000011	GU 16	0.283136[f]	0.000006

Superscript font refers to the respective analytical session for which standard data is presented in Table E.8, Appendix E.
m = measured, 2SE = 2 x standard internal error
M# = Merapi samples, GU# = Guntur samples

Table C.3. Oxygen isotope data ($\delta^{18}O$) for GVC, Salak and IVC mineral separates of volcanic rocks

	CPX	OL	PLAG
G01A	5.69	5.39	
G16	5.91		
G17	5.60		
G25	5.72		
G26	5.63		6.07
G30	5.78	5.42	
G35	5.76	5.32	
G33	5.68		
G40	5.55		
G42	5.52		
G44	5.81		
G46	5.94		
KI 31D	5.46		
KI 34	5.51		
KI 35	5.49		
KI 36	5.58		6.08
KI 63	5.38	5.02	
S100			6.03
S103	5.18		5.97
S106A	5.37		
S111			5.96
S112	5.44		6.07

G# = GVC rocks, KI# = IVC rocks, S# = Salak rocks
CPX, clinopyroxene; OL, olivine; PLAG, plagioclase.

Table D.1. Plagioclase mineral data

Sample	G01B	G01B	G01B	G01B	G01B	G01B	G01B	G01B	G11	G11	G11	G11	G11
Grain	P1	P1	P1	GM	P2	P2	P2	P3	P1	P1	P2	P2	P3
Position	C	M	R		C	M	R		R	C	C	R	C
SiO_2	43.43	44.08	44.84	47.03	44.37	45.38	45.37	44.94	54.05	53.55	48.25	47.47	54.01
TiO_2	0.02	0.01	0.02	0.03	0.01	0.03	0.03	0.03	0.03	0.04	0.02	0.02	0.04
Al_2O_3	34.45	33.91	33.44	32.29	33.43	33.12	32.96	33.65	28.27	28.69	31.61	31.73	28.57
Cr_2O_3	0.02	0.01	0.01	0.01	0.00	0.00	0.00	0.01	0.01	0.00	0.00	0.00	0.00
MgO	0.04	0.04	0.06	0.08	0.05	0.06	0.06	0.04	0.05	0.06	0.10	0.06	0.05
CaO	19.48	19.36	18.51	17.03	18.67	18.25	18.20	18.67	12.35	12.59	16.74	16.65	12.39
MnO	0.00	0.00	0.00	0.00	0.01	0.02	0.00	0.01	0.00	0.00	0.00	0.00	0.01
FeO	0.48	0.42	0.57	0.80	0.52	0.54	0.60	0.71	0.52	0.56	0.73	0.65	0.50
NiO	0.00	0.02	0.00	0.00	0.00	0.00	0.00	0.01	0.01	0.00	0.00	0.01	0.01
Na_2O	0.73	0.87	1.36	2.12	1.24	1.43	1.49	1.21	4.66	4.29	2.06	2.33	4.42
K_2O	0.01	0.01	0.03	0.06	0.02	0.03	0.03	0.02	0.26	0.28	0.17	0.06	0.30
Total	98.65	98.72	98.83	99.44	98.34	98.85	98.74	99.28	100.21	100.06	99.67	98.97	100.28
Si	8.18	8.29	8.41	8.74	8.37	8.50	8.51	8.40	9.80	9.72	8.92	8.84	9.78
Al	7.65	7.52	7.40	7.07	7.43	7.31	7.29	7.41	6.04	6.14	6.88	6.96	6.09
Fe(ii)	0.08	0.07	0.09	0.12	0.08	0.08	0.09	0.11	0.08	0.08	0.11	0.10	0.08
Ca	3.93	3.90	3.72	3.39	3.78	3.66	3.66	3.74	2.40	2.45	3.31	3.32	2.40
Na	0.27	0.32	0.49	0.76	0.45	0.52	0.54	0.44	1.64	1.51	0.74	0.84	1.55
K	0.00	0.00	0.01	0.01	0.00	0.01	0.01	0.00	0.06	0.07	0.04	0.01	0.07
Mg	0.01	0.01	0.02	0.02	0.01	0.02	0.02	0.01	0.01	0.02	0.03	0.02	0.01
Total	20.12	20.11	20.13	20.11	20.14	20.10	20.12	20.11	20.03	19.99	20.03	20.10	19.98
An	93.57	92.44	88.17	81.35	89.17	87.46	86.94	89.40	58.56	60.84	80.94	79.51	59.69
Ab	6.37	7.51	11.68	18.33	10.73	12.38	12.89	10.49	39.99	37.55	18.06	20.17	38.57
Or	0.06	0.05	0.15	0.32	0.10	0.15	0.17	0.10	1.45	1.62	1.00	0.32	1.74

Sample	G11	G11	G11	G11	G17	G17	G17	G17	G17	G17	G17	G17	G17
Grain	P3	P4	P4	P4	P1	P1	P1	P1	GM	P2	P3	P3	P3
Position	R	C	M	R	C	M2	M3	R			C	M1	M2
SiO_2	52.51	53.68	53.04	54.80	52.22	52.31	49.46	53.00	54.26	49.71	51.30	51.30	50.96
TiO_2	0.03	0.03	0.05	0.03	0.03	0.04	0.02	0.04	0.04	0.03	0.03	0.04	0.04
Al_2O_3	29.09	28.40	28.44	27.31	29.04	28.66	30.62	28.26	27.29	29.99	29.18	29.03	29.60
Cr_2O_3	0.01	0.00	0.00	0.01	0.00	0.00	0.00	0.00	0.00	0.00	0.00	0.01	0.01
MgO	0.06	0.05	0.06	0.07	0.05	0.06	0.04	0.05	0.07	0.06	0.04	0.04	0.06
CaO	12.96	12.51	12.74	11.43	13.01	12.59	15.01	12.15	10.95	14.37	13.44	13.51	13.91
MnO	0.00	0.02	0.00	0.00	0.02	0.03	0.01	0.00	0.00	0.02	0.00	0.00	0.04
FeO	0.59	0.60	0.59	0.62	0.39	0.60	0.49	0.59	0.53	0.44	0.56	0.52	0.67
NiO	0.00	0.01	0.00	0.01	0.02	0.00	0.01	0.01	0.00	0.02	0.00	0.00	0.00
Na_2O	4.14	4.44	4.30	4.97	4.33	4.60	3.29	4.83	5.57	3.70	4.10	4.20	3.98
K_2O	0.24	0.27	0.27	0.30	0.13	0.15	0.08	0.27	0.22	0.10	0.13	0.12	0.12
Total	99.63	100.01	99.50	99.55	99.24	99.01	99.06	99.21	98.92	98.42	98.78	98.75	99.37
Si	9.60	9.76	9.70	9.98	9.58	9.62	9.16	9.72	9.94	9.25	9.48	9.49	9.39
Al	6.27	6.08	6.13	5.86	6.28	6.21	6.68	6.11	5.89	6.58	6.35	6.33	6.42
Fe(ii)	0.09	0.09	0.09	0.09	0.06	0.09	0.08	0.09	0.08	0.07	0.09	0.08	0.10
Ca	2.54	2.44	2.50	2.23	2.56	2.48	2.98	2.39	2.15	2.86	2.66	2.68	2.74
Na	1.47	1.57	1.52	1.76	1.54	1.64	1.18	1.72	1.98	1.33	1.47	1.50	1.42
K	0.06	0.06	0.06	0.07	0.03	0.03	0.02	0.06	0.05	0.02	0.03	0.03	0.03
Mg	0.02	0.01	0.02	0.02	0.01	0.02	0.01	0.01	0.02	0.02	0.01	0.01	0.02
Total	20.03	20.01	20.02	20.00	20.06	20.10	20.10	20.11	20.12	20.13	20.09	20.11	20.12
An	62.48	59.92	61.16	54.99	61.95	59.70	71.25	57.26	51.45	67.85	63.91	63.58	65.45
Ab	36.14	38.52	37.31	43.30	37.32	39.48	28.29	41.22	47.33	31.61	35.33	35.75	33.90
Or	1.38	1.56	1.53	1.71	0.74	0.82	0.46	1.52	1.22	0.54	0.76	0.67	0.65

Sample	G17	G17	G17	G22	G22	G22	G22	G22	G22	G22	G22	G22	G22
Grain	P3	P3	GM	P1	P1	P1	P1	P1	P1	P2	P2	P2	P3
Position	M3	R		C	M1	M2	M3	M4	R	C	M	R	C
SiO_2	48.71	54.32	52.61	53.49	55.64	51.93	54.67	51.96	52.55	47.25	46.67	48.93	48.31
TiO_2	0.03	0.04	0.04	0.02	0.04	0.03	0.03	0.03	0.03	0.03	0.03	0.03	0.03
Al_2O_3	30.56	27.13	28.49	28.21	26.81	29.10	27.30	29.24	28.00	32.13	32.70	31.03	31.45
Cr_2O_3	0.00	0.00	0.00	0.00	0.00	0.01	0.00	0.01	0.02	0.00	0.01	0.01	0.00
MgO	0.05	0.06	0.06	0.04	0.04	0.03	0.05	0.06	0.07	0.03	0.04	0.06	0.04
CaO	15.49	11.21	12.29	11.84	10.30	13.23	11.02	13.28	12.10	16.74	17.29	15.74	15.97
MnO	0.00	0.02	0.02	0.00	0.00	0.00	0.00	0.00	0.00	0.02	0.00	0.00	0.01
FeO	0.59	0.58	0.59	0.46	0.45	0.45	0.44	0.48	0.56	0.53	0.47	0.65	0.48
NiO	0.00	0.00	0.00	0.02	0.01	0.00	0.00	0.00	0.00	0.01	0.00	0.01	0.00
Na_2O	2.98	5.41	4.73	4.87	5.69	4.30	5.50	4.23	4.81	2.30	1.94	2.87	2.69
K_2O	0.07	0.27	0.22	0.23	0.33	0.20	0.27	0.17	0.21	0.08	0.05	0.09	0.09
Total	98.48	99.02	99.05	99.18	99.30	99.28	99.28	99.47	98.35	99.12	99.21	99.42	99.06
Si	9.09	9.95	9.67	9.79	10.12	9.54	9.98	9.52	9.72	8.79	8.68	9.05	8.96
Al	6.72	5.86	6.17	6.08	5.75	6.30	5.87	6.32	6.11	7.04	7.17	6.76	6.88
Fe(ii)	0.09	0.09	0.09	0.07	0.07	0.07	0.07	0.07	0.09	0.08	0.07	0.10	0.07
Ca	3.09	2.20	2.42	2.32	2.01	2.60	2.15	2.61	2.40	3.34	3.45	3.12	3.18
Na	1.08	1.92	1.69	1.73	2.01	1.53	1.94	1.50	1.73	0.83	0.70	1.03	0.97
K	0.02	0.06	0.05	0.05	0.08	0.05	0.06	0.04	0.05	0.02	0.01	0.02	0.02
Mg	0.01	0.02	0.02	0.01	0.01	0.01	0.01	0.02	0.02	0.01	0.01	0.02	0.01
Total	20.10	20.10	20.11	20.06	20.04	20.10	20.09	20.08	20.11	20.11	20.09	20.09	20.09
An	73.89	52.57	58.20	56.58	49.09	62.24	51.78	62.83	57.47	79.68	82.89	74.80	76.28
Ab	25.71	45.93	40.55	42.11	49.05	36.65	46.71	36.23	41.36	19.85	16.84	24.68	23.22
Or	0.40	1.50	1.25	1.30	1.86	1.11	1.51	0.95	1.17	0.46	0.27	0.52	0.50

Grain: P, phenocryst; GM, groundmass. INC, inclusion (mineral included within is stated in parentheses)
Spot: C, core; M, mid point (number indicates relative position along transect from core to rim); R, rim
An, anorthite; Ab, albite; Or, orthoclase

Table D.1. Plagioclase mineral data continued

Sample	G22	G22	G22	G22	G23	G23	G23	G23	G23	G23	G23	G23	G24
Grain	P3	P3	P4	P4	P1	P2	P2	P2	INC (CPX)	P3	P4	P4	P1
Position	M	R	C	R		M1	M2	R		R	C-M	R	C
SiO_2	50.30	50.87	53.50	54.12	48.31	46.30	46.85	47.00	45.86	48.13	47.63	48.86	51.40
TiO_2	0.03	0.04	0.04	0.04	0.03	0.02	0.04	0.04	0.03	0.05	0.03	0.06	0.00
Al_2O_3	29.96	29.58	27.85	27.32	31.77	32.75	32.47	32.05	32.81	30.95	31.52	30.80	28.84
Cr_2O_3	0.00	0.01	0.00	0.00	0.00	0.00	0.00	0.01	0.00	0.01	0.00	0.00	0.00
MgO	0.06	0.07	0.07	0.06	0.08	0.07	0.07	0.08	0.04	0.10	0.07	0.25	0.08
CaO	14.24	13.84	11.93	11.41	16.41	17.52	17.29	16.89	18.00	16.00	16.49	15.60	13.08
MnO	0.04	0.01	0.03	0.00	0.00	0.00	0.00	0.00	0.02	0.00	0.00	0.02	0.00
FeO	0.47	0.61	0.58	0.50	0.65	0.60	0.66	0.66	0.76	0.73	0.58	0.82	0.59
NiO	0.00	0.00	0.00	0.00	0.00	0.00	0.00	0.00	0.00	0.00	0.00	0.00	0.00
Na_2O	3.64	3.85	4.90	5.24	2.56	1.89	2.12	2.16	1.62	2.78	2.47	2.81	4.22
K_2O	0.13	0.16	0.24	0.24	0.05	0.04	0.04	0.04	0.02	0.07	0.06	0.17	0.18
Total	98.86	99.03	99.13	98.94	99.87	99.19	99.53	98.93	99.15	98.81	98.85	99.38	98.38
Si	9.31	9.39	9.81	9.92	8.91	8.63	8.70	8.77	8.57	8.97	8.88	9.05	9.53
Al	6.53	6.44	6.02	5.90	6.90	7.19	7.10	7.04	7.22	6.80	6.92	6.72	6.30
Fe(ii)	0.07	0.09	0.09	0.08	0.10	0.09	0.10	0.10	0.12	0.11	0.09	0.13	0.09
Ca	2.82	2.74	2.34	2.24	3.24	3.50	3.44	3.37	3.60	3.20	3.29	3.10	2.60
Na	1.31	1.38	1.74	1.86	0.92	0.68	0.76	0.78	0.58	1.01	0.89	1.01	1.52
K	0.03	0.04	0.05	0.06	0.01	0.01	0.01	0.01	0.00	0.02	0.01	0.04	0.04
Mg	0.02	0.02	0.02	0.02	0.02	0.02	0.02	0.02	0.01	0.03	0.02	0.07	0.02
Total	20.09	20.09	20.07	20.08	20.10	20.12	20.13	20.10	20.11	20.13	20.11	20.11	20.10
An	67.86	65.91	56.63	53.90	77.74	83.50	81.67	80.97	85.93	75.78	78.42	74.66	62.51
Ab	31.43	33.19	42.04	44.74	21.95	16.30	18.11	18.78	13.96	23.85	21.27	24.36	36.46
Or	0.71	0.90	1.33	1.37	0.30	0.20	0.22	0.25	0.11	0.37	0.31	0.98	1.03

Sample	G24	G24	G24	G24	G24	G24	G26	G26	G26	G26	G26	G26	G26
Grain	P1	GM	P2	P2	P3	P3	P1	P1	P2	P2	P2	P2	P3
Position	R		C	R	C	R	C	R	C	M	M2	R	R
SiO_2	48.48	52.77	50.69	49.78	49.05	51.66	48.73	50.93	47.08	44.49	46.45	45.92	47.26
TiO_2	0.01	0.07	0.05	0.03	0.00	0.04	0.03	0.05	0.03	0.02	0.02	0.03	0.03
Al_2O_3	30.43	28.33	28.97	30.13	29.80	28.65	30.76	29.27	31.59	33.53	32.10	32.25	31.94
Cr_2O_3	0.00	0.01	0.00	0.00	0.01	0.01	0.00	0.01	0.00	0.00	0.00	0.00	0.00
MgO	0.06	0.06	0.09	0.08	0.07	0.08	0.06	0.05	0.08	0.05	0.07	0.03	0.05
CaO	14.92	12.33	13.31	14.74	14.72	12.76	15.20	13.77	16.77	18.89	17.34	17.77	16.68
MnO	0.00	0.00	0.00	0.01	0.00	0.00	0.00	0.01	0.00	0.00	0.00	0.00	0.00
FeO	0.72	0.94	0.61	0.66	0.62	0.69	0.72	0.95	0.58	0.43	0.60	0.73	0.68
NiO	0.01	0.00	0.00	0.00	0.01	0.02	0.01	0.00	0.00	0.01	0.00	0.00	0.01
Na_2O	3.26	4.70	4.06	3.29	3.44	4.36	3.18	3.87	2.39	1.09	2.01	1.71	2.25
K_2O	0.11	0.24	0.15	0.09	0.10	0.18	0.10	0.16	0.03	0.01	0.04	0.04	0.07
Total	98.01	99.44	97.92	98.81	97.81	98.44	98.77	99.07	98.55	98.52	98.63	98.48	98.97
Si	9.09	9.68	9.45	9.23	9.20	9.57	9.07	9.41	8.81	8.37	8.70	8.63	8.81
Al	6.72	6.12	6.37	6.59	6.59	6.26	6.75	6.38	6.97	7.44	7.09	7.14	7.01
Fe(ii)	0.11	0.14	0.09	0.10	0.10	0.11	0.11	0.15	0.09	0.07	0.09	0.12	0.11
Ca	3.00	2.42	2.66	2.93	2.96	2.53	3.03	2.73	3.36	3.81	3.48	3.58	3.33
Na	1.18	1.67	1.47	1.18	1.25	1.57	1.15	1.39	0.87	0.40	0.73	0.62	0.81
K	0.03	0.06	0.03	0.02	0.02	0.04	0.02	0.04	0.01	0.00	0.01	0.01	0.02
Mg	0.02	0.02	0.02	0.02	0.02	0.02	0.02	0.01	0.02	0.01	0.02	0.01	0.01
Total	20.15	20.11	20.11	20.07	20.14	20.10	20.14	20.10	20.13	20.10	20.12	20.11	20.10
An	71.22	58.38	63.88	70.90	69.88	61.16	72.14	65.66	79.33	90.48	82.45	84.99	80.06
Ab	28.13	40.26	35.28	28.60	29.58	37.83	27.31	33.42	20.49	9.46	17.31	14.80	19.54
Or	0.65	1.36	0.83	0.50	0.54	1.00	0.54	0.91	0.18	0.07	0.24	0.21	0.40

Sample	G26	G26	G26	G26	G27	G27	G27	G27	G27	G27	G27	G27	G30
Grain	P5	P5	P5	GM	P1	GM	P2	P2	P3	P3	GM	P4	INC (CPX)
Position	C	M	R		R		C	R	R	C		R	
SiO_2	47.98	46.57	50.16	52.52	49.84	50.64	51.63	51.89	49.72	46.82	52.80	52.32	47.16
TiO_2	0.03	0.02	0.05	0.05	0.05	0.06	0.04	0.04	0.04	0.00	0.03	0.06	0.04
Al_2O_3	31.35	32.31	29.74	28.77	29.92	28.92	28.34	29.35	30.58	31.65	28.09	27.75	32.31
Cr_2O_3	0.00	0.01	0.00	0.00	0.01	0.01	0.01	0.03	0.01	0.00	0.00	0.01	0.00
MgO	0.07	0.07	0.06	0.06	0.07	0.10	0.06	0.10	0.06	0.05	0.10	0.10	0.05
CaO	16.38	17.46	14.38	12.82	14.12	13.21	12.72	13.54	15.10	16.66	12.58	12.33	17.00
MnO	0.00	0.05	0.00	0.00	0.01	0.01	0.01	0.01	0.00	0.00	0.01	0.00	0.00
FeO	0.62	0.48	0.59	0.86	0.63	0.78	0.41	0.66	0.59	0.52	0.74	0.77	0.59
NiO	0.00	0.00	0.00	0.00	0.00	0.00	0.01	0.02	0.00	0.00	0.00	0.01	0.01
Na_2O	2.61	1.91	3.59	4.54	3.57	4.10	4.50	3.87	3.06	2.12	4.49	4.63	2.07
K_2O	0.09	0.04	0.12	0.22	0.10	0.13	0.13	0.10	0.09	0.04	0.15	0.18	0.09
Total	99.14	98.91	98.70	99.85	98.33	97.96	97.86	99.60	99.24	97.88	98.98	98.15	99.32
Si	8.92	8.70	9.31	9.60	9.28	9.45	9.61	9.50	9.18	8.81	9.71	9.71	8.76
Al	6.87	7.11	6.50	6.20	6.56	6.36	6.22	6.34	6.65	7.02	6.09	6.07	7.07
Fe(ii)	0.10	0.07	0.09	0.13	0.10	0.12	0.06	0.10	0.09	0.08	0.11	0.12	0.09
Ca	3.26	3.49	2.86	2.51	2.82	2.64	2.54	2.66	2.99	3.36	2.48	2.45	3.38
Na	0.94	0.69	1.29	1.61	1.29	1.48	1.62	1.38	1.09	0.77	1.60	1.67	0.75
K	0.02	0.01	0.03	0.05	0.02	0.03	0.03	0.02	0.02	0.01	0.03	0.04	0.02
Mg	0.02	0.02	0.02	0.02	0.02	0.03	0.02	0.03	0.02	0.01	0.03	0.03	0.01
Total	20.12	20.10	20.10	20.12	20.09	20.12	20.10	20.02	20.04	20.07	20.06	20.09	20.08
An	77.24	83.28	68.38	60.22	68.24	63.59	60.53	65.48	72.82	81.06	60.27	58.95	81.52
Ab	22.25	16.48	30.92	38.55	31.21	35.68	38.73	33.92	26.68	18.70	38.90	40.06	17.98
Or	0.51	0.24	0.70	1.23	0.55	0.73	0.74	0.60	0.50	0.24	0.84	1.00	0.50

Grain: P, phenocryst; GM, groundmass. INC, inclusion (mineral included within is stated in parentheses)
Spot: C, core; M, mid point (number indicates relative position along transect from core to rim); R, rim
An, anorthite; Ab, albite; Or, orthoclase

Table D.1. Plagioclase mineral data continued

Sample	G30	G30	G30	G30	G30	G30	G30	G30	G30	G30	G35	G35	G35
Grain	GM	GM	P1	P1	P1	P2	P2	P3	P3	P3	P1	P1	P2
Position	C	R	C	M	R	C	R	C	M	R	M	R	R
SiO_2	47.53	52.06	48.48	46.27	49.11	48.38	50.36	45.01	47.13	49.77	47.85	47.07	51.47
TiO_2	0.04	0.07	0.04	0.04	0.04	0.04	0.06	0.03	0.03	0.06	0.03	0.04	0.08
Al_2O_3	31.63	28.50	31.45	32.31	30.21	31.15	28.98	33.02	32.04	29.87	31.59	32.21	28.76
Cr_2O_3	0.00	0.01	0.01	0.00	0.01	0.00	0.02	0.00	0.01	0.00	0.00	0.01	0.01
MgO	0.08	0.08	0.07	0.07	0.10	0.08	0.08	0.05	0.08	0.10	0.09	0.07	0.09
CaO	16.59	12.86	16.00	16.53	14.83	15.88	13.71	17.96	16.84	14.61	16.28	17.24	13.15
MnO	0.00	0.01	0.03	0.02	0.00	0.02	0.00	0.00	0.02	0.03	0.00	0.01	0.00
FeO	0.83	0.81	0.56	0.52	0.74	0.67	0.90	0.65	0.73	0.85	0.66	0.74	0.86
NiO	0.00	0.00	0.00	0.01	0.00	0.00	0.02	0.00	0.01	0.00	0.01	0.00	0.00
Na_2O	2.36	4.35	2.77	2.35	3.24	2.64	3.83	1.58	2.17	3.40	2.50	1.92	4.23
K_2O	0.11	0.34	0.12	0.09	0.17	0.12	0.25	0.04	0.07	0.20	0.07	0.10	0.28
Total	99.16	99.09	99.50	98.21	98.45	98.98	98.19	98.34	99.14	98.89	99.08	99.40	98.93
Si	8.85	9.60	8.97	8.70	9.16	8.99	9.40	8.48	8.78	9.24	8.89	8.75	9.52
Al	6.94	6.19	6.85	7.16	6.64	6.82	6.38	7.33	7.03	6.54	6.92	7.05	6.27
Fe(ii)	0.13	0.12	0.09	0.08	0.12	0.10	0.14	0.10	0.11	0.13	0.10	0.11	0.13
Ca	3.31	2.54	3.17	3.33	2.96	3.16	2.74	3.63	3.36	2.91	3.24	3.43	2.60
Na	0.85	1.55	0.99	0.86	1.17	0.95	1.38	0.58	0.78	1.23	0.90	0.69	1.52
K	0.03	0.08	0.03	0.02	0.04	0.03	0.06	0.01	0.02	0.05	0.02	0.02	0.07
Mg	0.02	0.02	0.02	0.02	0.03	0.02	0.02	0.01	0.02	0.03	0.02	0.02	0.02
Total	20.12	20.11	20.11	20.16	20.12	20.08	20.13	20.14	20.10	20.12	20.10	20.08	20.13
An	79.03	60.85	75.64	79.10	70.98	76.35	65.51	86.08	80.75	69.54	77.96	82.77	62.20
Ab	20.33	37.26	23.69	20.39	28.04	22.96	33.08	13.70	18.83	29.31	21.65	16.65	36.21
Or	0.64	1.89	0.67	0.51	0.98	0.68	1.42	0.22	0.42	1.15	0.39	0.59	1.58
Sample	G35	G37A	G37A	G37A	G37A	G37A	G40	G40	G40	G40	G40	G40	G40
Grain	P3	GM	P1	P1	P2	P2	P1	P1	GM	P2	P2	P3	P3
Position	M		C-M	R	C-M	R	C	R		C	R	C	R
SiO_2	50.38	53.47	48.51	48.91	49.74	50.45	49.87	52.98	53.11	52.60	47.38	49.00	53.33
TiO_2	0.05	0.04	0.04	0.02	0.04	0.04	0.05	0.03	0.08	0.03	0.05	0.03	0.03
Al_2O_3	29.76	27.66	30.67	30.71	30.20	29.34	29.39	28.37	27.17	28.40	32.22	30.23	27.73
Cr_2O_3	0.00	0.01	0.01	0.00	0.00	0.02	0.02	0.02	0.00	0.00	0.01	0.00	0.02
MgO	0.10	0.09	0.06	0.06	0.06	0.07	0.08	0.06	0.09	0.06	0.07	0.06	0.09
CaO	14.28	11.85	15.63	15.24	14.79	13.61	13.99	12.14	11.35	12.64	16.92	15.09	12.26
MnO	0.02	0.00	0.00	0.01	0.01	0.01	0.01	0.01	0.03	0.00	0.00	0.02	0.00
FeO	0.62	0.70	0.54	0.58	0.55	0.59	0.65	0.67	0.72	0.51	0.65	0.66	0.70
NiO	0.00	0.00	0.01	0.00	0.01	0.00	0.02	0.01	0.01	0.01	0.00	0.02	0.02
Na_2O	3.57	4.80	2.73	2.96	3.20	3.79	3.64	4.72	5.30	4.49	2.10	3.06	4.80
K_2O	0.15	0.21	0.08	0.09	0.10	0.15	0.11	0.19	0.21	0.20	0.04	0.10	0.18
Total	98.91	98.83	98.27	98.59	98.69	98.06	97.84	99.22	98.07	98.91	99.44	98.26	99.16
Si	9.32	9.83	9.07	9.10	9.23	9.40	9.33	9.72	9.85	9.68	8.79	9.15	9.79
Al	6.49	5.99	6.75	6.73	6.60	6.44	6.48	6.13	5.94	6.16	7.04	6.66	6.00
Fe(ii)	0.10	0.11	0.08	0.09	0.08	0.09	0.10	0.10	0.11	0.08	0.10	0.10	0.11
Ca	2.83	2.33	3.13	3.04	2.94	2.72	2.81	2.39	2.26	2.49	3.36	3.02	2.41
Na	1.28	1.71	0.99	1.07	1.15	1.37	1.32	1.68	1.91	1.60	0.75	1.11	1.71
K	0.03	0.05	0.02	0.02	0.02	0.04	0.03	0.05	0.05	0.05	0.01	0.02	0.04
Mg	0.03	0.03	0.02	0.02	0.02	0.02	0.02	0.02	0.02	0.02	0.02	0.02	0.02
Total	20.08	20.05	20.06	20.07	20.05	20.07	20.09	20.08	20.14	20.06	20.07	20.08	20.08
An	68.31	57.03	75.65	73.58	71.45	65.95	67.54	58.07	53.56	60.20	81.45	72.72	57.94
Ab	30.85	41.75	23.89	25.89	27.96	33.18	31.81	40.83	45.24	38.69	18.30	26.70	41.03
Or	0.84	1.22	0.46	0.52	0.60	0.87	0.65	1.10	1.20	1.11	0.25	0.59	1.03
Sample	G41	G41	G41	G41	G41	G41	G41	G41	G41	G44	G44	G44	G44
Grain	P1	P1	GM	P2	P2	P2	P3	GM	GM	GM	P1	P2	P2
Position	M	R		C	M	R	R	C	R		R	C-M	R
SiO_2	50.54	47.82	48.46	48.05	49.70	49.11	48.48	48.53	49.14	47.45	47.12	46.30	47.16
TiO_2	0.03	0.03	0.00	0.03	0.01	0.03	0.00	0.04	0.06	0.01	0.02	0.02	0.03
Al_2O_3	29.70	30.66	30.95	31.14	30.51	30.93	30.59	30.23	30.19	32.66	32.44	32.60	33.09
Cr_2O_3	0.00	0.03	0.00	0.00	0.01	0.00	0.01	0.02	0.00	0.01	0.00	0.00	0.02
MgO	0.08	0.06	0.08	0.07	0.06	0.08	0.07	0.09	0.09	0.07	0.08	0.06	0.06
CaO	14.26	15.71	15.51	15.78	14.95	15.45	15.23	14.79	14.62	17.23	16.74	17.61	17.44
MnO	0.00	0.01	0.00	0.01	0.00	0.00	0.00	0.00	0.00	0.00	0.00	0.01	0.00
FeO	0.61	0.66	0.70	0.60	0.61	0.70	0.63	0.64	0.76	0.67	0.58	0.55	0.65
NiO	0.00	0.01	0.00	0.00	0.01	0.00	0.00	0.00	0.01	0.00	0.00	0.01	0.01
Na_2O	3.50	2.65	2.75	2.71	3.13	2.90	3.00	3.17	3.26	1.85	2.11	1.55	1.67
K_2O	0.12	0.08	0.10	0.09	0.11	0.10	0.11	0.11	0.12	0.04	0.05	0.03	0.04
Total	98.84	97.70	98.55	98.47	99.12	99.29	98.12	97.61	98.24	99.99	99.14	98.75	100.17
Si	9.35	9.00	9.03	8.97	9.19	9.08	9.07	9.13	9.18	8.75	8.76	8.66	8.68
Al	6.48	6.80	6.80	6.85	6.65	6.74	6.75	6.70	6.64	7.10	7.10	7.18	7.18
Fe(ii)	0.09	0.10	0.11	0.09	0.09	0.11	0.10	0.10	0.12	0.10	0.09	0.09	0.10
Ca	2.83	3.17	3.10	3.16	2.96	3.06	3.05	2.98	2.93	3.40	3.33	3.53	3.44
Na	1.26	0.97	0.99	0.98	1.12	1.04	1.09	1.15	1.18	0.66	0.76	0.56	0.60
K	0.03	0.02	0.02	0.02	0.03	0.02	0.03	0.03	0.03	0.01	0.01	0.01	0.01
Mg	0.02	0.02	0.02	0.02	0.02	0.02	0.02	0.02	0.02	0.02	0.02	0.02	0.02
Total	20.05	20.08	20.08	20.10	20.06	20.08	20.11	20.11	20.10	20.04	20.07	20.04	20.03
An	68.73	76.26	75.31	75.90	72.02	74.23	73.26	71.63	70.77	83.53	81.24	86.08	84.99
Ab	30.56	23.26	24.13	23.56	27.32	25.22	26.12	27.75	28.56	16.27	18.49	13.73	14.76
Or	0.71	0.48	0.56	0.54	0.65	0.54	0.62	0.62	0.67	0.21	0.28	0.19	0.26

Grain: P, phenocryst; GM, groundmass. INC, inclusion (mineral included within is stated in parentheses)
Spot: C, core; M, mid point (number indicates relative position along transect from core to rim); R, rim
An, anorthite; Ab, albite; Or, orthoclase

Table D.1. Plagioclase mineral data continued

Sample	G44	G44	G44	G44	G48	G48	G48	G48	G48	G48	G48	G48	G48
Grain	P3	GM	P4	P4	GM	GM	P1	P2	P2	P3	P3	P4	P4
Position	R		C	R			lath	C-M	R	C-M	R	C	R
SiO_2	46.50	45.98	47.15	50.68	55.16	54.95	55.77	49.88	51.85	47.82	51.92	54.41	53.07
TiO_2	0.03	0.02	0.01	0.05	0.06	0.06	0.08	0.05	0.06	0.03	0.07	0.06	0.02
Al_2O_3	32.55	32.87	32.43	29.95	27.57	27.71	27.42	30.58	29.86	32.25	29.06	28.24	28.89
Cr_2O_3	0.00	0.00	0.01	0.00	0.00	0.00	0.03	0.00	0.00	0.00	0.00	0.00	0.00
MgO	0.05	0.06	0.06	0.07	0.06	0.05	0.09	0.10	0.10	0.04	0.07	0.06	0.08
CaO	17.39	18.07	17.09	13.97	11.19	11.01	11.11	14.87	13.16	16.96	12.84	11.94	12.54
MnO	0.00	0.00	0.00	0.00	0.02	0.00	0.01	0.00	0.00	0.00	0.00	0.00	0.00
FeO	0.62	0.60	0.68	0.64	0.90	0.57	0.74	0.68	0.72	0.64	0.81	0.76	0.73
NiO	0.01	0.00	0.00	0.01	0.00	0.00	0.01	0.00	0.00	0.02	0.00	0.00	0.02
Na_2O	1.68	1.37	1.91	3.68	5.23	5.40	5.35	3.15	3.70	2.02	4.36	4.85	4.42
K_2O	0.03	0.03	0.05	0.12	0.36	0.29	0.24	0.09	0.17	0.05	0.23	0.30	0.21
Total	98.86	99.00	99.39	99.17	100.56	100.04	100.85	99.38	99.61	99.83	99.35	100.63	99.98
Si	8.68	8.59	8.75	9.34	9.96	9.95	10.02	9.19	9.48	8.82	9.54	9.83	9.66
Al	7.16	7.23	7.09	6.51	5.87	5.91	5.81	6.64	6.43	7.01	6.29	6.01	6.20
Fe(ii)	0.10	0.09	0.11	0.10	0.14	0.09	0.11	0.10	0.11	0.10	0.12	0.12	0.11
Ca	3.48	3.62	3.40	2.76	2.16	2.14	2.14	2.94	2.58	3.35	2.53	2.31	2.44
Na	0.61	0.49	0.69	1.31	1.83	1.90	1.86	1.13	1.31	0.72	1.55	1.70	1.56
K	0.01	0.01	0.01	0.03	0.08	0.07	0.06	0.02	0.04	0.01	0.05	0.07	0.05
Mg	0.01	0.02	0.02	0.02	0.02	0.01	0.02	0.03	0.03	0.01	0.02	0.02	0.02
Total	20.04	20.04	20.05	20.07	20.06	20.06	20.02	20.05	19.97	20.03	20.11	20.04	20.04
An	84.95	87.83	82.95	67.26	53.07	52.13	52.73	71.89	65.64	82.06	61.15	56.67	60.34
Ab	14.86	12.01	16.77	32.05	44.89	46.24	45.91	27.59	33.38	17.64	37.56	41.64	38.48
Or	0.19	0.16	0.28	0.69	2.04	1.62	1.36	0.51	0.98	0.29	1.29	1.68	1.19

Sample	G49	G49	G37A	G37A	G37A	G37A	G40	G40	G40	G40	G40	G40	G40
Grain	P1	P1	P1	P1	P2	P2	P1	P1	GM	P2	P2	P3	P3
Position	C	M1	C-M	R	C-M	R	C	R		C	R	C	R
SiO_2	56.23	54.58	48.51	48.91	49.74	50.45	49.87	52.98	53.11	52.60	47.38	49.00	53.33
TiO_2	0.01	0.02	0.04	0.02	0.04	0.04	0.05	0.03	0.08	0.03	0.05	0.03	0.03
Al_2O_3	26.62	27.61	30.67	30.71	30.20	29.34	29.39	28.37	27.17	28.40	32.22	30.23	27.73
Cr_2O_3	0.00	0.00	0.01	0.00	0.00	0.02	0.02	0.02	0.00	0.00	0.01	0.00	0.02
MgO	0.03	0.04	0.06	0.06	0.06	0.07	0.08	0.06	0.09	0.06	0.07	0.06	0.09
CaO	9.88	11.05	15.63	15.24	14.79	13.61	13.99	12.14	11.35	12.64	16.92	15.09	12.26
MnO	0.00	0.00	0.00	0.01	0.01	0.01	0.01	0.01	0.03	0.00	0.00	0.02	0.00
FeO	0.36	0.35	0.54	0.58	0.55	0.59	0.65	0.67	0.72	0.51	0.65	0.66	0.70
NiO	0.00	0.00	0.01	0.00	0.01	0.00	0.02	0.01	0.01	0.01	0.00	0.02	0.02
Na_2O	5.94	5.24	2.73	2.96	3.20	3.79	3.64	4.72	5.30	4.49	2.10	3.06	4.80
K_2O	0.37	0.28	0.08	0.09	0.10	0.15	0.11	0.19	0.21	0.20	0.04	0.10	0.18
Total	99.43	99.18	98.27	98.59	98.69	98.06	97.84	99.22	98.07	98.91	99.44	98.26	99.16
Si	10.20	9.96	9.07	9.10	9.23	9.40	9.33	9.72	9.85	9.68	8.79	9.15	9.79
Al	5.69	5.94	6.75	6.73	6.60	6.44	6.48	6.13	5.94	6.16	7.04	6.66	6.00
Fe(ii)	0.05	0.05	0.08	0.09	0.08	0.09	0.10	0.10	0.11	0.08	0.10	0.10	0.11
Ca	1.92	2.16	3.13	3.04	2.94	2.72	2.81	2.39	2.26	2.49	3.36	3.02	2.41
Na	2.09	1.85	0.99	1.07	1.15	1.37	1.32	1.68	1.91	1.60	0.75	1.11	1.71
K	0.09	0.07	0.02	0.02	0.02	0.04	0.03	0.05	0.05	0.05	0.01	0.02	0.04
Mg	0.01	0.01	0.02	0.02	0.02	0.02	0.02	0.02	0.02	0.02	0.02	0.02	0.02
Total	20.04	20.03	20.06	20.07	20.05	20.07	20.09	20.08	20.14	20.06	20.07	20.08	20.08
An	46.90	52.94	75.65	73.58	71.45	65.95	67.54	58.07	53.56	60.20	81.45	72.72	57.94
Ab	51.02	45.44	23.89	25.89	27.96	33.18	31.81	40.83	45.24	38.69	18.30	26.70	41.03
Or	2.08	1.62	0.46	0.52	0.60	0.87	0.65	1.10	1.20	1.11	0.25	0.59	1.03

Sample	G41	G41	G49	G49	G49	G49	G49	G49	G49	G49	G49	G51 L	G51 L
Grain	P1	P1	P1	P1	P2	P3	P3	P3	GM			P1	P1
Position	M	R	M2	R	R	C	M	R				M	R
SiO_2	50.54	47.82	57.07	52.18	55.79	56.62	54.17	54.85	53.56	52.94	55.66	51.80	57.42
TiO_2	0.03	0.03	0.03	0.01	0.04	0.01	0.02	0.00	0.03	0.02	0.04	0.03	0.03
Al_2O_3	29.70	30.66	26.63	29.30	27.75	27.33	28.35	27.76	28.63	29.24	27.74	29.34	25.69
Cr_2O_3	0.00	0.03	0.00	0.01	0.02	0.00	0.01	0.01	0.00	0.01	0.01	0.00	0.00
MgO	0.08	0.06	0.02	0.04	0.02	0.03	0.04	0.02	0.07	0.02	0.03	0.05	0.04
CaO	14.26	15.71	9.79	13.17	10.96	10.32	11.72	11.03	12.30	12.56	10.81	13.30	9.19
MnO	0.00	0.01	0.00	0.00	0.02	0.01	0.00	0.01	0.00	0.01	0.00	0.01	0.00
FeO	0.61	0.66	0.39	0.68	0.45	0.37	0.41	0.41	0.58	0.53	0.47	0.55	0.47
NiO	0.00	0.01	0.00	0.02	0.00	0.01	0.00	0.00	0.01	0.01	0.01	0.01	0.00
Na_2O	3.50	2.65	5.97	4.16	5.37	5.74	4.95	5.26	4.46	4.46	5.49	4.05	6.19
K_2O	0.12	0.08	0.36	0.22	0.41	0.31	0.24	0.38	0.31	0.24	0.36	0.22	0.51
Total	98.84	97.70	100.25	99.79	100.84	100.75	99.89	99.72	99.94	100.03	100.64	99.34	99.54
Si	9.35	9.00	10.25	9.54	10.01	10.14	9.83	9.96	9.74	9.63	10.01	9.51	10.39
Al	6.48	6.80	5.64	6.31	5.87	5.77	6.06	5.94	6.13	6.27	5.88	6.35	5.48
Fe(ii)	0.09	0.10	0.06	0.10	0.07	0.06	0.06	0.06	0.09	0.08	0.07	0.08	0.07
Ca	2.83	3.17	1.88	2.58	2.11	1.98	2.28	2.14	2.40	2.45	2.08	2.62	1.78
Na	1.26	0.97	2.08	1.48	1.87	1.99	1.74	1.85	1.57	1.57	1.91	1.44	2.17
K	0.03	0.02	0.08	0.05	0.09	0.07	0.06	0.09	0.07	0.06	0.08	0.05	0.12
Mg	0.02	0.02	0.01	0.01	0.01	0.01	0.01	0.01	0.02	0.01	0.01	0.01	0.01
Total	20.05	20.08	20.00	20.07	20.03	20.01	20.04	20.04	20.02	20.05	20.04	20.06	20.02
An	68.73	76.26	46.59	62.81	51.77	48.95	55.92	52.54	59.31	60.05	51.06	63.70	43.76
Ab	30.56	23.26	51.39	35.93	45.91	49.30	42.72	45.31	38.92	38.59	46.89	35.07	53.37
Or	0.71	0.48	2.02	1.26	2.32	1.75	1.36	2.15	1.77	1.36	2.05	1.23	2.87

Grain: P, phenocryst; GM, groundmass. INC, inclusion (mineral included within is stated in parentheses)
Spot: C, core; M, mid point (number indicates relative position along transect from core to rim); R, rim
An, anorthite; Ab, albite; Or, orthoclase

Table D.1. Plagioclase mineral data continued

Sample	G51 L	G51 L	G51 L	G51 L	G51 L	G51 D	G51 D	G51 D	G51 D	G51 D	G51 D	G51 D
Grain	P2	P2	P3	P3	P3	P4	P4	P4	P4	P4	P5	GM
Position	M	R	C	M	R	C	R	C	M	R	R	R
SiO_2	46.96	51.85	44.98	52.66	56.15	45.11	45.15	47.00	44.22	45.28	44.92	45.31
TiO_2	0.02	0.03	0.03	0.04	0.04	0.04	0.03	0.02	0.02	0.03	0.03	0.04
Al_2O_3	31.97	29.41	33.52	27.37	26.34	33.66	32.59	32.64	33.52	33.61	33.45	33.61
Cr_2O_3	0.00	0.00	0.00	0.00	0.00	0.00	0.00	0.01	0.00	0.00	0.01	0.00
MgO	0.03	0.04	0.03	0.05	0.05	0.06	0.06	0.07	0.05	0.06	0.05	0.05
CaO	16.75	13.50	18.69	11.46	10.00	18.61	17.83	17.45	18.81	18.43	18.43	18.55
MnO	0.00	0.00	0.00	0.00	0.00	0.01	0.00	0.00	0.00	0.02	0.00	0.02
FeO	0.55	0.51	0.63	0.57	0.52	0.54	0.85	0.58	0.49	0.66	0.56	0.66
NiO	0.00	0.01	0.00	0.01	0.00	0.01	0.00	0.00	0.00	0.02	0.00	0.00
Na_2O	2.32	3.99	1.28	4.83	5.78	1.26	1.54	2.11	1.13	1.25	1.31	1.23
K_2O	0.08	0.20	0.03	0.28	0.43	0.02	0.02	0.03	0.02	0.04	0.02	0.03
Total	98.68	99.54	99.18	97.25	99.32	99.31	98.08	99.92	98.25	99.39	98.78	99.50
Si	8.78	9.50	8.41	9.83	10.21	8.42	8.53	8.69	8.35	8.44	8.43	8.44
Al	7.04	6.35	7.39	6.02	5.64	7.40	7.26	7.11	7.46	7.39	7.40	7.38
Fe(ii)	0.09	0.08	0.10	0.09	0.08	0.08	0.13	0.09	0.08	0.10	0.09	0.10
Ca	3.35	2.65	3.75	2.29	1.95	3.72	3.61	3.46	3.80	3.68	3.70	3.70
Na	0.84	1.42	0.46	1.75	2.04	0.46	0.56	0.75	0.41	0.45	0.48	0.44
K	0.02	0.05	0.01	0.07	0.10	0.00	0.01	0.01	0.00	0.01	0.00	0.01
Mg	0.01	0.01	0.01	0.01	0.01	0.02	0.02	0.02	0.01	0.02	0.01	0.01
Total	20.13	20.05	20.12	20.06	20.03	20.10	20.12	20.13	20.13	20.09	20.11	20.09
An	79.60	64.41	88.85	55.83	47.66	89.00	86.42	81.92	90.07	88.86	88.50	89.13
Ab	19.93	34.45	10.98	42.53	49.88	10.89	13.46	17.89	9.82	10.92	11.38	10.71
Or	0.46	1.14	0.18	1.64	2.46	0.10	0.12	0.19	0.11	0.22	0.11	0.16

Sample	S102	S102	S102	S102	S102	S102	S102	S102	S102	S102	S102	S102	S102
Grain	P1	P1	P1	P1	P2	P2	P2	P2	P3	P4	P4	P4	P5
Position	C	M1	M2	R	C	M1	M2	R	R	C	M1	R	C
SiO_2	52.16	51.92	54.22	53.67	54.69	53.95	53.56	53.72	55.00	53.52	50.89	48.38	55.65
TiO_2	0.02	0.03	0.03	0.03	0.04	0.03	0.03	0.02	0.03	0.02	0.03	0.02	0.19
Al_2O_3	29.23	29.17	28.73	28.20	27.57	28.26	28.11	27.77	27.02	28.31	29.34	31.67	26.84
Cr_2O_3	0.01	0.00	0.00	0.00	0.00	0.01	0.00	0.01	0.00	0.01	0.01	0.00	0.00
MgO	0.06	0.04	0.05	0.05	0.05	0.05	0.05	0.05	0.05	0.05	0.05	0.10	0.07
CaO	13.15	13.10	12.06	11.83	11.09	11.72	11.73	11.45	10.65	11.86	13.65	16.09	10.24
MnO	0.02	0.01	0.02	0.00	0.01	0.01	0.00	0.00	0.00	0.00	0.00	0.00	0.07
FeO	0.42	0.43	0.43	0.52	0.41	0.53	0.54	0.57	0.56	0.44	0.44	0.62	0.34
NiO	0.00	0.00	0.00	0.00	0.00	0.00	0.01	0.00	0.01	0.01	0.00	0.00	0.13
Na_2O	4.33	4.34	5.01	5.05	5.42	5.13	5.07	5.26	5.79	5.07	4.09	2.74	5.93
K_2O	0.10	0.09	0.12	0.15	0.14	0.12	0.12	0.13	0.19	0.12	0.09	0.03	0.17
Total	99.50	99.13	100.66	99.50	99.41	99.81	99.21	98.96	99.31	99.40	98.58	99.64	99.23
Si	9.55	9.54	9.77	9.79	9.96	9.81	9.80	9.85	10.03	9.77	9.43	8.93	10.11
Al	6.31	6.32	6.10	6.06	5.92	6.06	6.06	6.00	5.81	6.09	6.41	6.89	5.75
Fe(ii)	0.06	0.07	0.06	0.08	0.06	0.08	0.08	0.09	0.08	0.07	0.07	0.10	0.05
Ca	2.58	2.58	2.33	2.31	2.16	2.28	2.30	2.25	2.08	2.32	2.71	3.18	1.99
Na	1.54	1.55	1.75	1.78	1.91	1.81	1.80	1.87	2.05	1.79	1.47	0.98	2.09
K	0.02	0.02	0.03	0.03	0.03	0.03	0.03	0.03	0.04	0.03	0.02	0.01	0.04
Mg	0.02	0.01	0.01	0.01	0.01	0.01	0.01	0.01	0.01	0.01	0.01	0.03	0.02
Total	20.07	20.08	20.06	20.08	20.05	20.08	20.08	20.10	20.11	20.09	20.11	20.11	20.05
An	62.34	62.18	56.70	55.96	52.64	55.41	55.76	54.20	49.88	56.01	64.55	76.36	48.39
Ab	37.10	37.33	42.63	43.20	46.60	43.92	43.58	45.06	49.08	43.31	34.95	23.49	50.67
Or	0.56	0.49	0.67	0.84	0.76	0.66	0.66	0.74	1.04	0.68	0.50	0.15	0.95

Sample	S102(XEN)	S102(XEN)	S102(XEN)	S102(XEN)	S102(XEN)	S102(XEN)	S102(XEN)	S102(XEN)	S102(XEN)	S102(XEN)	S106B	S106B	S106B
Grain	P1	P1	P1	P2	P2	P2	P3	P3	P4	P5	P1/GLOM	P1/GLOM	P1/GLOM
Position	C	M	R	C	M	R	C	R	R	R	R	M	
SiO_2	53.45	48.30	51.53	53.87	48.00	54.73	51.06	50.95	55.35	53.25	51.989	45.716	44.732
TiO_2	0.03	0.00	0.01	0.02	0.03	0.04	0.01	0.01	0.02	0.02	0.057	0.03	0.013
Al_2O_3	28.56	31.77	29.96	28.05	31.69	27.80	29.40	29.77	27.41	28.75	29.546	32.952	33.86
Cr_2O_3	0.00	0.00	0.00	0.00	0.00	0.03	0.00	0.02	0.01	0.01	0.007	0.004	0
MgO	0.05	0.06	0.06	0.04	0.07	0.08	0.07	0.04	0.07	0.05	0.086	0.059	0.029
CaO	12.34	16.56	14.38	11.83	16.37	11.71	13.89	14.28	11.13	12.66	13.977	17.996	18.865
MnO	0.00	0.01	0.00	0.00	0.00	0.00	0.01	0.00	0.01	0.01	0	0.037	0.013
FeO	0.46	0.51	0.52	0.48	0.51	0.60	0.59	0.59	0.63	0.62	0.715	0.632	0.54
NiO	0.01	0.00	0.00	0.00	0.01	0.00	0.00	0.00	0.01	0.01	0.016	0.011	0.011
Na_2O	4.59	2.28	3.64	4.94	2.41	4.90	3.79	3.64	5.38	4.44	3.969	1.504	1.035
K_2O	0.09	0.02	0.06	0.11	0.02	0.13	0.08	0.14	0.19	0.18	0.115	0.024	0.018
Total	99.57	99.50	100.15	99.34	99.10	100.01	98.90	99.46	100.21	100.00	100.48	98.97	99.12
Si	9.74	8.92	9.39	9.83	8.91	9.92	9.43	9.37	10.00	9.69	9.46	8.55	8.37
Al	6.14	6.92	6.44	6.03	6.93	5.94	6.40	6.45	5.84	6.16	6.34	7.26	7.47
Fe(ii)	0.07	0.08	0.08	0.07	0.08	0.09	0.09	0.09	0.09	0.09	0.11	0.10	0.08
Ca	2.41	3.28	2.81	2.31	3.25	2.27	2.75	2.81	2.15	2.47	2.72	3.61	3.78
Na	1.62	0.82	1.29	1.75	0.87	1.72	1.36	1.30	1.89	1.57	1.40	0.55	0.38
K	0.02	0.00	0.01	0.03	0.00	0.03	0.02	0.03	0.04	0.04	0.03	0.01	0.00
Mg	0.01	0.02	0.02	0.01	0.02	0.02	0.02	0.01	0.02	0.01	0.02	0.02	0.01
Total	20.01	20.03	20.03	20.04	20.06	19.99	20.06	20.07	20.04	20.03	20.08	20.09	20.09
An	59.47	79.98	68.36	56.59	78.92	56.51	66.65	67.88	52.73	60.54	65.63	86.74	90.87
Ab	40.02	19.91	31.30	42.77	20.98	42.76	32.90	31.31	46.18	38.45	33.73	13.12	9.02
Or	0.51	0.11	0.33	0.64	0.10	0.73	0.46	0.81	1.08	1.01	0.64	0.14	0.10

Grain: P, phenocryst; GM, groundmass. INC, inclusion (mineral included within is stated in parentheses)
Spot: C, core; M, mid point (number indicates relative position along transect from core to rim); R, rim
An, anorthite; Ab, albite; Or, orthoclase

Table D.1. Plagioclase mineral data continued

Sample	S106B	S106B	S106B	S106B	S106B	S106B	S106B	S106B	S110B	S110B	S110B	S110B	S110B
Grain	P2	P3	P3	P3	P4	P4	P5	GM	P1	P1	P2	P2	P2
Position	M-R	R	M	C	R	M			C	R	C	M	R
SiO_2	47.734	47.945	45.333	44.56	51.159	44.536	48.514	53.495	53.47	53.52	49.56	54.48	53.26
TiO_2	0.039	0.032	0.007	0.019	0.042	0.02	0.041	0.078	0.06	0.05	0.04	0.06	0.06
Al_2O_3	31.637	32.305	33.877	33.832	29.585	34.363	31.131	27.825	27.60	27.99	30.35	27.71	28.58
Cr_2O_3	0	0	0.01	0	0.006	0	0.003	0.007	0.02	0.00	0.00	0.00	0.01
MgO	0.042	0.065	0.05	0.04	0.081	0.045	0.047	0.057	0.08	0.06	0.06	0.10	0.07
CaO	16.482	16.869	18.555	18.676	13.851	19.091	15.404	11.882	11.28	11.77	14.84	11.30	12.31
MnO	0	0.006	0.022	0	0	0	0.018	0	0.03	0.03	0.04	0.00	0.00
FeO	0.813	0.722	0.597	0.643	0.657	0.474	0.736	1.113	0.59	0.59	0.58	0.58	0.68
NiO	0	0.014	0.002	0.011	0.008	0.013	0	0.001	0.00	0.00	0.00	0.00	0.00
Na_2O	2.274	2.217	1.158	1.175	3.803	0.821	2.991	4.808	5.33	5.04	3.18	5.25	4.77
K_2O	0.071	0.062	0.026	0.026	0.111	0.015	0.091	0.309	0.22	0.24	0.11	0.25	0.21
Total	99.09	100.24	99.64	98.98	99.30	99.38	98.98	99.58	98.67	99.30	98.75	99.73	99.94
Si	8.88	8.82	8.43	8.35	9.41	8.31	9.01	9.79	9.85	9.80	9.20	9.91	9.70
Al	6.93	7.00	7.42	7.47	6.42	7.55	6.82	6.00	5.99	6.04	6.64	5.94	6.13
Fe(ii)	0.13	0.11	0.09	0.10	0.10	0.07	0.11	0.17	0.09	0.09	0.09	0.09	0.10
Ca	3.28	3.32	3.70	3.75	2.73	3.82	3.07	2.33	2.22	2.31	2.95	2.20	2.40
Na	0.82	0.79	0.42	0.43	1.36	0.30	1.08	1.71	1.90	1.79	1.14	1.85	1.68
K	0.02	0.01	0.01	0.01	0.03	0.00	0.02	0.07	0.05	0.06	0.02	0.06	0.05
Mg	0.01	0.02	0.01	0.01	0.02	0.01	0.01	0.02	0.02	0.02	0.02	0.03	0.02
Total	20.07	20.08	20.07	20.12	20.06	20.06	20.12	20.09	20.13	20.10	20.06	20.07	20.09
An	79.69	80.50	89.72	89.65	66.38	92.70	73.62	56.71	53.22	55.57	71.62	53.56	58.10
Ab	19.90	19.15	10.13	10.21	32.98	7.21	25.87	41.53	45.52	43.07	27.78	45.05	40.71
Or	0.41	0.35	0.15	0.15	0.63	0.09	0.52	1.76	1.26	1.36	0.60	1.39	1.19

Sample	S110B	S110B	S110B	S110B	S110B	S110B	S110B	S110B	S110B	S111	S111	S111	S111
Grain	P3	P4	P5	P5	P5	GM	P6	P6	GM	GM	GM	P1	P1
Position	R		C	M	R		R	C				C	R
SiO_2	52.81	54.37	54.09	54.00	53.78	54.98	52.79	54.27	55.84	55.44	57.23	47.76	52.23
TiO_2	0.06	0.04	0.06	0.04	0.06	0.08	0.06	0.07	0.10	0.07	0.09	0.02	0.05
Al_2O_3	28.57	27.96	27.96	28.16	27.85	26.61	28.58	27.39	26.77	27.05	26.06	32.30	28.84
Cr_2O_3	0.01	0.00	0.00	0.00	0.00	0.00	0.00	0.00	0.00	0.00	0.01	0.01	0.00
MgO	0.06	0.07	0.06	0.08	0.08	0.09	0.07	0.07	0.05	0.06	0.06	0.08	0.07
CaO	12.44	11.68	11.56	11.92	11.80	10.61	12.42	11.15	10.23	11.04	9.06	16.92	12.92
MnO	0.02	0.00	0.01	0.01	0.00	0.01	0.00	0.01	0.00	0.00	0.01	0.02	0.00
FeO	0.66	0.45	0.49	0.51	0.56	0.94	0.67	0.56	0.81	1.22	0.99	0.77	0.95
NiO	0.00	0.02	0.00	0.02	0.00	0.02	0.00	0.00	0.00	0.01	0.00	0.00	0.00
Na_2O	4.65	5.20	5.14	4.94	5.15	5.72	4.75	5.44	5.82	5.50	6.41	2.07	4.23
K_2O	0.22	0.20	0.23	0.21	0.23	0.34	0.23	0.24	0.38	0.31	0.42	0.09	0.17
Total	99.49	99.99	99.58	99.90	99.50	99.39	99.58	99.21	99.97	100.70	100.33	100.03	99.47
Si	9.67	9.87	9.85	9.82	9.82	10.05	9.66	9.93	10.12	10.01	10.31	8.81	9.58
Al	6.16	5.98	6.00	6.03	6.00	5.73	6.16	5.90	5.71	5.76	5.53	7.02	6.24
Fe(ii)	0.10	0.07	0.07	0.08	0.09	0.14	0.10	0.09	0.12	0.18	0.15	0.12	0.14
Ca	2.44	2.27	2.26	2.32	2.31	2.08	2.44	2.19	1.98	2.14	1.75	3.34	2.54
Na	1.65	1.83	1.81	1.74	1.82	2.03	1.69	1.93	2.04	1.93	2.24	0.74	1.50
K	0.05	0.05	0.05	0.05	0.05	0.08	0.05	0.06	0.09	0.07	0.10	0.02	0.04
Mg	0.02	0.02	0.02	0.02	0.02	0.03	0.02	0.02	0.01	0.02	0.02	0.02	0.02
Total	20.09	20.08	20.07	20.06	20.11	20.13	20.12	20.10	20.08	20.10	20.08	20.06	20.07
An	58.90	54.77	54.71	56.44	55.16	49.68	58.33	52.41	48.22	51.69	42.82	81.46	62.18
Ab	39.87	44.10	44.01	42.36	43.58	48.45	40.38	46.24	49.66	46.61	54.82	18.05	36.83
Or	1.23	1.13	1.27	1.20	1.26	1.87	1.29	1.35	2.12	1.71	2.36	0.49	0.99

Sample	S111	S111	S111	S111	S112	S112	S112	S112	S112	S112	S112	S112	S112
Grain	P2	P3	P3	P4	P1	P1	P2	P2	P2	P2	P2	P3	P3
Position	R	C	R	R	CM	R	C	M1	M2	M3	R	C	M
SiO_2	53.69	47.89	47.83	45.66	50.22	50.92	52.54	50.17	52.93	51.17	51.71	54.10	53.53
TiO_2	0.05	0.05	0.00	0.01	0.03	0.04	0.06	0.03	0.04	0.04	0.04	0.02	0.03
Al_2O_3	28.60	32.04	31.75	34.05	26.12	29.69	28.63	30.21	28.41	29.05	28.78	27.71	28.17
Cr_2O_3	0.00	0.01	0.01	0.00	0.01	0.01	0.01	0.01	0.00	0.00	0.00	0.01	0.00
MgO	0.06	0.08	0.05	0.02	0.05	0.06	0.08	0.05	0.07	0.05	0.04	0.05	0.06
CaO	12.32	16.45	16.10	18.60	11.36	13.92	12.81	14.47	12.63	13.28	12.93	11.45	12.12
MnO	0.01	0.01	0.00	0.00	0.01	0.02	0.01	0.00	0.00	0.03	0.00	0.00	0.04
FeO	1.12	0.64	0.68	0.62	0.46	0.78	0.54	0.54	0.55	0.56	0.56	0.45	0.42
NiO	0.01	0.02	0.00	0.01	0.00	0.00	0.00	0.01	0.00	0.00	0.00	0.00	0.00
Na_2O	4.72	2.22	2.52	1.08	4.80	3.86	4.55	3.63	4.62	4.26	4.41	5.27	4.90
K_2O	0.20	0.07	0.06	0.02	0.20	0.13	0.16	0.10	0.15	0.12	0.16	0.22	0.20
Total	100.78	99.47	99.01	100.05	93.26	99.42	99.39	99.21	99.39	98.56	98.61	99.28	99.46
Si	9.71	8.86	8.89	8.44	9.80	9.37	9.63	9.26	9.69	9.48	9.56	9.88	9.78
Al	6.10	6.99	6.96	7.42	6.00	6.44	6.19	6.57	6.13	6.34	6.27	5.97	6.06
Fe(ii)	0.17	0.10	0.11	0.10	0.08	0.12	0.08	0.08	0.08	0.09	0.09	0.07	0.06
Ca	2.39	3.26	3.21	3.68	2.37	2.74	2.52	2.86	2.48	2.64	2.56	2.24	2.37
Na	1.66	0.80	0.91	0.39	1.82	1.38	1.62	1.30	1.64	1.53	1.58	1.87	1.74
K	0.05	0.02	0.01	0.00	0.05	0.03	0.04	0.02	0.03	0.03	0.04	0.05	0.05
Mg	0.02	0.02	0.01	0.00	0.01	0.02	0.02	0.01	0.02	0.01	0.01	0.01	0.02
Total	20.08	20.04	20.09	20.04	20.13	20.10	20.09	20.11	20.08	20.12	20.11	20.09	20.08
An	58.40	80.05	77.68	90.45	56.00	66.07	60.34	68.42	59.66	62.84	61.31	53.87	57.10
Ab	40.48	19.56	22.00	9.46	42.85	33.18	38.75	31.02	39.52	36.48	37.81	44.89	41.78
Or	1.12	0.39	0.32	0.09	1.15	0.75	0.91	0.56	0.83	0.68	0.88	1.24	1.12

Grain: P, phenocryst; GM, groundmass. INC, inclusion (mineral included within is stated in parentheses)
Spot: C, core; M, mid point (number indicates relative position along transect from core to rim); R, rim
An, anorthite; Ab, albite; Or, orthoclase

Table D.2. Clinopyroxene mineral data

Sample	G01B	G01B	G01B	G01B	G01B	G01B	G01B	G11	G11	G11
Grain	P1	P2	P2	P3	P3	GM	P4	P1	P2	INC (Plag P3)
Position		C	R	C	R		R			
SiO_2	50.58	50.99	49.97	51.30	50.93	48.84	50.81	50.48	50.95	50.78
TiO_2	0.51	0.51	0.73	0.61	0.67	0.80	0.65	0.63	0.58	0.53
Al_2O_3	2.42	2.01	3.04	2.46	2.77	4.03	2.56	2.22	2.19	2.43
Cr_2O_3	0.01	0.00	0.02	0.00	0.00	0.05	0.00	0.00	0.00	0.00
Fe_2O_3	4.43	4.56	4.66	3.33	3.72	5.37	3.70	3.25	2.51	2.43
FeO	4.47	4.38	3.79	5.44	4.82	3.57	4.59	10.55	10.60	10.60
MnO	0.24	0.26	0.20	0.26	0.24	0.21	0.23	0.46	0.45	0.44
MgO	15.61	15.84	15.10	15.34	15.23	14.82	15.25	13.61	13.50	13.12
CaO	21.35	21.39	22.00	21.61	21.88	21.61	21.90	18.71	19.23	19.63
Na_2O	0.22	0.25	0.28	0.25	0.27	0.27	0.28	0.36	0.36	0.35
K_2O	0.00	0.00	0.00	0.00	0.00	0.00	0.00	0.00	0.00	0.00
NiO	0.00	0.02	0.03	0.01	0.00	0.00	0.01	0.01	0.00	0.00
Total	99.83	100.20	99.81	100.61	100.54	99.56	99.98	100.29	100.37	100.30
Si	1.90	1.91	1.88	1.91	1.90	1.85	1.90	1.91	1.92	1.92
Al	0.11	0.09	0.13	0.11	0.12	0.18	0.11	0.10	0.10	0.11
Fe(ii)	0.14	0.14	0.12	0.17	0.15	0.11	0.14	0.33	0.33	0.33
Fe(iii)	0.12	0.13	0.13	0.09	0.10	0.15	0.10	0.09	0.07	0.07
Cr	0.00	0.00	0.00	0.00	0.00	0.00	0.00	0.00	0.00	0.00
Ti	0.01	0.01	0.02	0.02	0.02	0.02	0.02	0.02	0.02	0.02
Mn	0.01	0.01	0.01	0.01	0.01	0.01	0.01	0.01	0.01	0.01
Mg	0.87	0.88	0.85	0.85	0.84	0.83	0.85	0.77	0.76	0.74
Ca	0.86	0.86	0.89	0.86	0.87	0.88	0.88	0.76	0.78	0.80
Na	0.02	0.02	0.02	0.02	0.02	0.02	0.02	0.03	0.03	0.03
Total	4.04	4.04	4.04	4.03	4.03	4.05	4.03	4.03	4.02	4.02
Wo	42.89	42.61	44.59	43.48	44.13	44.23	44.31	38.61	39.78	40.76
En	43.62	43.93	42.59	42.96	42.73	42.19	42.93	39.10	38.85	37.91
Fs	13.50	13.46	12.82	13.56	13.14	13.58	12.76	22.29	21.37	21.33

Sample	G11	G17	G17	G17	G22	G22	G22	G22	G22	G23
Grain	P3	P1	P1	P1	P1	P1	P2	P2	P2	P1
Position		C	M	R	C	R	M	R	C	C
SiO_2	51.19	50.95	50.11	49.59	51.58	50.59	47.99	50.61	50.50	49.88
TiO_2	0.39	0.44	0.64	0.61	0.27	0.55	0.94	0.56	0.70	0.75
Al_2O_3	1.58	1.94	2.53	2.83	1.17	2.31	4.66	2.49	2.95	3.53
Cr_2O_3	0.00	0.00	0.01	0.00	0.00	0.00	0.01	0.00	0.00	0.00
Fe_2O_3	3.55	3.70	3.78	4.41	3.13	3.71	5.73	3.76	3.91	4.31
FeO	8.73	7.69	8.35	8.03	7.92	6.52	4.68	6.31	6.42	4.37
MnO	0.48	0.49	0.42	0.44	0.47	0.35	0.24	0.32	0.30	0.26
MgO	13.90	13.92	13.97	13.56	14.15	14.44	14.05	14.59	14.61	14.69
CaO	20.27	20.80	19.48	19.83	21.09	20.89	20.89	20.84	20.75	22.06
Na_2O	0.35	0.36	0.40	0.39	0.28	0.35	0.32	0.36	0.36	0.27
K_2O	0.00	0.00	0.00	0.00	0.00	0.00	0.00	0.00	0.00	0.00
NiO	0.00	0.01	0.02	0.00	0.01	0.00	0.02	0.00	0.00	0.01
Total	100.42	100.30	99.70	99.68	100.05	99.71	99.51	99.84	100.51	100.12
Si	1.93	1.92	1.90	1.89	1.95	1.91	1.83	1.91	1.89	1.87
Al	0.07	0.09	0.11	0.13	0.05	0.10	0.21	0.11	0.13	0.16
Fe(ii)	0.27	0.24	0.26	0.25	0.25	0.20	0.15	0.20	0.20	0.14
Fe(iii)	0.10	0.10	0.11	0.13	0.09	0.10	0.16	0.11	0.11	0.12
Cr	0.00	0.00	0.00	0.00	0.00	0.00	0.00	0.00	0.00	0.00
Ti	0.01	0.01	0.02	0.02	0.01	0.02	0.03	0.02	0.02	0.02
Mn	0.02	0.02	0.01	0.01	0.01	0.01	0.01	0.01	0.01	0.01
Mg	0.78	0.78	0.79	0.77	0.80	0.81	0.80	0.82	0.82	0.82
Ca	0.82	0.84	0.79	0.81	0.85	0.85	0.85	0.84	0.83	0.89
Na	0.03	0.03	0.03	0.03	0.02	0.03	0.02	0.03	0.03	0.02
Total	4.03	4.03	4.03	4.04	4.03	4.03	4.05	4.03	4.03	4.04
Wo	41.18	42.38	40.30	41.04	42.64	42.73	43.33	42.62	42.34	44.94
En	39.29	39.46	40.21	39.06	39.80	41.11	40.56	41.54	41.48	41.65
Fs	19.53	18.16	19.49	19.90	17.56	16.16	16.11	15.84	16.17	13.40

Grain: P, phenocryst; GM, groundmass; INC, inclusion (mineral included within is stated in parentheses); *mantling orthopyroxene; GLOM, glomerocryst. XEN = xenolith
Spot: C, core; M, mid point (number indicates relative position along transect from core to rim); R, rim
Wo, wollastonite; En, enstatite; Fs, ferrosilite

Table D.2. Clinopyroxene mineral data continued

Sample	G23	G23	G23	G23	G23	G23	G23	G24	G24	G24
Grain	P1	P2	P2	P3	P3	P4*	P4*	P1	P1	P1
Position	R	C	R	C	R		R	R	M	C
SiO_2	50.43	50.18	50.25	50.42	50.74	49.77	49.84	50.31	50.94	49.34
TiO_2	0.60	0.67	0.78	0.72	0.64	0.57	0.73	0.47	0.44	0.49
Al_2O_3	3.10	2.80	2.71	2.97	2.32	2.85	3.29	1.63	1.98	2.31
Cr_2O_3	0.00	0.00	0.00	0.00	0.00	0.01	0.01	0.02	0.02	0.01
Fe_2O_3	4.37	4.26	3.67	3.73	4.00	2.69	4.92	3.87	3.01	4.86
FeO	4.74	5.81	6.80	6.07	7.09	7.19	4.70	7.67	8.01	7.34
MnO	0.18	0.34	0.34	0.30	0.39	0.31	0.29	0.46	0.42	0.47
MgO	15.62	15.30	14.90	14.85	15.66	14.07	15.03	15.23	14.94	14.71
CaO	20.94	20.22	20.19	20.89	19.24	20.27	21.18	18.93	19.42	18.65
Na_2O	0.26	0.28	0.26	0.29	0.26	0.31	0.29	0.23	0.29	0.33
K_2O	0.00	0.00	0.00	0.00	0.00	0.00	0.00	0.00	0.00	0.00
NiO	0.03	0.00	0.00	0.00	0.00	0.01	0.00	0.00	0.02	0.03
Total	100.26	99.85	99.91	100.23	100.35	98.05	100.26	98.81	99.48	98.54
Si	1.88	1.89	1.89	1.89	1.90	1.91	1.87	1.92	1.93	1.90
Al	0.14	0.12	0.12	0.13	0.10	0.13	0.15	0.07	0.09	0.10
Fe(ii)	0.15	0.18	0.21	0.19	0.22	0.23	0.15	0.24	0.25	0.23
Fe(iii)	0.12	0.12	0.10	0.10	0.11	0.08	0.14	0.11	0.08	0.14
Cr	0.00	0.00	0.00	0.00	0.00	0.00	0.00	0.00	0.00	0.00
Ti	0.02	0.02	0.02	0.02	0.02	0.02	0.02	0.01	0.01	0.01
Mn	0.01	0.01	0.01	0.01	0.01	0.01	0.01	0.01	0.01	0.02
Mg	0.87	0.86	0.84	0.83	0.88	0.80	0.84	0.87	0.84	0.84
Ca	0.84	0.82	0.81	0.84	0.77	0.83	0.85	0.77	0.79	0.77
Na	0.02	0.02	0.02	0.02	0.02	0.02	0.02	0.02	0.02	0.02
Total	4.04	4.04	4.03	4.03	4.03	4.02	4.04	4.03	4.03	4.04
Wo	42.29	41.07	41.19	42.56	38.77	42.63	42.92	38.54	39.75	38.43
En	43.88	43.25	42.31	42.11	43.94	41.18	42.36	43.16	42.57	42.19
Fs	13.82	15.68	16.50	15.34	17.29	16.18	14.72	18.30	17.68	19.38

Sample	G24	G26	G26	G26	G27	G27	G30	G30	G30	G30
Grain	P2	P1	P2	P2	P1	P1	P1	P1	P2	P2
Position	R			R	R	M	M	C	C	M
SiO_2	49.34	49.31	49.14	49.26	51.30	50.66	50.65	49.52	48.03	48.67
TiO_2	0.66	0.75	0.88	0.65	0.40	0.47	0.61	0.84	0.99	0.98
Al_2O_3	2.67	3.33	4.06	3.19	1.66	2.37	2.85	3.42	4.99	5.06
Cr_2O_3	0.00	0.00	0.00	0.01	0.00	0.00	0.00	0.01	0.01	0.01
Fe_2O_3	4.46	5.17	4.71	5.19	2.76	3.55	3.62	4.35	5.34	4.31
FeO	7.80	5.12	5.55	5.76	10.07	7.86	6.49	5.89	5.40	6.08
MnO	0.44	0.35	0.35	0.39	0.57	0.45	0.30	0.32	0.21	0.26
MgO	14.42	14.70	14.24	14.96	14.68	14.77	15.31	14.61	13.75	13.81
CaO	18.83	20.71	20.81	19.70	18.35	19.31	20.02	20.58	20.68	20.69
Na_2O	0.33	0.31	0.34	0.30	0.30	0.35	0.29	0.29	0.37	0.35
K_2O	0.00	0.00	0.00	0.00	0.00	0.00	0.01	0.00	0.00	0.00
NiO	0.01	0.01	0.00	0.02	0.02	0.01	0.01	0.00	0.00	0.00
Total	98.95	99.77	100.08	99.44	100.10	99.79	100.15	99.83	99.77	100.23
Si	1.89	1.87	1.85	1.87	1.94	1.91	1.90	1.87	1.82	1.83
Al	0.12	0.15	0.18	0.14	0.07	0.11	0.13	0.15	0.22	0.22
Fe(ii)	0.25	0.16	0.17	0.18	0.32	0.25	0.20	0.18	0.17	0.19
Fe(iii)	0.13	0.15	0.13	0.15	0.08	0.10	0.10	0.12	0.15	0.12
Cr	0.00	0.00	0.00	0.00	0.00	0.00	0.00	0.00	0.00	0.00
Ti	0.02	0.02	0.02	0.02	0.01	0.01	0.02	0.02	0.03	0.03
Mn	0.01	0.01	0.01	0.01	0.02	0.01	0.01	0.01	0.01	0.01
Mg	0.82	0.83	0.80	0.85	0.83	0.83	0.85	0.82	0.78	0.78
Ca	0.77	0.84	0.84	0.80	0.74	0.78	0.80	0.83	0.84	0.83
Na	0.02	0.02	0.03	0.02	0.02	0.03	0.02	0.02	0.03	0.03
Total	4.04	4.05	4.04	4.05	4.02	4.03	4.03	4.04	4.05	4.04
Wo	38.93	42.29	42.95	40.31	37.49	39.59	40.78	42.22	43.22	43.27
En	41.49	41.75	40.90	42.60	41.71	42.14	43.38	41.72	40.01	40.20
Fs	19.59	15.96	16.15	17.09	20.80	18.27	15.84	16.05	16.78	16.52

Grain: P, phenocryst; GM, groundmass; INC, inclusion (mineral included within is stated in parentheses); *mantling orthopyroxene; GLOM, glomerocryst. XEN = xenolith
Spot: C, core; M, mid point (number indicates relative position along transect from core to rim); R, rim
Wo, wollastonite; En, enstatite; Fs, ferrosilite

Table D.2. Clinopyroxene mineral data continued

Sample	G30	G35	G35	G35	G35	G37A	G37A	G40	G40	G40
Grain	P2	P1	P2	P3	P3	P1	P2	P1	P2	P3
Position	R			C	R				M	
SiO_2	50.39	49.57	49.65	50.38	50.83	49.62	49.75	49.32	49.84	48.43
TiO_2	0.75	0.83	0.97	0.70	0.69	0.67	0.62	0.53	0.55	0.61
Al_2O_3	2.29	4.00	3.66	2.80	1.86	3.01	3.74	2.60	2.38	2.88
Cr_2O_3	0.00	0.01	0.01	0.01	0.00	0.00	0.01	0.00	0.00	0.02
Fe_2O_3	3.59	4.58	3.95	3.83	3.37	3.73	4.22	4.68	3.64	5.23
FeO	7.47	4.98	6.30	6.58	6.84	7.47	5.35	8.29	7.92	8.17
MnO	0.35	0.21	0.31	0.30	0.34	0.40	0.25	0.44	0.38	0.46
MgO	14.96	14.64	14.41	15.00	15.25	14.11	14.64	13.37	14.14	13.28
CaO	19.80	21.11	20.41	19.88	20.16	19.76	20.98	19.66	19.71	19.03
Na_2O	0.23	0.37	0.39	0.39	0.26	0.34	0.32	0.37	0.29	0.38
K_2O	0.00	0.00	0.00	0.00	0.00	0.00	0.00	0.00	0.00	0.00
NiO	0.01	0.00	0.00	0.01	0.01	0.01	0.01	0.00	0.00	0.02
Total	99.83	100.30	100.05	99.87	99.59	99.11	99.88	99.25	98.85	98.50
Si	1.90	1.86	1.87	1.90	1.92	1.89	1.87	1.89	1.91	1.88
Al	0.10	0.18	0.16	0.12	0.08	0.14	0.17	0.12	0.11	0.13
Fe(ii)	0.23	0.15	0.20	0.21	0.21	0.24	0.17	0.26	0.25	0.26
Fe(iii)	0.10	0.13	0.11	0.11	0.09	0.11	0.12	0.13	0.10	0.15
Cr	0.00	0.00	0.00	0.00	0.00	0.00	0.00	0.00	0.00	0.00
Ti	0.02	0.02	0.03	0.02	0.02	0.02	0.02	0.02	0.02	0.02
Mn	0.01	0.01	0.01	0.01	0.01	0.01	0.01	0.01	0.01	0.01
Mg	0.84	0.82	0.81	0.84	0.86	0.80	0.82	0.77	0.81	0.77
Ca	0.80	0.85	0.82	0.80	0.81	0.81	0.85	0.81	0.81	0.79
Na	0.02	0.03	0.03	0.03	0.02	0.03	0.02	0.03	0.02	0.03
Total	4.03	4.04	4.03	4.03	4.03	4.03	4.04	4.04	4.03	4.05
Wo	40.27	43.36	42.23	40.79	40.91	41.10	43.15	40.73	40.76	39.81
En	42.32	41.86	41.49	42.82	43.04	40.83	41.91	38.55	40.70	38.67
Fs	17.41	14.78	16.28	16.40	16.05	18.07	14.94	20.71	18.54	21.53

Sample	G41	G41	G41	G41	G44	G44	G44	G44	G44	G44
Grain	P1	P2	P2	P3	P1	P2	P3	P4	P5	P5
Position	C-M	M	R	M	R	M-R	R	M-R	C-M	R
SiO_2	50.09	51.33	49.70	50.06	51.15	50.61	52.39	51.43	49.79	49.46
TiO_2	0.66	0.48	0.69	0.73	0.52	0.57	0.42	0.48	0.62	0.72
Al_2O_3	2.58	2.62	3.54	3.69	1.75	3.53	1.88	1.54	2.71	4.06
Cr_2O_3	0.01	0.00	0.01	0.03	0.01	0.02	0.01	0.01	0.02	0.04
Fe_2O_3	4.27	3.18	3.83	3.64	2.35	2.67	1.52	2.66	3.31	3.68
FeO	6.78	6.46	6.76	6.90	9.65	6.71	8.77	8.88	9.27	5.85
MnO	0.35	0.27	0.31	0.31	0.49	0.30	0.36	0.45	0.40	0.28
MgO	15.14	15.67	14.27	14.54	14.52	14.86	16.00	15.16	13.61	14.55
CaO	19.50	19.98	20.12	20.18	18.95	20.44	18.91	19.10	19.14	20.71
Na_2O	0.30	0.34	0.38	0.33	0.29	0.29	0.25	0.24	0.35	0.26
K_2O	0.00	0.00	0.00	0.00	0.00	0.00	0.00	0.00	0.00	0.00
NiO	0.02	0.00	0.00	0.00	0.00	0.02	0.01	0.01	0.00	0.00
Total	99.69	100.32	99.60	100.41	99.67	100.02	100.51	99.96	99.23	99.61
Si	1.89	1.91	1.88	1.88	1.93	1.89	1.94	1.94	1.90	1.86
Al	0.12	0.12	0.16	0.16	0.08	0.16	0.08	0.07	0.12	0.18
Fe(ii)	0.21	0.20	0.21	0.21	0.30	0.21	0.27	0.28	0.29	0.18
Fe(iii)	0.12	0.09	0.11	0.10	0.07	0.07	0.04	0.07	0.09	0.10
Cr	0.00	0.00	0.00	0.00	0.00	0.00	0.00	0.00	0.00	0.00
Ti	0.02	0.01	0.02	0.02	0.01	0.02	0.01	0.01	0.02	0.02
Mn	0.01	0.01	0.01	0.01	0.02	0.01	0.01	0.01	0.01	0.01
Mg	0.85	0.87	0.80	0.81	0.82	0.83	0.88	0.85	0.77	0.82
Ca	0.79	0.80	0.81	0.81	0.77	0.82	0.75	0.77	0.78	0.84
Na	0.02	0.02	0.03	0.02	0.02	0.02	0.02	0.02	0.03	0.02
Total	4.04	4.03	4.03	4.03	4.02	4.02	4.01	4.02	4.03	4.03
Wo	39.76	40.60	41.81	41.59	38.92	42.22	38.32	38.75	39.98	42.91
En	42.95	44.29	41.28	41.68	41.52	42.69	45.12	42.80	39.54	41.95
Fs	17.29	15.10	16.91	16.73	19.57	15.09	16.57	18.45	20.48	15.14

Grain: P, phenocryst; GM, groundmass; INC, inclusion (mineral included within is stated in parentheses); *mantling orthopyroxene; GLOM, glomerocryst. XEN = xenolith
Spot: C, core; M, mid point (number indicates relative position along transect from core to rim); R, rim
Wo, wollastonite; En, enstatite; Fs, ferrosilite

Table D.2. Clinopyroxene mineral data continued

Sample	G48	G48	G48	G49	G49	G49	G49	G49	G49	G49
Grain	P1	P2	P3	GM	P1	P2	P2	P3	P4	P5
Position						M-R	R	C-M		
SiO_2	51.18	51.27	51.31	50.63	49.57	52.07	52.54	52.20	52.49	51.57
TiO_2	0.67	0.54	0.47	0.77	0.68	0.29	0.28	0.19	0.30	0.28
Al_2O_3	2.10	2.73	2.56	3.11	3.82	1.22	1.09	0.90	1.08	1.19
Cr_2O_3	0.02	0.02	0.00	0.00	0.00	0.00	0.03	0.02	0.00	0.01
Fe_2O_3	2.86	2.27	2.39	2.60	3.95	2.47	2.23	2.85	1.66	3.09
FeO	9.74	10.10	10.75	8.76	5.91	7.75	8.30	7.36	9.61	7.19
MnO	0.47	0.43	0.45	0.39	0.30	0.45	0.49	0.44	0.60	0.48
MgO	14.30	13.51	13.37	14.04	14.63	14.09	14.12	14.34	14.01	14.30
CaO	19.30	19.76	19.58	20.15	20.60	21.60	21.50	21.74	20.70	21.44
Na_2O	0.30	0.40	0.36	0.26	0.26	0.33	0.33	0.30	0.28	0.28
K_2O	0.00	0.00	0.00	0.01	0.00	0.00	0.01	0.00	0.00	0.00
NiO	0.02	0.00	0.01	0.00	0.00	0.00	0.00	0.00	0.00	0.01
Total	100.94	101.05	101.25	100.72	99.71	100.27	100.93	100.33	100.74	99.83
Si	1.92	1.92	1.92	1.89	1.87	1.95	1.96	1.96	1.96	1.95
Al	0.09	0.12	0.11	0.14	0.17	0.05	0.05	0.04	0.05	0.05
Fe(ii)	0.30	0.31	0.33	0.27	0.18	0.24	0.26	0.23	0.30	0.23
Fe(iii)	0.08	0.06	0.07	0.07	0.11	0.07	0.06	0.08	0.05	0.09
Cr	0.00	0.00	0.00	0.00	0.00	0.00	0.00	0.00	0.00	0.00
Ti	0.02	0.02	0.01	0.02	0.02	0.01	0.01	0.01	0.01	0.01
Mn	0.01	0.01	0.01	0.01	0.01	0.01	0.02	0.01	0.02	0.02
Mg	0.80	0.75	0.75	0.78	0.82	0.79	0.79	0.80	0.78	0.80
Ca	0.77	0.79	0.79	0.81	0.83	0.87	0.86	0.87	0.83	0.87
Na	0.02	0.03	0.03	0.02	0.02	0.02	0.02	0.02	0.02	0.02
Total	4.02	4.02	4.02	4.02	4.03	4.02	4.02	4.02	4.01	4.03
Wo	39.29	40.89	40.33	41.46	42.47	43.81	43.40	43.70	41.99	43.37
En	40.52	38.90	38.32	40.19	41.96	39.78	39.66	40.12	39.55	40.24
Fs	20.20	20.21	21.35	18.35	15.57	16.41	16.94	16.17	18.46	16.39

Sample	G49	G49	G49	G51 L	G51 L	G51 D	G51 D	G51 D	G51 D	G51 D
Grain	P6	GLOM	GLOM	P1	P1	P1	P1	P2	INC (OL)	P4
Position						M	R			
SiO_2	53.12	52.80	49.75	50.73	51.40	51.30	50.96	50.97	50.35	51.08
TiO_2	0.32	0.25	1.28	0.49	0.38	0.57	0.66	0.45	0.64	0.53
Al_2O_3	1.23	1.27	4.85	1.42	0.99	2.47	2.67	1.92	3.49	2.72
Cr_2O_3	0.01	0.00	0.01	0.00	0.01	0.02	0.00	0.01	0.14	0.00
Fe_2O_3	1.60	1.13	9.43	3.71	2.86	3.37	4.26	3.53	4.38	3.33
FeO	8.72	9.14	2.74	7.82	10.06	4.77	4.42	9.06	4.03	6.11
MnO	0.48	0.47	0.27	0.42	0.56	0.18	0.24	0.40	0.19	0.34
MgO	14.23	13.96	17.09	14.20	13.63	15.50	15.38	13.59	15.36	14.99
CaO	21.71	21.42	10.96	20.45	19.81	22.02	21.94	20.42	22.04	21.19
Na_2O	0.31	0.31	2.29	0.29	0.32	0.23	0.29	0.32	0.20	0.26
K_2O	0.00	0.00	0.82	0.00	0.00	0.00	0.00	0.00	0.00	0.00
NiO	0.02	0.00	0.00	0.02	0.02	0.00	0.01	0.01	0.00	0.00
Total	101.74	100.74	99.49	99.53	100.03	100.43	100.82	100.68	100.82	100.56
Si	1.96	1.97	1.87	1.93	1.95	1.91	1.89	1.92	1.87	1.90
Al	0.05	0.06	0.21	0.06	0.04	0.11	0.12	0.09	0.15	0.12
Fe(ii)	0.27	0.28	0.08	0.25	0.32	0.15	0.14	0.28	0.12	0.19
Fe(iii)	0.04	0.03	0.26	0.10	0.08	0.09	0.12	0.10	0.12	0.09
Cr	0.00	0.00	0.00	0.00	0.00	0.00	0.00	0.00	0.00	0.00
Ti	0.01	0.01	0.04	0.01	0.01	0.02	0.02	0.01	0.02	0.01
Mn	0.02	0.01	0.01	0.01	0.02	0.01	0.01	0.01	0.01	0.01
Mg	0.78	0.77	0.96	0.81	0.77	0.86	0.85	0.76	0.85	0.83
Ca	0.86	0.85	0.44	0.83	0.81	0.88	0.87	0.83	0.88	0.85
Na	0.02	0.02	0.17	0.02	0.02	0.02	0.02	0.02	0.01	0.02
Total	4.01	4.01	4.04	4.03	4.02	4.03	4.04	4.03	4.04	4.03
Wo	43.61	43.60	25.18	41.59	40.42	44.24	43.96	41.57	44.32	42.92
En	39.77	39.55	54.64	40.18	38.69	43.33	42.87	38.49	42.98	42.25
Fs	16.63	16.84	20.18	18.23	20.89	12.42	13.16	19.93	12.69	14.84

Grain: P, phenocryst; GM, groundmass; INC, inclusion (mineral included within is stated in parentheses); *mantling orthopyroxene; GLOM, glomerocryst. XEN = xenolith
Spot: C, core; M, mid point (number indicates relative position along transect from core to rim); R, rim
Wo, wollastonite; En, enstatite; Fs, ferrosilite

Table D.2. Clinopyroxene mineral data continued

Sample	G51 D	G51 D	S102	S102	S102	S102	S102(XEN)	S102(XEN)	S106B	S106B
Grain	P5	P1	P1*	P1*	P1*	P2	P1	P2	P1	P1
Position	R		M1	M2	R	R			R	M
SiO_2	49.15	51.50	51.59	50.48	51.24	50.91	52.38	52.78	49.92	50.27
TiO_2	0.91	0.41	0.34	0.44	0.37	0.38	0.35	0.49	0.68	0.56
Al_2O_3	3.81	1.81	1.20	1.99	1.47	1.53	1.75	1.83	3.42	2.86
Cr_2O_3	0.01	0.01	0.01	0.00	0.01	0.01	0.02	0.00	0.00	0.00
Fe_2O_3	4.76	3.64	3.59	4.12	3.70	3.14	1.21	0.79	4.23	4.25
FeO	4.31	6.00	8.20	8.02	7.36	8.70	11.52	9.63	6.79	5.34
MnO	0.20	0.34	0.57	0.58	0.50	0.55	0.62	0.48	0.35	0.29
MgO	14.36	15.88	14.36	13.54	15.54	13.37	13.46	15.15	15.10	15.25
CaO	21.91	20.60	20.41	20.31	19.48	20.68	19.64	19.64	19.28	20.49
Na_2O	0.30	0.20	0.32	0.43	0.23	0.35	0.36	0.27	0.33	0.33
K_2O	0.00	0.00	0.00	0.00	0.00	0.00	0.00	0.01	0.00	0.00
NiO	0.01	0.01	0.00	0.00	0.01	0.01	0.00	0.00	0.01	0.00
Total	99.72	100.40	100.59	99.91	99.91	99.61	101.31	101.07	100.11	99.64
Si	1.86	1.92	1.94	1.92	1.93	1.94	1.95	1.95	1.88	1.89
Al	0.17	0.08	0.05	0.09	0.07	0.07	0.08	0.08	0.15	0.13
Fe(ii)	0.13	0.19	0.26	0.25	0.23	0.28	0.36	0.30	0.21	0.17
Fe(iii)	0.13	0.10	0.10	0.12	0.10	0.09	0.03	0.02	0.12	0.12
Cr	0.00	0.00	0.00	0.00	0.00	0.00	0.00	0.00	0.00	0.00
Ti	0.03	0.01	0.01	0.01	0.01	0.01	0.01	0.01	0.02	0.02
Mn	0.01	0.01	0.02	0.02	0.02	0.02	0.02	0.02	0.01	0.01
Mg	0.81	0.88	0.81	0.77	0.87	0.76	0.75	0.83	0.85	0.86
Ca	0.89	0.82	0.82	0.83	0.79	0.84	0.78	0.78	0.78	0.83
Na	0.02	0.01	0.02	0.03	0.02	0.03	0.03	0.02	0.02	0.02
Total	4.04	4.03	4.03	4.04	4.03	4.03	4.01	4.01	4.04	4.04
Wo	44.99	41.07	41.07	41.72	39.15	42.51	40.34	39.94	39.54	41.79
En	41.05	44.06	40.22	38.71	43.45	38.24	38.49	42.89	43.10	43.30
Fs	13.96	14.86	18.71	19.56	17.40	19.25	21.17	17.17	17.36	14.91

Sample	S110B	S110B	S110B	S112	S112	S112	S112
Grain	P1	P2	P3	P1	P1	P2	P2
Position				M	R	C	R
SiO_2	50.64	51.01	51.13	50.99	50.36	50.48	48.17
TiO_2	0.70	0.68	0.63	0.26	0.51	0.52	1.21
Al_2O_3	2.21	2.17	1.98	1.07	1.89	1.80	4.92
Cr_2O_3	0.00	0.00	0.00	0.00	0.00	0.01	0.01
Fe_2O_3	3.65	3.55	3.77	3.97	4.20	4.08	4.34
FeO	9.05	8.95	8.61	7.85	7.51	8.90	7.57
MnO	0.47	0.45	0.44	0.51	0.47	0.47	0.39
MgO	14.33	14.19	14.54	13.70	13.95	13.54	13.34
CaO	19.26	19.70	19.65	21.13	20.67	20.15	19.83
Na_2O	0.31	0.36	0.34	0.29	0.29	0.32	0.33
K_2O	0.00	0.00	0.00	0.00	0.00	0.00	0.00
NiO	0.01	0.00	0.00	0.01	0.00	0.00	0.00
Total	100.61	101.06	101.07	99.78	99.84	100.26	100.10
Si	1.91	1.91	1.92	1.94	1.91	1.92	1.83
Al	0.10	0.10	0.09	0.05	0.08	0.08	0.22
Fe(ii)	0.28	0.28	0.27	0.25	0.24	0.28	0.24
Fe(iii)	0.10	0.10	0.11	0.11	0.12	0.12	0.12
Cr	0.00	0.00	0.00	0.00	0.00	0.00	0.00
Ti	0.02	0.02	0.02	0.01	0.01	0.01	0.03
Mn	0.02	0.01	0.01	0.02	0.02	0.02	0.01
Mg	0.80	0.79	0.81	0.78	0.79	0.77	0.75
Ca	0.78	0.79	0.79	0.86	0.84	0.82	0.81
Na	0.02	0.03	0.02	0.02	0.02	0.02	0.02
Total	4.03	4.03	4.03	4.03	4.04	4.04	4.04
Wo	39.21	40.04	39.69	42.75	42.03	41.05	41.69
En	40.59	40.13	40.86	38.58	39.47	38.38	39.02
Fs	20.20	19.82	19.46	18.67	18.50	20.57	19.29

Grain: P, phenocryst; GM, groundmass; INC, inclusion (mineral included within is stated in parentheses); *mantling orthopyroxene; GLOM, glomerocryst. XEN = xenolith
Spot: C, core; M, mid point (number indicates relative position along transect from core to rim); R, rim
Wo, wollastonite; En, enstatite; Fs, ferrosilite

Table D.3. Orthopyroxene mineral data

Sample	G11	G11	G11	G17	G17	G17	G17	G22	G22	G22
Grain	P1	P2	P3	P1	P2	P3	P4	P1	P2	P3
Position								C	C	R
SiO_2	51.99	50.98	52.82	51.58	51.87	51.21	50.51	53.36	52.95	52.34
TiO_2	0.29	0.29	0.19	0.27	0.21	0.22	0.28	0.21	0.17	0.26
Al_2O_3	1.33	1.48	0.93	1.06	0.93	1.04	1.65	0.75	0.64	1.30
Cr_2O_3	0.00	0.00	0.00	0.00	0.00	0.01	0.01	0.00	0.00	0.00
Fe_2O_3	1.74	3.13	1.25	2.74	2.60	3.52	3.35	1.90	2.36	1.97
FeO	21.36	20.73	22.73	18.91	18.36	19.45	21.47	16.85	16.39	17.69
MnO	0.71	0.66	0.80	0.80	0.79	0.89	0.73	0.52	0.56	0.62
MgO	21.33	20.98	21.24	22.49	23.15	21.98	20.26	24.95	24.96	23.85
CaO	1.62	1.74	1.46	1.57	1.39	1.46	1.65	1.62	1.53	1.43
Na_2O	0.05	0.04	0.01	0.02	0.00	0.01	0.04	0.01	0.01	0.04
K_2O	0.00	0.00	0.00	0.00	0.00	0.01	0.00	0.00	0.00	0.00
NiO	0.01	0.00	0.01	0.01	0.02	0.00	0.01	0.00	0.00	0.01
Total	100.43	100.04	101.43	99.43	99.30	99.78	99.97	100.17	99.57	99.50
Si	1.95	1.93	1.96	1.94	1.95	1.94	1.92	1.96	1.96	1.95
Al	0.06	0.07	0.04	0.05	0.04	0.05	0.07	0.03	0.03	0.06
Fe(ii)	0.67	0.65	0.70	0.59	0.57	0.61	0.68	0.52	0.50	0.55
Fe(iii)	0.05	0.09	0.03	0.08	0.07	0.10	0.10	0.05	0.07	0.05
Cr	0.00	0.00	0.00	0.00	0.00	0.00	0.00	0.00	0.00	0.00
Ti	0.01	0.01	0.01	0.01	0.01	0.01	0.01	0.01	0.00	0.01
Mn	0.02	0.02	0.03	0.03	0.03	0.03	0.02	0.02	0.02	0.02
Mg	1.19	1.18	1.18	1.26	1.30	1.24	1.15	1.37	1.38	1.32
Ca	0.07	0.07	0.06	0.06	0.06	0.06	0.07	0.06	0.06	0.06
Na	0.00	0.00	0.00	0.00	0.00	0.00	0.00	0.00	0.00	0.00
Total	4.01	4.02	4.01	4.02	4.02	4.03	4.03	4.02	4.02	4.02
Wo	3.27	3.51	2.91	3.13	2.76	2.90	3.34	3.17	3.00	2.84
En	59.75	58.74	58.87	62.51	64.07	60.86	57.10	67.85	67.99	66.08
Fs	36.98	37.76	38.23	34.36	33.17	36.23	39.56	28.98	29.00	31.08

Sample	G22	G23	G23	G23	G24	G24	G24	G24	G24	G27
Grain	P4	P1	P1	P4	P1* (cpx P1)	P2* (cpx P2)	P3	P4	P5	P1
Position	M	C	R	R	C	C				M
SiO_2	53.36	51.84	52.24	52.62	52.88	51.21	52.95	52.21	51.69	51.19
TiO_2	0.20	0.32	0.26	0.28	0.16	0.33	0.23	0.29	0.33	0.31
Al_2O_3	0.58	1.06	0.91	1.37	0.73	1.96	0.98	1.90	1.55	1.38
Cr_2O_3	0.00	0.00	0.00	0.01	0.00	0.00	0.01	0.00	0.02	0.00
Fe_2O_3	1.39	2.38	1.21	2.11	2.07	3.74	1.84	2.48	3.52	3.59
FeO	17.66	18.39	20.60	16.21	18.34	16.28	18.72	16.91	15.43	16.83
MnO	0.62	0.65	0.68	0.54	0.71	0.63	0.71	0.61	0.62	0.70
MgO	24.46	23.07	22.15	24.81	23.58	23.66	23.42	24.02	24.38	23.31
CaO	1.60	1.52	1.51	1.64	1.65	1.78	1.77	1.76	1.86	1.80
Na_2O	0.01	0.03	0.00	0.02	0.04	0.03	0.01	0.02	0.05	0.02
K_2O	0.00	0.00	0.00	0.00	0.00	0.00	0.00	0.00	0.00	0.00
NiO	0.02	0.00	0.01	0.00	0.00	0.00	0.00	0.00	0.00	0.01
Total	99.89	99.27	99.57	99.61	100.14	99.61	100.65	100.21	99.44	99.15
Si	1.97	1.96	1.91	1.94	1.96	1.91	1.96	1.93	1.93	1.93
Al	0.03	0.04	0.27	0.06	0.03	0.09	0.04	0.08	0.07	0.06
Fe(ii)	0.54	0.64	0.75	0.50	0.57	0.50	0.58	0.52	0.48	0.53
Fe(iii)	0.04	0.03	0.00	0.06	0.06	0.10	0.05	0.07	0.10	0.10
Cr	0.00	0.00	0.00	0.00	0.00	0.00	0.00	0.00	0.00	0.00
Ti	0.01	0.01	0.01	0.01	0.00	0.01	0.01	0.01	0.01	0.01
Mn	0.02	0.02	0.02	0.02	0.02	0.02	0.02	0.02	0.02	0.02
Mg	1.35	1.24	0.90	1.37	1.30	1.32	1.29	1.32	1.35	1.31
Ca	0.06	0.06	0.08	0.07	0.07	0.07	0.07	0.07	0.07	0.07
Na	0.00	0.00	0.00	0.00	0.00	0.00	0.00	0.00	0.00	0.00
Total	4.01	4.01	3.95	4.02	4.02	4.03	4.01	4.02	4.03	4.03
Wo	3.14	3.04	3.03	3.25	3.25	3.54	3.49	3.49	3.67	3.58
En	66.96	64.11	61.96	68.15	64.71	65.32	64.21	66.16	66.95	64.46
Fs	29.90	32.85	35.00	28.60	32.04	31.15	32.30	30.35	29.38	31.96

Grain: P, phenocryst; GM, groundmass; INC, inclusion (mineral included within is stated in parentheses); *mantling orthopyroxene; GLOM, glomerocryst. XEN = xenolith
Spot: C, core; M, mid point (number indicates relative position along transect from core to rim); R, rim
Wo, wollastonite; En, enstatite; Fs, ferrosilite

Table D.3. Orthopyroxene mineral data continued

Sample	G27	G27	G27	G27	G27	G37A	G37A	G37A	G37A	G37A
Grain	P1	P2	P3	P4	P5	P1	P1	P2	P3	P4
Position	R					M	R			
SiO_2	52.94	51.62	51.43	52.23	52.72	50.76	52.45	52.26	52.62	51.87
TiO_2	0.22	0.32	0.29	0.21	0.28	0.30	0.27	0.25	0.28	0.29
Al_2O_3	0.85	1.49	1.28	0.74	1.09	1.50	1.32	0.90	1.12	1.68
Cr_2O_3	0.00	0.00	0.00	0.00	0.00	0.02	0.00	0.00	0.01	0.00
Fe_2O_3	2.06	3.11	3.95	2.75	1.70	3.70	2.40	2.75	2.23	2.14
FeO	17.21	16.99	16.23	17.01	18.29	19.34	16.78	17.67	18.39	19.09
MnO	0.69	0.64	0.75	0.70	0.74	0.68	0.59	0.71	0.70	0.60
MgO	24.24	23.53	23.69	23.88	23.42	21.64	24.35	23.67	23.44	22.69
CaO	1.76	1.76	1.91	1.71	1.89	1.71	1.57	1.59	1.61	1.58
Na_2O	0.02	0.04	0.02	0.04	0.02	0.04	0.03	0.02	0.05	0.03
K_2O	0.00	0.00	0.00	0.00	0.00	0.00	0.00	0.00	0.00	0.00
NiO	0.02	0.00	0.01	0.01	0.01	0.01	0.00	0.00	0.00	0.00
Total	100.02	99.50	99.57	99.27	100.16	99.69	99.76	99.81	100.46	99.96
Si	1.96	1.93	1.93	1.95	1.95	1.92	1.94	1.95	1.95	1.94
Al	0.04	0.07	0.06	0.03	0.05	0.07	0.06	0.04	0.05	0.07
Fe(ii)	0.53	0.53	0.50	0.53	0.56	0.61	0.52	0.55	0.57	0.59
Fe(iii)	0.06	0.09	0.11	0.08	0.05	0.10	0.07	0.08	0.06	0.06
Cr	0.00	0.00	0.00	0.00	0.00	0.00	0.00	0.00	0.00	0.00
Ti	0.01	0.01	0.01	0.01	0.01	0.01	0.01	0.01	0.01	0.01
Mn	0.02	0.02	0.02	0.02	0.02	0.02	0.02	0.02	0.02	0.02
Mg	1.34	1.31	1.32	1.33	1.29	1.22	1.34	1.32	1.29	1.26
Ca	0.07	0.07	0.08	0.07	0.08	0.07	0.06	0.06	0.06	0.06
Na	0.00	0.00	0.00	0.00	0.00	0.00	0.00	0.00	0.00	0.00
Total	4.02	4.02	4.03	4.02	4.01	4.03	4.02	4.02	4.02	4.02
Wo	3.47	3.49	3.77	3.38	3.75	3.42	3.10	3.14	3.17	3.16
En	66.33	65.05	64.92	65.67	64.57	60.35	66.94	64.95	64.43	63.21
Fs	30.20	31.46	31.31	30.95	31.68	36.23	29.96	31.92	32.39	33.63

Sample	G37A	G37A	G40	G40	G40	G40	G40	G40	G40	G40
Grain	P5	P6	P1	P2	GM	P3	P4	P4	P5	P6
Position							R	C	M	
SiO_2	52.21	51.91	51.30	51.45	51.14	50.57	51.59	50.35	49.96	52.30
TiO_2	0.31	0.26	0.21	0.18	0.32	0.24	0.19	0.25	0.26	0.30
Al_2O_3	1.21	0.98	0.59	0.89	1.06	1.66	1.76	1.36	1.56	1.06
Cr_2O_3	0.01	0.01	0.00	0.00	0.00	0.01	0.00	0.01	0.02	0.00
Fe_2O_3	2.10	3.06	3.26	2.62	3.46	3.85	2.81	4.01	4.38	2.17
FeO	18.82	17.54	17.97	21.13	17.03	19.15	17.89	20.14	19.60	18.57
MnO	0.71	0.71	0.78	0.85	0.71	0.76	0.74	0.80	0.71	0.72
MgO	22.87	23.48	22.65	21.03	22.66	21.65	21.71	20.94	20.99	23.10
CaO	1.78	1.60	1.79	1.57	2.45	1.58	2.18	1.57	1.58	1.73
Na_2O	0.03	0.03	0.02	0.04	0.03	0.03	0.37	0.03	0.05	0.03
K_2O	0.00	0.00	0.00	0.00	0.00	0.00	0.01	0.00	0.00	0.00
NiO	0.03	0.00	0.00	0.00	0.01	0.02	0.00	0.00	0.03	0.00
Total	100.05	99.57	98.56	99.77	98.88	99.52	99.25	99.47	99.12	99.99
Si	1.95	1.94	1.95	1.95	1.94	1.92	1.94	1.92	1.92	1.95
Al	0.05	0.04	0.03	0.04	0.05	0.07	0.08	0.06	0.07	0.05
Fe(ii)	0.58	0.55	0.57	0.67	0.53	0.60	0.56	0.64	0.62	0.58
Fe(iii)	0.06	0.09	0.09	0.07	0.10	0.11	0.08	0.11	0.13	0.06
Cr	0.00	0.00	0.00	0.00	0.00	0.00	0.00	0.00	0.00	0.00
Ti	0.01	0.01	0.01	0.01	0.01	0.01	0.01	0.01	0.01	0.01
Mn	0.02	0.02	0.03	0.03	0.02	0.02	0.02	0.03	0.02	0.02
Mg	1.27	1.31	1.28	1.19	1.28	1.23	1.22	1.19	1.20	1.28
Ca	0.07	0.06	0.07	0.06	0.10	0.06	0.09	0.06	0.06	0.07
Na	0.00	0.00	0.00	0.00	0.00	0.00	0.03	0.00	0.00	0.00
Total	4.02	4.02	4.03	4.02	4.03	4.03	4.02	4.03	4.03	4.02
Wo	3.53	3.16	3.57	3.16	4.88	3.16	4.46	3.15	3.18	3.44
En	63.34	64.63	62.88	58.85	62.90	60.50	61.91	58.64	58.97	63.81
Fs	33.12	32.22	33.54	38.00	32.22	36.34	33.63	38.22	37.84	32.76

Grain: P, phenocryst; GM, groundmass; INC, inclusion (mineral included within is stated in parentheses); *mantling orthopyroxene; GLOM, glomerocryst. XEN = xenolith
Spot: C, core; M, mid point (number indicates relative position along transect from core to rim); R, rim
Wo, wollastonite; En, enstatite; Fs, ferrosilite

Table D.3. Orthopyroxene mineral data continued

Sample	G41	G41	G41	G41	G44	G44	G44	G44	G44	G44
Grain	P1	P2	P3	P4	P1	P1	INC (CPX)	P2	P3	P3
Position					C-M	R			M-R	R
SiO_2	53.25	52.94	52.18	52.11	53.60	53.37	53.31	52.78	52.13	53.61
TiO_2	0.29	0.36	0.32	0.35	0.23	0.25	0.29	0.34	0.32	0.26
Al_2O_3	1.73	1.58	1.59	1.42	1.40	1.97	1.51	1.12	1.21	1.80
Cr_2O_3	0.01	0.01	0.00	0.03	0.01	0.00	0.00	0.00	0.00	0.00
Fe_2O_3	1.68	1.48	2.93	2.67	0.76	1.22	2.12	1.33	2.70	1.43
FeO	16.26	17.73	16.02	16.24	18.11	16.13	15.22	19.10	17.20	15.77
MnO	0.52	0.59	0.51	0.52	0.51	0.46	0.50	0.73	0.59	0.48
MgO	25.15	24.02	24.46	24.34	24.49	25.55	25.89	22.99	23.72	25.92
CaO	1.68	1.81	1.89	1.84	1.50	1.35	1.59	1.88	1.86	1.38
Na_2O	0.04	0.03	0.03	0.02	0.02	0.04	0.02	0.04	0.04	0.02
K_2O	0.00	0.00	0.00	0.00	0.00	0.00	0.00	0.00	0.00	0.00
NiO	0.01	0.02	0.01	0.00	0.00	0.03	0.02	0.00	0.01	0.00
Total	100.61	100.57	99.94	99.54	100.62	100.36	100.48	100.31	99.78	100.68
Si	1.94	1.94	1.93	1.93	1.96	1.94	1.94	1.96	1.94	1.94
Al	0.07	0.07	0.07	0.06	0.06	0.08	0.06	0.05	0.05	0.08
Fe(ii)	0.49	0.54	0.49	0.50	0.55	0.49	0.46	0.59	0.53	0.48
Fe(iii)	0.05	0.04	0.08	0.07	0.02	0.03	0.06	0.04	0.08	0.04
Cr	0.00	0.00	0.00	0.00	0.00	0.00	0.00	0.00	0.00	0.00
Ti	0.01	0.01	0.01	0.01	0.01	0.01	0.01	0.01	0.01	0.01
Mn	0.02	0.02	0.02	0.02	0.02	0.01	0.02	0.02	0.02	0.01
Mg	1.37	1.31	1.35	1.35	1.33	1.39	1.41	1.27	1.32	1.40
Ca	0.07	0.07	0.07	0.07	0.06	0.05	0.06	0.07	0.07	0.05
Na	0.00	0.00	0.00	0.00	0.00	0.00	0.00	0.00	0.00	0.00
Total	4.01	4.01	4.02	4.02	4.01	4.01	4.02	4.01	4.02	4.01
Wo	3.30	3.58	3.72	3.64	2.96	2.66	3.09	3.75	3.68	2.69
En	68.75	66.15	67.01	66.95	67.32	70.16	70.21	63.67	65.29	70.59
Fs	27.95	30.27	29.27	29.40	29.72	27.18	26.70	32.58	31.04	26.72

Sample	G48	G48	G48	G48	G49	G49	G49	G49	G49	G49
Grain	P1	P2	P3	P4	GM	P1	P2	P2	P3	P4
Position										
SiO_2	52.57	54.04	52.52	53.05	53.11	52.90	52.16	52.42	52.36	53.14
TiO_2	0.28	0.21	0.31	0.29	0.17	0.23	0.09	0.13	0.16	0.17
Al_2O_3	1.30	0.62	0.80	0.80	0.41	0.96	0.38	0.43	0.63	0.55
Cr_2O_3	0.02	0.00	0.02	0.00	0.04	0.00	0.00	0.00	0.00	0.04
Fe_2O_3	2.05	0.32	1.97	1.01	0.00	0.00	2.09	2.09	1.31	0.63
FeO	17.48	19.87	19.98	21.15	23.44	23.05	20.77	21.26	21.96	22.23
MnO	0.60	0.65	0.64	0.74	0.89	0.85	0.97	0.92	0.98	0.94
MgO	24.00	23.51	22.48	21.88	20.77	20.94	21.94	21.85	21.48	21.88
CaO	1.53	1.76	1.76	2.02	1.43	1.46	1.13	1.16	1.11	1.14
Na_2O	0.06	0.03	0.03	0.05	0.03	0.01	0.03	0.04	0.02	0.01
K_2O	0.00	0.00	0.00	0.00	0.01	0.00	0.00	0.00	0.00	0.00
NiO	0.00	0.01	0.00	0.00	0.01	0.01	0.03	0.00	0.00	0.00
Total	99.88	101.02	100.50	100.99	100.31	100.41	99.58	100.30	100.00	100.75
Si	1.95	1.98	1.96	1.97	1.99	1.98	1.97	1.97	1.97	1.98
Al	0.06	0.03	0.04	0.04	0.02	0.04	0.02	0.02	0.03	0.02
Fe(ii)	0.54	0.61	0.62	0.65	0.74	0.72	0.65	0.66	0.69	0.69
Fe(iii)	0.06	0.01	0.05	0.03	0.00	0.00	0.06	0.06	0.04	0.02
Cr	0.00	0.00	0.00	0.00	0.00	0.00	0.00	0.00	0.00	0.00
Ti	0.01	0.01	0.01	0.01	0.00	0.01	0.00	0.00	0.00	0.00
Mn	0.02	0.02	0.02	0.02	0.03	0.03	0.03	0.03	0.03	0.03
Mg	1.32	1.28	1.25	1.21	1.16	1.17	1.24	1.22	1.20	1.21
Ca	0.06	0.07	0.07	0.08	0.06	0.06	0.05	0.05	0.04	0.05
Na	0.00	0.00	0.00	0.00	0.00	0.00	0.00	0.00	0.00	0.00
Total	4.02	4.00	4.02	4.01	4.00	4.00	4.02	4.02	4.01	4.00
Wo	3.04	3.47	3.50	4.01	2.89	2.97	2.26	2.30	2.23	2.27
En	66.24	64.50	61.99	60.62	58.57	59.12	61.05	60.49	60.05	60.78
Fs	30.72	32.02	34.51	35.37	38.53	37.91	36.70	37.21	37.72	36.95

Grain: P, phenocryst; GM, groundmass; INC, inclusion (mineral included within is stated in parentheses);
*mantling orthopyroxene; GLOM, glomerocryst. XEN = xenolith
Spot: C, core; M, mid point (number indicates relative position along transect from core to rim); R, rim
Wo, wollastonite; En, enstatite; Fs, ferrosilite

Table D.3. Orthopyroxene mineral data continued

Sample	G49	G49	G51 L	G51 L	S102	S102	S102	S102	S102	S102(XEN)
Grain	GLOM	GLOM	P1	P2	P1	P1	P2	P2	P1*	P1
Position					C	R			C	
SiO_2	52.58	53.26	51.47	51.07	51.68	50.82	50.98	52.27	51.33	51.88
TiO_2	0.11	0.12	0.26	0.37	0.21	0.22	0.25	0.16	0.21	0.19
Al_2O_3	0.54	0.54	1.14	0.92	1.00	0.65	0.71	0.66	0.98	1.23
Cr_2O_3	0.00	0.00	0.01	0.01	0.00	0.00	0.00	0.00	0.01	0.02
Fe_2O_3	1.26	0.31	2.49	2.06	2.67	2.70	2.29	2.29	2.64	2.18
FeO	21.86	22.90	21.83	21.41	21.43	22.96	22.61	21.14	21.56	20.81
MnO	0.91	0.95	0.88	0.79	1.02	1.13	1.06	1.03	0.96	0.92
MgO	21.66	21.56	20.77	20.51	21.00	19.64	19.91	21.56	20.81	21.54
CaO	1.10	1.08	1.43	1.95	1.46	1.44	1.44	1.52	1.43	1.49
Na_2O	0.03	0.03	0.04	0.03	0.04	0.00	0.04	0.02	0.02	0.03
K_2O	0.00	0.00	0.00	0.00	0.01	0.00	0.00	0.00	0.00	0.00
NiO	0.01	0.00	0.03	0.01	0.01	0.01	0.00	0.00	0.00	0.00
Total	100.07	100.74	100.34	99.12	100.52	99.57	99.27	100.64	99.96	100.30
Si	1.97	1.98	1.95	1.95	1.95	1.95	1.96	1.96	1.95	1.95
Al	0.02	0.02	0.05	0.04	0.04	0.03	0.03	0.03	0.04	0.05
Fe(ii)	0.68	0.71	0.69	0.68	0.67	0.73	0.72	0.66	0.68	0.65
Fe(iii)	0.04	0.01	0.07	0.06	0.08	0.08	0.07	0.06	0.08	0.06
Cr	0.00	0.00	0.00	0.00	0.00	0.00	0.00	0.00	0.00	0.00
Ti	0.00	0.00	0.01	0.01	0.01	0.01	0.01	0.00	0.01	0.01
Mn	0.03	0.03	0.03	0.03	0.03	0.04	0.03	0.03	0.03	0.03
Mg	1.21	1.20	1.17	1.17	1.18	1.13	1.14	1.21	1.18	1.21
Ca	0.04	0.04	0.06	0.08	0.06	0.06	0.06	0.06	0.06	0.06
Na	0.00	0.00	0.00	0.00	0.00	0.00	0.00	0.00	0.00	0.00
Total	4.01	4.00	4.02	4.02	4.02	4.02	4.02	4.02	4.02	4.02
Wo	2.21	2.16	2.88	3.97	2.92	2.91	2.93	3.02	2.88	2.99
En	60.45	60.11	58.14	58.03	58.48	55.38	56.39	59.60	58.24	60.10
Fs	37.33	37.73	38.98	38.00	38.60	41.71	40.68	37.39	38.88	36.91

Sample	S102(XEN)	S102(XEN)	S102(XEN)	S106B	S106B	S106B	S106B	S106B	S106B	S110B
Grain	P2	P3	P4	P1	P1	P2	P2	P3	P3	P1
Position				C	R	C	R	M	R	
SiO_2	52.80	53.37	53.27	51.78	52.71	52.59	52.04	51.82	53.12	52.09
TiO_2	0.16	0.22	0.26	0.31	0.32	0.35	0.29	0.36	0.24	0.36
Al_2O_3	0.67	0.65	1.02	2.35	2.09	2.35	1.71	2.46	1.15	1.06
Cr_2O_3	0.00	0.02	0.00	0.00	0.00	0.01	0.00	0.00	0.01	0.00
Fe_2O_3	1.08	1.37	1.55	3.03	1.73	1.69	2.24	2.71	2.12	2.06
FeO	23.18	17.88	18.38	15.37	16.50	16.56	17.04	15.81	16.10	20.07
MnO	1.11	0.63	0.75	0.55	0.48	0.52	0.56	0.54	0.57	0.72
MgO	20.78	24.24	24.10	24.61	24.80	24.53	23.87	24.49	25.04	22.08
CaO	1.47	1.69	1.33	1.71	1.63	1.73	1.69	1.71	1.73	1.83
Na_2O	0.01	0.03	0.03	0.04	0.01	0.04	0.03	0.02	0.04	0.02
K_2O	0.00	0.00	0.00	0.01	0.00	0.00	0.01	0.00	0.00	0.00
NiO	0.00	0.00	0.00	0.01	0.00	0.01	0.00	0.01	0.00	0.01
Total	101.25	100.09	100.68	99.77	100.27	100.38	99.47	99.92	100.10	100.31
Si	1.97	1.97	1.96	1.91	1.93	1.93	1.93	1.91	1.95	1.95
Al	0.03	0.03	0.04	0.10	0.09	0.10	0.07	0.11	0.05	0.05
Fe(ii)	0.72	0.55	0.56	0.47	0.50	0.51	0.53	0.48	0.49	0.62
Fe(iii)	0.03	0.04	0.04	0.08	0.05	0.05	0.06	0.07	0.06	0.06
Cr	0.00	0.00	0.00	0.00	0.00	0.00	0.00	0.00	0.00	0.00
Ti	0.00	0.01	0.01	0.01	0.01	0.01	0.01	0.01	0.01	0.01
Mn	0.04	0.02	0.02	0.02	0.01	0.02	0.02	0.02	0.02	0.02
Mg	1.16	1.33	1.32	1.36	1.35	1.34	1.32	1.35	1.37	1.23
Ca	0.06	0.07	0.05	0.07	0.06	0.07	0.07	0.07	0.07	0.07
Na	0.00	0.00	0.00	0.00	0.00	0.00	0.00	0.00	0.00	0.00
Total	4.01	4.01	4.01	4.02	4.01	4.01	4.02	4.02	4.02	4.02
Wo	2.93	3.33	2.62	3.39	3.22	3.43	3.37	3.39	3.39	3.64
En	57.76	66.41	65.97	67.92	68.25	67.82	66.24	67.67	68.31	61.26
Fs	39.31	30.26	31.41	28.69	28.53	28.75	30.39	28.94	28.29	35.10

Grain: P, phenocryst; GM, groundmass; INC, inclusion (mineral included within is stated in parentheses);
*mantling orthopyroxene; GLOM, glomerocryst. XEN = xenolith
Spot: C, core; M, mid point (number indicates relative position along transect from core to rim); R, rim
Wo, wollastonite; En, enstatite; Fs, ferrosilite

Table D.3. Orthopyroxene mineral data continued

Sample	S110B	S110B	S110B	S112	S112	S112	S112	S112
Grain	P1	P2	P3	P4	P1	P2	P2	P3
Position						C	R	
SiO_2	51.93	51.54	52.13	51.80	52.00	52.25	51.53	51.75
TiO_2	0.40	0.38	0.36	0.32	0.23	0.23	0.22	0.23
Al_2O_3	1.20	1.27	1.09	1.21	0.82	0.88	0.72	0.86
Cr_2O_3	0.01	0.01	0.00	0.00	0.00	0.01	0.00	0.00
Fe_2O_3	1.81	2.38	2.11	2.44	2.24	2.26	2.94	2.63
FeO	20.13	19.72	19.73	20.75	19.56	20.91	20.43	19.77
MnO	0.68	0.66	0.75	0.73	0.74	0.70	0.86	0.71
MgO	21.97	21.89	22.26	21.56	22.51	21.76	21.62	22.11
CaO	1.83	1.88	1.81	1.71	1.44	1.67	1.43	1.67
Na_2O	0.03	0.03	0.04	0.03	0.02	0.03	0.03	0.01
K_2O	0.00	0.00	0.00	0.00	0.00	0.00	0.00	0.00
NiO	0.00	0.00	0.00	0.00	0.00	0.00	0.01	0.02
Total	99.99	99.77	100.28	100.55	99.56	100.70	99.78	99.76
Si	1.95	1.94	1.95	1.94	1.96	1.95	1.95	1.95
Al	0.05	0.06	0.05	0.05	0.04	0.04	0.03	0.04
Fe(ii)	0.63	0.62	0.61	0.65	0.61	0.65	0.64	0.62
Fe(iii)	0.05	0.07	0.06	0.07	0.06	0.06	0.08	0.07
Cr	0.00	0.00	0.00	0.00	0.00	0.00	0.00	0.00
Ti	0.01	0.01	0.01	0.01	0.01	0.01	0.01	0.01
Mn	0.02	0.02	0.02	0.02	0.02	0.02	0.03	0.02
Mg	1.23	1.23	1.24	1.21	1.26	1.21	1.22	1.24
Ca	0.07	0.08	0.07	0.07	0.06	0.07	0.06	0.07
Na	0.00	0.00	0.00	0.00	0.00	0.00	0.00	0.00
Total	4.01	4.02	4.02	4.02	4.02	4.02	4.02	4.02
Wo	3.68	3.77	3.61	3.42	2.88	3.31	2.86	3.34
En	61.33	61.13	61.73	59.89	62.53	60.18	60.07	61.32
Fs	35.00	35.10	34.66	36.69	34.59	36.51	37.07	35.34

Grain: P, phenocryst; GM, groundmass; INC, inclusion (mineral included within is stated in parentheses); *mantling orthopyroxene; GLOM, glomerocryst. XEN = xenolith
Spot: C, core; M, mid point (number indicates relative position along transect from core to rim); R, rim
Wo, wollastonite; En, enstatite; Fs, ferrosilite

Table D.4. Olivine mineral data

Sample	G01B	G01B	G01B	G01B	G23	G26	G26	G26	G26	G26
Grain	P1	P1	P2	P3	P1	P1	P2	P2	P3	P4
Position	C	R	C				C	R		C
SiO_2	36.25	36.67	36.72	36.86	36.96	34.87	34.73	35.38	35.65	35.30
TiO_2	0.02	0.02	0.02	0.02	0.02	0.02	0.02	0.03	0.02	0.02
Al_2O_3	0.00	0.00	0.00	0.00	0.00	0.00	0.00	0.00	0.00	0.00
Cr_2O_3	0.00	0.00	0.01	0.01	0.00	0.00	0.00	0.00	0.00	0.00
MgO	36.13	36.15	35.82	36.01	35.29	26.44	27.00	27.12	31.85	27.74
CaO	0.11	0.13	0.13	0.12	0.14	0.20	0.18	0.17	0.15	0.16
MnO	0.51	0.50	0.51	0.54	0.54	0.82	0.86	0.86	0.68	0.82
FeO	26.57	27.06	26.79	26.30	27.54	37.43	37.44	38.15	31.94	36.17
NiO	0.02	0.01	0.01	0.03	0.00	0.01	0.00	0.01	0.01	0.04
Na_2O	0.02	0.02	0.00	0.02	0.00	0.02	0.00	0.00	0.01	0.00
K_2O	0.00	0.00	0.00	0.00	0.00	0.00	0.00	0.00	0.00	0.00
Total	99.63	100.56	100.00	99.88	100.50	99.80	100.23	101.71	100.32	100.24
Si	0.97	0.98	0.98	0.98	0.99	0.99	0.98	0.98	0.98	0.99
Al	0.00	0.00	0.00	0.00	0.00	0.00	0.00	0.00	0.00	0.00
Fe(ii)	0.60	0.60	0.60	0.59	0.61	0.89	0.88	0.89	0.73	0.85
Mn	0.01	0.01	0.01	0.01	0.01	0.02	0.02	0.02	0.02	0.02
Mg	1.45	1.43	1.43	1.43	1.40	1.12	1.14	1.12	1.30	1.16
Ca	0.00	0.00	0.00	0.00	0.00	0.01	0.01	0.01	0.00	0.00
Total	3.03	3.03	3.02	3.02	3.02	3.02	3.02	3.02	3.03	3.02
Fo	70.8	70.4	70.5	70.9	69.6	55.7	56.2	55.9	64.0	57.8
Fa	29.2	29.6	29.5	29.1	30.4	44.3	43.8	44.1	36.0	42.2
Sample	G26	G30	G30	G35	G35	G35	G51 D	S106B	S106B	S106B
Grain	P4	P1	P2	P1	P2	P3	P1	INC	P1	P2
Position	R								M	M
SiO_2	34.40	36.02	35.39	34.98	35.69	36.07	37.42	36.27	35.28	35.09
TiO_2	0.04	0.01	0.02	0.02	0.02	0.02	0.03	0.01	0.04	0.02
Al_2O_3	0.00	0.00	0.00	0.00	0.00	0.00	0.00	0.00	0.00	0.00
Cr_2O_3	0.02	0.00	0.00	0.00	0.00	0.01	0.01	0.00	0.00	0.00
MgO	26.80	33.48	30.56	29.75	31.14	32.77	36.18	32.79	28.36	27.32
CaO	0.19	0.17	0.15	0.21	0.19	0.23	0.14	0.17	0.19	0.19
MnO	0.86	0.53	0.58	0.67	0.64	0.59	0.42	0.58	0.81	0.82
FeO	37.26	29.83	32.65	33.88	32.41	30.74	26.38	29.60	35.56	36.65
NiO	0.01	0.01	0.00	0.02	0.01	0.02	0.01	0.01	0.00	0.01
Na_2O	0.01	0.00	0.03	0.04	0.00	0.01	0.02	0.01	0.02	0.01
K_2O	0.00	0.00	0.00	0.00	0.00	0.00	0.00	0.00	0.00	0.00
Total	99.59	100.06	99.39	99.58	100.11	100.45	100.61	99.44	100.24	100.10
Si	0.98	0.98	0.98	0.98	0.98	0.98	0.99	0.99	0.98	0.99
Al	0.00	0.00	0.00	0.00	0.00	0.00	0.00	0.00	0.00	0.00
Fe(ii)	0.89	0.68	0.76	0.79	0.75	0.70	0.58	0.67	0.83	0.86
Mn	0.02	0.01	0.01	0.02	0.01	0.01	0.01	0.01	0.02	0.02
Mg	1.14	1.35	1.26	1.24	1.28	1.33	1.43	1.33	1.18	1.14
Ca	0.01	0.01	0.00	0.01	0.01	0.01	0.00	0.00	0.01	0.01
Total	3.03	3.03	3.02	3.03	3.02	3.03	3.01	3.02	3.02	3.02
Fo	56.2	66.7	62.5	61.0	63.1	65.5	71.0	66.39	58.71	57.06
Fa	43.8	33.3	37.5	39.0	36.9	34.5	29.0	33.61	41.29	42.94

Grain: P, phenocryst; GM, groundmass; INC, inclusion
Spot: C, core; M, mid point (number indicates relative position along transect from core to rim); R, rim
Fo, forsterite; Fa, fayalite

Table D.4. Oivine mineral data continued

Sample	S111	S111	S111	S111	S111	S111	S111
Grain	P1	P2	P3	P4	P5	P6	P7
Position					R	M	
SiO_2	34.90	35.14	36.42	35.50	35.91	37.17	36.46
TiO_2	0.01	0.05	0.04	0.04	0.02	0.00	0.02
Al_2O_3	0.00	0.00	0.00	0.00	0.00	0.00	0.00
Cr_2O_3	0.01	0.00	0.01	0.00	0.05	0.01	0.03
MgO	26.21	25.64	29.66	27.76	27.87	32.56	28.50
CaO	0.20	0.22	0.18	0.20	0.19	0.18	0.20
MnO	0.82	0.82	0.71	0.79	0.75	0.62	0.75
FeO	38.26	38.66	33.94	36.29	36.14	30.96	35.52
NiO	0.01	0.04	0.03	0.02	0.01	0.01	0.01
Na_2O	0.00	0.00	0.00	0.05	0.01	0.04	0.00
K_2O	0.00	0.00	0.00	0.00	0.00	0.00	0.00
Total	100.42	100.56	100.99	100.65	100.94	101.53	101.48
Si	0.99	0.99	1.00	0.99	1.00	1.00	1.00
Al	0.00	0.00	0.00	0.00	0.00	0.00	0.00
Fe(ii)	0.90	0.91	0.78	0.85	0.84	0.69	0.81
Mn	0.02	0.02	0.02	0.02	0.02	0.01	0.02
Mg	1.10	1.08	1.21	1.15	1.15	1.30	1.17
Ca	0.01	0.01	0.01	0.01	0.01	0.01	0.01
Total	3.02	3.01	3.01	3.01	3.01	3.01	3.00
Fo	55.0	54.2	60.9	57.7	57.9	65.2	58.9
Fa	45.0	45.8	39.1	42.3	42.1	34.8	41.1

Grain: P, phenocryst; GM, groundmass; INC, inclusion
Spot: C, core; M, mid point (number indicates relative position along transect from core to rim); R, rim
Fo, forsterite; Fa, fayalite

Table D.5. Fe-Ti oxide mineral data

Sample	G01B	G01B	G01B	G01B	G01B	G11	G11	G11	G17	G17
Grain	INC	GM	P1	P1	P2	P1	P2	P3	INC (OPX)	P1
Position			C	R						
SiO_2	0.03	0.07	0.06	0.05	0.02	0.05	0.06	0.07	0.06	0.06
TiO_2	10.22	10.44	10.51	10.50	10.83	12.18	11.34	10.72	11.28	12.22
Al_2O_3	4.63	4.26	4.31	4.25	4.26	2.28	2.98	3.15	2.48	1.30
Cr_2O_3	0.19	0.09	0.11	0.13	0.14	0.09	0.08	0.06	0.04	0.09
Fe_2O_3	45.61	44.64	44.48	44.77	44.50	43.39	44.12	45.10	44.79	43.05
FeO	35.17	35.32	35.40	35.42	35.96	38.40	38.10	36.40	39.41	40.91
MnO	0.42	0.36	0.31	0.40	0.37	0.44	0.44	0.38	0.50	0.46
MgO	3.76	3.53	3.61	3.56	3.53	2.45	2.24	2.88	1.36	0.59
CaO	0.02	0.07	0.00	0.02	0.00	0.00	0.01	0.05	0.00	0.01
Total	100.05	98.77	98.79	99.09	99.60	99.28	99.37	98.81	99.92	98.68
Si	0.01	0.02	0.02	0.01	0.01	0.02	0.02	0.02	0.02	0.02
Ti	2.22	2.30	2.32	2.31	2.37	2.72	2.53	2.39	2.53	2.80
Al	1.58	1.47	1.49	1.47	1.46	0.80	1.04	1.10	0.87	0.47
Cr	0.04	0.02	0.03	0.03	0.03	0.02	0.02	0.01	0.01	0.02
Fe(iii)	9.92	9.86	9.82	9.86	9.75	9.70	9.84	10.06	10.03	9.87
Fe(ii)	8.50	8.67	8.68	8.67	8.76	9.54	9.45	9.03	9.81	10.43
Mn	0.10	0.09	0.08	0.10	0.09	0.11	0.11	0.09	0.13	0.12
Mg	1.62	1.54	1.58	1.55	1.53	1.09	0.99	1.27	0.60	0.27
Ca	0.01	0.02	0.00	0.01	0.00	0.00	0.00	0.02	0.00	0.00
Total	24.00	24.00	24.00	24.00	24.00	24.00	24.00	24.00	24.00	24.00
TiO_2	11.23	11.54	11.62	11.57	11.86	12.97	12.12	11.63	11.81	12.70
Fe_2O_3	50.12	49.38	49.22	49.37	48.75	46.17	47.16	48.90	46.91	44.76
FeO	38.65	39.08	39.16	39.06	39.39	40.86	40.72	39.47	41.28	42.54

Sample	G22	G22	G22	G23	G23	G23	G23	G24	G24	G24
Grain	P1	INC (OPX)	P2	GM	GM	INC (CPX)	INC	P1	GM	P2
Position	C		C							
SiO_2	0.03	0.05	0.04	0.05	0.04	0.08	0.08	0.07	0.06	0.06
TiO_2	11.80	10.90	11.02	8.62	8.74	11.55	10.26	11.68	12.97	11.21
Al_2O_3	2.86	3.10	3.03	5.50	5.54	4.04	4.09	3.19	2.35	3.41
Cr_2O_3	0.04	0.06	0.06	0.07	0.08	0.07	0.06	0.06	0.08	0.05
Fe_2O_3	43.44	44.56	44.54	46.71	47.00	43.28	45.43	42.92	40.44	43.54
FeO	38.98	37.71	39.04	33.27	33.65	37.10	35.03	38.57	39.50	38.16
MnO	0.48	0.36	0.51	0.30	0.29	0.36	0.31	0.46	0.50	0.49
MgO	1.91	2.19	1.40	3.89	3.90	3.19	3.64	2.10	1.86	2.06
CaO	0.00	0.02	0.07	0.05	0.02	0.12	0.12	0.00	0.04	0.00
Total	99.54	98.96	99.70	98.44	99.27	99.79	99.02	99.05	97.80	98.97
Si	0.01	0.02	0.01	0.02	0.01	0.02	0.02	0.02	0.02	0.02
Ti	2.63	2.44	2.47	1.90	1.91	2.53	2.26	2.61	2.95	2.51
Al	1.00	1.09	1.06	1.89	1.89	1.39	1.41	1.12	0.84	1.19
Cr	0.01	0.02	0.01	0.02	0.02	0.02	0.01	0.01	0.02	0.01
Fe(iii)	9.70	9.98	9.97	10.27	10.25	9.49	10.01	9.60	9.20	9.74
Fe(ii)	9.68	9.39	9.71	8.13	8.16	9.04	8.58	9.59	9.99	9.49
Mn	0.12	0.09	0.13	0.07	0.07	0.09	0.08	0.11	0.13	0.12
Mg	0.85	0.97	0.62	1.69	1.68	1.39	1.59	0.93	0.84	0.91
Ca	0.00	0.01	0.02	0.01	0.01	0.04	0.04	0.00	0.01	0.00
Total	24.00	24.00	24.00	24.00	24.00	24.00	24.00	24.00	24.00	24.00
TiO_2	12.52	11.70	11.65	9.73	9.78	12.56	11.31	12.54	13.96	12.06
Fe_2O_3	46.11	47.82	47.08	52.72	52.57	47.08	50.08	46.07	43.52	46.86
FeO	41.37	40.48	41.27	37.55	37.64	40.36	38.61	41.40	42.52	41.07

Grain: P, phenocryst; GM, groundmass; GLOM, glomerocryst; INC, inclusion (mineral included within is stated in parentheses) XEN = xenolith
Spot: C, core; M, mid point (number indicates relative position along transect from core to rim); R, rim

Table D.5. Fe-Ti oxide mineral data continued

Sample	G26	G26	G26	G27	G27	G27	G27	G30	G30	G30
Grain	INC (CPX)	P1	P2	P1	GM	P2	P3	INC (CPX)	P1	P1
Position									C	R
SiO_2	0.06	0.07	0.05	0.09	0.08	0.08	0.07	0.07	0.07	0.05
TiO_2	10.04	11.43	11.65	11.52	16.58	11.11	11.27	11.72	12.80	12.86
Al_2O_3	4.21	3.90	3.70	3.80	1.43	4.20	4.55	5.57	4.76	4.72
Cr_2O_3	0.06	0.05	0.03	0.07	0.04	0.07	0.04	0.18	0.08	0.09
Fe_2O_3	46.26	42.78	42.90	43.04	34.70	43.09	42.82	41.65	39.64	39.82
FeO	34.90	39.13	39.39	38.05	44.49	37.98	37.56	36.34	39.05	39.26
MnO	0.38	0.45	0.41	0.50	0.59	0.50	0.45	0.38	0.40	0.51
MgO	3.77	1.78	1.78	2.50	0.85	2.29	2.75	4.08	2.78	2.67
CaO	0.01	0.00	0.00	0.00	0.04	0.00	0.00	0.00	0.00	0.01
Total	99.69	99.58	99.91	99.56	98.82	99.31	99.51	99.97	99.59	99.99
Si	0.02	0.02	0.01	0.02	0.03	0.02	0.02	0.02	0.02	0.01
Ti	2.19	2.54	2.58	2.55	3.77	2.46	2.48	2.53	2.81	2.81
Al	1.44	1.36	1.29	1.32	0.51	1.46	1.57	1.88	1.63	1.62
Cr	0.01	0.01	0.01	0.02	0.01	0.02	0.01	0.04	0.02	0.02
Fe(iii)	10.12	9.51	9.52	9.52	7.89	9.55	9.43	8.98	8.69	8.71
Fe(ii)	8.48	9.67	9.71	9.35	11.25	9.36	9.19	8.71	9.52	9.54
Mn	0.09	0.11	0.10	0.12	0.15	0.13	0.11	0.09	0.10	0.12
Mg	1.63	0.78	0.78	1.10	0.38	1.00	1.20	1.74	1.21	1.16
Ca	0.00	0.00	0.00	0.00	0.01	0.00	0.00	0.00	0.00	0.00
Total	24.00	24.00	24.00	24.00	24.00	24.00	24.00	24.00	24.00	24.00
TiO_2	11.00	12.25	12.40	12.44	17.31	12.05	12.29	13.06	13.99	13.99
Fe_2O_3	50.72	45.83	45.67	46.47	36.23	46.75	46.73	46.43	43.33	43.31
FeO	38.27	41.92	41.93	41.08	46.46	41.20	40.98	40.51	42.68	42.70

Sample	G30	G30	G35	G35	G37A	G37A	G40	G40	G41	G41
Grain	P2	GM	P1	P2	P1	P2	P1	P2	P1	GM
Position										
SiO_2	0.08	0.02	0.04	0.04	0.06	0.08	0.05	0.05	0.07	0.08
TiO_2	11.66	12.18	15.23	18.48	11.01	11.39	12.37	12.47	10.26	13.28
Al_2O_3	5.30	0.85	0.99	1.39	3.52	3.51	2.36	2.31	4.59	2.35
Cr_2O_3	0.10	0.02	0.08	0.10	0.08	0.07	0.07	0.11	0.06	0.11
Fe_2O_3	40.93	43.37	38.32	31.65	44.49	43.51	42.10	42.21	44.72	40.91
FeO	38.12	41.11	44.05	45.34	36.76	37.44	40.71	40.13	35.65	39.76
MnO	0.37	0.40	0.40	0.50	0.42	0.41	0.53	0.46	0.39	0.47
MgO	2.73	0.29	0.57	1.55	2.97	2.76	0.99	1.48	3.35	2.19
CaO	0.00	0.04	0.00	0.00	0.00	0.00	0.00	0.00	0.00	0.04
Total	99.28	98.26	99.68	99.04	99.30	99.18	99.19	99.22	99.08	99.18
Si	0.02	0.00	0.01	0.01	0.02	0.02	0.02	0.02	0.02	0.02
Ti	2.56	2.82	3.45	4.16	2.44	2.53	2.80	2.81	2.26	2.97
Al	1.82	0.31	0.35	0.49	1.22	1.22	0.84	0.82	1.58	0.83
Cr	0.02	0.01	0.02	0.02	0.02	0.02	0.02	0.02	0.01	0.03
Fe(iii)	8.99	10.04	8.70	7.14	9.85	9.66	9.52	9.51	9.85	9.16
Fe(ii)	9.30	10.58	11.11	11.36	9.05	9.24	10.23	10.05	8.72	9.89
Mn	0.09	0.10	0.10	0.13	0.10	0.10	0.13	0.12	0.10	0.12
Mg	1.19	0.13	0.26	0.69	1.30	1.21	0.44	0.66	1.46	0.97
Ca	0.00	0.01	0.00	0.00	0.00	0.00	0.00	0.00	0.00	0.01
Total	24.00	24.00	24.00	24.00	24.00	24.00	24.00	24.00	24.00	24.00
TiO_2	12.85	12.60	15.60	19.36	11.94	12.34	12.99	13.15	11.32	14.14
Fe_2O_3	45.12	44.87	39.27	33.16	48.22	47.12	44.23	44.52	49.35	43.54
FeO	42.03	42.53	45.13	47.49	39.84	40.54	42.77	42.33	39.33	42.32

Grain: P, phenocryst; GM, groundmass; GLOM, glomerocryst; INC, inclusion (mineral included within is stated in parentheses) XEN = xenolith
Spot: C, core; M, mid point (number indicates relative position along transect from core to rim); R, rim

Table D.5. Fe-Ti oxide mineral data continued

Sample	G41	G44	G44	G48	G48	G48	G49	G49	G49	G49
Grain Position	P2	P1	P2	P1	INC	GM	GM	P1	GM2	P2
SiO_2	0.07	0.09	0.07	0.00	0.00	0.05	0.18	0.04	0.04	0.04
TiO_2	10.13	9.83	9.99	0.97	10.87	3.03	14.21	13.60	13.07	11.20
Al_2O_3	4.84	4.53	4.36	2.76	1.69	1.34	0.75	1.00	0.86	2.25
Cr_2O_3	0.09	0.11	0.10	0.09	0.13	0.03	0.09	0.08	0.08	0.08
Fe_2O_3	44.61	45.33	45.52	64.86	46.56	60.95	37.80	41.37	41.79	44.49
FeO	35.98	35.64	35.78	27.68	37.64	32.02	42.18	41.97	41.27	39.75
MnO	0.36	0.37	0.37	0.79	0.37	0.21	0.55	0.62	0.65	0.48
MgO	3.12	3.10	3.14	2.47	2.09	0.92	0.42	0.73	0.60	0.93
CaO	0.00	0.00	0.00	0.04	0.01	0.06	0.06	0.00	0.04	0.00
Total	99.20	99.00	99.33	99.66	99.36	98.60	96.23	99.42	98.39	99.22
Si	0.02	0.03	0.02	0.00	0.00	0.02	0.06	0.01	0.01	0.01
Ti	2.23	2.17	2.20	0.22	2.45	0.70	3.34	3.09	3.01	2.54
Al	1.67	1.57	1.50	0.97	0.60	0.48	0.28	0.36	0.31	0.80
Cr	0.02	0.03	0.02	0.02	0.03	0.01	0.02	0.02	0.02	0.02
Fe(iii)	9.81	10.01	10.03	14.57	10.48	14.08	8.90	9.41	9.63	10.08
Fe(ii)	8.80	8.75	8.76	6.91	9.42	8.22	11.04	10.61	10.57	10.01
Mn	0.09	0.09	0.09	0.20	0.09	0.05	0.15	0.16	0.17	0.12
Mg	1.36	1.36	1.37	1.10	0.93	0.42	0.20	0.33	0.27	0.42
Ca	0.00	0.00	0.00	0.01	0.00	0.02	0.02	0.00	0.01	0.00
Total	24.00	24.00	24.00	24.00	24.00	24.00	24.00	24.00	24.00	24.00
TiO_2	11.17	10.82	10.94	1.04	11.43	3.15	15.08	14.03	13.60	11.74
Fe_2O_3	49.17	49.92	49.86	69.36	48.97	63.49	40.14	42.68	43.47	46.61
FeO	39.66	39.25	39.19	29.60	39.59	33.35	44.78	43.30	42.93	41.65

Sample	G49	G51 L	G51 D	G51 D	G51 D	G51 D	S102	S102	S102(XEN)	S102(XEN)
Grain Position	GLOM	P1	P1 C	P1 R	P2	GM	P1	P2	P1	P2
SiO_2	0.04	0.03	0.01	0.04	0.03	0.04	0.10	0.06	0.05	0.11
TiO_2	12.27	13.44	12.92	12.86	10.58	10.58	11.64	12.85	9.68	46.52
Al_2O_3	0.88	1.52	1.40	1.42	4.37	4.28	2.41	2.09	2.84	0.05
Cr_2O_3	0.07	0.03	0.07	0.07	0.10	0.12	0.02	0.01	0.06	0.00
Fe_2O_3	43.94	42.66	43.18	42.64	45.66	45.58	43.53	41.30	47.13	0.00
FeO	41.00	41.51	40.78	40.50	36.00	36.02	39.58	40.24	37.59	46.67
MnO	0.46	0.48	0.53	0.54	0.37	0.39	0.52	0.62	0.48	1.26
MgO	0.63	1.43	1.34	1.32	3.57	3.53	1.33	1.37	1.50	1.63
CaO	0.01	0.00	0.00	0.04	0.03	0.00	0.00	0.02	0.00	0.19
Total	99.29	101.11	100.22	99.43	100.70	100.53	99.12	98.55	99.32	96.42
Si	0.01	0.01	0.00	0.01	0.01	0.01	0.03	0.02	0.01	0.04
Ti	2.80	2.98	2.90	2.91	2.29	2.30	2.63	2.92	2.18	10.78
Al	0.32	0.53	0.49	0.50	1.48	1.46	0.85	0.74	1.00	0.02
Cr	0.02	0.01	0.02	0.02	0.02	0.03	0.00	0.00	0.01	0.00
Fe(iii)	10.04	9.47	9.69	9.64	9.89	9.90	9.83	9.38	10.61	0.00
Fe(ii)	10.41	10.24	10.17	10.18	8.67	8.69	9.93	10.16	9.40	12.03
Mn	0.12	0.12	0.13	0.14	0.09	0.09	0.13	0.16	0.12	0.33
Mg	0.29	0.63	0.60	0.59	1.53	1.52	0.59	0.62	0.67	0.75
Ca	0.00	0.00	0.00	0.01	0.01	0.00	0.00	0.01	0.00	0.06
Total	24.00	24.00	24.00	24.00	24.00	24.00	24.00	24.00	24.00	24.00
TiO_2	12.62	13.77	13.33	13.40	11.47	11.48	12.29	13.62	10.25	49.92
Fe_2O_3	45.20	43.71	44.57	44.41	49.50	49.45	45.94	43.75	49.93	0.00
FeO	42.18	42.52	42.10	42.19	39.03	39.07	41.77	42.63	39.82	50.08

Grain: P, phenocryst; GM, groundmass; GLOM, glomerocryst; INC, inclusion (mineral included within is stated in parentheses) XEN = xenolith
Spot: C, core; M, mid point (number indicates relative position along transect from core to rim); R, rim

Table D.5. Fe-Ti oxide mineral data continued

Sample	S106B	S106B	S106B	S110B	S110B	S110B	S111	S111	S111	S112
Grain	P1	P2	P3	INC	P1	P2	P1	P2	P3	P1
Position	C	C								
SiO_2	0.08	0.07	0.07	0.08	0.07	0.08	0.07	0.10	0.05	0.05
TiO_2	11.05	11.32	15.56	15.95	18.18	15.03	10.29	12.77	11.18	13.32
Al_2O_3	4.24	3.66	1.85	3.11	2.46	2.69	4.37	2.74	3.66	2.53
Cr_2O_3	0.03	0.05	0.07	0.01	0.04	0.03	0.16	0.24	0.14	0.03
Fe_2O_3	43.72	43.25	37.35	34.37	31.46	37.93	44.32	41.08	43.62	41.14
FeO	37.57	38.13	42.54	41.35	45.19	42.08	37.46	39.94	38.31	41.53
MnO	0.43	0.44	0.47	0.51	0.58	0.59	0.40	0.42	0.42	0.51
MgO	2.67	2.25	1.82	2.61	1.68	1.96	2.19	1.89	2.11	1.31
CaO	0.00	0.00	0.03	0.02	0.00	0.03	0.00	0.01	0.00	0.01
Total	99.79	99.15	99.75	98.00	99.66	100.42	99.26	99.19	99.48	100.42
Si	0.02	0.02	0.02	0.02	0.02	0.02	0.02	0.03	0.01	0.02
Ti	2.43	2.52	3.47	3.58	4.05	3.32	2.28	2.86	2.49	2.96
Al	1.46	1.28	0.65	1.09	0.86	0.93	1.52	0.96	1.27	0.88
Cr	0.01	0.01	0.02	0.00	0.01	0.01	0.04	0.06	0.03	0.01
Fe(iii)	9.62	9.63	8.35	7.71	7.00	8.38	9.84	9.20	9.70	9.16
Fe(ii)	9.19	9.44	10.56	10.31	11.18	10.33	9.24	9.94	9.46	10.27
Mn	0.11	0.11	0.12	0.13	0.14	0.15	0.10	0.11	0.10	0.13
Mg	1.16	0.99	0.81	1.16	0.74	0.86	0.96	0.84	0.93	0.58
Ca	0.00	0.00	0.01	0.01	0.00	0.01	0.00	0.00	0.00	0.00
Total	24.00	24.00	24.00	24.00	24.00	24.00	24.00	24.00	24.00	24.00
TiO_2	11.97	12.21	16.30	17.40	19.17	15.82	11.17	13.61	12.01	13.88
Fe_2O_3	47.35	46.66	39.14	37.50	33.17	39.90	48.14	43.80	46.85	42.86
FeO	40.69	41.13	44.57	45.11	47.65	44.28	40.69	42.58	41.14	43.26

Sample	S112	S112	S112	S112
Grain	P2	P3	P4	P4
Position			C	R
SiO_2	0.05	0.03	0.06	0.04
TiO_2	13.78	13.52	13.45	13.46
Al_2O_3	2.34	2.39	2.44	2.48
Cr_2O_3	0.02	0.04	0.02	0.03
Fe_2O_3	41.01	40.57	40.16	40.84
FeO	41.56	40.31	40.31	40.79
MnO	0.58	0.52	0.49	0.49
MgO	1.60	1.94	1.86	1.77
CaO	0.00	0.05	0.00	0.00
Total	100.93	99.37	98.79	99.90
Si	0.01	0.01	0.02	0.01
Ti	3.05	3.03	3.03	3.00
Al	0.81	0.84	0.86	0.87
Cr	0.01	0.01	0.00	0.01
Fe(iii)	9.07	9.08	9.04	9.10
Fe(ii)	10.21	10.03	10.09	10.11
Mn	0.14	0.13	0.12	0.12
Mg	0.70	0.86	0.83	0.78
Ca	0.00	0.01	0.00	0.00
Total	24.00	24.00	24.00	24.00
TiO_2	14.30	14.32	14.32	14.15
Fe_2O_3	42.56	42.98	42.76	42.95
FeO	43.14	42.70	42.92	42.90

Grain: P, phenocryst; GM, groundmass; GLOM, glomerocryst; INC, inclusion (mineral included within is stated in parentheses) XEN = xenolith
Spot: C, core; M, mid point (number indicates relative position along transect from core to rim); R, rim

Appendix E. Analytical techniques

E.1. Preparation of whole-rock powders

Samples from IVC, Merapi and Guntur were provided as rock powders by J. Baker and J. Gamble, R. Gertisser and R. Hall respectively. The following method was used to obtain powdered samples of GVC and Salak volcanic rocks collected in this study.

Rock samples of 1-2kg were sawn into smaller blocks to remove weathered edges and visible xenoliths. Any saw marks remaining on the rocks were removed with graphite paper and samples were then cleaned with de-ionised water. The blocks were broken into chips less than 1cm using a Fritsch stainless steel jaw crusher and any visible xenoliths were removed from the samples. Each sample was divided into two using the 'cone and quartering' technique. One half of the sample was powdered in an agate ball mill for approximately 30 minutes. All equipment was thoroughly cleaned prior to use and between each sample.

E.2. Major element Analysis

Major element contents of GVC and Salak samples were determined on fused glass discs produced by the Fusion method (spectroflux 105) using the Automated Philips PW2404 X-ray fluorescence spectrometer at the University of Edinburgh.

Approximately 5g of powdered rock sample was dried overnight at 110°C to eliminate moisture. 0.8-0.9g of the dried sample was then added to a platinum crucible of which the mass had been accurately recorded. The combined mass of the crucible and rock powder was then noted. The sample was covered with a platinum lid and ignited in a furnace at 1100°C for 20 minutes. After cooling, the crucible was reweighed and the loss on ignition calculated. Flux (spectroflux 105) was added at five times the weight of the ignited sample plus 0.03g extra to compensate for loss of volatiles from the flux. The sample was then mixed into the flux with a clean spatula. The sample and flux were fused at 1100°C for 20mins, removed

from the furnace and swirled to ensure the sample had completely dissolved in the flux. After cooling, the sample was reweighed and a small amount of flux was added to obtain a 5:1 flux to sample ratio ±0.0003g. The flux-sample mixture was fused in the crucible over a burner for 3 minutes, swirled thoroughly, placed on burner for another 2 minutes, swirled again and immediately cast on a hot plate at 220°C. The sample was left to anneal under a glass cover for 5 minutes. When cool, the glass disc was removed from the hotplate and any excess glass was trimmed with pliers. The sample was labelled on the back of the fused disc, placed in a self-sealing polythene bag and stored in dessicator. Machine calibration was achieved and data quality monitored by running in-house rock standards.

E.3. Mineral analysis

Mineral analyses were performed on carbon-coated polished slides of selected rock samples of GVC and Salak volcanic rocks using a Cameca SX 100 at the NERC facility, University of Manchester. The accelerating voltage was 15kV, and the beam current was 2nA. Detection limits for Al, Mg, K, Ca, Ti are 0.01 or lower, Na, Si, Cr, Ni are around 0.03, while Fe is slightly higher around 0.08. Element precision is dependant on the mineral being analysed, but was typically less than 1% for Ca, Ti, Si, Al, Mg. Between 1-2% for Fe, 2.7% for Ni and around 4% for Na, K, Mn and Cr.

E.4. Trace element Analysis

Trace element concentrations were determined on the PerkinElmer ELAN 6000 quadrupole ICP-MS at the University of Durham. Full details of the analytical procedure and instrument operating conditions are given by Ottley et al. (2003); a summary is presented here. Samples were processed in batches of 30, including several blanks and internal rock standards in each batch. 0.1g ± 0.001 of powdered rock sample was placed in a Teflon beaker to which a 1:4

HNO_3-HF mixture was added. The beakers were then sealed and placed on a hot plate (150°C) for at least 24 hours, followed by evaporation and then repeat additions and dry-downs of HNO_3 to ensure removal of HF. 2.5ml of 16N HNO_3 was added to each beaker and was diluted with approximately 10mls of MilliQ H_2O. The samples were then spiked with 1ml of 1pmm Re-1ppm Rh solution. This solution was diluted in 50mls followed by a 1:10 dilution prior to analysis, resulting in an overall dilution of 1:5000.

The sample solution was introduced into the plasma using a cross-flow nebuliser assembly and a Scott double-pass spray chamber at an uptake rate of ~ 1 ml per minute. Sample analysis began 50 seconds after initial uptake. In between samples the instrument aspirated a 3% HNO_3 wash solution for 3 minutes. Data was acquired by peak hopping, with dwell times between 10-60ms, depending on individual elemental detection limits (Ottley et al., 2003). The mass spectrum swept 25 times for each reading and two replicate readings were obtained for each analysis.

Calibration of the ELAN was achieved during each session via the use of in-house standards and international reference materials: W2, BHVO-1, AGV1, BE-N and BIR1 together with procedural blanks (3 per batch). Accuracy of the analytical method was good, as shown by the good agreement of analyses with those of international standards (Table E.1). Total procedural blanks were typically low and maximum blank concentrations (n = 70) are displayed in Table E.1. Multiple analyses of blanks and standards during each session, e.g. at the start, mid-way, and at the end of a run, allowed any drift in the instrument calibration to be detected. Table E.2 shows sample reproducibility, measured by replicate analysis of an internal rock standard, KI 202. Comparisons between XRF (Sitorus, 1990) and ICP-MS (this study) measurements for Zr in IVC volcanic rocks are shown in Fig. E.1 The XRF and ICP-MS data show excellent agreement suggesting that dissolution of accessory minerals, such as zircon, was successful during sample preparation for ICP-MS analysis.

Table E.1. Accepted element abundances of international rock standards compared to those measured in this study

	BIR1			W2			BHVO-1			AGV1		
	Accepted	This study		Accepted	This study		Accepted	This study		Accepted	This study	
PPM	value	value (n = 26)	1SD	value	value (n = 13)	1SD	value	value (n = 23)	1SD	value	value (n = 12)	1SD
Sc	44	43	4.70	35	36	1	31.8	31	2	12.1	12	1
Ti (wt%)	0.96	0.97	0.08	1.06	1.07	0.07	2.71	2.79	0.12	1.06	1.03	0.06
V	313	334	16.60	262	272	8	317	319	10	123	121	4
Cr	382	418.4	25.2	93	92.5	3.4	289	295.1	8.5	12	7.0	3.4
Mn (wt%)	0.171	0.18	0.01	0.163	0.17	0.01	0.168	0.17	0.01	0.096	0.10	0.01
Co	51.4	55	2	44	45	1	45	45	1	15.1	16	0
Ni	166	199.8	8.2	70	81.4	2.1	121	134.7	3.4	17	16.7	0.7
Cu	126	120	5	103	104	3	136	138	3	60	58	2
Zn	71	69	8	77	84	27	105	108	5	88	84	3
Ga	16	15	1	20	18	0	21	21	1	20	20	0
Rb	0.27	0.2	0.0	20	20.2	0.4	11	9.5	0.2	67	67.2	1.2
Sr	108	110	12	194	201	9	403	391	22	662	676	32
Y	16	16	1	24	23	0	27.6	28	0	21	20	0
Zr	22	15	0	94	91	2	179	175	2	225	229	3
Nb	2	0.57	0.02	7.9	7.66	0.09	19	19.39	0.18	15	14.52	0.14
Cs	0.45	0.00	0.02	0.99	0.89	0.04	0.13	0.10	0.03	1.26	1.24	0.04
Ba	7.7	7	0	182	177	4	139	138	3	1221	1219	25
La	0.88	0.6	0.0	11.4	10.8	0.2	15.8	15.6	0.3	38	37.9	0.7
Ce	2.5	1.9	0.0	24	23.4	0.4	39	37.8	0.6	66	66.8	1.2
Pr	0.5	0.38	0.01	5.9	3.18	0.04	5.7	5.62	0.09	6.5	8.65	0.19
Nd	2.5	2.5	0.1	14	13.9	0.2	25.2	26.3	0.4	34	33.2	0.6
Sm	1.08	1.11	0.04	3.25	3.38	0.04	6.2	6.31	0.10	5.9	5.85	0.12
Eu	0.54	0.51	0.02	1.1	1.11	0.01	2.06	2.07	0.03	1.66	1.68	0.03
Gd	1.9	1.94	0.04	3.6	3.86	0.06	6.4	6.55	0.13	5.2	4.83	0.10
Tb	0.41	0.38	0.01	0.63	0.65	0.01	0.96	0.98	0.01	0.71	0.67	0.01
Dy	2.4	2.54	0.08	3.8	3.87	0.06	5.2	5.33	0.07	3.8	3.53	0.06
Ho	0.5	0.57	0.02	0.76	0.80	0.01	0.99	1.00	0.01	0.73	0.67	0.01
Er	1.8	1.62	0.06	2.5	2.15	0.02	2.4	2.43	0.02	1.61	1.73	0.03
Tm	0.27	0.27	0.01	0.38	0.34	0.01	0.33	0.35	0.01	0.32	0.27	0.01
Yb	1.7	1.64	0.07	2.05	2.07	0.02	2.02	2.01	0.02	1.67	1.65	0.03
Lu	0.26	0.27	0.01	0.33	0.33	0.00	0.291	0.30	0.00	0.28	0.27	0.01
Hf	0.58	0.59	0.02	2.56	2.42	0.04	4.38	4.47	0.04	5.1	5.12	0.09
Ta	0.062	0.05	0.01	0.5	0.50	0.01	1.23	1.26	0.01	0.92	0.91	0.01
tot Pb	3.2	3.2	0.3	9.3	7.9	0.2	2.6	2.2	0.1	36	35.7	0.7
Th	0.031	0.03	0.00	2.2	2.21	0.07	1.08	1.26	0.03	6.5	6.34	0.20
U	0.01	0.01	0.00	0.53	0.49	0.01	0.42	0.42	0.01	1.89	1.87	0.06

	BE-N			NBS688			detection	detection	maximum blank
	Accepted	This study		Accepted	This study		limit	limit	measured
PPM	value	value (n = 11)	1SD	value	value (n = 14)	1SD	solid ng g^{-1}	soln pg ml^{-1}	(n = 70, ppm)
Sc	22	23	1	38	38	2	212	42	1
Ti (wt%)	2.61	2.66	0.13	1.17	1.16	0.07	6380	1280	0.00
V	235	233	9	242	252	8	273	55	0
Cr	360	368.1	15.6	332	333.1	11.7	532	106	1.6
Mn (wt%)	0.2	0	0	0.167	0	0	231	46	0
Co	61	62	2	49	49	2	19.5	3.9	0
Ni	267	300.9	10.4	158	173.4	5.5	897	179	0.6
Cu	72	72	3	96	87	3	128	26	0
Zn	120	121	4	84	79	13			65
Ga	17	18	1	17	16	0	34.3	6.9	0
Rb	47	48.2	1.5	1.91	2.0	0.1	13.4	2.7	0.0
Sr	1370	1538	138	169.2	174	7	43	0.64	0
Y	30	31	1	17	21	0	20.9	4.2	0
Zr	265	273	5	61	56	1	25.2	5	3
Nb	100	117.56	1.49	5	4.33	0.06	9.72	1.9	0.02
Cs	0.8	0.75	0.04	0.24	0.02	0.04	3.79	0.8	0.05
Ba	1025	1059	24	200	178	4	111	22	3
La	82	82.1	1.6	5.3	5.3	0.1	3.73	0.75	0.0
Ce	152	147.9	2.2	13	12.0	0.2	12.2	2.4	0.0
Pr	16.9	17.96	0.35	2.4	1.82	0.03	2.57	0.51	0.03
Nd	70	69.9	1.1	9.6	8.9	0.1	13.2	2.6	0.0
Sm	12	12.42	0.21	2.5	2.44	0.03	2.84	0.57	0.05
Eu	3.6	3.72	0.04	1.01	0.99	0.01	1.78	0.36	0.01
Gd	9	10.18	0.19	3.2	3.12	0.08	3.01	0.6	0.03
Tb	1.3	1.33	0.02	0.52	0.54	0.01	0.3	0.06	0.01
Dy	6.29	6.41	0.08	3.4	3.42	0.05	2.12	0.42	0.04
Ho	1.03	1.09	0.01	0.81	0.74	0.01	0.4	0.08	0.01
Er	2.48	2.44	0.04	2.1	2.07	0.03	0.23	0.05	0.01
Tm	0.37	0.33	0.02	0.29	0.33	0.01	0.4	0.08	0.00
Yb	1.8	1.85	0.03	2.05	2.09	0.03	0.44	0.09	0.01
Lu	0.24	0.27	0.00	0.35	0.35	0.01	0.12	0.02	0.01
Hf	5.4	5.79	0.09	1.55	1.53	0.03	4.46	0.89	0.07
Ta	5.5	6.15	0.06	0.31	0.30	0.01	0.68	0.14	0.01
tot Pb	4	4.1	0.1	3.3	3.3	0.6	25.4	5.1	2.1
Th	11	10.72	0.28	0.33	0.35	0.02	2.73	0.55	0.01
U	2.4	2.43	0.07	0.31	0.29	0.03	0.78	0.16	0.00

Accepted standard values taken from Potts et al., 1992

Table E.2. Comparison of trace element concentrations of the internal standard (KI 202) analysed in each batch

PPM	KI 202	KI 202	KI 202	KI 202	KI 202	KI 202	KI 202	KI 202	KI 202	AVERAGE	1SD	2SD	RSD
Sc	17	18	17	17	17	17	18	16	16	17	0.6	1.3	3.8
Ti (wt%)	0.75	0.85	0.82	0.81	0.82	0.82	0.82	0.72	0.76	0.80	0.0	0.1	5.3
V	179	182	179	173	176	176	177	179	166	176	4.6	9.3	2.6
Cr	2.6	2.2	1.2	2.8	2.8	2.8	2.8	2.4	1.8	2.4	0.6	1.1	23.7
Mn (wt%)	0.15	0.16	0.16	0.15	0.16	0.16	0.16	0.15	0.15	0.15	0.0	0.0	2.3
Co	37	39	39	38	38	38	38	38	36	38	1.0	2.1	2.7
Ni	4.7	4.7	4.0	4.0	3.6	3.7	3.7	4.8	4.1	4.2	0.5	1.0	11.4
Cu	38	40	38	39	39	39	40	39	36	39	1.3	2.6	3.4
Zn	62	67	67	68	70	68	71	66	63	67	2.9	5.9	4.4
Ga	17	18	18	17	17	17	17	17	17	17	0.5	1.0	2.9
Rb	62.8	72.6	72.1	71.0	70.7	70.9	71.5	71.3	66.2	69.9	3.2	6.5	4.6
Sr	342	427	429	412	411	412	412	381	387	401	27.5	55.0	6.9
Y	26	28	28	28	28	28	28	28	26	27	0.9	1.9	3.4
Zr	168	180	181	178	177	177	177	179	165	176	5.6	11.1	3.2
Nb	7.90	8.41	8.55	8.38	8.34	8.34	8.40	8.36	7.84	8.28	0.2	0.5	2.9
Cs	2.88	3.11	3.09	3.06	3.04	3.05	3.05	3.00	2.84	3.01	0.1	0.2	3.1
Ba	484	628	646	646	643	640	641	655	602	621	53.4	106.9	8.6
La	19.4	20.6	21.1	21.1	21.0	20.8	20.9	21.5	19.7	20.7	0.7	1.4	3.4
Ce	39.9	41.3	42.0	42.0	42.2	42.0	42.1	43.2	39.5	41.6	1.2	2.3	2.8
Pr	5.20	5.36	5.40	5.37	5.43	5.30	5.36	5.52	5.06	5.33	0.1	0.3	2.5
Nd	21.2	22.1	22.2	22.2	22.5	22.2	22.4	22.8	20.9	22.1	0.6	1.2	2.8
Sm	4.57	4.74	4.81	4.79	4.82	4.79	4.85	4.93	4.53	4.76	0.1	0.3	2.7
Eu	1.14	1.23	1.24	1.20	1.22	1.21	1.23	1.26	1.14	1.21	0.0	0.1	3.5
Gd	4.44	4.79	4.75	4.75	4.74	4.73	4.86	4.86	4.46	4.71	0.2	0.3	3.2
Tb	0.70	0.76	0.74	0.75	0.76	0.76	0.75	0.76	0.71	0.74	0.0	0.0	3.3
Dy	4.12	4.41	4.39	4.40	4.43	4.40	4.40	4.50	4.18	4.36	0.1	0.2	2.8
Ho	0.86	0.92	0.94	0.92	0.92	0.92	0.92	0.93	0.88	0.91	0.0	0.1	2.9
Er	2.42	2.53	2.62	2.59	2.60	2.54	2.57	2.59	2.41	2.54	0.1	0.2	3.1
Tm	0.42	0.43	0.44	0.41	0.41	0.40	0.42	0.42	0.38	0.41	0.0	0.0	3.9
Yb	2.55	2.72	2.73	2.70	2.71	2.71	2.70	2.72	2.56	2.68	0.1	0.1	2.7
Lu	0.42	0.46	0.46	0.45	0.45	0.45	0.45	0.45	0.43	0.45	0.0	0.0	3.0
Hf	4.41	4.65	4.73	4.63	4.63	4.62	4.69	4.71	4.42	4.61	0.1	0.2	2.5
Ta	0.77	0.81	0.81	0.81	0.82	0.81	0.82	0.81	0.77	0.80	0.0	0.0	2.4
tot Pb	10.4	11.5	11.6	11.6	11.6	11.6	11.6	11.7	10.5	11.3	0.5	1.0	4.6
Th	7.33	8.00	8.25	8.24	8.27	8.14	8.20	8.29	7.46	8.02	0.4	0.7	4.6
U	1.78	1.93	1.99	1.968	2.01	1.962	1.983	2.02	1.79	1.94	0.1	0.2	4.7

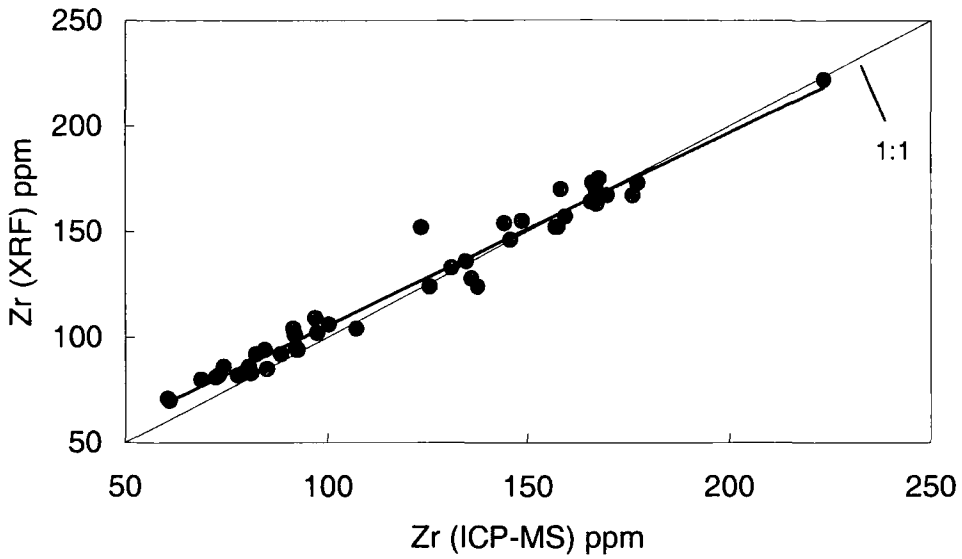

Fig. E.1. Comparison of ICP-MS versus XRF Zr concentration data for IVC volcanic rocks. XRF data from Sitorus (1990).

E.5. Radiogenic Isotope analysis

E.5.1. Sample dissolution Sr, Nd and Hf

Sample preparation for Sr, Nd and Hf isotope analysis was undertaken at the Arthur Holmes Isotope Geology Laboratory (AHIGL), University of Durham. The sample dissolution procedure and separation of Hf and Nd from rock samples is based on that presented by Dowall et al. (2003). The separation procedure for Sr in this study differs from that outlined in Dowall et al. (2003) and is described in more detail in E.5.2.

The initial sample dissolution procedure is identical for Sr, Nd and Hf. Around 150mg of whole rock powder was dissolved in a 3:1 HF/HNO_3 mixture in sealed Teflon beakers and left on a hotplate at 120°C for at least 24 hours. Once the powder had dissolved the solution was evaporated under clean air extraction. Care was taken when drying-down samples to not bake the samples, as this can cause the formation of fluoride compounds, which can be difficult to re-dissolve. 1ml of 16N HNO_3 was added to each beaker, which was then heated and placed on the hotplate for several hours. The HNO_3 was then evaporated. This step was

repeated again to ensure the removal of any remaining HF. 1ml of 12N HCl was then added to each sample, which was heated to ensure dissolution and then dried down. 1ml of 1N HCl was added to the samples, which were put back on the hot plate with the top tightly sealed. The solution was then centrifuged in pre-cleaned (with 6N HCl and then MilliQ H_2O) centrifuge tubes. After centrifugation, the supernatant acid solution was put through a series of cation and anion exchange columns to separate Sr-Nd-Hf bearing fractions.

E.5.2. Separation of Sr

At this stage a 200µl aliquot of sample was removed from the centrifuge tube and placed into a clean beaker and dried down. 100μl of 3N HNO_3 was added to each beaker, which was then sealed and placed back on the hotplate. The micro-column technique used to separate Sr is based on that published by Charlier et al. (2006). The Sr spec. resin was cleaned before and between use (if the resin was reused a second time) with ~1 cm height of MilliQ H_2O, which was agitated with small plastic pipette to ensure fluid flow through the resin. The resin cleaning and pre-conditioning procedure is given in Table E.3. After pre-conditioning the sample was loaded very carefully on to the resin with clean pipette tips for each sample. Beakers were then rinsed with MilliQ H_2O and filled with ~ 1ml of 6N HCl. The beakers were placed on the hotplate while 50μl 3N HNO_3, 100μl 3N HNO_3, 150μl 3N HNO_3, 200μl 3N HNO_3 were carefully pipetted onto the resin and allowed to drain through before every new volume of HNO_3 was added (Table. E.3). The Sr beakers were then removed from the hotplate, after cooling, the contents were emptied to waste and the beakers were rinsed with MilliQ H_2O. The Sr was then released from the resin by 100μl MilliQ H_2O which was collected from the columns, followed by 200μl MilliQ H_2O that was also collected. 15μl of concentrated HNO_3 was then added to each beaker. The samples were then ready to run on the mass spectrometer (after sample dilution).

Table E.3. Procedure for cleaning and pre-conditioning of Sr spec. resin and separation of the Sr fraction from the sample solution

Reagent	Volume (ml)	Action	Purpose
6N HCl	2 CV	Elute	Remove residual Sr
18.2MΩ H_2O	1 CV		Washes off HCl
3N HNO_3	200 μl		Pre-conditions column
3N HNO_3	200 μl		
Load sample (in 100μl 3N HNO_3) elute to waste and clean beakers (0.5 ml 6N HCl and sweat on hotplate)			
3N HNO_3	50 μl	Elute	Carefully releases bulk sample from resin
	100 μl		
	150 μl		
	200 μl		
18.2MΩ H_2O	100 μl	Collect	Releases Sr
18.2MΩ H_2O	200 μl		

CV = column volume

E.5.3. Separation of Nd and Hf

The separation of Nd and Hf from the sample solution follows the 2-stage ion exchange chemical separation procedure in Dowall et al. (2003). However, slight changes were made to the volumes of reagent processed, so a summary of the procedure is presented in Tables E.4-E.7.

The Nd cut from the first-stage cation column was dried down and 1ml of 3% HNO_3 diluent was added to each beaker. The solution was transferred into 2ml micro-centrifuge tubes pre-cleaned with Teflon distilled HCl. The Hf cut from the first stage cation column was dried down on the hotplate and 1ml 0.52N H_2SO_4 & 5% H_2O_2 was added to each vial. Once the Hf residue had dissolved, the solution was loaded on the second-stage anion columns. After the 0.52N H_2SO_4 - 5% H_2O_2 solution had eluted through the anion-exchange resin the column tip was checked for yellow colouration, if the liquid was still yellow, then the second step in Table E.7 was repeated and an additional 5mls of 0.52N H_2SO_4 – 5% H_2O was eluted through the resin. After the Hf cut was collected, samples were dried down at 220°C to evaporate concentrated H_2SO_4. Some of the columns leak a small amount of resin,

therefore, H_2O_2 was added to oxidise and remove the organic resin beads. After evapoartion, 0.5ml of 3% HNO_3 diluent was added to each beaker along with 1 drop of 29N HF.

Table E.4. Procedure for cleaning and pre-conditioning of Bio-Rad AG50W-X8 cation-exchange resin

Reagent	Volume (ml)	Purpose
29N HF	10	Removes residual Hf
18.2MΩ H_2O	10	Washes off HF
6N HCl	10	Removes residual Nd and Sr; converts resin to chloride form
18.2MΩ H_2O	10	Washes off HCl
1N HCl	10	Conditions column prior to loading sample

Modified from Dowall et al. (2003)

Table E.5. Procedure for separation of Nd and Hf bearing fractions

Reagent	Volume (ml)	Action	Purpose
1N HCl	1	Load sample and collect	Collects Hf and other HFSE and Period 1 transition elements
1N HF – 1N HCl	3	Collect	Collects Hf and other HFSE and Period 1 transition elements
1N HF – 1N HCl	13	Elute	Removes bulk sample plus Rb
2.5N HCl	14	Elute	Removes Sr and other alkaline earth elements
2N HNO_3	10	Elute	Removes Ba
6N HCl	12	Collect	Nd plus other REE

Modified from Dowall et al. (2003)

Table E.6. Procedure for cleaning and pre-conditioning of Bio-Rad AG1-X8 anion-exchange resin.

Reagent	Volume (ml)	Purpose
29N HF	5	Removes residual Hf
18.2MΩ H_2O	5	Washes off HF
12N H_2SO_4	4	Converts resin to sulphate form
18.2MΩ H_2O	5	Washes off H_2SO_4
0.52N H_2SO_4 – 5% H_2O_2	6	Conditions column prior to loading sample

Modified from Dowall et al. (2003)

Table E.7. Procedure for separation of Hf and Zr from Ti

Reagent	Volume (ml)	Action	Purpose
0.52N H_2SO_4 - 5% H_2O_2	1	Load and elute	Removes Ti and other Period 1 transition elements
0.52N H_2SO_4 - 5% H_2O_2	5	Elute	Removes Ti and other Period 1 transition elements
1N HF – 2N HCl	4	Collect	Collects Hf, Zr and other HFSE

Modified from Dowall et al. (2003)

E.5.4. Analysis

Sr, Nd and Hf fractions were measured for isotope ratios using the AHIGL ThermoElectron Neptune Multi-collector Plasma Mass Spectrometer (MC-ICP-MS). Detailed instrument operating conditions (including cup configurations and interference corrections) are presented in Nowell et al. (2003) and Dowall et al. (2003). The basic analytical method used for each element on the Neptune comprises a static multi-collection routine of 1 block of 50 cycles with an integration time of 4 seconds per cycle; total analysis time 3.5 minutes. However, a static multi-collection routine of 9 blocks of 10 cycles with an integration time of 4 seconds per cycle was initially used for Nd and Hf cuts analysed in 2002 (see Tables E.8 and Appendix C).

After chemistry, Sr samples (in 1ml of 3%HNO_3) were introduced into the Neptune using an ESI PFA50 nebuliser and a dual cyclonic–Scott Double Pass spray chamber. With this sample introduction set up, and the normal H skimmer cone, the sensitivity for Sr on the Neptune is typically ~60V total Sr ppm^{-1} at an uptake rate of 90µl min^{-1}. Prior to analysis a small aliquot was first tested to establish the Sr concentration of each sample by monitoring the size of the ^{84}Sr beam (^{88}Sr was too high in non-diluted aliquot to measure directly) from which a dilution factor was calculated to yield a beam of approximately 20V ^{88}Sr.

Instrumental mass bias was corrected for using a $^{88}Sr/^{86}Sr$ ratio of 8.375209 (the reciprocal of the $^{86}Sr/^{88}Sr$ ratio of 0.1194) and an exponential law.

The REE cuts containing the Nd fraction (in 1ml of 3% HNO_3) were introduced into the Neptune using an ESI PFA50 nebuliser and a dual cyclonic–Scott Double Pass spraychamber. With this sample introduction set up, and the normal H skimmer cone, the sensitivity for Nd on the Neptune is 60-80V total Nd ppm^{-1} at an uptake rate of 90µl min^{-1}. Instrumental mass bias was corrected for using a $^{146}Nd/^{145}Nd$ ratio of 2.079143 (equivalent to the more commonly used $^{146}Nd/^{145}Nd$ ratio of 0.7219) and an exponential law. The $^{146}Nd/^{145}Nd$ ratio is used for correcting mass bias since at Durham Nd isotopes are measured on a total REE-cut and this is the only Ce and Sm-free stable Nd isotope ratio. This approach requires a correction for isobaric interferences from Sm on ^{144}Nd, ^{148}Nd and ^{150}Nd (see Nowell and Parrish (2002)).

Hf samples (in 0.5ml 3%HNO_3 – 1N HF) were introduced using an ESI PFA50 nebuliser together with a Cetac Aridus desolvator. With this sample introduction set up, and the high sensitivity X skimmer cone, which was used in most analytical sessions (Table E.8), the sensitivity for Hf on the Neptune was 400-450V total Hf ppm^{-1} at an uptake rate of 90µl min^{-1}. Instrumental mass bias was corrected for using a $^{179}Hf/^{177}Hf$ ratio of 0.7325 and an exponential law. Corrections for isobaric interferences from Yb and Lu on ^{176}Hf were made by monitoring $^{172\text{-}173}Yb$ and ^{175}Lu and using the approach of Nowell and Parrish (2002).

E.5.5. Accuracy, precision, reproducibility and repeatability of data

Samples were analysed on several separate occasions. Data quality was monitored over the separate sessions by frequent analysis of standard reference materials throughout each run. Details of individual standards run are given in Table E.8 and a summary of all standard data is presented in Table E.9. The reproducibility of the $^{87}Sr/^{86}Sr$, $^{143}Nd/^{144}Nd$ and $^{176}Hf/^{177}Hf$

ratios for the respective standard solutions in each of the individual analytical sessions are better than 42 ppm in all cases, and generally better than 20 ppm (Table E.8). The average standard isotope ratios measured lie within error of respective accepted values. Nd is analysed as part of a total REE cut, therefore, pure standards and Sm doped standards were run to test the accuracy of the interfering element corrections. Table E.9 shows good agreement between the pure Nd and Sm doped Nd isotopic standard ratios, which illustrates the accuracy of the interference correction procedure. Sr-Nd-Hf isotope data presented in this thesis are plotted relative to NBS 987, J&M and JMC 475 standard values of 0.71024 (Thirlwall, 1991), 0.511110 (Royse et al., 1998) and 0.282160 (Nowell, et al., 1998) respectively.

Table E.8. Reproducibility and accuracy of Sr, Nd and Hf isotope ratios for standard solutions measured in individual runs

$^{87}Sr/^{86}Sr$	07/08/2003 (a)	02/10/2003 (b)	27/05/2004 (c)	09/08/2004 (d)		
n =	14	12	14	13		
NBS 987	0.710267	0.710275	0.710246	0.710259		
2SD abs	0.000015	0.000012	0.000009	0.000008		
2SD ppm	21.0	17.1	12.9	11.7		
$^{143}Nd/^{144}Nd$	27/06/2002 (a)	29/07/2003 (b)	30/07/03 A (c)	30/07/03 B (d)	17/11/2003 (e)	08/10/2004 (f)
n =	18	15	5	9	13	14
J&M all	0.511099	0.511112	0.511115	0.511101	0.511104	0.511108
2SD abs	0.000020	0.000008	0.000003	0.000005	0.000009	0.000013
2SD ppm	38.9	14.8	6.4	10.2	17.2	25.7
n =	14	8	3	5	7	7
J&M - pure	0.511098	0.511110	0.511114	0.511102	0.511104	0.511105
2SD abs	0.000021	0.000008	0.000004	0.000004	0.000009	0.000009
2SD ppm	41.4	15.5	8.1	7.5	17.2	18.5
n =	4	7	2	4	6	7
J&M - Sm doped	0.511102	0.511114	0.511116	0.511101	0.511103	0.511111
2SD abs	0.000016	0.000004	0.000001	0.000007	0.000009	0.000013
2SD ppm	31.1	8.4	2.8	13.7	18.6	26.0
$^{176}Hf/^{177}Hf$	H-cone	Aridus + X-CONE				
	28/06/2002 (a)	23/07/2003 (b)	24/07/2003 (c)	10/12/2003 (d)	11/12/2003 (e)	11/08/2004 (f)
n =	11	10	9	11	8	13
JMC 475	0.282160	0.282145	0.282146	0.282143	0.282143	0.282154
2SD abs	0.000008	0.000002	0.000004	0.000005	0.000004	0.000007
2SD ppm	28.4	5.8	12.7	18.2	13.4	24.2

Letters in parentheses refer to corresponding analytical session of sample data presented in Appendix C

Table E.9. Average reproducibility and accuracy of Sr, Nd and Hf isotope ratios for standard solutions measured during this study

Element and Standard	Ratio	Accepted or reported value	Number of standards run	Mean measured value	Error (± 2SD absolute)	Error (± 2SD ppm)
Sr (NBS 987)	$^{87}Sr/^{86}Sr$	0.710240[i]	53	0.710262	0.000011	15.7
Nd (J&M - pure)	$^{143}Nd/^{144}Nd$	0.51111[ii]	44	0.511106	0.000009	18.0
Nd (J&M - Sm doped)	$^{143}Nd/^{144}Nd$	0.51111[ii]	30	0.511108	0.000009	16.7
Nd (J&M all)	$^{143}Nd/^{144}Nd$	0.51111[ii]	74	0.511106	0.000010	18.9
Hf (JMC 475 - H-CONE)	$^{176}Hf/^{177}Hf$	0.282160[iii]	11	0.282160	0.000008	28.4
Hf (JMC 475 - ARIDUS X-CONE)	$^{176}Hf/^{177}Hf$	0.282160[iii]	51	0.282146	0.000004	14.8

References: i, Thirlwall, 1991; ii, Royse et al., 1998; iii, Nowell et al., 1998.
Aridus and X-cone long-term average at Durham = 0.282145, 2RSD=26 ppm, n = 79 (Nowell et al., 2003; Pearson and Nowell, 2005).

Total procedural blanks (TPB) for Sr, Nd and Hf were determined by ICP-MS on the PerkinElmer ELAN 6000 quadrupole at the University of Durham. Throughout the course of this study TPBs were below 1.2 ng for Sr, 219 pg for Nd and 73 pg for Hf. Sr blanks were typically < 300pg. The higher value of 1.2ng was probably a result of moving to a new laboratory. These values are considered insignificant in relation to the quantity of Sr, Nd and Hf typically processed from the volcanic rocks (~12μg, ~3μg and 200-500ng respectively).

E.6. Stable isotope analysis

Oxygen isotope analyses of mineral separates were performed by laser-fluorination at Royal Holloway, University of London using the procedures outlined by (Macpherson et al. 2000). Around 10mg of clinopyroxene, olivine and plagioclase were separated from crushed and sieved samples by handpicking under a binocular microscope. Care was taken to avoid phenocrysts containing inclusions and cracks, or that showed signs of alteration. The mineral separates were then cleaned with distilled water, dried and then cleaned in acetone. The

mineral separates were then picked through again to obtain 2mg of the cleanest crystals. In general around 5-15 crystal fragments were used for a single analysis.

In-house standard values of SC olivine 2 and GMG II over the period of study were +5.24‰ ± 0.04 (1σ, n = 6) and +5.69‰ ± 0.08 (1σ, n = 15); within 0.01‰ of their accepted values. Precision and accuracy within runs were similar to the overall standard results. Oxygen yields were greater than 98% for olivine (n = 4), 93% for plagioclase and between 92-94% (n = 20) for clinopyroxene. Although the yields for plagioclase and clinopyroxene are slightly low, they were consistent over the three sessions. Replicate analyses of olivine, plagioclase and clinopyroxene were within 0.06‰, 0.09‰ and 0.04‰ respectively. Oxygen results are reported as per mille deviations relative to the standard mean ocean water (SMOW) standard, given by the relationship:

$$\delta^{18}O(‰) = \left[\left(\frac{^{18}O/^{16}O_{sample}}{^{18}O/^{16}O_{SMOW}}\right) - 1\right] x1000$$

Table F.1. Element distribution coefficients used in geochemical modelling

	OL	OPX	CPX	PLAG	MT
Rb	0.021	0.022	0.033	0.113	0.15
Ba	0.044	0.072	0.038	0.440	0.183
Th	0.260	0.048	0.035	0.059	0.235
K	0.013	0.017	0.010	0.178	0.045
Sr	0.048	0.048	0.139	2.512	0.11
Y	0.028	0.343	0.860	0.076	0.322
Yb	0.283	0.423	0.661	0.052	0.218
U	0.083	0.008	0.016	0.112	0.110
La	0.087	0.068	0.130	0.183	0.150
Nb	0.027	0.351	0.168	0.275	0.837
Zr	0.030	0.061	0.197	0.098	0.727
Hf	0.370	0.101	0.297	0.031	0.353
Ta	0.059	0.079	0.123	0.057	1.113
Ti	0.034	0.423	0.350	0.052	9.5

Distribution coefficients calculated as average values for basaltic-andesitic-dacitic systems taken from the GERM database (http://earthref.org/GERM/index.html).
OL, olivine; OPX, orthopyroxene; CPX, clinopyroxene; PLAG, plagioclase; MT, magnetite.

The Ph.D. Game

BEGINNING Throw away sanity to start	1. Supervisor gives you project title. Go on 3 spaces.	2. 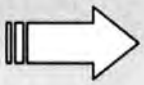	3. You are full of enthusiasm Have another turn.	4. Realise supervisor has given nothing but project title.	5. Go to library, you can't understand catalogue. Miss one turn.	6. 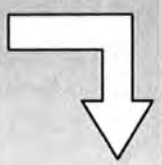
14. 	13. Unlucky for some, you become disillusioned. Miss one turn.	End of first year 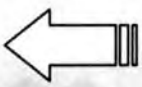	10. Beer monster strikes, spend 1 turn recovering.	9. Use beer to buy technical assistance. Go on two spaces.	8. Need supervisors help. Miss one turn finding him.	7. Important reference is in Japanese. Back two spaces.
15. You become depressed. Miss two turns.	16. You become more depressed. Miss three turns.	17. Change Project. Go back to beginning	18. Change supervisor. Go on 6 spaces	19. Demonstrate to get some extra cash. Go on 2 spaces	20. 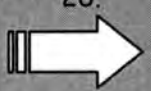	21. Lab demos take up too much of your time. Back 4 spaces
28. You begin to think you'll never finish. You are probably right.	27. 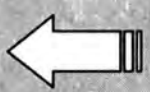	26. Work every weekend for 5 months. Go on 6 spaces.	25. End of second year. No results, who cares, throw again.	24. Labs closed for 8 months due to building move. Go back to 15.	23. Samples labelled incorrectly. Go back to 20.	22. 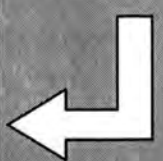
29. 	30. You spend more time complaining than working! Miss one turn.	31. You realise your mates are earning 5 times your grant, have a good cry.	32. You are asked why you started a PhD. Miss a turn finding a reason.	33. You are offered a job, you may continue or retire from the game.	34. Start writing up, now you are really depressed. Miss 5 turns	35. 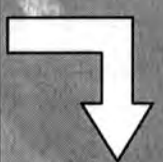
42. Your PhD is awarded congrats, now join dole queue	41. You are asked to resubmit thesis. Back to 33.	40. You decide PhD isn't worth the bother, withdraw now. Game over.	39. It proves impossible to write-up and work. Go to 33.	38. Your thesis will disprove external examiners work. Go back to 28.	37. Your data have just been published by rival group. Go back to 28.	36. End of third year 

Modified from the J. I. version (2001).